

EFP-98 Terrigene aflejrings kildebjergartspotentiale – slutrapport

EFP-98/1313-98-0022

Jørgen A. Bojesen-Koefoed, Hans Peter Nytoft,
Henrik I. Petersen og Per Rosenberg



EFP-98 Terrigene aflejrings kildebjergartspotentiale – slutrapport

EFP-98/1313-98-0022

Jørgen A. Bojesen-Koefoed, Hans Peter Nytoft,
Henrik I. Petersen og Per Rosenberg

A F S L U T N I N G S S K E M A
for projekter inden for energiforskningsprogrammet.

EFP-98

Journalnr.: 1313/98-0022

Område: Olie og naturgas

Titel: Terrigene aflejrings kildebjergartspotentiale (petroleum source potential of terrigenous source rocks)

Tilsagnshaver: Danmarks og Grønlands Geologiske Undersøgelse (GEUS), Thoravej 8, 2400 København NV, Projektansvarlig: Erik Thomsen

Projektleder: Jørgen A. Bojesen-Koefoed

Deltagende virksomheder/institutioner: GEUS, se dog vedlagte liste

Projektets finansiering: (x 1.000 kr.)

EFP-tilsagn: (faktisk udbetalt)..... 2300

Anden finansiering: (faktisk modtaget).....

Egenfinansiering: (faktisk ydet)..... 2370

Total:..... 4670

Anden finansieringskilde:

Sammenfatning:

EFP-98 projektet "Terrigene aflejrings kildebjergartspotentiale" havde til formål at undersøge:

- organisk-rige terrigene bjergarters evne til at danne og afgive olie og gas.
- sammensætningen af olie og gas dannet fra sådanne kildebjergarter
- relationer mellem generativt potentiale, olietype og GOR og den optisk erkendbare kerogensammensætning.
- relationer mellem den kemisk erkendbare fordeling af "gas-prone", "oil-prone" og "inert" kerogen og den optisk erkendbare kerogensammensætning.
- de kinetiske aspekter af dannelse af olie og gas fra terrigene kildebjergarter.
- effekten af øget thermal modenhed på ovenfor nævnte forhold.
- mulige forskelle i kildebjergartspotentiale i forhold til geologisk alder og hermed udgangsmaterialets kemiske sammensætning. Herunder især mulige forskelle mellem terrigent materiale af gymnosperm oprindelse (ældre end midt-Kridt), og materiale af angiosperm oprindelse (yngre end midt-Kridt).
- muligheder for forbedret matematisk/numerisk modellering af olie-gas dannelse fra terrigene aflejringer.

De to sidstnævnte punkter har af praktiske/tekniske årsager måttet delvist opgives eller nedprioriteres, således som beskrevet i årsrapport pr. 31.1.2000.

Bortset herfra er samtlige opstillede punkter mere eller mindre indgående behandlet i de publicerede arbejder. Arbejdet har været samlet omkring dannelse af olie fra kul og kulskefibre, samt karakteristik og genkendelse af terrigene olier. Olie dannelse fra kul har været stærkt omdiskuteret, og undertiden rejses stadig tvivl om hvorvidt det er muligt. Imidlertid viser projektets resultater at det finder sted, og det har kunnet sandsynliggøres på hvilken måde kuls sammensætning kan spille en vigtig rolle for de kinetiske aspekter af olie dannelse fra kul. Undersøgelser af biomarkere, herunder omfattende syntesearbejder, har ført til en meget bedre forståelse af oprindelsen af biomarkere, der anses for karakteristiske for terrigene, henholdsvis marine, aflejringer, og et større antal hidtil ukendte biomarkører er identificeret. Dette har styrket mulighederne for at se kausale sammenhænge mellem oliers biomarker-signatur og kildebjergarters aflejringsmiljø. Samlet har projektet bidraget med megen væsentlig ny viden, der i internationalt perspektiv vil være nyttig i efterforskningsammenhæng.

Engelsk resume (abstract):

The objectives of the EFP-98 research project "Petroleum source potential of terrigenous source rocks" were to investigate:

- The capacity of organic-rich terrigenous deposits to generate and expel petroleum liquids
- The composition of petroleum liquids generated from such sources
- The relationships between generation potential, petroleum characteristics, and the kerogen composition
- Relationships between the pyrolytically defined distribution of gas-prone, oil-prone, and inert kerogen and the kerogen composition as defined optically
- Kinetics of petroleum generation from terrigenous deposits
- Maturity effects on the generation of petroleum liquids from terrigenous deposits
- Possible relationships between generation capacity and geological age, e.g. differences between gymnosperm-derived versus angiosperm-derived kerogen
- Improved numerical/mathematical modelling of the generation of petroleum liquids from terrigenous deposits.

With the exception of the latter two objectives, which for technical/practical reasons described elsewhere (yearly report January 31st, 2000) had to assume lower priority or be excluded from the project, all objectives mentioned have been addressed in varying degrees of detail; the results have been reported in a number of published papers and conference contributions. The work has been focused on the generation of petroleum liquids from coals and coaly shales, and the characteristics and diagnostic features of such liquids. Although generation of petroleum from coals has been, and occasionally still is, debated, the results of the project clearly demonstrate its feasibility and validity. Moreover, relationships between coal composition and the kinetics of petroleum formation have been shown. Detailed biomarker analyses, including extensive synthesis work, have led to an improved understanding of the significance and origin of certain biomarkers that are assumed to be diagnostic of terrigenous or marine source depositional environments, and a number of unknown compounds have been identified. The results offer insights into hitherto unknown causalities between petroleum composition and source depositional environments. The project has contributed important new information that is potentially useful for petroleum exploration both within Danish territory as well as internationally.

Resultatudnyttelse og evt. nye aktiviteter:

Projektets resultater bidrager generelt til en forøget forståelse af petroleumssystemer baseret på terrestriske aflejringer, og prospektiviteten af bassiner domineret af sådanne systemer. Specifikt har projektet bidraget til en dybere forståelse af petroleumssystemer i Nordsøen og Vietnam, og herigennem forbedret definitionen af playtyper.

Projektets afrapporteringsform sikrer en stor udbredelse af resultaterne, til gavn for olie-gas efterforskning på Dansk område, såvel som internationalt.

Rapporter, publikationer, symposier m.v.:

Se vedlagte liste

Tilsagnshaver: GEUS Dato:.....26. januar.2001 Underskrift:.....

Energistyrelsen:

Deltagere

Følgende personer (i alfabetisk orden) har bidraget til nærværende forskningsprojekt:

C. Andersen, konsulent, GEUS
J. Andsbjerg, seniorforsker, GEUS
P. H. Anh, VPI, Ho Chi Minh City, Vietnam
J. A. Bojesen-Koefoed, seniorforsker, GEUS (*projektleder*)
D. Christensen, ingeniør
F. G. Christiansen, statsgeolog, GEUS
G. Dam, seniorforsker, GEUS (fra 1.12.2000: DONG)
Y. Desezar, overlaborant, GEUS
P. T. Dien, VPI, Hanoi
M. G. Fowler, senior scientist, GSC Calgary, Canada
M.-B. H. Frost, ingeniør
J. Halskov, tegner, GEUS
B. F. Hjortkjær, stipendiat, GEUS
A. Jensen, ingeniør
D. Kiel-Dühring, overlaborant, GEUS
C. Guvad, laboratoriekoordinator, GEUS
T. K. C. Jørgensen, ingeniør
R. B. Larsen, ingeniør
J. Lautrup, fotograf, GEUS
K. Lund, ingeniør
A. Mathiesen, seniorrådgiver, GEUS
E. Melskens, tegner, GEUS
L. H. Nielsen, seniorforsker, GEUS
L. L. Nielsen, overlaborant, GEUS
H. P. Nytoft, seniorrådgiver, GEUS
L. K. Núñez-Betelu, University of the Basque Country, Spanien
M. Pearson, University of Aberdeen, Scotland
G. K. Pedersen, lektor, Geologisk Institut, Københavns Universitet
H. I. Petersen, seniorforsker, GEUS
T. Richardt, ingeniør
P. Rosenberg, seniorrådgiver, GEUS
P. Schiøler, seniorforsker, GEUS
F. Surlyk, professor, Geologisk Institut, Københavns Universitet
S. Sølberg, tegner, GEUS
S. W. Sørensen, ingeniør
L. Thanh, VPI, Hanoi, Vietnam
L. H. Thiem, Petrovietnam, Hanoi, Vietnam
E. Thomsen, statsgeolog, GEUS
J. V. Thomsen, ingeniør
H. Vosgerau, forsker, GEUS
H. Wielens, seniorgeolog, GSC Halifax, Nova Scotia, Canada
H. Zhou, stipendiat, University of Aberdeen, Scotland

Publicerede arbejder m.v.

Langt hovedparten af resultaterne af forskningsprojektet "Terrigene aflejrings kildebjergartspotentiale" er afrapporteret i form af diverse internationale publikationer som angivet nedenfor, kopi vedlagt (posters og foredrag dog undtagne).

Abstracts

1. Nytoft, H. P., Thomsen, J. V, Jørgensen, T. K. C., Bojesen-Koefoed, J. A: & Petersen, H. I. 1999. Hopa-15-17(21)-dienes in sediments: precursors of diahopanes? *19th International Meeting on Organic Geochemistry, Istanbul, 6-10 september 1999; Abstracts vol. #1, 13-14*
2. Bojesen-Koefoed, J. A., Nytoft, H. P. & Petersen, H. I. 1999. Landwards - seawards directional facies changes in Middle Jurassic oil-prone coals recorded by composition of derived oils, Søgne Basin, Central Graben, North Sea. *19th International Meeting on Organic Geochemistry, Istanbul, 6-10 september 1999; Abstracts vol. #1, 181-182*
3. Nytoft, H. P. & Bojesen-Koefoed, J. A. 2000. 21-methyl-28-norhopanes: a new series of rearranged hopanes related to 18 α -neohopanes. *Gordon Research Conference on Organic Geochemistry, Holderness, New Hampshire, USA, 13-18 aug 2000*
4. Nytoft, H. P. & Bojesen-Koefoed, J. A. (*fremsendt*) Carbon number distribution of 18 α -neohopanes and related compounds. *20th International Meeting on Organic Geochemistry, Nancy, September 2001*
5. Zhou, H., Pearson, M., Bojesen-Koefoed, J. A. & Nytoft, H. P. (*fremsendt*) Geochemical correlation of seep oils and hydrocarbon sourcing, Nuussuaq Basin, west Greenland. *20th International Meeting on Organic Geochemistry, Nancy, September 2001*

Posters

1. Nytoft, H. P., Bojesen-Koefoed, J. A., Christensen, D., Frost, M.-B. H., Jensen, A. Larsen, R. B. & Richardt, T. 1998. Hydrogenation and acid-induced rearrangement of hop-17(21)-enes, neohop-13(18)-enes and hopadienes: some factors controlling the distribution of hopanes and rearranged hopanes. *Gordon Research Conference on Organic Geochemistry, New Hampshire, USA*
2. Bojesen-Koefoed, J. A., Nytoft, H. P. & Petersen, H. I. 1999. Landwards - seawards directional facies changes in Middle Jurassic oil-prone coals recorded by composition of derived oils, Søgne Basin, Central Graben, North Sea. *19th International Meeting on Organic Geochemistry, Istanbul, 6-10 september 1999*

3. Zhou, H., Pearson, M., Bojesen-Koefoed, J. & Nytoft, H. P. 2000. Geochemical correlation of West Greenland seep oils. *BOGS*, 5-7 jul. 2000
4. Nytoft, H. P. & Bojesen-Koefoed, J. A. 2000. 21-methyl-28-norhopanes: a new series of rearranged hopanes related to 18 α -neohopanes. *Gordon Research Conference on Organic Geochemistry, Holderness, New Hampshire, USA, 13-18 aug 2000*

Foredrag

1. Bojesen-Koefoed, J. A., Christiansen, F. G., Nytoft, H. P., & Petersen, H. I. 1998. Petroleum source potential and the importance of marine versus terrigenous organic matter input: a comparative study of mid-Cretaceous deposits from Ellesmere Island, Northwest Territories, Canada. *Fifteenth Annual Meeting of the Society for Organic Petrology, Halifax, Nova Scotia, Canada*
2. Petersen, H. I., Bojesen-Koefoed, Nytoft, H. P., & Rosenberg, P. 1998. Composition and depositional environment of petroleum-generating Middle Jurassic coals, Danish North Sea. *Fifteenth Annual Meeting of the Society for Organic Petrology, Halifax, Nova Scotia, Canada*
3. Nytoft, H. P., Thomsen, J. V, Jørgensen, T. K. C., Bojesen-Koefoed, J. A: & Petersen, H. I. 1999. Hopa-15-17(21)-dienes in sediments: precursors of dihopanes? *19th International Meeting on Organic Geochemistry, Istanbul, 6-10 september 1999*
4. Andersen, C., Mathiesen, A., Nielsen, L. H., Tiem, P. V. & Dien, P. T., 1999. Petroleum Systems in the Northern part of the Song Hong basin, Gulf of Tonkin - Vietnam. *Tectonics, Stratigraphy and Petroleum and Mineral Systems of Palawan, Borneo and Surrounding Areas. An International Conference, Philliphines 1999.*
5. Petersen, H. I., Andersen, C., ielsen, L. H. 2000 Hydrocarbon potential of the northeastern Song Hong Basin: implications from immature terrestrial source rocks. Extended abstract, *25th Anniversary of PetroVietnam, Technical Conference, September 2000, Hanoi, Vietnam, 196-204*

Artikler og "extended abstracts"

1. Bojesen-Koefoed, J. A., Christiansen, F. G., Nytoft, H. P., & Petersen, H. I.. 1998. Petroleum source potential and the importance of marine versus terrigenous organic matter input: a comparative study of mid-Cretaceous deposits from Ellesmere Island, Northwest Territories, Canada. "Extended Abstract", Mukhopadhyay, P. K., Avery, M. P., Calder, J. H. & Goodarzi, F. (eds): *Fifteenth Annual Meeting of the Society for Organic Petrology, Abstracts and Program, vol. 15, p. 57-60*

2. Petersen, H. I., Bojesen-Koefoed, Nytoft, H. P., & Rosenberg, P. 1998. Composition and depositional environment of petroleum-generating Middle Jurassic coals, Danish North Sea. "Extended Abstract", Mukhopadhyay, P. K., Avery, M. P., Calder, J. H. & Goodarzi, F. (eds): *Fifteenth Annual Meeting of the Society for Organic Petrology, Abstracts and Program, vol. 15, p. 67-70*
3. Petersen, H. I. & Vosgerau, H. 1999. Composition and organic maturity of Middle Jurassic coals, North-East Greenland: evidence for liptinite-induced suppression of huminite reflectance. *International Journal of Coal Geology*, **41**, 257-274
4. Nytoft, H. P. Bojesen-Koefoed, J. A. & Christiansen, F. G. 2000, C₂₆ and C₂₈₋₃₄ 28-norhopanes in sediments and petroleum. *Organic Geochemistry*, **31**, 25-39
5. Petersen, H. I., Andersen, C., Nielsen, L. H. 2000. Hydrocarbon potential of the northeastern Song Hong Basin: implications from immature terrestrial source rocks. Extended abstract, *25th Anniversary of PetroVietnam, Technical Conference, September 2000, Hanoi, Vietnam*, 196-204
6. Petersen, H. I & Rosenberg, P. 2000 The relationship between the composition and rank of humic coals and their activation energy distributions for the generation of bulk petroleum. *Petroleum Geoscience* **6**, 137-149
7. Petersen, H. I., Andsbjerg, J., Bojesen-Koefoed, J. A. & Nytoft, H. P. 2000. Coal-generated oil: source rock evaluation and petroleum geochemistry of the Lulita oilfield, Danish North Sea. *Journal of Petroleum Geology* **23**, 55-90
8. Vosgerau, H., Bojesen-Koefoed, J. A., Petersen, H. I. & Surlyk, F. 2000. Forest fires, climate, and sea-level changes in a coastal plain shallow marine succession (Early - Middle Oxfordian Jakobsstigen Formation, North-East Greenland). *Journal of Sedimentary Research* **70**, 408-418
9. Petersen, H. I., Andersen, C. Anh, P. H., Bojesen-Koefoed, J. A., Nielsen, L. H., Nytoft, H. P., Rosenberg, P. & Thanh, L. 2001. Petroleum potential of Oligocene lacustrine mudstones and coals at Dong Ho, Vietnam - an immature outcrop analogue to possible terrestrial source rocks in the greater Song Hong Basin. *Journal of Asian Earth Sciences* **19**, 135-154

Manuskripter

1. Nytoft, H. P. & Bojesen-Koefoed, J. A.: 17 α 21 α (H)-hopanes: natural and synthetic. *Organic Geochemistry, genfremsendt efter revision.*
2. Bojesen-Koefoed, J. A., Dam, G., Hjortkjær, B. F., Nytoft, H. P., Pedersen, G. K. & Petersen, H. I. Drowning of a nearshore peatforming environment, Atane Formation (Cretaceous) at

Asuk, West Greenland: sedimentology, organic petrography and geochemistry. Organic Geochemistry, *under revision after review*

3. Petersen, H. I., Bojesen-Koefoed, J. A. & Nytoft, H. P. Source rock evaluation of Middle Jurassic coals, north-east Greenland by artificial maturation: aspects of petroleum generation from coal. AAPG Bulletin, *under revision after review*
4. Bojesen-Koefoed, J. A., Christiansen, F. G., Núñez-Betelu, L. K., Nytoft, H. P. & Petersen, H. I. Cretaceous source rocks in the Arctic: hydrous pyrolysis of black shales from Ellesmere Island, Northwest Territories, Canada – implications for exploration on- and offshore West Greenland and in the Melville Bay region. AAPG Bulletin, *under revision after review*

Videre arbejde

Udover de publicerede arbejder er flere manuskripter under planlægning eller i arbejde, herunder:

1. Nytoft, H. P., Bojesen-Koefoed, J. A., Christiansen, F. G. & Fowler, M. G. Oleanane or lupane - reappraisal of the presence of oleanane in Late Cretaceous - Tertiary oils and sediments. *in prep.*
2. Nytoft, H. P., Thomsen, J. V, Jørgensen, T. K. C., Lund, K., Bojesen-Koefoed, J. A., Petersen, H. I. & Sørensen, S. W. Hopa-15,17(21)-dienes in sediments. precursors of dihopanes. *in prep.*

Endvidere gennemfører Hongxiu ("Joy") Zhou et Ph.D. studium ved University of Aberdeen, Scotland i forlængelse af en del af nærværende projekt. Hongxiu ("Joy") Zhou's Ph.D. arbejde finder sted under vejledning af M. Pearson (University of Aberdeen) og Jørgen A. Bojesen-Koefoed (GEUS), og forventes afsluttet i løbet af 2002.

Udover de publicerede resultater findes en mindre mængde analyseresultater fra undersøgelser i Vestgrønland og fra undersøgelser i den norske del af Søgne Bassinet i Nordsøen, der endnu ikke er under publikation. Dette arbejder afventer mulighed for publikation i forbindelse med kommende forskningsprojekter. Publikation vil i så fald ske med skyldig reference til både nærværende og eventuelle kommende forskningsprojekter.

Hopa-15,17(21)-dienes in sediments: Precursors of diahopanes?

Hans Peter Nytoft, Jens Valdemar Thomsen, Toni Kennet Corleoné Jørgensen,
Jørgen A. Bojesen-Koefoed and Henrik Ingermann Petersen

Geological Survey of Denmark and Greenland (GEUS), Thoravej 8,
DK 2400 Copenhagen NV, Denmark

Synthetic C₃₀ Hopa-15,17(21)-diene has been known for some time, and a C₃₀ 17,21-epoxyhopane which can easily be converted to hopa-15,17(21)-diene has been isolated from a fern (Berti *et al.*, 1966). However, there seems to be no record of hopa-15,17(21)-dienes in sediments. We have identified a series of C₂₉-C₃₂ hopa-15,17(21)-dienes in thermally immature sediments ranging in age from recent (< 100 years) to Ordovician by comparison with standards synthesized from the corresponding hop-17(21)-enes. Synthesis involved epoxidation with 3-chloroperoxybenzoic acid and subsequent hydrochloric acid treatment. The hopadienes have been found in coals, marine sediments and lacustrine sediments, and their widespread occurrence suggests a bacterial origin. The distribution of hopa-15,17(21)-diene and hop-17(21)-ene homologs is usually very similar which indicates a genetic relationship between the hopadienes and the hop-17(21)-enes. In recent sediments we have only found the C₃₀ members of both series whereas in older sediments other homologs are present as well. A high content of both series has been found in highly immature samples with huminite reflectances of 0.2 - 0.3 % R_o. Hopadienes have so far not been found in samples with a huminite reflectance higher than 0.4 % R_o. The hopa-15,17(21)-dienes have very characteristic mass spectra. The base peak is m/z 144 + R. Other significant ions are M⁺ (4 %) and M⁺ - CH₃ (50-60 %). Hydrogenation of the C₃₀ hopa-15,17(21)-diene in 0.1 N perchloric acid/acetic acid gave a mixture of regular hopanes and a compound with the same mass spectrum and retention time as the 17 α (H)-15 α -methyl-27-norhopane ("17 α (H)-diahopane" or compound "X") which has been found in crude oils and mature sediments (Moldowan *et al.*, 1991; Farrimond *et al.*, 1996). It is thus probable that diahopanes in sediments are formed from the ubiquitous hopa-15,17(21)-dienes via clay catalysis. Work is currently underway to check (by NMR) that the synthetic and "natural" diahopanes are identical.

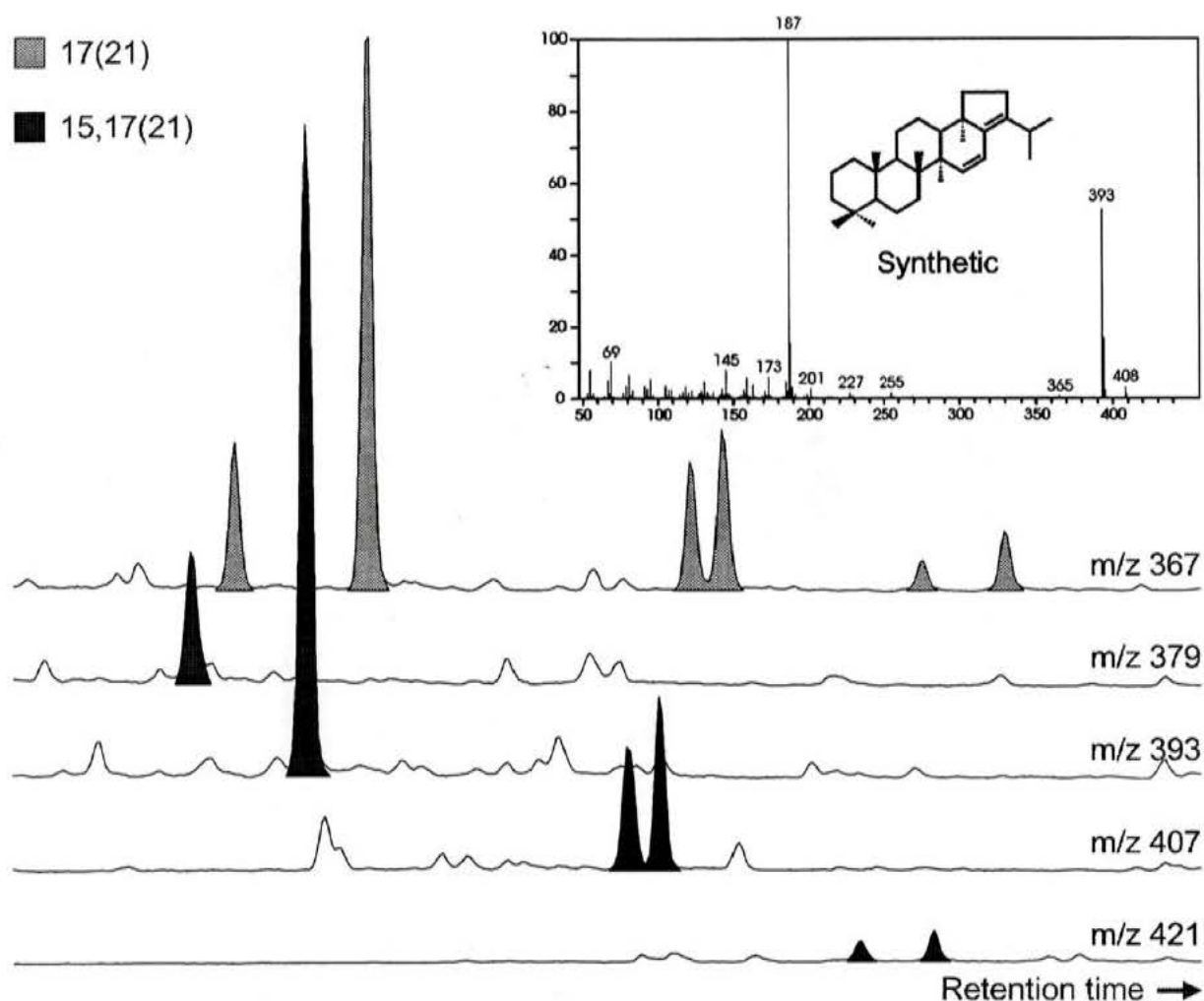


Fig. 1 Ion chromatograms showing C_{29} - C_{32} hop-17(21)-enes (m/z 367) and C_{29} - C_{32} hopa-15,17(21)-dienes (m/z 379,393,407 & 421) in a low rank Jurassic coal from Bornholm, Denmark

Berti, G., Bottari F., Marsili A. and Morelli I. (1966) A triterpenoid epoxide from polypodium vulgare *Tetrahedron Letters* 979-982.

Farrimond P. and Telnaes N. (1996) Three series of rearranged hopanes in Toarcian sediments (northern Italy). *Org. Geochem.* **25**, 165-177.

Moldowan J. M., Fago F. J., Carlson R. M. K., Young D. C., van Duyne G., Clardy J., Schoell M., Pillinger C. T and Watt D. S. (1991) Rearranged hopanes in sediments and petroleum. *Geochim. Cosmochim. Acta* **55**, 3333-3353.

**Landwards - seawards directional facies changes in Middle Jurassic
oil-prone coals recorded by composition of derived oils, Sogne Basin,
Central Graben, North Sea**

J. A. BOJESEN-KOEFOED¹, H. P. NYTOFT¹ and H. I. PETERSEN¹

¹ Geological Survey of Denmark and Greenland (GEUS), Thoravej 8,
DK-2400 Copenhagen NV, Denmark

The Bryne Formation (Bajonian – Callovian/Oxfordian) of the Søgne Basin, situated in the northern part of the Danish Central Graben, North Sea contains a succession of oil-prone coals, which have been penetrated and cored in a number of exploration wells. The coals, which were exhaustively described by Petersen *et al.* (1998), have acted as sources for commercial accumulations of oil and gas/condensate in the Harald Field, the Lulita Field and the Trym Field. The precursor peats were deposited in a paralic coastal plain environment. The nearshore setting of the depositional environment caused a subtle influence of relative sea-level changes on the composition of the peats. Hence, detailed organic petrographic and geochemical analyses of a large number of samples have allowed the discrimination of 4 seams, which were deposited under a comparatively rapid rise in relative sea-level (seams T1-T4) and 2 seams which were deposited during periods of more slowly rising relative sea-level (seams R1-R2). All seams show more or less well-developed directional changes in organic facies, corresponding to variations along a landwards – seawards transect of the palaeoenvironment of deposition, and the changes are recurring in the composition of hydrocarbons extracted from the coals. In particular, pristane/phytane ratios, the abundance of tricyclic triterpanes relative to pentacyclic triterpanes, and sterane and homohopane distributions serve to trace directional facies changes. In general, along a landwards to seawards trend pristane/phytane ratios decrease, the proportion of tricyclic triterpanes increase, the distribution of regular steranes shifts in favour of C₂₇ steranes, C₃₀ regular steranes are observed, and homohopane indices increase.

Sandstones, which are present overlying and interfingering with the oil-prone coals in the Bryne Formation host commercial accumulations of oil and gas, and a number of oil samples have been analysed from the West Lulu-1, West Lulu-3 (Harald Field), Lulita-1 (Lulita-Field), and 3/7-4 (Trym Field) wells. The wells are situated in varying positions relative to the Middle Jurassic palaeocoastline, and the geochemical variations with palaeogeographic position which were noted in the coals are recurring in the oil samples. Hence, from the West

Lulu-3 well, situated in the most landward position relative to the palaeocoastline, via the West Lulu-1 well to the Lulita-1 and 3/7-4 wells, which are situated closer to the palaeocoastline, a number of geochemical parameters change in a way that can be predicted from the observed changes in facies of the associated coals. These parameters include pristane/phytane ratios, the proportions of tricyclic triterpanes, and sterane and homohopane distributions. The landwards – seawards changes in oil composition are very similar to the observations made by McCaffrey *et al.* (1994) in their study of Beaufort Sea oils. The observed variations in oil composition imply simple vertical secondary migration pathways, with little lateral mixing of the expelled oils, and add further to prove the Bryne Formation coals as the sources for the oil accumulations in the Søgne Basin.

References

- McCaffrey, M., Dahl, J. E., Sundararaman, P., Moldowan, J. M. and Schoell, M. (1994) Source rock quality determination from oil biomarkers II – A case study using Tertiary-reservoired Beaufort Sea oils. *AAPG Bulletin* 78, 1527-1540
- Petersen, H. I., Andsbjerg, J., Bojesen-Koefoed, J. A., Nytoft, H. P. and Rosenberg, P. (1998) Petroleum potential and depositional environments of Middle Jurassic coals and non-marine deposits, Danish Central Graben, with special reference to the Søgne Basin. *Geology of Denmark Survey Bulletin* 36, 78pp.

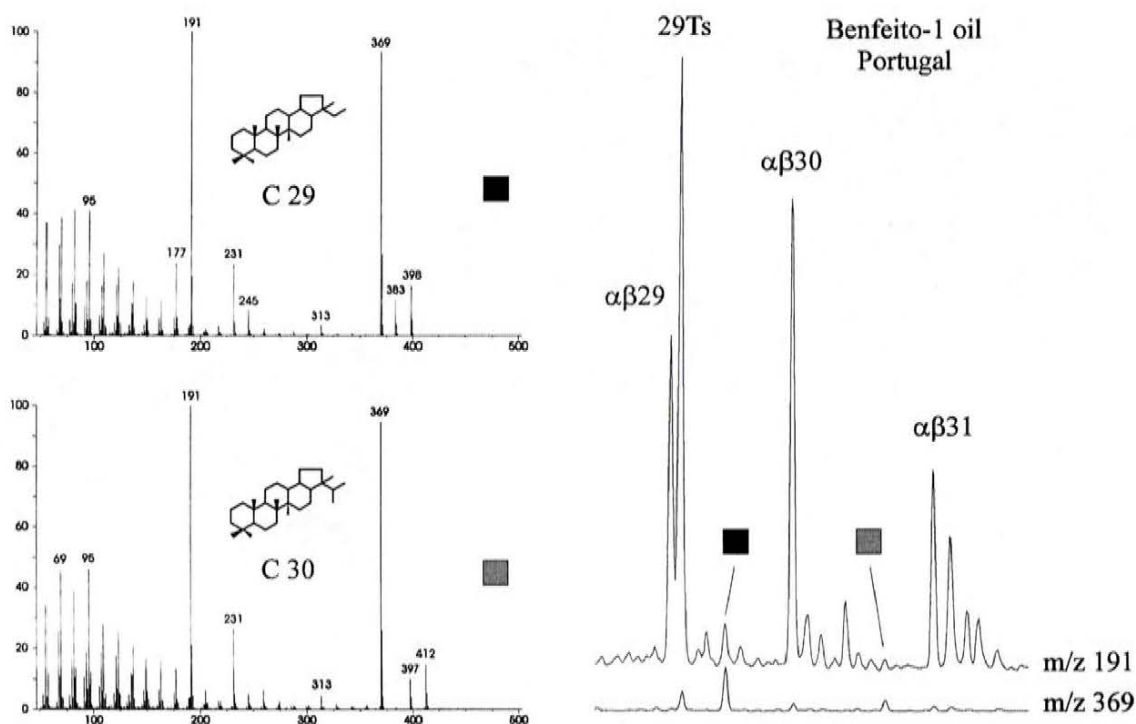
21-Methyl-28-norhopanes: a new series of rearranged hopanes related to 18 α -neohopanes.

Hans Peter Nytoft*, Jørgen A. Bojesen-Koefoed

Geological Survey of Denmark and Greenland, Thoravej 8, DK 2400 Copenhagen NV, Denmark

A new series of hopanes (C₂₉-C₃₁) has been tentatively identified as 21-methyl-28-norhopanes based on their mass spectra. Mass spectra were obtained from HPLC-purified compounds. All members of the series have an extremely large m/z 369 fragment (~90 % of m/z 191) corresponding to loss of the side chain because of the quaternary C21 carbon atom. The mass spectra also show similarities with the mass spectra of 28-norhopanes. The C₂₉ 21-methyl-28-norhopane elutes halfway between the C₃₀ diahopane and C₂₉ moretane. The C₂₉ 21-methyl-28-norhopane is always the dominant member of the series. The content of the C₃₀ compound is typically 5 times smaller, and the C₃₁ compound is absent in many samples. A C₃₀ A-ring methylated 21-methyl-28-norhopane (2 α -Me?) with a retention time only marginally longer than that of the corresponding non methylated compound has been noted.

The content of 21-methyl-28-norhopanes is usually low, but in some cases 21-methyl-28-norhopanes are more abundant than diahopanes. The restricted carbon number distribution of the new series is similar to that of 18 α -neohopanes. The content of C₂₉ 21-methyl-28-norhopane relative to 29Ts is relatively constant irrespective of the 29Ts/(29Ts + 29H) ratio suggesting a relationship between the two series. This was substantiated by laboratory hydrogenation of synthetic 30-norneohop-13(18)-ene in acid solution which in addition to regular hopanes and neohopanes yielded about 1% C₂₉ 21-methyl-28-norhopane.



CARBON NUMBER DISTRIBUTION OF 18 α -NEOHOPANES AND RELATED COMPOUNDS

H. P. Nytoft and J. A. Bojesen-Koefoed

Geological Survey of Denmark and Greenland (GEUS), 8 Thoravej, DK-2400 NV
Copenhagen, Denmark

Several series of rearranged hopanes such as C(14a)-Homo-26-nor-17 α -hopanes, 17 α -diahopanes, and the unidentified early-eluting hopane series have a carbon number distribution similar to that of regular hopanes. In contrast, 18 α -neohopanes are dominated by the C₂₇ and C₂₉ compounds (Ts and C₂₉Ts). The C₃₀ 18 α -neohopane (C₃₀Ts) is found in relatively low concentrations, and the higher members of the series have to our knowledge not been reported. However, in fractions obtained by reverse-phase HPLC of triterpane concentrates from crude oils we have recently found compounds which, based on mass spectral data and GC- and HPLC retention-times are tentatively identified as C₃₁ and C₃₂ 18 α -neohopanes (22S + 22R). The concentration of the higher carbon number 18 α -neohopanes is very low and in the *m/z* 191 ion chromatogram they are masked by various coeluting compounds. In case of C₃₁ 18 α -neohopanes, the main interfering compounds are gammacerane, a C₃₁ hexahydrobenzohopane and C₃₂ methylhopanes.

The most likely precursors of 18 α -neohopanes are neohop-13(18)-enes formed by acid catalyzed isomerization of the corresponding hop-17(21)-enes, which are abundant in immature sediments. In addition, at least C₃₀ neohop-13(18)-ene can be formed by isomerization of other triterpenes as well. We suspected that the peculiar carbon number distribution of 18 α -neohopanes was caused both by different reactivities of the various hop-17(21)-enes and by carbon number dependant equilibria of the two types of compounds. In order to test this, C₂₇, C₂₉, C₃₀ and C₃₁-22R hop-17(21)-enes were synthesized, and an equal mixture of the four compounds were subjected to acid catalyzed isomerization in 0.1 N perchloric acid/acetic acid at 35°C. The relative initial isomerization rates (C₃₀ = 1) and relative content of neohop-13(18)-enes (13(18) + 17(21) = 1) at equilibrium were as follows: C₂₇: (120, > 0.99), C₂₉: (4, > 0.95), C₃₀: (1, ~0.70), C₃₁: (0.2, ~0.30), thus confirming the hypothesis. Since neohop-13(18)-enes can be converted back to hop-17(21)-enes, which are much easier to hydrogenate to yield regular hopanes, even high concentrations of C₃₀ neohop-

13(18)-ene, is not sufficient to ensure a high concentration of C₃₀ neohopane. Prolonged acid treatment of the hopene mixtures gradually leads to formation of various other triterpenes, and again the lower carbon number compounds are formed much faster. Such compounds are likely precursors of some of the saturated triterpenes found in oils. Two triterpane series (Fig. 1) with a carbon number distribution similar to that of 18 α -neohopanes have been found in crude oils from clay-rich source rocks. One series appears to be the saturated counterparts of the spiro-triterpenes (Hauke et al., 1994), whereas the other series is tentatively identified as 21-methyl-28-norhopanes. Members of both series have been produced in low yields by acid- or clay-catalyzed isomerization of the corresponding neohop-13(18)-enes followed by hydrogenation in acid. 21-methyl-28,30-bisnorhopane was also produced in fair yield by isomerization of synthetic 30-norhopa-15,17(21)-diene followed by hydrogenation suggesting an additional generation mechanism for this series.

Hauke, V., Trendel, J. M., Albrecht, P., Connan, J., 1994. Spiro-Triterpenes from Clay-Catalysed Rearrangement of Hopenes: NMR Structural Elucidation and Occurrence in a Recent Sediment. *Tetrahedron Letters*. 2227-2230.

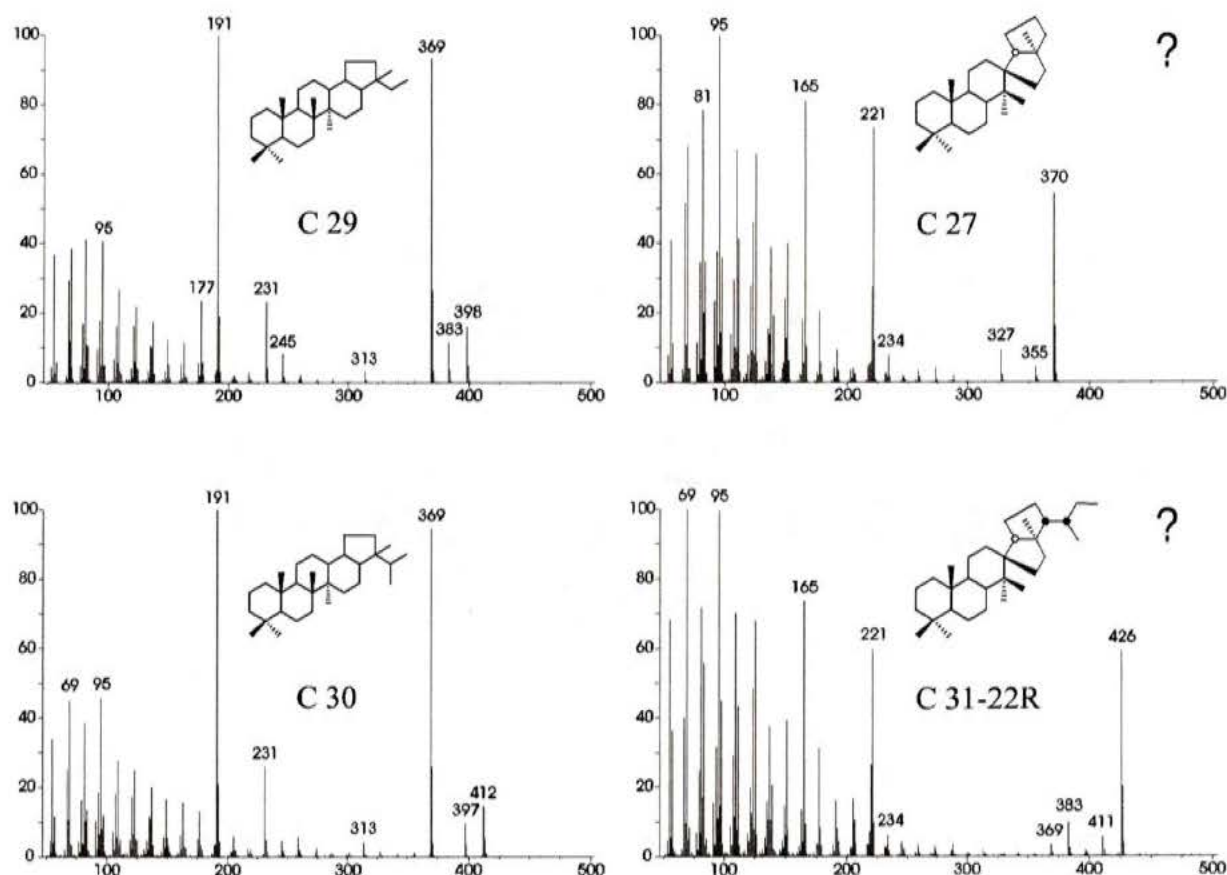


Fig. 1. Mass spectra of 21-methyl-28-norhopanes (left) and putative spiro-triterpanes (right) isolated by reverse phase HPLC from a crude oil (Mona-1 well, Danish North Sea).

**GEOCHEMICAL CORRELATION OF SEEP OILS
AND HYDROCARBON SOURCING,
NUUSSUAQ BASIN, WEST GREENLAND**

Hongxiu ZHOU¹, Mike PEARSON², Jørgen BOJESSEN-KOEFOED³ and Hans-Peter NYTOFT³

^{1,2} OPG, Department of Geology, University of Aberdeen, AB24 3UE, Scotland

³ Geological Survey of Denmark and Greenland (GEUS), Thoravej 8, DK-2400 Copenhagen NV, Denmark

The West Greenland Nuussuaq Basin was formed during the opening of the Labrador Sea in the Late Mesozoic. Cretaceous to Early Tertiary sedimentary fill is preserved underneath Tertiary basalt cover which may have been several kilometers thick. Late Palaeogene to post-glacial phases of uplift have exhumed the basalt and underlying sediments in the east of the basin, where onshore oil staining and seepage in the volcanic succession has attracted recent oil exploration interest. Six exploratory wells have been drilled on the Nuussuaq Peninsula. An understanding of the petroleum system and mixed sourcing of the seeps are important in the assessment of exploration risks, both onshore and offshore, in this frontier area.

Oils samples used in this correlation study are mainly extracted from bituminous vugs in basaltic cores of three wells and outcropping basalts. A limited number of shales in drill cuttings have been examined as potential source rocks. Techniques applied to basalt and sedimentary rock bitumens include aliphatic and aromatic biomarker quantitation, carbon IRMS, FTIR and fluid inclusion /fluorescence.

The investigation has focussed on two major oil types (Marraat and Eqaalulik) and their mixtures in the Nuussuaq area. Analysed basalt-hosted bitumens ('oils') are generally at low maturity levels, within the early oil window; but significant variations exist. Marraat oil seems to have lower maturity than Eqaalulik oil and stable carbon isotope ratios and biomarker data indicate that

Egalulik oil contributes no greater than 50% to mixtures. However many of the mixed oils have even lower maturities suggesting a simple mixing model of two sources is inadequate. Use of aromatic sulphur compound (ASC) distributions may help to resolve this mixing complexity. Some oils previously-regarded as identical have different ASC distributions.

Thermal maturities of the sediments below the basalt are surprisingly low. Few of the examined shales has been effective source for the basalt-hosted bitumens which are therefore presumed to have migrated from the downfaulted basin to the west. The presence of angiosperm-derived biomarkers in Marraat oils limits possible sources to a Late Cretaceous to Early Tertiary age range in the present offshore area. Multiple phases of migration may have occurred in response to basin faulting and inversion of the eastern margin.

REFERENCES:

- Bojesen-Koefoed, J.A. *et. al.*, 1999. Oil seepage onshore West Greenland: evidence of multiple source rocks and oil mixing, *Petroleum Geology of Northwest Europe: Proceedings of the 5th Conference*, 805-814.
- Chalmers, J.A., 2000. Offshore evidence for Neogene uplift in central West Greenland, *Global and Planetary Change* 24, 311-318.

¹ Corresponding author, email: joy.zhou@abdn.ac.uk

Fifteenth Annual Meeting of The Society for Organic Petrology

July 26-30, 1998
Halifax, Nova Scotia, Canada

Abstracts and Program
Volume 15

TSOP - Halifax'98



"Sailing into the New Millennium"

Edited by
P. K. Mukhopadhyay, M. P. Avery, J. H. Calder, F. Goodarzi

Organized and Hosted by

Global Geoenergy Research Ltd.
Geological Survey of Canada
Nova Scotia Department of Natural Resources
Canadian Society for Coal Science and Organic Petrology

Petroleum Source Potential and the Importance of Marine Versus Terrigenous Organic Matter Input: a comparative study of mid-Cretaceous deposits from Ellesmere Island, Northwest Territories, Canada

BOJESSEN-KOEFOED, J.A., CHRISTIANSEN, F.G., NYTOFT, H.P., PETERSEN, H.I., Geological Survey of Denmark and Greenland (GEUS), 8 Thoravej, DK-2400 Copenhagen NV, Denmark

Rich petroleum source rocks are present in several intervals in the Aptian-Coniacian succession in many basins over most of the World (e.g. Hallam, 1987), and are held to be the source for 29% of world's original petroleum reserves (Klemme and Ulmishek, 1992).

In the Sverdrup Basin (Arctic Canada), such deposits are represented by the Hassel Formation (Albian), and by the basal part of the Kanguk Formation (Cenomanian-Maastrichtian). This basal part of the formation is informally known as the "Bituminous Member" (Cenomanian-Turonian).

A large database of Rock-Eval/TOC analyses of samples from a number of localities on Ellesmere Island documents the presence of intervals of highly prolific petroleum source rocks in both the Hassel Formation and the Bituminous Member of the Kanguk Formation (Núñez-Betulu, 1993, 1994).

Two thermally immature samples, one collected from the Hassel Formation and one collected from the Bituminous Member of the Kanguk Formation, were selected for a detailed study by seven stages of hydrous pyrolysis (72h at temperatures ranging from 220°C to 330°C), Rock-Eval/TOC screening analysis, pseudo-activation energy distribution analysis, pyrolysis-gas chromatography, biomarker analysis and organic petrographic

analysis.

Although both the Hassel Formation and the Kanguk Formation consist mainly of marine deposits, differences in kerogen composition between the samples are distinct.

The Hassel Formation contains high proportions of terrigenous organic debris (Table 1). The unpyrolysed sample yields a Hydrogen Index of 333 (T_{max} 419°, R_o 0.45%), which upon hydrous pyrolysis-induced passage through the oil window decreases to 155 (T_{max} 452°, R_o 1.34%), roughly following the "type III" evolution path in the T_{max} vs. HI diagram. The pseudo-activation energy distribution yielded by the unpyrolysed sample is skewed, with a fair proportion of the total generation potential in the higher activation energy range, which remains after hydrous pyrolysis at 330° C/72h. Pyrolysis-GC data show that upon passage through the "oil window", the Hassel Formation source rocks will generate both oil and gas over a wide range of thermal maturities, and that significant potential remains after hydrous pyrolysis at 330° C/72h (Fig.1). In general, the characteristics of extractable liquids correspond well to the kerogen composition, showing clear odd-number *n*-alkane predominance, high pristane/phytane ratios, high proportions of waxy components and sesqui- and diterpanes, predominance of C₂₉-steranes, high proportions of moretanes, and absence of tricyclic triterpanes. The *n*-alkane distribution present after hydrous pyrolysis at 330° C is characterized by relatively high proportions of waxy (*n*C₂₂₊) components (*n*C₁₅₋₂₂/*n*C₂₃₋₃₀ = 2.6), and a "convex-up" trend of decreasing abundance with increasing carbon number. The pristane/phytane ratio is 2.7.

The Kanguk Formation Bituminous Member contains only minor proportions of recognizable terrigenous organic components (Table 1). The unpyrolysed sample yields a Hydrogen Index of 358 (T_{max} 411°, R_o 0.32%), which upon hydrous pyrolysis-induced passage through the oil window decreases to 80 (T_{max} 452°, R_o not available), roughly following the "type II" evolution path in the T_{max} vs. HI diagram. The pseudo-activation energy distribution yielded by the unpyrolysed sample is fairly narrow, with a limited proportion of the total generation potential in the higher activation energy range. Pyrolysis-GC data show that upon passage through the "oil window", the Kanguk Formation source rock will generate both oil and gas, but over a rather narrow range of thermal maturities, and that the generation potential for liquid petroleum is largely exhausted after hydrous pyrolysis at 330° C/72h (Fig.1). In general, the characteristics of extractable liquids correspond well to the kerogen composition, showing little odd- or even-number *n*-alkane predominance, low pristane/phytane ratios, moderate proportions of waxy components, few sesqui- and diterpanes, predominance of C₂₇-steranes, very high proportions of 28,30-bisnorhopane, and presence of tricyclic triterpanes. The *n*-alkane distribution shown by the extractable liquids after hydrous pyrolysis at 330° C is characterized by moderate proportions of waxy (*n*C₂₂₊) components (*n*C₁₅₋₂₂/*n*C₂₃₋₃₀ = 3.1), and a "concave-up" trend of decreasing abundance with increasing carbon number. The pristane/phytane ratio is 1.8.

Although both samples represent excellent petroleum source rocks, they will give rise to widely differing types of petroleum upon maturation, and their generation characteristics differ markedly.

Despite deposition in a marine environment, the Hassel Formation shales represent A terrigenous source rocks, containing high proportions of "Type III" kerogen. However, contrary to common conceptions regarding the principal products generated from such deposits, the data presented show that the rocks will generate high proportions of liquid petroleum products in addition to gas. Furthermore, the results indicate that petroleum generation takes place over a wide range of thermal maturities, and that both oil (C₆₊) and gas (C₁₋₅) are generated even at very high levels of thermal maturity. The very modest proportions of liptinite present suggest that vitrinite also contributes to the liquid petroleum potential, supporting the results of Petersen *et al.* (this volume and in review) and Petersen and Rosenberg (in review).

The Kanguk Formation Bituminous Member shales represent A marine source rocks, containing high proportions of "type II" kerogen. The results of the present study confirm the general view regarding the principal petroleum products generated from such deposits. Hence, upon maturation, the Kanguk Formation Bituminous Member source rock will generate predominantly liquid petroleum products in addition to large amounts of gas. Generation of liquid petroleum is restricted to a rather narrow range of thermal maturities, whereas at high levels of thermal maturity, the generation products are more or less exclusively in the gas fraction (C₁₋₅).

The presence of prolific source rocks of Albian and Cenomanian-Turonian age in the region, combined with the widespread occurrence of source rocks of similar age elsewhere in the world, is very encouraging for exploration on- and offshore western Greenland, where recent discoveries of extensive oil seepage onshore in the Disko-Nuussuaq area (Bojesen-Koefted *et al.*, in press; Christiansen *et al.*, 1996) have renewed interest in petroleum exploration in this region, and discredited the area's long held reputation of being, at best, gas-prone.

Fifteenth Annual Meeting of The Society for Organic Petrology

July 26-30, 1998
Halifax, Nova Scotia, Canada

Abstracts and Program
Volume 15

TSOP - Halifax '98



"Sailing into the New Millennium"

Edited by
P. K. Mukhopadhyay, M. P. Avery, J. H. Calder, F. Goodarzi

Organized and Hosted by
Global Geoenergy Research Ltd.
Geological Survey of Canada
Nova Scotia Department of Natural Resources
Canadian Society for Coal Science and Organic Petrology

condensate and 25 billion Nm³ gas (Danish Energy Agency, 1996). Oil samples recovered from Middle Jurassic sandstones have a typical terrestrial signature, including pr/ph ratios between 4.09 and 4.24, a hopane distribution which maximizes at C₃₀, and bulk isotope $\delta^{13}\text{C}$ ratios of up to or greater than -26 parts/mol, which is significantly heavier than the common oils generated from marine Upper Jurassic shales in the Danish Central Graben (Petersen et al., 1995, 1996). A terrestrial source is further supported by comparison of Harald Field oils and extracts of Middle Jurassic coals which show a similar and generally C₂₉ sterane-dominated C₂₇₋₂₉ sterane distribution.

The Middle Jurassic deposits in the northeastern part of the Danish Central Graben are included in the Bryne Formation, which is 130-300 m thick in the Harald Field area. A nonmarine to marginal marine unit (50-100 m thick) in the middle of the formation contains 6 coal seams with a cumulative thickness of 0.60-5.05 m and a maximum coal seam thickness of 1.3 m (Petersen et al., submitted). Peat formation in the coastal precursor mires occurred during an overall transgressive period, and peat accumulation was to a large extent related to the rate of water table rise, linked to relative sea-level rise, and to the associated marine influence (Petersen and Andsbjerg, 1996). Seams R1, R1a (seam split of R1) and R2 were formed during a comparatively slow relative sea-level rise, whereas seams T1 to T4 were formed during a faster relative sea-level rise. This is reflected in the composition of the coals. In a sequence stratigraphic context, all the seams are situated in transgressive systems tracts.

The coals are petrographically characterised by a low content of liptinite (0.8-7.8 vol.%) and significant amounts of allochthonous or *in situ* formed inertinite and fluorescent vitrinite (Petersen et al., submitted). Towards the palaeo-shoreline, the coal facies generally represent a wet peat-forming mire due to a continuously high-standing water table, whereas more landward reaches of the precursor peats may have been more subjected to a fluctuating water table and desiccation. Pyroinertinite and char in the seams suggest the presence of wildfires in the ancient mires. Laterally, towards the palaeo-coastline, all coal seams have increased proportions of C₂₇ steranes (relative to C₂₈₋₂₉ steranes) and higher C₃₅-homohopane indices, which suggest a stronger, prolonged marine influence on the coastal reaches of the mires. The most landward and fresh-water influenced parts of the seams have higher proportions of C₂₉ sterane and the highest pr/ph ratios. However, seams T1 to T4, formed during an accelerated rise in relative sea level, show characteristics suggesting that the precursor peats of these seams had an overall stronger marine influence than the precursor peats of seams R1, R1a and R2, which formed during a comparatively slow relative sea-level rise. This includes, in the same well-position, a general higher pyrite content, a general higher proportion of C₂₇ sterane and a higher C₃₅-homohopane index in the T-seams than in the R-seams (Petersen et al., submitted). Furthermore, in a direction towards the palaeo-shoreline, equal proportions of C₂₇ and C₂₉ steranes occur first in coal extracts of the T-seams compared to R-seams.

The majority of the vitrinite reflectance values are in the range 0.81-0.89%R_r indicating that the coals with respect to thermal maturity are situated within the range of peak oil generation in the oil window. In the T-seams, observed reflectance values between 0.75 and 0.78%R_r are slightly retarded. Element analyses of vitrinite concentrates show that the vitrinite in these samples is enriched in hydrogen (per-hydrous). FT-i.r. analyses demonstrate that the lower reflectance values of the per-hydrous vitrinite may be related to a lower degree of aromatisation shown by a lower response in aryl hydrogen vibrations in the 900-700 cm⁻¹ range on FT-i.r. spectra (Petersen and Rosenberg, submitted).

The variation in the geochemical and petrographic composition of the coal seams is as shown above, inherited from the depositional environment of the precursor peats and influences the petroleum generative potential. T-seams that formed during a comparatively fast relative sea-level rise, which promoted waterlogged, anoxic and marine-influenced conditions, generally have the highest average HI values and S₁+S₂ contents, and for individual seams an increase in the average HI values is generally recorded in a seaward direction (Petersen et al., submitted). The depositional conditions of the T-seams also favoured the formation of the per-hydrous vitrinite yielding retarded reflectance values. Rock-Eval analysis of the vitrinite concentrates shows that the hydrogen-enriched vitrinite results in higher HI values (240-255) and S₁+S₂ contents (up to 200.98 mg HC/g rock) than obtained from the 'normal' vitrinite (HI = 199-208; S₁+S₂ up to 179.02 mg HC/g rock). These data suggest that petroleum generation from the coals is strongly related to the vitrinite component and not to the liptinite content, which rarely exceeds 4 vol.%. This is supported by multivariate statistical modeling of the data yielding a model explaining 71% of the variation in the remaining generative potential represented by S₂ (corr. coef.: 0.85). Components with a significant positive influence on S₂ are the TOC content, the vitrinite maceral group, the vitrinite macerals collotelinite and telinite, the vitrinite-rich microlithotypes vitrite, clarite and duroclarite, and the liptinite maceral resinite (Petersen et al., 1996; Petersen et al., submitted).

Despite the level of maturity of the coals, about 13-30% of the carbon in the coals will participate in petroleum formation during further maturation, and Py-GC data from extracted coal samples indicate that the

Composition and organic maturity of Middle Jurassic coals, North-East Greenland: evidence for liptinite-induced suppression of huminite reflectance

H.I. Petersen^{*}, H. Vosgerau

Geological Survey of Denmark and Greenland, Thoravej 8, Copenhagen DK-2400 NV, Denmark

Received 18 August 1998; accepted 18 March 1999

Abstract

Middle Jurassic coals from Kuhn Ø, North-East Greenland, may contain up to 85 vol.% liptinite, principally resinite (up to 68.6 vol.%). The coals are thus petrographically comparable to the Middle Jurassic Muslingebjerg Formation coals at Hochstetter Forland approximately 40–50 km to the north, and they are inherently excellent petroleum source rocks. Liptinite-poor (≤ 6.0 vol.%) coal samples from both Kuhn Ø and Hochstetter Forland yield mean random huminite reflectance values of $0.49\text{--}0.53\%R_o$, implying a rank of sub-bituminous A. Above a threshold value somewhere between 3 and 24 vol.% resinite and 6 and 35 vol.% total liptinite, significant reflectance suppression is induced, and between 24 and 69 vol.% resinite and 35 and 85 vol.% total liptinite, a nearly linear inverse relationship exists between the content of liptinite/resinite and the mean random reflectance values. At the highest liptinite/resinite contents, reflectance suppression may be up to $0.23\%R_o$. The reflectance suppression is related to bitumen-adsorption caused by bitumen-expulsion from resinite, and total reflectance distributions of the huminite fractions suggest that the reflectance of all huminite macerals is lowered with increasing liptinite/resinite content. © 1999 Elsevier Science B.V. All rights reserved.

Keywords: liptinite; resinite; reflectance suppression; Middle Jurassic; North-East Greenland

^{*} Corresponding author. Tel.: +45-38-14-23-45; Fax: +45-38-14-20-50; E-mail: hip@geus.dk

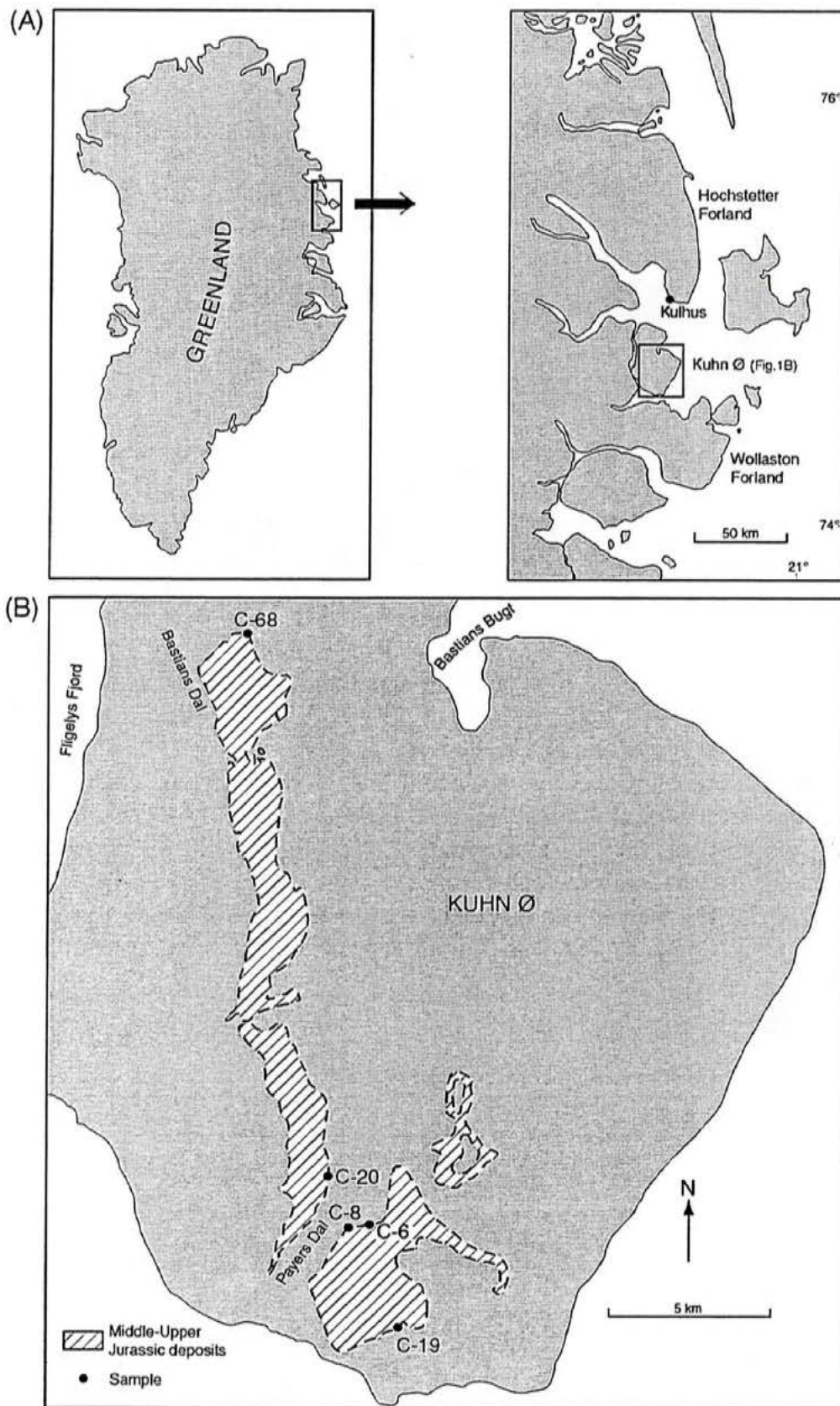
1. Introduction

Coal seams from the Middle Jurassic Muslingebjerg Formation on Hochstetter Forland, North-East Greenland, are unusual with an extraordinarily high content of liptinite macerals, in particular resinite (Bojesen-Koefoed et al., 1996; Petersen et al., 1998). The abundance of hydrogen-rich liptinite components results in a high hydrocarbon generative potential for these coals. Two huminite-rich samples yielded random reflectance values of $0.50\%R_o$ and $0.49\%R_o$, indicating a sub-bituminous A rank (Petersen et al., 1998). Petroleum generation from coal, particularly resinite, has been suggested from marginally marine strata in the Beaufort–Mackenzie Basin in Canada (0.40 – $0.60\%R_o$) by Snowdon and Powell (1982) and in the Gippsland Basin in Australia ($0.50\%R_o$) by Shanmugam (1985). Khorasani (1987) stated that resinite generates petroleum at low maturities corresponding to a reflectance range of approximately 0.43 – $0.56\%R_o$. Furthermore, results from artificial coalification of resin/resinite (Stout, 1995), and of peat containing resin globes ('Cyrilla facies', Okefenokee Swamp of Georgia; Cohen and Bailey, 1997) support an early generation from resinite. In the light of this, the composition and maturity of Middle Jurassic Muslingebjerg Formation coals on Kuhn Ø approximately 40–50 km south of Hochstetter Forland are an interesting aspect in a regional petroleum perspective. The source rock potential and organic geochemistry will be elucidated in detail from ongoing organic geochemical and pyrolysis studies of the coals.

In contrast to the Muslingebjerg Formation coals from Hochstetter Forland, the coals from Kuhn Ø have never been analysed in detail. A few coal samples from Kuhn Ø were collected during fieldwork in 1994 within the framework of the 'Wollgan project' which was a research project involving Statoil, Saga Petroleum, Amoco, the Norwegian Petroleum Directorate and the Geological Institute, University of Copenhagen. The coal seams of the Muslingebjerg Formation were not the main subject of the fieldwork, which is the reason why only five samples were collected. The samples, however, provide the opportunity to carry out a preliminary petrographic investigation of the coals. Furthermore, recognition of a relationship between liptinite content and reflectance suppression is of general significance due to the wide use of reflectance measurements as a maturity parameter in petroleum exploration. Huminite/vitrinite reflectance measurements are generally considered to be a reliable method for estimating the thermal maturity of organic matter. However, reflectance anomalies manifested by lowered reflectance values compared to the regional rank gradient are reported for both dispersed vitrinite in sedimentary successions and for coals of various ages.

The aims of the present study are (1) to describe the petrographic composition of the Kuhn Ø coals, and (2) to investigate the influence of the high content of liptinite/re-

Fig. 1. (A) Map showing the location of Hochstetter Forland and Kuhn Ø in North-East Greenland. The coal samples from the Muslingebjerg Formation at Hochstetter Forland were sampled from the outcrop at Kulhus. (B) Detailed map of Kuhn Ø, showing the sample sites of the Middle Jurassic coals in Bastians Dal (C-68) and Payers Dal (C-6, C-8, C-19, C-20) (Modified from Alsgaard et al., in press).



sinite on the huminite reflectance values of the Kuhn Ø and Hochstetter Forland Muslingebjerg Formation coals.

2. Geology and coal samples

Ten outcrop coal samples from the Middle Jurassic coal-bearing Muslingebjerg Formation of Hochstetter Forland and Kuhn Ø were used in this study (Fig. 1). The five samples from Hochstetter Forland were taken from coal seams 2, 3 and 4 at the type locality at Kulhus, southwestern Hochstetter Forland, where the Muslingebjerg Formation is at least 20 m thick and consists of four coal seams interbedded with lagoonal siltstones and sandstones and subordinate shoreface sandstones (Clemmensen and Surlyk, 1976; Petersen et al., 1998) (Fig. 1). Seams 2, 3 and 4 are between 1.15 and 3.45 m thick. Each coal seam contains three organic facies cycles that are petrographically characterised by an increasing content of liptinite, in particular resinite, from the base towards the top, resulting in exceptionally petroleum-prone coals. The precursor peats accumulated on a coastal plain, and peat-formation was linked to rises in relative sea level. A detailed organic petrographic and geochemical description of the Hochstetter Forland coals, together with an interpretation of the peat-forming mires and associated siliciclastic depositional environments, is presented in Bojesen-Koefoed et al. (1996) and Petersen et al. (1998). The five samples from Kulhus used in the present study contain between 3.8 and 65.6 vol.% total liptinite and between 0.4 and 44.0 vol.% resinite (Table 1).

In Payers Dal, central Kuhn Ø, coal (locally up to approximately 0.15 m thick) of the Muslingebjerg Formation overlies weathered crystalline basement or thin fluvial deposits of the Bastians Dal Formation; coal samples C-6, C-8, C-19 and C-20 were collected from this coal (Fig. 1). Coal sample C-68 is from a coal-bearing outcrop of the Muslingebjerg Formation discovered during the 1994 fieldwork in Bastians Dal, central Kuhn Ø (Fig. 1). The outcrop contains three coal seams, approximately 1.0–1.5 m thick. They are partially interbedded with fluvial deposits of the same type as the fluvial

Table 1
Petrographic composition of samples from Hochstetter Forland^a

Sample	061	090	101	130	131
Seam	2	2	3	4	4
Seam interval (cm)	35–45	305–315	55–65	180–185	185–192
Lithotype	banded	dull	dull	bright	banded
Huminite (vol.%)	91.0	42.0	24.8	89.2	63.2
Inertinite (vol.%)	1.2	15.2	3.0	4.2	1.4
Liptinite (vol.%)	3.8	35.0	65.6	6.0	33.8
Resinite (vol.%)	0.4	24.2	44.0	2.4	25.6
Minerals (vol.%)	4.0	7.8	6.6	0.6	1.6

^aSee also Petersen et al. (1998).

conglomerates and pebbly sandstones of the underlying Bastians Dal Formation (Alsgaard et al., in press).

3. Methods

Maceral analysis of the polished blocks of the Kuhn Ø samples was carried out in oil immersion using a Zeiss incident light microscope equipped with visible and blue-light sources, and a Swift point counter. Five-hundred points (macerals, minerals) were recorded in each sample. Identification of the low rank macerals followed the recommendations of the International Committee for Coal and Organic Petrology (1963, 1971, 1975) and Stach et al. (1982).

Random reflectance values of the 10 coals were determined by 50–100 measurements per sample on homogeneous eu-ulminite using a Leitz MPV-SP system, which was calibrated against a standard with a reflectance value of 0.515% R_o . Reflectance measurements on resinite were performed with the same equipment.

Table 2
Petrographic composition of samples from Kuhn Ø

Petrography (vol.%)	C-6 Payers Dal	C-8 Payers Dal	C-19 Payers Dal	C-20 Payers Dal	C-68 Bastians Dal
Textinite	0	2.6	0.2	1.4	0
Textoulminite	0	0.2	0	0	1.0
Eu-ulminite	4.2	5.4	6.6	3.8	17.2
Attrinite	3.6	3.8	0.8	1.8	0.6
Densinite	10.2	5.0	17.8	5.2	31.8
Porigelinite	0	0.4	0.2	0.2	4.0
Corpohuminite	0.2	0	0	0	0.4
Gelinite	2.4	0.4	1.4	0	7.4
Fusinite	0	0.4	0.2	0	1.6
Semifusinite	0.6	0.6	0	0	3.4
Inertodetrinite	17.2	5.4	7.0	0.4	20.2
Macrinite	6.6	1.4	0.6	0.2	3.2
Sporinite	1.2	0.2	0.4	0	0.4
Cutinite	4.8	7.0	2.2	2.0	1.2
Resinite	30.8	54.4	56.4	68.6	0.8
Suberinite	0	0	0.2	0	0.6
Liptodetrinite	13.4	12.4	5.0	14.4	2.4
Exsudatinite	0	0.2	0	0	0
Pyrite	2.4	0.2	0	0.2	0.4
Other minerals	2.4	0	1.0	1.8	3.4
Huminite	20.6	17.8	27.0	12.4	62.4
Inertinite	24.4	8.0	7.8	0.6	28.4
Liptinite	50.2	74.0	64.2	85.0	5.4
Minerals	4.8	0.2	1.0	2.0	3.8

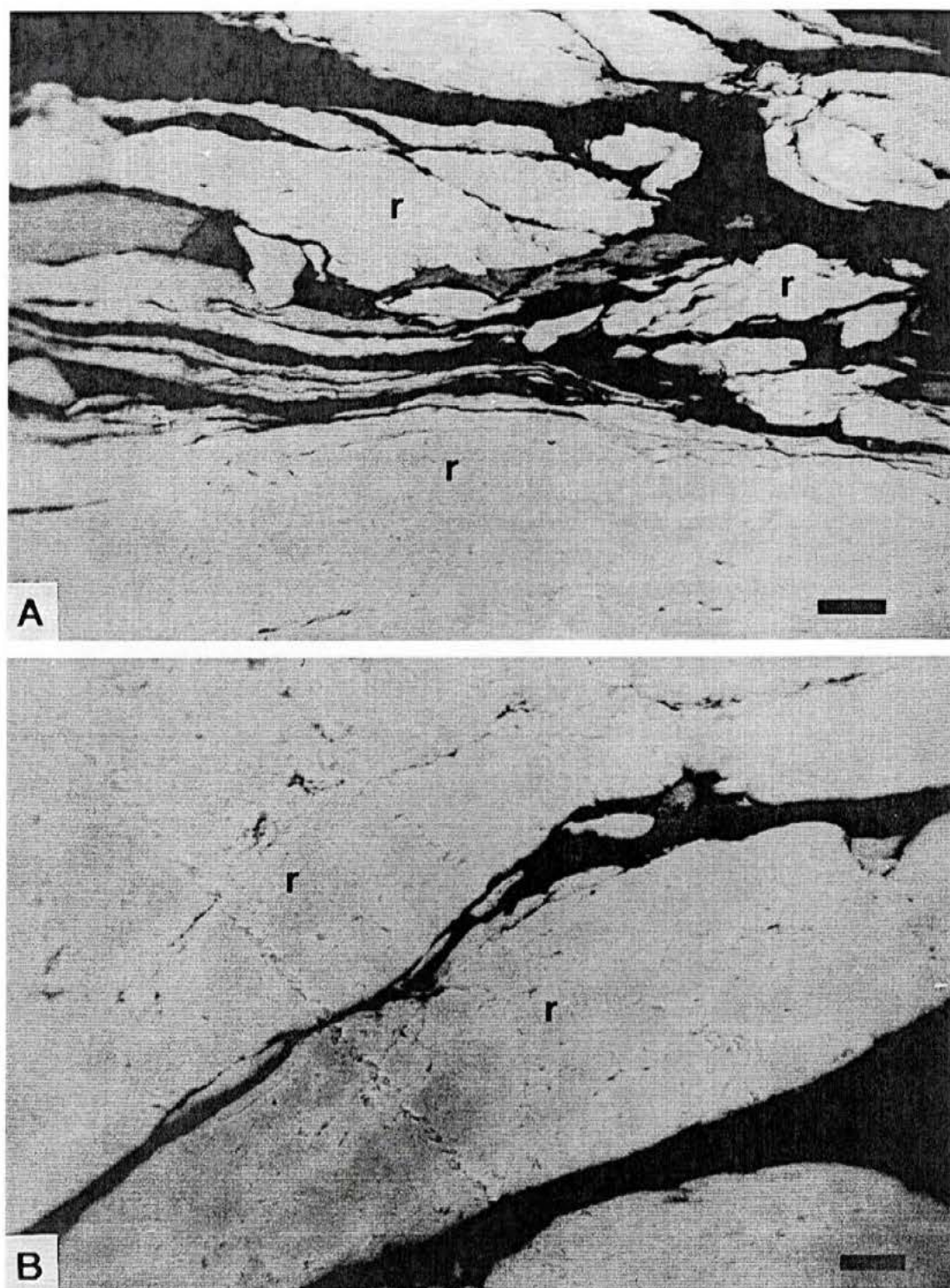


Fig. 2. Black and white photomicrographs of mainly orange-yellowish fluorescing resinite in coal samples from Payers Dal, Kuhn Ø. Reflected light, fluorescence inducing blue-light excitation, oil immersion. Scale bar $\sim 30 \mu\text{m}$. (A) Abundance of resinite (r) in sample C-19. (B) Large resinite (r) particles in sample C-19. (C) Resinite (r) and liptodetrinite (arrows) in sample C-20. (D) Resinite (r) and cutinite (arrows) in sample C-8.

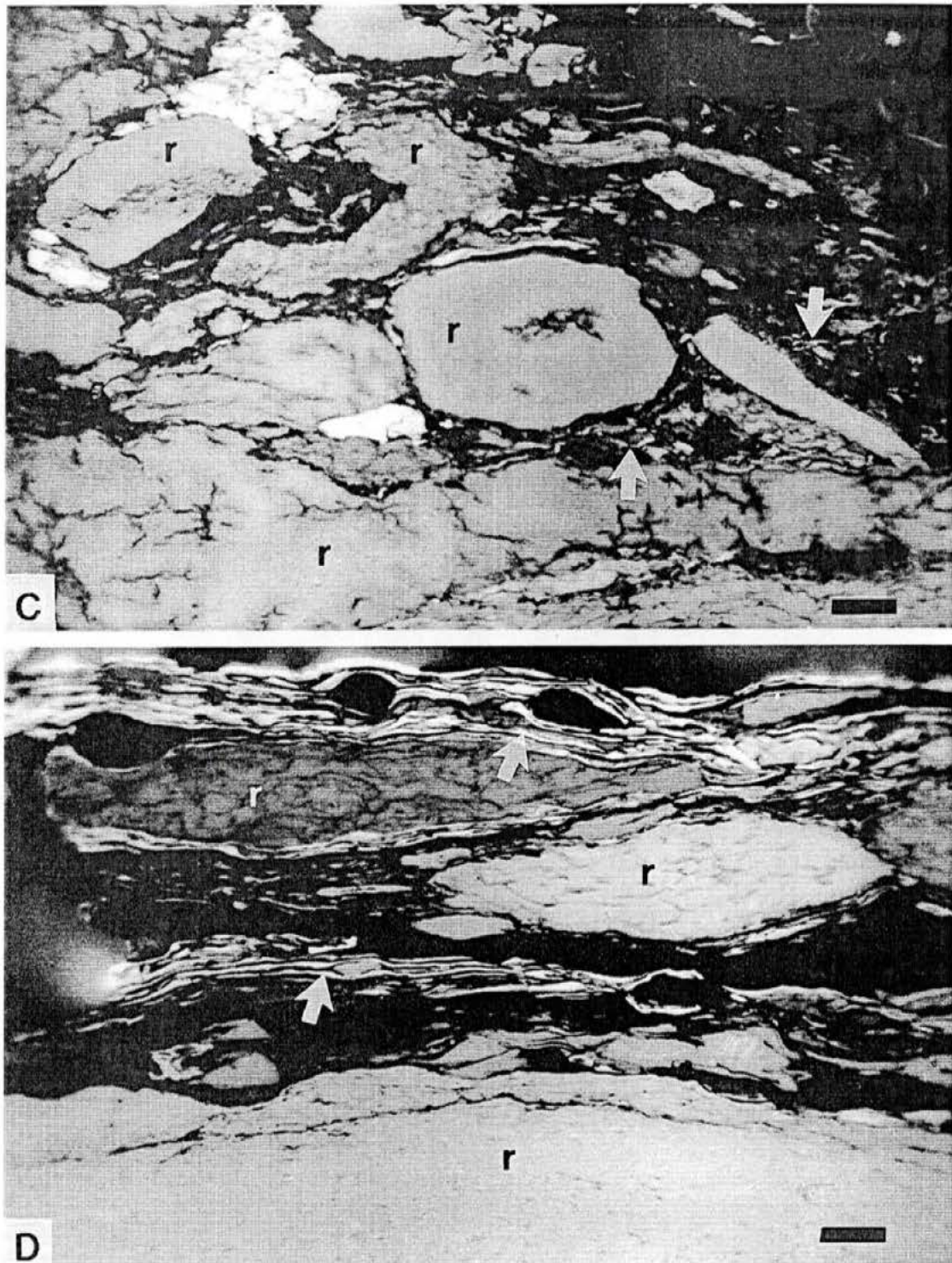


Fig. 2 (continued).

A digital automatic image analysis system (PIA) was used to measure the total reflectance distribution of the huminite fraction in four samples. The PIA system consists of a reflected light microscope equipped with a CCD TV-camera, and an automatic scanning stage and autofocus device. The system was calibrated against a

standard with a reflectance of 0.515% R_o . A total of 270 fields covering a measure area of $800 \times 1200 \mu\text{m}$ were measured in each sample.

4. Results

4.1. Organic petrographic composition of the Kuhn Ø coals

The four samples from Payers Dal contain between 12.4 and 27.0 vol.% huminite primarily composed of attrinite, densinite and eu-ulminite (Table 2). Additionally, huminite macerals with preserved tissue structure (textinite, textoulminite) and humic gels (gelinite, corpohuminite, porigelinite) are present. The inertinite content, mainly inertodetrinite and macrinite (Table 2), varies from 0.6 to 24.4 vol.%. In sample C-6, which contains the highest proportion of inertinite, fine-grained inertodetrinite is laminated with liptodetrinite and mineral matter, and also occurs as rounded, densely packed particles. The most characteristic feature of the coals is, however, the large amounts of liptinite, ranging from 50.2 to 85.0 vol.% (Table 2). The most dominant liptinite maceral is resinite (30.8–68.6 vol.%) followed by liptodetrinite (up to 14.4 vol.%), cutinite (up to 7.0 vol.%) and minor amounts of sporinite (Fig. 2). In samples C-6 and C-8, the secondary liptinite maceral, exsudatinite, has been observed in inertinite. The mineral matter content of the samples ranges from 0.2 to 4.8 vol.%, with 2.4 vol.% of mainly minute pyrite crystals in sample C-6 (Table 2). The pyrite content in the other three samples is negligible.

Sample C-68 from Bastians Dal deviates from the other four samples by containing 62.4 vol.% huminite, mainly represented by densinite (31.8 vol.%) and eu-ulminite (17.2 vol.%) (Table 2). Significant proportions of humic gels, primarily gelinite and porigelinite, are also present. The inertinite maceral group amounts to 28.4 vol.% and is to a large extent represented by inertodetrinite (20.2 vol.%). Liptinite macerals only constitute 5.4 vol.%, and mineral matter amounts to 3.8 vol.% (Table 2).

Table 3

Random reflectance measurements on eu-ulminite (% R_o) and resinite (% R_{res})

Sample	% R_o (minimum value)	% R_o (maximum value)	% R_o (mean value)	% R_{res} (minimum value)	% R_{res} (maximum value)	% R_{res} (mean value)
C-20	0.26	0.36	0.30	0.05	0.10	0.08
C-8	0.25	0.42	0.30	–	–	–
C-19	0.25	0.45	0.34	–	–	–
101	0.31	0.51	0.40	–	–	–
C-6	0.33	0.50	0.40	0.05	0.11	0.08
131	0.36	0.47	0.43	–	–	–
090	0.40	0.54	0.47	–	–	–
130	0.41	0.56	0.49	–	–	–
061	0.47	0.55	0.50	–	–	–
C-68	0.45	0.60	0.53	0.05	0.13	0.09

4.2. Random reflectance measurements of the Kuhn Ø and Hochstetter Forland coals

Mean random reflectance values from the Kuhn Ø samples range from 0.30 to 0.53% R_o with the highest mean value obtained from the huminite-rich sample C-68 and the lowest mean values obtained from the liptinite/resinite-rich samples C-8 and C-20 (Table 3). In these two latter samples, the measured eu-ulminite reflectance range is from 0.25 to 0.42% R_o and 0.26 to 0.36% R_o , respectively, whereas it is from 0.45 to 0.60% R_o in sample C-68 (Table 3). The reflectance ranges for samples C-6 and C-19 are 0.33–0.50% R_o (mean: 0.40% R_o) and 0.25–0.45% R_o (mean: 0.34% R_o), respectively.

The mean random reflectance values from the Hochstetter Forland coals lie between 0.40% R_o and 0.50% R_o (Table 3), a variation which occurs within only ca. 10 m. The

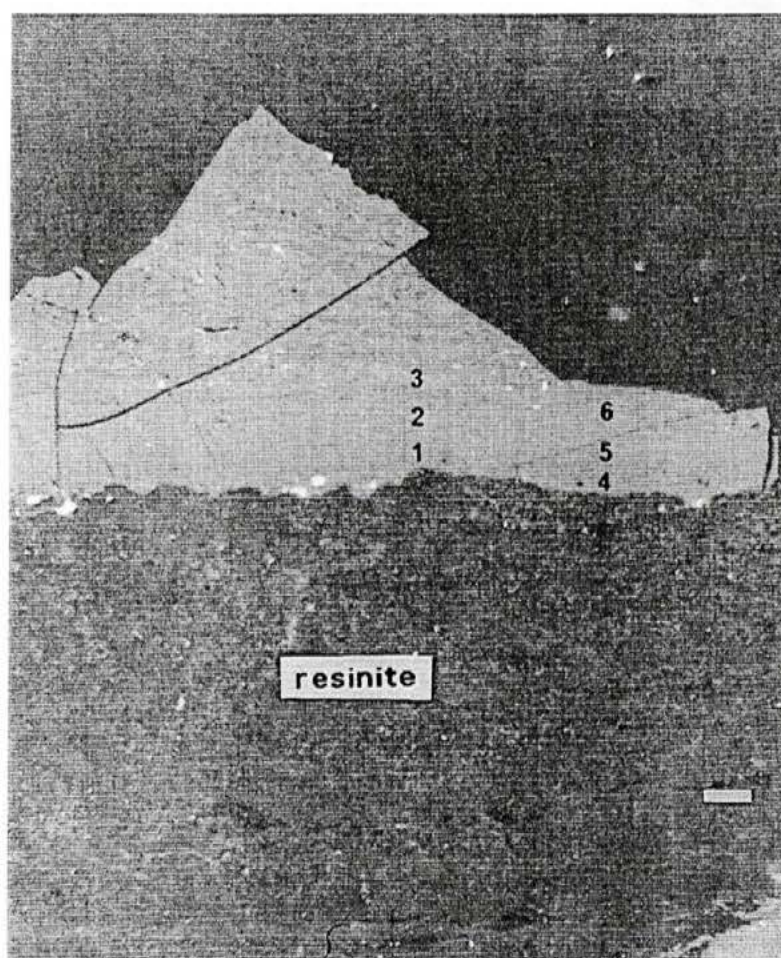


Fig. 3. Huminite in contact with a large resinite particle. At the boundary with the resinite, the huminite is notably darker than huminite further away from the resinite. This is emphasized by eu-ulminite reflectance measurements showing values of 0.22% R_o (line 1) and 0.20% R_o (line 2) immediately adjacent to the contact, and values up to 0.30% R_o approximately 30 μm away from the resinite. Line 1: 1 = 0.22% R_o , 2 = 0.26% R_o , 3 = 0.30% R_o ; line 2: 4 = 0.20% R_o , 5 = 0.26% R_o , 6 = 0.28% R_o (Sample C-19, Payers Dal, Kuhn Ø; reflected white light, oil immersion; scale bar $\sim 15 \mu\text{m}$).

lowest mean value is from sample 101 (55–65 cm interval in seam 3; reflectance range: 0.31–0.51% R_o), which contains 65.6 vol.% liptinite (resinite: 44.0 vol.%), and the highest mean value from sample 061 (35–45 cm interval in seam 2; reflectance range: 0.47–0.55% R_o), which only contains 3.8 vol.% liptinite. The other Hochstetter Forland coal samples yield mean random reflectances in between these outer limits and contain intermediate amounts of liptinite/resinite (Tables 2 and 3).

In huminite that is in direct contact with large resinite particles, it is possible to detect an increase in the random reflectance value of the huminite away from the resinite. Over a distance of ca. 30 μm away from a resinite particle in sample C-19, the reflectance value of eu-ulminite increases by 0.08% R_o as shown by the two 'measure lines' (line 1: 0.22% R_o < 0.26% R_o < 0.30% R_o ; line 2: 0.20% R_o < 0.26% R_o < 0.28% R_o) (Fig. 3). Similarly, reflectance values of up to 0.28% R_o are obtained from eu-ulminite in the centre of a huminite particle in sample C-8, whereas the reflectance value decreases to 0.21% R_o at the boundary to the resinite (Fig. 4). In another example, eu-ulminite at the boundary to resinite yields mean random reflectance values between 0.20 and 0.22% R_o , while values up to 0.29% R_o are obtained away from the resinite particle (Fig. 5).

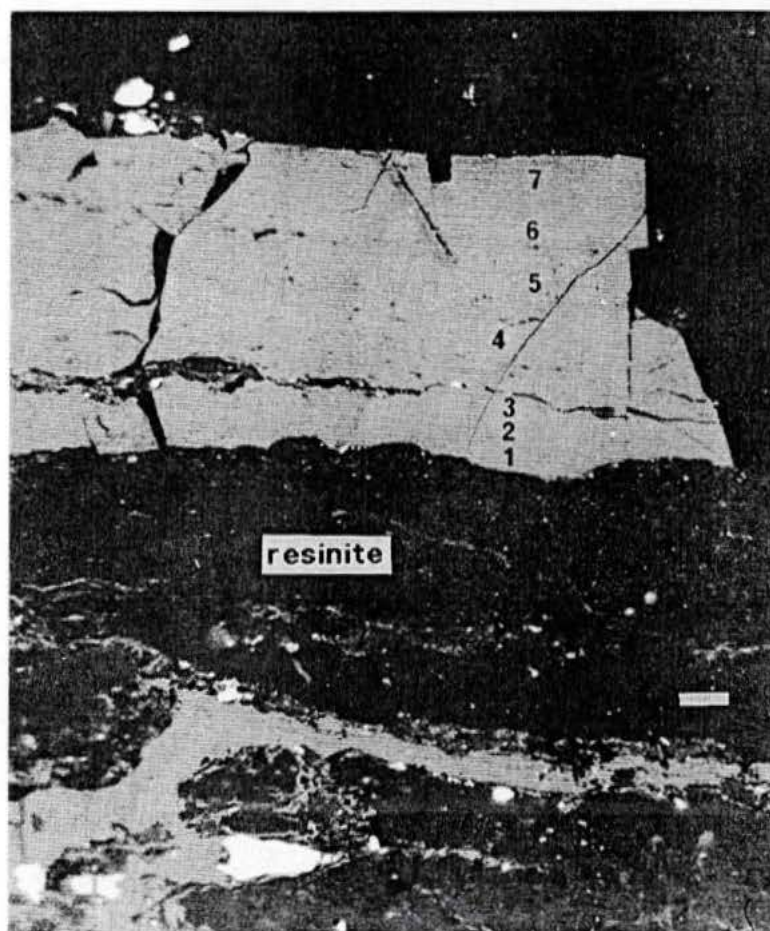


Fig. 4. Eu-ulminite reflectance values showing a decrease from approximately 0.28% R_o to 0.21% R_o towards the resinite particle. 1 = 0.21% R_o , 2 = 0.24% R_o , 3 = 0.28% R_o , 4 = 0.28% R_o , 5 = 0.26% R_o , 6 = 0.27% R_o , 7 = 0.24% R_o (Sample C-8, Payers Dal, Kuhn Ø; reflected white light, oil immersion; scale bar $\sim 15 \mu\text{m}$).

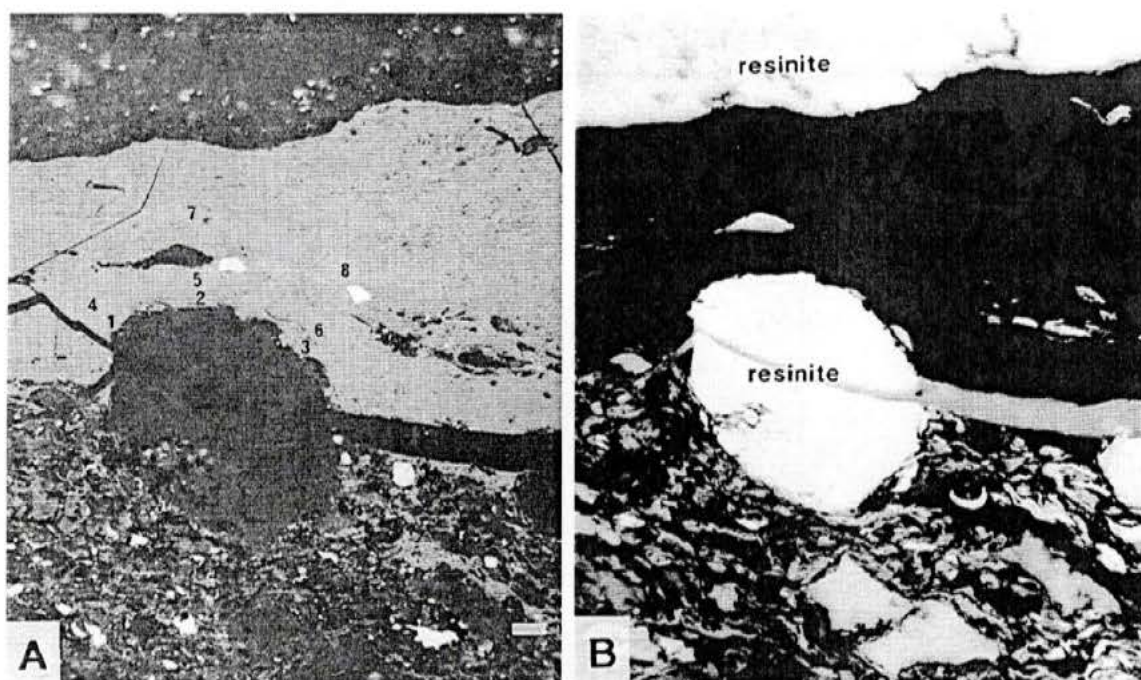


Fig. 5. (A) Eu-ulminite reflectance values between $0.20\%R_o$ and $0.22\%R_o$ are recorded immediately adjacent to the boundary with the oval resinite particle. Away from the resinite, the reflectance values increase to a maximum of $0.29\%R_o$. 1 = $0.22\%R_o$, 2 = $0.20\%R_o$, 3 = $0.22\%R_o$, 4 = $0.29\%R_o$, 5 = $0.26\%R_o$, 6 = $0.25\%R_o$, 7 = $0.28\%R_o$, 8 = $0.29\%R_o$. (B) Same field as (A) but seen under fluorescence-inducing blue-light excitation. Resinite is strongly fluorescing, in particular the oval resinite particle and the large resinite body above the huminite band [Sample C-8, Payers Dal, Kuhn Ø; oil immersion; (A) reflected white light, (B) reflected blue-light; scale bar $\sim 15 \mu\text{m}$].

Random reflectance measurements were carried out on homogeneous parts of resinite particles in samples C-6, C-20 and C-68. The measurements yield very narrow reflectance ranges ($0.05\text{--}0.13\%R_{\text{res}}$). The majority of the reflectance values lie in the range $0.05\text{--}0.09\%R_{\text{res}}$, resulting in mean random reflectance values of $0.08\%R_{\text{res}}$ and $0.09\%R_{\text{res}}$ (Table 3).

4.3. Total reflectance distributions of the huminite fractions

The lower reflectance boundary of the huminite fraction was set to $0.16\%R_o$ on the image analysis system. This was done by excluding all materials with a reflectance value below this threshold from the reflectance measure range by means of an 'erosion option' in the image analysis programme. The threshold value effectively excluded the liptinite macerals from the total reflectance measurements as shown by the random reflectance range and mean random reflectance values of resinite (Table 3), the primary liptinite maceral in the coals. Mineral matter was also excluded in this way. Based on the reflectance range of random reflectance measurements on eu-ulminite (Table 3), where the highest measured value is $0.60\%R_o$ (but generally the maximum values are lower), the upper reflectance limit of the huminite fraction was set to $0.60\%R_o$ on the image analysis system. The measurable reflectance range was thus constrained to 0.16--

0.60% R_o , corresponding to the reflectance range of the huminite fraction in the coals. The upper reflectance limit of 0.60% R_o also excludes the inertinite from the measurements. The four analysed samples (C-68, 090, C-6, C-20) exhibit an increasing content

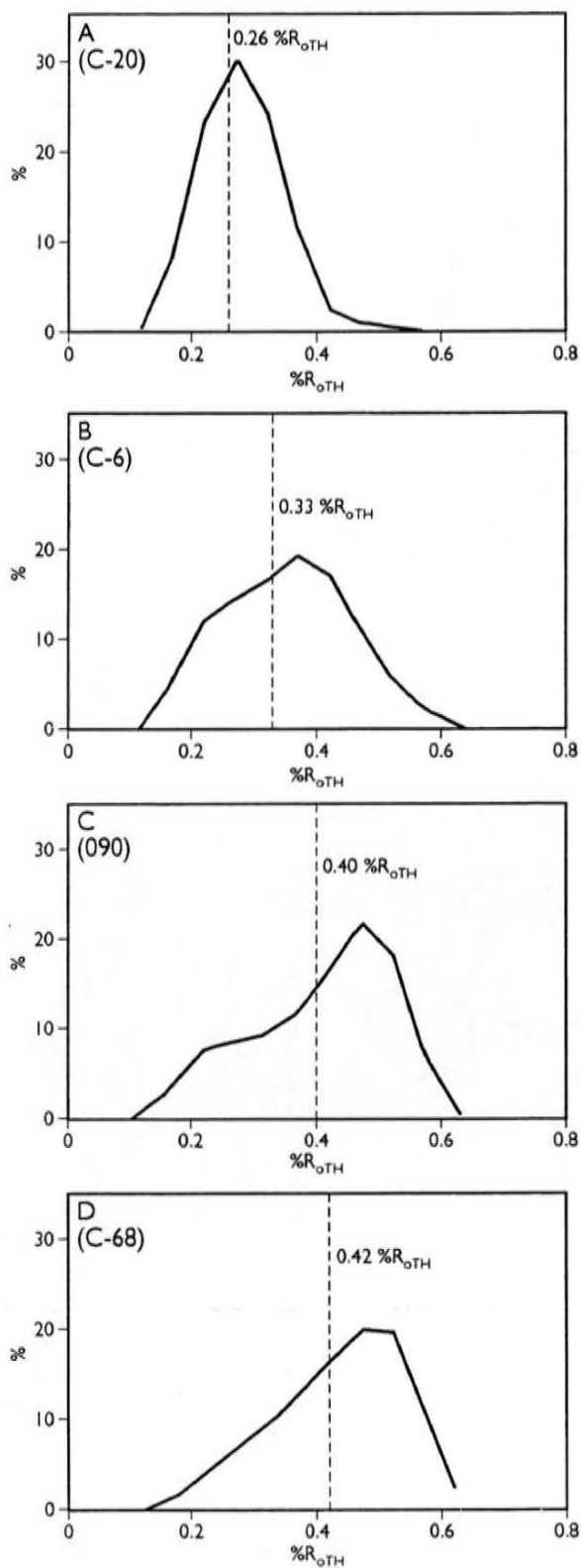


Table 4

Total reflectance distributions ($\%R_{\text{OTH}}$) of the huminite fractions and the relative proportions of the huminite subgroups

Reflectance range/petrography	C-20	C-6	090	C-68
0.10–0.15% R_{OTH}	0.6%	0.3%	0.2%	0.1%
0.15–0.20% R_{OTH}	8.8%	5.0%	2.8%	1.2%
0.20–0.25% R_{OTH}	23.7%	11.8%	7.0%	3.8%
0.25–0.30% R_{OTH}	29.7% ^a	14.1%	8.1%	6.4%
0.30–0.35% R_{OTH}	23.6%	16.4%	8.8%	9.2%
0.35–0.40% R_{OTH}	10.2%	19.0% ^a	11.2%	12.4%
0.40–0.45% R_{OTH}	2.1%	16.7%	15.9%	16.0%
0.45–0.50% R_{OTH}	0.7%	10.1%	21.3% ^a	19.7% ^a
0.50–0.55% R_{OTH}	0.4%	4.8%	17.6%	19.3%
0.55–0.60% R_{OTH}	0.2%	1.6%	6.4%	10.2%
0.60–0.65% R_{OTH}	0%	0.2%	0.7%	1.7%
Mean ^b	0.26% R_{OTH}	0.33% R_{OTH}	0.40% R_{OTH}	0.42% R_{OTH}
Humotelinite	41.9%	20.4%	48.6%	29.2%
Humodetrinite	56.5%	67.0%	41.0%	51.9%
Humocollinite	1.6%	12.6%	10.4%	18.9%

^a Reflectance range in which the total reflectance distribution maximises.

^b Mean of the total reflectance distribution.

of liptinite/resinite from 5.4 vol.% liptinite and 0.8 vol.% resinite to 85.0 vol.% liptinite and 68.6 vol.% resinite (Tables 1 and 2). From sample C-68, with the lowest liptinite/resinite content, to sample C-20, with the highest liptinite/resinite content, the total reflectance distributions of the huminite fractions show two pronounced characteristics (Fig. 6; Table 4): (1) the mean reflectance of the total reflectance distribution decreases with increasing liptinite/resinite content; and (2) the maximum of the total reflectance curve is at lower reflectance values with increasing liptinite/resinite content.

5. Discussion

Four of the coal samples from Kuhn Ø contain extraordinarily high proportions of liptinite, in particular resinite, and are thus similar to the ‘dull coal facies’ of the Muslingebjerg Formation coal seams from Hochstetter Forland (Petersen et al., 1998). The coals are also petrographically comparable to the Jurassic–Lower Cretaceous Canadian ‘needle coals’ discussed by Snowden et al. (1986) and Goodarzi et al. (1993).

Fig. 6. Total reflectance distributions of the huminite fractions of samples C-20, C-6, 090 and C-68 illustrating the lowering of the reflectance of the entire huminite fraction with increasing liptinite/resinite content. (A) Liptinite: 85.0 vol.%, resinite: 68.6 vol.%. Mean of total reflectance distribution: 0.26% R_{OTH} . Mean random reflectance: 0.30% R_{O} (Sample C-20). (B) Liptinite: 50.2 vol.%, resinite: 30.8 vol.%. Mean of total reflectance distribution: 0.33% R_{OTH} . Mean random reflectance: 0.40% R_{O} (Sample C-6). (C) Liptinite: 35.0 vol.%, resinite: 24.2 vol.%. Mean of total reflectance distribution: 0.40% R_{OTH} . Mean random reflectance: 0.47% R_{O} (Sample 090). (D) Liptinite: 5.4 vol.%, resinite: 0.8 vol.%. Mean of total reflectance distribution: 0.42% R_{OTH} . Mean random reflectance: 0.53% R_{O} (Sample C-68).

The huminite-rich coal sample from Bastians Dal, central Kuhn Ø, is petrographically similar to the 'banded coal facies' of the Hochstetter Forland coals. This sample, however, may not be representative of the petrographic composition of the three coal seams in Bastians Dal as suggested by the significant coal facies variation in the coal seams from Kulhus, Hochstetter Forland. Liptinite-rich intervals may thus be present in the seams in Bastians Dal. The petrography emphasises that the Kuhn Ø coals, like the coals from Hochstetter Forland, are an excellent petroleum source rock.

The mean random huminite reflectance values vary from 0.30 to 0.53% R_o , and a clear relationship between the reflectance values and the content of liptinite/resinite in the coals is evident (Fig. 7). Samples C-68, 061 and 130, which have low liptinite/resinite contents, yield mean random reflectance values between 0.49% R_o and 0.53% R_o , corresponding to a sub-bituminous A rank, which is supposed to be the 'true' rank of the coals. Between a resinite content of approximately 24 vol.% and 69 vol.% and a total liptinite content of 35 vol.% and 85 vol.%, the reflectance values show a more or less linear decrease with increasing content of liptinite/resinite (correlation coefficient_{liptinite}: -0.91 ; correlation coefficient_{resinite}: -0.93). Due to the extraordinary high resinite content, the suppression is mainly determined by the resinite content (Fig. 7). The samples (C-8, C-20) with the highest liptinite/resinite content yield a mean random reflectance of 0.30% R_o , which corresponds to a reflectance suppression of up to

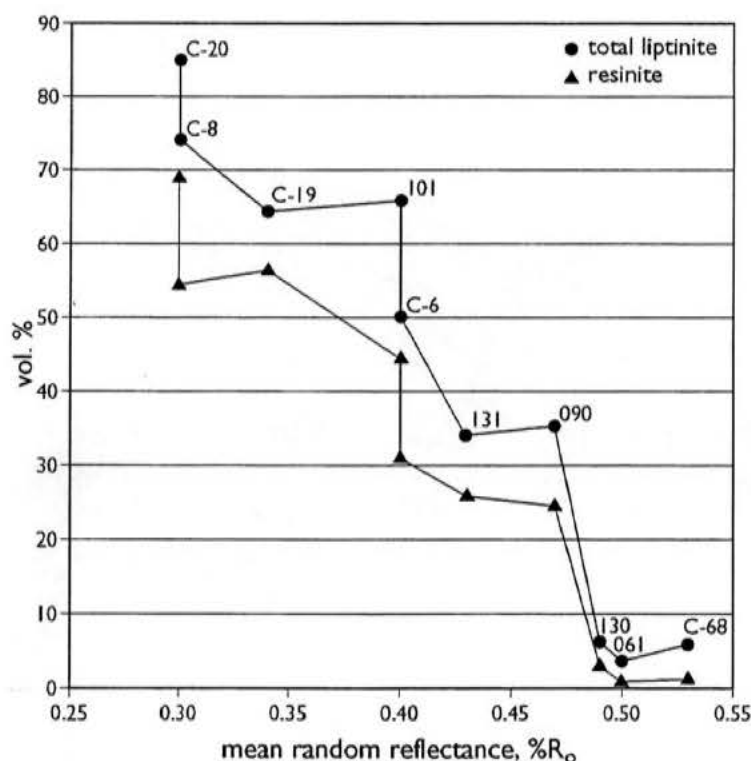


Fig. 7. Correlation between mean random reflectance values and liptinite/resinite content. Huminite reflectance suppression starts somewhere between a resinite content of 3–24 vol.% and a total liptinite content of 6–35 vol.%. Between 24 and 69 vol.% resinite and 35 and 85 vol.% total liptinite, a more or less linear inverse correlation exists (correlation coefficient_{liptinite}: -0.91 ; correlation coefficient_{resinite}: -0.93). Reflectance suppression of up to 0.23% R_o occurs in the samples with the highest liptinite/resinite content.

0.23% R_o . Fig. 7 suggests that significant suppression starts above a threshold value somewhere between a resinite content of 3–24 vol.% and a total liptinite content of 6–35 vol.%. A threshold value of ca. 20% total liptinite above which significant vitrinite reflectance suppression occurs has been proposed by Murchison et al. (1991).

The total reflectance populations show a clear shift towards lower reflectance values of the huminite fraction with increasing liptinite/resinite content (decreasing mean values, % R_{oTH}), which suggests that all huminite macerals attain a lower reflectance with increasing liptinite/resinite content (Fig. 6; Table 4). The relative proportions of humodetrinite, which generally is lower-reflecting than humotelinite, show that this shift is not controlled by the abundance of humodetrinite in the samples (Table 4).

An interesting question is what mechanism causes this suppression-effect. Lowered reflectance values have primarily been explained by two different mechanisms. One mechanism is related to initial hydrogen-rich vitrinitic precursor material, and it has been suggested that the rate of reflectance increase of hydrogen-rich huminite/vitrinite occurs at a reduced rate compared to 'normal' huminite/vitrinite due to different reaction kinetics (Newman and Newman, 1982; Price and Barker, 1985; Hao and Chen, 1992; Huang, 1996; Newman et al., 1997). This is supported by aromatic out-of-plane CH vibrations in the region 900–700 cm^{-1} , which show a lower degree of aromatisation in perhydrous huminite/vitrinite compared to 'normal' huminite/vitrinite (Suárez-Ruiz et al., 1994; Petersen and Rosenberg, 1998). In this situation, the mechanism for the suppression-effect is inherited from the early history of the huminite/vitrinite-precursor, and it may thus be appropriate to use the term 'retardation' (e.g., Petersen and Rosenberg, 1998). The other major mechanism is related to a high liptinite content of the kerogen or coal (Hutton and Cook, 1980; Kalkreuth, 1982; Murchison et al., 1991; Gentzis and Goodarzi, 1994; Goodarzi et al., 1994). The high content of liptinite in the coal or kerogen may induce a lower reflectance value due to bitumen-expulsion from liptinite into the huminite/vitrinite structure. It may be suggested that the adsorbed bitumen reduces the rate of cross-linking and condensation of the aromatic framework (i.e., maturation) resulting in suppressed reflectance values (Diessel, 1992, p. 218). Such a liptinite-induced lowering in reflectance has, for example, been shown by an increasing vitrinite reflectance suppression with an increase in alginite content in an alginite-rich torbanite from Joadja, Australia (Hutton and Cook, 1980), and a gradual reflectance reduction with an increase in the total liptinite content in Cretaceous coals of British Columbia, Canada, has been documented by Kalkreuth (1982).

Under the microscope, huminite immediately in contact with a large resinite body in the Kuhn Ø and Hochstetter Forland coals may be notably darker than huminite of the same particle further away from the boundary between the two macerals. This is detectable by an increase in the mean random reflectance value of the eu-ulminite away from the resinite particle (Figs. 3–5). In the examples from samples C-8 and C-19, the reflectance value may increase by ca. 0.08% R_o in a line away from the resinite, suggesting that bitumen-impregnation of huminite in close contact with resinite actually occurs. Thus, the evidence presented in this study suggests that the lowered reflectance values of the Kuhn Ø and Hochstetter Forland coals are caused by diffusion of bitumen from resinite into the huminite. Additionally, the high liptinite/resinite content may have promoted hydrogen-enrichment of the huminitic organic matter. Mastalerz et al.

(1993) demonstrated that the hydrogen content of vitrinite increases as the liptinite content increases. Furthermore, Price and Barker (1985) believe that the variance in hydrogen content in the huminite/vitrinite macerals is one of the most important controlling factors on reflectance, and in liptinite-rich coal or kerogen, this hydrogen-enrichment is favoured during diagenesis.

Although both the bitumen-impregnated and 'normal' huminite of the Kuhn Ø and Hochstetter coals have experienced the same thermal history, the reflectance measurements carried out on the suppressed eu-ulminite clearly underestimate the thermal maturity of the 'normal' eu-ulminite. The reflectance evidence for bitumen-expulsion at this low maturation stage suggests, combined with the observation of exsudatinite, an early generation from resinite, which is in agreement with several other studies (Snowdon and Powell, 1982; Shanmugam, 1985; Khorasani, 1987).

6. Conclusions

(1) The four samples from Payers Dal, Kuhn Ø, contain significant proportions of liptinite, in particular resinite, whereas the sample from Bastians Dal is huminite-rich. The four liptinite-rich samples are thus petrographically similar to the 'dull coal facies' and the huminite-rich sample to the 'banded coal facies' of the Muslingebjerg Formation coals at Kulhus, Hochstetter Forland, 40–50 km to the north. The excellent petroleum potential of the 'dull coal facies' at Hochstetter Forland has been demonstrated by Bojesen-Koefoed et al. (1996) and Petersen et al. (1998), and the occurrence of similar coal facies at Kuhn Ø thus enlarges the area with documented potential coal source rocks in North-East Greenland.

(2) The mean random reflectance values of the coals are strongly influenced by the liptinite/resinite content. The 'true' rank of the coals from Kuhn Ø and Hochstetter Forland is sub-bituminous A ($0.49\text{--}0.53\%R_o$), which is shown by random reflectance measurements carried out on liptinite-poor (≤ 6.0 vol.%) samples.

(3) Increasing liptinite/resinite content induces reflectance suppression, and above a threshold value somewhere between a resinite content of 3–24 vol.% and a total liptinite content of 6–35 vol.%, significant suppression starts. Between a resinite content of 24–69 vol.% and a total liptinite content of 35–85 vol.%, a more or less linear inverse correlation exists between the liptinite/resinite content and the mean random reflectance value. The samples with the highest liptinite/resinite content yield a mean random reflectance of $0.30\%R_o$, which corresponds to a reflectance suppression of up to $0.23\%R_o$. The decreasing mean value ($\%R_{TH}$) of the total reflectance distribution of the huminite fraction with increasing liptinite/resinite content suggests that the reflectance of all huminite macerals is lowered.

(4) Reflectance measurements show that reflectance suppression is related to bitumen-adsorption caused by bitumen-expulsion from resinite, which probably caused a reduction of the rate of cross-linking and condensation of the aromatic framework, and possibly also to the high liptinite/resinite content which may have favoured the formation of hydrogen-enriched huminite.

Acknowledgements

This study received financial support from the Danish Energy Research Programme (EFP-98), grant no. 1313/98-0022. We are grateful to Amoco Norway Oil for allowing us to use the coal samples from Kuhn Ø. J.R. Ineson (GEUS) improved the English, and S. Sølberg and J. Halskov (both GEUS) prepared the drawings. This paper is published with the permission of the Geological Survey of Denmark and Greenland (GEUS). IJCG reviewers F. Goodarzi, R.W.T. Wilkins and J. Newman are thanked for their valuable comments.

References

- Alsgaard, P.C., Felt, V.L., Vosgerau, H., Surlyk, F., in press. The Jurassic of Kuhn Ø, North-East Greenland. In: Surlyk, F., Ineson, J.R. (Eds.), *The Jurassic of Denmark and Greenland*. Geol. Denm. Surv. Bull.
- Bojesen-Koefoed, J.A., Christiansen, F.G., Petersen, H.I., Piasecki, S., Stemmerik, L., Nytoft, H.P., 1996. Resinite-rich coals of northeast Greenland—a hitherto unrecognized, highly oil-prone Jurassic source rock. *Bull. Can. Petrol. Geol.* 44, 458–473.
- Clemmensen, L.B., Surlyk, F., 1976. Upper Jurassic coal-bearing shoreline deposits, Hochstetter Forland, East Greenland. *Sediment. Geol.* 15, 193–211.
- Cohen, A.D., Bailey, A.M., 1997. Petrographic changes induced by artificial coalification of peat: comparison of two planar facies (Rhizophora and Cladium) from the Everglades-mangrove complex of Florida and a domed facies (Cyrilla) from the Okefenokee Swamp of Georgia. *Int. J. Coal Geol.* 34, 163–194.
- Diessel, C.F.K., 1992. Coal-bearing Depositional Systems. Springer-Verlag, Heidelberg, pp. 471–505.
- Gentzis, T., Goodarzi, F., 1994. Reflectance suppression in some Cretaceous coals from Alberta, Canada. In: Mukhopadhyay, P.K., Dow, W.G. (Eds.), *Vitrinite Reflectance as a Maturity Parameter—Applications and Limitations*, ACS Symposium Series 570, pp. 93–110.
- Goodarzi, F., Harrison, J.C., Wall, J.H., 1993. Stratigraphy and petrology of Lower Cretaceous coal, southeastern Melville Island, District of Franklin, Arctic Canada. In: Christie, R.L., McMillan, N.J. (Eds.), *The Geology of Melville Island, Arctic Canada*, Geol. Surv. Can. Bull., Vol. 450, pp. 229–245.
- Goodarzi, F., Snowdon, L., Gentzis, T., Pearson, D., 1994. Petrological and chemical characteristics of liptinite-rich coals from Alberta, Canada. *Mar. Petrol. Geol.* 11, 307–319.
- Hao, F., Chen, J., 1992. The cause and mechanism of vitrinite reflectance anomalies. *J. Petrol. Geol.* 15, 419–434.
- Huang, W.-L., 1996. Experimental study of vitrinite maturation: effects of temperature, time, pressure, water, and hydrogen index. *Org. Geochem.* 24, 233–241.
- Hutton, A.C., Cook, A.C., 1980. Influence of alginite on reflectance of vitrinite from Joadja, NSW, and some other coals and oil shales containing alginite. *Fuel* 59, 711–714.
- International Committee for Coal and Organic Petrology (ICCP), 1963. *International Handbook of Coal Petrography*, 2nd edn. Centre National de la Recherche Scientifique, Paris.
- International Committee for Coal and Organic Petrology (ICCP), 1971. Supplement to the 2nd edition of the *International Handbook of Coal Petrography*. Centre National de la Recherche Scientifique, Paris.
- International Committee for Coal and Organic Petrology (ICCP), 1975. Supplement to the 2nd edition of the *International Handbook of Coal Petrography*. Centre National de la Recherche Scientifique, Paris.
- Kalkreuth, W.D., 1982. Rank and petrographic composition of selected Jurassic–Lower Cretaceous coals of British Columbia, Canada. *Bull. Can. Petrol. Geol.* 30, 112–139.
- Khorasani, G.K., 1987. Oil-prone coals of the Walloon Coal Measures (Jurassic), Surat Basin, Australia. In: Scott, A.C. (Ed.), *Coal and Coal-bearing Strata: Recent Advances*. Geol. Soc. London Spec. Publ., Vol. 32, pp. 303–310.
- Mastalerz, M., Wilks, K.R., Bustin, R.M., 1993. Variation in vitrinite chemistry as a function of associated liptinite content; a microprobe and FTIR investigation. *Org. Geochem.* 20, 555–562.

- Murchison, D.G., Pearson, J., Raymond, A.C., 1991. Anomalies in vitrinite reflectance gradients. *Bull. Soc. Geol. France* 162, 183–191.
- Newman, J., Newman, N.A., 1982. Reflectance anomalies in Pike River coals: evidence of variability in vitrinite type, with implications for maturation studies and 'Suggate rank'. *N. Z. J. Geol. Geophys.* 25, 233–243.
- Newman, J., Price, L.C., Johnston, J.H., 1997. Hydrocarbon source potential and maturation in Eocene New Zealand vitrinite-rich coals. *J. Petrol. Geol.* 20, 137–163.
- Petersen, H.I., Rosenberg, P., 1998. Reflectance retardation (suppression) and source rock properties related to hydrogen-enriched vitrinite in Middle Jurassic coals, Danish North Sea. *J. Petrol. Geol.* 21, 247–263.
- Petersen, H.I., Bojesen-Koefoed, J.A., Nytoft, H.P., Surlyk, F., Therkelsen, H., Vosgerau, H., 1998. Relative sea-level changes recorded by paralic liptinite-rich coal facies cycles, Middle Jurassic Muslingebjerg Formation, Hochstetter Forland, Northeast Greenland. *Int. J. Coal Geol.* 36, 1–30.
- Price, L.C., Barker, C.E., 1985. Suppression of vitrinite reflectance in amorphous rich kerogen—a major unrecognized problem. *J. Petrol. Geol.* 8, 59–84.
- Shanmugam, G., 1985. Significance of coniferous rain forests and related organic matter in generating commercial quantities of oil, Gippsland Basin, Australia. *AAPG Bull.* 69, 1241–1254.
- Snowdon, L.R., Powell, T.G., 1982. Immature oil and condensate—modification of hydrocarbon generation model for terrestrial organic matter. *AAPG Bull.* 66, 775–788.
- Snowdon, L.R., Brooks, P.W., Goodarzi, F., 1986. Chemical and petrological properties of some liptinite-rich coals from British Columbia. *Fuel* 65, 459–472.
- Stach, E., Mackowsky, M.-T.H., Teichmüller, M., Taylor, G.H., Chandra, D., Teichmüller, R., 1982. *Stach's Textbook of Coal Petrology*. Gebrüder Borntraeger, Berlin–Stuttgart, 535 pp.
- Stout, S.A., 1995. Resin-derived hydrocarbons in fresh and fossil dammar resins and Miocene rocks and oils in the Mahakam Delta, Indonesia. In: Anderson, K.B., Crelling, J.C. (Eds.), *Amber, Resinite, and Fossil Resins*, ACS Symposium Series 617, pp. 43–75.
- Suárez-Ruiz, I., Jiménez, A., Iglesias, M.J., Laggoun-Defarge, F., Prado, J.G., 1994. Influence of resinite on huminite properties. *Energy and Fuels* 8, 1417–1424.



C₂₆ and C₂₈–C₃₄ 28-norhopanes in sediments and petroleum

Hans Peter Nytoft*, Jørgen A. Bojesen-Koefoed, Flemming G. Christiansen

Geological Survey of Denmark and Greenland, Thoravej 8, DK 2400 Copenhagen NV, Denmark

Received 24 February 1999; accepted 20 October 1999

(Returned to author for revision 18 May 1999)

Abstract

A complete series of 28-norhopanes (C₂₆ and C₂₈–C₃₄) has been detected in oil samples and rock extracts from West Greenland and the North Sea. Only the C₂₈ members of the series (28,30-bisnorhopanes) and the related 25,28,30-trisnorhopanes have been described in the literature. 28,30-Bisnorhopanes are often the only 28-norhopanes in oils and sediments, and their isotopic composition can be different from that of the regular hopanes, suggesting that 28,30-bisnorhopanes have a different origin. In other cases, 28-norhopanes and regular hopanes have a similar distribution of homologues, and there is no isotopic evidence for a different origin of the two series. When the complete series of 28-norhopanes is present, it is usually accompanied by high concentrations of the corresponding demethylated aromatic 8,14-secohopanes. The 28-norhopanes seem to be less resistant to biodegradation than regular hopanes, and there is a preferential demethylation of the low-molecular-weight 28-norhopanes. C₂₅ and C₂₇–C₃₁ 25,28-bisnorhopanes have been identified in biodegraded oils. The C₂₈–C₃₄ 28-norhopanes are best studied using the *m/z* 355 mass chromatogram, since this fragment is comparatively intense and the interference from other compounds is usually low. The 17β(H),21α(H)/(17α(H),21β(H) + 17β(H),21α(H)) ratios of the C₂₉ and C₃₀ 28-norhopanes can be used as maturity parameters. In immature samples, a large proportion of the 28-norhopanes (especially C₂₈ and C₃₀) occurs in the bitumen. However, hydrous pyrolysis experiments have shown that 28-norhopanes are also part of the kerogen. © 2000 Elsevier Science Ltd. All rights reserved.

Keywords: 28-Norhopanes; 25,28-Bisnorhopanes; Demethylated aromatic 8,14-secohopanes; Biodegradation; Maturity parameters; Hydrous pyrolysis; West Greenland; North Sea

1. Introduction

In addition to the ubiquitous pentacyclic triterpanes of the hopane series (e.g. Ensminger et al., 1974; van Dorsselaer et al., 1974; Ourisson et al., 1979), a few series of demethylated hopanes have been found. Hopanes demethylated at C-10 (25-norhopanes) are probably the best known, and it is now generally accepted that the 25-norhopanes result from microbial demethylation of hopanes during biodegradation of petroleum in reservoirs (Moldowan and McCaffrey, 1995; Peters et al., 1996). A series of hopanes with unbranched side chains

(30-norhopanes) was detected by Seifert et al. (1984) in biodegraded oil seep samples from Greece. Later they were also found in nonbiodegraded oils (Moldowan et al., 1992), and it was suggested that the normal hopanes and the 30-norhopanes had similar bacterial precursors except for the presence or absence of the C-30 methyl group. The C₂₉-member of the series is the same as the common C₂₉ 17α(H),21β(H)-hopane. The 30-norhopanes have been shown to be widely distributed in crude oils derived from carbonate source rocks (Subroto et al., 1991). The 30-norhopanes seem to be more resistant to biodegradation than regular hopanes, but 25,30-bisnorhopanes have been found in severely biodegraded oils (Subroto et al., 1991). The origin and geochemistry of these two series of demethylated hopanes are fairly well understood. However, this is not the case for the 28-norhopanes. The C₂₈ members of the series (3 isomers of

* Corresponding author. Tel.: +45-38-142348; fax: +45-38-142050.

E-mail address: hpn@geus.dk (H.P. Nytoft).

28,30-bisnorhopane) have been found (Seifert et al., 1978) in extremely high abundance in the Miocene Monterey Formation, California, USA. The concentration of 28,30 bisnorhopanes in these sediments is highly variable (Curiale and Odermatt, 1989). They are also found in sediments and oils from the North Sea and surrounding areas (Bjørøy et al., 1980; Grantham et al., 1980) and several other places, and are often accompanied by the further nuclear demethylated 25,28,30-trisnorhopanes. It has been shown that 28,30-bisnorhopanes only occur as free compounds in bitumen and are not liberated from kerogen by pyrolysis (Moldowan et al., 1984; Noble et al., 1985; Tannenbaum et al., 1986). No biological precursor for 28,30-bisnorhopanes has yet been found, and their origin is still unclear. In the Monterey Formation, it was found that 28,30-bisnorhopanes differed isotopically from the common 17 α (H)-hopanes, and it was suggested that 28,30-bisnorhopanes originated from a different source (chemoautotrophic bacteria). Since 28-norhopanes larger than C₂₈ had not been found, it was suggested that C₂₈ demethylation occurred on a specific 30-norhopene (Schoell et al., 1992).

In this paper we report the occurrence of the complete series of 28-norhopanes (C₂₆ and C₂₈–C₃₄) in oils and sediments from West Greenland and the North Sea. The C₂₉–C₃₄ 28-norhopanes are often, but not always, present in samples containing 28,30-bisnorhopanes. It is shown that the C₂₉–C₃₀ members of the series are useful as maturity indicators.

2. Experimental

2.1. Samples

Samples from West Greenland included cores and oil seeps from the Nuussuaq area. The geology of the area and the geochemistry of the various oil types found there have been described previously (Christiansen et al., 1996; Bojesen-Koefoed et al., 1999). Samples from the North Sea consisted of crude oils generated from source rocks of Jurassic age and solvent extracts of immature source rocks of similar type and age (cores or cuttings). Most of the samples were from the Danish part of the North Sea, but a few oil samples from the British and Norwegian sectors were also analysed. Twenty-one North Sea samples with a relatively high content of 28-norhopanes are listed in Table 1. The remaining samples were Ellesmere Island, Arctic Canada, outcrops (Bojesen-Koefoed et al., 1998) and one bitumen from the Orinoco Belt, Venezuela. An immature shale from the B-1 well, German (previously Danish) North Sea was used for hydrous pyrolysis. Both solvent extracted samples (4) and unextracted samples (8) were pyrolysed.

2.2. Extraction and separation

Sediments were extracted with a dichloromethane:methanol mixture (93:7 v/v) using a soxtec system. The asphaltenes were removed from oils and extracts by precipitation in *n*-pentane, and the maltenes were fractionated by MPLC (Radke et al., 1980). MPLC was also used to prepare fractions enriched in saturated triterpanes. Reverse-phase HPLC on a Hyperprep ODS, 8 μ m, 250 \times 10 mm or a Vydac 201 TP1010, 10 μ m, 250 \times 10 mm column yielded individual triterpanes or mixtures of a few. The mobile phase was typically acetone:acetonitrile (70:30 v/v at 3 ml/min. The detector was a Waters R 401 differential refractometer.

2.3. Gas chromatography (GC)

Gas chromatography was performed using a Hewlett–Packard 5890 instrument equipped with a splitless injector and an HP-1 capillary column (25 m \times 0.20 mm i.d., film thickness 0.11 μ m). The temperature program was 5.0°C/min from 80 to 300°C, followed by 15 min at 300°C.

2.4. Gas chromatography–mass spectrometry (GC–MS)

Gas chromatography–mass spectrometry (GC–MS) was carried out on a Hewlett–Packard 5890 gas chromatograph connected to a HP5971 mass selective detector. The GC was fitted with a HP-5 capillary column (25 m \times 0.20 mm i.d., film thickness 0.11 μ m). The temperature program was 30°C/min from 70 to 100°C and 4°C/min from 100 to 300°C followed by 12 min at 300°C. Splitless injection was used. The samples were dissolved in isooctane, and the concentration was usually 0.5 mg/100 μ l. When the content of 28-norhopanes was low, the concentration was 1–5 mg/100 μ l. The MS was operated in electron impact (EI) mode with an electron energy of 70 eV. Analysis was done in the full data acquisition (SCAN) mode by scanning from 50 to 600 amu at 1.1 cycles/s and in the selected ion monitoring (SIM) or multiple ion detection mode with each of 20 ions being monitored for 30 ms dwell times. Samples with a low content of 28-norhopanes were also analyzed in SIM mode with only 3 ions being monitored (m/z 191.2: 100 ms, m/z 217.2: 100 ms, m/z 355.3: 600 ms). All mass chromatograms are from the total saturate fraction of oils or extracts, but all mass spectra have been obtained from HPLC-purified fractions. All the mass spectra are shown without background subtraction. The distribution of hopanes and 28-norhopanes were calculated from peak areas in the m/z 191 and m/z 355 mass chromatograms. The separation of C₂₉ and C₃₀ 28-norhopanes were as shown in Fig. 7, and integration was done without the use of curve-fitting software to improve separation. Sterane isomerization was

Table 1

Biomarker ratios, samples from the North Sea (21 samples) and an immature shale, B-1 well, German North Sea subjected to hydrous pyrolysis for 72 h at various temperatures (13 samples)

Natural samples/hydrous pyrolysis 72h			Maturity parameters						28-Norhopane/hopane		C ₂₈ –C ₃₀ 28-Norphopanes		
Well/field	Depth	Sample type	<i>m/z</i> 217	<i>m/z</i> 191	<i>m/z</i> 191	<i>m/z</i> 355	<i>m/z</i> 355	<i>m/z</i> 355	<i>m/z</i> 191	<i>m/z</i> 191	<i>m/z</i> 355	<i>m/z</i> 355	<i>m/z</i> 355
			C ₂₉ Sterane 20S/ 20S + 20R	C ₃₁ Hopane 22S/ 22S + 22R	C ₃₀ 28N Hopane 22S/ 22S + 22R	C ₃₀ 28N Hopane 22S/ 22S + 22R	C ₂₉ 28N Hopane β α / β α + α β	C ₃₀ 28N Hopane β α / β α + α β	28N/ 29H	30N/ 31H	% C ₂₈	% C ₂₉	% C ₃₀
B-1	8620'	Cuttings	0.08	0.35	0.28	0.26	0.40	0.07	2.38	1.29	21	7	71
B-1	8700'	Cuttings	0.10	0.45	0.42	0.41	0.32	0.12	5.48	1.92	48	8	43
B-1	8820'	Cuttings	0.10	0.42	0.38	0.39	0.33	0.13	5.23	0.66	62	8	29
B-1	8880'	Cuttings	0.10	0.44	0.39	0.40	0.42	0.17	3.64	0.53	57	10	34
Bo-1	8500'	Cuttings	0.09	0.41	0.27	0.28	0.44	0.19	3.49	0.15	83	6	11
Bo-1	8520'	Cuttings	0.11	0.44	0.31	0.34	0.57	0.33	0.41	0.09	43	23	34
Bo-1	8550'	Cuttings	0.12	0.44	0.32	0.34	0.60	0.36	0.24	0.06	40	24	36
E-1X	9784'	Core	0.16	0.54	0.51	0.54	0.55	0.40	0.12	0.12	16	28	57
E-1X	9786'	Core	0.14	0.53	0.49	0.52	0.52	0.42	0.15	0.18	18	21	61
E-1X	9789'	Core	0.15	0.53	0.49	0.53	0.55	0.40	0.21	0.19	17	23	60
E-8X	n.a.	Oil	0.27	0.56	0.50	0.50	0.64	0.52	0.30	0.06	48	28	24
Jens-1	9540'	Cuttings	0.31	0.57	–	0.64	0.64	0.53	0.68	0.07	69	17	14
Jens-1	9560'	Cuttings	0.32	0.57	–	0.62	0.65	0.51	0.53	0.07	62	20	18
Jens-1	9600'	Cuttings	0.31	0.57	–	0.61	0.64	0.53	0.33	0.07	47	24	29
Valdemar-2H	n.a.	Oil	0.31	0.57	–	0.61	0.71	0.64	0.13	0.05	35	33	32
Valdemar-2H	n.a.	Oil	0.31	0.57	–	0.65	0.72	0.61	0.12	0.05	33	35	32
Rita-1X	12380'	Cuttings	0.42	0.58	–	0.64	0.70	0.64	0.20	0.06	41	30	29
Rita-1X	12420'	Cuttings	0.40	0.58	–	0.64	0.70	0.67	0.14	0.07	32	28	40
Brent	n.a.	Oil	0.46	0.59	–	0.64	0.74	0.74	0.79	0.11	46	30	24
Mona-1	12242-12380'	Oil	0.50	0.59	–	0.63	0.71	0.68	0.59	0.08	46	30	24
30/6-C14	3436.7 m	Oil	0.51	0.58	–	–	0.73	0.65	0.74	0.14	36	33	31
B-1	8480-9020'	Untreated	0.08	0.39	0.34	0.35	0.34	0.13	7.48	1.39	51	8	41
B-1	8480-9020'	240°	0.08	0.40	0.35	0.35	0.34	0.14	6.74	1.20	54	11	35
B-1	8480-9020'	250°	0.09	0.40	0.35	0.35	0.30	0.13	6.29	1.33	51	9	40
B-1	8480-9020'	260°	0.10	0.42	0.38	0.42	0.28	0.11	3.40	0.83	51	12	37
B-1	8480-9020'	288°	0.12	0.38	0.38	0.38	0.23	0.17	2.72	0.83	49	13	38
B-1	8480-9020'	300°	0.23	0.44	0.44	0.43	0.26	0.21	2.27	0.75	52	13	35
B-1	8480-9020'	315°	0.29	0.50	0.49	0.49	0.32	0.30	1.57	0.54	48	17	35
B-1	8480-9020'	330°	0.43	0.55	0.54	0.54	0.48	0.46	1.06	0.40	40	23	37
B-1	8480-9020'	345°	0.46	0.51	–	0.58	0.59	0.54	1.02	0.46	46	20	34
B-1	8480-9020'	E260 ^a	0.08	0.23	0.22	0.24	0.11	0.06	0.82	0.42	30	25	45
B-1	8480-9020'	E300°	0.18	0.39	0.40	0.39	0.17	0.20	0.31	0.30	22	34	44
B-1	8480-9020'	E330°	0.44	0.54	0.53	0.56	0.47	0.46	0.22	0.26	20	39	41
B-1	8480-9020'	E260° E330°	0.46	0.55	0.53	0.56	0.49	0.48	0.23	0.28	20	42	38

^a E: solvent extracted sample, E260 E: solvent extracted sample, pyrolysed 260/72, solvent extracted again before final hydrous pyrolysis.

measured using peak heights in the m/z 217 mass chromatogram.

2.5. Combined gas chromatography–isotope ratio mass spectrometry (GC–IRMS)

Fractions containing > 75% triterpanes were prepared using MPLC. The GC–IRMS analyses were performed by Geolab Nor, Norway. The experimental procedure has been described by Bjorøy et al. (1993).

2.6. Hydrous pyrolysis

Hydrous pyrolysis was carried out in stainless-steel HPLC-columns (Knauer A0021, 4 mm id., 120 mm length). The columns were filled with 0.7–1.0 g of finely ground rock and 1 ml of water. Sealed columns were heated for 72 h at temperatures ranging from 240 to 345°C in a block of aluminium equipped with temperature sensors and heating cartridges. After cooling, the columns were thoroughly washed out with water. The rock was recovered on 0.45 µm polycarbonate filters and dried at room temperature. The water phase was not used.

3. Results and discussion

3.1. Mass spectra of 28-norhopanes

In 1992, a typical terrigenous, high-wax oil (the “Marraat oil”) was found on the Nuussuaq peninsula, West Greenland (Christiansen et al., 1996). During drilling in 1993–1995, more oils were discovered, both in cores of volcanics and underlying sediments and at the surface in the vicinity of the drill sites. At least five distinct oil types have now been recognized in the area (Bojesen-Koefoed et al., 1999). One of these (the “Eqalulik oil”) was probably generated from a lacustrine source rock. Unlike the Marraat oil, it contains no terrigenous triterpenoids and has a low sterane content. However, it contains abundant C_{28} ring-A methylated steranes and the corresponding mono- and triaromatic methyl steranes are present. A gas chromatogram of the saturate fraction of an Eqalulik-type oil (Bojesen-Koefoed et al., 1999) shows a very high content of hopanes. The m/z 191 mass chromatogram of the Eqalulik oil (Fig. 1) shows the presence of 28,30-bisnorhopane and regular C_{27} – C_{35} hopanes, but several other compounds can also be seen. Analysis in scan mode revealed a series of compounds with the base peak at m/z 191 and molecular ions at m/z 398, 412, 426, 440 and 454. They all have a small M-15 fragment and a relatively intense m/z 355 fragment. The m/z 355 fragment corresponds to loss of the side chain from a nuclear demethylated hopane. The base peak at m/z 191 and a very small m/z 177

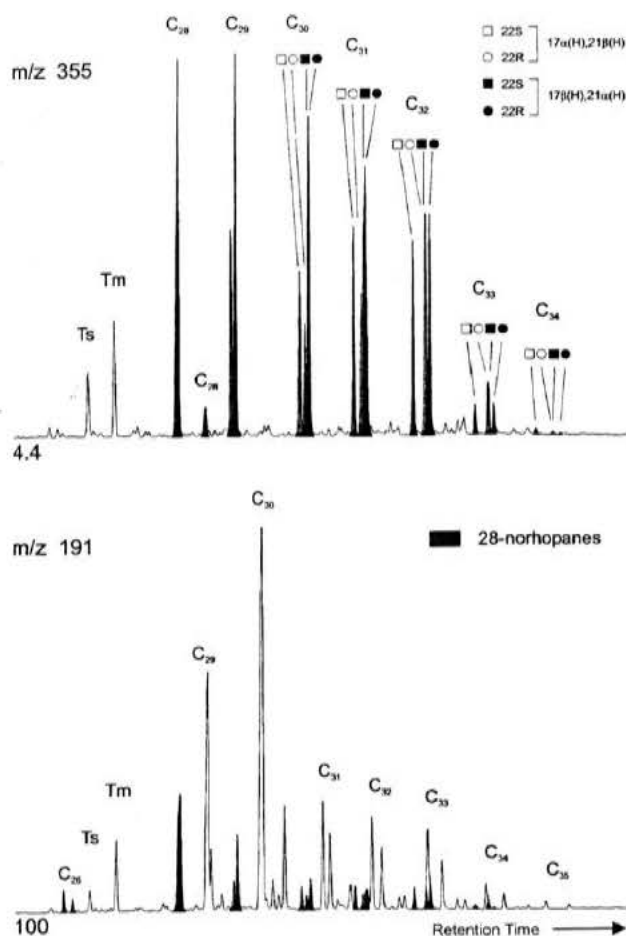


Fig. 1. m/z 191 (bottom) mass chromatogram showing the distribution of hopanes and 28-norhopanes in the Eqalulik oil, West Greenland, GEUS No. 439001-647, GANE No. 1 well, 638.45 m, and the m/z 355 mass chromatogram (top) showing only the 28-norhopanes. Both regular hopanes and 28-norhopanes have a similar distribution of homologues suggesting a common origin. The C_{30} 17 α (H),21 β (H)-hopane has an increased response in the m/z 191 mass chromatogram due to a m/z 191 fragment from both halves of the molecule. The chromatograms are normalized to the largest peak.

fragment show that the methyl group is missing in the ring C/D part of the ring system and not in ring A/B. The only possibilities for missing methyl groups are then at C-14 or C-18. The spectra of the new series are in many ways similar to the spectrum of 28,30-bisnorhopane. The ring A/B fragment (m/z 134 + R) is relatively weak irrespective of stereochemistry at C-17 and C-21, and all spectra contain a m/z 217 ion. These mass spectral features and the fact that these compounds have only been found in oils and sediments containing 28,30-bisnorhopanes, strongly suggest that this is the C_{29} – C_{33} members of the 28-norhopane series, although definite proof can only be obtained after comparison with synthetic reference material. Clean mass spectra of C_{34} 28-norhopanes could not be obtained, but traces can be seen in the m/z 355 mass chromatograms (Figs. 1 and 2). The 191 mass chromatogram (Fig. 1) also revealed two

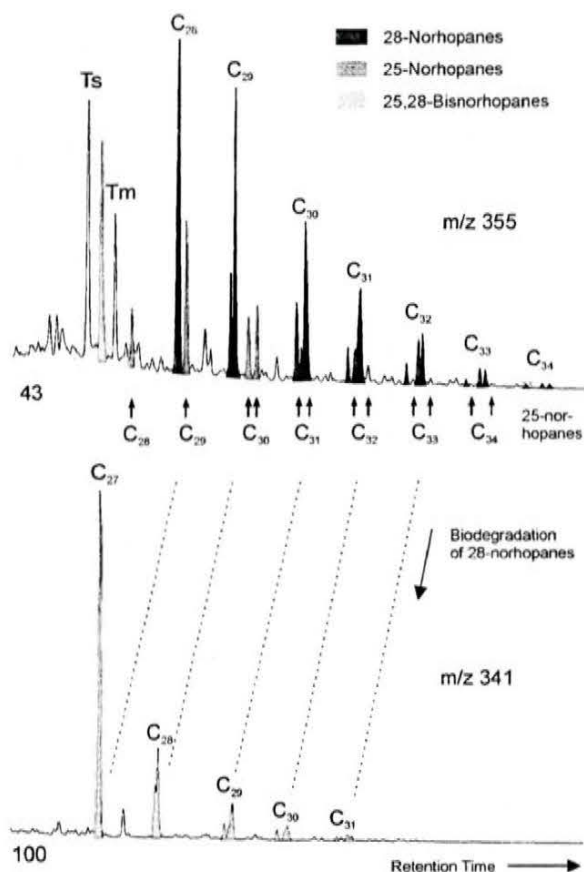


Fig. 2. m/z 355 (top) mass chromatogram showing the distribution of 25-norhopanes and 28-norhopanes in a biodegraded oil from the Oseberg area, Norway. 25-norhopanes with more than 30 carbon atoms are obscured by the more abundant 28-norhopanes. The arrows below the baseline show their retention times. The m/z 341 mass chromatogram (bottom) shows the 25,28-bisnorhopanes formed by degradation of 28-norhopanes. Note the preferential degradation of low molecular weight 28-norhopanes.

compounds eluting approximately 1/2 carbon number earlier than $18\alpha(\text{H})$ -22,29,30-trisnorneohopane (T_s). This is where a pair of C_{29} tricyclic terpanes is usually found, but because the sample was almost devoid of other tricyclics these compounds had to be something else. In order to get mass spectra of pure compounds it was necessary to use reverse phase HPLC to remove the coeluting methylsteranes. The two compounds have identical mass spectra which are similar to those of $17\alpha(\text{H})$ -22,29,30-trisnorhopane (T_m) and especially T_s , except that they have a molecular ion at m/z 356 instead of m/z 370 and a fragment at m/z 135 (ring D + E) instead of m/z 149. The mass spectra of the late eluting isomer and T_s are shown in Fig. 5. The mass spectral data suggest that these compounds are two isomeric 22,28,29,30-tetrakisnorhopanes, but the exact stereochemistry has not been determined. The ratio in the Eqlulik oil is 6:4 (Fig. 1). Hydrous pyrolysis at 330°C of a solvent-extracted, immature Jurassic shale from the North Sea produced both isomers in the same ratio. The

late eluting isomer was also found in a biodegraded bitumen from the Orinoco Belt in Venezuela.

The C_{28} – C_{34} 28-norhopanes are best studied using the m/z 355 mass chromatogram (Fig. 1). With the exception of the C_{27} hopanes and 25-norhopanes, other hopanes do not produce this fragment, and interference from other compounds in the m/z 355 mass chromatogram is usually low. If the m/z 356 mass chromatogram is used instead, the C_{26} 28-norhopanes can also be detected, but the signal from the C_{28} – C_{34} 28-norhopanes is approximately 4 times weaker. In oils generated from source rocks containing terrestrial higher plants, various non-hopanoid C_{27} – C_{30} triterpanes are encountered, and some of the C_{29} triterpanes produce a m/z 355 fragment (e.g. Rullkötter et al., 1982a; Curiale 1991; Armanios et al., 1994). 24-Norlupane has been found in oils from the Mackenzie Delta-Beaufort region (Curiale, 1991) and in sediments from Baffin Bay (ten Haven et al., 1992) together with 28,30-bisnorhopanes. 24-norlupane elutes a little earlier than 30-norhopane and is clearly separated from 28,30-bisnorhopanes and the C_{29} 28-norhopanes. In seeps from the Nuussuaq area, West Greenland, mixtures of the Marraat oil and the Eqlulik oil have often been found. The Marraat oil contains abundant 24,28-bisnorlupanes (Rullkötter et al., 1982a; Christiansen et al., 1996) and oleanane + lupane (Nytoft et al., 1997). $17\beta(\text{H})$ -28-norlupane and $17\alpha(\text{H})$ -28-norlupane are also present. However, the content of the 28-norlupanes is very low, and it was necessary to concentrate the 28-norlupanes using normal-phase and reverse-phase HPLC in order to get clean spectra. Synthetic 28-norlupanes from Chiron were used for comparison. The spectra of C_{29} 28-norhopanes and of 28-norlupanes are very similar, but the ratios of ions m/z 355/398 are below 1:1 in the spectra of 28-norlupanes, whereas the C_{29} 28-norhopanes display a 3:2 ratio of these ions (Fig. 3). When both types of compounds are present in a sample, GC-separation is usually not a problem. The $17\alpha(\text{H})$ -28-norlupane elutes just after the $18\alpha(\text{H})$ -30-norhopane ($C_{29}T_s$), and the later eluting $17\beta(\text{H})$ -28-norlupane has a retention time shorter than that of the C_{29} $17\alpha(\text{H})$, $21\beta(\text{H})$ -28-norhopane.

3.2. 25-Norhopanes and 25,28-bisnorhopanes

In some cases, both 25-norhopanes and 28-norhopanes occur in the same sample, but the two series have very different mass spectra and retention times. All 25-norhopanes give a relatively intense m/z 177 fragment (ring A + B) which is slightly smaller than the ring D + E fragment (e.g. Rullkötter and Wendisch, 1982). They produce a m/z 355 fragment, but it is small compared to that from the isomeric 28-norhopanes. The ratio 355/molecular ion is greater than 2 for C_{30} – C_{34} 28-norhopanes but less than 0.5 for the 25-norhopanes. Fig. 2 shows the m/z 355 mass chromatogram of the saturated

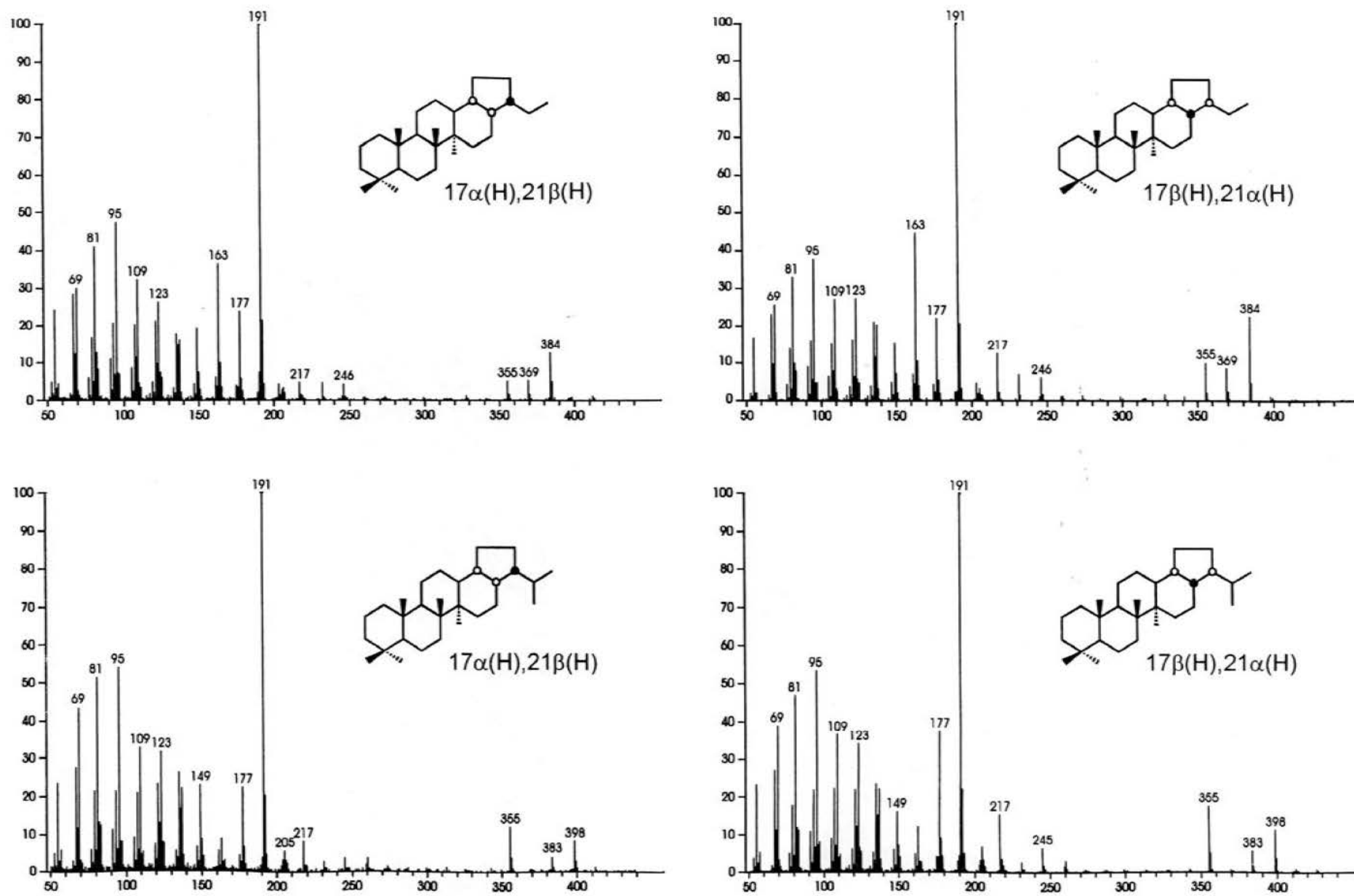


Fig. 3. Mass spectra of C_{28} 28-norhopanes (28,30-bisnorhopanes) and C_{29} 28-norhopanes from the Eqaulik oil, West Greenland, outcrop samples, mixture of GEUS no. 414852 + 414853 + 414857 + 414862.

fraction from a crude oil containing both series of norhopanes (Oseberg area, Norwegian North Sea). The geology and geochemistry of the area have been described by Dahl and Yücker (1991). The oil also contains *n*-alkanes which indicate a mixture of biodegraded and undegraded oils. The 25-norhopanes elute almost at the same time as the next lower carbon number isomeric 28-norhopanes, and only the C_{28} – C_{29} 28-norhopanes are completely separated from the C_{29} – C_{30} 25-norhopanes. The higher-carbon-number 25-norhopanes and 28-norhopanes coelute. In Fig. 2 the retention times of C_{31} – C_{34} 25-norhopanes are shown with arrows below the baseline. The retention times were obtained from another sample (bitumen from Venezuela) which contains the complete series of 25-norhopanes and no 28-norhopanes with more than 28 carbon atoms. It is believed that 25,28,30-trisnorhopanes are the degradation products of 28,30-bisnorhopanes (Volkman et al., 1983a; Moldowan et al., 1984). The mass spectra of 25,28,30-trisnorhopanes have an intense m/z 341 fragment corresponding to the loss of the side chain. The m/z 341 mass chromatogram of the Oseberg oil (Fig. 2) shows that higher 25,28-bisnorhopanes are also present (C_{28} – C_{31}). C-25 demethylation of the regular hopanes occurs preferentially among low-molecular-weight hopanes (Moldowan and McCaffrey 1995; Peters et al., 1996) and Fig. 2 shows that this also applies to 28-norhopanes. Although the absolute concentrations of the various hopanes in the Oseberg oil have not been measured, the m/z 177/191 and 341/355 ratios indicate that the 28-norhopanes are less resistant to biodegradation than regular hopanes. In this case, it is not possible to measure the relative degradation rates of the two series because the original biodegraded oil had probably been diluted by a later charge of undegraded oil whose concentrations of regular hopanes and 28-norhopanes are not known. In a sample of Brent oil (British North Sea), a high concentration of 25,28,30-trisnorhopane was found, and 25,28-bisnorhopanes up to C_{30} could also be detected. However, the concentration relative to 25,28,30-trisnorhopane was only a third of that found in the Oseberg sample. The Brent oil sample did not contain 25-norhopanes, which again shows that 28-norhopanes are more easily degraded than the regular hopanes.

As mentioned earlier, a 22,28,29,30-tetrakisnorhopane was found in a bitumen sample from the Orinoco Tar Belt in Venezuela. This sample also had a high content of 28,30-bisnorhopanes and 25,28,30-trisnorhopanes. The two 22,25,29,30-tetrakisnorhopanes (Rullkötter and Wendisch, 1982; Volkman et al., 1983a, 1983b) were also present. A 22,25,28,29,30-pentakisnorhopane could then be expected, and a low content of such a compound was indeed found after reverse-phase HPLC-fractionation of the bitumen. It had a molecular ion at m/z 342 (71%) and intense ions at m/z 135 (100%) and m/z 177 (70%). 25,28,30-trisnorhopane from the bitumen had m/z 370 (77%), m/z 163 (100%) and m/z 177 (75%).

3.3. Stereochemistry and elution order of 28-norhopanes

In the Miocene Monterey Formation, Moldowan et al. (1984) identified three epimeric 28,30-bisnorhopanes: 17 α (H),21 β (H)-, 17 β (H),21 α (H)-, and 17 β (H),21 β (H)-. The order of thermodynamic stability is 17 β (H),21 α (H) > 17 α (H),21 β (H) > 17 β (H),21 β (H). The diagenetically first-formed epimer is thought to be 17 α (H),21 β (H)- because it predominates in immature shale. Two C_{29} 28-norhopanes have been found in samples from West Greenland and the North Sea. The highest content of the first eluting compound is found in immature samples. In mature samples, the later eluting isomer predominates, and the ratio is approximately 3:7. This is similar to the ratios of the 17 α (H),21 β (H)- and 17 β (H),21 α (H)-28,30-bisnorhopanes found in mature samples by Moldowan et al. (1984). Based on this observation and the elution order of the normal hopanes and moretanes, the first eluting peak is assigned the $\alpha\beta$ -structure and the later eluting peak the $\beta\alpha$ -structure. The C_{30} – C_{34} 28-norhopanes have an additional asymmetric centre at C-22, giving four possible $\alpha\beta$ and $\beta\alpha$ epimers. The 22R and 22S diastereomers of the C_{30} 17 α (H),21 β (H)-28-norhopanes are well-resolved, but like the normal C_{31} moretanes (Larcher et al., 1987) and “moretane-like” 8,14-secohopanes (Fazeelat et al., 1995), the corresponding pair of 17 β (H),21 α (H)-28-norhopanes are not resolved giving only three peaks (Fig. 1). With increasing length of the side chain, the separation of the 17 β (H),21 α (H)-28-norhopanes increases, but instead this leads to coelution of the 22R 17 α (H),21 β (H)-28-norhopanes and 22S 17 β (H),21 α (H)-28-norhopanes (Fig. 1). The 17 β (H),21 β (H)-28,30-bisnorhopane coelutes with the 17 α (H),21 β (H)-30-norhopane under our GC-conditions, but it can clearly be seen in the m/z 355 mass chromatogram (Fig. 1). Similarly, small amounts of the 17 β (H),21 β (H)-epimers of the higher 28-norhopanes may be present, but it was not possible to obtain mass spectra of sufficiently pure compounds to confirm this.

Isothermal gas chromatography was carried out on an HP-5 column at 270°C. Straight lines were obtained when retention times of 28-norhopanes were plotted against those of the regular hopanes with the same stereochemistry, which show that the 28-norhopanes are also a pseudohomologous series. Plots of the natural logarithms of the retention times versus carbon number of 28-norhopanes were linear for compounds with 31 and more carbon atoms, but the C_{30} members of the series were slightly displaced to higher retention times. This deviation from linearity has previously been found for C_{31} hopanes and moretanes (Larcher et al., 1987) and C_{31} 8,14-secohopanes (Fazeelat et al., 1995).

The assignment of stereochemistry is substantiated by the elution order of 28-norhopanes on reverse phase HPLC columns. A triterpane concentrate of an Equisetum-type oil

was separated on a C₁₈ column and 80 fractions were collected. GC/MS analysis in scan mode of selected fractions showed that both normal hopanes and 28-norhopanes had the same elution order: $\alpha\beta$ 22S < $\alpha\beta$ 22R < $\beta\alpha$ 22S < $\beta\alpha$ 22R. 28-norhopanes had much longer retention times than isomeric regular hopanes and moretanes. This allowed the complete separation of the C₂₉ 17 β (H),21 α (H)-28-norhopane from the C₂₉ 17 β (H),21 α (H)-hopane which coelute using our GC procedure (Fig. 1). All mass spectra in Figs. 3 and 4 were obtained using these fractions.

3.4. 28-Norhopanes as maturity indicators

Moldowan et al. (1984) found that the percentage D/E *cis* of the total 28,30-bisnorhopanes = $\alpha\beta/(\alpha\beta + \beta\alpha + \beta\beta)$ was a useful maturation parameter which could supplement the sterane 20S/(20S + 20R) ratio. This parameter is seldom if ever used because separation of the 17 α (H),21 β (H)- and 17 β (H),21 α (H)-28,30-bisnorhopanes is only possible under special GC-conditions. However, it is possible to get a reasonable separation of the C₂₉ and C₃₀ $\alpha\beta$ and $\beta\alpha$ isomers on a standard 25 m column (Fig. 7). Table 1 shows the distribution of C₂₉ and C₃₀ 28-norhopanes in 21 samples of different maturities together with 20S/(20S + 20R) ratios of C₂₉ steranes and 22S/(22S + 22R) ratios of C₃₁ hopanes for comparison. The samples are Jurassic source rocks from the North Sea or crude oils sourced from such rocks. Although many of the samples from West Greenland have a higher content of 28-norhopanes, they are not included because most are Eqaalilik-type oils with almost no steranes and a distribution of 28-norhopanes very similar to that shown in Fig. 1. When steranes and 28-norhopanes were present in samples from West Greenland, there was evidence of mixing of different oil types (Bojesen-Koefoed et al., 1999), which means that 28-norhopanes and steranes probably come from different sources. As shown in Table 1 and Fig. 6, $\beta\alpha/(\alpha\beta + \beta\alpha)$ ratios of C₂₉ 28-norhopanes increase faster than $\beta\alpha/(\alpha\beta + \beta\alpha)$ ratios of C₃₀ 28-norhopanes, but eventually both reach 0.7 in samples with sterane 20S/(20S + 20R) ratios above 0.4. This means, that the $\beta\alpha/(\alpha\beta + \beta\alpha)$ ratio of the C₂₉ and C₃₀ 28-norhopanes can be utilized as an indicator of thermal maturity until the start of the oil window, and this maturity parameter could be particularly useful if the samples contain few or no steranes.

Isomerization at C-22 of the C₃₀–C₃₄ 17 α (H),21 β (H) 28-norhopanes seems to follow the isomerization of regular homohopanes. However, only the 22S/(22S + 22R) ratios of the C₃₀ 28-norhopanes could be measured. Isomerization ratios were measured from the *m/z* 355 and *m/z* 191 mass chromatograms (Table 1). When the content of 28-norhopanes was high, both ions gave similar ratios, but in mature samples with a low 28-

norhopane content, the *m/z* 191 signal-to-noise ratio was too low for accurate measurements. The 22S/(22S + 22R) ratio of C₃₀ 28-norhopanes in early oil window rank samples is 0.6–0.65. Values do not increase further with increasing maturity.

3.5. Hydrous pyrolysis

A thermally immature sample from the B-1 well, German North Sea was subjected to hydrous pyrolysis for 72 h at temperatures ranging from 240 to 345°C. Rock-Eval data from some of these experiments have been published previously (Bojesen-Koefoed et al., 1995). Eight unextracted and four extracted samples were pyrolysed (Table 1). The 28-norhopane/hopane ratios in extracts of pyrolysed samples were measured from the *m/z* 191 mass chromatogram. The ratios between 28-norhopanes and regular hopanes with the same side chain (C₂₈N/C₂₉H and C₃₀N/C₃₁H) decreased with increasing pyrolysis temperature and were especially low in pyrolysates of extracted samples. It has been shown previously that pyrolysis of extracted samples and kerogen from the Monterey Formation did not produce 28,30-bisnorhopanes (Moldowan et al., 1984; Noble et al., 1985; Tannenbaum et al., 1986), which suggests that the 28,30-bisnorhopanes are only found in the bitumen and are not part of the kerogen. Similarly, our results show that a high proportion of the 28-norhopanes exists in the bitumen of the unpyrolysed immature shale. Increasing hydrous pyrolysis temperatures then leads to a gradual dilution of the 28-norhopanes with regular hopanes liberated from the kerogen. However, it is also evident that some of the 28-norhopanes have been incorporated into the kerogen. The extracted samples were still able to produce significant amounts of 28-norhopanes by hydrous pyrolysis, and the C₂₉ and C₃₀ 28-norhopanes produced at 260°C had a much lower $\beta\alpha/(\alpha\beta + \beta\alpha)$ ratio (lower maturity) than those extracted from the untreated sample. This also explains the decrease in the $\beta\alpha/(\alpha\beta + \beta\alpha)$ ratio of in particular the C₂₉ 28-norhopanes when unextracted samples are pyrolysed at temperatures below 300°C. Extracts of immature samples are dominated by C₂₈ and C₃₀ 28-norhopanes. The relative content of C₂₉ and C₃₁–C₃₄ 28-norhopanes is low in immature samples, but increases with increasing hydrous pyrolysis temperature. A similar trend can be seen for “natural” samples (Table 1; Fig. 7), and ultimately this leads to a distribution of 28-norhopanes similar to that shown in Fig. 2. Recently Murray et al. (1998) published a hydro-pyrolysis study (not hydrous pyrolysis) of six dichloromethane-extracted Kimmeridge Clay samples. Sample Nos. 2–6 were taken from a single well in the Central Graben region of the North Sea. By coincidence, their sample no. 2 is almost identical to that used for our hydrous pyrolysis experiments, although their sample is

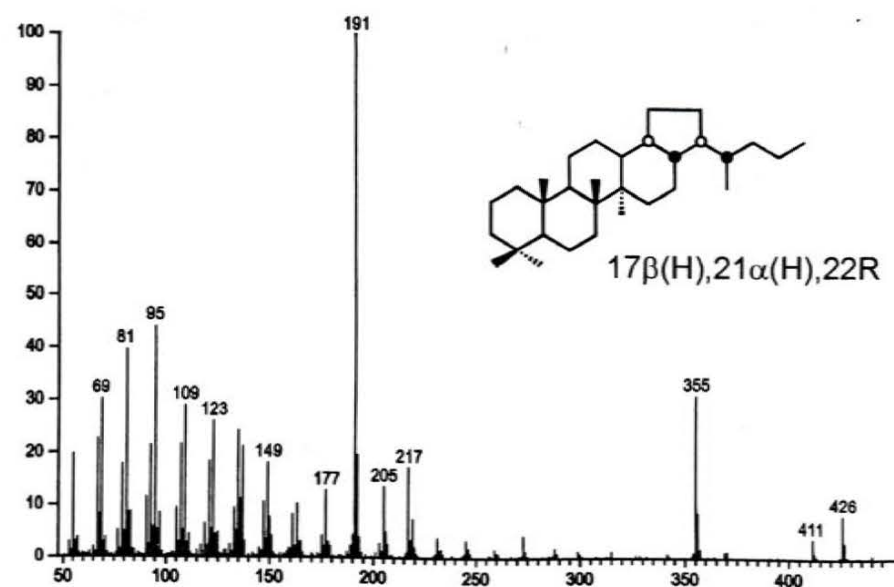
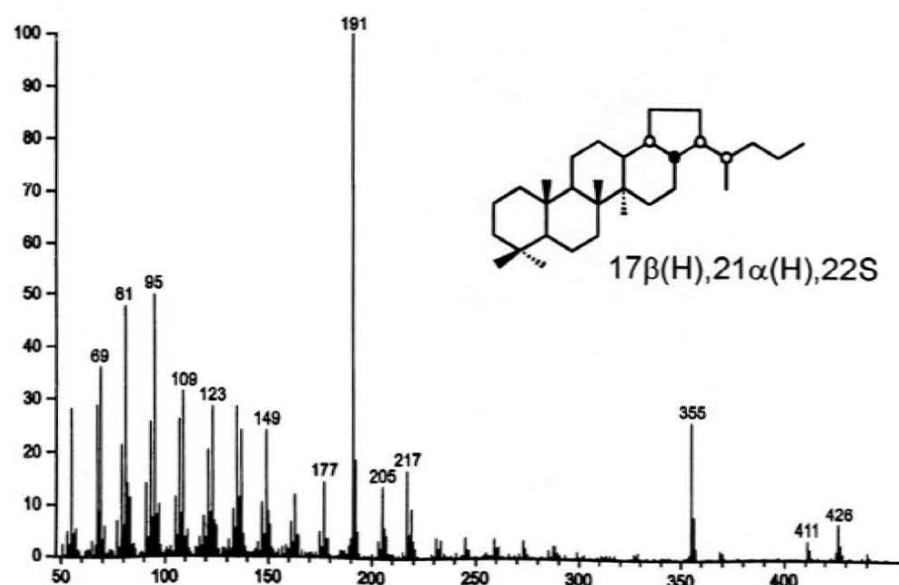
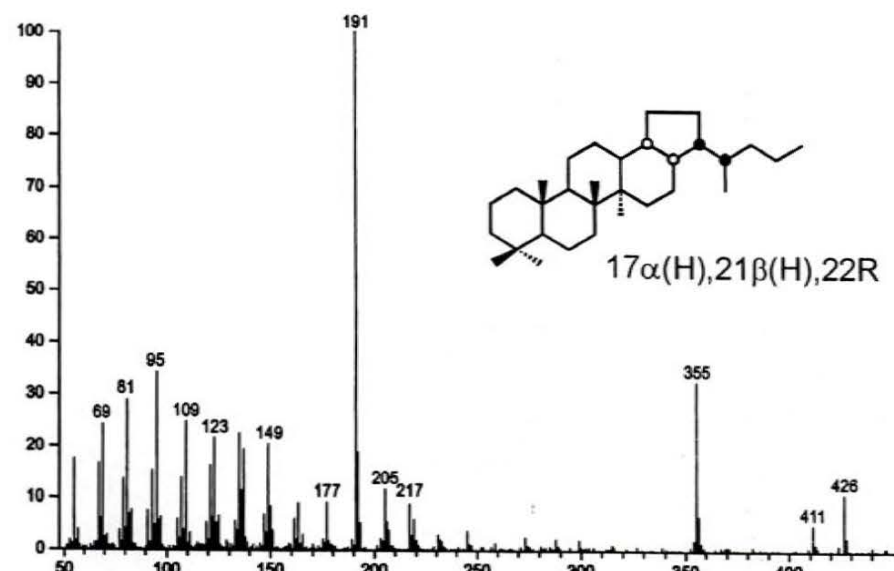
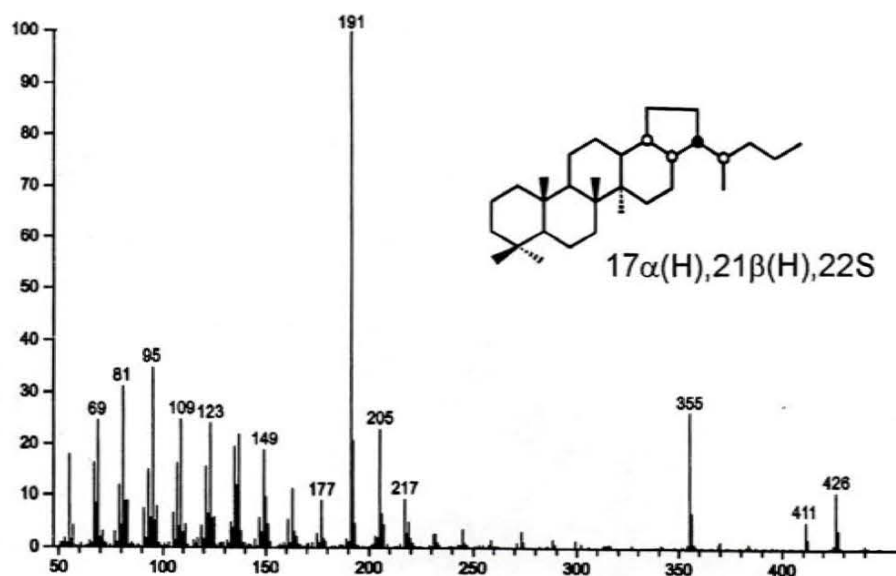


Fig. 4. Mass spectra of C₃₁ 28-norhopanes from the Eqaulik oil, West Greenland, outcrop samples, mixture of GEUS no. 414852 + 414853 + 414857 + 414862.

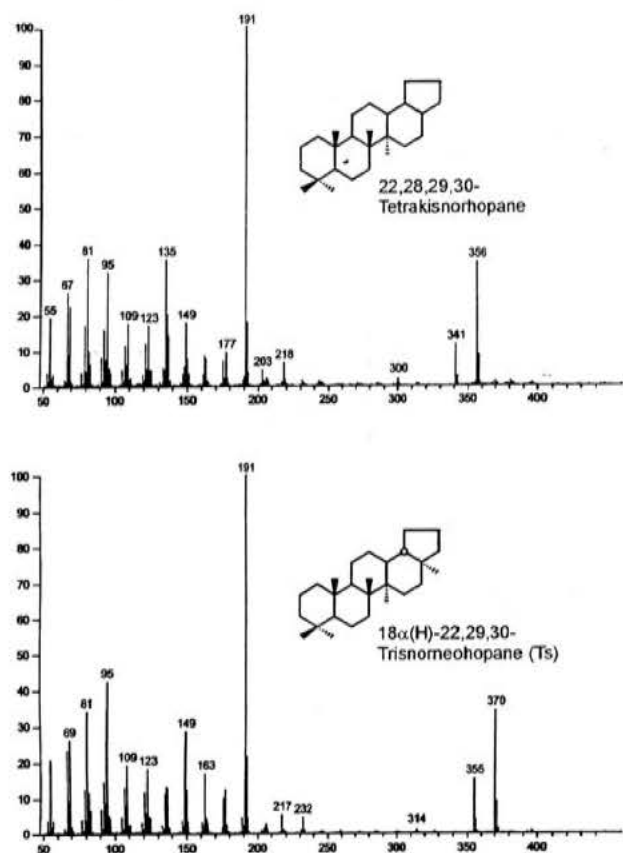


Fig. 5. Mass spectra of 22,28,29,30-tetrakisnorhopane and T_s , from the Eqaalulik oil, West Greenland, outcrop samples, mixture of GEUS no. 414852 + 414853 + 414857 + 414862.

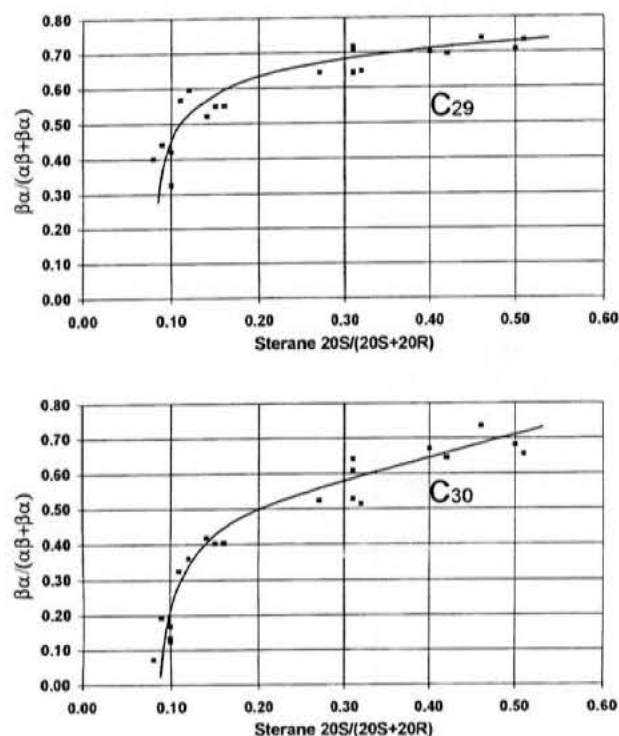


Fig. 6. $\beta\alpha/(\alpha\beta+\beta\alpha)$ ratios of C₂₉ and C₃₀ 28-norhopanes versus C₂₉ sterane 20S/(20S+20R) of 21 samples (Table 1) from the North Sea.

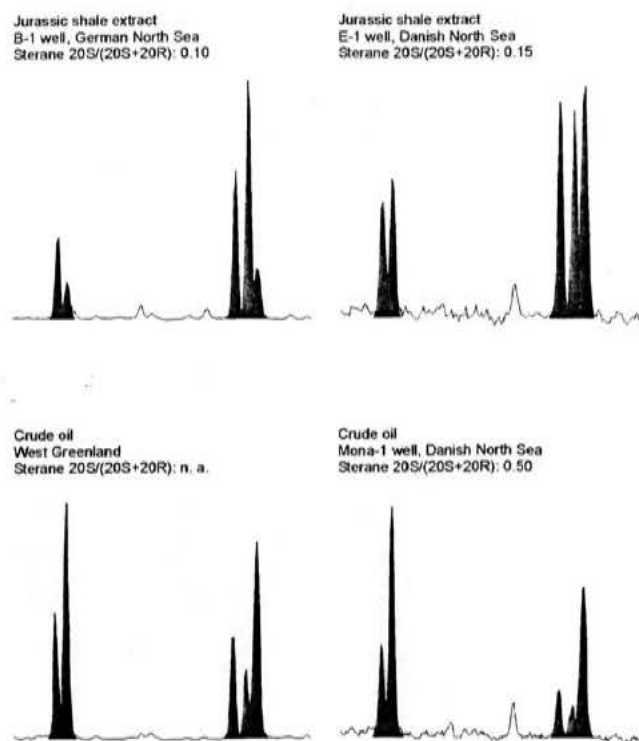


Fig. 7. m/z 355 mass chromatograms showing the distribution of C₂₉ and C₃₀ 28-norhopanes in four samples of different maturities.

slightly more mature: TOC=9.4%, T_{\max} =425, HI=646, Sterane 20S/(20S+20R)=0.12. Data for our sample: TOC=8.5%, T_{\max} =421, HI=393, Sterane 20S/(20S+20R)=0.10. The content of 28,30-bisnorhopanes in their sample was relatively high, and although higher carbon number 28-norhopanes were not mentioned in the paper, it is evident from the m/z 191 mass chromatogram (Fig. 2 in Murray et al., 1998) that both C₂₉ and C₃₀ 28-norhopanes are abundant as well. C₂₉ and C₃₀ 28-norhopanes are also found in the hydro-pyrolysis oil. C₂₉ 28-norhopane ratios could not be measured from the m/z 191 mass chromatogram because of coelution with the C₂₉ 17 β (H),21 α (H)-hopane, but the C₃₀ 28-norhopanes in the hydro-pyrolysis oil indeed had a less mature composition than the rock extract, again confirming that 28-norhopanes can be kerogen-bound.

3.6. Precursors for 28-norhopanes

The regular hopanes in geological samples are mainly the diagenetic alteration products of C₃₀ hopanes and C₃₅ biohopanoids with 4–6 functional groups in the side chain, compounds used by bacteria as membrane reinforcers (e.g. Rohmer et al., 1992). In contrast, the search for biological precursors of the 28,30-bisnorhopanes has been less successful, and the origin of 28,30-bisnorhopanes has been the subject of much speculation. Hopanoids such as adipedatol (found in ferns) which already possess a 30-norhopane skeleton and are functionalized

on the C-28 methyl group have been proposed as precursors. (e.g. Seifert et al., 1978; Grantham et al., 1980; Schoell et al., 1992). 28,30-bisnorhopanes and the related 25,28,30-trisnorhopanes can have $\delta^{13}\text{C}$ variations which exceed those in lipids derived from primary producers, and this could suggest that both compounds were derived from sediment-dwelling bacteria which utilised porewater CO_2 as a carbon source (Schouten et al., 1997, and refs. therein). The isotopic composition of this CO_2 is dependent on the intensities of sulfate reduction and methanogenesis (Blair and Carter, 1992), thus giving variable isotopic compositions in compounds synthesized by sedimentary organisms living on porewater CO_2 . The 28,30-bisnorhopanes in an immature oil from the Monterey Formation were found to be considerably depleted in ^{13}C compared to the regular hopanes and the whole oil (Schoell et al., 1992), whereas $\delta^{13}\text{C}$ values in the Polish Menilite were almost identical (Köster et al., 1998). However, it is very likely that there is more than one mechanism for formation of 28,30-bisnorhopanes. It seems that 28,30-bisnorhopanes are most often formed alone, whereas the complete series of 28-norhopanes is more rare. There is no evidence in the literature that higher carbon number 28-norhopanes have been detected in Monterey Formation samples. Similarly, extremely high amounts of 28,30-bisnorhopanes have been found in sediments from Ellesmere Island, Arctic Canada (Bojesen-Koefoed et al., 1998), but no higher carbon number 28-norhopanes were reported. Since higher carbon number 28-norhopanes could also be kerogen bound, hydrous pyrolysis was carried out on two samples at seven temperatures in the range from 220 to 330°C. No higher carbon number 28-norhopanes were found in any of the pyrolysed samples. The Eqaulik oil from West Greenland (lacustrine?) is completely different. The isotopic composition of regular hopanes and 28-norhopanes has been measured and it was found that both types of hopanes were equally depleted in ^{13}C (Table 2); therefore, there is no isotopic evidence for different origins of the two types of hopanes. Furthermore, the distribution of regular hopane homologues and 28-norhopanes with the same side chain is almost identical (Fig. 1). In North Sea oils and sediments, an intermediate situation could exist. We have analysed a large number of oils and sediments from the North Sea using GC-MS in SIM-mode (m/z 191 and 355). Most of the samples were oils and sediment extracts from the Danish sector, but a few oils from both the British (Brent and Forties), and Norwegian sectors (Oseberg, Fig. 2) were also analysed. All samples containing 28,30-bisnorhopanes also contained the higher carbon number 28-norhopanes, and the higher carbon number 28-norhopanes were never found in samples without 28,30-bisnorhopanes. An immature shale from the B-1 well, German North Sea Sector, which had a high content of both regular hopanes and 28-norhopanes

Table 2

Stable carbon isotope ratios of hopanes and 28-norhopanes in the Eqaulik oil, West Greenland, GEUS No. 439001-654, GANE No. 1 well, 640.10 m, (A) and an immature Jurassic shale, B-1 well, 8480-9020', German North Sea (B)

Sample	A	B
17 α (H),21 β (H), 30-norhopane	-35.4	-
17 α (H),21 β (H), hopane	-34.7	-
22S 17 α (H), 21 β (H) homohopane	-36.9	-30.3
22R 17 α (H), 21 β (H) homohopane	-36.8	-28.9
22S 17 α (H), 21 β (H) bishomohopane	-35.5	-
22R 17 α (H),21 β (H) bishomohopane	-35.1	-
17 α (H),21 β (H) + 17 β (H),21 α (H)28,30 bisnorhopane	-36.7	-25.4
17 α (H),21 β (H), 28-norhopane	-34.1	-
22S 17 α (H),21 β (H) 28-norhomohopane	-36.7	-28.3
22R 17 α (H),21 β (H) 28-norhomohopane	-35.9	-28.3
22S + R 17 β (H), 21 α (H) 28-norhomohopane	-37.6	-
22S 17 α (H),21 β (H) 28-norbishomohopane	-35.9	-
22S + R 17 β (H),21 α (H) 28-norbishomohopane	-33.9	-

was chosen for GC-IRMS analysis. The concentration (from the GC-IRMS chromatogram) of 28,30-bisnorhopane was at least 5 times higher than the concentration of any of the other hopanes, and it was enriched in ^{13}C by 3–5‰ compared to both the C_{31} hopanes and the C_{30} 28-norhopanes. These results also indicate that the complete series of 28-norhopanes and the regular hopanes could sometimes be formed from the same precursors, but when an extremely high content of 28,30-bisnorhopane is found, some of it could have a different origin.

28,30-Bisnorhopenes could be the immediate precursors of 28,30-bisnorhopanes. In a Gulf of California sediment, Rullkötter et al. (1982b) found 28,30-bisnorhopanes and a C_{28} triterpene which was tentatively identified as 28,30-bisnorhop-17(18)-ene. Sinninghe Damsté (1997) has identified a 28,30-bisnorhop-13(18)-ene in Cenomanian-Turonian black shales from the North Atlantic Ocean. The identification was based on comparison of its mass spectral data with those of the neohop-13(18)-ene series. We have found a compound with the same mass spectrum in an immature lacustrine? Jurassic sediment from southern Sweden (Fig. 8) and in a Lower Cretaceous carbonaceous claystone, Bornholm, Denmark with a huminite reflectance value of 0.24% Rr (Petersen et al., 1996). A small amount of a later eluting isomer with almost the same mass spectrum was also present. The samples also contained small amounts of 28,30-bisnorhopane, and 28,30-bisnorhop-13(18)-ene is a likely precursor in these samples. Measurement of the ^{13}C content in both compounds could have given more information, but unfortunately the samples were too small and the content of 28,30-bisnorhopanes too low for such a measurement. The only C_{28} monounsaturated triterpene found is 28,30-bisnorhop-13(18)-ene, whereas the content

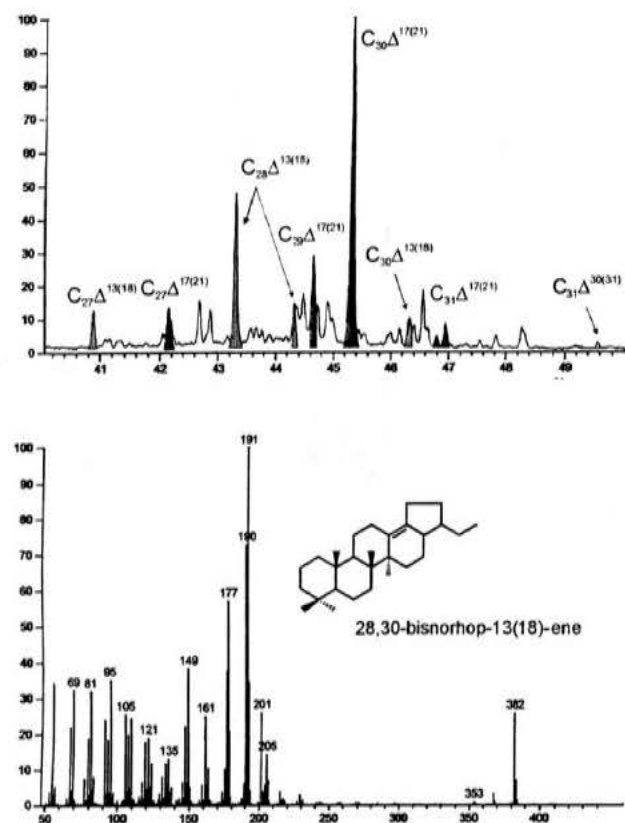


Fig. 8. Total ion chromatogram (full scan) of the hopene fraction from an immature lacustrine sediment from southern Sweden. The mass spectrum of the major (first eluting) C_{28} Hop-13(18)-ene is shown below.

of C_{27} and C_{29} – C_{31} hop-17(21)-enes is high compared to that of the corresponding neohop-13(18)-enes. This means that 28,30-bisnorhop-13(18)-ene is probably produced by some unknown organism and not by rearrangement of a C_{28} hop-17(21)-ene or other C_{28} triterpene, unless the absence of a methyl group at C-18 increases the rate of rearrangement reactions described for the C_{30} triterpenes (Ageta et al., 1987). Similarly, the hydrogenation of the C_{28} hop-13(18)-ene could be comparatively easy, whereas the usual neohop-13(18)-enes are difficult to hydrogenate unless severe conditions are used. Less than 0.01 mg of the major 28,30-bisnorhop-13(18)-ene was isolated 90% pure from one of the samples (Fig. 8) using reverse-phase HPLC. Hydrogenation in 0.1 N perchloric acid/acetic acid using platinum dioxide as a catalyst gave mainly 28,30-bisnorhopanes as expected, but due to the limited amount of 28,30-bisnorhop-13(18)-ene available, more systematic hydrogenation experiments have not been possible. The role of 28,30-bisnorhop-13(18)-ene is still enigmatic however, and we have not found it in any of the immature samples with a very high content of 28,30-bisnorhopanes, although small amounts of the normal neohop-13(18)-enes and hop-17(21)-enes were still present, which suggests that other more important precursors must exist.

Recently a series of 28-norhopanoic acids (C_{29} – C_{31}) was identified in Neogene upwelling sediments (Yamamoto et al., 1997). It was found that the ratio of 28-norhopanoic acids over total hopanoic acids was parallel to that of 28,30-bisnorhopane over total hopanes. The 28-norhopanoic acids are thus obvious precursors of 28-norhopanes. C_{29} –28-bisnorhopanoic acid was the major 28-norhopanoic acid. Decarboxylation will yield 28,30-bisnorhopane.

Finally, it must be mentioned that small amounts of 28-norhopanes can be formed by laboratory hydrogenation of the normal neohop-13(18)-enes. We have hydrogenated synthetic C_{29} – C_{31} neohop-13(18)-enes (>99% pure) in 0.1 N perchloric acid/acetic acid using platinum dioxide as a catalyst. Neohopanes and regular hopanes were the main products. Minor products (all below 2%) were 8,14-secohopanes (Schmitter et al., 1982), 28-norhopanes, 25-norhopanes and several unidentified compounds. 28,30-bisnorhopanes were formed from 30-norneohop-13(18)-ene and C_{29} 28-norhopanes were formed from neohop-13(18)-ene etc. Similarly, there is a possibility that 28-norhopanes can be formed in sediments under the influence of clay, but we consider it unlikely that more than trace amounts are formed this way in natural samples.

3.7. Demethylated D-ring aromatic 8,14-secohopanes

A relatively high concentration of demethylated D-ring aromatic 8,14-secohopanes is found in samples containing the full series of 28-norhopanes, suggesting common precursors of the two series. Demethylated aromatic 8,14-secohopanes lacking probably the C-28 methyl group (m/z 351) were first identified by Killips (1991). The normal Ring D aromatic 8,14-secohopanes (m/z 365) were found by Hussler et al., (1984). The latter are particularly abundant in carbonates, but can be found in most oils and sediments. We have analysed a large number of Jurassic oils and sediments from the Danish North Sea and found both series in all samples. In Upper Jurassic oils and sediments, the complete series of saturated 28-norhopanes is usually present, and these samples also have a high content of the demethylated aromatic 8,14-secohopanes, whereas samples of Middle Jurassic age contain no 28-norhopanes and only a small amount of demethylated aromatic 8,14-secohopanes. The Eqaalulik oil from West Greenland has a content of demethylated aromatic 8,14-secohopanes exceeding that of the usual aromatic 8,14-secohopanes, and the distribution of homologs is very similar to that of the 28-norhopanes, albeit with a relatively lower content of the C_{28} compounds. In samples from Ellesmere Island with a very high content of 28,30-bisnorhopane and no higher 28-norhopanes, a relatively low content of all demethylated aromatic 8,14-secohopanes was found, again suggesting an alternative source for

28,30-bisnorhopanes in these samples. A low content of demethylated aromatic 8,14-secohopanes can also be found in samples without 28-norhopanes and even in oils from carbonate source rocks. This probably means that they can also be formed from the same precursors as the normal aromatic 8,14-secohopanes. During aromatization, the C-28 methyl group is lost from some molecules instead of being moved to C-21. In mature samples, the demethylated aromatic 8,14-secohopanes show pairs of C_{28} and C_{29} homologues as shown by Killops (1991), and double pairs of the C_{30} – C_{34} homologues. Two of the four C_{30} isomers coelute, giving rise to three peaks with a relative abundance of 1:2:1 (Fig. 9). We call this series the A-series. In immature samples, an equal number of additional isomers of a second series (B-series) is present. Only the C_{28} members of the isomer-series A and B can be separated on standard capillary columns. Of the C_{29} and C_{30} members, only the first eluting isomer of the series A and the last eluting isomer of the series B are separated. Otherwise, various degrees of coelution of the series A and series B isomers prevail. The series B is almost absent in the mature Oseberg oil (Fig. 9). The normal D-ring aromatic 8,14-secohopanes

also have a late eluting series which is most prominent in immature samples (as shown by Köster et al., 1997), whereas it is almost absent in mature samples (as shown by Hussler et al., 1984). We have found that the relative content of this later eluting series closely follows the B/(A + B) ratio for the demethylated aromatic 8,14-secohopanes suggesting a similar stereochemistry, possibly at C-8. In mature samples, small amounts of an additional earlier eluting series of demethylated aromatic 8,14-secohopanes (series C) can be seen, and the ratio C/A is around 0.1 in mature samples like the Oseberg oil (Fig. 9). The C_{28} series B isomers coelute with the C_{29} series C isomers. All isomers have nearly identical mass spectra, and assignment of stereochemistry to the various series awaits further research.

Like their saturated counterparts, the demethylated aromatic 8,14-secohopanes can lose one more methyl group (probably C-25) during biodegradation, and there is also a preferential degradation of the low-molecular-weight compounds. In a biodegraded oil from the Norwegian Oseberg area, the complete C_{28} – C_{34} series of demethylated aromatic 8,14-secohopanes could be seen in the m/z 351 mass chromatogram (Fig. 9), and the corresponding series of aromatic 25,28-bisnor-8,14-secohopanes (C_{27} – C_{29} only) was tentatively identified in the m/z 337 ion chromatogram. The aromatic 25,28-bisnor-8,14-secohopanes have only been found in samples which also contain saturated 25,28-bisnorhopanes.

4. Conclusions

28,30-Bisnorhopanes have been known for more than 20 years, and they are the only 28-norhopanes in oils and source rocks from many locations. The complete series of C_{26} and C_{28} – C_{34} 28-norhopanes has now been found in oils and source rocks from West Greenland and the North Sea. The C_{28} – C_{34} 28-norhopanes have only been found in samples containing 28,30-bisnorhopanes. When the complete series of 28-norhopanes is present, there is (so far) no isotopic evidence for different origins of 28-norhopanes and regular hopanes, but this needs further investigation. The C_{28} and C_{30} 28-norhopanes dominate in the bitumen of immature sediments, whereas larger proportions of C_{29} and C_{31} – C_{34} 28-norhopanes are part of the kerogen. 28-Norhopanes are more easily degraded than the regular hopanes. C_{25} and C_{27} – C_{31} 25,28-bisnorhopanes have been identified in biodegraded samples. A relatively high concentration of demethylated D-ring aromatic 8,14-secohopanes is found in samples containing the full series of 28-norhopanes, suggesting common precursors of the two series. The 28-norhopanes can be seen in the m/z 191 mass chromatogram, but since their mass spectra also have a strong m/z 355 fragment, they are best studied in the m/z 355 mass chromatogram. The $\beta\alpha/(\alpha\beta + \beta\alpha)$ ratio of

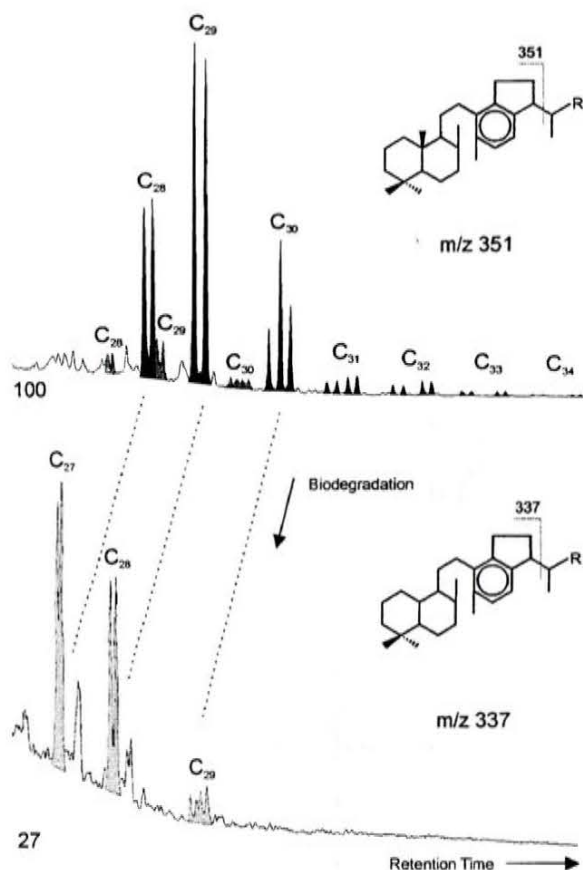


Fig. 9. m/z 351 (top) mass chromatogram showing the distribution of the A-series 28-nor aromatic 8,14-secohopanes (black) and the minor, early eluting C-series (grey) in a biodegraded oil from the Oseberg area, Norway. Biodegradation leads to 25,28-bisnor aromatic 8,14-secohopanes (m/z 337 (bottom)).

C₂₉ and C₃₀ 28-norhopanes can be utilized as an indicator of thermal maturity until the start of the oil window.

Acknowledgements

Technical assistance of Mohammad Amin Dejkam, Ditte Kiel-Dühring, Carsten Guvad and Lisbeth Løvig Nielsen is greatly acknowledged. We thank L. Koldo Núñez-Betelu for Ellesmere Island samples and Birger Dahl for Oseberg area samples. SK energi, Kalundborg provided samples of Orinoco bitumen. Funding for field work and analyses was provided partially by the Government of Greenland, Minerals Office. Additional financial support was provided by the Danish Energy Research Programme (EFP-98), grant 1313/98-0022. Finn Steffens and his crew on *Maja S* are thanked for good seamanship and assistance at coastal outcrops. We also thank Jon R. Ineson, Mark A. McCaffrey and Michel Rohmer for their constructive reviews of the manuscript. This paper was published with the permission of the Geological Survey of Denmark and Greenland (GEUS).

Associate Editor—P. Farrimond

References

- Ageta, H., Shiojima, K., Arai, Y., 1987. Acid-induced rearrangement of triterpenoid hydrocarbons belonging to the hopane and migrated hopane series. *Chemical and Pharmaceutical Bulletin* 35, 2705–2716.
- Armanios, C., Alexander, R., Kagi, R.I., Sosrowidjojo, I.B., 1994. Fractionation of sedimentary higher-plant derived pentacyclic triterpanes using molecular sieves. *Organic Geochemistry* 21, 531–543.
- Bjørøy, M., Hall, K., Vigran, J.O., 1980. An organic geochemical study of Mesozoic shales from Andøya, North Norway. In: Douglas, A.G., Maxwell, J.R. (Eds.), *Advances in organic geochemistry* 1979. Pergamon Press, Oxford, pp. 77–91.
- Bjørøy, M., Hall, P. B., Moe, R. P., 1993. Stable carbon isotope variation of *n*-alkanes in Central Graben oils. In: Telnæs, N., G. van Graas, K. Oygard (Eds.), *Advances in Organic Geochemistry* 1993, *Organic Geochemistry*. Vol. 22, pp. 355–381.
- Blair, N.E., Carter, W.D., 1992. The carbon isotope geochemistry of acetate from a methanogenic marine sediment. *Geochimica et Cosmochimica Acta* 56, 1247–1258.
- Bojesen-Koefoed, J. A., Nytoft, H. P., Amin Dejkam, M., 1995. Hydrous pyrolysis of Upper Farsund Formation (Volgian-Ryazanian) "hot shales" from the southern central Trough, German North Sea Sector. In: J. O. Grimalt, C. Dorronsoro (Eds.), *Selected papers from the 17th International Meeting on Organic Geochemistry Donastia-San Sebastián, The Basque Country, Spain*. 4–8 September 1995. A.I.G.O.A., Donastia-San Sebastián, pp. 542–544.
- Bojesen-Koefoed, J. A., Christiansen, F. G., Nytoft, H. P., Pedersen, A. K., 1999. Oil seepage onshore West Greenland: evidence of multiple source rocks and oil mixing. In: A.S. Fleet, S. Boldy (Eds.), *Petroleum Geology of NW-Europe*, proceedings of the 5th Conference, Geological Society of London, London.
- Bojesen-Koefoed, J. A., Christiansen, F. G., Nytoft, H. P., Petersen, H. I., 1998. Petroleum source potential and the importance of marine versus terrigenous organic matter input: a comparative study of mid-Cretaceous deposits from Ellesmere Island, Northwest Territories, Canada. In: P. K. Mukhopadhyay, M. P. Avery, J. H. Calder, F. Goodarzi (Eds.), *Abstracts of the 15th Annual Meeting of The Society for Organic Petrology*, 29–30 July 1998, Halifax, Nova Scotia, Canada. Vol. 15, pp. 57–59.
- Christiansen, F.G., Bojesen-Koefoed, J.A., Dam, G., Nytoft, H.P., Larsen, L.M., Pedersen, A.K., Pulvertaft, T.C.R., 1996. The Marraat oil discovery on Nuussuaq, West Greenland: evidence for a latest Cretaceous–earliest Tertiary oil prone source rock in the Labrador Sea — Melville Bay region. *Bulletin of Canadian Petroleum Geology* 44, 39–54.
- Curiale, J.A., Odermatt, J.R., 1989. Short-term biomarker variability in the Monterey formation, Santa Maria Basin. *Organic Geochemistry* 14, 1–13.
- Curiale, J.A., 1991. The petroleum geochemistry of Canadian Beaufort Tertiary "non-marine" oils. *Chemical Geology* 93, 21–45.
- Dahl, B., Yüklér A., 1991. The role of petroleum geochemistry in basin modeling of the Oseberg Area, North Sea. In: R.K. Merrill (Ed.), *AAPG Source and Migration Processes and Evaluation Techniques*, pp. 65–85.
- Ensminger, A., van Dorsselaer, A., Spyckerelie, Ch., Albrecht, P., Ourisson, G., 1974. Pentacyclic triterpenes of the hopane type as ubiquitous geochemical markers: origin and significance. In: Tissot, B., Biennier, F. (Eds.), *Advances in organic geochemistry* 1973. Editions Technip, Paris, pp. 245–260.
- Fazeelat, T., Alexander, R., Kagi, R.I., 1995. Molecular structures of sedimentary 8,14-secohopanes inferred from their gas chromatographic retention behaviour. *Organic Geochemistry* 23, 641–646.
- Grantham, P.J., Posthuma, J., De Groot, K., 1980. Variation and significance of the C₂₇ and C₂₈ triterpane content of a North Sea core and various North Sea crude oils. In: Douglas, A.G., Maxwell, J.R. (Eds.), *Advances in organic geochemistry*, 1979. Pergamon Press, Oxford, pp. 29–38.
- ten Haven, H.L., Peakman, T.M., Rullkötter, J., 1992. Early diagenetic transformation of higher-plant triterpenoids in deep-sea sediments from Baffin Bay. *Geochimica et Cosmochimica Acta* 56, 2001–2024.
- Hussler, G., Connan, J., Albrecht, P., 1984. Novel families of tetra- and hexacyclic aromatic hopanoids predominant in carbonate rocks and crude oils. *Organic Geochemistry* 6, 39–49.
- Killops, S.D., 1991. Novel aromatic hydrocarbons of probable bacterial origin in a Jurassic lacustrine sequence. *Organic geochemistry* 17, 25–36.
- Köster, J., van Kaam-Peters, H.M.E., Koopmans, M.P., de Leeuw, J.W., Sinninghe Damsté, J.S., 1997. Sulphurisation of homohopaneoids: effects on carbon number distribution, speciation, and 22S/22R epimer ratios. *Geochimica et Cosmochimica Acta* 61, 2431–2452.
- Köster, J., Rospondek, M., Schouten, S., Kotarba, M., Zubrzycki, A., Sinninghe Damsté, J.S., 1998. Biomarker geochemistry of a foreland basin: the Oligocene Menilite formation in the Flysch Carpathians of Southeast Poland. *Organic Geochemistry* 29, 649–669.

- Larcher, A.V., Alexander, R., Kagi, R.I., 1987. Changes in configuration of extended moretanes with increasing sediment maturity. *Organic Geochemistry* 11, 59–63.
- Moldowan, J.M., Seifert, W.K., Arnold, E., Clardy, J., 1984. Structure proof and significance of stereoisomeric 28,30-bisnorhopanes in petroleum and petroleum source rocks. *Geochimica et Cosmochimica Acta* 48, 1651–1661.
- Moldowan, J.M., Lee, C.Y., Sundaraman, P., Salvatori, T., Alajbeg, A., Gjukic, B., Demaison, G.J., Slougui, N.-E., Watt, D.S., 1992. Source correlation and maturity assessment of select oils and rocks from the Central Adriatic Basin (Italy and Yugoslavia). In: Moldowan, J.M., Albrecht, P., Philp, R.P. (Eds.), *Biological Markers in Sediments and Petroleum*. Prentice Hall, Englewood Cliffs, New Jersey, pp. 370–401.
- Moldowan, J.M., McCaffrey, M.A., 1995. A novel microbial hydrocarbon degradation pathway revealed by hopane demethylation in a petroleum reservoir. *Geochimica et Cosmochimica Acta* 59, 1891–1894.
- Murray, I.P., Love, G.D., Snape, C.E., Bailey, N.J.L., 1998. Comparison of covalently-bound aliphatic biomarkers released via hydropyrolysis with their solvent-extractable counterparts for a suite of Kimmeridge clays. *Organic Geochemistry* 29, 1487–1505.
- Noble, R., Alexander, R., Kagi, R.I., 1985. The occurrence of bisnorhopane, trisnorhopane and 25-norhopanes as free hydrocarbons in some Australian shales. *Organic Geochemistry* 8, 171–176.
- Nytoft, H. P., Bojesen-Koeft, J. A., Christiansen, F. G., Fowler, M. G., 1997. HPLC-separation of coeluting lupane and oleanane — confirmation of the presence of lupane in oils derived from terrigenous source rocks of Cretaceous–Tertiary age. In: Abstracts Part I from the 18th International Meeting on Organic Geochemistry, Maastricht, The Netherlands. 22–26 September 1997, Forschungszentrum Jülich, pp. 313–314.
- Ourisson, G., Albrecht, P., Rohmer, M., 1979. The hopanoids: palaeochemistry and biochemistry of a group of natural products. *Pure & Applied Chemistry* 51, 709–729.
- Petersen, H.I., Bojesen-Koeft, J.A., Nytoft, H.P., 1996. Depositional environment and burial history of a Lower Cretaceous carbonaceous claystone, Bornholm, Denmark. *Bulletin of the Geological Society of Denmark* 43, 133–142.
- Peters, K.E., Moldowan, J.M., McCaffrey, M.A., Fago, J.F., 1996. Selective biodegradation of extended hopanes to 25-norhopanes in petroleum reservoirs. Insights from molecular mechanics. *Organic Geochemistry* 24, 765–783.
- Radke, M., Willsch, H., Welte, D.H., 1980. Preparative hydrocarbon group determination by automated Medium Pressure Liquid Chromatography. *Analytical Chemistry* 52, 406–411.
- Rohmer, M., Bissert, P., Neunlist, S., 1992. The hopanoids, procaryotic triterpenoids and precursors of ubiquitous molecular fossils. In: Moldowan, J.M., Albrecht, P., Philp, R.P. (Eds.), *Biological Markers in Sediments and Petroleum*. Prentice Hall, Englewood Cliffs, New Jersey, pp. 1–17.
- Rullkötter, J., Wendisch, D., 1982. Microbial alteration of 17 α (H)-hopanes in Madagascar asphalts: removal of C-10 methyl group and ring opening. *Geochimica et Cosmochimica Acta* 46, 1545–1553.
- Rullkötter, J., Leythaeuser, D., Wendisch, D., 1982a. Novel 23,28-bisnorlupanes in Tertiary sediments. Widespread occurrence of nuclear demethylated triterpanes. *Geochimica et Cosmochimica Acta* 47, 2501–2510.
- Rullkötter, J., Von der Dick, H., Welte, D.H., 1982b. Organic petrography and extractable hydrocarbons of sediment from the Gulf of California, Deep Sea Drilling Project Leg 64. In: Curray, J.R., Moore, D.G. et al. (Eds.), *Initial reports of the deep sea drilling project. 64*, U.S. Govt. Printing Office, Washington, pp. 837–853.
- Schmitter, J.M., Sucrow, W., Arpino, P.J., 1982. Occurrence of novel tetracyclic geochemical markers: 8,14-seco-hopanes in a Nigerian crude oil. *Geochimica et Cosmochimica Acta* 46, 2345–2350.
- Schouten, S., Schoell, M., Rijpstra, W.I.C., Sinninghe Damsté, J.S., de Leeuw, J.W., 1997. A molecular stable carbon isotope study of organic matter in immature Miocene Monterey sediments, Pismo basin. *Geochimica et Cosmochimica Acta* 61, 2065–2082.
- Schoell, M., McCaffrey, M.A., Fago, F.J., Moldowan, J.M., 1992. Carbon isotopic compositions of 28,30-bisnorhopanes and other biological markers in a Monterey crude oil. *Geochimica et Cosmochimica Acta* 56, 1391–1399.
- Seifert, W.K., Moldowan, J.M., Smith, G.W., Whitehead, E.V., 1978. First proof of structure of a C28-pentacyclic triterpane in petroleum. *Nature* 271, 436–437.
- Seifert, W.K., Moldowan, J.M., Demaison, G.J., 1983. Source correlation of biodegraded oils. In: Schenck, P.A., de Leeuw, J.W., Ljmbach, G.W.M. (Eds.), *Advances in Organic Geochemistry*. Pergamon Press, Oxford, pp. 633–643.
- Sinninghe Damsté, J. S., 1997. C₂₇–C₃₀ neohop-13(18)-enes and their aromatic derivatives in sediments: indicators for water column stratification?. In: Abstracts of the 18th International Meeting on Organic Geochemistry, Maastricht, The Netherlands. 22–26 September 1997, Forschungszentrum Jülich, pp. 659–660.
- Subroto, E.A., Alexander, R., Kagi, R.I., 1991. 30-Norhopanes: their occurrence in sediments and crude oils. *Chemical Geology* 93, 179–192.
- Tannenbaum, E., Ruth, E., Huizinga, B.J., Kaplan, I.R., 1986. Biological marker distribution in coexisting kerogen, bitumen and asphaltene in Monterey formation diatomite, California. *Organic Geochemistry* 10, 531–536.
- Van Dorsselaer, A., Ensminger, A., Spyckerelle, C., Dastillung, M., Sieskind, O., Arpino, P., Albrecht, P., Ourisson, G., Brooks, P.W., Gaskell, S.J., Kimble, B.J., Philp, R.P., Maxwell, J.R., Eglinton, G., 1974. Degraded and extended hopane derivatives (C₂₇ to C₃₅) as ubiquitous geochemical markers. *Tetrahedron Letters* 14, 1349–1352.
- Volkman, J.K., Alexander, R., Kagi, R.I., Woodhouse, G.W., 1983a. Demethylated hopanes in crude oils and their applications in petroleum geochemistry. *Geochimica et Cosmochimica Acta* 47, 785–794.
- Volkman, J.K., Alexander, R., Kagi, R.I., Rullkötter, J., 1983. GC–MS characterisation of C₂₇ and C₂₈ triterpanes in sediments and petroleum. *Geochimica et Cosmochimica Acta* 47, 1033–1040.
- Yamamoto, M., Ogihara, S., Yamamoto, S., Naraoka, H., Ishiwatari, R., 1997. Identification and occurrences of 28-norhopanoic acids in Neogene upwelling sediments. In: Abstracts of the 18th International Meeting on Organic Geochemistry, Maastricht, The Netherlands. 22–26 September 1997, Forschungszentrum Jülich, pp. 471–472.

HYDROCARBON POTENTIAL OF THE NORTH-EASTERN SONG HONG BASIN: IMPLICATIONS FROM IMMATURE TERRESTRIAL SOURCE ROCKS

H.I. Petersen
C. Andersen
L.H. Nielsen

Geological Survey of Denmark and Greenland

ABSTRACT

The majority of the liquid petroleum in Southeast Asia is generated from lake-related facies in Palaeogene syn-rift successions. The North-eastern part of the Song Hong basin, NE of the Vinh Ninh and Song Lo fault zones, contains a number of Cenozoic halfgrabens with Palaeogene syn-rift sediments. Inversion movements have exposed oil-prone, immature Oligocene alluvial-fluvial silt- and sandstones, lacustrine mudstones and 10 – 15 cm thick coals at Dong Ho on the Vietnamese mainland in the Quang Ninh province and on Bach Long Vi island in the Gulf of Bac Bo (Gulf of Tonkin).

Hydrogen Index (HI) values from 200 – 690; the mudstones contain up to ~17 wt.% TOC. Outcrop and submarine mud-/siltstone samples from Bach Long Vi island contain up to ~7 wt.% TOC and yield HI values up to 702. The coals correspond to kerogen type III and the organic matter in the mudstones and siltstones to kerogen types I and II. The activation energy (E_a) distributions of the mudstones are characterised by a prominent principal E_a -value, and the E_a -distributions and the evolution in T_{max} HI and extract yield during artificial maturation (hydrous pyrolysis) indicate significant petroleum formation over a relatively narrow temperature range. In contrast, the coals may have a more gradual generation. Artificial maturation results in a change in extract composition towards higher proportions of saturated hydrocarbons, which together with an ability to generate long-chain n-alkanes upon expulsion would result in a waxy paraffinic crude oil.

Continuous, high amplitude seismic reflections in the Paleogene syn-rift successions of the northern Song Hong basin may indicate the presence of lacustrine facies, which may be analogous to the source rocks exposed at Dong Ho and on Bach Long Vi island. This may imply the existence of a highly prolific terrestrial-sourced petroleum system in the north-eastern Song Hong basin.

INTRODUCTION

Since 1995 Vietnam Petroleum Institute, a subsidiary of Petrovietnam, and the Geological Survey of Denmark and Greenland (GEUS) have conducted several joint studies on the development and hydrocarbon potential of the Cenozoic Song Hong basin located on the Northern Vietnamese continental shelf (Nielsen and Dien, 1997; Andersen and Dien, 1998; Petersen et al., 1998). The studies have included seismic interpretation with seismic facies and structural analyses, source rock investigations based on organic petrographic and geochemical analyses and determination of activation energy distributions and hydrocarbon yields, in addition to biostratigraphic, lithostratigraphic and sequence stratigraphic analyses. The main results of the studies have been published recently or are in press (Dien et al., 1997, 1998a, b, 1999; Nielsen et al., 1997, 1999; Andersen et al., 1998, 1999; Petersen et al., in press). This paper focuses on the source rock aspects by reviewing the results of comprehensive organic petrographic and geochemical analyses of immature outcrop samples from Dong Ho and Bach Long Vi island.

GEOLOGICAL BACKGROUND

The north-eastern part of the Song Hong Basin, north-east of the Vinh Ninh and Song Lo fault zones

(Figure 1), contains a number of Cenozoic halfgrabens with Paleogene syn-rift sediments unconformably overlain by younger post-rift sediments. Paleogene syn-rift successions of many Southeast Asian Cenozoic basins include lacustrine carbonaceous mudstones and paralic coals, which constitute good to excellent source rocks, and the majority of the liquid petroleum in Southeast Asia is generated from these lake-related facies (Noble et al., 1991; Wang and Sun, 1994; Williams et al., 1995; Sladen, 1997; Todd et al., 1997; Lee and Watkins, 1998; Wan Hsiaiah, 1999). The Beibu Wan and Pearl River Mouth basins on the Chinese shelf and the Cuu Long basin located on the Vietnamese shelf are examples of prospective basins along the northern and western margin of the East Vietnam Sea (South China Sea) (Figure 1), where the dominant source rock is Paleogene lacustrine mudstones (e.g. Wang and Sun, 1994; Todd et al., 1997; Zhu et al., 1999). In the Nam Con basin further to the Southeast, paralic carbonaceous mudstones and coastal plain coals are suggested as the primary source rocks (Todd et al., 1997).

The Cenozoic basin-fill succession of the greater Song Hong basin is considered to be dominated by kerogen type III organic matter, and generally the Song Hong basin is mainly regarded as a gas-prone basin (Hao et al., 1995, 1998; Ha, 1998; Chen et al., 1998; Nielsen et al., 1999). However, inversion movements in the north-eastern Song Hong Basin have exposed oil-prone, immature Paleogene (probably of Oligocene age) alluvial-fluvial silt- and sandstones, lacustrine mudstones and 10–15 cm thick coals at Dong Ho on the Vietnamese mainland in the Quang Ninh province, and onshore and below sea-level on Bach Long Vi island in the Gulf of Bac Bo (Gulf of Tonkin) (Dien et al., 1999) (Figure 1). Importantly, a more regional occurrence of the lacustrine mudstones in the Northeastern part of the Song Hong basin is suggested by mapping of undrilled, Paleogene halfgrabens (Rangin et al., 1995; Andersen et al., 1998, 1999), where several seismic sections show syn-rift successions with distinct, continuous high-amplitude reflectors, a seismic facies pattern often interpreted as lacustrine shale-prone units (Figure 2). This suggests a more widespread offshore existence of the prolific Paleogene source rocks north-east of the Vinh Ninh and Song Lo fault zones.

Hydrocarbons have also been encountered in the Hanoi Trough, which forms the onshore extension of the Song Hong basin. On the basis of maturity modelling, these hydrocarbons may have been generated from Middle Miocene coals (Nielsen et al., 1999), however geochemical data suggest a contribution from lacustrine mudstones (unpublished data, GEUS).

POTENTIAL SOURCE ROCKS: THE DONG HO AND BACH LONG VI ISLAND OUTCROPS

The deposits at Dong Ho consists of faintly laminated to structureless, grey to black and dark brown, carbonaceous mudstones interbedded with clayey sandstones and coal seams up to 15 cm thick. The carbonaceous mudstones were deposited in oxygen-deficient fresh water to marine-influenced lakes, whereas the coals represent fresh water peat deposits (Traynor and Sladen, 1997; Petersen et al., in press). The Oligocene deposits on Bach Long Vi island are exposed due to basin inversion during the Pliocene and (?) Quaternary in the north-eastern Song Hong basin. The onshore and submarine outcrops on Bach Long Vi island consist of mudstones, siltstones and coals (Dien et al., 1999), but in contrast to the Dong Ho outcrop, the deposits on Bach Long Vi island are much less well-known. However, organic petrographic and geochemical analyses carried out on siltstone samples suggest a lacustrine, oxygen-poor depositional environment for these deposits (unpublished data, GEUS).

The carbonaceous mudstones from Dong Ho contain up to ~17 wt.% TOC (Petersen et al., in press), whereas onshore and submarine samples from Bach Long Vi Island contain up to ~7 wt.% TOC (Dien et al., 1999). The primary organic components in the carbonaceous mudstones from Dong Ho are fluorescing amorphous organic matter (AOM), which is intimately associated with the mineral matter and liptodetrinite (Petersen et al., in press). The fluorescing AOM is considered mainly to be derived from degraded algae.

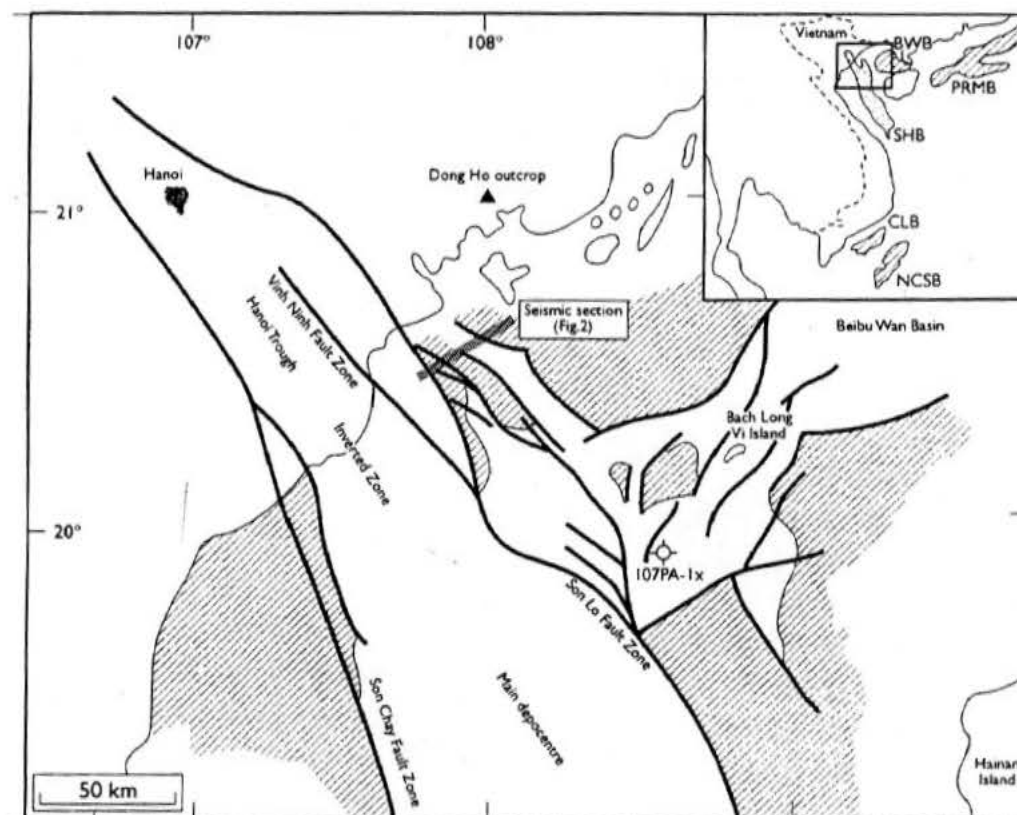


Figure 1. Map of the northern Gulf of Bac Bo showing the structural outline of the northern part of the Song Hong Basin, the Dong Ho and Bach Long Vi island outcrops, well 107 PA-1x, and the seismic line shown in figure 2. BWB: Beibu Wan Basin; CLB: Cuu Long Basin; NCSB: Nam Con Son Basin; PRMB: Pearl River Mouth Basin; SHB: Song Hong Basin. Hatched areas: post-rift sediments resting directly on pre-Cenozoic basement in the offshore area (After Petersen et al., in press).

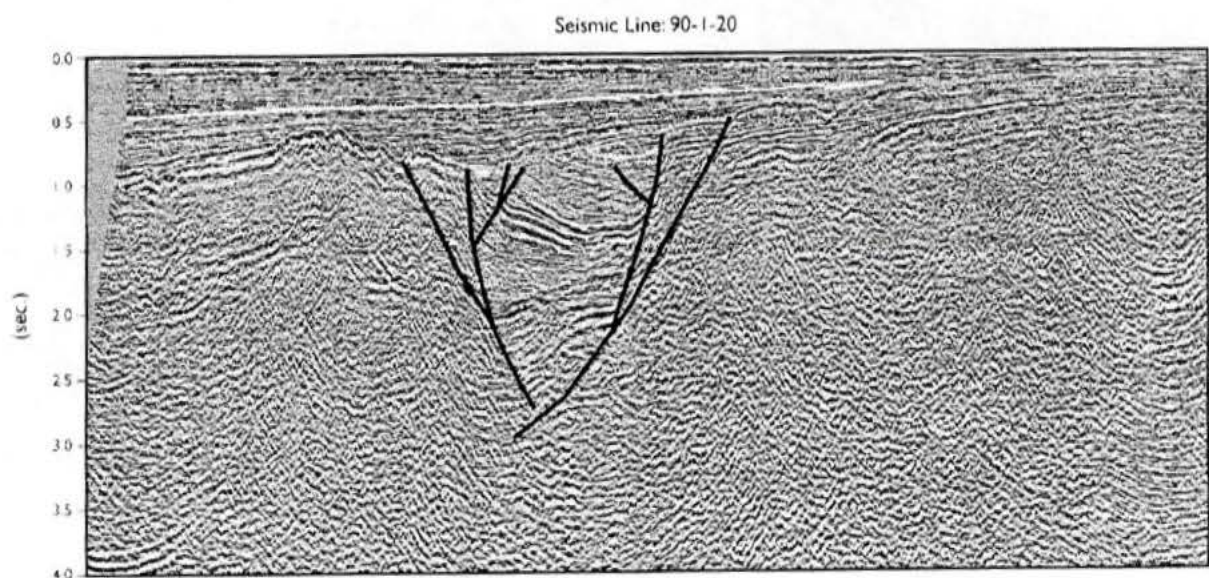


Figure 2. Seismic line 90-1-020 crossing the narrow Palaeogene Kiem An graben structure (see also Figure 1). The interval of continuous, high amplitude reflections between 1.1–1.5 sec. in the syn-rift prism probably represent Oligocene lacustrine shales (After Andersen et al., 1998).

Another important component is alginite with a morphology similar to extant fresh water to brackish *Botryococcus* algae. The organic matter in the mudstones from Dong Ho corresponds thus mainly to kerogen types I and II. The organic matter from Bach Long Vi island is primarily composed of fluorescing AOM, followed by liptodetrinite, alginite (mainly *Botryococcus*-type) and huminite (unpublished data, GEUS). Thus, this organic matter also corresponds mainly to kerogen types I and II.

Hydrogen Index (HI) values of the Dong Ho mudstones range up to 690 and S_2 yields are up to 117 mg HC/g rock (Petersen et al., in press), whereas HI values from the siltstones from Bach Long Vi island may be as high as 702 (Dien et al., 1999) (Figure 3). Hence, the carbonaceous mudstones and siltstones from Dong Ho and Bach Long Vi island are highly oil-prone.

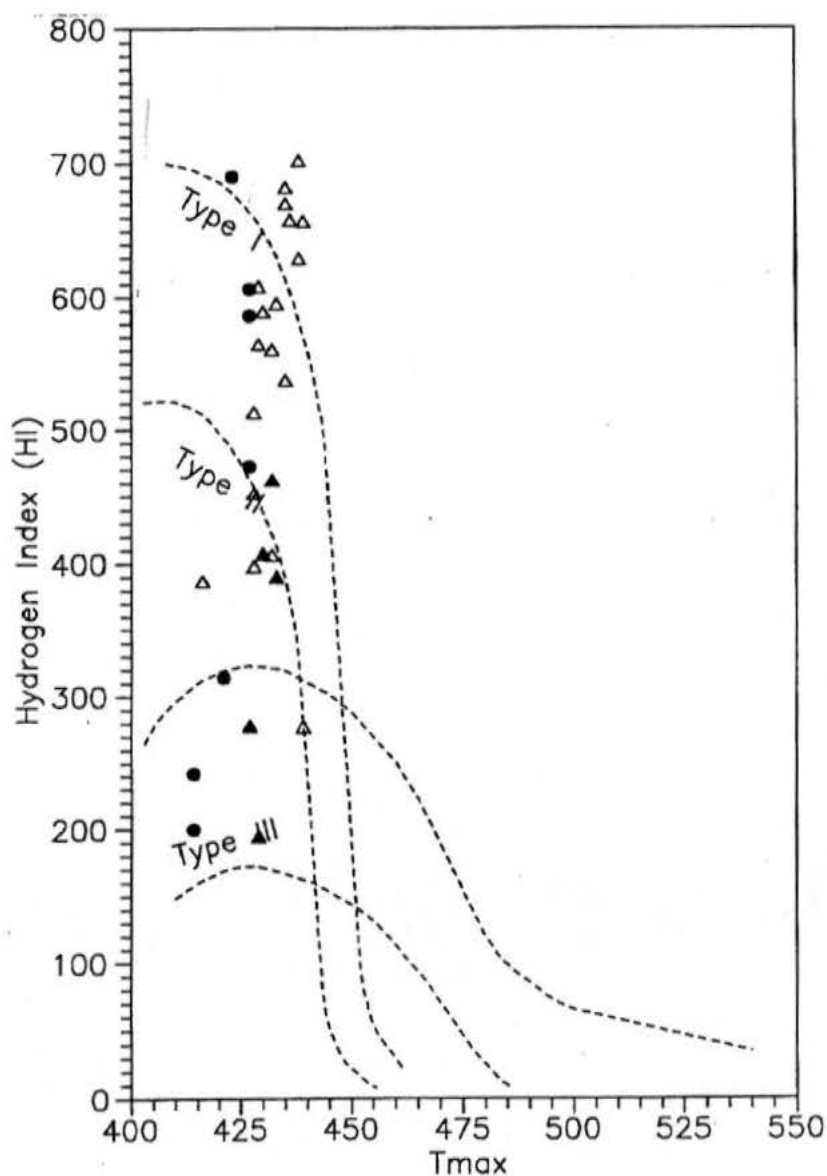


Figure 3. Hydrogen Index vs T_{max} diagram showing the excellent source potential of the coals and lacustrine mud- and siltstones from Dong Ho and Bach Long Vi island. Dots: Dong Ho (data partly from Petersen et al., in press); Black triangle: Bach Long Vi island (GEUS data); Open triangle: Bach Long Vi island (data from Dien et al., 1999).

Determination of activation energies (E_a) have been carried out on the carbonaceous mudstones from Dong Ho. Slightly asymmetric E_a -distributions were found, and the range of E_a -values is consistent with the heterogeneous composition of the organic matter and accordingly a wide range of chemical bonds (Petersen et al., in press). The significant magnitude of the E_a -peaks, however, reflects the dominance of kerogen types I and II, with more uniform chemical bonds in the mudstones. Determination of the E_a -distributions of samples from Bach Long Vi island is in progress, but considering the dominance of kerogen types I and II in the siltstones from Bach Long Vi island, E_a -distributions similar to those of the Dong Ho samples may be expected. This E_a -distribution has a profound influence on the generation characteristics of the mud- and siltstones.

During artificial maturation (stepwise hydrous pyrolysis at 240°C/72h, 270°C/72h, 300°C/72h and 330°C/72h) the carbonaceous mudstones and siltstones from Dong Ho and Bach Long Vi island follow the maturation path for kerogen type II on the HI vs. T_{max} diagram. The mudstones and siltstones show a small to insignificant change in T_{max} and a significant decrease in HI, in particular from a hydrous pyrolysis temperature of 300°C/72h to 330°C/72h. This small change in T_{max} and the marked decrease in HI indicate extensive petroleum formation, which is related to the large E_a -peaks, as a narrow E_a -distribution typically results in a lack of change in T_{max} due to generation of petroleum (Tissot et al., 1987). Calculations suggest that about 40–50% of the organic carbon in the mudstones from Dong Ho participates in petroleum formation during artificial maturation, and the majority of the generation potential is realised over the interval 270°C/72h to 330°C/72h (Petersen et al., in press). Gas-to-Oil Ratios (GOR) as low as 0.3 indicate primary generation of fluid petroleum. The mud- and siltstones will generate a crude oil with a typical terrestrial geochemical signature.

The mudstones from Dong Ho in particular, but also the siltstones from Bach Long Vi island, show a marked increase in extract yields above 300°C/72h together with a change towards higher proportions of saturated hydrocarbons. Gas chromatograms of the saturated fraction of the extracts from the Dong Ho mudstones hydrous-pyrolysed at 330°C/72h have a broad, slightly bimodal *n*-alkane distribution with long-chain *n*-alkanes extending to at least nC_{35} , whereas gas chromatograms from siltstones from Bach Long Vi island hydrous-pyrolysed at 330°C/72h have broad, light-end skewed *n*-alkane distributions with high proportions of long-chain *n*-alkanes in the waxy end ($> nC_{22}$). The Pr/Ph ratios range from 1.3 to around 3.

The humic coals from Dong Ho contain up to ~67 wt.% TOC, and are mainly composed of huminite (kerogen type III) derived from woody tissues of higher land plants. The coals further contain much less proportions of liptodetrinite, cutinite and sporinite also derived from higher land plants. The coals from Dong Ho yield HI values up to 314 and S_2 yields up to 179 mg HC/g rock (Petersen et al., in press), and a coal sample from Bach Long Vi island yield a HI value of 387 and a S_2 yield of 190 mg HC/g rock (Dien et al., 1999). These values indicate a potential for generation of both gas and crude oil. The HI of humic coals with low contents of liptinite is primarily controlled by specific huminite macerals, and secondly by the content of liptinite (Petersen and Rosenberg, 2000).

E_a -distributions of the coals are broad and slightly asymmetric, and the general complex composition of the coals and the thermally robust aromatic nature of the huminite are responsible for the broad E_a -distributions (Tegelaar and Noble, 1994; Pepper and Corvi, 1995). During artificial maturation the coals follow the maturation path for kerogen type III, and in contrast to the mud- and siltstones they show a more gradual increase in T_{max} and decrease in HI (Petersen et al., in press).

Calculations show that only about 17% of the organic carbon in the Dong Ho coals participates in petroleum formation during artificial maturation, but a largely constant GOR close to 0.6 up to a pyrolysis

temperature of 330°C/72h suggest that the coals are able to generate fluid petroleum over a wide range of temperatures. In addition, pyrograms obtained from pyrolysis-gas chromatography of solvent extracted samples show the ability of the coals to generate abundance of long-chain *n*-alkanes (nC_{15+}) (Petersen et al., in press), which may facilitate hydrocarbon expulsion from the coal matrix (Isaksen et al., 1998). Like the lacustrine source rocks the extract composition changes towards a higher proportion of saturated hydrocarbons with increasing hydrous pyrolysis temperature. The gas chromatograms of hydrous-pyrolysed coal samples (330°C/72h) have broad, unimodal and heavy-end skewed *n*-alkane distributions with a predominance of odd-numbered *n*-alkanes in the nC_{22+} range and Pr/Ph ratios above 5, which is typically for petroleum derived from a terrestrial source. Thus, the coals would generate a waxy paraffinic crude oil.

SUMMARY OF POTENTIAL SOURCE ROCKS

The Dong Ho and Bach Long Vi island outcrops contain two types of source rocks: humic coals/kerogen type III and kerogen types I and II. The data strongly indicate that mature equivalents to the Oligocene source rocks exposed at Dong Ho and Bach Long Vi island are capable of generating large quantities of fluid hydrocarbons with a typical terrestrial geochemical signature. However, the two source rock types will have different generation characteristics. The mud- and siltstones will generate large quantities of crude oil over a relatively restricted temperature range, i.e. depth interval, whereas the coals will generate crude oil, although minor quantities, over a wider temperature range (depth interval), but they will probably continue to generate after the mudstones have been completely depleted in petroleum potential.

IMPLICATIONS FOR OFFSHORE EXPLORATION IN THE SONG HONG BASIN

Widespread formation of Paleogene extensional grabens and halfgrabens in the Gulf of Bac Bo was followed by Late Oligocene – Early Miocene post-rift subsidence. The tectonic regime changed during Middle – Late Miocene time; basement inversion led to formation of conspicuous compression structures over the former depocentres between the major basin bounding faults, the Song Chay Fault Zone to the southwest and the Vinh Ninh and Song Lo Fault Zones to the northeast (Figure 1). The basin inversion culminated in Late Miocene time with formation of a significant unconformity that deeply truncates the inversion structures. However renewed basin subsidence is witnessed by a southward thickening, mostly undisturbed cover of post-uppermost Miocene sediments.

A number of narrow Paleogene grabens and halfgrabens have been mapped north-east of the Song Lo Fault Zone in the northernmost part of the Gulf of Tonkin, and the syn-rift deposits may occasionally exceed a thickness of 5 km. The syn-rift sediments have only been partly penetrated in one well, namely 107 PA-1x (Figure 1), where massive conglomerates and sandstones are overlain by alternating sandstones, siltstones and mudstones with TOC contents mostly below 0.5 wt.%. The seismic reflection pattern in the syn-rift succession at the well location differs considerably from the correlating interval characterised by continuous, high amplitude reflections between 1.1–1.5 sec. in the graben structure displayed in Figure 2. This shale-prone seismic facies is widespread in the NW–SE oriented grabens (Andersen et al., 1998, 1999). Thus, the oil-prone Paleogene syn-rift successions have not been drilled in the northeastern Song Hong basin and no direct ties can be made from the offshore Paleogene successions to the isolated Dong Ho outcrop. However, the Bach Long Vi island outcrop is part of an inverted Paleogene syn-rift succession, which can be seismically correlated to the syn-rift prism shown in Figure 2. This and the mapped shale-prone seismic facies suggest that successions of oil-prone, lacustrine, carbonaceous shales with minor coal seams similar to the outcrops may be preserved in the Paleogene syn-rift prisms in the halfgrabens.

Maturity modelling suggests that large parts of the undrilled, shale-prone Paleogene interval characterised by continuous, high amplitude reflectors presently are in the oil and condensate window (Andersen et al., 1998, 1999; Nielsen et al., 1999). Therefore, prolific Paleogene source kitchens may exist in the syn-rift prisms in the northern part of the Gulf of Tonkin Northeast of the Song Lo Fault Zone.

ACKNOWLEDGEMENT

Several research projects on the development and hydrocarbon potential of the Song Hong basin have been carried out in the past 5 years by the Geological Survey of Denmark and Greenland (GEUS) together with Vietnam Petroleum Institute (VPI), a subsidiary of the national state-owned Petrovietnam. The Danish contributions have been funded through grants from the Danish Energy Research Programme and Danida (Danish International Development Assistance), while VPI and Petrovietnam have funded the Vietnamese contributions and provided data for the projects. The projects have in part been carried out under the auspices of CCOP (Coordinating Committee for Coastal and Offshore Geoscience Programmes in East and Southeast Asia). Petrovietnam and VPI are thanked for access to samples and permission to publish the results.

REFERENCES

1. Andersen, C., Dien, P.T. (Eds), 1998. *Basin analysis and modelling of the Cenozoic Song Hong Basin, Vietnam*. Final report to phase II, Hanoi. (Confidential).
2. Andersen, C., Tiem, P.V., Mathiesen, A., Nielsen, L.H., 1998. Some new thermal maturity modelling results using Yýkler 1D software and seismic facies mapping in the northern part of the Song Hong Basin. In: Toan, T.N., Quy, N.H., Ngoc, N.V. (Eds), *Proceedings of Conference on Vietnam Petroleum Institute, 20 years development and prospects*. Hanoi, May 1998, p. 273 – 284.
3. Andersen, C., Mathiesen, A., Nielsen, L.H., Tiem, P.V., Dien, P.T., 1999. *Petroleum systems in the northern part of the Song Hong Basin, Gulf of Tonkin – Vietnam*. *Proceedings on CD-ROM from: Tectonics, stratigraphy and petroleum and mineral systems of Palawan, Borneo and surrounding areas. An international conference 29/11 – 3/12/1999, Palawan Island, Philippines*.
4. Chen Honghan, Li Sitian, Sun Yongchuan, Zhang Qiming, 1998. *Two petroleum systems charge the YA13-1 gas field in Yinggehai and Qiongdongnan Basins, South China Sea*. *American Association of Petroleum Geologists Bulletin* 82, p. 757 – 772.
5. Dien, P.T., Nielsen, L.H., Andersen, C., Nhuan, D.V., 1997. *Late Mesozoic to Cenozoic basin development along the north-west margin of the East Vietnam Sea*. *Petrovietnam Review*, 4/1997, p. 5 - 10.
6. Dien, P.T., Nielsen, L.H., Andersen, C., Nhuan, D.V., 1998a. *Late Mesozoic to Cenozoic basin development along the north-west margin of the East Vietnam Sea*. *AAPG Annual Convention, Utah, May 17 – 28; Abstract*, p. 1 – 6.
7. Dien, P. T., Nielsen, L.H., Andersen, A., Tiem, P.V., Nhuan, D.V., 1998b. *Late Mesozoic –Cenozoic events along the north-west margin of the East Vietnam Sea*. In: Toan, T.N, Quy, N.H., Ngoc, N.V (Eds), *Proceedings of Conference on Vietnam Petroleum Institute, 20 year development and prospects*. Hanoi, May 1998, p. 25 – 131.
8. Dien, P.T., Quy, N.H., Tiem, P.V., Tai, P.S., Andersen, C., Nielsen L.H., 1999. *Basin analysis and petroleum system of the Song Hong Basin*. In: Hiep et al. (Eds), *Geology and petroleum in Vietnam*. In occasion of the 36th CCOP and annual session, October 26–29, and 34th CCOP Steering Committee Meeting, November 1–2, 1999, Hanoi, Vietnam, p. 44 – 67.

9. Ha, N.B., 1998. *Studying source rocks in the Song Hong sedimentary Basin*. In: Toan, T.N., Quy, N.H., Ngoc, N.V. (Eds), Conference on Vietnam Petroleum Institute, 20 years development and prospects. Hanoi, May 1998, p. 186 – 204.
10. Hao Fang, Sun Yongchuan, Li Sitian, Zhang Qiming, 1995. Overpressure retardation of organic-matter maturation and petroleum generation: A case study from the Yinggehai and Qiongdongnan Basins, South China Sea. *American Association of Petroleum Geologists Bulletin* 79, p. 551 – 562.
11. Hao Fang, Li Sitian, Sun Yongchuan, Zhang Qiming, 1998. Geology, compositional heterogeneities, and geochemical origin of the Yacheng gas field, Qiongdongnan Basin, South China Sea. *American Association of Petroleum Geologists Bulletin* 82, p. 1372 – 1384.
12. Isaksen, G.H., Curry, D.J., Yeakel, J.D., Jenssen, A.I., 1998. *Controls on the oil and gas potential of humic coals*. *Organic Geochemistry* 29, p. 23 – 44.
13. Lee, G.H., Watkins, J.S., 1998. Seismic sequence stratigraphy and hydrocarbon potential of the Phu Khanh Basin, offshore central Vietnam, South China Sea. *American Association of Petroleum Geologists Bulletin* 82, p. 1711 – 1735.
14. Nielsen, L.H., Dien, P.T. (Eds), 1997. *Basin analysis and modelling of the Cenozoic Song Hong Basin, Vietnam*. Final report to phase I, Vol. 1 & 2: 12 technical reports including enclosures. (Confidential).
15. Nielsen, L.H., Bidstrup, T., Mathiesen, A., Dien, P.T., Tiem, P.V., 1997. *The Cenozoic Song Hong Basin, Vietnam; a highly prospective basin*. Abstract in: Tectonics, stratigraphy and petroleum systems of Borneo. Brunei June 22–25, 1997, p. 48.
16. Nielsen, L.H., Mathiesen, A., Bidstrup, T., Vejbaek O.V., Dien, P.T., Tiem, P.V., 1999. *Modelling of hydrocarbon generation in the Cenozoic Song Hong Basin, Vietnam: A highly prospective basin*. *Journal of Asian Earth Sciences* 17, p. 269 – 294.
17. Noble, R.A., Wu, C.H., Atkinson, C.D., 1991. *Petroleum generation and migration from Talang Akar coals and shales off-shore N.W. Java, Indonesia*. *Organic Geochemistry* 17, p. 363 – 374.
18. Pepper, A.S., Corvi, P.J., 1995. Simple kinetic models of petroleum formation. Part 1: oil and gas generation from kerogen. *Marine and Petroleum Geology* 12, p. 291 – 319.
19. Petersen, H.I., Rosenberg, P., 2000. The relationship between the composition and rank of humic coals and their activation energy distributions for the generation of bulk petroleum. *Petroleum Geoscience* 6, p. 139 – 147.
20. Petersen, H.I., Bojesen-Koefoed, J.A., Nielsen, L.H., Nytoft, H.P., 1998. *Organic petrography and geochemistry of three samples from Dong Ho, Vietnam*. EFP-97 project: Description of the petroleum system(s) of the Song Hong Basin, Vietnam. Danmarks og Grønlands Geologiske Undersøgelse Rapport 1998/49, 38 pp. and Appendix 1 – 4.
21. Petersen, H.I., Andersen, C., Anh, P.H., Bojesen-Koefoed, J.A., Nielsen, L.H., Nytoft, H.P., Rosenberg, P., Thanh, L., in press. *Petroleum potential of Oligocene lacustrine mudstones and coals at Dong Ho, Vietnam: An outcrop analogue to terrestrial source rocks in the greater Song Hong Basin*. *Journal of Asian Earth Sciences*.
22. Rangin, C., Klein, M., Roques, D., Le Pichon, X., Truong, L.V., 1995. *The Red River fault system in the Tongkin Gulf, Vietnam*. *Tectonophysics* 243, p. 209 – 222.
23. Sladen, C., 1997. Exploring the lake basins of east and Southeast Asia. In: Fraser, A.J., Matthews, S.J.,

- Murphy, R.W., (Eds.), *Petroleum Geology of Southeast Asia*. Geological Society London Special Publication 126, p. 49 – 76.
24. Tegelaar, E.W., Noble, R.A., 1994. Kinetics of hydrocarbon generation as a function of the molecular structure of kerogen as revealed by pyrolysis-gas chromatography. *Organic Geochemistry* 22, p. 543 – 574.
 25. Tissot, B.P., Pelet, R., Ungerer, P.H., 1987. *Thermal history of sedimentary basins, maturation indices, and kinetics of oil and gas generation*. American Association of Petroleum Geologists Bulletin 71, p. 1445 – 1466.
 26. Todd, S.P., Dunn, M.E., Barwise, A.J.G., 1997. *Characterizing petroleum charge systems in the Tertiary of SE Asia*. In: Fraser, A.J., Matthews, S.J., Murphy, R.W., (Eds.), *Petroleum Geology of Southeast Asia*. Geological Society London Special Publication 126, p. 25 – 47.
 27. Traynor, J.J., Sladen, C., 1997. Seepage in Vietnam: Onshore and offshore examples. *Marine and Petroleum Geology* 14, p. 345 – 362.
 28. Wan Hasiah, A., 1999. Oil-generating potential of Tertiary coals and other organic-rich sediments of the Nyalau Formation, onshore Sarawak. *Journal of Asian Earth Sciences* 17, p. 255 – 267.
 29. Wang, C., Sun, Y., 1994. Development of Paleogene depressions and deposition of lacustrine source rocks in the Pearl River Mouth Basin, northern margin of the South China Sea. *American Association of Petroleum Geologists Bulletin* 78, p. 1711 – 1728.
 30. Williams, H.H., Fowler, M., Eubank, R.T., 1995. *Characteristics of selected Palaeogene and Cretaceous lacustrine source basins of Southeast Asia*. In: Lambiase, J.J., (Ed.), *Hydrocarbon habitat in rift basins*. Geological Society London Special Publication 80, p. 241 – 282.
 31. Zhu, W., Li, M., Wu, P., 1999. *Petroleum systems of the Zhu III Subbasin, Pearl River Mouth Basin, South China Sea*. *American Association of Petroleum Geologists Bulletin* 83, p. 990 – 1003.

The relationship between the composition and rank of humic coals and their activation energy distributions for the generation of bulk petroleum

H. I. Petersen and P. Rosenberg

Geological Survey of Denmark and Greenland (GEUS), Thoravej 8, DK-2400 Copenhagen NV, Denmark

ABSTRACT: Activation energy (E_a) distributions and pre-exponential factors (A) of 27 humic coals of varying composition, rank, age and origin are discussed. The petrography and rank of the coals have been correlated to the distribution of E_a and the Hydrogen Index (HI). The HI is positively correlated to vitrinitic and liptinitic constituents; in particular, the vitrinite maceral collotelinite has a strong influence on the HI. Inertinitic constituents have a negative effect on the HI. A higher value of the peak position of the E_a distributions is mainly controlled by the thermal maturity and to a lesser extent by the proportion of collotelinite. A number of other vitrinitic components result in a lower E_a peak position. The peak width of the E_a distributions is broadened by high vitrinite reflectance values and higher proportions of collotelinite and the microlithotypes vitrite and vitrinertite. Liptinitic and inertinitic constituents, in particular the microlithotype clarodurite, narrow the peak width.

KEYWORDS: *coal composition, coal rank, activation energy, source rock*

INTRODUCTION

Coals have a heterogeneous petrographic composition, corresponding to a complex mixture of kerogen types I, II, III and IV. Typical bulk chemical analyses of coal reflect the relative abundance of the organic constituents and, due to the dominance of organic matter derived from terrestrial woody tissues, coals will commonly plot within the kerogen type III band ($H/C=0.6-0.9$) on the 'van Krevelen diagram' (Tissot & Welte 1984), although they may contain significant proportions of oil-prone hydrogen-rich components. Therefore coals have, in general, been considered poor oil-prone source rocks. However, an increasing number of worldwide oil discoveries and seeps with typical terrestrial organic geochemical signatures have challenged this common opinion (e.g. Cook & Struckmeyer 1986; Clayton *et al.* 1991; Huang *et al.* 1991; Noble *et al.* 1991; Killips *et al.* 1994; Scott & Fleet 1994; Petersen *et al.* 1998; Boreham *et al.* 1999; Bojesen-Koefoed *et al.* 1999). These crude oils generated from coal-bearing strata also demonstrate the capability of coals to expel oil. Several features have been suggested to facilitate oil expulsion from coals, including a two-phase migration theory (Huc *et al.* 1986), the microlithotype composition (Durand & Paratte 1983; Bertrand 1989; Stout 1994), the natural fracture system of coals (Close 1993), a continuous evolution and destruction of the micropore system during organic matter maturation (Durand & Paratte 1983; Katz *et al.* 1991), and the ability of the coals to generate abundant long-chain aliphatic hydrocarbons (Isaksen *et al.* 1998).

Coal types

Coals can be divided into sapropelic and humic coals, the latter being the topic of this study. Sapropelic coals represent subaquatic muddy deposits composed of finely degraded plant remains, reworked peat, spores/pollen and algae (Taylor *et al.*

1998). In contrast, humic coals represent ancient peat deposits that formed by accumulation of organic matter primarily derived from woody land plants. In general, humic coals are mainly composed of constituents belonging to the maceral groups huminite (brown coal) or vitrinite, which is the hard coal equivalent of huminite. Huminite- or vitrinite-rich humic coals are, in particular, typical of Carboniferous and Upper Cretaceous-Tertiary coals (Taylor *et al.* 1998). The individual constituents (macerals) of the huminite/vitrinite maceral group are primarily derived from complex humic substances formed during decomposition of cellulose and lignin in woody plant material. Humic coals can also contain significant amounts of inertinite, which essentially is derived from the same precursors as huminite/vitrinite. However, inertinite has experienced a higher degree of oxidation, for example during wildfire. Inertinite-rich humic coals occur for instance among Permian-Carboniferous 'Gondwana' coals, Middle Jurassic coals in NW Europe and Cretaceous coals of North America (e.g. Falcon & Snyman 1986; Taylor *et al.* 1989; Cadle *et al.* 1993; Lamberson *et al.* 1996; Petersen *et al.* 1998). The last and least abundant organic constituents of humic coals are hydrogen-rich components of the liptinite maceral group.

Activation energies of humic coals

The organic composition of humic coals is thus more complex than the composition of the organic matter in typical marine or lacustrine source rocks. The activation energy (E_a) distribution is dependent on the various bond types present in the organic matter (i.e. its molecular structure) (Tegelaar & Noble 1994; Pepper & Corvi 1995), and the heterogeneity of humic coals results in broad asymmetric E_a distributions for the generation of bulk petroleum. Ungerer (1990) reports mean activation energies between 47 and 60 kcal/mole for coals, and Ungerer & Pelet (1987) display the E_a distribution of a Tertiary Mahakam coal with a 'tail' up to 70 kcal/mole. Likewise, a Scottish coal

Table 1. Reflectance values, maceral group composition (vol.%, mineral matter free), age and origin of the coals

Sample	%R _o	Vitrinite	Inertinite	Liptinite	Age and origin
Brunner	0.36	82	13	5	Middle Eocene/New Zealand
Dong Ho 3	0.41	88	1	11	Oligocene/Vietnam
PSOC 1488	0.44	88	8	4	Paleocene/USA
Id2	0.44	90	4	6	Tertiary/Indonesia
PSOC 1445	0.47	76	17	7	Late Cretaceous/USA
PSOC 1502	0.52	60	33	7	Late Cretaceous/USA
PSOC 1493	0.53	83	10	7	Carboniferous/USA
Co2	0.54	78	17	5	Tertiary/Colombia
Id1	0.55	91	3	6	Tertiary/Indonesia
Co1	0.59	77	17	6	Tertiary/Colombia
Au1	0.62	27	69	4	Permian/Australia
Au2	0.63	37	56	7	Permian/Australia
Vz1	0.66	80	14	6	Tertiary/Venezuela
SA3	0.68	37	56	7	Permian/South Africa
SA2	0.71	20	74	6	Permian/South Africa
US1	0.73	74	16	10	Carboniferous/USA
Au5	0.73	53	35	12	Permian/Australia
SA5	0.74	19	71	10	Permian/South Africa
SA4	0.75	42	50	8	Permian/South Africa
WL 4468	0.76	81	17	2	Middle Jurassic/North Sea
PSOC 1451	0.77	79	15	6	Carboniferous/USA
Au3	0.84	62	32	6	Permian/Australia
Un1	0.84	63	18	19	?/USA
WL 4506	0.87	65	33	2	Middle Jurassic/North Sea
Au4	1.11	40	59	1	Permian/Australia
PSOC 1500	1.25	94	6	0	Late Cretaceous/USA
PSOC 1516	1.43	91	9	0	Carboniferous/USA

shows an asymmetric E_a distribution with main activation energies between 52 and 55 kcal/mole and a 'tail' up to 66 kcal/mole (Jarvie 1991). This suggests that humic coals and kerogen type III generate petroleum over a wider temperature range (depth range) than kerogen types I and II (Tissot *et al.* 1987). Typical pre-exponential factors (A), assuming first-order parallel reactions, are in the range of 10^{14} to 10^{18} s⁻¹ (Ungerer & Pelet 1987).

Aims of this article

It is thus evident that increased knowledge of the petroleum generation capability and characteristics of humic coals or kerogen type III is needed to evaluate the petroleum potential of strata dominated by terrestrial organic matter in exploration areas, and to improve modelling of the generation history of potential humic coal source rocks. No studies covering the compositional variability of humic coals have systematically examined the correlation between the petrographic composition and the activation energies for bulk petroleum formation as determined by open-system pyrolysis. The present dataset comprises 27 samples of humic coals of varying rank, petrographic composition, age and geographical origin, which makes possible a general correlation between the kinetic data and source rock potential of humic coals, and their rank and petrography. In this study the aims are:

- (1) to present E_a distributions and pre-exponential factors (A) of the coals;
- (2) to correlate the petrography and rank of the coals with their oil and gas generative potential represented by the Hydrogen Index (HI);
- (3) to correlate the petrography and rank of the coals with the E_a distributions represented by the E_a peaks, which is relevant for the timing of petroleum generation;

- (4) to correlate the petrography and rank of the coals with the width of the E_a distributions, which is related to the chemical nature of the organic matter (Tegelaar & Noble 1994; Pepper & Corvi 1995).

SAMPLE MATERIAL

A total of 27 humic coal samples have been selected for this study. The samples represent coals from the Carboniferous (4), Permian (9), Middle Jurassic (2), Late Cretaceous (3) and Tertiary (8) (Table 1). The Carboniferous coals are from the USA, the Permian samples, which represent 'Gondwana coals', are from Australia and South Africa, the Middle Jurassic coals are from the Danish North Sea, the Upper Cretaceous coals are from the USA, while the Tertiary coals are from Colombia, Indonesia, New Zealand, USA, Venezuela and Vietnam (Table 1). The Un1 sample is from the USA, but the age is unknown.

METHODS

Organic petrography

Polished blocks (pellets) of the coals were prepared for random reflectance measurements and reflected light microscopy. Huminite and vitrinite reflectance measurements were conducted in monochromatic light and oil immersion. The petrographic composition of the coals was determined by standard point-counting in oil immersion using white light and fluorescence-inducing blue light. In each sample 500 particles (macerals, mineral matter) and 500 microlithotypes were counted. A total of 10 different microlithotypes were counted in the coals, and 14 different macerals from the vitrinite, inertinite and liptinite groups together with pyrite and 'other minerals' were detected in the hard coals (Tables 2, 3). The analysis procedures and maceral and microlithotype identifications

Table 2. *Maceral composition (vol.%) of the coals*

Sample	Other minerals	Pyrite	Macrinite	Inertodetrinite	Semifusinite	Fusinite	Suberinite	Resinite	Liptodetrinite	Cutinite	Sporinite	Corpogelinite	Gelinite	Collodetrinite	Collotelinite	Telinite
Brunner	1	1	1	10	2	0	0	0	3	0	1	1	11	66	3	0
Dong Ho 3	2	0	0	0	1	0	0	0	7	2	1	5	17	55	8	2
PSOC 1488	1	0	2	5	1	1	1	2	1	1	0	7	6	35	29	8
Id2	0	0	1	2	0	0	0	2	2	1	0	3	11	60	17	1
PSOC 1445	1	0	5	10	1	2	4	2	1	1	0	9	5	46	10	3
PSOC 1502	2	0	8	21	2	2	0	1	2	2	2	4	6	37	9	2
PSOC 1493	2	1	4	5	1	1	0	0	5	1	1	2	2	34	36	5
Co2	0	0	2	11	2	2	0	0	3	2	0	3	9	51	14	1
Id1	1	0	0	1	1	0	2	0	3	0	0	5	11	65	9	2
Co1	2	0	4	7	4	2	0	0	3	2	1	12	3	51	7	2
Au1	1	0	13	46	5	5	0	0	2	1	0	1	0	18	4	4
Au2	2	0	14	30	6	4	0	0	3	2	2	1	1	24	10	1
Vz1	1	0	2	9	4	0	1	0	3	1	1	7	4	52	15	0
SA3	3	1	16	36	1	2	0	0	3	1	3	1	3	20	9	1
SA2	1	1	23	46	2	1	0	0	3	2	1	0	0	10	10	0
US1	1	2	4	10	1	0	0	0	5	2	2	0	2	41	30	0
Au5	1	1	6	23	3	2	0	0	5	3	4	0	2	32	18	0
SA5	2	0	18	48	2	1	0	0	4	3	3	0	1	12	6	0
SA4	3	0	10	35	1	2	0	1	3	2	3	0	1	22	17	0
WL 4468	3	1	2	13	0	1	0	0	1	1	0	0	5	42	31	0
PSOC 1451	3	0	6	7	1	1	0	0	2	1	4	3	2	22	46	2
Au3	1	0	8	19	2	2	0	1	3	1	2	5	3	27	24	2
Un1	1	0	2	15	0	1	0	0	8	4	5	0	3	34	26	1
WL 4506	0	0	3	25	3	2	0	0	1	0	1	0	4	31	30	0
Au4	2	0	20	31	5	2	0	0	1	0	0	0	2	22	15	0

For the PSOC 1500 and PSOC 1516 samples the macerals were not counted due to the high rank.

Table 3. Microlithotype composition (vol.%) of the coals

Sample	Vitrite	Liptite	Inertite	Clarite	Durite	Vitrinerite	Duroclarite	Clarodurite	Vitrineroliptite	Carbominerite
Brunner	27	0	0	15	0	26	26	2	0	4
Dong Ho 3	47	0	0	39	0	4	9	0	0	1
PSOC 1488	58	0	2	18	0	6	12	2	0	2
Id2	46	0	1	33	0	7	10	2	0	1
PSOC 1445	37	0	3	12	2	15	22	6	2	1
PSOC 1502	17	0	5	4	2	30	25	14	1	2
PSOC 1493	46	0	5	21	1	6	11	2	1	7
Co2	31	0	3	16	1	28	19	1	0	1
Id1	48	0	0	33	0	10	8	0	0	1
Co1	21	0	6	25	0	19	25	1	0	3
Au1	6	0	23	0	8	30	9	23	0	1
Au2	7	0	17	2	2	33	14	23	0	2
Vz1	27	0	3	20	0	27	21	1	0	1
SA3	14	0	23	3	12	16	10	13	1	8
SA2	7	0	38	2	21	11	7	9	0	5
US1	34	0	3	17	2	11	22	4	1	6
Au5	12	0	9	12	2	15	29	16	2	3
SA5	4	0	24	1	30	14	5	17	0	5
SA4	16	0	21	4	8	18	14	12	2	5
WL 4468	55	0	3	2	1	18	6	6	0	9
PSOC 1451	41	0	4	16	2	10	19	3	1	4
Au3	28	0	12	10	3	19	12	13	0	3
Un1	23	0	2	16	6	10	29	8	3	3
WL 4506	36	0	14	5	1	31	10	3	0	0
Au4	13	0	24	0	2	51	1	4	0	5
PSOC 1500	59	0	1	0	0	29	0	0	0	11
PSOC 1516	71	0	2	0	0	18	0	0	0	9

follow the standards outlined in Taylor *et al.* (1998) and ICCP (1998). A brief introduction to the maceral and microlithotype terminology is presented below.

Maceral and microlithotype terminology

Vitrinite macerals are derived from decomposition of cellulose- and lignin-rich parenchymatous and woody tissues of land plants, and they have a greyish colour under the reflected light microscope. Telinite is characterized by recognizable cell walls of plant tissue, whereas collotelinite has a homogeneous appearance. Collodetrinite consists of a mottled vitrinitic ground-mass composed of particles less than 10 µm in size, whereas gelinite and corpogelinite are homogeneous and structureless infillings of cracks/other voids and cells, respectively. The inertinite macerals represent oxidized organic matter and appear light grey to white in reflected light. Fusinite and semifusinite are both characterized by preserved cellular structure of plant tissue, but the cellular structure of semifusinite has a poorer preservation and the reflectance is lower. Inertodetrinite represents discrete inertinitic fragments with a particle size less than 10 µm in the maximum dimension, whereas macrinite occurs as an amorphous matrix or as structureless particles with the smallest diameter above 10 µm. The liptinite macerals sporinite, cutinite, resinite and suberinite are derived from spores/pollen, cuticular layers and cuticles of stems and leaves, resins and suberin in corkified cell walls, respectively. Liptodetrinite includes finely detrital liptinitic constituents. The liptinite macerals are recognized by their morphology and fluorescence in reflected blue light.

Maceral associations are called microlithotypes. The mono-maceral microlithotypes vitrite, liptite and inertite contain not less than 95% of vitrinite (V), liptinite (L) and inertinite (I) respectively. Clarite, durite and vitrinerite are bimaceral microlithotypes. In clarite, V+L>95%, in durite I+L>95%,

and in vitrinerite V+I>95%. Duroclarite, clarodurite and vitrineroliptite are trimaceral microlithotypes and all maceral groups are represented by more than 5%, but in duroclarite V>I, L, in clarodurite I>V, L, and in vitrineroliptite L>I, V. Carbominerite contains between 20 and 60% minerals (or between 5 and 20% where the mineral is pyrite).

During analysis of the low rank coals the terminology of the huminite maceral group was used. The petrographic data and the mean random reflectance values were used as variables in the multivariate statistical correlation to the HI values and the E_a . However, the modelling necessitates a uniform dataset, and therefore the huminite macerals were translated into vitrinite macerals. Thus, 'textinite+textoulminite' was translated into 'telinite', 'eu-ulminite' was translated into 'collotelinite', 'atrinite+densinite' was translated into 'collodetrinite', 'porigelinite+gelinite' was translated into 'gelinite', and finally 'corpohuminitite' was translated into 'corpogelinite'. This has no influence on the obtained results, but is only a technical adjustment of the data.

Determination of activation energies

As recommended by Jarvie (1991) and Schenk & Horsfield (1998), the non-extracted coal samples were pyrolysed using a Vinci Rock-Eval 5 instrument. The discrete E_a distributions and the pre-exponential factors were estimated from four pyrograms representing heating rates of 5, 10, 25 and 50 K/min by using Vinci standard (Optkin1) non-linear optimization/least squares minimizing function and assuming parallel first-order reactions with a unique pre-exponential factor for all reactions. The maximum pyrolysis temperature was 650°C. In order to be able to calculate the HI, the total organic carbon (TOC) content was determined by means of a LECO IR-212 apparatus.

The E_a distributions are characterized by three components. One is the total area of the E_a distribution, which corresponds

to the HI, another is the position of the peak of the E_a distribution (ideally linearly related to $\log A$), and the final one is the width of the E_a distribution. The HI was calculated by the instrument software using the TOC value. To extract the E_a peak position and the peak width, a peak fitting, using the Gauss distribution, was applied to the centre of the E_a distributions. The two parameters were extracted from the Gauss curve as the Gauss peak position (hereafter ' E_a peak') and the Gauss peak width at half peak height (hereafter 'peak width'). This procedure enables simple regressions to be performed between the petrographic composition, which is multivariate, and the three univariate target parameters (HI, E_a peak, peak width).

Multivariate regression analysis

Multivariate regression analysis was used to evaluate the dataset. The reflectance values and the normalized data of the maceral group, maceral and microlithotype analyses were used in the multivariate calibration (Tables 1–3), and the target parameters extracted from the E_a distribution curves were thus (1) the HI (representing the petroleum generative potential), (2) the centre of the Gauss curve fitted to the E_a main population (peak of E_a distribution), and (3) the width of a Gauss curve fitting the E_a distribution. Before modelling, the variables were scaled to unit variances in order to avoid dominance from variables high in variance over variables low in variance but with significant influence on the target parameter. This allows the variables to be equally weighted with respect to variance prior to estimation of their importance on the model. However, as a rule of thumb, if the standard deviation of a variable over the dataset is less than four times the standard deviation of the analytical method, scaling should not be performed or the variable should be deleted (Wold 1987). Taylor *et al.* (1998) have reported repeatability of maceral analyses counted on 500 particles to be approximately 1.3 (standard deviation) in the level below 10%. The repeatability of microlithotype analysis has not been reported, but is presumed to be within the same range. For maceral group analysis and reflectance measurements intercalibrations indicate reproducibility to be better than approximately 4–7% relative (standard deviation) and 0.05 (standard deviation), respectively. Consequently, it was decided to delete variables from the microlithotype and maceral analyses that varied within the range 0–7 vol.%. Both the reflectance values and the maceral group analyses have standard deviations higher than four times the reproducibility. Noise and thus uncertainty from the independent variables will not, provided the above precautions are taken, be modelled. Modelling beyond the systematic variation of the variables would lead to principal components that cannot be validated, and the modelling will be stopped. Another stop criterion is, of course, the estimated uncertainty of the target parameter.

Correlation was performed with the computer software 'Sirius' using partial least squares (PLS) regression analyses (Kvalheim & Karstang 1987; Martens & Næs 1991), and principal components were verified by the cross-validation procedure proposed by Wold (1978). Outliers were identified by using the Soft Independent Modelling of Class Analogies (SIMCA) method (Wold 1976), and confirmed by scrutiny of the raw data.

The scope of the regression analyses is to identify which variables influence the E_a distributions and to study the relationships between these variables and the E_a distributions (and not to create a model, from which the E_a distributions can be predicted). One weakness in the dataset is data closure (normalized variables). This means that a positive correlation by

some variables to a target parameter automatically induces negative correlation by others. It is not possible to overcome this problem and it must be considered when the results are evaluated.

RESULTS

Coal rank and petrography

The samples yield random vitrinite (huminite) reflectance values from 0.36% R_o to 1.43% R_o which corresponds to ranks from lignite (soft brown coal) to medium volatile bituminous (Table 1). Petrographically the coals exhibit a wide variation. The vitrinite content on a mineral matter free (mmf) basis ranges between 19 vol.% and 94 vol.%, whereas the inertinite content ranges from 1–74 vol.% (mmf) (Table 1). The liptinite maceral group ranges between 0 and 19 vol.% (mmf) with the majority of the samples containing less than 8 vol.% (mmf). The vitrinite values close to 90 vol.% (mmf) or above are, in general, related to the Tertiary low rank coals (% R_o = 0.41–0.55) and the two coals of highest rank (% R_o = 1.25–1.43). At this high rank, macerals of the liptinite group have attained a reflectance very similar to the corresponding vitrinite and they have lost all or most of their fluorescence ability (Teichmüller 1982; Taylor *et al.* 1998). The most common macerals are collodetrinite, collotelinite, inertodetrinite and macrinite, but a significant variation between the samples is evident (Table 2). The microlithotypes likewise exhibit a significant variation, but vitrite, inertite, clarite, vitrinertite, duroclarite and clarodurite are most common (Table 3).

Hydrogen Index and activation energy

The HI values span from 96 to 327 mg HC/g TOC (Table 4). Among the eight coals with the lowest HI values (96–145 mg HC/g TOC), three have the highest maturity (highest rank) of all coal samples and three are inertinite-rich Gondwana coals (≥ 50 vol.% inertinite). The highest HI value is obtained from the Carboniferous US1 sample, and interestingly two Australian Gondwana coals are also among the four samples with highest HI. These two samples have inertinite contents between 32 vol.% and 35 vol.%. With respect to HI values, the coals of similar age are scattered over the entire HI spectrum represented by the sample set.

The E_a distributions are presented in four groups, where groups 1 to 3 each represent the following constrained reflectance intervals:

- group 1 includes coals with reflectance values from 0.41% R_o to 0.59% R_o ;
- group 2 includes coals with reflectance values from 0.71% R_o to 0.77% R_o ;
- group 3 include coals with reflectance values from 1.11% R_o to 1.43% R_o .

This may permit a visual comparison of the E_a distribution of coals with the rank parameter eliminated. Group 4 includes the remaining coals ordered with respect to increasing rank. All coals yield a broad E_a distribution corresponding to a complex organic composition with a variety of chemical bonds present in the organic matter (Fig. 1a–d). It is shown by groups 1–4 that the peak position of the E_a distribution increases with increasing maturity. In group 1 it is centred around 54–58 kcal/mole, in group 2 around 60–62 kcal/mole, and in group 3 around 64–66 kcal/mole. It can also be noted that the E_a distributions of the most strongly coalified samples (group 3 and samples

Table 4. Target parameters and A factors

Sample	R_o (%)	Hydrogen index (mg HC/g TOC)	Peak position (kcal/mole)	Peak width (kcal/mole)	A factor (s^{-1})
Brunner	0.36	161	59.2	7.37	1.551×10^{16}
Dong Ho 3	0.41	197	58.4	4.55	4.126×10^{15}
PSOC 1488	0.44	115	54.7	5.12	2.322×10^{14}
Id2	0.44	221	57.7	7.53	4.592×10^{15}
PSOC 1445	0.47	202	54.4	4.25	1.808×10^{14}
PSOC 1502	0.52	167	54.5	4.26	1.726×10^{14}
PSOC 1493	0.53	145	60.7	5.53	1.863×10^{16}
Co2	0.54	212	59.2	4.88	4.247×10^{15}
Id1	0.55	249	56.6	4.73	7.065×10^{14}
Co1	0.59	151	57.6	4.86	9.705×10^{14}
Au1	0.62	97	58.9	4.85	2.368×10^{15}
Au2	0.63	183	54.7	3.38	1.320×10^{14}
Vz1	0.66	260	60.7	4.26	1.201×10^{16}
SA3	0.68	154	58.3	3.94	2.158×10^{15}
SA2	0.71	120	60.8	4.48	7.221×10^{15}
US1	0.73	327	62.0	4.87	1.709×10^{16}
Au5	0.73	275	58.2	3.38	1.590×10^{15}
SA5	0.74	163	60.4	3.42	7.425×10^{15}
SA4	0.75	142	62.3	4.15	3.046×10^{16}
WL 4468	0.76	237	62.4	4.89	1.889×10^{16}
PSOC 1451	0.77	213	61.0	4.75	9.337×10^{15}
Au3	0.84	260	52.5	3.16	2.921×10^{13}
Un1	0.84	270	62.1	3.88	2.259×10^{16}
WL 4506	0.87	172	63.6	4.83	2.810×10^{16}
Au4	1.11	136	63.5	5.33	9.517×10^{15}
PSOC 1500	1.25	132	65.0	5.83	1.729×10^{16}
PSOC 1516	1.43	96	66.0	6.03	1.961×10^{16}

Un1 and WL 4506 in group 4) still attain a Gauss-like shape, with a 'tail' of comparatively low E_a values.

The pre-exponential factor varies significantly within the individual groups. In group 1 variations within two decades are found with a mean value of $A_{\text{mean}} = 3.8 \times 10^{15} \text{ s}^{-1}$. Group 2 exhibits a somewhat smaller variation, but is also more constrained in maturity, and the pre-exponential factors of the group yield a mean value of $A_{\text{mean}} = 1.3 \times 10^{16} \text{ s}^{-1}$. The pre-exponential factors of group 3 are not higher than in group 2 (group 3, $A_{\text{mean}} = 1.5 \times 10^{16} \text{ s}^{-1}$). The pre-exponential factors of group 4 vary within three decades. However, the group does not reveal a clear correlation between the maturity and the A values. Despite the tendency to an increase in the peak position of the E_a distribution and the pre-exponential factors with increasing maturity, the variations within the groups with a restricted reflectance range is pronounced. This stresses the complexity of the correlation between the E_a distribution, petrographic composition and rank, and justifies a multivariate regression analysis.

Multivariate calibration

In order to avoid modelling of analytical noise, the following variables were removed from the dataset:

- Macerals: telinite, sporinite, cutinite, resinite, suberinite, fusinite, semifusinite, pyrite and 'other minerals'.
- Microlithotypes: vitrinitertoliptite and liptite.

The presence of these variables are all low and consequently with high uncertainty.

Correlation to the Hydrogen Index

The correlation to the HI resulted in a three principal components model. The first component explained 55% of the

variance in HI, the second 22% and the third 8.5% of the variance. Thus, some 85% of the variance in HI could be explained using these three principal components. Figure 2 shows the predicted values of HI versus the measured values. Although considered acceptable compared to the uncertainty in measuring HI, the explained variance of 85% results in a fairly low slope of the correlation curve (0.87) and interception with the y -axis at a relatively high value. This indicates that the petrographic composition cannot fully describe the HI. The correlation coefficient of 0.93 is, however, considered satisfactory. WL 4506 is difficult to model, and including this coal results in a weaker model explaining about 81% of the variance in HI. However, from a statistical point of view, using SIMCA, WL 4506 is not an outlier, but it was decided to leave it out.

Five coals were regarded as outliers, namely PSOC 1451, PSOC 1488, PSOC 1493, Id1 and Un1. PSOC 1451 and PSOC 1493 both have very high collotelinites contents (36 vol.% and 46 vol.%, respectively) compared to the other coals, which all have contents below 31 vol.%. Id1 has a low content of collotelinite (9 vol.%) and at the same time a high HI (249), which is abnormal compared to the other coals. Conversely PSOC 1488 has a high content of collotelinite (59 vol.%) and a low HI (115), which is also abnormal. Un1 is extreme with respect to the liptinite content (19 vol.%, mmf), as all other coal samples have liptinite contents lower than 12 vol.% (mmf).

The variables with a significant influence on HI are the vitrinite reflectance, the maceral groups inertinite and liptinite (vitrinite is deleted from the model since the three maceral groups are normalized), the macerals macrinite, inertodetrinite, liptodetrinite, gelinite, collodetrinite and collotelinite and finally the microlithotypes vitrite and inertite.

A variable plot, also called a loading plot, using the two first principal components is shown in Fig. 3. In this plot, collotelinite, liptinite and liptodetrinite plot very close to each other and to HI, indicating a strong correlation between these

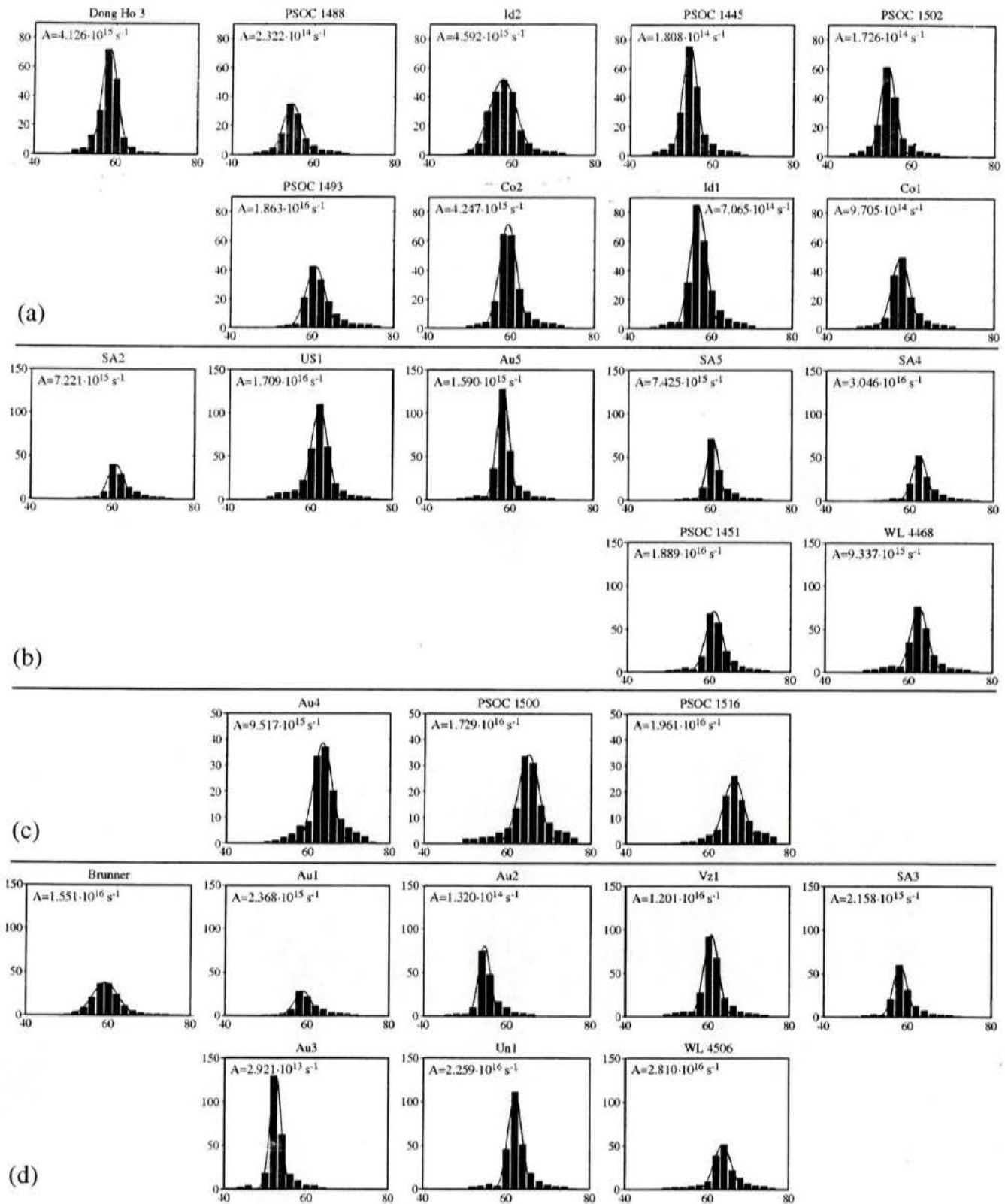


Fig. 1. Activation energy (E_a) distributions for the humic coals. Note the broad E_a distributions whose main population can be approximated by a Gauss curve. The two target correlation parameters ' E_a peak position' and ' E_a peak width' were extracted from the Gauss curves. (a) group 1: brown coals (huminitic reflectance values from 0.41% R_o to 0.59% R_o) with E_a distributions centred around 54–58 kcal/mole; (b) group 2: hard coals (vitrinite reflectance values from 0.71% R_o to 0.77% R_o) with E_a distributions centred around 60–62 kcal/mole; (c) group 3: hard coals (vitrinite reflectance values from 1.11% R_o to 1.43% R_o) with E_a distributions centred around 64–66 kcal/mole; (d) group 4: the remaining coals ranged according to increasing reflectance values (0.36–0.87% R_o). X-axis: activation energies (kcal/mole); y-axis: initial petroleum potential (mg/g TOC). See also Table 1.

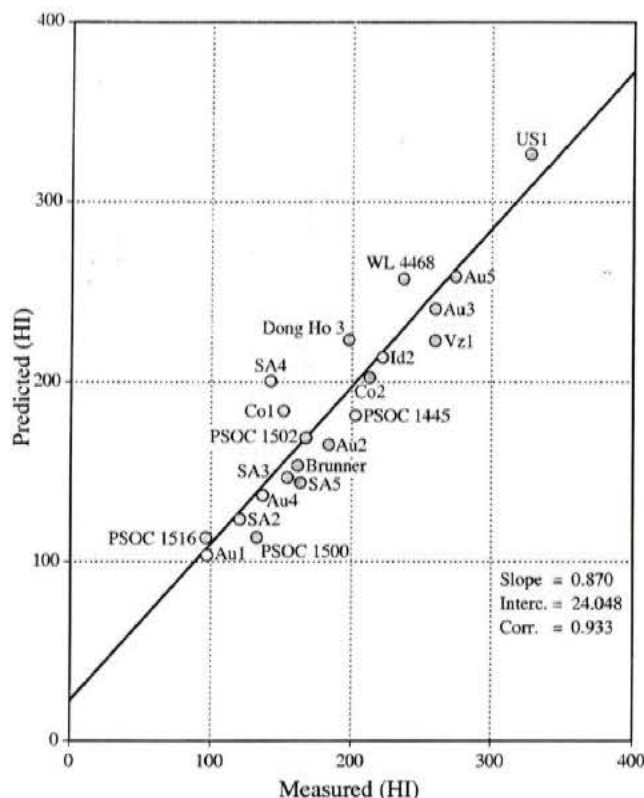


Fig. 2. Predicted versus measured HI. The model explains 85% of the variation in HI, and a correlation coefficient of 0.93 is considered satisfactory.

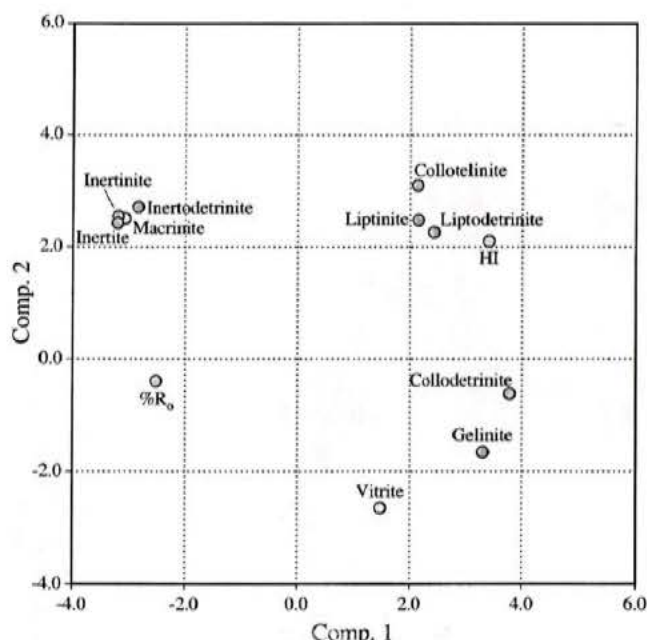


Fig. 3. Variable plot using principal components 1 and 2. Collotelinitite, liptinite and liptodetrinite plot very close to each other and to the HI indicating a strong correlation between these macerals and HI. The vitrinite reflectance ($\%R_o$; thermal maturity) plots opposite indicating a negative correlation to HI.

macerals and the HI. The vitrinite reflectance value shows a negative correlation to HI. Gelinite and collodetrinite have a smaller yet positive correlation to HI, while inertite, inertinite, macrinite and inertodetrinite have a small negative correlation

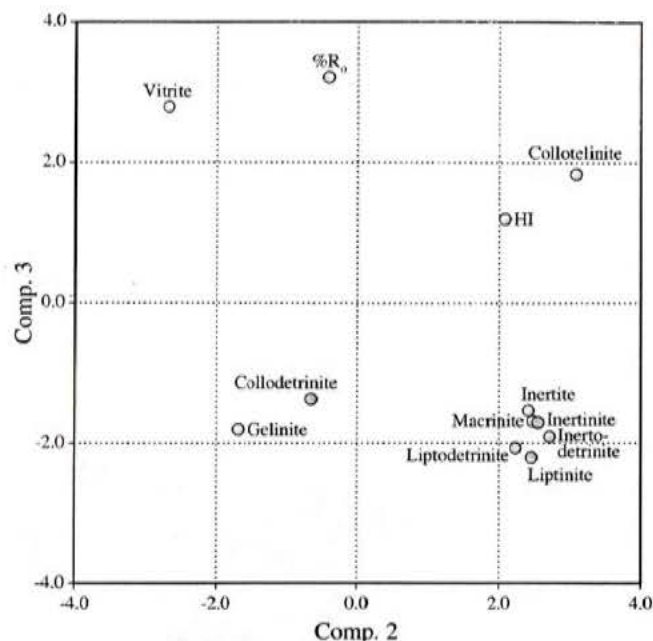


Fig. 4. Variable plot using principal components 2 and 3. Again a strong positive correlation is found between collotelinitite and the HI.

to HI. In Fig. 4, the variables are plotted using principal components 2 and 3. Again a strong positive correlation is found between collotelinitite and HI. A small positive correlation between vitrinite reflectance and HI is seen, whereas gelinite and collodetrinite show a negative correlation. The remaining variables are almost without significance in this plot.

Principal components are vectors in the variable space that represent the variation in the dataset and, at the same time, best describe the target parameter. Principal components are therefore a combination of the variation in the dataset as a whole and are normally not amenable to direct interpretation; e.g. principal component 1 is a combination of almost all variables. This is evidenced in Figs 3 and 4 by studying the projection of the variables on the axes.

Studying the loading plots can sometimes lead to erroneous conclusions, since each loading plot only represents two dimensions in the reduced dataset (which, in this case, is three dimensional). An example is the reflectance value, which in Fig. 3 appears to be negatively correlated to HI while in Fig. 4 it appears to be positively correlated. In a three-dimensional plot, however, the reflectance value is negatively correlated. Therefore the so-called target projection is both simpler and safer to use when the overall relationship between the target parameter and the included variables is studied. In the target projection in Fig. 5 the overall modelled correlation between the variables and HI is shown. As expected, the inertinitic constituents exhibit a negative correlation to HI, while liptinitic and vitrinitic constituents are positively correlated. The vitrinite reflectance shows a small negative correlation to HI. As also indicated in the two variables-plot (Figs 3 and 4), collotelinitite is by far the most influential parameter.

Correlation to peak position of the E_a distribution

A plot of the E_a peak positions versus the reflectance values shows a clear tendency in the dataset towards a relationship between high vitrinite reflectance values and E_a distributions at

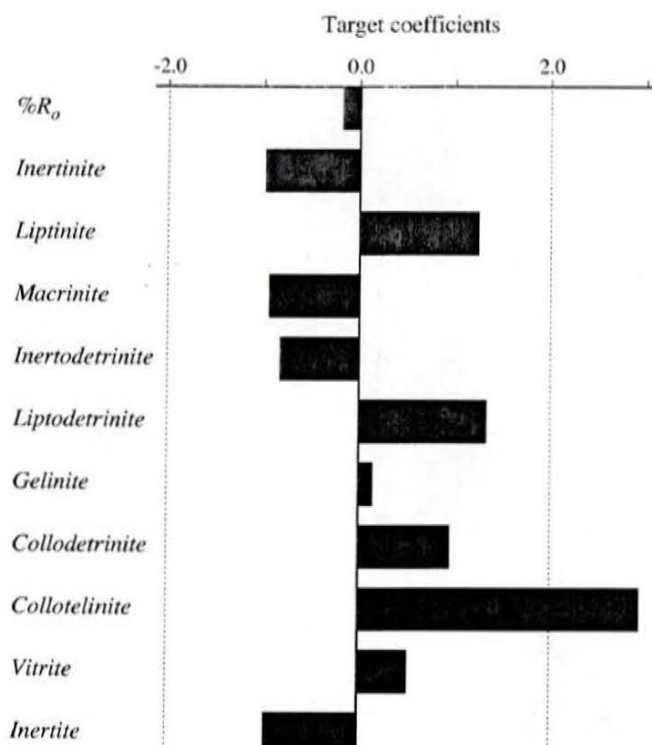


Fig. 5. Target projection of the partial least squares regression (PLSR) model, which gives a measure of the correlation between individual variables and HI. Collotelinite, liptodetrinite and liptinite are, in particular, positively correlated to the HI.

higher values (Fig. 6). The relationship is not consistent for all coals, however, and the petrographic data were thus included in a multivariate correlation.

A three-component model explaining 82% of the variance in the E_a peak position could be established. Considering the relatively high uncertainty in fitting a Gauss curve shape to the discrete distributed E_a values, an explained variance of 82% is satisfactory. The response from the model demonstrates a satisfactory correlation between the predicted and the measured values of the E_a peak positions (correlation coefficient: 0.92) (Fig. 7).

The target projection plot is in agreement with the raw data plot in Fig. 6 with respect to the influence from the vitrinite reflectance value on the E_a peak position (Fig. 8). Other variables included in the model are corpogelinite, gelinite, collodetrinite, clarite, duroclarite and clarodurite, which all have a negative correlation to the peak position. The dominant influence is found from the vitrinite reflectance value, corpogelinite and clarodurite. Including collotelinite in the model does not improve the model, but including this component results in a weak positive correlation between the peak position and collotelinite.

Dong Ho 3 and Co1 are regarded as outliers to the model. Dong Ho 3 has an extremely high gelinite content (almost 17 vol.%), while the remaining coals all have contents lower than 11 vol.%. Co1 has an atypically high content of corpogelinite (12 vol.%) as all other coals contain less than 9 vol.%.

Correlation to peak width of the E_a distribution

The correlation model to the peak width explains almost 93% of the variance in the peak width by using 4 components. The response from the model is excellent with a slope of 0.94 and correlation coefficient between the predicted and the measured peak width of 0.97 (Fig. 9).

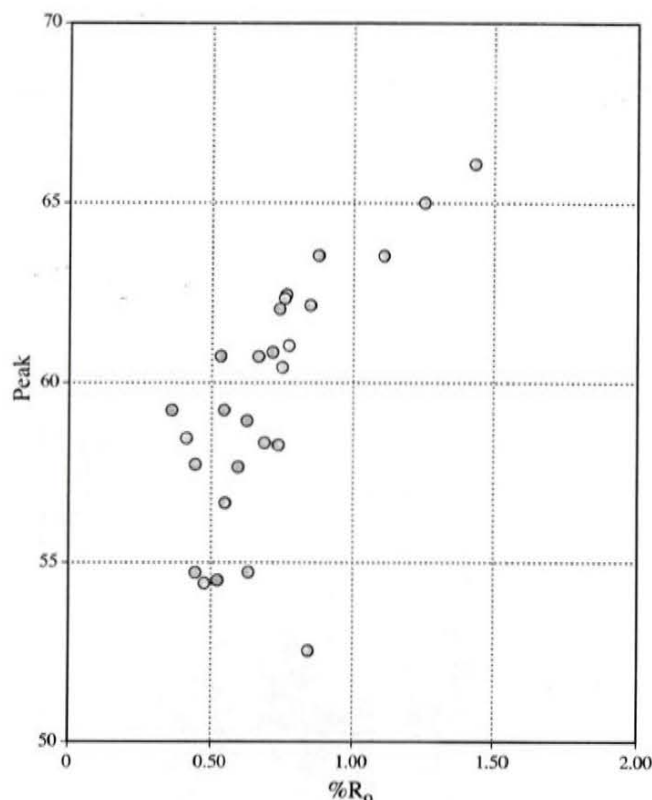


Fig. 6. The E_a peak position (kcal/mole) versus reflectance value plot shows a tendency in the dataset towards a relationship between high vitrinite reflectance values and E_a distributions at higher values.

The following variables are considered of importance to the model: (1) the vitrinite reflectance value; (2) the maceral groups inertinite and liptinite; (3) the macerals macrinite, inertodetrinite, liptodetrinite, gelinite, collodetrinite and collotelinite; and (4) the microlithotypes vitrinite, inertite, durite, vitrinertite, duroclarite and clarodurite. From the target projection, the overall importance of the variables can be studied (Fig. 10). Of minor overall importance is macrinite, gelinite, collodetrinite, collotelinite and inertite. Vitrinite and to some degree vitrinertite, and high vitrinite reflectance values broaden the peak, whereas inertinite, liptinite, inertodetrinite, liptodetrinite, durite, duroclarite and clarodurite have the opposite effect.

Brunner, PSOC 1502, Id2, Au1 and Au3 are regarded as outliers. Brunner and Id2 are both extreme in the peak width, 7.37 kcal/mole and 7.53 kcal/mole respectively, compared to the remaining coals which all have peak widths below 6.03 kcal/mole (the majority below 5 kcal/mole). For PSOC 1502, Au1 and Au3, no single variable can explain why they are outliers.

DISCUSSION

By using the reflectance values and the petrographic composition of the coals in a multivariate calibration, it is possible to correlate some of these components to the E_a distribution with respect to the curve area (Hydrogen Index), E_a peak position and the span of the E_a (peak width of the E_a distribution).

The E_a peak and the pre-exponential factor A

By assuming a unique pre-exponential factor and first-order parallel reactions in the estimation of the E_a distributions, the

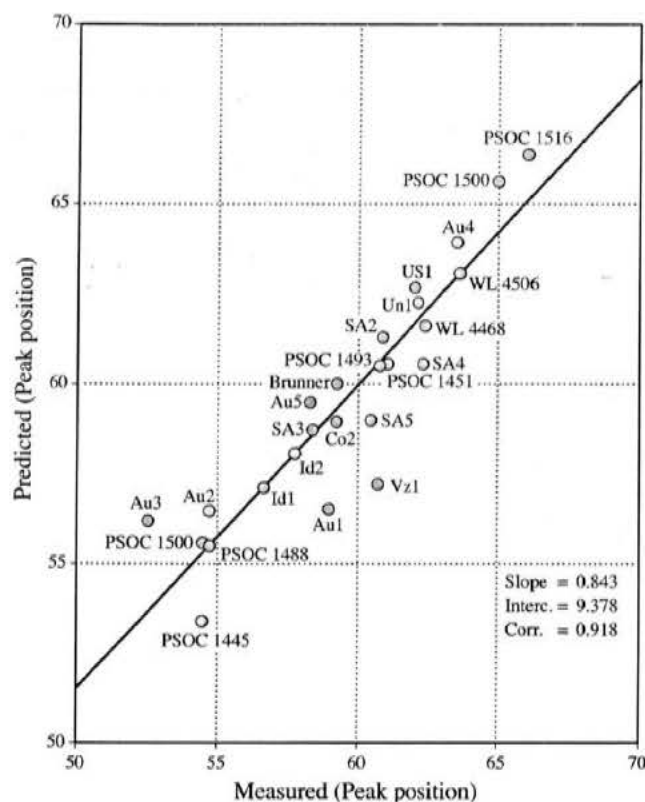


Fig. 7. Predicted versus measured E_a peak position. The model explains 82% of the variation in the peak position, and a correlation coefficient of 0.92 is considered satisfactory.

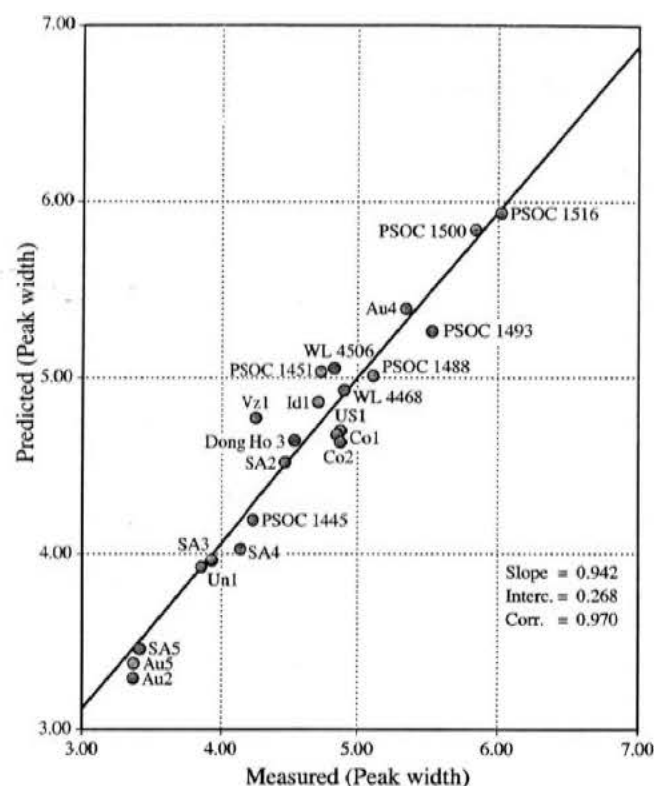


Fig. 9. Predicted versus measured peak width of the E_a distribution. The model explains about 93% of the variation in the peak width, and a correlation coefficient of 0.97 and a slope of 0.94 indicate an excellent response from the model.

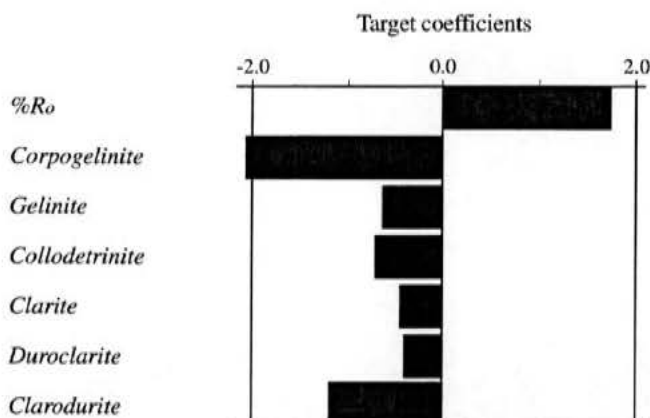


Fig. 8. Target projection of the partial least squares regression (PLSR) model, which gives a measure of the correlation between individual variables and E_a peak position. Higher vitrinite reflectance values (thermal maturity) pull the peak position to higher E_a values, whereas a number of vitrinite macerals and vitrinite-rich microlithotypes pull the peak position to lower E_a values.

optimized pre-exponential factor functions as a mathematically fitting factor (Schaefer *et al.* 1990). The pre-exponential factor is logarithmically related to the E_a peak as shown in Fig. 11. The correlation coefficient is rather poor (0.80), indicating a relatively large error in fitting the E_a distributions or in establishing the pre-exponential factors. Removing the high rank coals (PSOC 1516, PSOC 1500, Au4) from the dataset improves the correlation coefficient to 0.90, which is comparable to the

correlation shown by Pepper & Corvi (1995). The lack of fit of the high maturity coals may be caused by a change in reaction kinetics due to aromatization and condensation reactions at high maturity (Schenk & Horsfield 1998; Boreham *et al.* 1999), or it is perhaps caused by incomplete pyrolysis of high maturity coals at the relatively low final temperature of 650°C. Roughly, a linear correlation exists between the E_a peak and the pre-exponential factor; thus modelling of the pre-exponential factor will not substantially increase the level of information compared to modelling of E_a .

Organic petrography and Hydrogen Index

The correlation between the organic petrography and HI shows a very similar relationship to that previously found by Petersen *et al.* (1996, 1998) in studies of oil- and gas/condensate-generating coals from the Middle Jurassic Bryne Formation in the Sogne Basin in the Danish North Sea. In these studies, it was also found that collotelinite has a very significant influence on the hydrocarbon generative potential. Additionally, telinite, the vitrinite maceral group, the microlithotypes vitrite (also important in the present study), clarite and duroclarite were modelled to have a strong influence on the hydrocarbon generative potential of the coals in the Sogne Basin. Influence from liptinitic constituents on the HI obtained from the Bryne Formation coals was only weak, probably due to the generally low liptinite content of the coal seams. In the present study, the wider span of liptinite contents has resulted in the inclusion of the liptinite maceral group and liptodetrinite; the positive correlation of these hydrogen-rich components to the HI is not surprising. In all three studies, inertinitic components have a negative correlation to HI indicating that these components act

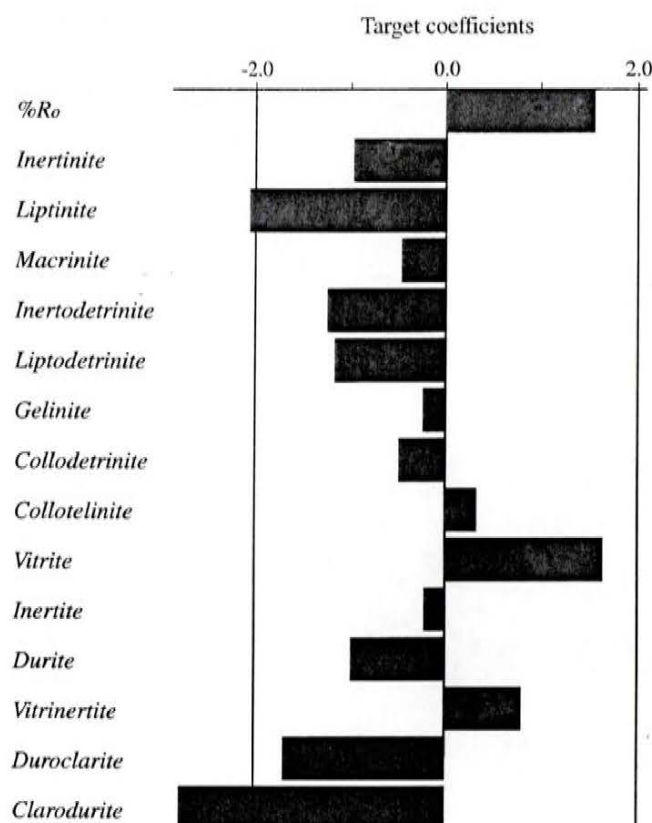


Fig. 10. Target projection of the partial least squares regression (PLSR) model, which gives a measure of the correlation between individual variables and peak width of the E_a distribution. The vitrinite reflectance (thermal maturity), the maceral collotelinite and the microlithotypes vitrite and vitrinertite broaden the peak width. A number of inertinitic and liptinitic constituents have the opposite effect.

by 'diluting' the petroleum-prone constituents, which results in a reduction in the amounts of generated hydrocarbons. The vitrinite reflectance, and thus the thermal maturity, plays a small, yet significant, role.

It has been shown that the positive correlation of mainly vitrinite-rich constituents with HI from the earlier studies can be expanded from the very narrow span of Middle Jurassic coals with essentially similar rank and from a single basin in the North Sea to worldwide coals from various geological settings and with various rank, petrographic composition and age. It is notable that due to the lower reflectance of collodetrinite, and since this maceral is generally regarded to have a higher hydrogen content and inclusions of submicroscopic lipid material (ICCP 1998; Taylor *et al.* 1998) compared to the other vitrinite macerals, it is widely assumed that collodetrinite is the major vitrinitic petroleum generator. However, this study and the previous studies by Petersen *et al.* (1996, 1998) indicate that the single most important maceral with respect to HI in humic coals is collotelinite. With respect to the HI, collotelinite in this study behaves rather similarly to liptinite and liptodetrinite as illustrated by the two variables plot (Figs 3 and 4). Whether paraffinic oil or mainly gas/condensate is generated from these macerals is, according to Isaksen *et al.* (1998), dependent on their capability to generate sufficient amounts of long-chain aliphatic compounds (in particular above nC_{13}). We suggest that this may be favoured by the presence of hydrogen-enriched vitrinite, as the Middle Jurassic Bryne Formation coals, the primary source for oil accumulations in the

Sogne Basin, contain hydrogen-enriched vitrinite and low amounts of liptinite (Petersen & Rosenberg 1998; Petersen *et al.* 1996, 1998).

Organic petrography and the E_a peak

The E_a distribution of coals of different geographical origins, age and rank shows no clear interpretable relationship to any of these characteristics besides a shift towards a higher peak position of the E_a distributions with increasing maturity (rank) (Fig. 1a–d). A shift towards a higher peak position of the E_a distributions with increasing maturity within the present maturity range (0.36–1.43% R_o) was also noted by Schaefer *et al.* (1990), Jarvie (1991) and Schenk & Horsfield (1998). The shift towards a higher principal E_a is due to elimination of lower activation energies during thermal stress. According to Schenk & Horsfield (1998), this increase continues up to a vitrinite reflectance of 1.70% R_o (low volatile bituminous rank) after which it decreases and, due to the co-variance of the principal E_a and the pre-exponential factor, the factor also decreases above 1.70% R_o . Within groups 1–3 with narrow reflectance ranges (Fig. 1a–c) the variation in the E_a distributions is most likely associated with organic petrographic differences (Tables 1–3). This is in agreement with the correlation between the E_a distribution and the molecular structure of kerogen as revealed by pyrolysis–gas chromatography shown by Tegelaar & Noble (1994). Effects from the mineral matrix (catalysis, retention of S_2 ; Jarvie 1991; Dembicki Jr 1992; Pelet 1994) can be neglected due to the low amounts of mineral matter in these humic coals (Table 2). The organic petrographic influence is, for example, shown by the variation in the E_a distributions in group 2 (Fig. 1b); except for PSOC 1451 the absolute values are clearly higher for the vitrinite-rich coals (US1, Au5, WL 4468) compared to the inertinite-rich coals (SA2, SA5, SA4).

As shown above, the E_a peak position is clearly influenced by the maturity (reflectance value) (Figs 6, 8). However, it is not always possible to predict the E_a peak position from the reflectance value alone (Fig. 6). Multivariate calibration indicates that the vitrinitic constituents have significant influence on the E_a peak position. These constituents serve to shift the E_a peak to a lower E_a than predicted from the reflectance value alone. It is notable that neither liptinite nor inertinite alone influence the position of the E_a peak. However, this might very well change in coals richer in liptinite. Inertinite is regarded as 'inert' with respect to petroleum generation (coals up to 74 vol.% inertinite are included in this model). The E_a distribution is influenced by the ability of generated bitumen to escape the coal. According to Stout (1994) petroleum expulsion from the 'massive' microlithotype vitrite (typically dominated by collotelinite) is retarded due to trapment within the microporosity of the vitrinite, whereas expulsion is favoured by a mixture of liptinite and vitrinite (e.g. collodetrinite and clarite). Additionally, inertinite-rich microlithotypes may favour petroleum expulsion (Bertrand 1989). These results are in good agreement with the present correlation as collodetrinite, clarite and the inertinite-rich microlithotypes duroclarite and clarodurite show a negative correlation to the E_a peak position, i.e. these components draw the peak position to lower E_a . Inclusion of collotelinite in the model does not improve the correlation and it is therefore left out; if included, however, collotelinite shows a weak positive correlation to the peak position, i.e. it draws the position to a higher E_a . In contrast, the strong negative influence from corpogelinite and gelinite is more difficult to explain.

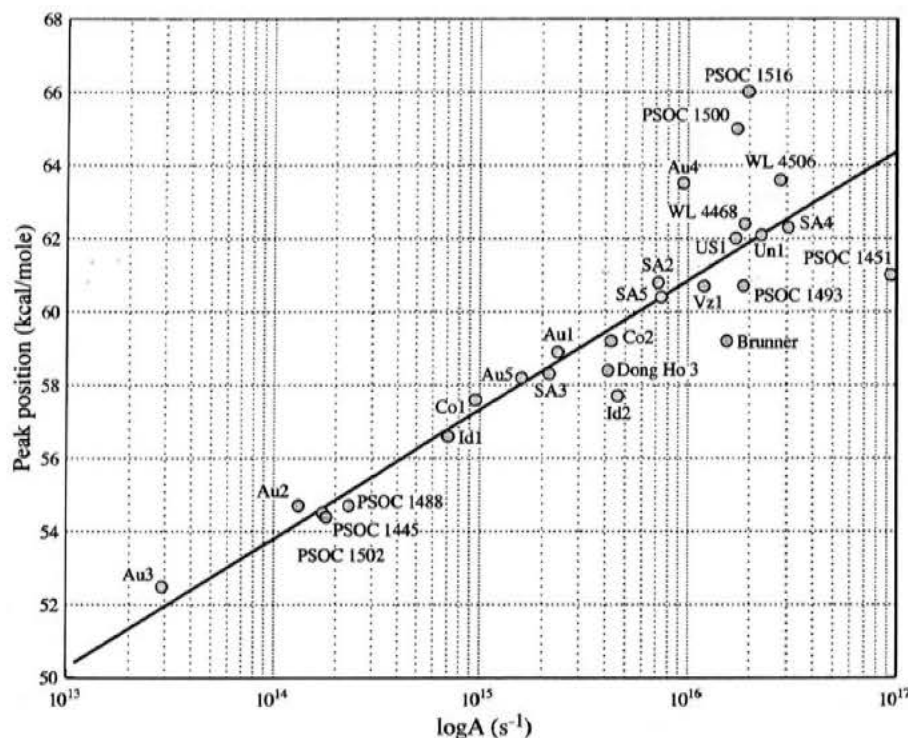


Fig. 11. Correlation between E_a peak position of the Gauss curve and $\log A$ indicating a linear correlation ($r^2=0.80$ for all coals; $r^2=0.90$ when deleting the coals of highest rank: PSOC 1516, PSOC 1500 and Au4).

Organic petrography and peak width of the E_a distribution

A more complex relationship exists with respect to the width of the E_a distribution. The width increases with increasing reflectance value corresponding to increasing thermal maturity of the organic matter. The broad E_a distributions with a 'front' of comparatively low E_a values shown by the most mature coal samples (group 3 and samples Un1 and WL 4506 in group 4) suggest that these coals have retained a generative potential. The coal samples of this study constitute a natural maturation series, and the broad E_a distributions of the high rank coals may thus reflect the creation of new petroleum potential by structural changes in the coal matrix as recently shown by Schenk & Horsfield (1998). These processes are not reproducible in the laboratory, and timing predictions of petroleum formation based on artificially matured coals may thus not be fully reliable (Schenk & Horsfield 1998). Generation of high molecular bitumen with low activation energies during maturation may broaden the E_a distribution. Primary oil generation is caused by partial decomposition of the bitumen, which is a process involving activation energies from 34 to 67 kcal/mole (Lewan 1994). The microlithotype vitrinite also seems to broaden the E_a distribution (Fig. 10). Liptinitic and inertinitic components result in a narrower E_a distribution; this may be related to a more uniform distribution of bonding energies in liptinite, as shown by published E_a distributions of kerogen types I and II (e.g. Tissot *et al.* 1987; Ungerer 1990), and in inertinite, which is very carbon-rich. The trimacerites duroclarite and clarodurite also narrow the width. This may tentatively be explained by a combination of the presence of liptinite and considerable amounts of inertinite, and expulsion efficiency.

CONCLUSIONS

- (1) The key characteristics of the E_a distributions, including the HI, of a suite of worldwide humic coals have been correlated satisfactorily to the coals' petrographic composition and rank (huminitic/vitrinitic reflectance values). The

complex correlations reflect the heterogeneous nature of humic organic matter (humic coals and kerogen type III). Overall it can be concluded that vitrinite and, in particular, the vitrinite maceral type, is the major factor controlling the source rock properties of humic coals.

- (2) The hydrocarbon generation potential expressed by HI shows a similar relationship to the petrographic composition as found in previous studies of Middle Jurassic humic coals from the Danish sector of the North Sea (Petersen *et al.* 1996, 1998). These results have thus been extended to cover humic coals that vary in petrographic composition, rank, age and geographical origin.
- (3) The most important single parameter for the HI and thus the hydrocarbon generation potential is collotelinite and not collodetrinite as generally believed, although collodetrinite still is important. Liptodetrinite, the liptinite maceral group and the microlithotype vitrinite also have a positive influence on HI, whereas inertinitic constituents have a negative influence, probably because these components act as diluents of petroleum-prone components. The rank shows only minor overall influence on the HI.
- (4) The E_a peak position is mainly controlled by the reflectance value (thermal maturity) and to a lesser extent by collotelinite. A number of vitrinitic constituents, however, tend to lower the E_a peak position, whereas liptinitic and inertinitic components are almost without influence.
- (5) The huminitic/vitrinitic reflectance (thermal maturity), collotelinite and the microlithotypes vitrinite and vitrinertite result in broader E_a distributions as measured as the width of the fitted Gauss curve. Liptinitic and inertinitic constituents, in particular the microlithotype clarodurite, narrow the E_a distribution.
- (6) These results reflect the compositional heterogeneity of humic coals and stress the importance of considering the compositional variability when evaluating the source rock potential of coal-bearing strata and when modelling the generation history of potential humic coal source rocks.

We would like to thank the Danish Energy Research Programme (grant no. 1313/98-0022) for the support. J. A. Bojesen-Koefoed (GEUS) and J. Ineson (GEUS) are thanked for constructive comments on the manuscript, and S. Solberg (GEUS) is thanked for technical support. *Petroleum Geoscience* reviewers B. Horsfield and H. J. Schenk are thanked for their valuable comments. The paper is published with the permission of the Geological Survey of Denmark and Greenland.

REFERENCES

- BERTRAND, P. R. 1989. Microfacies and petroleum properties of coals as revealed by a study of North Sea Jurassic coals. *International Journal of Coal Geology*, **13**, 575–595.
- BOJESEN-KOEFOED, J. A., CHRISTIANSEN, F. G., NYTOFT, H. P. & PEDERSEN, A. K. 1999. Oil seepage onshore West Greenland: evidence of multiple source rocks and oil mixing. In: Fleet, A. J. & Boldy, S. A. R. (eds) *Petroleum Geology of Northwest Europe: Proceedings of the 5th Conference*. The Geological Society, London, 305–314.
- BOREHAM, C. J., HORSFIELD, B. & SCHENK, H. J. 1999. Predicting the quantities of oil and gas generated from Australian Permian coals, Bowen Basin using pyrolytic methods. *Marine and Petroleum Geology*, **16**, 165–188.
- CADLE, A. B., CAIRNCROSS, B., CHRISTIE, A. D. M. & ROBERTS, D. L. 1993. The Karoo Basin of South Africa: type basin for the coal-bearing deposits of southern Africa. *International Journal of Coal Geology*, **23**, 117–157.
- CLAYTON, J. L., RICE, D. D. & MICHAEL, G. E. 1991. Oil-generating coals of the San Juan Basin, New Mexico and Colorado, U.S.A. *Organic Geochemistry*, **17**, 735–742.
- CLOSE, J. C. 1993. Natural fractures in coal. In: Law, B. E. & Rice, D. D. (eds) *Hydrocarbons from coal*. American Association of Petroleum Geologists Studies in Geology, **38**, 119–132.
- COOK, A. C. & STRUCKMEYER, H. 1986. The role of coal as a source rock for oil. In: Glenie, R. (ed.) *Second South-Eastern Australia Oil Exploration Symposium*. Petroleum Exploration Society of Australia, 419–429.
- DEMBICKI, H. Jr 1992. The effects of the mineral matrix on the determination of kinetic parameters using modified Rock Eval pyrolysis. *Organic Geochemistry*, **18**, 531–539.
- DURAND, B. & PARATTE, M. 1983. Oil potential of coals: a geochemical approach. In: Brooks, J. (ed.) *Petroleum Geochemistry and Exploration of Europe*. Geological Society London Special Publication, **12**, 255–264.
- FALCON, R. M. S. & SNYMAN, C. P. 1986. An introduction to coal petrography: atlas of petrographic constituents in the bituminous coals of southern Africa. *The Geological Society of South Africa Review Paper*, **2**.
- HUANG, D., ZHANG, D., LI, J. & HUANG, X. 1991. Hydrocarbon genesis of Jurassic coal measures in the Turpan Basin, China. *Organic Geochemistry*, **17**, 827–837.
- HUC, A. Y., DURAND, B., ROUCACHET, M., VANDENBROUCKE, M. & PITTON, J. L. 1986. Comparison of three series of organic matter of continental origin. *Organic Geochemistry*, **10**, 65–72.
- ICCP 1998. The new vitrinite classification (ICCP System 1994). *Fuel*, **77**, 349–358.
- ISAKSEN, G. H., CURRY, D. J., YEAKEL, J. D. & JENSSEN, A. I. 1998. Controls on the oil and gas potential of humic coals. *Organic Geochemistry*, **29**, 23–44.
- JARVIE, D. M. 1991. Factors affecting Rock-Eval derived kinetic parameters. In: Curiale, J. A., Alexander, R. & Brooks, P. W. (eds) *Organic geochemistry of hydrocarbon basins*. Chemical Geology, **93**, 79–99.
- KATZ, B. J., KELLEY, P. A., ROYLE, R. A. & JORJORIAN, T. 1991. Hydrocarbon products of coals as revealed by pyrolysis-gas chromatography. *Organic Geochemistry*, **17**, 711–722.
- KILLOPS, S. D., WOOLHOUSE, A. D., WESTON, R. J. & COOK, R. A. 1994. A geochemical appraisal of oil generation in the Taranaki Basin, New Zealand. *American Association of Petroleum Geologists Bulletin*, **78**, 1560–1585.
- KVALHEIM, O. M. & KARSTANG, T. V. 1987. A general-purpose program for multivariate data analysis. *Chemometrics and Intelligent Laboratory Systems*, **2**, 235–237.
- LAMBERSON, M. N., BUSTIN, R. M., KALKREUTH, W. D. & PRATT, K. C. 1996. The formation of inertinite-rich peats in the mid-Cretaceous Gates Formation: implications for the interpretation of mid-Albian history of paleowildfire. *Palaeogeography, Palaeoclimatology, Palaeoecology*, **120**, 235–260.
- LEWAN, M. D. 1994. Assessing natural oil expulsion from source rocks by laboratory pyrolysis. In: Magoon, L. B. & Dow, W. G. (eds) *The petroleum system – from source to trap*. American Association of Petroleum Geologists Memoir, **60**, 201–210.
- MARTENS, H. & NÆS, T. 1991. *Multivariate calibration*. John Wiley, New York.
- NOBLE, R. A., WU, C. H. & ATKINSON, C. D. 1991. Petroleum generation and migration from Talang Akar coals and shales offshore N.W. Java, Indonesia. *Organic Geochemistry*, **17**, 363–374.
- PELET, R. 1994. Comments on the paper 'The effects of the mineral matrix on the determination of kinetic parameters using modified Rock-Eval pyrolysis' by H. Dembicki Jr., *Org. Geochem.*, **18**, 531–539 (1992). *Organic Geochemistry*, **21**, 979–981.
- PEPPER, A. S. & CORVI, P. J. 1995. Simple kinetic models of petroleum formation Part I: oil and gas generation from kerogen. *Marine and Petroleum Geology*, **12**, 291–319.
- PETERSEN, H. I. & ROSENBERG, P. 1998. Reflectance retardation (suppression) and source rock properties related to hydrogen-enriched vitrinite in Middle Jurassic coals, Danish North Sea. *Journal of Petroleum Geology*, **21**, 247–263.
- , — & ANDSBJERG, J. 1996. Organic geochemistry in relation to the depositional environments of Middle Jurassic coal seams, Danish Central Graben, and implications for hydrocarbon generative potential. *American Association of Petroleum Geologists Bulletin*, **80**, 47–62.
- , ANDSBJERG, J., BOJESEN-KOEFOED, J. A., NYTOFT, H. P. & ROSENBERG, P. 1998. Petroleum potential and depositional environments of Middle Jurassic coals and non-marine deposits, Danish Central Graben, with special reference to the Søgne Basin. *Geology of Denmark Survey Bulletin*, **36**.
- SCHAEFER, R. G., SCHENK, H. J., HARDELAUF, H. & HARMS, R. 1990. Determination of gross kinetic parameters for petroleum formation from Jurassic source rocks of different maturity levels by means of laboratory experiments. *Organic Geochemistry*, **16**, 115–120.
- SCHENK, H. J. & HORSFIELD, B. 1998. Using natural maturation series to evaluate the utility of parallel reaction kinetics models: an investigation of Toarcian shales and Carboniferous coals, Germany. *Organic Geochemistry*, **29**, 137–154.
- SCOTT, A. C. & FLEET, A. J. 1994. *Coal and Coal-bearing Strata as Oil-prone Source Rocks?* Geological Society, London, Special Publication, **77**.
- STOUT, S. A. 1994. Chemical heterogeneity among adjacent coal microlithotypes – implications for oil generation and primary migration from humic coal. In: Scott, A. C. & Fleet, A. J. (eds) *Coal and Coal-bearing Strata as Oil-prone Source Rocks?* Geological Society, London, Special Publications, **77**, 93–106.
- TAYLOR, G. H., LIU, S. Y. & DIESSEL, C. F. K. 1989. The cold-climate origin of inertinite-rich Gondwana coals. *International Journal of Coal Geology*, **11**, 1–22.
- , TEICHMÜLLER, M., DAVIS, A., DIESSEL, C. F. K., LITKE, R. & ROBERT, P. 1998. *Organic petrology*. Gebrüder Borntraeger, Berlin.
- TEGELAAR, E. W. & NOBLE, R. A. 1994. Kinetics of hydrocarbon generation as a function of the molecular structure of kerogen as revealed by pyrolysis-gas chromatography. *Organic Geochemistry*, **22**, 543–574.
- TEICHMÜLLER, M. 1982. *Fluoreszenz von Liptiniten und Vitriniten in Beziehung zu Inkohlungsgrad und Verkokungsverhalten*. Geologisches Landesamt Nordrhein-Westfalen, Krefeld.
- TISSOT, B. P. & WELTE, D. H. 1984. *Petroleum formation and occurrence*. Springer-Verlag, Berlin.
- , PELET, R. & UNGERER, P. H. 1987. Thermal history of sedimentary basins, maturation indices, and kinetics of oil and gas generation. *American Association of Petroleum Geologists Bulletin*, **71**, 1445–1466.
- UNGERER, P. 1990. State of the art of research in kinetic modelling of oil formation and expulsion. *Organic Geochemistry*, **16**, 1–25.
- & PELET, R. 1987. Extrapolation of the kinetics of oil and gas formation from laboratory experiments to sedimentary basins. *Nature*, **327**, 52–54.
- WOLD, S. 1976. Pattern recognition by means of disjoint principal components model. *Pattern Recognition*, **8**, 127–139.
- 1978. Cross-validatory estimation of the number of components in factor and principal component model. *Technometrics*, **20**, 397–405.
- 1987. Principal component analysis. *Chemometrics and Intelligent Laboratory Systems*, **2**, 37–52.

COAL-GENERATED OIL: SOURCE ROCK EVALUATION AND PETROLEUM GEOCHEMISTRY OF THE LULITA OILFIELD, DANISH NORTH SEA

H. I. Petersen^{*,†}, J. Andsbjerg^{*}, J. A. Bojesen-Koefoed^{*} and H. P. Nytoft^{*}

Controversy still exists as to whether coals can source commercial accumulations of oil. The Harald and Lulita fields, Danish North Sea, are excellent examples of coal-sourced petroleum accumulations, the coals being assigned to the Middle Jurassic Bryne Formation. Although the same source rock is present at both fields, Lulita primarily contains waxy crude oil in contrast to Harald which contains large quantities of gas together with secondary oil/condensate. A compositional study of the coal seams at well Lulita-1Xc (Lulita field) was therefore undertaken in order to investigate the generation there of liquid petroleum.

Lulita-1Xc encountered six coal seams (0.15–0.25 m thick) which are associated with reservoir sandstones. The coals have a complex petrography dominated by vitrinite, with prominent proportions of inertinite and only small amounts of liptinite. Peat formation occurred in coastal-plain mires; the coal seams at Lulita-1Xc represent the waterlogged, oxygen-deficient and occasionally marine-influenced coastal reaches of these mires. Vitrinite reflectance values (mostly 0.82–0.84 %Ro) indicate that the coals are thermally mature. Most of the coal samples have Rock-Eval Hydrogen Index values above 220 mg HC/g TOC, although the HI values may be increased due to the presence of extractable organic matter. Oil–source rock correlations indicate that there are similarities between crude oil samples (and an oil-stained sandstone extract) from the Lulita field, and extracts from the Bryne Formation coals immediately associated with the reservoir sandstones; from this, we infer that the coals have generated the crude oil at Lulita. The presence in the coals of oil-droplets, exsudatinite and micrinite is further evidence that they have generated liquid petroleum. The generation of aliphatic-rich crude oil by the coals in the Lulita field area, and the coals' high expulsion efficiency, may have been facilitated by a combination of the coals' favourable petrographic composition and their capability to generate long-chain n-alkanes (C₂₂₊). Moreover, all the Lulita coal seams are relatively thin and this may have facilitated oil saturation to the expulsion threshold. We suggest that during further maturation of the coals, 19–22% of the organic carbon will potentially participate in petroleum-generation, of which about 42–53% will be in the gas-range and 47–58% in the oil-range.

^{*}Geological Survey of Denmark and Greenland, Thoravej 8, DK-2400 Copenhagen NV, Denmark.

[†]corresponding author (email: hip@geus.dk)

INTRODUCTION

The Søgne Basin in the Danish North Sea (Fig. 1) contains two commercial oilfields, *Harald* and *Lulita* (Fig. 2). The *Harald* field has separate reservoirs in Upper Cretaceous/Danian chalk (*Harald East*) and Middle Jurassic Bryne Formation sandstones (*Harald West*) (Fig. 2). The structure at *Harald East* is related to displacement of the chalk above a salt diapir, whereas that at *Harald West* is formed by a tilted Jurassic fault block. The reservoirs contain primary gas and secondary condensate/crude oil, and expected recoverable reserves are currently estimated to be 18.2 billion Nm³ (643 billion ft³) of gas and 5.5 million m³ (34.6 million bbl) of crude oil/condensate (Danish Energy Agency, 1999).

Oil/condensate tests from wells in the *Harald* field have a clearly terrestrial organic-geochemical signature which is very similar to that of extracts of coals from the Middle Jurassic Bryne Formation; detailed maturity and compositional studies have demonstrated that the coals are the source rock for this petroleum accumulation (Petersen *et al.*, 1996, 1998). The *Lulita* field is located to the east of *Harald*, and consists of a fault-created structural trap where Middle Jurassic Bryne Formation sandstones are the reservoir (Fig. 2). Reserves at *Lulita* are much smaller than those at *Harald* and have recently been downgraded from expected recoverable reserves of 2 million m³ (12.6 million bbl) oil and 1 billion Nm³ (35 billion ft³) gas to 0.3 million m³ (1.9 million bbl) crude oil and 0.3 billion Nm³ (11 billion ft³) gas (Danish Energy Agency, 1998, 1999). Thus, in contrast to the primary gas accumulations at *Harald*, the *Lulita* accumulation consists of waxy crude oil with an overlying gas cap.

With the exception of some suppressed values (Petersen and Rosenberg, 1998), coals from wells *West Lulu-1*, *-2*, and *-3* and *Lulu-1* yield vitrinite reflectance values of 0.81–0.89 %R_o, which conventionally indicate a thermal maturity corresponding to peak oil generation within the oil window. However, Price (1991) suggested that the oil window for coal commences by 0.8 %R_o and ends by approximately 1.6–2.0 %R_o; therefore, the Bryne Formation coals may only just have entered the petroleum generating phase. This would be consistent with pyrolysis experiments demonstrating that the coals are still capable of generating considerable amounts of liquid petroleum upon further maturation. This includes well *Amalie-1* (about 11 km south of *Lulu-1*), where the coals are buried to a depth of about 5 km and accordingly yield vitrinite reflectance values of 1.3 %R_o.

Multivariate regression analyses have shown that the petroleum generation potential of the Bryne Formation coals can be positively correlated to the presence of vitrinitic macerals (particularly telinite and collotelinite); a recent study has shown that this correlation seems to be valid for humic coals world-wide independent of age or maturity (Petersen and Rosenberg, *in press*). Other studies have indicated that the expulsion of generated crude oil from coals may be facilitated by the presence of specific microlithotypes (i.e. associations of macerals); by the large amounts of gases generated by the coals (primary HC migration in gaseous solution); and by the ability of the coals to generate long-chain *n*-alkanes (e.g. Durand and Paratte, 1983; Bertrand, 1989; Price, 1991; Stout, 1994; Isaksen *et al.*, 1998). However, controversy still exists as to whether coals can generate commercial quantities of crude oil.

A detailed organic petrographic and geochemical study of the coals in the Søgne Basin was therefore considered to be desirable and in this context the nature of the coals in the *Lulita* field is clearly of great interest. This study focuses on the analysis of Bryne Formation seams at well *Lulita-1Xc* (*Lulita* field) and of *Lulita* oils in order to: (1) investigate why the *Lulita* field, in contrast to the *Harald* field, is oil-dominated; (2) understand why the coals expelled oil; and (3) establish an oil–source rock correlation.

GEOLOGICAL SETTING

The Søgne Basin is situated in the NE of the Danish Central Graben, which is part of the Mesozoic Central Graben rift system (Fig. 1). Differential subsidence in the Danish Central

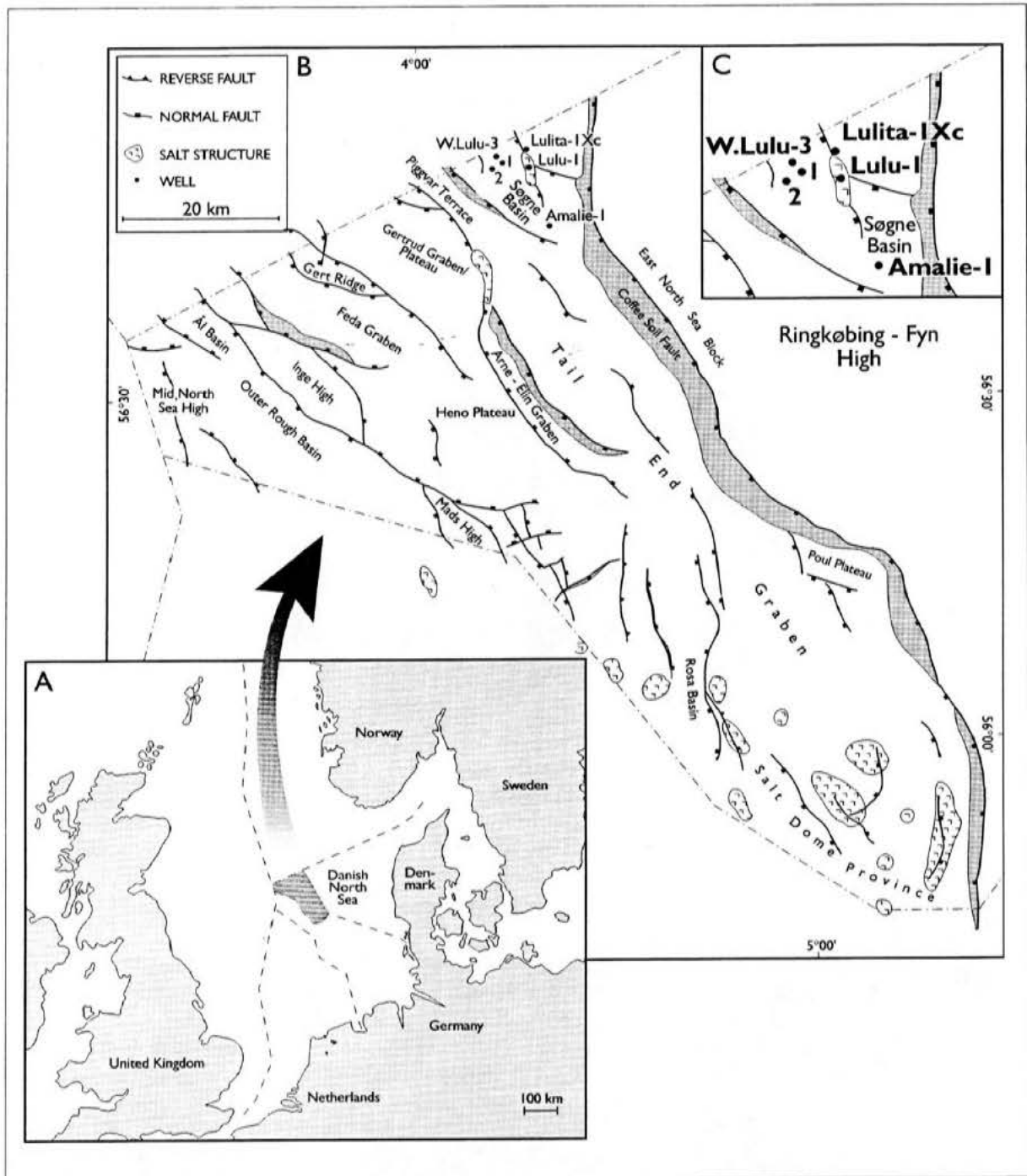


Fig. 1(a). Location of the Danish Central Graben in the North Sea. **(b).** Structural map of the Danish Central Graben with the Søgne Basin in the NE corner. **(c).** Map of the Søgne Basin with the location of the West Lulu-1, -2, and -3 and Lulu-1 wells in the Harald field, and the Lulita-IXc well in the Lulita field.

Graben along north-south and NW-SE trending faults started during the Middle Jurassic, and the Søgne Basin and the Tail End Graben began to subside as separate half-grabens (Gowers and Sæbøe, 1985; Møller, 1986). Asymmetric subsidence in the Søgne Basin was connected with Middle Jurassic boundary fault activity, especially along segments of the Coffee Soil Fault (e.g. Gowers and Sæbøe, 1985; Møller, 1986; Cartwright, 1991; Korstgård et al., 1993).

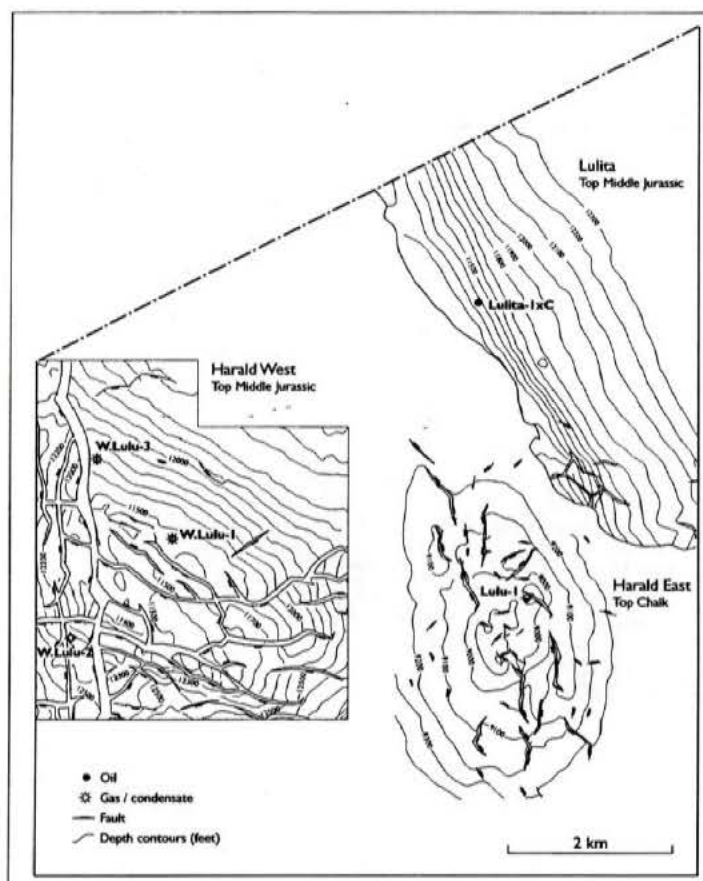


Fig. 2. Structural outline of reservoirs in the *Harald* field (comprising *Harald West* and *Harald East*) and the *Lulita* field in the Søgne Basin (slightly modified from Danish Energy Agency, 1999). Note the locations of the wells referred to in this study.

Middle Jurassic sandstones with interbedded mudstones and coals in the northern part of the Danish Central Graben are included in the Upper Bajocian to Upper Callovian/lowermost Oxfordian Bryne Formation (Fig. 3) (Jensen *et al.*, 1986; Andsbjerg and Dybkjær, 1997), and were first encountered by the *Lulu-1* well (Figs. 1 and 2). The Bryne Formation is 130- to 300-m thick in wells in the Danish part of the Søgne Basin; it wedges-out on structural highs, and may be thicker in the deepest parts of the basin. The formation is divided by a sequence boundary into a fluvial-dominated lower part, and a paralic- and marginal-marine dominated upper part (Andsbjerg, 1997; Andsbjerg and Dybkjær, 1997). The lower part corresponds to sequence *Bat-1A* according to the sequence-stratigraphic model of Andsbjerg (1997). The coal seams are mostly present in the upper part, consisting of the sequences *Cal-1A* and *Cal-1B* of Andsbjerg (*ibid.*). Marine influences increase upwards through the Bryne Formation, and the coal-bearing upper parts are overlain by marine deposits from which they are separated by a sequence boundary.

PALAEOGEOGRAPHY AND COAL SEAM FORMATION

The coals in the Bryne Formation comprise nine separate seams (from the base: T1, R1, R1a, T2, T2a, X, R2, T3 and T4). These vary in thickness from more than 1 m to less than 0.1 m, and in areal extent from local to regional. The areally-extensive R1 and T4 seams are present throughout most of the Søgne Basin (Petersen *et al.*, 1998) (Figs. 4a and 5d). The precursor mire of the T2 seam was also relatively extensive (Fig. 5a), but peat formation was temporarily hindered in the *Lulita-1Xc*–*Lulu-1* area due to flooding from the north (Fig. 5b).

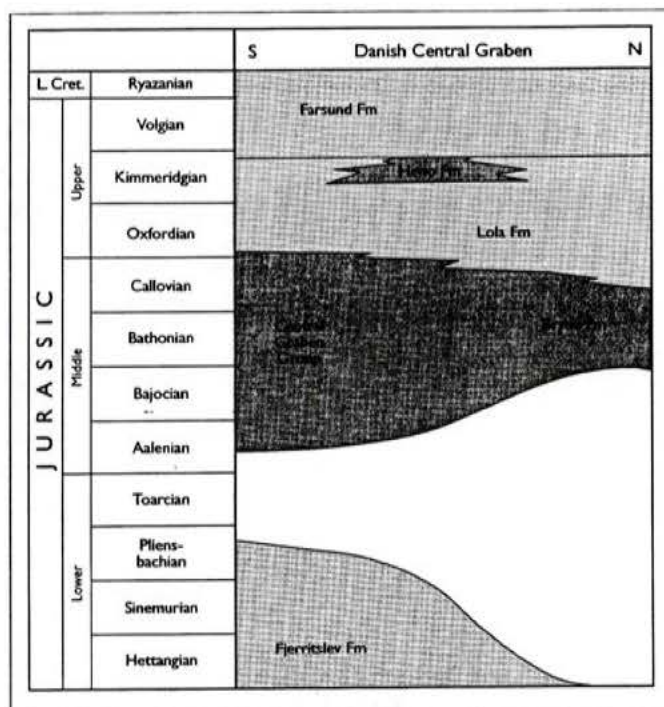


Fig. 3. Jurassic stratigraphy of the Danish Central Graben (after Andsbjerg, 1997). Middle Jurassic deposits in the Søgne Basin are assigned to the Bryne Formation; the coal-bearing interval is of Late Bathonian to Callovian age.

The thickest coal seams and the cumulatively greatest thickness of coal (up to 5.05 m) occur in the area of wells *West Lulu-1*, -2 and -3 landward of an approximately north-south trending palaeo-coastline close to, and parallel with, the *Amalie-1*, *Lulu-1*, and *Lulita-1Xc* wells. Precursor peats were deposited on coastal plains, and the coals are generally interbedded with fluvial/estuarine channel, lagoonal, tidal-influenced channel and shoreface deposits (Petersen and Andsbjerg, 1996; Petersen *et al.*, 1996, 1998) (Fig. 6). All the coal seams are part of transgressive systems tracts, and peat formation was largely controlled by rises in water table caused by rises in relative sea-level. The R-seams were formed during a slower rise in relative sea-level, whereas the T-seams were formed during a comparatively fast rise in relative sea-level which favoured a stable and high-standing water table and a stronger marine influence during peat formation.

The coastal reaches of all the peat mires were generally subjected to prolonged and continuous waterlogging, while more landward areas were prone to more subtle water-table fluctuations. Slight doming of the peat surface may occasionally have occurred. The mires' coastal reaches were most exposed to marine influences, which have been detected (e.g. by increased proportions of C_{27} steranes and the presence of C_{30} steranes) for all coal seams towards the palaeo-coastline (Petersen *et al.*, 1998). In agreement with this depositional scenario, interbedded shoreface and offshore deposits are more common towards the palaeo-coastline (in the *Amalie-1*, *Lulu-1* and *Lulita-1Xc* wells) (Fig. 6).

The differing depositional conditions for the peats had a considerable impact on the resulting organic geochemical and petrographic composition — and source rock potential — of coals in the *Harald* field (Petersen *et al.*, 1996, 1998). In general, T-seam coals comprise better source rocks than do R-seams coals. In addition, those parts of a coal seam representing the coastal reaches of the precursor peat mire, in which marine influence and waterlogging were most pronounced, have a higher generative potential than do more landward parts.

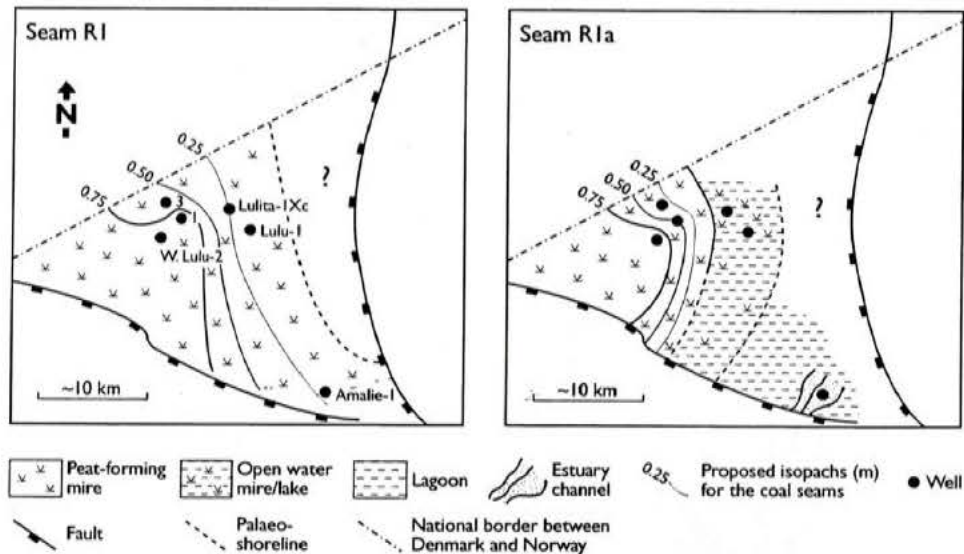


Fig. 4a and b. Palaeogeographic maps showing the areal extent of the precursor mires for the R1 and R1a coal seams. Although flooding of the precursor peat for the R1 seam occurred at the *West Lulu-1* and *West Lulu-3* locations, peat development continued without any interruption at *West Lulu-2*. A resumption of peat accumulation at *West Lulu-1* and *-3* led to the development of the precursor for seam R1a. (Slightly modified from Petersen *et al.*, 1998).

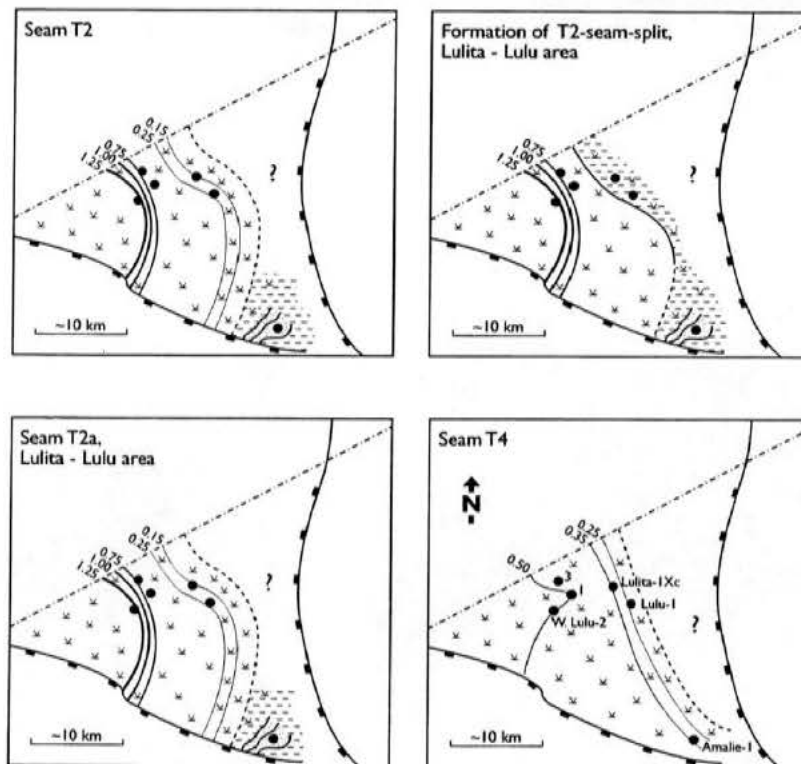


Fig. 5a-d. Palaeogeographic maps showing the areal extent of the precursor mires for the T2, T2a and T4 coal seams. Also shown (5b) is the interval between deposition of the precursor peats for the T2 and T2a seams in the *Lulita-1Xc* and *Lulu-1* area, during which flooding from the north temporarily hindered peat formation; this flooding is preserved as a siliciclastic band splitting seam T2 into two. During deposition of this seam-split and the following precursor peat for the T2a seam, the precursor peat for seam T2 continued to form without any interruption in the area of the *West Lulu* wells. (Modified from Petersen *et al.*, 1998).

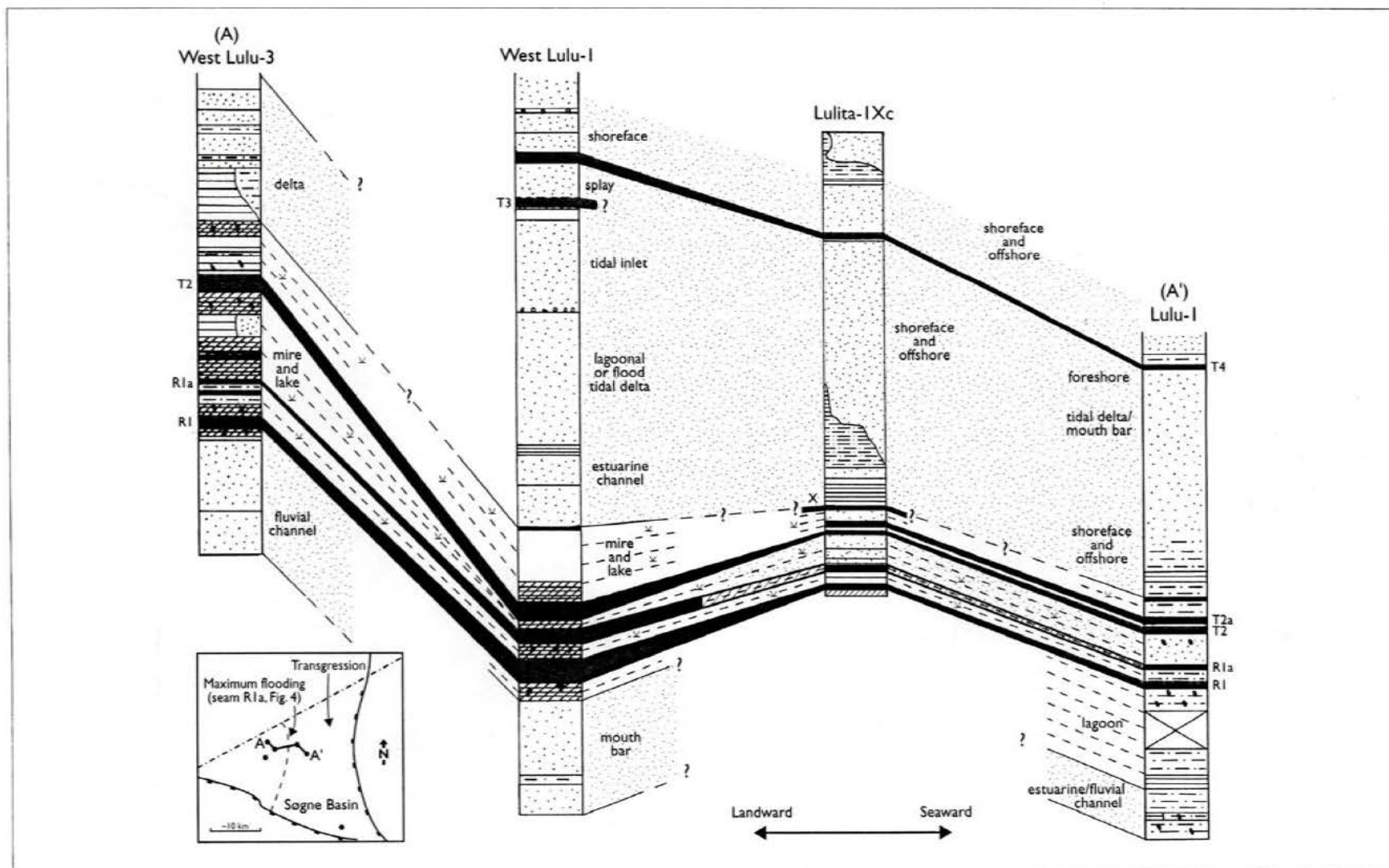


Fig. 6. Correlation (not to scale) of the *West Lulu-3*, *West Lulu-1*, *Lulita-1Xc* and *Lulu-1* wells. Marine sediments are dominant in the *Lulita-1Xc* and *Lulu-1* wells, which are located closer to the palaeo-coastline. The insert map indicates that flooding was from the north and that the most extensive flooding occurred during accumulation of the precursor peat for the R1a seam.

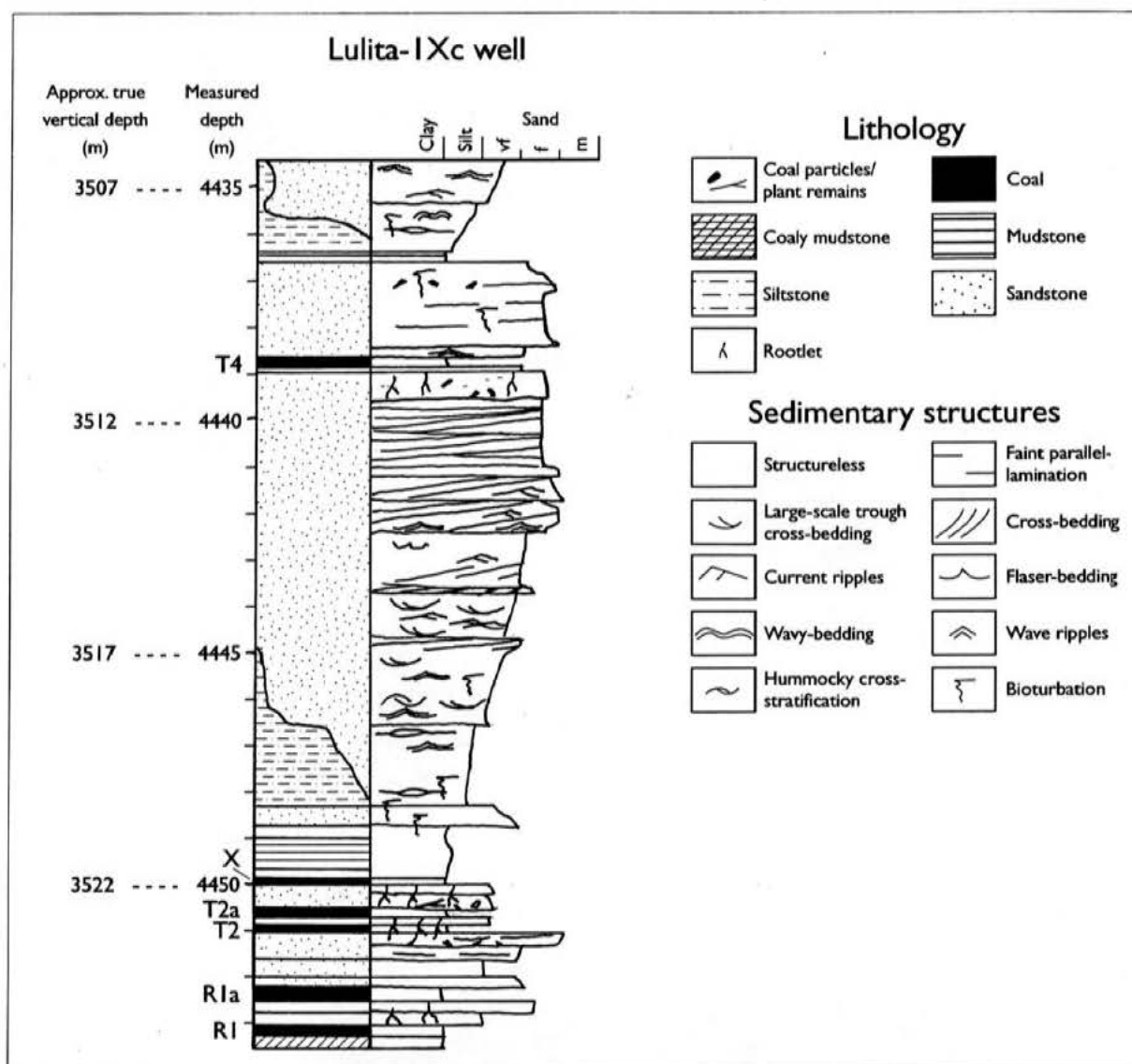


Fig. 7. Sedimentological log of the coal-bearing interval of the *Lulita-1Xc* well.

SEDIMENTOLOGY OF THE COAL-BEARING INTERVAL AT THE LULITA-1XC WELL

Lulita-1Xc is a cored, deviated sidetrack of the *Lulita-1* well, and contains six coal seams in the interval corresponding to sequences *Cal-1A* and *Cal-1B* (Fig. 7). Five of the seams (R1, R1a, T2, T2a, X) occur in a single zone between depths of about 4,450 m and 4,454 m, corresponding to a true vertical depth of about 3,524 m. A carbonaceous mudstone, approximately one-metre thick, and representing a restricted marine environment overlies seam X. Above this mudstone is an 0.4-m thick, upward-fining, strongly bioturbated, massive to heterolithic sandstone representing a transgressive sand-sheet; this is overlain by 0.75-m of bioturbated offshore mudstones that become increasingly heterolithic with abundant sand lenses and laminae upwards. The succession continues with approximately 1.5 m of heterolithic, very fine-grained sandstone showing wave ripples, hummocky cross-stratification and some bioturbation, and approximately 4 m of upward-coarsening, mainly very fine-grained sandstone with poorly defined low-angle cross-bedding with trough cross-bedded and ripple cross-

Table 1.
Core samples collected from the Lulita-1Xc well.

Sample no.	Measured depth* (m)	Material/Coal seam	Interval in coal seams (m)
736	4436.44 – 4436.47	carb. mudstone (c. 0.08 m)	-
737	4438.65 – 4438.70	seam T4 (c. 0.23 m)	0.18 – 0.23
738	4438.70 – 4438.78		0.10 – 0.18
739	4438.78 – 4438.83		0.05 – 0.10
740	4438.83 – 4438.88		0.00 – 0.05
742	4449.72 – 4449.78	seam X (0.21 m)	0.15 – 0.21
743	4449.78 – 4449.83		0.10 – 0.15
744	4449.83 – 4449.88		0.05 – 0.10
745	4449.88 – 4449.93		0.00 – 0.05
746	4450.54 – 4450.60	seam T2a (c. 0.15 m)	0.09 – 0.15
747	4450.60 – 4450.64		0.05 – 0.09
748	4450.64 – 4450.69		0.00 – 0.05
749	4450.84 – 4450.88	seam T2 (c. 0.15 m)	0.11 – 0.15
750	4450.88 – 4450.94		0.05 – 0.11
751	4450.94 – 4450.99		0.00 – 0.05
752	4452.21 – 4452.44	seam R1a (0.23 m)	0.00 – 0.23
753	4453.00 – 4453.25	seam R1 (0.25 m)	0.00 – 0.25
754	4506.93 – 4506.98	carbonaceous mudstone	-
755	4506.98 – 4507.03	coal/carb. mudstone	-
756	4507.03 – 4507.26	carbonaceous mudstone	-
757	4507.43 – 4507.51	coaly mudstone	-
758	4507.51 – 4507.76	carbonaceous mudstone	-
759	4507.76 – 4508.25	coal (sample 1)	-
760	4507.76 – 4508.25	coal (sample 2)	-
741	4439.72	oil-stained sandstone	-

*True vertical depth is approximately 928 m lower than measured depth

laminated intervals. The heterolithic sandstone and upward-coarsening sandstone represent the offshore transition and lower shoreface, respectively.

The lower shoreface succession is erosively overlain by 2.8 m of low-angle cross- and parallel-bedded, fine- to medium-grained sandstone occurring mainly as upward-fining beds. This part of the succession is interpreted to represent upper shoreface and beach deposits, and is separated from coal seam T4 by 0.6-m of thoroughly rooted sandstone, probably representing a barrier environment. The complete succession between R1 and T4 represents a transgressive-regressive cycle of shelf deposition overlain by a prograding shoreface terminated by beach and barrier deposits. The sandstones between seams X and T4 are dark and have a strong petroleum odour resulting from crude oil-staining.

SAMPLES AND ANALYTICAL METHODS

A total of 25 drill-core samples were collected from floor to roof (channel samples) from the coal seams (such that the samples represent the total thickness of the seams) and associated carbonaceous mudstones of the *Lulita-1Xc* well (Table 1). The upper sample suite (753–736) comprises coal seams R1 to T4 and an overlying mudstone, which are assigned to the paralic/marginal-marine *Cal-1A* and *-1B* sequences. The lower sample suite (754–760) were taken from the underlying, fluvial-dominated *Bat-1a* sequence.

Samples were crushed to a grain size of 63 μm to 1 mm and embedded in epoxy, the preparation procedure taking into account the grain size as well as density-induced particle separation.

Table 2.
Maceral types, derivation and generative potential.

	Maceral types	Derivation	Generative potential*
Vitrinite group	Telinite	Derived from woody	++
	Collotelinite	plant tissues	+++
	Collodetrinite	composed of	++
	Gelinite	lignin and cellulose	+
	Corpogelinite		+
Inertinite group	Fusinite	Formed by charring	n.i.
	Semifusinite	or oxidation of	n.i.
	Macrinite	organic matter of	n.i.
	Inertodetrinite	diverse origin	n.i.
	Char		n.i.
Liptinite group	Sporinite	Originate from H-rich	++
	Cutinite	plant materials such	++
	Resinite	as spores/pollen,	++
	Alginite	resins and algae	+++
	Liptodetrinite		++
Generation products	Exsudatinite	Constituents related	-
	Micrinite	to petroleum generation	-
	Oil-droplets	during maturation	-

*Relative positive influence on the generation potential based on the studies by Petersen *et al.* (1998) and Petersen and Rosenberg (*in press*).
n.i.: no importance or negative influence

Petrographic analyses

Polished particulate mounts suitable for reflected light microscopy in oil immersion were prepared from 16 coal and carbonaceous mudstone samples. Vitrinite reflectance ($\%R_o$) measurements (random) were carried out on the vitrinite maceral collotelinite by means of a *Leitz MPV-SP* system and *Leica MPVGEOR* software following the standards outlined by Taylor *et al.* (1998). Maceral and microlithotype (20-point eyepiece reticule) analyses were conducted in combined reflected white light and fluorescence-inducing blue light using a Zeiss incident light microscope and a Swift point counter. Five hundred macerals and 500 microlithotypes were counted per sample. Procedures for maceral and microlithotype identification followed ICCP (1998) and Taylor *et al.* (1998).

The maceral types and generation products recorded in this study are listed in Table 2, together with their botanical derivation and also their relative importance in terms of petroleum generation based on studies of the Bryne Formation coals and of world-wide vitrinite-rich ('humic') coals (Petersen *et al.*, 1998; Petersen and Rosenberg, *in press*). The relatively minor importance of the liptinite macerals is due to their low abundances in the Bryne Formation coals. Micrinite and exsudatinite are so-called 'secondary' macerals formed during maturation and are taken to indicate petroleum generation.

Microlithotypes

Associations of macerals are referred to as "microlithotypes", and the microlithotypes *vitrite*, *liptite* and *inertite* contain not less than 95% of vitrinite (V), liptinite (L) and inertinite (I) respectively. *Clarite*, *durite* and *vitrinertite* are bimaceralic microlithotypes and in clarite, $V+L > 95\%$, in durite $I+L > 95\%$, and in vitrinertite $V+I > 95\%$.

Table 3.
Maceral composition (vol.%) and vitrinite reflectance values.

Sample no.	Seam	Interval (m)	T+ Ct — vitrinite —	Cd	G+ Co	Lipt	F+ Sf — inertinite —	In	Ma	Py	Min	%R _o
736	-	-	42.4	24.2 ¹	3.6	6.0 ²	0.2	2.2	0.0	3.0	18.4 ³	-
737	T4	0.18–0.23	48.4	35.8	8.4	1.4	1.6	3.6	0.4	0.0	0.4	-
738		0.10–0.18	52.0	29.0	9.0	4.4	1.2	3.6	0.6	0.0	0.2	-
739		0.05–0.10	22.6	24.4	2.6	8.2	11.8	21.6	6.6	0.6	1.6	-
740		0.00–0.05	24.6	29.0	4.2	3.0	14.4	17.2	5.2	0.4	2.0	-
742	X	0.15–0.21	34.6	27.8	4.2	4.0	9.6	15.4	4.2 ⁴	0.0	0.2	-
743		0.10–0.15	34.8	20.6	6.4	1.8	19.8	12.2 ⁵	3.6	0.0	0.8	0.82
744		0.05–0.10	27.0	29.8	3.6	5.0	7.2	22.6	3.4	0.0	1.4	-
745		0.00–0.05	30.4	36.0	4.4	7.8	3.6	15.0	1.2	0.0	1.6	0.82
746	T2a	0.09–0.15	24.6	20.4	2.6	5.4	8.4	26.4	8.8	1.6	1.8	-
747		0.05–0.09	28.2	38.8	4.8	4.8	4.2	15.2	3.4	0.2	0.4	0.75
748		0.00–0.05	38.6	29.4	4.2	2.2	2.6	14.4	4.0	0.2	4.4	-
749	T2	0.11–0.15	65.2	19.6	10.4	0.0	0.2	2.0	0.0	0.2	2.4	0.84
750		0.05–0.11	14.0	32.4	4.8	2.8	6.4	30.6	5.6	0.8	2.6	0.83
751		0.00–0.05	22.6	39.0	8.6	2.6	6.6	15.2	3.0	0.4	2.0	-
753	RI	0.00–0.25	19.2	37.4	5.4	4.8	4.0	17.2	4.6	0.8	6.6	0.83

T+Ct: telinite+collotelinite; Cd: collodetrinite; G+Co: gelinite+corpogelinite;

Lipt: liptinite; F+Sf: fusinite+semifusinite; In: inertodetrinite; Ma: macrinite;

Py: pyrite; Min: other minerals

¹includes vitrodetrinite

²includes 0.6 vol.% alginite

³includes 2.8 vol.% fluorescing mineral matter

⁴includes 0.4 vol.% naturally-formed char

⁵includes 0.4 vol.% micrinite

Duroclarite, *clarodurite* and *vitrinertoliptite* are trimaceralic microlithotypes and all maceral groups are represented by more than 5%. In *duroclarite* V > I, L; in *clarodurite* I > V, L; and in *vitrinertoliptite* L > I, V. *Carbominerite* contains between 20 and 60% minerals (or between 5 and 20% where the mineral is pyrite).

Vitrite, clarite and *duroclarite* are positively related to the generative potential of the Bryne Formation coals (Petersen et al., 1998), but in addition microlithotypes may influence the expulsion efficiency of coals (Durand and Paratte, 1983; Bertrand, 1989; Stout, 1994).

Organic geochemical analyses

All samples were analysed for total organic carbon (TOC) content by combustion in a *LECO IR-212* induction furnace, and pyrolysed on a *Vinci Rock-Eval 5* instrument. In addition, fourteen solvent-extracted samples were analysed for TOC content by means of a *LECO CS-200* induction furnace and pyrolysed in a *Vinci Rock-Eval 6* instrument. Samples for TOC determination were treated with HCl to remove carbonate-bonded carbon before combustion.

A total of 15 samples were solvent-extracted by means of CH₂Cl₂/CH₃OH (93 vol./7 vol.), and the solvent-extract's asphaltenes were precipitated by addition of 40-fold *n*-pentane. The remaining maltenes were separated into saturated and aromatic hydrocarbons (HCs) and heteroatomic compounds, and the saturated HC fractions were analysed by gas chromatography (GC) by means of a *Hewlett Packard 5890* gas chromatograph fitted with a 25 m HP-1 WCOT column and flame ionisation detection (FID). Additionally, the saturated HC fractions were analysed by selected ion monitoring (m/z 191, m/z 217, m/z 218) gas chromatography/mass

Table 4.
Microlithotype composition (vol. %).

Sample no.	Seam	Interval (m)	V	L	I	Cl	D	Vitrn	Ducl	Cldu	VitrI	Carb
737	T4	0.18–0.23	65.3	0.0	2.7	8.6	0.0	14.5	7.8	0.0	0.0	1.1
738		0.10–0.18	61.5	0.0	1.3	19.3	0.4	7.4	9.5	0.4	0.0	0.2
739		0.05–0.10	19.9	0.2	15.4	8.9	4.9	19.0	13.1	14.2	0.0	4.4
740		0.00–0.05	23.0	0.0	19.4	0.9	1.1	33.7	10.9	5.2	0.0	5.8
742	X	0.15–0.21	35.3	0.2	10.5	2.1	0.0	27.1	16.5	7.9	0.2	0.2
743		0.10–0.15	35.9	0.0	24.1	3.8	0.0	24.3	8.2	2.9	0.0	0.8
744		0.05–0.10	23.3	0.0	4.4	0.6	0.6	32.6	19.6	15.2	0.8	2.9
745		0.00–0.05	33.0	0.2	1.3	3.8	0.0	19.0	31.5	5.8	0.2	5.2
746	T2a	0.09–0.15	23.4	0.4	14.1	0.6	2.7	17.3	9.2	17.3	0.0	15.0
747		0.05–0.09	34.3	0.2	5.4	3.1	0.2	27.8	20.9	5.0	0.2	2.9
748		0.00–0.05	47.3	0.0	4.9	1.3	2.4	19.5	5.6	7.7	0.2	11.1
749	T2	0.11–0.15	83.1	0.0	0.2	0.4	0.0	10.0	2.3	0.2	0.0	3.8
750		0.05–0.11	21.6	0.2	12.1	1.2	2.7	37.5	7.0	10.3	0.0	7.4
751		0.00–0.05	35.4	0.0	8.3	1.9	0.2	35.6	7.6	5.7	0.0	5.3
753	R1	0.00–0.25	29.5	0.0	7.0	2.5	0.2	31.5	8.9	4.1	0.0	16.3

V: vitrite; L: liptite; I: inertite; Cl: clarite; D: durite; Vitrn: vitrinertite; Ducl: duroclarite; Cldu: clarodurite; VitrI: vitrinertoliptite; Carb: carbominerite+minerals

spectrometry (GC/MS) using a *Hewlett Packard 5890* series II gas chromatograph equipped with a 25 m HP-5 WCOT column and coupled to a *Hewlett Packard 5971A* quadrupole mass spectrometer. The saturated HC fraction of two *Lulita* oil-samples were likewise analysed by GC and GC/MS.

Two solvent-extracted coal samples (743, 749) were subjected to temperature programmed pyrolysis-gas chromatography (Py-GC) using a custom-made pyrolysis unit coupled to a *Hewlett Packard 5890A* gas chromatograph equipped with a 50 m Chrompack CP-Sil-8CB WCOT column and FID. The pyrolysis unit and the column were joined by 1 m of pre-column used for cold trapping of effluents in liquid nitrogen prior to chromatography. Gas-range (C_{1-5}) and oil-range (C_{6+}) components were determined by the construction of a horizontal baseline on blank-subtracted pyrograms at zero-level before elution of the C_1 peak, and splitting the integrated pyrogram into a gas and oil fraction (Pepper and Corvi, 1995).

RESULTS

Organic petrography

Maceral compositions and vitrinite reflectance measurements for the 16 coal and mudstone samples analysed are given in Table 3; the maceral compositions (mineral matter free: m.m.f.) are plotted in Fig. 8. Table 4 shows the coal samples' microlithotype compositions.

With the exception of sample 747 which yielded a vitrinite reflectance value of 0.75 % R_o , reflectance values lie between 0.82 % R_o and 0.84 % R_o (Table 3), indicating a high volatile bituminous B rank for the coals.

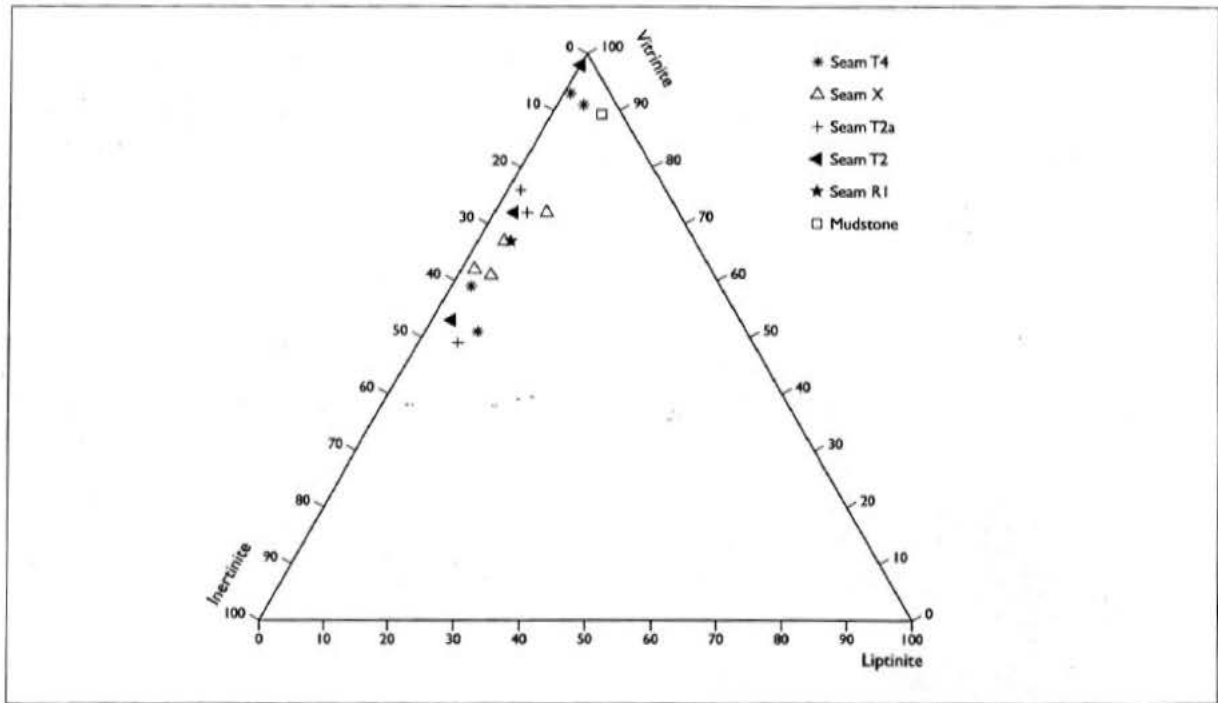


Fig. 8. Maceral group composition (vol.%, mineral matter free) of the coal seams and a carbonaceous mudstone from *Lulita-IXc*. The coals and mudstone are dominated by vitrinite, but contain a prominent proportion of inertinite. The liptinite content is generally low.

Coal seam R1

Sample 753 from the 0.25-m thick R1 seam is dominated by vitrinite (67 vol.%, mineral matter free (m.m.f.)), and has a prominent proportion of inertinite (28 vol.%, m.m.f.) but a low content of liptinite (Fig. 8). Most of the vitrinite and inertinite is composed of detrital macerals, e.g. collodetrinite, inertodetrinite and macrinite particles (Table 3). The sample's microlithotype composition (Table 4) is dominated by vitrite and vitrinertite; the rather high content of carbominerite is due to a mineral content of 6.6 vol.% (Table 3).

Coal seam T2

The lower and (in particular) upper parts of this 0.15-m thick seam are characterised by a large amount of vitrinite (up to 98 vol.%, m.m.f.), whereas the middle part contains a very high content of inertinite (44 vol.%, m.m.f.) (Fig. 8; Table 3). The liptinite content is low. Collodetrinite dominates the vitrinite maceral group in the lower to middle part of the seam, while telinite+collotelinite are very abundant in the upper part (Table 3).

Gelinite+corpogelinite are abundant constituents in the lower and upper parts of seam T2. The inertinite is mainly composed of inertodetrinite, but fusinite, semifusinite, and macrinite (the latter sometimes occurring as large, massive particles) are common (Table 3; Plate 1a, b - see page 87). Naturally-formed char also occurs (Plate 1c). The mineral matter and pyrite content are low (Table 3). The microlithotype composition (Table 4) shows a very high amount of vitrite in the top of the seam, and significant amounts of vitrinertite and inertite in the lower and middle parts.

Table 5.
Screening data.

Screening data.							
Sample	Seam	TOC (wt.%)	T _{max} (°C)	S ₁ S ₂		HI	HI _{extr} *
				(mg HC/g rock)			
736	-	39.31	431	10.39	135.38	344	-
737	T4	78.73	442	13.58	184.86	235	199
738		75.20	433	15.48	206.90	275	225
739		76.27	437	16.21	168.44	221	210
740		78.16	435	20.28	157.50	202	-
742	X	64.31	436	19.00	187.90	292	-
743		75.20	435	18.70	195.18	260	190
744		83.04	436	15.71	172.76	208	197
745		75.94	435	13.50	180.34	237	-
746	T2a	68.53	435	15.40	158.60	231	180
747		75.94	435	16.80	191.80	253	208
748		64.85	439	13.28	148.80	229	-
749	T2	83.53	437	14.85	190.38	228	208
750		74.75	438	16.73	135.88	182	170
751		66.18	436	15.53	170.74	258	-
752	R1a	37.86	438	7.39	73.68	195	174
753	R1	56.86	436	12.13	124.78	219	165
754	-	20.97	437	2.47	40.08	191	-
755	-	44.41	434	6.37	102.74	231	191
756	-	15.15	435	2.32	29.68	196	-
757	-	38.24	434	6.30	77.92	204	160
758	-	11.35	438	1.31	13.92	123	-
759	-	64.22	435	10.87	161.64	252	214
760	-	57.75	439	7.74	111.26	193	-

* HI_{extr}: Hydrogen Index of solvent extracted samples

Coal seam T2a

Seam T2a, 0.15-m thick, is dominated by vitrinite but contains much inertinite, particularly in the upper part (45 vol.%, m.m.f.) (Fig. 8; Table 3). The liptinite content does not exceed 6 vol.% (m.m.f.). Except for the middle part of the seam, telinite+collotelinite dominate over collodetrinite (Table 3). Inertodetrinite dominates the inertinite group (Table 3) and it often exhibits a faint microlamination, imparting an allochthonous appearance to the particles. In the middle interval of the seam, exsudatinite and micrinitised sporinite are present. In general, the mineral matter content is low (Table 3), and the upper part of the seam contains framboidal and massive pyrite. In terms of microlithotypes (Table 4), vitrite decreases up through the seam. The middle part contains significant amounts of vitrinertite and duroclarite, whereas the high inertinite content in the upper part accounts for the high contents of both inertite and clarodurite.

Coal seam X

This seam, which is 0.21-m thick, is dominated by vitrinite (up to 72 vol.%, m.m.f.), but contains significant amounts of inertinite (up to 36 vol.%, m.m.f.), especially in the middle part of the seam (Fig. 8; Table 3). The liptinite content reaches nearly 8 vol.% in the basal part (Table 3). In the lower half of the seam, the vitrinite maceral group is dominated by collodetrinite, whereas telinite+collotelinite dominates the upper half (Table 3). Inertodetrinite is generally the characteristic inertinite maceral, but the 0.10–0.15 m interval (sample 743) has a very high content of fusinite and semifusinite (Table 3). The inertodetrinite commonly occurs together with liptodetrinite and has a typical microlaminated allochthonous appearance. Very large, naturally-formed char particles were observed (Plate 2). During fluorescence-

Table 6.
Extract yields, GC and GC/MS data.

Sample	Seam	Extract yield (mg SOM/g OC)	Pr/Ph	Steranes			
				29 $\alpha\alpha\alpha$ 20S/(20S+20R)	% $\alpha\beta\beta$ C ₂₇	% $\alpha\beta\beta$ C ₂₈	% $\alpha\beta\beta$ C ₂₉
737	T4	36.4	2.88	0.48	37.2	27.4	35.4
738		32.1	3.15	0.47	36.7	27.6	35.7
739		31.2	2.92	0.47	34.7	27.5	37.7
743	X	51.2	3.38	0.47	26.9	26.2	47.0
744		26.7	4.13	0.44	24.4	24.7	50.9
746	T2a	39.5	4.03	0.46	29.1	26.1	44.8
747		36.3	4.23	0.45	28.4	26.6	45.0
749	T2	25.1	3.45	0.46	35.6	27.2	37.2
750		33.8	3.16	0.49	33.1	26.1	40.9
752	R1a	26.2	4.62	0.45	17.6	22.1	60.4
753	R1	28.2	4.65	0.47	26.7	25.4	47.9
755	-	24.0	6.29	0.35	14.8	21.4	63.8
757	-	20.5	5.60	0.30	14.0	25.6	60.5
759	-	35.7	6.62	0.40	12.8	16.9	70.3
741	sst. extract	835	-	0.50	32.4	28.2	39.4
Lulita oil		-	2.9	0.55	37.5	27.6	34.9
Lulita oil		-	3.0	0.49	37.4	29.0	33.6
Harald oil*		-	3.7	0.49	34.4	26.5	29.1
Harald oil*		-	4.1	0.55	35.5	25.8	38.7
Harald oil**		-	4.3	0.48	37.1	24.1	38.8
Harald oil**		-	4.2	0.54	38.8	26.1	39.7

*West Lulu-1

** West Lulu-3

inducing blue-light irradiation, 'bleed' of oil-droplets from fusinitic structures may occur. Characteristic microlithotypes with generally high values throughout the seam are vitrite (up to 35.9 vol.%), vitrinertite (up to 32.6 vol.%), and duroclarite (up to 31.5 vol.%) (Table 4).

Coal seam T4

The lower half of this 0.23-m thick seam contains a high proportion of inertinite (38–41 vol.%, m.m.f.), whereas the upper half is strongly dominated by vitrinite (92–95 vol.%, m.m.f.) (Fig. 8; Table 3). The liptinite content reaches slightly more than 8 vol.% in the lower half. Collodetrinite and telinite+collotelinite occur in more or less equal proportions in the lower part of the seam, while the latter two macerals clearly dominate the upper part (Plate 3a, b; Table 3). Gelinitic vitrinite is likewise prominent in the upper half. The inertinite in the lower part is dominated by inertodetrinite, which appears to be very fine-grained and allochthonous (Table 3). The mineral matter and pyrite content is low. A micrinitised cutinite was observed (Plate 4), and yellowish fluorescing oil-droplets associated with fissures in telinite and collotelinite are a very characteristic feature of the seam (Plate 5a, b, c). The high content of inertinite in the lower part of the seam is consistent with the abundance of the microlithotypes inertite, vitrinertite and clarodurite, whereas vitrite and clarite are characteristic for the upper part (Table 4).

Sample 736, a carbonaceous mudstone

The 0.08-m thick carbonaceous mudstone above seam T4 contains a significant amount of vitrinite, mainly composed of collotelinite, telinite and collodetrinite (Fig. 8; Table 3). The inertinite content is negligible whereas the liptinite content amounts to 6.0 vol.%; part of this

has been identified as alginite (Plate 6). In addition, about 3 vol.% intimately associated fluorescing organic matter and mineral matter is present; the mudstone also contains a significant proportion of mainly framboidal pyrite (Table 3).

Organic geochemistry

The results of organic-geochemical analyses are given in Tables 5-7 for the coal, mudstone and oil samples analysed. A total of 24 TOC and *Rock-Eval* data is given in Table 5, and extract yields and GC and GC/MS data of 15 extracted coal and mudstone samples and 6 oil samples in Table 6. Table 7 lists coal-extract and oil compositions, data which is plotted in Fig. 9.

The TOC values of the samples range from 11.4 to 83.8 wt.% (Table 5), and *Rock-Eval*-derived T_{\max} values are generally between 435°C and 439°C. In general, *Rock-Eval* pyrolysis yields (S_1 and S_2) increase from the base to the top of the sampled interval, and the highest values are obtained from seams X and T4 (S_1 up to 20.28 mg HC/g rock, S_2 up to 206.90 mg HC/g rock) (Table 5). Hydrogen Index (HI) values range from 123 mg HC/g TOC to 344 mg HC/g TOC. Most of the samples from the coal seams yield HI values above 220 mg HC/g TOC, while the highest HI value is from the topmost carbonaceous mudstone containing alginite (Table 5). The fourteen solvent-extracted samples typically yield slightly higher T_{\max} values and significantly lower HI values compared to their non-extracted counterparts (Table 5).

Extract yields from the coals and carbonaceous mudstones (Table 6) range from 20.5 to 51.2 mg SOM/g OC, whereas the extract yield from the oil-stained sandstone between seams X and T4 amounts to 835 mg SOM/g OC. The composition of the maltene fractions from the coals and carbonaceous mudstones is dominated by heteroatomic compounds (NSOs) (Fig. 9; Table 7). By contrast, more than half of the oil-stained sandstone-extract is composed of saturated HCs, followed by aromatic HCs and NSO compounds.

The gas chromatograms of the saturated HC fractions from extracts of the coals and carbonaceous mudstones show broad, light-end skewed or slightly bimodal *n*-alkane distributions, with high proportions of long-chain *n*-alkanes in the waxy end ($> nC_{22}$) (Fig. 10). Normal alkanes up to about nC_{36-38} are recorded, and the waxy *n*-alkanes decrease in abundance with increasing carbon-chain length along a largely sigmoidal trend. Several of the gas chromatograms show slight enhancement of nC_{15} , nC_{17} and nC_{19} (Fig. 10). Acyclic isoprenoids are present in rather modest proportions relative to normal alkanes. The pristane/phytane (Pr/Ph) ratios range from 2.9 to 6.6 with a clearly decreasing tendency from the basal to the topmost samples (Table 6). The Pr/Ph ratios are generally higher in the R1 and R1a seams than in the T-seams and seam X.

The gas chromatograms of the *Lulita* crude oil show characteristics very similar to those recorded for the coal and mudstone samples (in particular samples from the T-seams and seam X), although the Pr/Ph ratios are slightly lower than for most coal and mudstone samples (Fig. 10; Table 6). For comparison, Fig. 10 also shows a gas chromatogram of a saturated HC fraction from an oil generated by the marine shales in the Upper Jurassic Farsund Formation, which are the principal source rocks for the crude oil in the Danish North Sea. The oil was collected in a nearby well, and the maturity is comparable to that of the *Lulita* oil. Differences between this oil and the *Lulita* oil are evident with respect to *n*-alkane distribution, Pr/Ph ratio and the proportion of acyclic isoprenoids relative to *n*-alkanes.

Differences between samples from the T-seams and R-seams in the distribution of triterpane (m/z 191 fragmentogram) and sterane (m/z 217 and m/z 218 fragmentograms) biological markers are evident (Fig. 11). With respect to triterpanes, samples from both the T-seams and R-seams show a predominance of C_{30} $\alpha\beta$ hopane, fair proportions of $\beta\alpha$ -hopanes relative to $\alpha\beta$ -hopanes, high proportions of diahopanes, and an absence of 28,30-bisnorhopane. However, samples from the R-seams show Ts/Tm ratios <1 , whereas samples from the T-seams show

Table 7.
Composition of coal extracts and Lulita oils.

Sample	Seam	Asphaltenes	Saturates	Aromatics	NSO	Saturates	Aromatics	NSO
		(mg/g OC)				(%)		
737	T4	7.4	2.8	12.2	14.0	9.6	42.2	48.2
738		7.6	1.9	10.6	12.0	7.9	43.2	48.9
739		8.5	2.7	8.3	11.7	11.7	36.7	51.7
743	X	13.6	6.6	12.9	18.1	17.5	34.3	48.2
744		6.4	2.6	7.6	10.1	12.8	37.4	49.8
746	T2a	9.4	4.8	10.1	15.2	16.1	33.5	50.4
747		8.3	3.3	11.1	13.6	11.7	39.5	48.8
749	T2	4.8	2.5	9.3	8.5	12.1	45.8	42.1
750		5.4	5.9	10.3	12.2	20.8	36.3	42.9
752	R1a	5.8	3.0	7.9	9.5	14.9	38.7	46.4
753	R1	7.5	3.0	8.1	9.6	14.5	39.0	46.5
755	-	7.2	2.3	5.9	8.6	13.5	35.1	51.4
757	-	7.7	2.1	3.5	7.2	16.6	27.4	56.1
759	-	13.6	3.0	6.1	13.0	13.6	27.6	58.8
741	sst. extr.	74.3	416.9	191.7	152.1	54.8	25.2	20.0
Lulita oil	-	-	-	-	-	63.2	20.0	16.8
Lulita oil	-	-	-	-	-	62.8	22.3	14.9

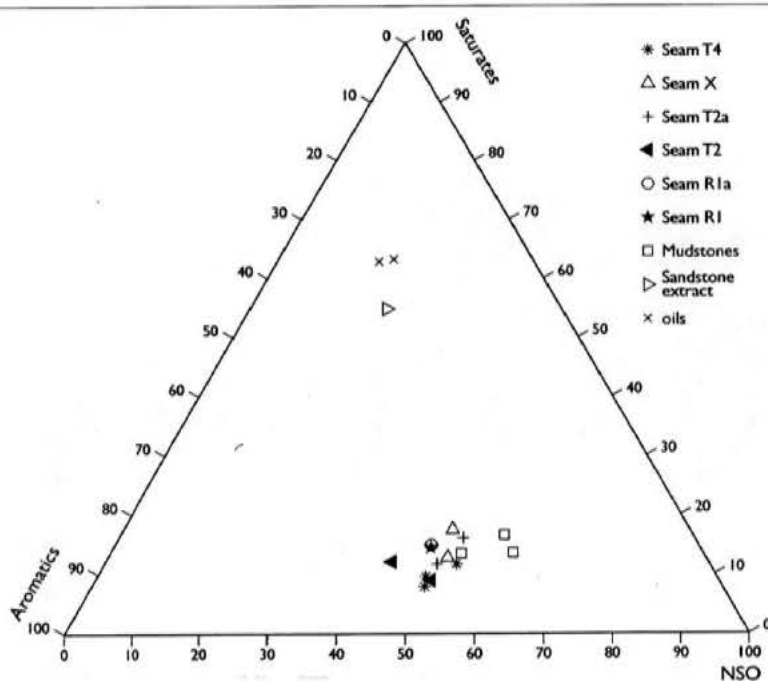


Fig. 9. The distribution of saturated and aromatic HCs and NSO compounds in the coal and carbonaceous mudstone extracts, in the oil-stained sandstone extract and in the *Lulita* crude oil. The coal and carbonaceous mudstone extracts are dominated by NSO compounds and aromatic HCs, whereas the crude oil and sandstone extract are enriched in saturated HCs due to the selective expulsion of long-chain *n*-alkanes.

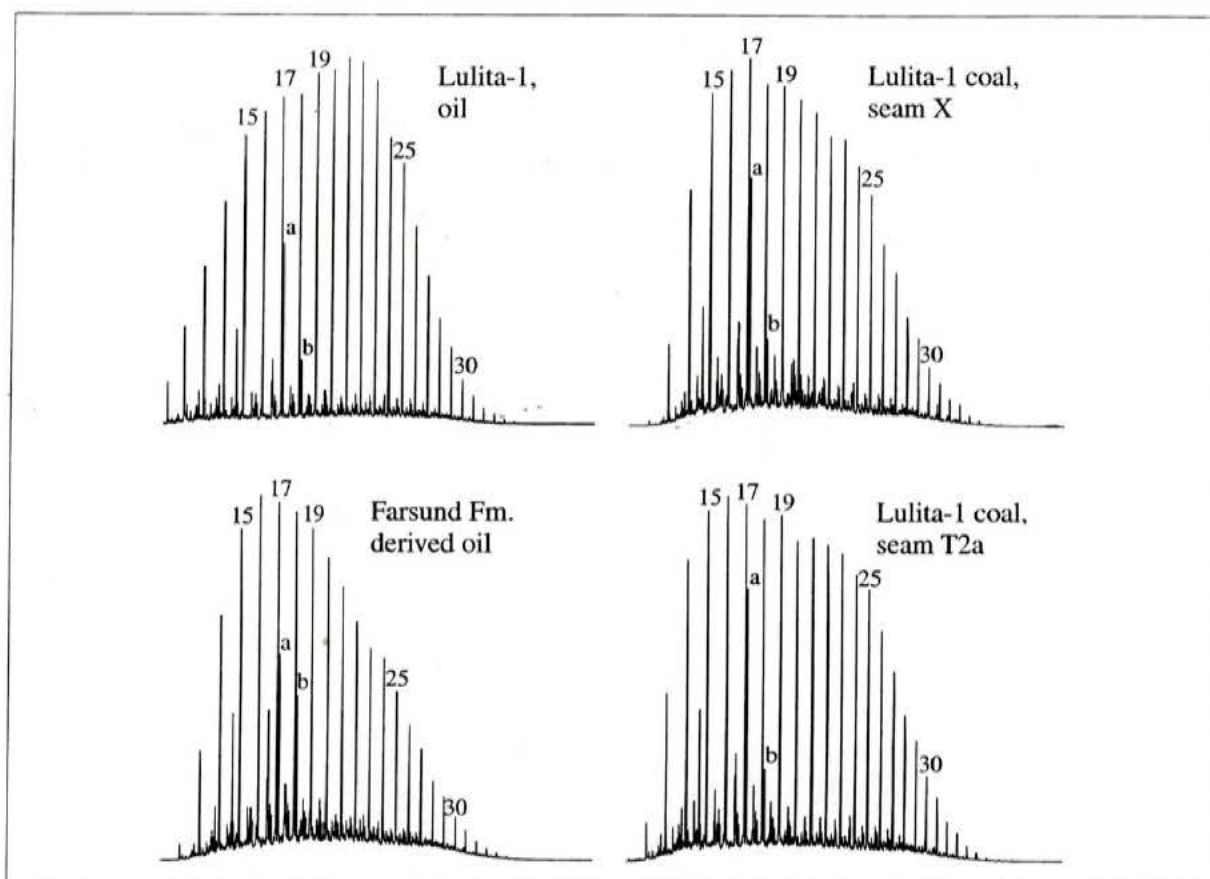


Fig. 10. Gas chromatograms of the saturated HC fractions of the *Lulita* crude oil, of two Middle Jurassic Bryne Formation coal extracts, and of an oil generated by the Upper Jurassic Farsund Formation from a nearby well. Numbers refer to *n*-alkane carbon number; a: pristane; b: phytane.

Ts/Tm ratios >1. Moreover, norhopane/hopane ratios are significantly lower in samples from the T-seams than in samples from the R-seams. Samples from the R1, R1a and X seams show a marked predominance of the C₂₉ regular steranes (and diasteranes) over both the C₂₇ and C₂₈ homologues, with C₂₇/C₂₉ regular sterane ratios significantly less than unity (Fig. 11; Table 6). The C₃₀ steranes are absent. By contrast, samples from the T-seams show much higher proportions of the C₂₇ regular steranes (and diasteranes), with C₂₇/C₂₉ regular sterane ratios close to unity (occasionally above 1), and frequently the presence of C₃₀ steranes (Fig. 11; Table 6).

Estimated hopane/sterane ratios (highest m/z 191 peak to highest m/z 217 peak) are moderate to high for all samples. Samples from the T-seams generally yield values in the range 3–5, whereas samples from the R-seams (as well as the mudstone samples) generally show considerably higher values.

The triterpane and sterane distributions of crude oil from the *Lulita* field are very similar to those of samples from the T-seams (Figs. 11 and 12; Table 6). The estimated hopane/sterane ratio is slightly greater than 3. By contrast, oils derived from the Farsund Formation with comparable maturity show lower proportions of dihopanes and $\beta\alpha$ -hopanes, somewhat higher proportions of extended hopanes, C₂₇/C₂₉ regular sterane ratios above unity, the presence of C₃₀ steranes and, invariably the presence of 28,30-bisnorhopane (Fig. 11). Estimated hopane/sterane ratios are generally 1.5–2.5.

Homohopane 22S-22R epimerisation has reached equilibrium in all samples, whereas the C₂₉ regular sterane 20S/(20S+20R) epimerisation ratios range from 0.44 to 0.49 in the coals, and from 0.30 to 0.40 in the carbonaceous mudstones (Table 6). The oil-stained sandstone

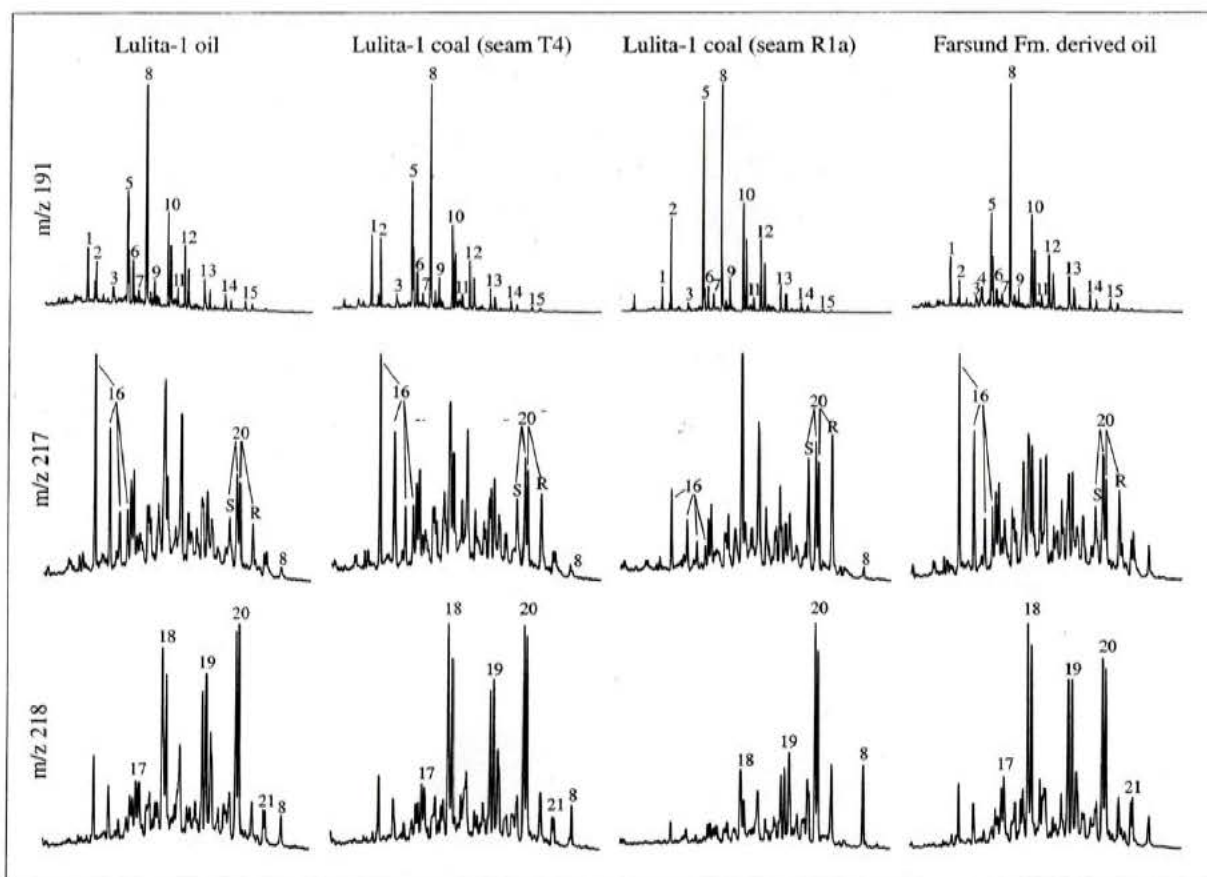


Fig. 11. Ion fragmentograms m/z 191, m/z 217 and m/z 218 of a *Lulita* field crude oil, two Middle Jurassic Bryne Formation coal extracts, and an oil generated by the Upper Jurassic Farsund Formation from a nearby well.

Peak identification:

- | | |
|--|--|
| 1: trisnorneohopane (Ts); | 14: $\alpha\beta$ -tetrakishomohopane (22S + 22R isomers); |
| 2: trisnorhopane (Tm); | 15: $\alpha\beta$ -pentakishomohopane (22S + 22R isomers); |
| 3: nordiahopane; | 16: C_{27} diasteranes (isomers); |
| 4: 28,30-bisnorhopane; | 17: C_{26} regular steranes ($\alpha\beta\beta$ -isomers); |
| 5: $\alpha\beta$ -norhopane; | 18: C_{27} regular steranes ($\alpha\beta\beta$ -isomers); |
| 6: diahopane; | 19: C_{28} regular steranes ($\alpha\beta\beta$ -isomers); |
| 7: $\beta\alpha$ -norhopane (normoretane); | 20: C_{29} regular steranes ($\alpha\beta\beta$ -isomers are shown in the m/z 218 fragmentograms, and $\alpha\alpha\alpha$ S, $\alpha\alpha\alpha$ R and $\alpha\beta\beta$ isomers in the m/z 217 fragmentograms); |
| 8: $\alpha\beta$ -hopane; | 21: C_{30} regular steranes ($\alpha\beta\beta$ -isomers). |
| 9: $\beta\alpha$ -hopane (moretane); | |
| 10: $\alpha\beta$ -homohopane (22S + 22R isomers); | |
| 11: $\beta\alpha$ -homohopane (homomoretane); | |
| 12: $\alpha\beta$ -bishomohopane (22S + 22R isomers); | |
| 13: $\alpha\beta$ -trishomohopane (22S + 22R isomers); | |

Note: due to very high hopane/sterane ratios in certain samples, hopane (peak 8) appear in the m/z 217 and m/z 218 fragmentograms. Furthermore, co-eluting norhopane (peak 5) contributes to the C_{29} 20R regular sterane isomer peak in the m/z 217 fragmentograms, thereby rendering 20S/(20S+20R) sterane epimerization ratios spurious.

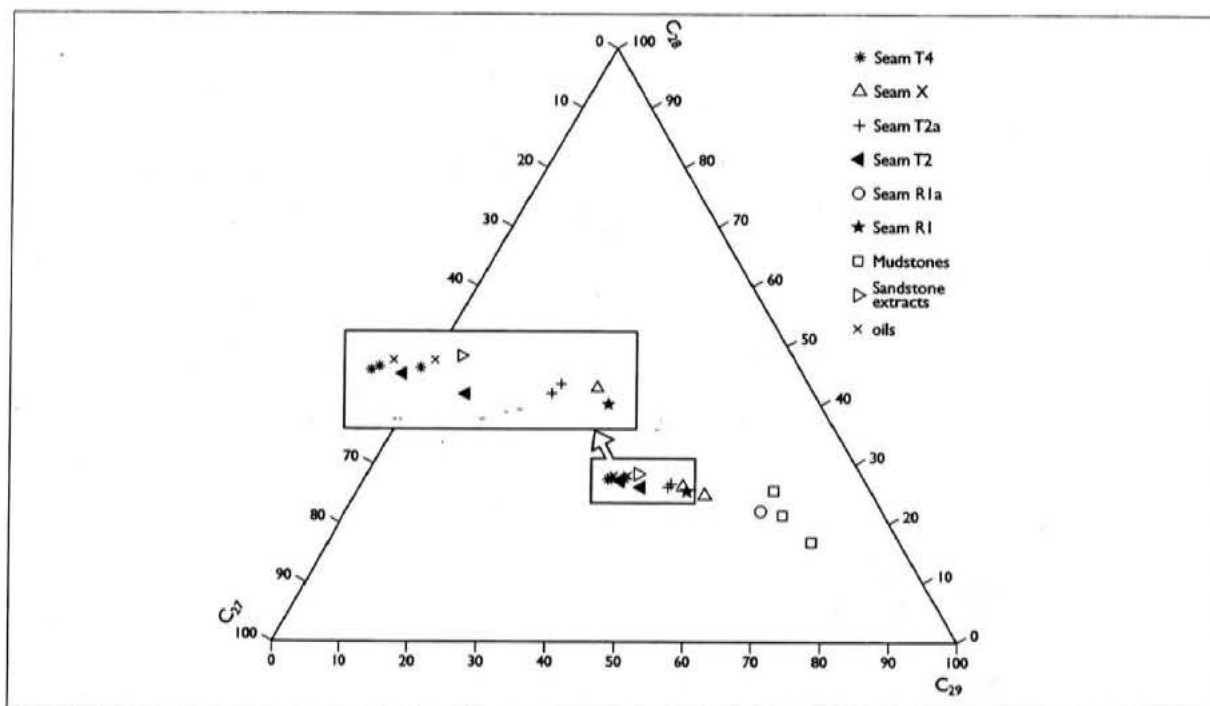


Fig. 12. C_{27-29} sterane distributions in the coal and carbonaceous mudstone extracts, and in the *Lulita* crude oil and oil-stained sandstone extract. The sterane distributions of the crude oil and extracts from coal seams T2 and T4 in particular show a very high degree of similarity.

extract yields a ratio of 0.50, and the two *Lulita* crude oils ratios of 0.49 and 0.55 (Table 6).

The pyrograms of the two solvent-extracted coal samples (743 and 749; Fig. 13) show that the proportion of unresolved pyrolysate is low in both, but that detailed pyrolysate compositions differ notably. The C_{6+} fraction of the pyrolysate of sample 743 shows a number of prominent peaks which are identified as (or tentatively assigned to) benzene, toluene, xylenes, phenol, naphthalene, methylnaphthalenes and other alkylated aromatic or phenolic compounds. These peaks protrude above a fairly prominent series of *n*-alkene/alkane doublets, which extend to at least to nC_{32} along an irregularly decreasing trend of abundance. Conversely, sample 749 has fewer recognisable compounds. Moreover, the C_{6+} fraction of the pyrolysate is entirely dominated by benzene, toluene, xylenes and phenol, whereas *n*-alkene/alkane compounds are sparse, and decrease in abundance along a very regular trend until nC_{24} , which is the largest *n*-alkyl compound to be recognised.

DISCUSSION

Palaeoenvironment of the coal seams: composition and source rock implications

At the *Harald* field, the depositional conditions of precursor peats had a considerable influence on the source-rock potential of the resulting coals (*see above*). A palaeoenvironmental interpretation of the coal seams at *Lulita-1Xc* is therefore of great relevance. In terms of the overall palaeogeography of the Søgne Basin (Petersen *et al.*, 1998), the *Lulita-1Xc* well is located close to the palaeo-coastline (Figs. 4 and 5), and this is supported by the occurrence there of marine sediments in the coal-bearing interval (Figs. 6 and 7). The coal seams at *Lulita-1Xc* are therefore considered to represent the coastal reaches of the precursor peat mires, and the petrographic and geochemical compositions of these seams should therefore be comparable to those of the seams at wells *Lulu-1* and *Amalie-1*. There are limited

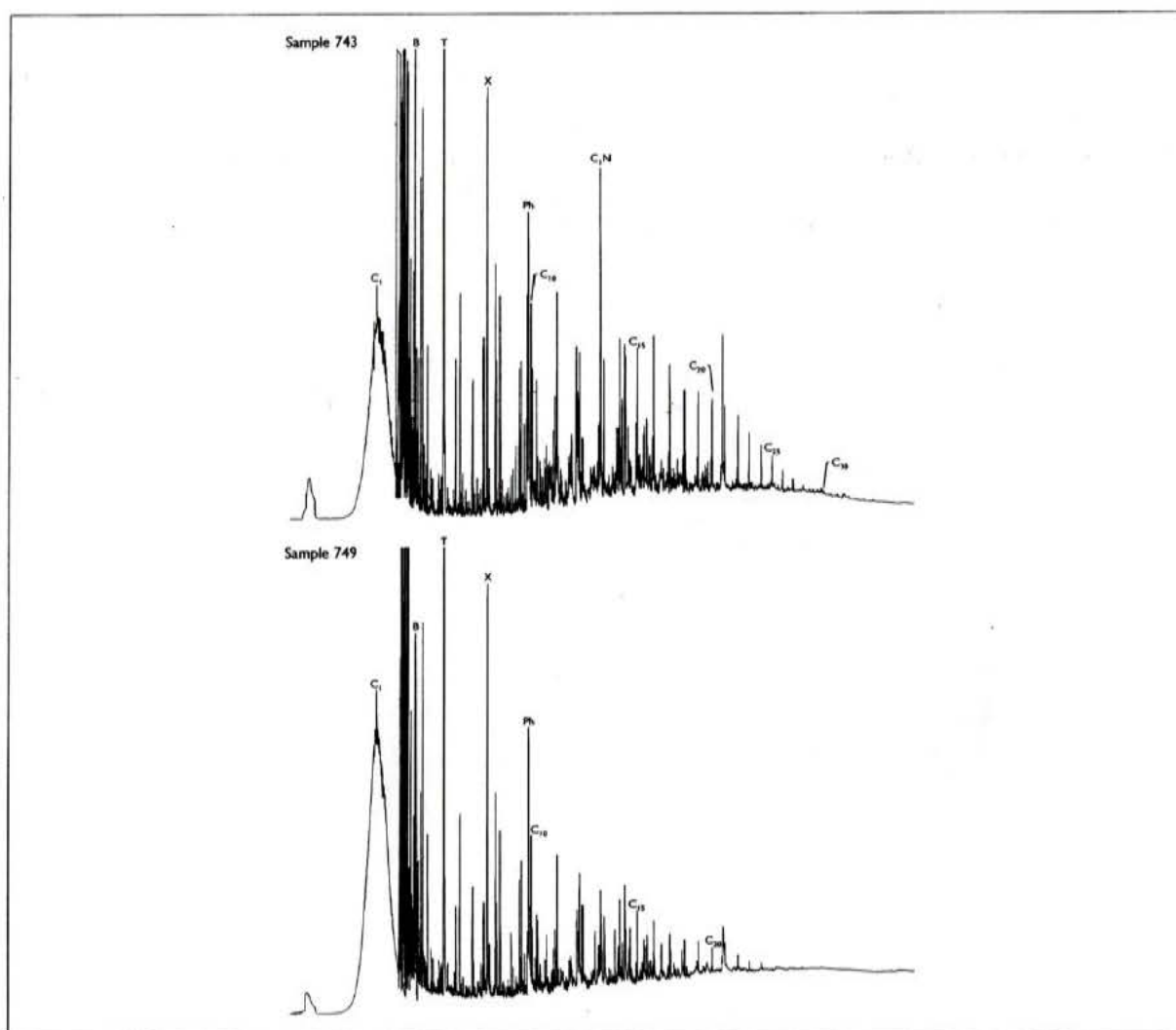


Fig. 13. Pyrograms of the solvent-extracted samples 743 and 749 from seams X and T2, respectively. A prominent series of *n*-alkene/alkane doublets extends to at least nC_{32} in sample 743, whereas the series extends to only nC_{24} in sample 749. The pyrograms show that the coals are still able to generate long-chain *n*-alkanes typical of terrestrial waxy crude oils. Compound identification: C_1 : methane; B: benzene; T: toluene; X: m+p xylene; Ph: phenol; C_1N : methyl-naphthalenes; C_{10} , C_{15} , C_{20} , C_{25} , C_{30} : *n*-alkene/alkane doublets.

petrographic differences between the seams formed during either comparatively slow or faster rises in relative sea-level due to a generally high-standing water table in the coastal reaches of the mires; this reduced the influence from water table fluctuations on the peats.

Overall the Bryne Formation sequences comprise a landward-stepping succession, with increasing marine influence upwards. The nature of the carbonaceous mudstones and coals from the lower, fluvial-dominated sequence *Bat-1A* (samples 754-760) are consistent with this pattern; the organic-geochemical data in Table 6 reveals the strongest terrestrial influence on the organic matter. Thus C_{29} steranes, which in a primary peat deposit can be related to terrestrial OM (Huang and Meinschein, 1979; Philp, 1994), dominate significantly over C_{27} steranes, which is mainly related to marine algae (e.g. Hunt, 1996) (Table 6). In addition, these samples' Pr/Ph ratios are the highest of any of the analysed samples. However, the coals of the fluvial-dominated sequence have the lowest generative potential of the coals in the *Lulita-1Xc* well (Table 5).

Depositional environments of seams R1 and R1a

In wells *West Lulu-1*, -2, -3 and *Lulu-1*, seams R1, R1a and T2 are situated within an interval approximately 3–5 m thick. The presence of these seams in the coaly interval between measured depths of 4,450 and 4,454 m at *Lulita-1Xc* fits neatly into the regional pattern (Figs. 6 and 7). Seam R1 at *Lulita-1Xc* is dominated by detrital macerals; it has a significant proportion of mineral matter (Tables 3 and 4), which suggests a precursor mire influenced by nearby siliciclastic depositional systems. In addition, C_{29} steranes dominate over C_{27} steranes (Table 6), and the precursor mire was probably not subjected to any significant marine influence.

Seam R1a is immediately above seam R1 and this seam also occurs in wells *West Lulu-3* and -1. A TOC content of about 38 wt% (Table 5) shows that the seam has not developed as a true coal but rather as a coaly mudstone. The low proportion of C_{27} steranes and a Pr/Ph ratio of 4.62 indicate the absence of marine influences and a strong input of terrestrial organic matter (Table 6).

Depositional conditions have resulted in a favourable composition in terms of generative potential for the R1 seam, whereas the R1a seam (in agreement with the lower content of organic matter and absence of marine influence) has a lower generative potential (Table 5).

Depositional environments of seams T2 and T2a

About 1 m above the coaly mudstone equivalent to the R1a seam are two seams, each 0.15-m thick, separated by approximately 0.15-m of silt- and mudstone with an abundance of bifurcating roots (Fig. 7). The lower seam (T2) has a high proportion of vitrinite in the lower and upper parts and an inertinite-rich middle part (Table 3). Massive, groundmass-like macrinite, naturally-formed char and large amounts of inertodetrinite occur in the interval 0.05–0.11 m within the seam (Table 3). A temporary drop in the mire's water table, allowing burning of the peat, is suggested by the occurrence of naturally-formed char which is derived from heat-affected humified organic matter (Petersen, 1998), in contrast to fusinite which is formed by the burning of fresh plant tissues. The associated inertodetrinite and groundmass-like macrinite support the interpretation of a fluctuating water table, as these macerals may have formed by oxidation of the peat surface (Moore *et al.*, 1996). In contrast to the lower and in particular the upper part of the seam, where a high proportion of the petroleum-prone macerals collotelinite and collodetrinite are present (Table 3), the abundance of inertinite in the middle part decreases the source rock potential considerably (Table 5). The distribution of the C_{27} and C_{29} steranes, with a significant proportion of C_{27} , is in agreement with the interpretation that seam T2 accumulated during a comparatively faster rise in relative sea-level than the underlying seam R1 (Petersen and Andsbjerg, 1996).

The upper seam (T2a) represents a seam split from T2. This implies that the coastal reaches of the precursor peat of seam T2 were drowned, perhaps due to outpacing of the rate of peat accumulation by the rate of rise in relative sea level. In fact, the T2 seam in *Lulu-1* contains an 0.08-m thick siliciclastic interval approximately in the middle of the seam, which could imply that the drowning event reached this location (Fig. 5b). The very high content of vitrinite and the low mineral-matter content at the top of seam T2 exclude a gradual drowning of the peat, and probably indicate a more 'sudden' drowning event. However, neither the sterane distribution nor the pyrite content indicate direct marine flooding. Following a drop in the water table, peat accumulation was resumed. The microlamination of the inertodetrinite in the upper seam suggests some redistribution of the organic matter in the original mire, in particular in the upper part, where framboidal pyrite additionally indicates a marine influence on the mire (Cohen *et al.*, 1984; Phillips and Bustin, 1996), although the sterane distribution suggests only limited marine influence during peat formation (Table 6). The seam is rather rich in petroleum-prone macerals like collotelinite and collodetrinite (Table 3), and some gas

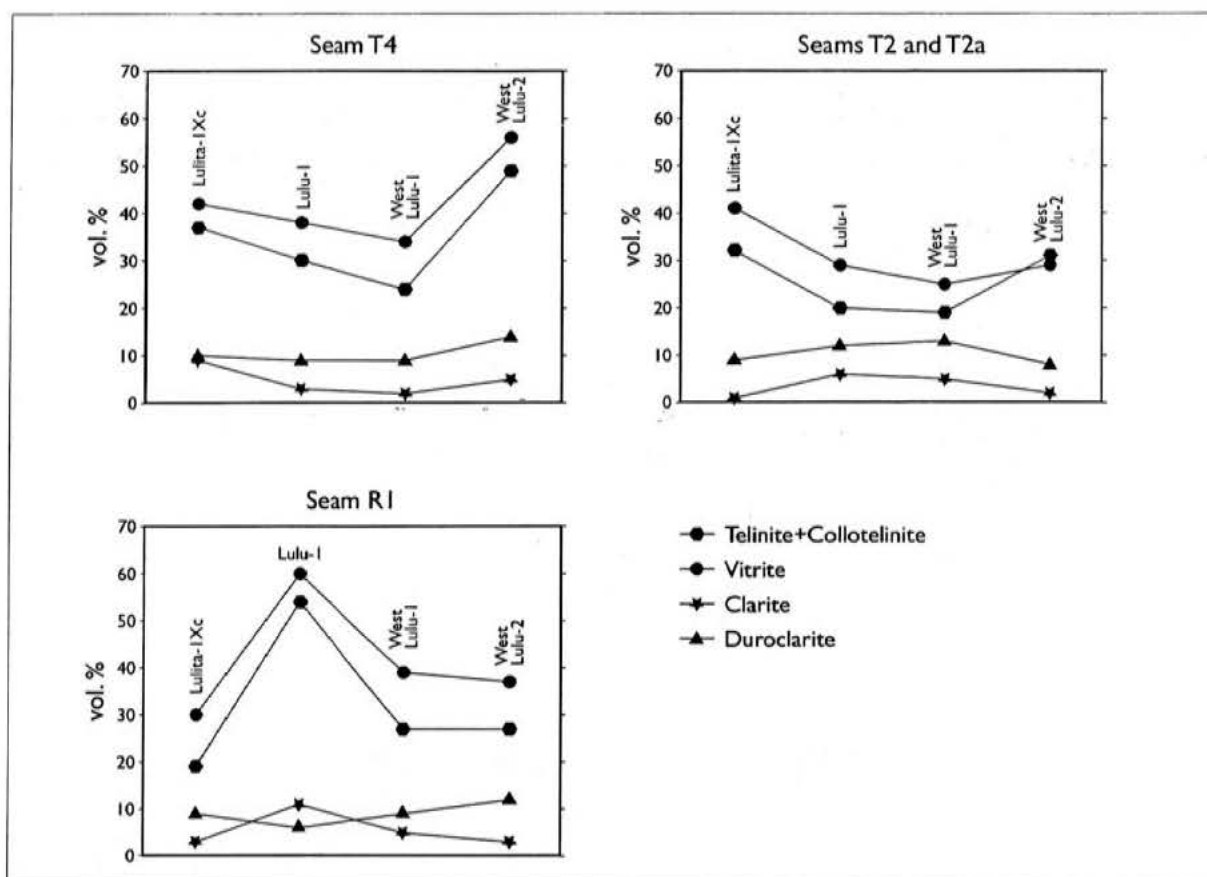


Fig. 14. The proportion of petroleum-prone components in seams T4, T2+T2a and R1 in the *Lulita-IXc*, *Lulu-1*, *West Lulu-1* and *West Lulu-2* wells. Compared to *West Lulu-1* and *Lulu-1*, seam T4 in *Lulita-IXc* is enriched in these components; seams T2+T2a in *Lulita-IXc* are in particular enriched in telinite+collotelinite compared to the other wells. Seam X in *Lulita-IXc* likewise has a very favourable composition.

chromatograms show a slight increase in the C_{15} , C_{17} , and C_{19} *n*-alkanes which suggest a primary contribution to the biomass from algae (Fig. 10) (Peters and Moldowan, 1993, p. 141). This composition is highly favourable in terms of the source rock potential (Table 5).

Depositional environment of seam X

The 0.21-m thick seam X may represent a more local episode of peat accumulation. The proportion of C_{29} steranes and the complete absence of pyrite (Tables 3 and 6) indicate that the precursor mire for this seam was predominantly freshwater. The microlaminated inertodetrinite and liptodetrinite suggest that weakly-flowing water was present in the precursor mire, and the inertodetrinite may therefore partly be allochthonous. However, the occasional increased content of fusinite and semifusinite also points to an *in situ* wildfire-derivation for part of the inertinite (e.g. Scott, 1989). The co-occurrence of naturally-formed char in the coal suggests a temporarily low-standing water table allowing burning of the peat itself. The X seam contains a considerable proportion of petroleum-prone collotelinite, collodetrinite and liptinite macerals (Table 3), and a primary contribution to the biomass from algae is detected from a slight increase in the C_{15} , C_{17} , and C_{19} *n*-alkanes in some gas chromatograms (Fig. 10) (Peters and Moldowan, 1993, p. 141). Thus, despite the non-marine influence during peat accumulation and the abundance of inertinite macerals, the composition is highly favourable in terms of its source-rock potential (Table 5).

Depositional environments of seam T4 and the overlying carbonaceous mudstone

The 0.23-m thick T4 seam at *Lulita-1Xc* overlies a transgressive-regressive cycle of transgressive shelf deposits, which is overlain by a transition to lower shoreface and upper shoreface to beach deposits. This siliciclastic succession is very similar to that overlain by the T4 seam in the *Lulu-1* well (Petersen *et al.*, 1998). Rootlets extend from the coal seam into the underlying fine-grained sand containing coal particles. Very fine-grained, probably allochthonous inertodetrinite occurs in the lower part, together with significant proportions of wildfire-derived semifusinite and fusinite. The increase in vitrinite content, and particularly in the petroleum-prone maceral collotelinite, towards the top of seam T4 in *Lulita-1Xc* indicates the establishment of an anoxic and stagnant peat mire. The sterane distribution is characterised by the dominance of C_{27} steranes over the C_{29} steranes in the upper part of the seam (Table 6). The very high proportion of the C_{27} steranes in seam T4 compared to that in the underlying seams is consistent with increasing marine influence between seams R1 and T4, reflecting the landward-stepping and overall transgressive nature of the Bryne Formation. These depositional conditions resulted in a coal seam whose composition was highly favourable in terms of petroleum generative potential (Table 5).

Above coal seam T4, which represents the last peat-forming period before fully-marine conditions prevailed in the Søgne Basin, is an approximately 0.08-m thick carbonaceous mudstone. The mudstone was deposited in an oxygen-deficient, lacustrine to brackish open-water mire as indicated by the comparatively high content of mainly framboidal pyrite, the high content of vitrinite, the high mineral matter content, and the occurrence of alginite occasionally having a morphology similar to the extant *Botryococcus* genus. This is the first documented observation of mudstones containing Type I kerogen in the Bryne Formation in wells from the Danish part of the Søgne Basin.

Thermal maturity and source rock evaluation of the coals*Thermal maturity*

Most of the vitrinite reflectance values for the *Lulita-1Xc* coals range between 0.82 % R_o and 0.84 % R_o (Table 3), and the average T_{max} value of the coals and carbonaceous mudstones is 436 °C (Table 5). According to conventional practice, this indicates that the coals are well within the oil window. However, according to the oil window as defined by Price (1991) (approximately 0.8–2.0 % R_o), the coals are only in an early stage of petroleum generation. This may partly explain the relatively small amount of oil in the *Lulita* field. The true vertical depth of the coals is from about 3,510 to 3,525 m (Fig. 7), and the vitrinite reflectance values are thus in agreement with the values obtained from the Bryne Formation coals in the other wells in the Søgne Basin.

An exception is sample 747; this has an R_o of 0.75 % which is probably retarded. Vitrinite reflectance retardation (suppression) has previously been documented in these coals, and retarded reflectance values lie between 0.75 % R_o and 0.78 % R_o (Petersen and Rosenberg, 1998). The slower maturation was caused by the higher hydrogen content of the vitrinite which was inherited as a result of the oxygen-deficient, waterlogged and marine-influenced conditions in the precursor mires, conditions which favoured bacterial activity.

In addition, the close association of the coal seams and the reservoir sandstones may have caused petroleum impregnation of the coals. The difference between the HI values of the coals and the solvent-extracted counterparts (Table 5) illustrates that extractable organic matter is present in the coals. The average T_{max} value of 436 °C for *Lulita-1Xc* is 4–12 °C lower than the average values calculated for the other wells (Petersen *et al.*, 1996, 1998), and this could also imply suppression of T_{max} . However, the average T_{max} value of the solvent-extracted samples is only 3 °C higher than the average value of the non-extracted samples,

Depositional environments of seam T4 and the overlying carbonaceous mudstone

The 0.23-m thick T4 seam at *Lulita-IXc* overlies a transgressive-regressive cycle of transgressive shelf deposits, which is overlain by a transition to lower shoreface and upper shoreface to beach deposits. This siliciclastic succession is very similar to that overlain by the T4 seam in the *Lulu-I* well (Petersen *et al.*, 1998). Rootlets extend from the coal seam into the underlying fine-grained sand containing coal particles. Very fine-grained, probably allochthonous inertodetrinite occurs in the lower part, together with significant proportions of wildfire-derived semifusinite and fusinite. The increase in vitrinite content, and particularly in the petroleum-prone maceral collotelinite, towards the top of seam T4 in *Lulita-IXc* indicates the establishment of an anoxic and stagnant peat mire. The sterane distribution is characterised by the dominance of C_{27} steranes over the C_{29} steranes in the upper part of the seam (Table 6). The very high proportion of the C_{27} steranes in seam T4 compared to that in the underlying seams is consistent with increasing marine influence between seams R1 and T4, reflecting the landward-stepping and overall transgressive nature of the Bryne Formation. These depositional conditions resulted in a coal seam whose composition was highly favourable in terms of petroleum generative potential (Table 5).

Above coal seam T4, which represents the last peat-forming period before fully-marine conditions prevailed in the Søgne Basin, is an approximately 0.08-m thick carbonaceous mudstone. The mudstone was deposited in an oxygen-deficient, lacustrine to brackish open-water mire as indicated by the comparatively high content of mainly framboidal pyrite, the high content of vitrinite, the high mineral matter content, and the occurrence of alginite occasionally having a morphology similar to the extant *Botryococcus* genus. This is the first documented observation of mudstones containing Type I kerogen in the Bryne Formation in wells from the Danish part of the Søgne Basin.

Thermal maturity and source rock evaluation of the coals*Thermal maturity*

Most of the vitrinite reflectance values for the *Lulita-IXc* coals range between 0.82 % R_o and 0.84 % R_o (Table 3), and the average T_{max} value of the coals and carbonaceous mudstones is 436 °C (Table 5). According to conventional practice, this indicates that the coals are well within the oil window. However, according to the oil window as defined by Price (1991) (approximately 0.8–2.0 % R_o), the coals are only in an early stage of petroleum generation. This may partly explain the relatively small amount of oil in the *Lulita* field. The true vertical depth of the coals is from about 3,510 to 3,525 m (Fig. 7), and the vitrinite reflectance values are thus in agreement with the values obtained from the Bryne Formation coals in the other wells in the Søgne Basin.

An exception is sample 747; this has an R_o of 0.75 % which is probably retarded. Vitrinite reflectance retardation (suppression) has previously been documented in these coals, and retarded reflectance values lie between 0.75 % R_o and 0.78 % R_o (Petersen and Rosenberg, 1998). The slower maturation was caused by the higher hydrogen content of the vitrinite which was inherited as a result of the oxygen-deficient, waterlogged and marine-influenced conditions in the precursor mires, conditions which favoured bacterial activity.

In addition, the close association of the coal seams and the reservoir sandstones may have caused petroleum impregnation of the coals. The difference between the HI values of the coals and the solvent-extracted counterparts (Table 5) illustrates that extractable organic matter is present in the coals. The average T_{max} value of 436 °C for *Lulita-IXc* is 4–12 °C lower than the average values calculated for the other wells (Petersen *et al.*, 1996, 1998), and this could also imply suppression of T_{max} . However, the average T_{max} value of the solvent-extracted samples is only 3 °C higher than the average value of the non-extracted samples,

which implies that significant suppression of this maturity parameter is not caused by petroleum impregnation.

The 20S/(20S+20R) epimer ratios of the C₂₉ $\alpha\alpha\alpha$ steranes of the R1, R1a, T2, T2a, X and T4 seams range between 0.44 and 0.49, and are thus more or less in equilibrium (Table 6). The lowermost three samples (755, 757, 759) yield ratios of only 0.30–0.40. However, these low values are caused by high proportions of hopanes in the extracts and thus co-elution of the C₂₉-hopane (norhopane), which yields minor m/z 217 and m/z 218 ion fragments, and the $\alpha\alpha\alpha$ 20R sterane epimer.

Source rock potential

Coal seams R1, R1a, T2, T2a, X and T4 of the *Lulita-IXc* well yield HI values of between 182 and 292 mg HC/g TOC; the majority lie between 221 and 292 mg HC/g TOC (Table 5). The average HI values of seams R1, R1a, T2, T2a, X and T4 at *Lulita-IXc* — 219, 195, 223, 237, 249 and 233 mg HC/g TOC, respectively — are higher than average values for the same seams in all other wells in the Danish part of the Søgne Basin (Petersen *et al.*, 1998, their table 11). However, the lower HI values of the solvent-extracted samples show that the HI values are influenced by the presence of extractable organic matter (heavy oil ?) in the coals, although the extracted samples still yield high HI values. The average HI value of the fourteen solvent-extracted samples is 192 mg HC/g TOC, compared to 228 mg HC/g TOC for their non-extracted counterparts. Average S₁+S₂ pyrolysis yields from seams T2, T2a, X and T4 in *Lulita-IXc* are likewise higher than for the same seams in all other wells.

Also of interest are the HI values of the more deeply-buried carbonaceous mudstones (and coal samples) from 4,506.93–4,508.25 m (measured depth), i.e. samples 760–754 (Table 5). These lie, except for one sample, within the same range of values as the overlying coals at *Lulita-IXc*. This is because the composition of the disseminated organic matter in the mudstones typically consists of the same terrestrial organic material as that in the coals (Petersen *et al.*, 1998). The first observed exception from this 'normal' carbonaceous mudstone composition is the thin mudstone above seam T4, which has a HI value of 344 mg HC/g TOC (Table 5). The increased HI value is due to a combination of the presence of Type I kerogen (alginite) and the intimately associated fluorescing organic matter and minerals, which may contain degraded algal material.

The generally high HI values recorded at *Lulita-IXc* are consistent with the coastal palaeo-environmental location of the well, and the general pattern of increasing HI values from landward to coastal well locations (Petersen *et al.*, 1998). Likewise, the higher HI values in the T-seams (and seam X) compared to the R-seams follow the trend seen in the other wells in the Danish part of the Søgne Basin. This is related to the depositional environment in the coastal reaches of the precursor mires; and also to the comparatively fast relative sea-level rise during T-seam formation, as these conditions promoted the development of continuously waterlogged, oxygen-deficient mires. These conditions of restricted oxygen availability and occasionally marine influence favoured the formation of vitrinitic macerals. In particular, hydrogen-enriched vitrinite formed due to the removal of oxygen from the organic matter by anaerobic bacteria. Hydrogen-enriched vitrinite has a higher generative potential than does "normal" vitrinite (Petersen and Rosenberg, 1998). The detailed chemistry of vitrinite may therefore have an influence on source rock potential, and vitrinite in general exerts a significant influence on the generative potential of the coals in the Søgne Basin.

Multivariate regression analysis comprising both maceral and microlithotype data as well as TOC values from 81 coal samples from the Bryne Formation in the Søgne Basin was used to investigate the variation in Rock-Eval S₂ (the remaining generative potential) (Petersen *et al.*, 1998). This study showed that S₂ is strongly positively correlated to TOC content also to vitrinite-rich components particularly collotelinite, telinite, vitrite, clarite and duroclarite. A similar statistical analysis of 21 humic coals from all parts of the World stressed, beside the

importance of liptinite, the significant influence of collotelinite on the HI (Petersen and Rosenberg, *in press*).

With these models in mind, it is interesting to note that seams T2/T2a and T4 at *Lulita-IXc* on average contain significantly high values of telinite+collotelinite and vitrite (Fig. 14). The average content of these components exceeds their average contents in the same seams in wells *Lulu-1* and *West Lulu-1* from the *Harald* field. In well *West Lulu-2*, these components are present with higher average proportions in seam T4. In addition *Lulita-IXc* contains seam X which is also rich in the petroleum-prone components telinite+collotelinite, vitrite and duroclarite (Tables 3 and 4). Seam R1 in *Lulu-1* is also very enriched in petroleum-prone components; however, this seam is only 0.06-m thick in this well, thus limiting its source potential at this location. The average liptinite content in general varies between 2 and 5 vol.% in the seams independent of the well, and cannot therefore be a decisive factor influencing the generative potential. According to the statistical models of Petersen *et al.* (1998) and Petersen and Rosenberg (*in press*), four of the six coal seams in *Lulita-IXc* have a petrography favourable for petroleum generation. The generative potential of the coals at *Lulita-IXc* is further improved by the probable presence of algal material, as indicated by the enhanced proportions of nC_{15} , nC_{17} , and nC_{19} and the prominent proportions of C_{27} steranes.

Evidence in the seams for liquid petroleum generation

Direct evidence for liquid petroleum generation in the coals comes from oil-droplets associated with cleats in telinite and collotelinite (Plate 5a, b, c), a feature which has been demonstrated in various coals (Teichmüller, 1974a; Cook and Struckmeyer, 1986; L. Stasiuk, *pers. comm.*, 1999). Exsudatinite and micrinite were observed (Plate 4), lending further support to the liquid petroleum generative capability of the coals. Exsudatinite is an orange to yellowish fluorescing bituminous substance generated from liptinite and hydrogen-enriched vitrinite during maturation (Teichmüller, 1974a, b; Taylor *et al.*, 1998). Micrinite is a high-reflecting maceral generated from liptinite macerals and hydrogen-enriched vitrinite during maturation from approximately what corresponds to the late sub-bituminous stage of coalification (about 0.65 % R_o), and its formation is related to the generation of petroleum (Teichmüller, 1974b; Taylor *et al.*, 1998).

Reflections on the petroleum expulsion efficiency

The coal seams at *Lulita-IXc* have uniformly high HI values (Table 5), which is not the case for the seams in the *Harald* field area. These high HI values for the thin *Lulita-IXc* seams may have facilitated crude oil-saturation to the expulsion threshold; by contrast, the wider range of (favourable and less favourable) HI values in the generally thicker seams at *Harald* may have hindered effective saturation and expulsion (e.g. Petersen *et al.*, 1996, their fig. 11).

The occurrence of oil-droplets in cleats in telinite and collotelinite may support the views of Close (1993), that the natural fracture system in a coal may constitute very significant pathways for the flow of liquid petroleum. The abundance of fractures seems to increase with increasing rank, thereby increasing the permeability. Expulsion of generated crude oil may be further influenced by the transmission of lithostatic pressure to crude oil in the pore spaces present, for example, in fusinite (Plate 1). The presence of inertinite-rich microlithotypes (Plate 3a), which are very common in the *Lulita-IXc* coals, associated with more deformable microlithotypes such as vitrite (Plate 3b), will improve this expulsion mechanism (Bertrand, 1989). According to Durand and Paratte (1983), the *Rock-Eval* S_2 peak of coals up to 1.5 % R_o consists mainly of petroleum-like components, and at maturities higher than 0.7 % R_o crude oil is formed by most coals. These authors considered that, due to the continuous evolution of the coal structure during maturation, trapping of the generated crude oil in the micropores of

the coal is of minor importance below 1.5 %R_o. According to Isaksen *et al.* (1998), polar aromatic and heteroatomic compounds are preferentially absorbed by the coal matrix compared to aliphatic compounds, resulting in the selective expulsion of mainly aliphatic products. Oil-prone coals must therefore be able to generate relatively high proportions of *n*-alkanes, in particular in the C₁₅₊ range. The pyrolysis-gas chromatography (Py-GC) we performed on two *Lulita-IXc* coals yielded long-chain *n*-alkanes above nC₂₀ (Fig. 13). An excess of these *n*-alkanes relative to the multi-phase equilibrium between the different constituents in the coal matrix will lead to the expulsion of an aliphatic-rich crude oil (Isaksen *et al.*, 1998). This phenomenon is clearly shown by the composition of the extract from the oil-stained sandstone situated between the X and T4 seams (Fig. 9; Table 7).

By combining Py-GC and *Rock-Eval* data, the chemically-inert, gas-prone (C₁₋₅) and oil-prone (C₆₊) proportions of the TOC can be calculated (Pepper and Corvi, 1995). These calculations demonstrate that about 78–81% of the organic carbon is inert, leaving 19–22% to participate in petroleum formation; of this, approximately 42–53% will be in the gas-range and 47–58% in the oil-range. Gas-to-oil ratios (GOR) are therefore 0.74 (sample 743) and 1.11 (sample 749). These proportions of oil-range components are lower than those obtained from the same seams in the other wells, where 72–82% of the petroleum products are in the oil-range (Petersen *et al.*, 1998); also, they appear to conflict with the high HI values of the *Lulita-IXc* coals. However, the coals' HI values have been raised by the presence of extractable organic matter (Table 5). In addition, qualitative microscopic observations under blue light show that the vitrinite in the *Harald* field coals are commonly more strongly fluorescing than the vitrinite from *Lulita-IXc*. This stronger fluorescence is caused by the presence of absorbed and poorly extractable bitumen, which may account for the generation of abundant long-chain *n*-alkanes during pyrolysis of *Harald* field coals. This suggests that the *Harald* field coals are not able to expel liquid petroleum effectively at their present maturity. This may partly be due to the varying HI in the seams (see above). Thus, the lower proportions of crude oil generated by the *Lulita-IXc* coals during further maturation may simply reflect the expulsion efficiency of these coals.

Oil-source rock correlations

Based on the results presented above, there is a clear correlation between *Lulita* field crude oils and the Bryne Formation coals. The m/z 218 fragmentograms of the saturated HC fractions of the coal extracts, oil-stained sandstone extract, and two *Lulita* crude oils all contain a significant proportion of C₂₉ steranes, and the sterane distributions are very similar (Figs. 11 and 12). The similarity of the sterane distributions of the extracts from the T4 seam and the *Lulita* crude oils is particularly evident.

Crude oils represent an integration of products generated from source rocks, which are not necessarily homogeneous in terms of chemical characteristics or generation capability. Thus, oil compositions are biased towards the composition of the more prolific and/or volumetrically important parts of the source rock succession; no single sample of a source rock will correlate exactly with the generated oil. At *Lulita-IXc*, we have shown that the marine-influenced T-seams (in particular seam T4) and the X seam represent the most prolific source rocks in the succession. Their correlation to *Lulita* crude oils is valid for all the parameters investigated, including the distributions of *n*-alkanes, acyclic isoprenoids, triterpanes and steranes, as well as for hopane/sterane ratios.

The correlation is further supported by stable carbon isotope data (Fig. 15). The "Galimov curves" confirm the close similarity between the oils from the *Harald* and *Lulita* fields and the Bryne Formation coal extracts.

In Fig. 16, $\Delta\delta^{13}\text{C}$ is plotted versus Pr/Ph ratio for *Lulita* and *Harald* field oils, an oil sourced by the Farsund Formation, and Bryne Formation coal extracts. This plot emphasises the terrestrial nature of the *Lulita* and *Harald* oils. The *Lulita* oils plot close to the "marine"

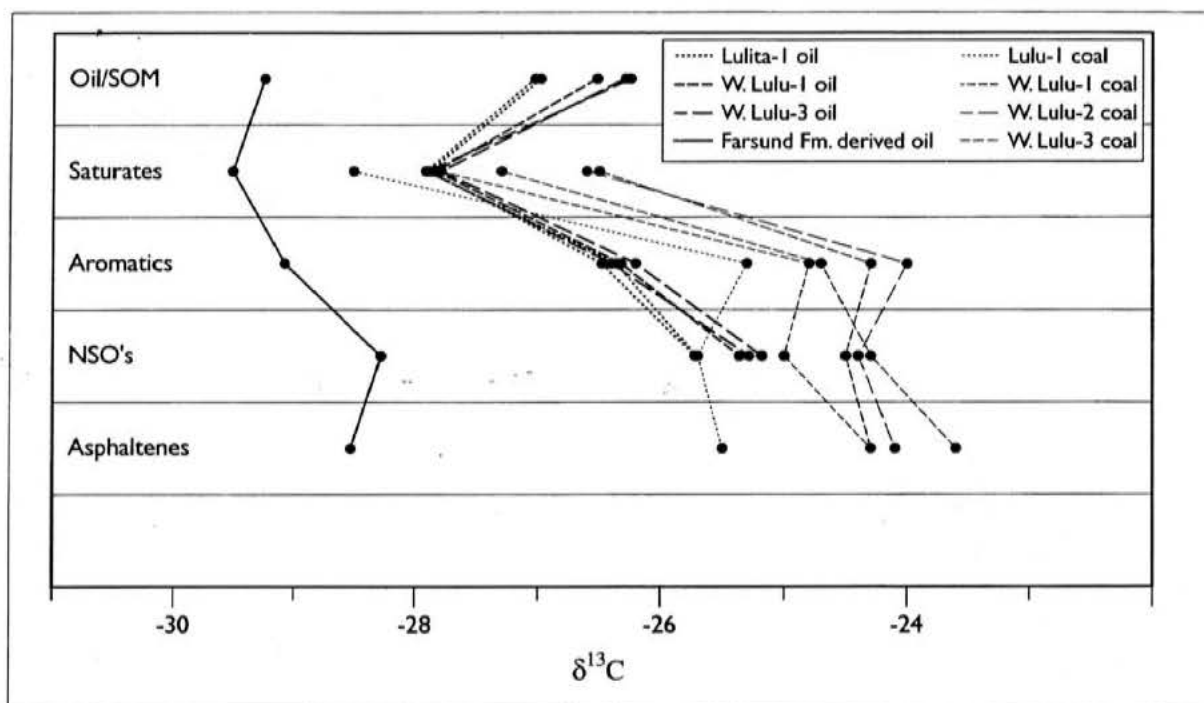


Fig. 15. "Galimov" curves for oil from the *Lulita* and *Harald* fields (wells West Lulu-1 and -3), a "typical" oil from the Farsund Formation, and for Bryne Formation coal extracts. The *Lulita* and *Harald* field oils clearly resemble the coal extracts; the oil derived from the Farsund Formation is isotopically lighter. Coal extracts from wells West Lulu-2 and -3 have the heaviest isotopic ratios; these wells are situated in the most landward location relative to the palaeo-coastline.

field, and this is consistent with the location of the *Lulita* well close to the palaeo-coastline. It is also consistent with the most marine-influenced coals (e.g. seam T4) having the highest generative potential. In fact, two samples from this seam show a dominance of C_{27} steranes.

In contrast, there is a distinct absence of correlation between the *Lulita* oil and the oil derived from the shales in the Farsund Formation. These shales are the source of all the commercial oil accumulations in the Danish North Sea (Damtoft *et al.*, 1992) except *Harald* and *Lulita*. Fig. 15 shows that $\delta^{13}C$ ratios for *Harald* and *Lulita* oils and Bryne Formation coal extracts are significantly heavier than those of oil generated by the Farsund Formation. Significant differences between the *Lulita* oils and the oil derived from the Farsund Fm. shales are also apparent on the gas chromatograms and m/z 218 fragmentograms (Figs. 10 and 11).

In summary, our data shows that the Bryne Formation coals, in particular those in the marine-influenced T-seams, have generated and expelled liquid petroleum. We infer that these coals have generated the *Lulita* oil accumulation.

CONCLUSIONS

(1) The *Lulita* field (Søgne Basin, Danish North Sea) is an excellent example of a coal-sourced oil accumulation. Source rocks are coals in the Middle Jurassic Bryne Formation. These coals also sourced the larger volumes of petroleum at the nearby *Harald* field, which in contrast to *Lulita*, is dominated by gas and condensate.

(2) The *Lulita-1Xc* well penetrated six relatively-thin coal seams (0.15-0.25 m thick). The coals have a complex petrography dominated by vitrinite with prominent proportions of inertinite but low contents of liptinite.

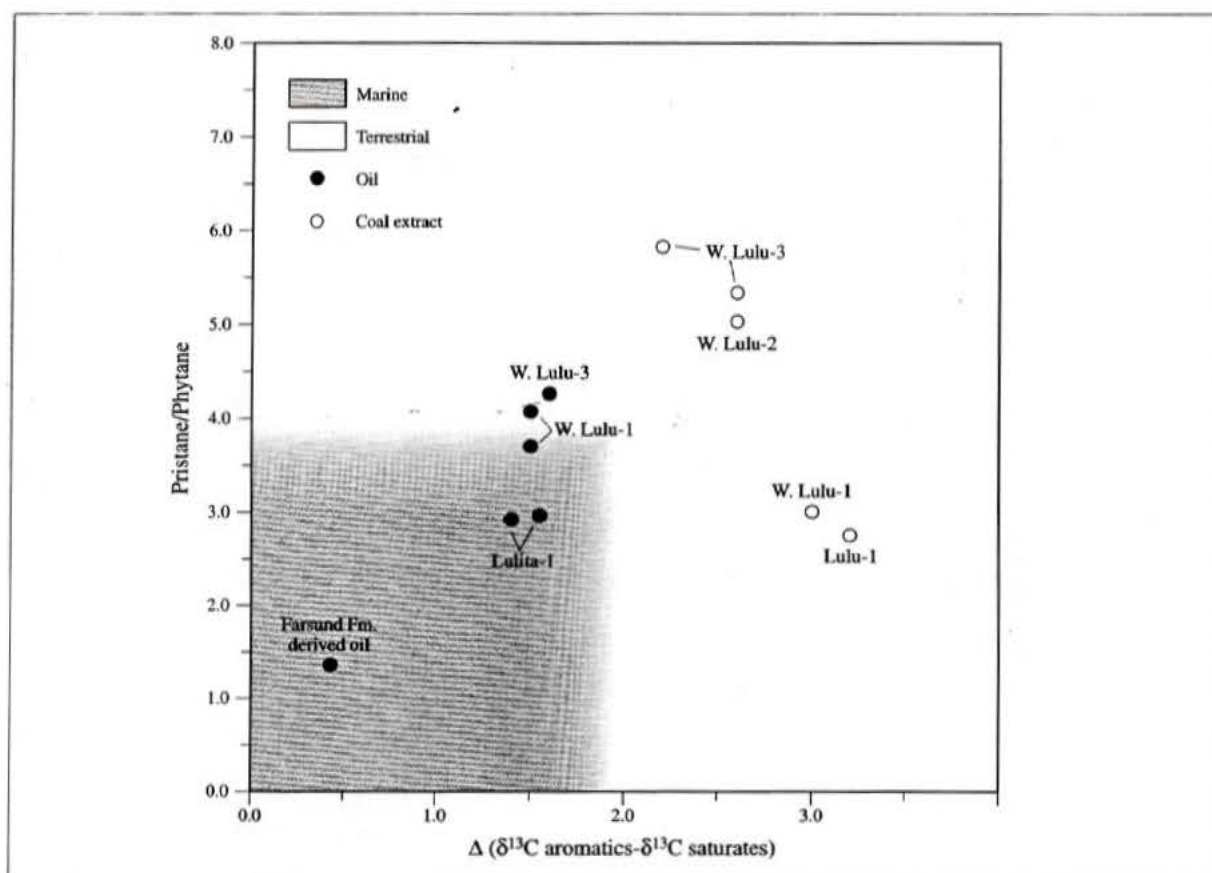


Fig. 16. Plot of $\Delta\delta^{13}\text{C}$ ($\delta^{13}\text{C}$ aromatic- $\delta^{13}\text{C}$ saturates) versus Pr/Ph ratio for oils from the *Lulita* and *Harald* fields (West Lulu-1 and West Lulu-3). Also plotted are a "typical" oil derived from the Farsund Formation, and extracts of Bryne Formation coals.

(3) The coal seams at this location represent the coastal reaches of coastal plain peat mires, which were in general waterlogged, oxygen-deficient, and occasionally marine-influenced although fluctuations in the water tables occurred. The lowermost coaly interval encountered by the well is the most terrestrial, whereas the uppermost coal seam (T4) is the most marine-influenced. Above seam T4, there occurs a thin, carbonaceous mudstone containing alginite and an abundance of framboidal pyrite which represents a freshwater to brackish open water mire. The depositional conditions of the precursor peats had a favourable impact on the composition of the resulting coals in terms of their source rock potential.

(4) The *Lulita-1Xc* coals have comparatively high Rock-Eval S_1+S_2 yields. The seams have uniformly distributed high HI values, and the average HI value for each coal seam is higher than the average HI values of equivalent seams in other wells in the Søgne Basin. The HI value of the carbonaceous mudstone above seam T4 is particularly high due to the presence of alginite (Type I kerogen). It also contains intimately associated fluorescing organic materials and mineral matter. *Lulita-1Xc* coals are rich in components such as telinite, collotelinite, vitrite and duroclarite which are positively correlated to S_2 and HI. The coastal position of the precursor mires may in addition have favoured the formation of hydrogen-enriched vitrinite. Furthermore, gas chromatograms suggest the presence of algal material in the seams. The combination of the coals' uniformly distributed high HI values, their favourable composition and the comparatively small seam thickness at *Lulita-1Xc* may have facilitated oil saturation to the expulsion threshold. Expulsion of aliphatic crude oil may have been facilitated by the

ability of the coals to generate long-chain *n*-alkanes, and the co-occurrence of deformable and undeformable microlithotypes.

(5) According to conventional theory, the vitrinite reflectance and Tmax values we measured indicate that the *Lulita-IXc* coals are well within the oil window. However, according to the maturity scale for coals proposed by Price (1991), the coals may in fact only be in the early phase of oil-generation. This may partly explain why the volume of oil at the *Lulita* field is small.

(6) We predict that on further maturation, about 19-22% of the organic carbon within the coals will generate petroleum, of which approximately 42-53% will be in the gas-range and 47-58% in the oil-range.

(7) By means of geochemical correlation, we have demonstrated that the Bryne Formation coals (in particular seams T2 and T4) immediately associated with the reservoir sandstones have generated the crude oil at the *Lulita* field. The presence of oil-droplets, exsudatinites and micrinite in the coals is further direct evidence of this.

(8) The source potential of Bryne Formation coals at the *Harald* field is lower than it is at *Lulita*. We suggest that this may be due to (i) the less favourable petrographic composition of some of the coals; (ii) an uneven distribution of the generative potential (HI) in the seams; (iii) the greater seam thickness at *Harald* than at *Lulita-IXc*, which may have hampered effective oil saturation to the expulsion threshold. Gas and condensates generated by the coals were, however, expelled. The total volume of petroleum accumulated at *Harald* is much larger than it is at *Lulita* because of the greater cumulative thickness at *Harald* of the coal seams.

ACKNOWLEDGEMENTS

This study was supported financially by the Danish Energy Research Programme (EFP-98), grant no. 1313/98-0022. Stuart Watt (GEUS) is thanked for constructive comments on the paper. The paper is published with the permission of the Geological Survey of Denmark and Greenland (GEUS). Journal reviewers N. Morton (*Birkbeck College, University of London*), L. C. Price (*USGS, Denver*), A.C. Scott (*Royal Holloway, University of London*) and A. R. Scott (*Bureau of Economic Geology, The University of Texas at Austin*) are thanked for their valuable comments.

REFERENCES

- ANDSBJERG, J., 1997. Sedimentology and sequence stratigraphy of the Bryne Formation, Middle Jurassic, Danish Central Graben. In: ANDSBJERG, J. (Ed.), *Sedimentology and sequence stratigraphy of Middle Jurassic deposits. Danish and Norwegian Central Graben. Danm. Grøn. Geol. Unders. Rapport*, **1997/68(2)**, 60 pp.
- ANDSBJERG, J. and DYBKJÆR, K., 1997. Jurassic sequence stratigraphy of the Danish Central Graben. In: ANDSBJERG, J. (Ed.), *Sedimentology and sequence stratigraphy of Middle Jurassic deposits. Danish and Norwegian Central Graben. Danm. Grøn. Geol. Unders. Rapport*, **1997/68(1)**, 31 pp.
- BERTRAND, P. R., 1989. Microfacies and petroleum properties of coals as revealed by a study of North Sea Jurassic coals. *Int. J. Coal Geol.*, **13**, 575-595.
- CARTWRIGHT, J. A., 1991. The kinematic evolution of the Coffee Soil Fault. In: ROBERTS, A. M., YIELDING, G. and FREEMAN, B. (Eds.), *The geometry of normal faults. Geol. Soc. London Spec. Publ.*, **56**, 29-40.
- CLOSE, J. C., 1993. Natural fractures in coal. In: LAW, B. E. and RICE, D. D. (Eds.), *Hydrocarbons from coal. AAPG Studies in Geol.*, **38**, 119-132.

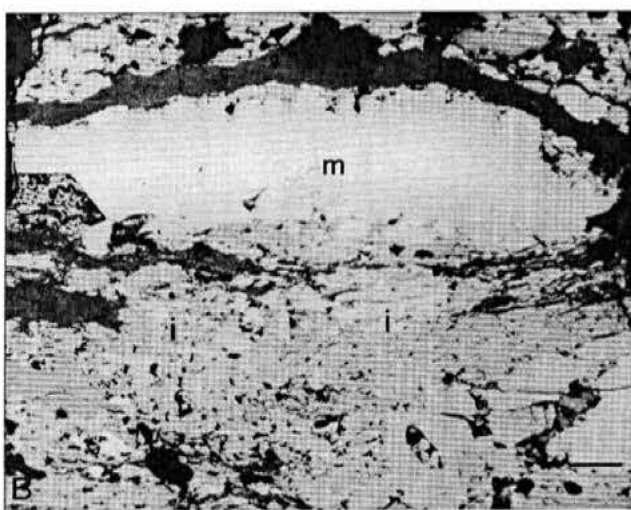
- COHEN, A. D., SPACKMAN, W. and DOLSEN, P., 1984. Occurrence and distribution of sulfur in peat-forming environments of southern Florida. *Int. J. Coal Geol.*, **4**, 73–96.
- COOK, A. C. and STRUCKMEYER, H., 1986. The role of coal as a source rock for oil. In: GLENIE, R. C. (Ed.), Second South-Eastern Australia Oil Exploration Symposium. Petroleum Exploration Society of Australia, 419–429.
- DAMTOFT, K., NIELSEN, L. H., JOHANNESSEN, P. N., THOMSEN, E. and ANDERSEN, P. R., 1992. Hydrocarbon plays of the Danish Central Trough. In: SPENCER, A. M. (Ed.), Generation, accumulation and production of Europe's hydrocarbons II. Spec. Publ. European Association of Petroleum Geoscientists, **2**, 35–58.
- DANISH ENERGY AGENCY, 1998. Oil and gas production in Denmark 1997. Danish Energy Agency, Ministry of Environment and Energy, Copenhagen, 78 pp.
- DANISH ENERGY AGENCY, 1999. Oil and gas production in Denmark 1998. Danish Energy Agency, Ministry of Environment and Energy, Copenhagen, 99 pp.
- DURAND, B. and PARATTE, M., 1983. Oil potential of coals: a geochemical approach. In: BROOKS, J. (Ed.), Petroleum geochemistry and exploration of Europe. *Geol. Soc. London Spec. Publ.*, **12**, 255–264.
- GOWERS, M. B. and SÆBØE, A., 1985. On the structural evolution of the Central Trough in the Norwegian and Danish sectors of the North Sea. *Mar. Petrol. Geol.*, **2**, 298–318.
- HUANG, W.-Y. and MEINSCHIN, W. G., 1979. Sterols as ecological indicators. *Geochim. Cosmochim. Acta*, **43**, 739–745.
- HUNT, J. M., 1996. Petroleum geochemistry and geology. W. H. Freeman and Company, New York, 743 pp.
- ICCP, 1998. The new vitrinite classification (ICCP System 1994). *Fuel*, **77**, 349–358.
- ISAKSEN, G. H., CURRY, D. J., YEAKEL, J. D. and JENSSEN, A. I., 1998. Controls on the oil and gas potential of humic coals. *Org. Geochem.*, **29**, 23–44.
- JENSEN, T. F., HOLM, L., FRANDBSEN, N. and MICHELSEN, O., 1986. Jurassic – Lower Cretaceous lithostratigraphic nomenclature for the Danish Central Trough. *Danm. Geol. Unders. Ser. A*, **12**, 65 pp.
- KORSTGÅRD, J. A., LERCHE, I., MOGENSEN, T. E. and THOMSEN, R. O., 1993. Salt and fault interactions in the northeastern Danish Central Graben: observations and inferences. *Bull. Geol. Soc. Denm.*, **40**, 197–255.
- MOORE, T. A., SHEARER, J. C. and MILLER, S. L., 1996. Fungal origin of oxidised plant material in the Palangkaraya peat deposit, Kalimantan Tengah, Indonesia: implications for “inertinite” formation in coal. *Int. J. Coal Geol.*, **30**, 1–23.
- MØLLER, J. J., 1986. Seismic structural mapping of the Middle and Upper Jurassic in the Danish Central Trough. *Danm. Geol. Unders. Ser. A*, **13**, 37 pp.
- PEPPER, A. S. and CORVI, P. J., 1995. Simple kinetic models of petroleum formation. Part 1: oil and gas generation from kerogen. *Mar. Petrol. Geol.*, **12**, 291–319.
- PETERS, K. E. and MOLDOWAN, J. M., 1993. The biomarker guide – interpreting molecular fossils in petroleum and ancient sediments. Prentice Hall, New Jersey, 363 pp.
- PETERSEN, H. I., 1998. Morphology, formation and palaeo-environmental implications of naturally formed char particles in coals and carbonaceous mudstones. *Fuel*, **77**, 1177–1183.
- PETERSEN, H. I. and ANDSBJERG, J., 1996. Organic facies development within Middle Jurassic coal seams, Danish Central Graben, and evidence for relative sea-level control on peat accumulation in a coastal plain environment. *Sed. Geol.*, **106**, 259–277.
- PETERSEN, H. I. and ROSENBERG, P., 1998. Reflectance retardation (suppression) and source rock properties related to hydrogen-enriched vitrinite in Middle Jurassic coals, Danish North Sea. *Journ. Petrol. Geol.*, **21**, 247–263.
- PETERSEN, H. I. and ROSENBERG, P., *in press*. The relationship between the composition and rank of humic coals and their activation energy distributions for the generation of bulk petroleum. *Petrol. Geosci.*
- PETERSEN, H. I., ROSENBERG, P. and ANDSBJERG, J., 1996. Organic geochemistry in relation to the depositional environments of Middle Jurassic coal seams, Danish Central Graben, and implications for hydrocarbon generative potential. *AAPG Bull.*, **80**, 47–62.
- PETERSEN, H. I., ANDSBJERG, J., BOJESSEN-KOEFOED, J. A., NYTOFT, H. P. and ROSENBERG, P., 1998. Petroleum potential and depositional environments of Middle Jurassic coals and non-marine deposits, Danish Central Graben, with special reference to the Søgne Basin. *Geol. Denm. Surv. Bull.*, **36**, 78 pp.
- PHILLIPS, S. and BUSTIN, R. M., 1996. Sulfur in the Changuinola peat deposit, Panama, as an indicator of the environments of deposition of peat and coal. *Jour. Sed. Research*, **66**, 184–196.

- PHILP, R. P., 1994. Geochemical characteristics of oils derived predominantly from terrigenous source materials. In: SCOTT, A. C. and FLEET, A. J. (Eds.), Coal and coal-bearing strata as oil-prone source rocks? *Geol. Soc. London Spec. Publ.*, **77**, 71–91.
- PRICE, L. C., 1991. On the origin of the Gulf Coast Neogene oils. *Transactions – Gulf Coast Ass. Geol. Soc.*, **XLI**, 524–541.
- SCOTT, A. C., 1989. Observations on the nature and origin of fusain. *Int. J. Coal Geol.*, **12**, 443–475.
- STOUT, S. A., 1994. Chemical heterogeneity among adjacent coal microlithotypes – implications for oil generation and primary migration from humic coals. In: SCOTT, A. C. and FLEET, A. J. (Eds.), Coal and coal-bearing strata as oil-prone source rocks? *Geol. Soc. London Spec. Publ.*, **77**, 93–106.
- TAYLOR, G. H., TEICHMÜLLER, M., DAVIS, A., DIESSEL, C. F. K., LITTKE, R. and ROBERT, P., 1998. Organic petrology. Gebrüder Borntraeger, Berlin, Stuttgart, 704 pp.
- TEICHMÜLLER, M., 1974a. Entstehung und Veränderung bituminöser Substanzen in Kohlen in Beziehung zur Entstehung und Umwandlung des Erdöls. *Fortschr. Geol. Rheinld. u. Westf.*, **24**, 65–112.
- TEICHMÜLLER, M., 1974b. Über neue Macerale der Liptinit-Gruppe und die Entstehung von Micrinit. *Fortschr. Geol. Rheinld. u. Westf.*, **24**, 37–64.
-

a



b



c

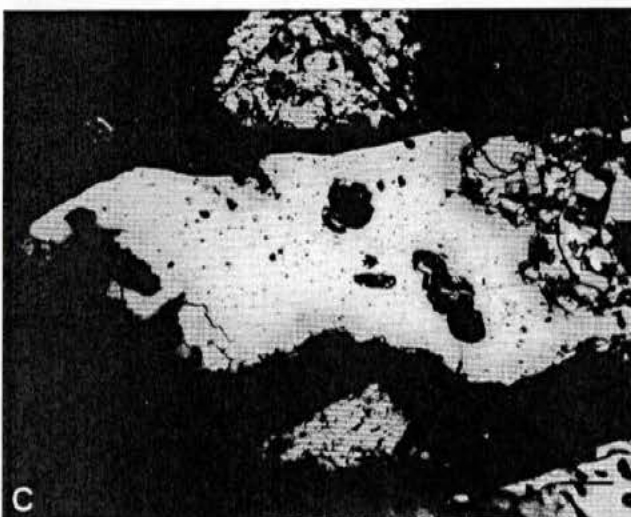


Plate 1a. High-reflecting, partly crushed fusinite (f) and broken, lower-reflecting semifusinite (sf) together with an abundance of inertodetrinite and macrinite; b. "massive" macrinite (m) and inertodetrinite (i); c. naturally-formed char particle.

All photomicrographs from sample 750, seam T2, 0.05 to 0.11 m interval; reflected white light, oil immersion; scale bar approx. 30 μm .



Plate 2. Very large particle of naturally-formed char (sample 743, seam X, 0.10 to 0.15 m interval; reflected white light, oil immersion; scale bar approx. 30 μm).

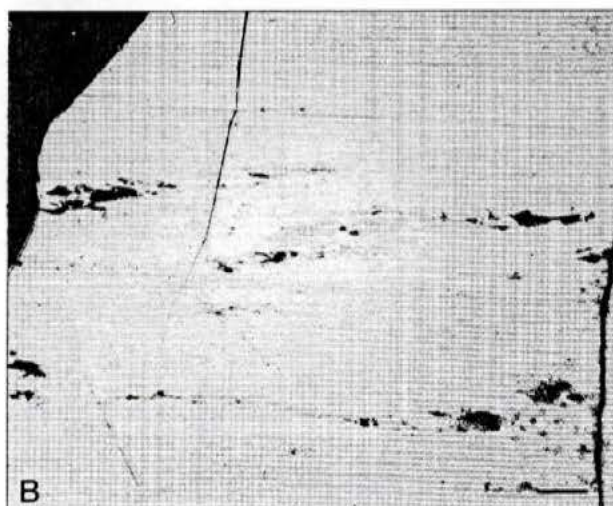
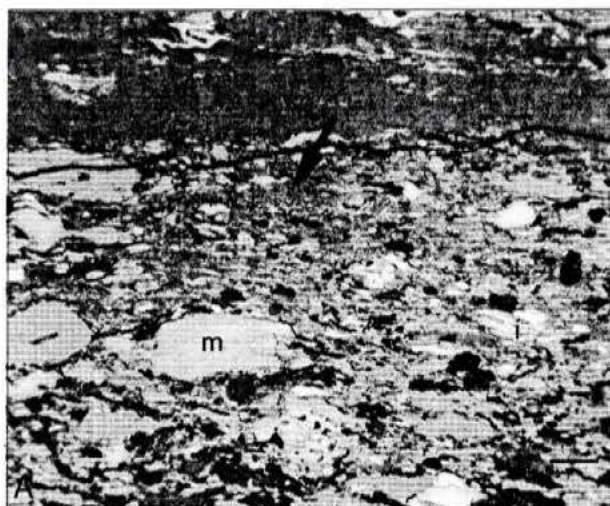


Plate 3a. Abundant inertodetrinite (i), macrinite (m), and sporinite and liptodetrinite (dark particles) in a groundmass of collodetrinite (arrow) (sample 739, seam T4, 0.05 to 0.10 m interval);
b. collotelinite (sample 738, seam T4, 0.10 to 0.18 m interval).

Both photomicrographs in reflected white light, oil immersion; scale bar approx. 30 μm .

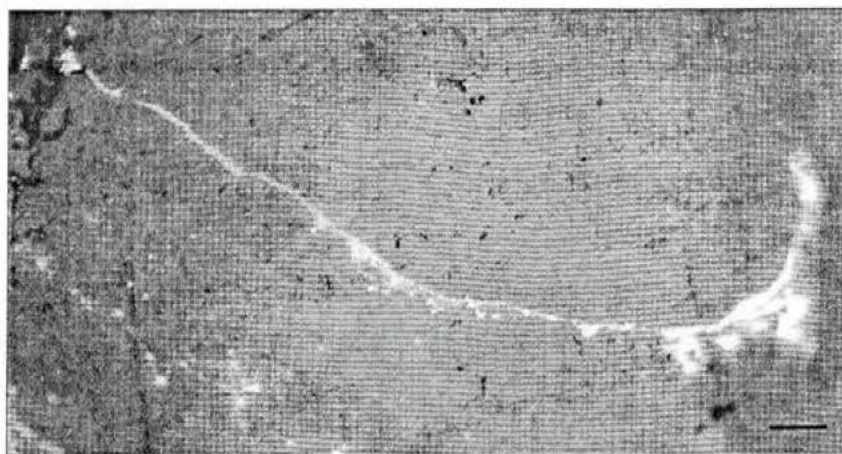


Plate 4. Micritised cutinite (sample 739, seam T4, 0.05 to 0.10 m interval; reflected white light, oil immersion; scale bar approx. 20 μm)

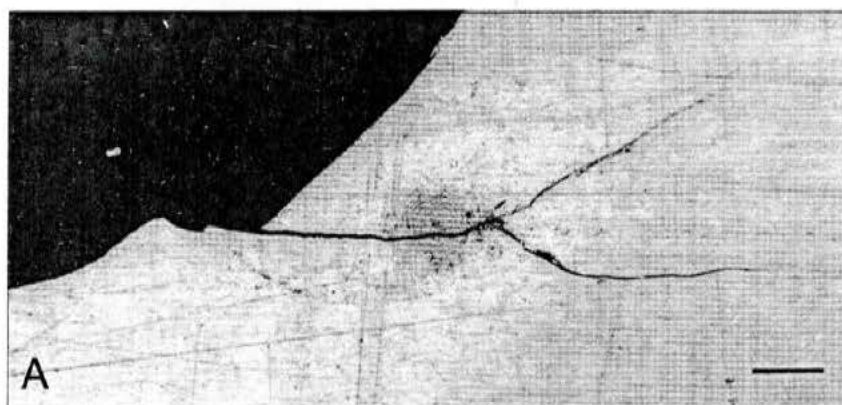


Plate 5. (a, b, c) Oil-droplets in association with cleats in collotelinite; picture (c) shows the same field as (b) under blue-light irradiation which makes the yellowish fluorescence of the oil-droplets visible (sample 737, seam T4, 0.18 to 0.23 m interval; photomicrographs (a) and (b) in reflected white light, oil immersion; photomicrograph (c) in reflected blue light, oil immersion; scale bar approx. 30 μm).



Plate 5c.

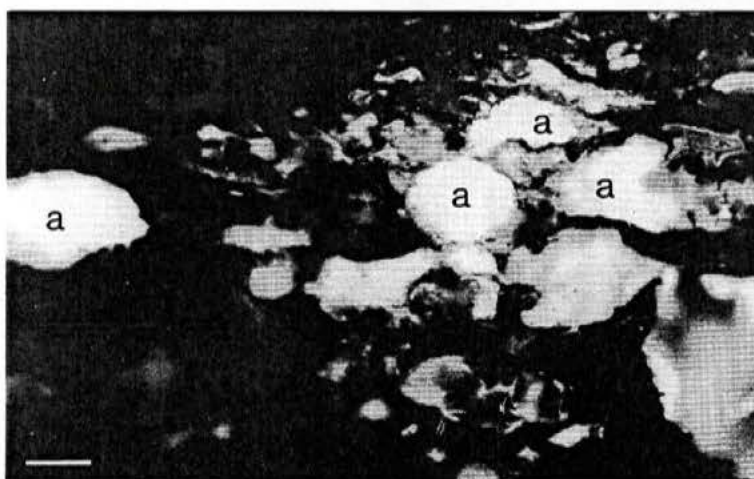


Plate 6. Alginite (a) in the 0.08-m thick carbonaceous mudstone above seam T4 (sample 736, reflected blue light, oil immersion; scale bar approx. 30 μ m).

FOREST FIRES, CLIMATE, AND SEA-LEVEL CHANGES IN A COASTAL PLAIN-SHALLOW MARINE SUCCESSION (EARLY-MIDDLE OXFORDIAN JAKOBSSTIGEN FORMATION, NORTH-EAST GREENLAND)

HENRIK VOSGERAU¹*, JØRGEN A. BOJESSEN-KOEFOED², HENRIK I. PETERSEN², AND FINN SURLYK¹

¹ Geological Institute, University of Copenhagen, Øster Voldgade 10, DK-1350 Copenhagen K, Denmark

² Geological Survey of Denmark and Greenland, Thoravej 8, DK-2400 Copenhagen NV, Denmark

ABSTRACT: The Lower-Middle Oxfordian Jakobsstigen Formation of North-East Greenland was deposited in a semi-enclosed marine embayment along the western margin of the rifted seaway between Greenland and Norway. It consists of rhythmically interbedded coastal-plain and shallow marine deposits, reflecting repeated alternation of two markedly different environments. The formation is 128 m thick and forms an overall coarsening-upward unit. The basic motif is a high-order sequence, 0.1–10 m thick, consisting of a thin, laterally extensive carbonaceous mudstone overlain by coarsening-upward offshore-transition-zone and shoreface heteroliths and sandstones. The mudstone was deposited during early base-level rise in a shallow, flat-bottomed lake or lagoon on a flat, low-lying coastal plain. The plain was subsequently flooded during maximum rise in sea level, followed by shoreface progradation during late rise, stillstand, and early fall. The boundary between coastal-plain and shallow-marine deposits represents the maximum flooding surface, separating the transgressive and highstand systems tracts. The organic material of the carbonaceous coastal-plain mudstones is dominated by inertinite macerals resulting from wildfires. In the shallow-marine sediments the organic material contains a high proportion of huminite and a significantly lower proportion of inertinite macerals, indicating wetter conditions and a lower frequency of wildfires in the hinterland during times of shoreface deposition. The different climatic regimes may reflect high-order sea-level fluctuations that exerted an important influence on the areal extent of the marine environments in large areas of the rifted seaway between Greenland and Norway due to the flat, low-gradient basin floor and overall shallow-water conditions. Periods of late rise and highstand were characterized by a humid climate, possibly caused by higher precipitation in the nearby source areas related to evaporation over the extensive sea. During lowstands only the topographically deeper parts of the rift complex remained submerged and a drier continental climate prevailed. The carbonaceous mudstones were deposited in the transitional period from the drier to the more humid climate corresponding to early sea-level rise. This was the time of large seasonal variations with optimum conditions for wildfires in the vegetated hinterland. This time interval was also characterized by onset of base-level rise in the low-lying coastal plain, where the wildfire-derived inertinite was trapped in shallow lakes and lagoons.

INTRODUCTION

The Lower-Middle Oxfordian Jakobsstigen Formation of North-East Greenland consists of rhythmically interbedded thin, laterally extensive carbonaceous mudstones and coarsening-upward heteroliths and sandstones. Surlyk and Clemmensen (1983) interpreted the mudstones as deposited offshore under poorly oxygenated conditions followed by shoreface progradation reflected by the coarsening-upward nature of the overlying heteroliths and sandstones. Organic geochemical and coal petrographic analyses of the carbonaceous mudstones suggest, however, that they were deposited in shallow lakes or lagoons on a coastal plain and contain evidence for wildfires.

Stacked coarsening-upward parasequences composed of shallow-marine sediments are separated by marine flooding surfaces (Van Wagoner et al. 1990). In the Jakobsstigen Formation coarsening-upward shallow-marine heteroliths and sandstones are separated by coastal-plain mudstones. The basic unit consists of a thin coastal-plain mudstone separated by a flooding surface from overlying offshore-transition-zone to shoreface heteroliths and sandstones. The main focus in the facies description is on the terrestrially influenced coastal-plain mudstones preserved below the flooding surfaces. The organic geochemical and coal petrographic composition of the mudstones was treated by Bojesen-Koefoed et al. (1997). The aim of this paper is to describe and interpret the abrupt, rhythmic changes between the markedly different environments and relate them to variations in climate and sea level.

GEOLOGICAL SETTING

The Lower-Middle Oxfordian Jakobsstigen Formation was deposited in the Wollaston Forland basin of North-East Greenland, situated on the western margin of the Jurassic rift complex between Greenland and Norway (Surlyk 1977, 1990, 1991). The paleogeographic setting was a rift-controlled embayment limited by the Greenland craton to the west, closed to the north and open to marine circulation to the south. Jurassic rifting was initiated in the Late Bajocian and reached a climax in the Volgian. During deposition of the Jakobsstigen Formation the basin was limited to the east by the crestal margin of a slightly westwards to southwestwards tilted block; the crest formed elongated islands or peninsulas that broadened and were attached to the mainland to the north (Fig. 1). The overall sediment transport was axial from north to south.

The Early-Middle Oxfordian age of the formation is based on finds of dinoflagellate cysts (Fig. 2, Table 1), boreal Bathonian-Callovian ammonites in the underlying Pelion Formation, lower Upper Oxfordian ammonites in the overlying Bernbjerg Formation, and a few occurrences of the ammonite *Cardioceras alphacordatum* Spath in the lower and middle part of the formation indicating the Lower Oxfordian *Cardioceras cordatum* Chronozone (Maync 1947; Sykes and Surlyk 1976; Surlyk 1977).

METHODS

The Jakobsstigen Formation was studied in the type section, the valley *Cardiocerasdal* in southwest Wollaston Forland (triangle in Fig. 1). A total of 38 samples were collected for organic petrographic, geochemical, and biostratigraphic analysis.

Microscopic analyses of polished blocks of the mudstone samples and the heterolithic sample were carried out in oil immersion using a Zeiss incident-light microscope equipped with visible and ultraviolet light sources, and a Swift point counter. A total of 500 points were recorded in each sample, but it was possible to obtain only 300 points in the kerogen concentrate from the heterolithic facies. Inertinite reflectance measurements were performed by means of a Leitz MPV-SP system, which was calibrated against a standard with a reflectance value of 0.893% R_o . Between 250 and 300 measurements were made on each sample. Sample preparation, analysis methods, and maceral nomenclature follow the standards outlined in Taylor et al. (1998).

Total organic carbon (TOC) was determined on carbonate-free samples by means of a LECO IR212 induction furnace. Total sulfur was determined

* Current address: Geological Survey of Denmark and Greenland, Thoravej 8, DK-2400 Copenhagen NV, Denmark

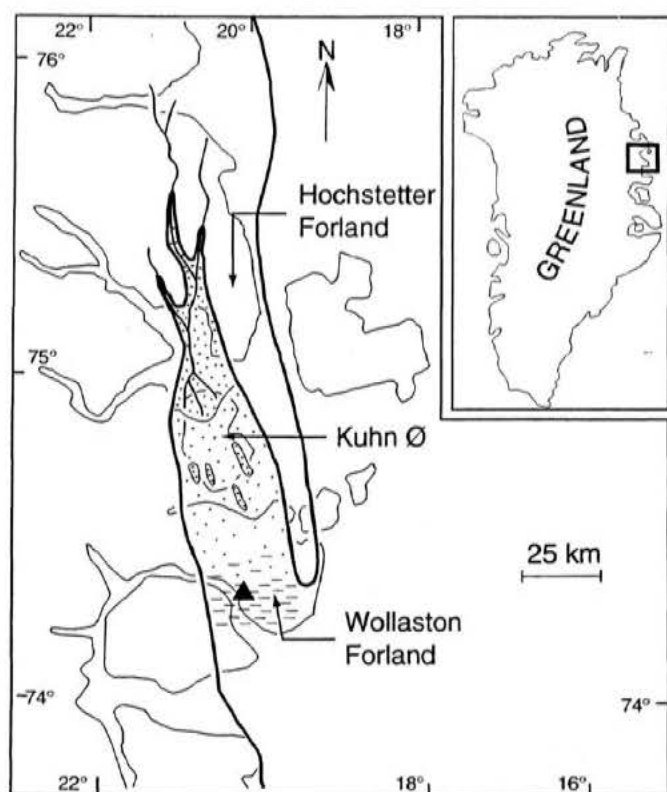


FIG. 1.—Early Oxfordian paleogeography of the Wollaston Forland area. Triangle marks the location of Cardiocerasdal (after Surlyk 1990).

by using a Metalyt 90S CS-analyzer. Gas chromatography of saturated extract fractions was performed using a Hewlett-Packard 5890 gas chromatograph (25m HP1 WCOT column, splitless injection).

SEDIMENTARY FACIES

The Jakobsstigen Formation is 128 m thick in Cardiocerasdal, and consists of alternating coastal-plain and shallow-marine deposits (Fig. 2). The rhythmic alternation between pale-colored shoreface sandstones and thin, dark, carbonaceous mudstones gives the formation a characteristic, horizontally striped appearance in the field (Fig. 3). The two facies associations and their constituent facies are described below.

Offshore-Transition to Shoreface Facies Association (1)

The facies of this association form coarsening-upward units. The units are described in the following, beginning with the most fine-grained facies, which normally form the lower part of the units.

Heterolithic Mudstone and Sandstone (1a).—The heterolithic facies consists of wave and current cross-laminated sandstones with thin organic-rich mudstone drapes. The facies shows a very uniform development throughout the formation. Wave ripple crests are mainly oriented NE–SW (Fig. 4). The primary structures are commonly obscured because of weathering and strong bioturbation. The facies include a fine-grained subfacies with a mudstone/sandstone ratio of about 0.4, which is commonly overlain by a coarse-grained subfacies with a mudstone/sandstone ratio of about 0.15. The sandstones are carbonate cemented and very fine grained. The facies contains spores, pollen, marine dinoflagellate cysts, and macrofossils, mainly belemnites, and bivalves. Analysis of a kerogen concentrate of the heterolithic facies (sample 99–573, Fig. 2) shows that the organic matter is characterized by a high proportion of huminite (76 vol. %) and a sig-

nificantly lower proportion of inertinite (13 vol. %). Naturally formed char (see Petersen 1998) is not recorded (Table 2). The fine-grained heteroliths show the highest degree of bioturbation (up to 100%) and seem to have the lowest ichnodiversity (Fig. 5). They dominate the association in the lower part of the formation, whereas the coarse-grained heteroliths dominate in the upper part. The two subfacies commonly form coarsening-upward successions.

The heterolithic facies were deposited in a marine environment, as reflected by the abundant marine dinoflagellate cysts and macrofossils. The orientations of wave ripple crests suggest a NE–SW trending coastline. The high degree of bioturbation in the fine-grained heteroliths reflects slow sedimentation and little physical reworking. The fine-grained heteroliths are interpreted as deposited in the offshore transition–lower shoreface zone, whereas the coarse-grained heteroliths were deposited during higher-energy conditions and are interpreted as formed in the lower to middle shoreface zone. A coarsening-upward succession of the two facies therefore reflects upward shallowing caused by lower to middle shoreface progradation over the offshore transition zone (e.g., Elliott 1986).

Cross-Bedded Sandstone (1b).—In the upper part of the formation the heterolithic facies (1a) is commonly overlain by cross-bedded sandstones with sets up to 2 m thick (Figs. 2, 5). The foresets are tangential and are separated by single or double mud drapes and reactivation surfaces. The sandstones in some cases also show low-angle master bedding separated by thinner cross-bedded or climbing-ripple cross-laminated sets. Paleocurrent directions indicated by the cross-bedding and the low-angle master bedding are towards the southwest (Fig. 4). The low-angle master bedding surfaces may be wave or current rippled and draped by thin mudstones. Sporadic current-ripple cross-laminae dip in the direction opposite to that of the master bedding (Fig. 4). The cross-bedded sandstones show a gradual contact with the underlying heterolithic facies, whereas the upper boundary is a sharp erosion surface. Logs up to 1 m long occur locally. The degree of bioturbation is low, and the trace-fossil assemblage is dominated by *Monocraterion tentaculatum* Torell and meter-long vertical U-burrows of *Diplocraterion habichi*.

The single or double mud drapes, reactivation surfaces, and bimodal cross-lamination suggest deposition in subtidal sandwaves (Visser 1980; Boersma and Terwindt 1981; Smith 1988; Wood and Hopkins 1989). The climbing-ripple cross-laminated sets, migrating down the low-angle master bedding, reflect suspension fallout into deeper water and possibly deposition in mouth bars (cf. Elliott 1974; Gjelberg and Steel 1995).

Planar-Laminated Sandstone (1c).—In a few cases a planar-laminated sandstone, about 10 cm thick, overlies the cross-bedded sandstone (1b). It has a bimodal grain-size distribution of fine-grained and subordinate coarse-grained sand. It is not bioturbated, and the lower and upper boundaries are erosional (Fig. 5). The planar lamination, coarse grain size, and lack of bioturbation suggest upper-flow-regime plane-bed deposition in the foreshore (Clifton et al. 1971).

The facies association forms coarsening-upward units consisting of heterolithic mudstones and sandstones gradually overlain by cross-bedded sandstones that locally are overlain by a thin planar-laminated sandstone. It is interpreted as formed by progradation of subtidal sandwaves and in some cases mouth bars over offshore-transition-zone to middle-shoreface deposits. The paleogeographic setting, the tidal indications, and the dominance of southwestward-directed ebb currents suggest deposition in a tide-dominated delta (cf. Wood and Hopkins 1989; Allen and Posamentier 1993). Tidal currents were most likely amplified by the funnel-shaped geometry of the basin, which formed a structurally controlled estuary (Surlyk and Clemmensen 1983).

Coastal-Plain Facies Association (2)

The coastal-plain facies association consists of thin carbonaceous mudstones and rare inclined heterolithic sandstone and mudstone beds. In the

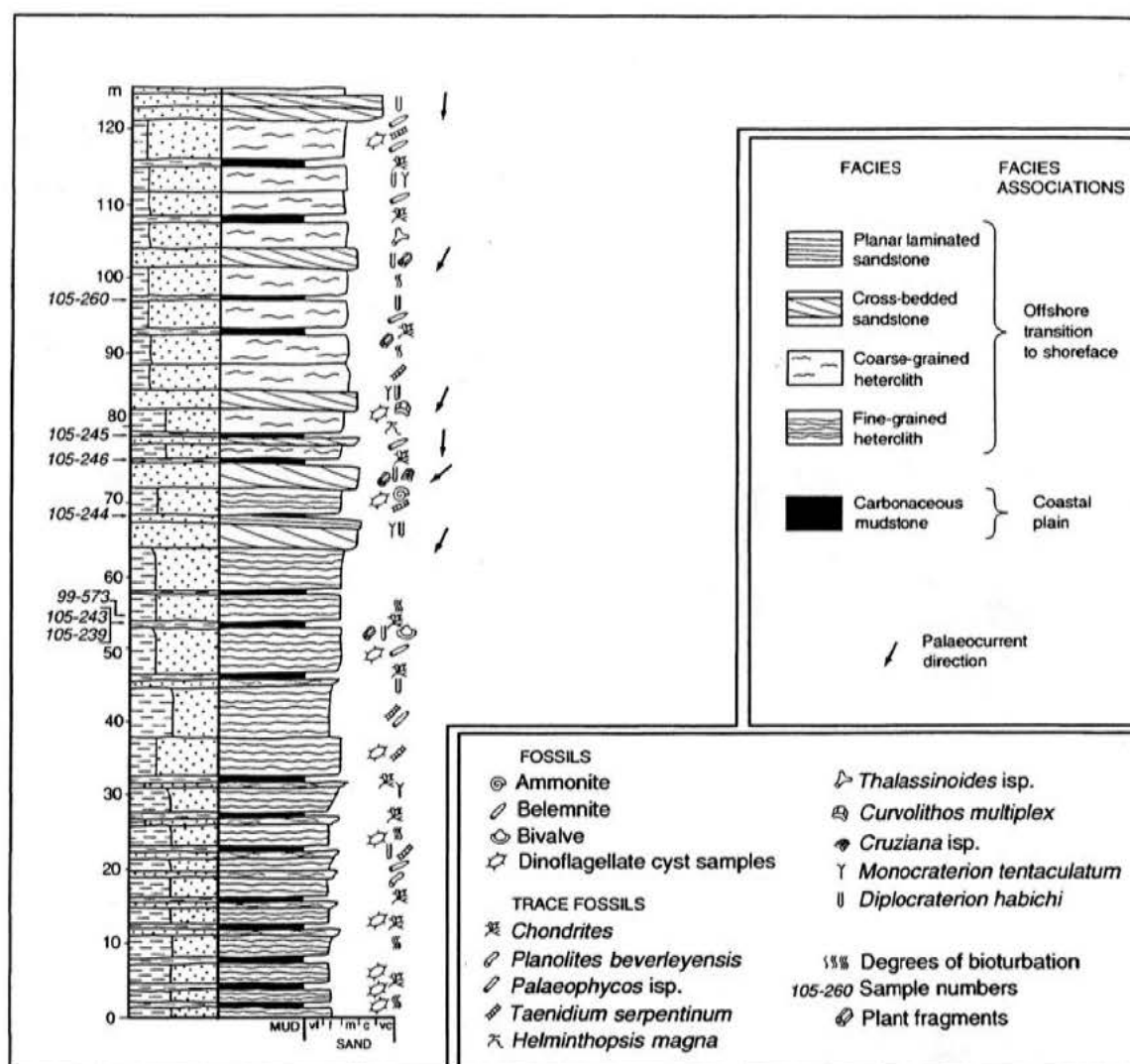


FIG. 2.—Section of the Jakobsstigen Formation, northwest side of Cardiocersdal, Wollaston Forland (location shown in Figure 1) with the thickest and most lateral continuous mudstones marked. Examples of higher-order sequences are shown in Figure 5.

TABLE 1.—List of dinoflagellate cysts identified in samples collected from the sandy marine sediments of the Jakobsstigen Formation, Cardiocersdal.

<i>Chytroisphaeridia cerastes</i> Davey 1979
<i>Endoscrinium galerium</i> (Deflandre) Vozzhennikova 1967
<i>Gonyaulacysta jurassica</i> (Deflandre) Sarjeant 1982
<i>Leptodinium subtile</i> Klement 1960
<i>Liesbergia</i> (<i>Trichodinium</i>) <i>scarburghense</i> Sarjeant 1964
<i>Nannoceratopsis pellucida</i> (Deflandre) Evitt 1961
<i>Pareodinia</i> sp.
<i>Pareodinia ceratophora</i> (Deflandre) Below 1990
<i>Kalyptea diceras</i> (Cookson and Eisenack) Fisher and Riley 1980
<i>Pareodinia stegasta</i> (Sarjeant) Below 1990
<i>Rhynchodiniopsis cladophora</i> (Deflandre) Below 1981
<i>Rigaudella aemula</i> (Deflandre) Below 1982
<i>Rigaudella filamentosa</i> (Cookson and Eisenack) Below 1982
<i>Seriodinium crystallinum</i> (Deflandre) Klement 1960
<i>Surculosphaeridium</i> sp.
<i>Wanaea fimbriata</i> Sarjeant 1961

The dinoflagellate cysts indicate an Early–Middle Oxfordian age, especially by the presence of *Chytroisphaeridia cerastes* Davey 1979, *Liesbergia* (*Trichodinium*) *scarburghense* Sarjeant 1964, *Kalyptea diceras* (Cookson and Eisenack) Fisher and Riley 1980, *Rigaudella aemula* (Deflandre) Below 1982, *Seriodinium crystallinum* (Deflandre) Klement 1960 and *Wanaea fimbriata* Sarjeant 1961 (S. Piasecki, personal communication, 1998).

description and interpretation of the mudstone the main focus is on the petrographic composition and geochemistry of the organic matter. The position of the investigated samples is shown in Figure 2.

Carbonaceous Mudstone (2a).—The carbonaceous mudstones are 1–20 cm thick and tabular, and the thickest can be followed laterally for more than 1 km, with distance limited by outcrop (Fig. 3). They are dark gray to black, structureless, or with fine horizontal lamination and in some places small lenses of current cross-laminated very fine-grained sandstones. Grain-size analysis of the inorganic fraction shows a mean composition of 40 wt % clay, 30 wt % silt, and 30 wt % sand. About ten carbonaceous mudstone beds were investigated for their palynological, geochemical, or coal petrographic composition. The mudstones do not contain dinoflagellate cysts, marine macrofossils, spores, or pollen. Total organic carbon (TOC) and total sulfur (TS) contents are 7–21 wt % and 0.08–7.4 wt %, respectively (Table 2). Solvent extract yields are low, ranging from 8 to 51 mg/g TOC, and the extract compositions are dominated by heteroatomic compounds. Distributions of normal alkanes are generally skewed towards short-chain-length compounds, which show a strong even-carbon-number predominance. In the nC_{22+} range, slight odd-carbon-number predominance prevails. Hopane and sterane biological markers indicate low thermal maturity, and notable features include enhancement of homohopanes and $\alpha\beta\beta$ -ster-

TABLE 2.—Organic petrographical composition and screening data, Jakobsstigen Formation, Cardiocerasdal.

Organic Petrographic Composition and Screening Data								
Volume %							Wt.-%	
Sample	Huminite	Liptinite	Inertinite	Char	Other Minerals	Pyrite	TOC	TS
105-260	4	0	53	3	33	7	15.82	0.79
105-246	7	0	52	2	37	2	20.46	5.1
105-245	11	0	58	3	27	1	20.93	1.1
105-244	5	1	49	1	41	3	19.57	4.5
105-243	4	0	41	0	51	4	9.21	7.4
105-242	4	0	52	1	41	2	15.87	3.9
105-241	5	0	49	2	43	1	15.88	2.7
105-240	4	0	44	0	51	1	15.66	3.8
105-239	6	0	41	1	51	1	16.65	5.4
105-223	12	3	36	0	45	4	7.12	0.78
99-573	76*	1*	13*	0*	5*	5*	0.61	—

* Kerogen concentrate of shoreface sandstone.

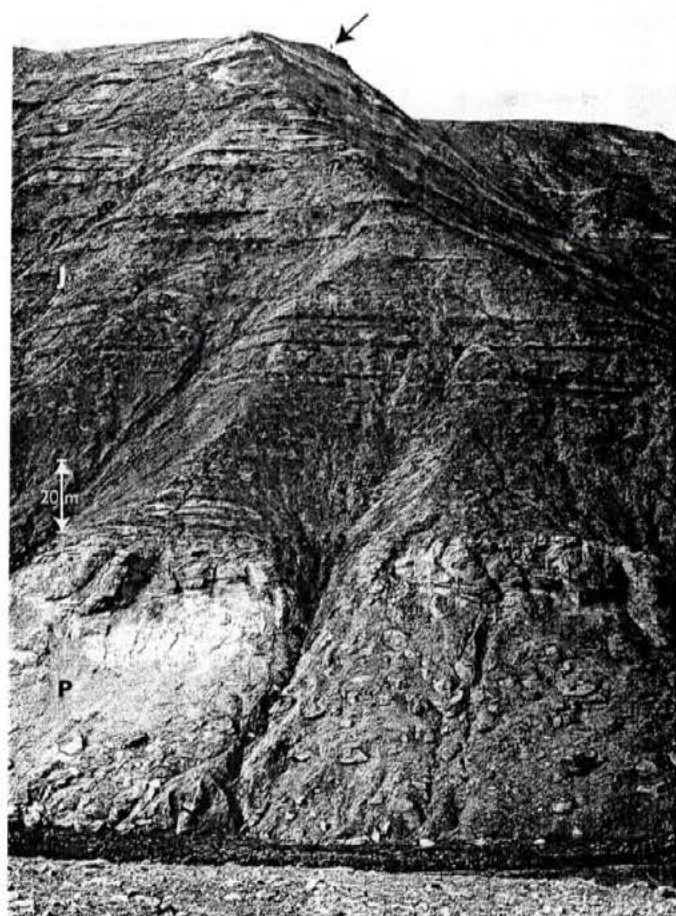


FIG. 3.—The Middle Jurassic sandy Pelion Formation (P) overlain by the horizontally striped cliffs exposing the Lower-Middle Oxfordian Jakobsstigen Formation (J), 128 m thick, Cardiocerasdal, Wollaston Forland. Arrow points at person for scale.

anes, and very low hopane/sterane ratios (Bojesen-Koefoed et al. 1997). Pyrite, amounting to 1–7 vol. %, is present as framboidal or weathered pyrite (Table 2), but the content may be underestimated because of very small crystal sizes. These observations suggest an almost total absence of terrigenous lipids, a predominance of microbially derived *n*-alkanes, and a

saline depositional environment (Casagrande 1987; Grimalt and Albaiges 1987; Fu Jiamo et al. 1990; Genik 1993; Brown and Cohen 1995).

The organic-matter fraction of the mudstones is dominated by inertinite (36–58 vol. %), with angular and fragile inertodetrinite particles being the far most prominent constituent. The huminite fraction is dominated by the maceral attrinite, representing detrital humified organic matter. The huminite content is very low (4–7 vol. %), except for samples 105–245 and 105–223, in which it reaches 11 and 12 vol. %, respectively. Small amounts of liptinite are present in only two samples and is thus a negligible constituent, whereas minor amounts of char are observed in the majority of the samples (Table 2). Reflectance measurements of the inertinite fraction show a wide range with two pronounced reflectance populations with average values of 1.73 % R_o and 4.91 % R_o , respectively (Bojesen-Koefoed et al. 1997).

Abundant sand-filled *Chondrites* descend from the overlying heterolithic deposits. The burrow fill is coarser grained and the content of silt and clay is less than in the sand laminae of the mudstone. The mudstones commonly contain gypsum and are cemented with carbonate. Carbonate cement is particularly notable in the coarser-grained burrow fills, which are flattened because of early compaction. Thin bands of carbonate-cemented organic matter bend slightly around the burrow fills, showing that some compaction took place after cementation.

The mudstones in most cases rest on a sharp erosion surface with a relief of a few centimeters. In one case, small root casts were observed below a thin carbonaceous mudstone (too thin to be marked in Figure 2 but occurring approximately at the 60 m level). The contact with the overlying heterolithic sandstones is either a sharp erosion surface or gradational. In the latter case the mudstones become sandy and bioturbated in the upper part (Fig. 6).

The fine grain size, the horizontal lamination, and occasional lenses of current-ripple cross-laminated very fine-grained sand suggest that the mudstones were deposited from suspension and weak bottom currents. An al-

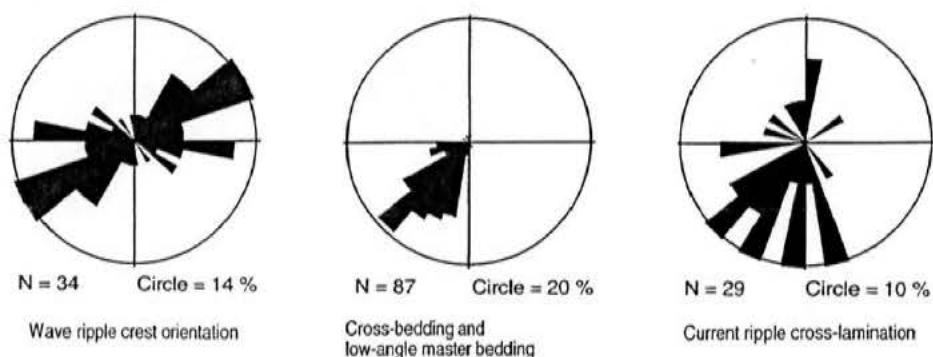


FIG. 4.—Paleocurrent data from the Jakobsstigen Formation, Cardiocerasdal. The data are grouped into wave-ripple crest orientation, cross-bedding and low-angle master bedding, and current-ripple cross-lamination.

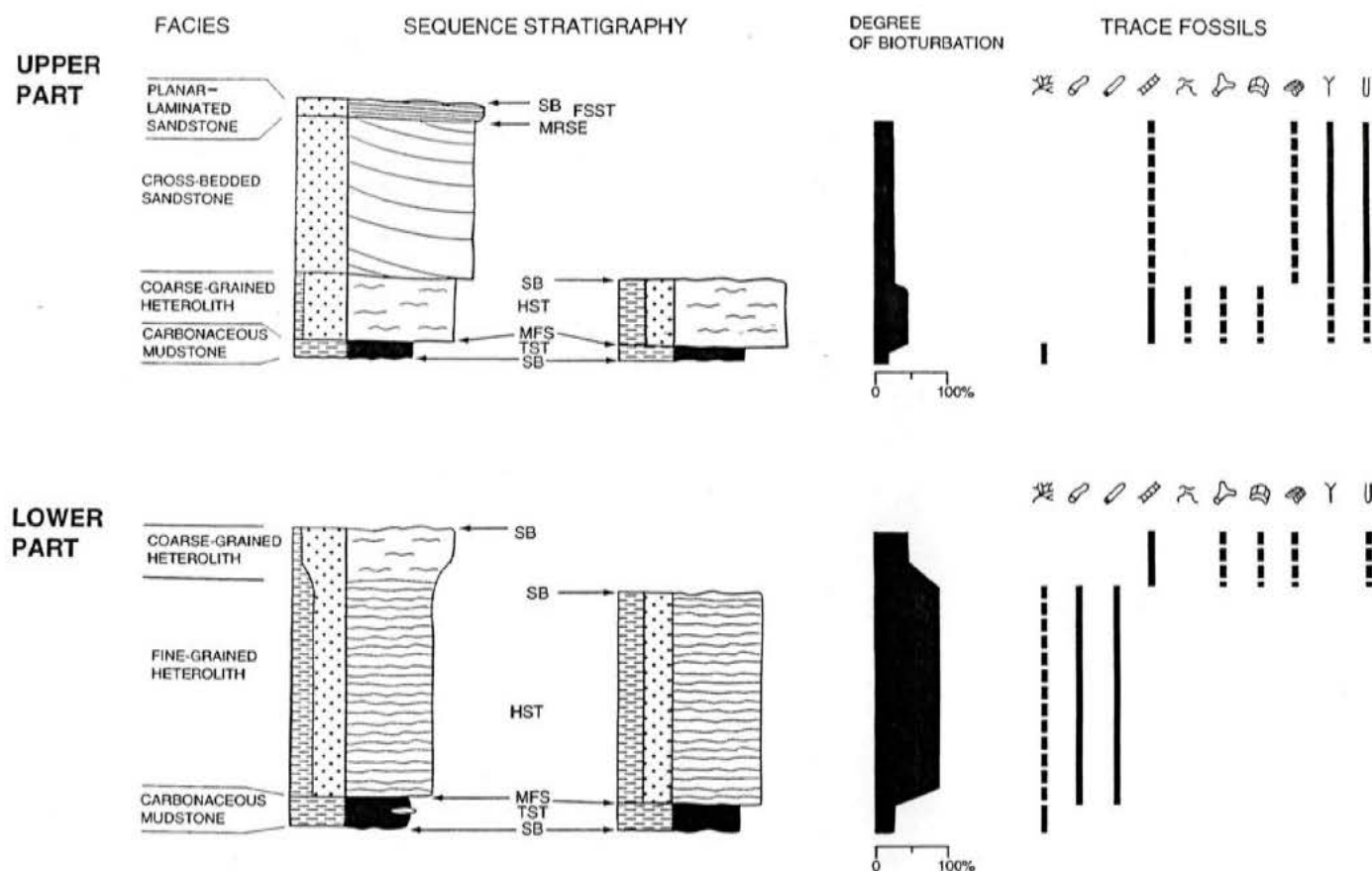


FIG. 5.—Schematic logs of high-order sequences from the lower and upper part of the Jakobsstigen Formation characterized by containing a basal thin coastal-plain mudstone; key surfaces are marked. Logs of well-developed and less developed sequences are shown to the left and right, respectively. The sequences vary in thickness from 0.1 m to 10 m. SB, sequence boundary; TST, transgressive systems tract; MFS, maximum flooding surface; MRSE, marine regressive surface of erosion; HST, highstand systems tract; FSST, falling-stage systems tract. For key to trace fossils, see Figure 2. The solid and broken lines indicate abundant or local occurrences of the trace fossils, respectively.

lochthonous origin of the inertinite is corroborated by the absence of rootlets below all but one bed. The exception is the organic-rich layer with rootlets, which has the highest content of humified organic matter of all samples (12 vol. %), indicating that *in situ* plants originally were present and possibly contributed to the formation of the bed (sample 105–223,

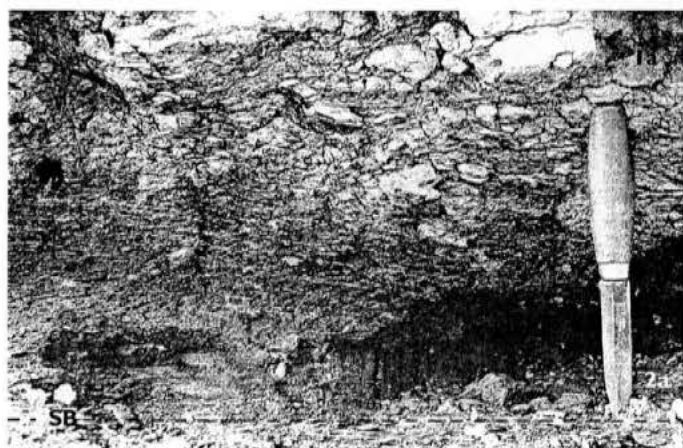


FIG. 6.—Carbonaceous mudstone (2a) with a sandy and bioturbated upper part and a gradational boundary with overlying heterolithic mudstone and sandstone (1a) (c. 55 m in Fig. 2). Knife is 19 cm long.

Table 2). In contrast, rootlets were not observed below the bed represented by sample 105–245, although the content of huminite is 11 vol. %.

The commonly poorly sorted, angular, and fragile nature of the inertodetrinite particles indicate that they represent fine splinters of fossil charcoal (fusinite, semifusinite), and the lack of a distinct microlamination suggests transport by wind to the site of deposition (Jones 1993; Taylor et al. 1998). Char represents heat-affected, degassed, humified organic matter (Petersen 1998), and its presence in the carbonaceous mudstones supports a fire-derived origin for the inertodetrinite macerals. The wide range of reflectances in the inertinite (charcoal) reflects the temperatures generated during the fires (cf. Cope and Chaloner 1985; Scott 1989; Jones et al. 1991; Scott and Jones 1994). The two main inertinite reflectance populations of the present study are interpreted to reflect ground fires and crown fires, respectively (Bojesen-Koefoed et al. 1997).

The presence of small rootlets under one carbonaceous mudstone with humified organic matter reflects emergent or nearly emergent conditions. The great lateral extent and tabular geometry of the thin mudstones and the low relief of the underlying erosion surfaces suggest deposition in a flat, low-lying coastal plain. The high pyrite contents with framboidal pyrite suggest syngenetic precipitation (Cohen et al. 1984; Casagrande 1987; Diessel 1992; Brown and Cohen 1995), and the geochemical composition of the solvent extract points to saline conditions. The complete absence of marine palynomorphs, body fossils, and trace fossils (except for *Chondrites*, which clearly descend from the overlying shallow-marine deposits) shows that the depositional environment was unfavorable for living organ-

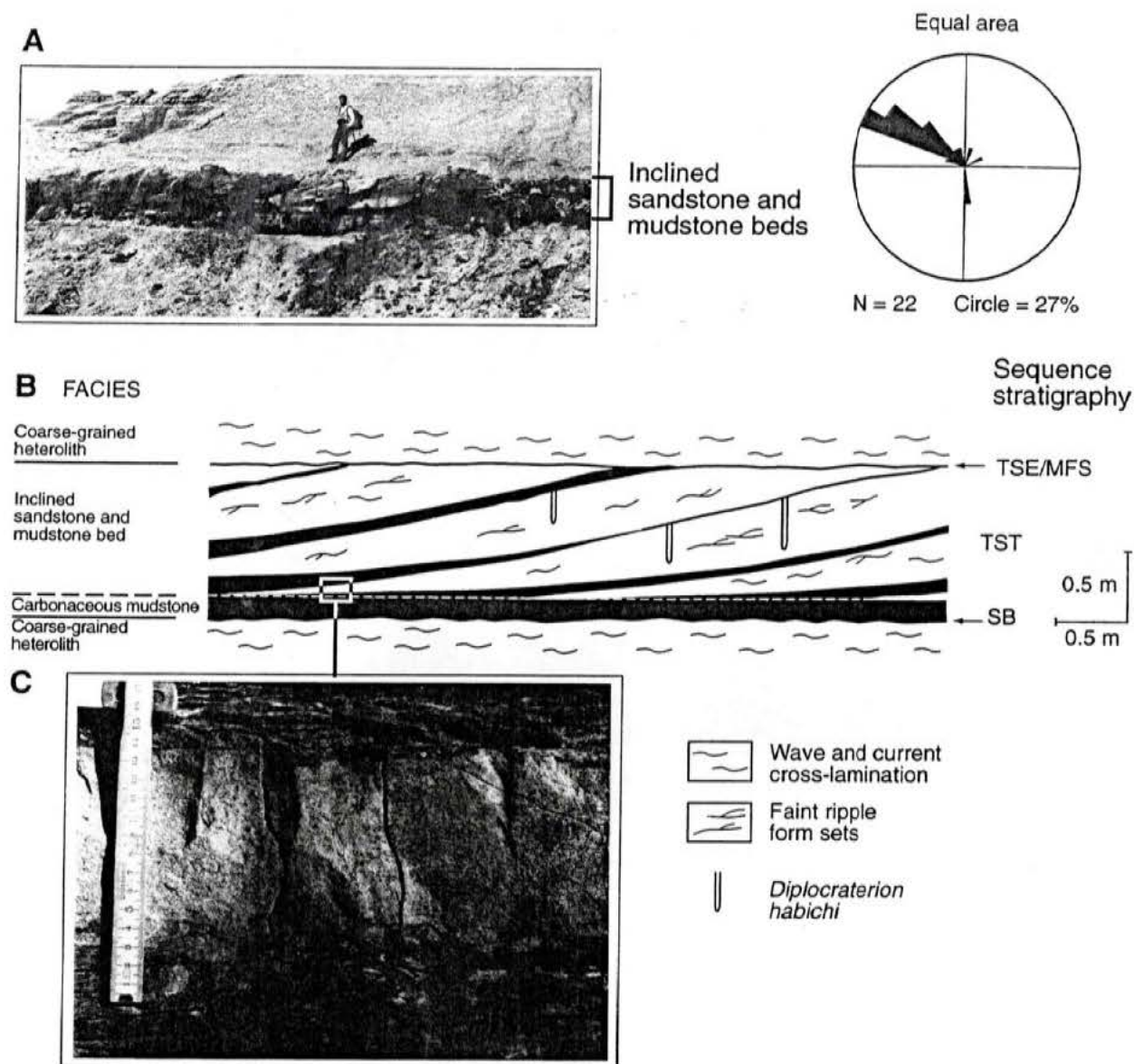


FIG. 7.—**A**) A set of Northwestward-inclined heterolithic sandstone and mudstone beds from the 60 m level in Figure 2. **B**) Sketch showing facies architecture and sequence stratigraphic interpretation of the inclined heterolithic strata. SB, sequence boundary; TST, transgressive systems tract; TSE, transgressive surface of erosion; MFS, maximum flooding surface. **C**) Detail of inclined heterolithic strata showing the gradational lower boundary and sharp irregular upper boundary of a sandstone bed in strike section.

isms except for halophilic microorganisms such as cyanobacteria, archaeobacteria, and possibly certain microalgae (Bojesen-Koeboed et al. 1997).

The mudstones are accordingly interpreted as deposited in shallow, flat-bottomed lakes or lagoons on a flat, low-lying coastal plain that was largely barren of higher plant vegetation. The fact that the fill of the *Chondrites* burrows are carbonate cemented shows that cementation took place after deposition of the carbonaceous mudstones. The burrow-fill cementation and the total lack of body fossils suggest that the cement was formed by percolating pore water enriched in carbonate by dissolution of fossils of the overlying shallow marine heteroliths and sandstones. The lack of marine microfossils and macrofossils in the mudstones also suggests that saline conditions were caused mainly by saltwater intrusion into the coastal plain during rising sea level, and not by random inundations. The infiltration of sea water and high rates of evaporation rendered the lakes saline and hindered higher plant vegetation on emergent areas. However, conditions fa-

vorable for autochthonous peat accumulation may have existed in places, as seen by the occasional presence of huminite and rootlets. The cause of the absence of spores and pollen in the carbonaceous mudstones is uncertain because they are very resistant to destruction and would be able to survive long periods of oxidation. The gypsum may be syngenetic, caused by evaporation of saline water. It is more likely, however, that the gypsum is related to weathering of pyrite.

Inclined Heterolithic Sandstone and Mudstone Bed (2b).—On the southeast side of the Cardiocerasdal valley (Fig. 1) a tabular set, 1 m thick, of inclined alternating fine- to medium-grained sandstone beds and dark gray to black, organic-rich mudstone beds overlies a carbonaceous mudstone (2a), c. 15 cm thick (Fig. 7). The set occurs approximately at the 60 m level in Figure 2 and can be followed laterally for more than 500 m. The lower set boundary is erosional but can be difficult to recognize because mudstone commonly occurs both below and above the surface. The

inclined sandstone and mudstone beds dip and thin out downwards to the lower set boundary with an angle of 2–29°, averaging 15°. The upper set boundary is a sharp erosion surface, which is overlain by coarse-grained heteroliths (1a). The down-dip length of the inclined beds is 4 to 6 m. They dip towards the northwest (Fig. 7). The beds contain no macrofossils. Unfortunately no samples were collected to test the content of microfossils.

The inclined sandstone beds are up to 0.5 m thick and are overall thicker than the interbedded mudstones. They have an almost sigmoidal shape in dip section, the uppermost convex part being partly removed by erosion. The grain size does not seem to change up-dip within beds. The sandstone beds are structureless or in some places contain faint ripple form sets separated by thin mud laminae. The degree of bioturbation is high, with *Diplocraterion habichi* and *Planolites beverleyensis* Billings as the dominant trace fossils. The boundary with an overlying inclined mudstone bed is sharp, commonly irregular, with a relief of a few centimeters (Fig. 7C).

The inclined mudstone beds typically are 10–15 cm thick, locally up to 35 cm. In places they thin up-dip so that the inclined sandstone beds are in direct contact in the upper part of the set. The mudstones are either structureless, planar laminated, parallel to the inclined bed surface, or contain faint sandy ripple formsets. Subrounded rip-up mudstone clasts occur locally down-dip, and sand-filled *Chondrites* may descend from overlying inclined sandstone beds. The mudstone layers become sandy and bioturbated in the upper part, and the boundary with the overlying inclined sandstone is gradational (Fig. 7C).

The alternation of faint ripple formsets and thin mudstone laminae in the inclined sandstones reflects varying flow regime. The sharp irregular top surfaces of the inclined sandstone beds indicate erosion during the highest-energy conditions, followed by mud deposition during periods of low energy. The inclined mudstone beds are very similar to the carbonaceous mudstone facies (2a) and were probably also deposited from suspension and weak bottom currents. However, the presence of subrounded rip-up mudstone clasts in the lower part reflects erosion of nearby mudstone deposits and deposition during higher-energy conditions. The sandy upper parts of an inclined mudstone bed reflect a gradual transition to higher-energy conditions and more intense bioturbation.

Inclined heterolithic strata are usually interpreted as formed by lateral point-bar migration in meandering channels that experienced considerable fluctuation in discharge as a result of seasonal or tidal changes (e.g., Bridges and Leeder 1976; Thomas et al. 1987; Noe-Nygaard and Surlyk 1988). It is not possible from the faint ripple formsets to determine whether paleocurrent directions were at right angles to the dip of the inclined beds, an important criterion for recognition of point-bar deposits (Stewart 1983). The northwestward inclination of the sandstone and mudstone beds is, however, perpendicular to the overall southwestward paleocurrent direction indicated by cross-bedding and cross-lamination from the other facies (Fig. 4). This supports the interpretation of the inclined beds as point-bar deposits. The down-dip continuation of the inclined mudstone beds suggests that they do not represent fluvial point-bar deposits, because clay and mud deposited during low discharge would have tended to be eroded from the deeper parts of fluvial channels. In contrast, clay and mud may be preserved from the whole point-bar surface in tidally influenced channels because of a relatively even distribution of stream velocity within the channel (Shanley et al. 1992). The sigmoidal shape of the inclined sandstone beds indicates that the upper set boundary represents only minor erosion (Bridges and Leeder 1976). The set thickness of 1 m of the inclined beds therefore approximates the depth of the channel in which point-bar migration took place. Channel erosion into the underlying carbonaceous mudstone facies (2a) is reflected by the presence of subrounded mudstone clasts but was probably limited because of cohesion and consolidation of the mud. The inclined sandstones with faint ripple formsets separated by thin mudstone laminae might reflect varying energy conditions caused by daily or monthly tidal cycles. The inclined mudstone beds are probably too thick to reflect simple settling from suspension during the time available over daily or

monthly slackwater intervals; more likely they reflect seasonal variations (cf. Thomas et al. 1987). Similar alternations are known to have formed in estuaries with annual fluctuations in the position of the turbidity maximum related to annual fluctuations in fluvial discharge (Thomas et al. 1987; Allen 1992; Shanley et al. 1992; Shanley and McCabe 1993; Ainsworth and Walker 1994). Although the inclined sandstone beds are strongly bioturbated, the marine influence was limited, as suggested by the absence of marine macrofossils.

The point-bar deposits are interpreted as reflecting seasonal variation in fluvial discharge during lateral migration of tidally influenced fluvial channels on the coastal plain. During seasons of low fluvial discharge organic-rich mud represented by the underlying carbonaceous mudstone (2a) continued to be deposited from suspension and by weak bottom currents on point bars, whereas sand was deposited during seasons of high fluvial discharge.

STACKING PATTERN OF FACIES ASSOCIATIONS

The Jakobsstigen Formation overlies shallow-marine, high-energy shelf sandstones of the Middle Jurassic Pelion Formation. It consists of small coarsening-upward units that stack in an overall coarsening-upward pattern, 128 m thick, and was formed by long-term progradation following initial maximum transgression. The basic coarsening-upward units are bounded by erosion surfaces reflecting fall in relative sea level and are therefore considered high-order depositional sequences. They are 0.1–10 m thick and commonly show a “blocky” vertical grain-size motif (Fig. 5). They consist of deposits of the coastal-plain facies association overlain by the offshore-transition to shoreface facies association. Some of the investigated coastal-plain mudstones are only a few centimeters thick. Mudstone laminae with a similar thickness are abundant within the heteroliths but cannot be followed laterally because of the presence of poorly exposed intervals and because diagenesis commonly makes their recognition difficult. The laminae of the heterolithic wavy-bedded facies may thus be confused with the coastal-plain mudstones. The total number of higher-order sequences is therefore uncertain, and in order to be determined would require analysis of each mudstone lamina for its organic composition or content of marine microfossils.

The basal thin coastal-plain mudstone of a high-order sequence is separated from the underlying shallow-marine deposits by a low-relief erosion surface (Fig. 5). The surface was probably formed by subaerial erosion of upper shoreface and foreshore sands and marks the onset of a basinward shift in facies, caused by a high-frequency sea-level fall. It is considered a high-order sequence boundary (cf. Van Wagoner et al. 1990). The paleogeographic setting during the fall in sea level, and subsequent stages of a sea-level cycle, is illustrated in Figure 8.

The widespread carbonaceous mudstones were deposited during onset of sea-level rise. The slow rise in relative sea level resulted in base-level rise on the coastal plain (e.g., Demarest and Kraft 1987; Devine 1991; Hartley 1993; Aitken 1994; Archer et al. 1994). The rise in base level forced deposition of the terrestrial sediment in a landward direction and resulted in the formation of extensive, shallow and flat-bottomed lakes or lagoons on the coastal plain (Fig. 8). These environments acted as traps for terrestrially derived mud and sand and for inertinite particles formed by wildfires. During continued base-level rise, meandering tidally influenced fluvial channels were locally developed on the coastal plain.

The carbonaceous mudstones and the inclined heterolithic sandstone and mudstone beds are topped by a sharp transgressive surface, formed by marine ravinement during maximum rate of relative sea-level rise when the coastal plain was flooded (Figs 5, 7, 8). More gradual transitions probably reflect damping of wave energy during transgression of the very flat, low-gradient and extensive coastal plain. The transgressive surface (which must commonly be amalgamated with the maximum flooding surface because no transgressive marine deposits are recognized) separates the thin trans-

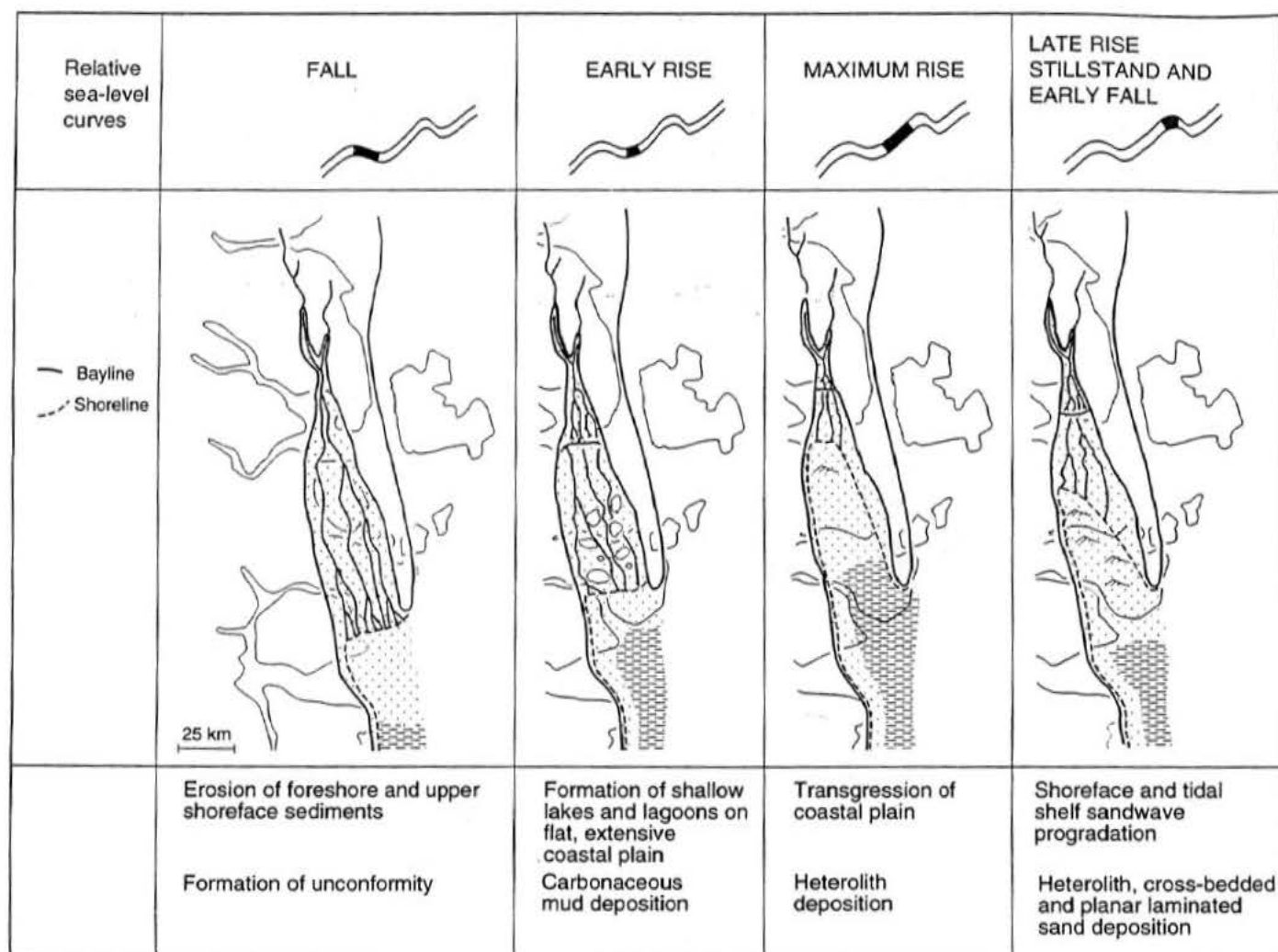


Fig. 8.—Paleogeographic changes during a sea-level cycle. Early–Middle Oxfordian, the Wollaston Forland area, North-East Greenland.

gressive systems tract represented by the coastal-plain mudstone from the sandy, shallow-marine, highstand systems tract.

The coarsening-upward offshore-transition to shoreface facies association was formed by progradation during late rise, stillstand, and early fall (Fig. 8). The erosion surface underlying the planar-laminated sandstone at the top of some coarsening-upward units (Fig. 5) may have formed during early fall, resulting in foreshore erosion of the underlying facies. If this is correct the boundary may represent onset of a minor forced regression (Posamentier et al. 1992).

Farther north in the embayment, the Jakobsstigen Formation is developed as a shallow-marine, tidally influenced sandstone succession that does not show any vertical trends or organization (Surlyk 1991; Alsgaard et al. in press). The basin floor formed a very low-angle homoclinal ramp, as seen by the facies distribution, which does not indicate any differentiation into a shelf, slope, and deeper-water basin. Sediment accumulation was very sensitive to fluctuations in relative sea level because of the flat, low-gradient basin floor and the shallow water depths. Even minor rises resulted in northwards flooding of large areas up the axis of the basin. Slow rise, stillstand, and onset of fall, on the other hand, resulted in rapid axial progradation over tens of kilometers over very short time intervals. This pattern is well known from slightly older shallow-marine deposits of the Pelion Formation in the Jameson Land basin farther to the south (Heinberg and Birkelund 1984; Engkilde and Surlyk in press).

DISCUSSION

The organic-matter fraction of the carbonaceous beds consists almost entirely of inertinite. Inertinite may form by fires, atmospheric oxidation, or fungal decomposition. The formation of inertinite by fires is well documented both in laboratories (Scott 1989; Jones and Chaloner 1991; Jones et al. 1991; Scott and Jones 1991; Jones 1993) and in recent environments (e.g., Cohen 1973; Scott and Jones 1994), and the occurrence of char in the carbonaceous mudstones is an undisputed sign of pyrolyzation (cf. Rosenberg et al. 1996). A peat-forming mire with a fluctuating water table may result in the formation of inertinite with a semifusinitic reflectance from desiccation and fungal decomposition of organic matter, and in addition to inertodetrinite and structured inertinite, amorphous inertinite (macrinite) may form from oxidation of gelified humic matter (Diessel 1992; Moore et al. 1996; Taylor et al. 1998). The formation at the peat surface results in a close association of the inertinite with humified organic matter in the peat/coal. None of these characteristics occur in the carbonaceous mudstones except for a minor amount of macrinite and occasionally huminite. The large amounts of inertinite in the mudstones therefore suggest periodically common wildfires in peat swamps of the hinterland.

The most favorable conditions for wildfires occur in climates with seasonal rainfall, with periodic droughts (Edwards 1984; Sellwood and Price 1993; Scott and Jones 1994; Lamberson et al. 1996). Drier periods and

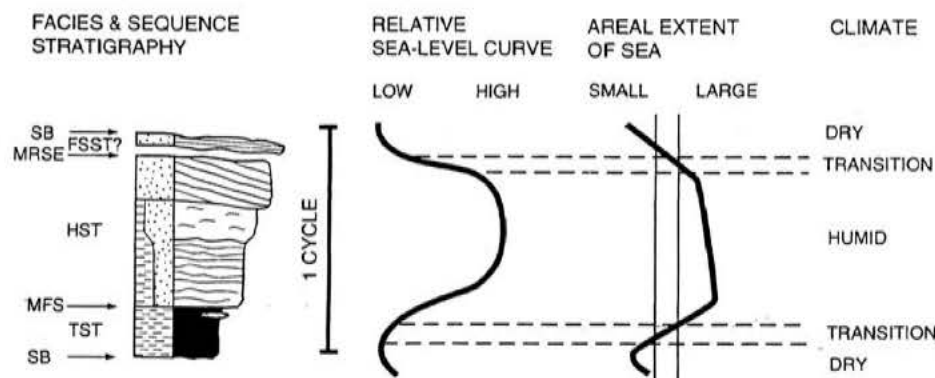


Fig. 9.—Relation between relative sea level, areal extent of sea, and climate. SB, sequence boundary; TST, transgressive systems tract; MFS, maximum flooding surface; MRSE, marine regressive surface of erosion; HST, highstand systems tract; FSST, falling-stage systems tract.

drawdown of the groundwater table result in drying out of the peat, causing conditions favorable for ignition by lightning. Seasonal variation in rainfall during deposition of the coastal-plain deposits is supported by the alternating sandy and muddy point-bar deposits interpreted as reflecting considerable seasonal fluctuations in fluvial discharge.

The organic material in the shallow-marine sediments is characterized by a considerably higher proportion of huminite, absence of char, and a significantly lower proportion of inertinite than in the coastal-plain mudstone. This suggests that generally wetter conditions and a lower frequency of wildfires prevailed during deposition of the marine sediments than during coastal-plain deposition. It is accordingly suggested that the marine and coastal-plain deposits represent different climatic regimes.

The global distribution of geological climatically significant features suggests that the Wollaston Forland area was located in a humid climatic belt characterized by seasonally wet conditions during Late Jurassic times (fig. 7 in Hallam 1985), favorable for seasonal fire events. Orbitally forced variations in solar radiation may cause considerable latitudinal migration of climate belts (Matthews and Perlmutter 1994). However, this cannot easily explain the climatic variations reflected by the Jakobsstigen Formation because the area was situated at a paleo-latitude of c. 50° in the Oxfordian (fig. 8 in Scotese 1994), characterized by subhumid conditions during both climatic minima and maxima (fig. 4 in Matthews and Perlmutter 1994). Nevertheless, regional paleogeography may have a large effect on climatic variations (Chandler et al. 1992; Matthews and Perlmutter 1994). Sea-level fluctuations exerted an important influence on the areal extent of the marine coverage because of the very low basin-floor gradient. This was not only the case for the Wollaston Forland basin but also characterized all of the Jurassic seaway between Greenland and Norway. Sea-level fluctuations probably also influenced the regional climate, because the introduction of a shallow sea into a continental region can cause an increase of atmospheric humidity and precipitation (Hallam 1984). Periods of transgression and highstand seem to have been associated with a humid climate, possibly caused by a high degree of precipitation related to evaporation from the extensive sea. Conditions of maximum humidity existed at the time of maximum transgression. No sediments are preserved to document the climatic conditions during lowstands, because these periods are represented by unconformities forming high-order sequence boundaries. During lowstands, however, only the topographically deeper parts of the seaway remained inundated, and drier continental climate conditions most likely prevailed. A strong interaction is therefore interpreted to have existed between fluctuations in relative sea level, areal extent of the sea, and regional climate (Fig. 9). During humid periods corresponding to periods of sea-level rise, seasonal variations were suppressed and everwet conditions existed. Large seasonal variations and thereby optimum conditions for wildfires probably existed in the transitional periods between humid and drier climates. Seasonal variations may, however, also have prevailed during the drier periods, but these cannot be documented (see above). The transition period from a humid to a drier climate was unfavorable for rich vegetation

growth because of erosion and base-level fall (Fig. 9). In contrast, the transition period from drier to humid climate was a time of base-level rise, and conditions favorable for vegetation growth developed in the hinterland. The carbonaceous mudstones were deposited during this time interval.

The high-order sequences are thus interpreted to reflect repeated fluctuations in climate between wet and drier climate. The uncertainty concerning the total number of sequences in the Jakobsstigen Formation and the lack of detailed time control does not allow inferences about causal factors governing the cyclic nature of the succession.

SUMMARY

The Lower-Middle Oxfordian Jakobsstigen Formation was deposited in the Wollaston Forland basin of North-East Greenland, situated at the western margin of the Jurassic rifted seaway between Greenland and Norway. The basin was funnel-shaped, elongated north-south, and open to marine circulation to the south. The overall sediment transport was from north to south along the axis of the basin.

The formation consists of coarsening-upward units, 0.1–10 m thick, which are limited by unconformities reflecting fall in relative sea level and are considered high-order sequences. They consist of a thin coastal-plain facies association overlain by a coarsening-upward shallow-marine facies association. The coastal-plain facies association consists of dark gray to black carbonaceous mudstones and rare inclined heterolithic beds. The carbonaceous mudstones are up to 20 cm thick, have a tabular geometry, and can be followed laterally for more than 1 km. They do not contain dinoflagellate cysts, spores, pollen, marine macrofossils, or indigenous trace fossils. The total organic carbon content (TOC) is 7–21 wt %, and the organic matter is dominated by angular, inertinite macerals formed by wildfires. Solvent extract yields are very low, but a geochemical composition of even-carbon-number n-alkane predominance, very low hopane/sterane ratios, and enhancement of homohopanes and $\alpha\beta\beta$ -steranes suggests a saline depositional environment. The presence of small root casts under one bed with a high huminite content reflects emergent or nearly emergent conditions. The mudstones were deposited in shallow, flat-bottomed lakes or lagoons on a low-lying, low-relief coastal plain that was largely barren of higher plant vegetation. The marine influence was caused mainly by salt-water intrusion into the coastal plain during early rise in sea level, and not by random inundations. At one locality, a 1-m-thick set of inclined heterolithic beds overlies a carbonaceous mudstone. It is interpreted as a point-bar deposit, showing seasonal variation in fluvial discharge during lateral migration of tidally influenced fluvial channels on the coastal plain.

The offshore-transition to shoreface facies association forms coarsening-upward units starting with faintly wave or current cross-laminated, strongly bioturbated heteroliths with abundant marine dinoflagellate cysts and macrofossils. The organic matter of the facies is characterized by a high proportion of huminite and a significantly lower proportion of inertinite. The heterolithic facies is commonly overlain by cross-bedded sandstones with

single or double mud drapes and reactivation surfaces. In a few cases a planar-laminated sandstone, about 10 cm thick, overlies the cross-bedded sandstone. The offshore-transition to shoreface facies association reflects a shallowing-upward development caused by progradation by the shoreface or foreshore over the offshore-transition zone in a tidally influenced environment.

The coastal-plain facies association overlies a low-relief, high-order sequence boundary. The surface above the coastal-plain deposits, separating them from shallow-marine strata, represents the maximum flooding surface. It demarcates the transgressive systems tract, represented by the thin coastal-plain mudstone, from the sandy, shallow-marine highstand systems tract.

Sediment accumulation was very sensitive to fluctuations in relative sea level because of the very flat, low-gradient basin floor and shallow water depths. Even minor rises resulted in flooding of large areas up the axis of the rift basin. Slow rise, stillstand, and onset of fall, on the other hand, resulted in axial progradation over tens of kilometers over short time intervals. Therefore, high-order sea-level fluctuations exerted an important influence on the areal extent of the marine environments, not only in the Wollaston Forland basin but also throughout the seaway between Greenland and Norway.

The different maceral composition of the organic material of the two facies associations implies that deposition of the offshore-transition to shoreface association took place under wetter conditions and lower frequency of wildfires in the hinterland than during deposition of the coastal-plain association. The wet-dry cycles were probably related to high-order sea-level fluctuations. Periods of transgression and highstand were characterized by a humid climate caused by a high degree of precipitation related to evaporation from an extensive sea. During lowstands only the topographically deeper parts of the seaway were inundated and drier continental climate prevailed. Large seasonal variations and thereby optimum conditions for wildfires existed in the transition from drier to humid climate, a time of base-level rise and conditions favorable for vegetation growth. The coastal-plain mudstones were deposited during this time interval. The high-order sequences of the Jakobsstigen Formation are interpreted to reflect a strong interaction between fluctuations in relative sea level, areal extent of the sea, and climate and frequency of wild fires.

ACKNOWLEDGMENTS

The present study was supported by a grant to F. Surlyk from Amoco Norway Oil Co., Norwegian Petroleum Directorate, Saga Petroleum a.s., and Statoil a.s. Support from the Danish Natural Science Research Council is also acknowledged. We are grateful to L.B. Clemmensen, C. Bjerrum, and Journal reviewer S. Hesselbo and an anonymous reviewer for very useful, constructive comments. J. Callomon and S. Piasecki are thanked for providing biostratigraphic information. R. Madsen, O. Bang Berthelsen, and B.M. Schark provided technical support in preparation of the figures.

REFERENCES

- AINSWORTH, R.B., AND WALKER, R.G., 1994, Control of estuarine valley-fill deposition by fluctuations of relative sea-level, Cretaceous Bearpaw-Horseshoe Canyon transition, Drumheller, Alberta, Canada, in Dalrymple, R.W., Boyd, R., and Zaitlin, B.A., eds., *Incised-Valley Systems: Origin and Sedimentary Sequences*: SEPM, Special Publication 51, p. 159-174.
- AITKEN, J.F., 1994, Coal in a sequence stratigraphic framework: *Geoscientist*, v. 4, p. 9-12.
- ALLEN, G.P., 1992, Sedimentary processes and facies in the Gironde estuary: a recent model for macrotidal estuarine systems, in Smith, D.G., Reinson, G.E., Zaitlin, B.A., and Rahmani, R.A., eds., *Clastic Tidal Sedimentology*: Canadian Society of Petroleum Geologists, Memoir 16, p. 29-40.
- ALLEN, G.P., AND POSAMANTIER, H.W., 1993, Sequence stratigraphy and facies model of an incised valley fill: the Gironde estuary, France: *Journal of Sedimentary Petrology*, v. 63, p. 378-391.
- ALSGAARD, P.C., FELT, V.L., VOSGERAU, H., AND SURLYK, F., in press, Jurassic geology of Kuhn Ø, North-East Greenland, in Surlyk, F., and Ineson, J.R., eds., *The Jurassic of Denmark and Greenland*: Geology of Denmark, Survey Bulletin.
- ARCHER, A.W., FELDMAN, H.R., KVALE, E.P., AND LANIER, W.P., 1994, Comparison of drier- to wetter-interval estuarine roof facies in the Eastern and Western Interior coal basins, USA: *Palaeogeography, Palaeoecology, Palaeoclimatology*, v. 106, p. 171-185.
- BOERSMA, J.R., AND TERWINDT, J.H.J., 1981, Neap-spring tide sequences of intertidal shoal deposits in a mesotidal estuary: *Sedimentology*, v. 28, p. 151-170.
- BOJSEN-KOEFØED, J.A., PETERSEN, H.I., SURLYK, F., AND VOSGERAU, H., 1997, Organic petrography and geochemistry of inertinite-rich mudstones, Jakobsstigen Formation, Upper Jurassic, northeast Greenland: indications of forest fires and variations in relative sea-level: *International Journal of Coal Geology*, v. 34, p. 345-370.
- BRIDGES, P.H., AND LEEDER, M.R., 1976, Sedimentary model for intertidal mudflat channels, with examples from the Solway Firth, Scotland: *Sedimentology*, v. 23, p. 533-552.
- BROWN, K.E., AND COHEN, A.D., 1995, Stratigraphic and micropetrographic occurrences of pyrite in sediments at the confluence of carbonate and peat-forming depositional systems, southern Florida, U.S.A.: *Organic Geochemistry*, v. 22, p. 105-126.
- CASAGRANDE, D.J., 1987, Sulphur in peat and coal, in Scott, A.C., ed., *Coal and Coal-Bearing Strata: Recent Advances*: Geological Society of London, Special Publication 32, p. 87-105.
- CHANDLER, M.A., RIND, D., AND RUDY, R., 1992, Pangean climate during the Early Jurassic: GCM simulations and the sedimentary record of paleoclimate: *Geological Society of America, Bulletin*, v. 104, p. 543-559.
- CLIFTON, H.E., HUNTER, R.E., AND PHILLIPS, R.L., 1971, Depositional structures and processes in the non-barred high-energy nearshore: *Journal of Sedimentary Petrology*, v. 41, p. 651-670.
- COHEN, A.D., 1973, Petrology of some Holocene peat sediments from Okefenokee swamp-marsh complex of southern Georgia: *Geological Society of America, Bulletin*, v. 84, p. 3867-3878.
- COHEN, A.D., SPACKMAN, W., AND DOLSEN, P., 1984, Occurrence and distribution of sulfur in peat-forming environments of southern Florida: *International Journal of Coal Geology*, v. 4, p. 73-96.
- COPE, M.J., AND CHALONER, W.G., 1985, Wildfire: An interaction of biological and physical processes, in Tiffney, B.H., ed., *Geological Factors and the Evolution of Plants*: New Haven, Connecticut, Yale University Press, p. 257-277.
- DEMAREST, J.M., AND KRAFT, J.C., 1987, Stratigraphic record of quaternary sea-levels: Implications for more ancient strata, in Nummedal, D., Pilkey, O.H., and Howard, J.D., eds., *Sea-Level Fluctuation and Coastal Evolution*: SEPM, Special Publication 41, p. 223-239.
- DEVINE, P.E., 1991, Transgressive origin of channelled estuarine deposits in the Point Lookout Sandstone, Northwestern New Mexico: A model for Upper Cretaceous, cyclic regressive parasequences of the U.S. Western Interior: *American Association of Petroleum Geologists, Bulletin*, v. 75, p. 1039-1063.
- DIESSEL, C.F.K., 1992, *Coal-Bearing Depositional Systems*: Berlin, Springer-Verlag, 721 p.
- EDWARDS, D., 1984, Fire regimes in the biomes of South Africa, in Booysen, P.D.V., and Tainton, N.M., eds., *Ecological Effects of Fire in South African Ecosystems*: *Ecological Studies* 48, p. 19-37.
- ELLIOTT, T., 1974, Interdistributary bay sequences and their genesis: *Sedimentology*, v. 21, p. 611-622.
- ELLIOTT, T., 1986, Siliciclastic shorelines, in Reading, H.G., ed., *Sedimentary Environments and Facies*: Oxford, U.K., Blackwell, p. 155-188.
- ENGKILDE, M., AND SURLYK, F., in press, Sequence stratigraphy of shallow marine sandstones of the Middle Jurassic Pelion and Fossilbjerget Formations, East Greenland, in Surlyk, F., and Ineson, J.R., eds., *The Jurassic of Denmark and Greenland*: Geology of Denmark, Survey Bulletin.
- FU, J., SHENG, G., XU, J., EGLINTON, G., GOWAR, A.P., JIA, R., FAN, S., AND PENG, P., 1990, Application of biological markers in the assessment of palaeoenvironments of Chinese non-marine sediments: *Organic Geochemistry*, v. 16, p. 769-779.
- GENIK, G.J., 1993, Petroleum geology of Cretaceous-Tertiary rift basins in Niger, Chad, and Central African Republic: *American Association of Petroleum Geologists, Bulletin*, v. 77, p. 1405-1434.
- GIELBERG, J., AND STEEL, R.J., 1995, Helvetiafjellet Formation (Barremian-Aptian), Spitsbergen: characteristics of a transgressive succession, in Steel, R.J., Felt, V., Johannessen, E.P., and Mathieu, C., eds., *Sequence Stratigraphy on the Northwest European Margin*: Norwegian Petroleum Society (NPF), Special Publication 5, Amsterdam, Elsevier, p. 571-593.
- GRIMALT, J., AND ALBAIGES, J., 1987, Sources and occurrence of C_{12} - C_{22} n-alkane distributions with even-carbon-number preference in sedimentary environments: *Geochimica et Cosmochimica Acta*, v. 51, p. 1379-1384.
- HALLAM, A., 1984, Continental humid and arid zones during the Jurassic and Cretaceous: *Palaeogeography, Palaeoclimatology, Palaeoecology*, v. 47, p. 195-223.
- HALLAM, A., 1985, A review of Mesozoic climates: *Geological Society of London, Journal*, v. 142, p. 433-445.
- HARTLEY, A.J., 1993, A depositional model for the Mid-Westphalian to late Westphalian B coal measures of South Wales: *Geological Society of London, Journal*, v. 150, p. 1121-1136.
- HEINBERG, C., AND BIRKELUND, T., 1984, Trace-fossil assemblages and basin evolution of the Vardekloft Formation (Middle Jurassic, central East Greenland): *Journal of Paleontology*, v. 58, p. 362-397.
- JONES, T.P., 1993, New morphological and chemical evidence for a wildfire origin for fusain from comparisons with modern charcoal: *The Palaeontological Association, Special Papers in Palaeontology*, no. 49, p. 113-123.
- JONES, T.P., AND CHALONER, W.G., 1991, Fossil charcoal, its recognition and palaeoatmospheric significance: *Palaeogeography, Palaeoclimatology, Palaeoecology* (Global and Planetary Change Section), v. 97, p. 39-50.
- JONES, T.P., SCOTT, A., AND COPE, M., 1991, Reflectance measurements and the temperature of formation of modern charcoals and implications for studies of fusain: *Société Géologique de France, Bulletin*, v. 162, p. 193-200.
- LAMBERSON, M.N., BUSTIN, R.M., KALKREUTH, W.D., AND PRATT, K.C., 1996, The formation of inertinite-rich peats in the mid-Cretaceous Gates Formation: implications for the interpre-

- tation of mid-Albian history of paleowildfire: *Palaeogeography, Palaeoclimatology, Palaeoecology*, v. 120, p. 235–260.
- MATTHEWS, M.D., and PERLMUTTER, M.A., 1994, Global cyclostratigraphy: an application to the Eocene Green River Basin, in de Boer, P.L., and Smith, D.G., eds., *Orbital Forcing and Cyclic Sequences*: International Association of Sedimentologists, Special Publication 19, p. 459–481.
- MAYNE, W., 1947, Stratigraphie der Jurabildungen Ostgrönlands zwischen Hochstetterbugten (75°N.) und dem Kejser Franz Joseph Fjord (73°N.): *Meddelelser om Grønland*, v. 132, 223 p.
- MOORE, T.A., SHEARER, J.C., and MILLER, S.L., 1996, Fungal origin of oxidised plant material in the Palangkaraya peat deposit, Kalimantan Tengah, Indonesia: implications for 'inertinite' formation in coal: *International Journal of Coal Geology*, v. 30, p. 1–23.
- NOE-NYGAARD, N., and SURLYK, F., 1988, Washover fan and brackish bay sedimentation in the Berriasian–Valanginian of Bornholm, Denmark: *Sedimentology*, v. 35, p. 197–217.
- PETERSEN, H.L., 1998, Morphology, formation and palaeo-environmental implications of naturally formed char particles in coals and carbonaceous mudstones: *Fuel*, v. 77, p. 1177–1183.
- POSAMENTIER, H.W., ALLEN, G.P., JAMES, D.P., and TESSON, M., 1992, Forced regressions in a sequence stratigraphic framework: concepts, examples, and exploration significance: *American Association of Petroleum Geologists, Bulletin*, v. 76, p. 1687–1709.
- ROSENBERG, P., PETERSEN, H.L., and THOMSEN, E., 1996, Combustion char morphology related to combustion temperature and coal petrology: *Fuel*, v. 75, p. 1071–1082.
- SCOTSE, C.R., 1994, Late Jurassic paleogeographic map, in Klein, G.D., ed., *Pangea: Paleoclimate, Tectonics, and Sedimentation during Accretion, Zenith, and Breakup of a Supercontinent*: Geological Society of America, Special Paper 288.
- SCOTT, A.C., 1989, Observations on the nature and origin of fusain, in Lyons, P.C., and Alpern, B., eds., *Peat and Coal: Origin, Facies, and Depositional Models*: *International Journal of Coal Geology*, v. 12, p. 443–475.
- SCOTT, A.C., and JONES, T.P., 1991, Microscopical observations of recent and fossil charcoal: *Microscopy and Analysis*, p. 13–15.
- SCOTT, A.C., and JONES, T.P., 1994, The nature and influence of fire in Carboniferous ecosystems: *Palaeogeography, Palaeoclimatology, Palaeoecology*, v. 106, p. 91–112.
- SELLWOOD, B.W., and PRICE, G.D., 1993, Sedimentary facies as indicators of Mesozoic Palaeoclimate: Royal Society [London], *Philosophical Transactions, Series B*, v. 341, p. 225–233.
- SHANLEY, K.W., and McCABE, P.J., 1993, Alluvial architecture in a sequence stratigraphic framework: a case history from the Upper Cretaceous of southern Utah, USA, in Flint, S.S., and Bryant, I.D., eds., *The Geological Modelling of Hydrocarbon Reservoirs and Outcrop Analogues*: International Association of Sedimentologists, Special Publication 15, p. 21–56.
- SHANLEY, K.W., McCABE, P.J., and HETTINGER, R.D., 1992, Tidal influence in Cretaceous fluvial strata from Utah, USA: a key to sequence stratigraphic interpretation: *Sedimentology*, v. 39, p. 905–930.
- SMITH, D.G., 1988, Tidal bundles and mud couplets in the McMurray Formation, north-eastern Alberta, Canada: *Bulletin of Canadian Petroleum Geology*, v. 36, p. 216–219.
- STEWART, D.J., 1983, Possible suspended-load channel deposits from Wealden Group (Lower Cretaceous) of southern England, in Collinson, J.D., and Lewin, J., eds., *Modern and Ancient Fluvial Systems*: International Association of Sedimentologists, Special Publication 6, p. 369–384.
- SURLYK, F., 1977, Stratigraphy, tectonics and palaeogeography of the Jurassic sediments of the areas north of Kong Oscar Fjord, East Greenland: *Grønlands Geologiske Undersøgelse, Bulletin*, v. 123, 56 p.
- SURLYK, F., 1990, Timing, style and sedimentary evolution of Late Palaeozoic–Mesozoic extensional basins of East Greenland, in Hardman, R.F.P., and Brooks, J., eds., *Tectonic Events Responsible for Britain's Oil and Gas Reserves*: Geological Society of London, Special Publication 55, p. 107–155.
- SURLYK, F., 1991, Sequence stratigraphy of the Jurassic–lowermost Cretaceous of East Greenland: *American Association of Petroleum Geologists, Bulletin*, v. 75, p. 1468–1488.
- SURLYK, F., and CLEMMENSEN, L.B., 1983, Rift propagation and eustasy as controlling factors during Jurassic inshore and shelf sedimentation in northern East Greenland: *Sedimentary Geology*, v. 34, p. 119–143.
- SYKES, R.M., and SURLYK, F., 1976, A revised ammonite zonation of the Boreal Oxfordian and its application in northeast Greenland: *Lethaia*, v. 9, p. 421–436.
- TAYLOR, G.H., TEICHMÜLLER, M., DAVIS, A., DIESSEL, C.F.K., LITKE, R., and ROBERT, P., 1998, *Organic petrology*: Berlin, Gebrüder Borntraeger, 704 p.
- THOMAS, R.G., SMITH, D.G., WOOD, J.M., VISSER, J., CALVERLEY-RANGE, E.A., and KOSTER, E.H., 1987, Inclined heterolithic stratification—terminology, description, interpretation and significance: *Sedimentary Geology*, v. 53, p. 123–179.
- VAN WAGONER, J.C., MITCHUM, R.M., CAMPHO, K.M., and RAHMANIAN, V.D., 1990, Siliciclastic sequence stratigraphy in well logs, cores, and outcrops: *American Association of Petroleum Geologists, Methods in Exploration Series* 7, 55 p.
- VISSER, M.J., 1980, Neap-spring cycles reflected in Holocene subtidal large-scale bedform deposits: a preliminary note: *Geology*, v. 8, p. 543–546.
- WOOD, J.M., and HOPKINS, J.C., 1989, Reservoir sandstone bodies in estuarine valley fill: Lower Cretaceous Glauconitic Member, Little Bow Field, Alberta, Canada: *American Association of Petroleum Geologists, Bulletin*, v. 73, p. 1361–1382.

Received 24 June 1996; accepted 27 May 1999.



Petroleum potential of Oligocene lacustrine mudstones and coals at Dong Ho, Vietnam — an outcrop analogue to terrestrial source rocks in the greater Song Hong Basin

H.I. Petersen^{a,*}, C. Andersen^a, P.H. Anh^b, J.A. Bojesen-Koefoed^a, L.H. Nielsen^a, H.P. Nytoft^a, P. Rosenberg^a, L. Thanh^c

^aGeological Survey of Denmark and Greenland (GEUS), Thoravej 8, DK-2400 Copenhagen, NV, Denmark

^bVietnam Petroleum Institute, VPI, Ho Chi Minh City Branch, R.020 Block G1, Thanh Da Hotel, Binh Thanh Dist, Ho Chi Minh City, Viet Nam

^cVietnam Petroleum Institute, VPI, Yen Hoa, Cau Giay, Hanoi, Viet Nam

Received 28 August 1999; accepted 19 March 2000

Abstract

The outcrop of Oligocene age at Dong Ho, northern Vietnam, may constitute an immature analogue to offshore terrestrial source rocks in the greater Song Hong Basin. The outcrop includes an interval with two source rocks: (1) highly oil-prone carbonaceous mudstones containing kerogen types IIA and IIA/I, and with TOC contents from 6.48 to 16.89 wt%, and HI values from 472 to 690; and (2) oil-prone humic coals (kerogen type III) with HI values from 200 to 242. The mudstones were deposited in oxygen-deficient lakes, which on occasion were subject to marine influence, and the coals accumulated in freshwater peat-forming mires. The coals have broad activation energy (E_a) distributions, while the mudstones have E_a distributions characterised by a pronounced principal E_a . During artificial maturation about 16–17% of the organic carbon in the coals and 45–50% of the organic carbon in the mudstones participated in petroleum formation. The two source rocks primary generate oil and secondary generate gas, however, the mudstones realised the majority of their potential over a more narrow temperature range than the coals. The excellent generative potential of the terrestrial source rocks at Dong Ho is encouraging for offshore exploration for reservoirs charged by Cenozoic rift-lake successions. © 2001 Elsevier Science Ltd. All rights reserved.

1. Introduction

In many Asian Cenozoic basins lacustrine mudstones and paralic coals are widely distributed and constitute good to excellent source rocks (e.g. Noble et al., 1991; Wang and Sun, 1994; Williams et al., 1995; Lee and Watkins, 1998; Ratanasthien et al., 1999; Wan Hsiaiah, 1999). The major part of the petroleum in Southeast Asia is generated from mudstones containing non-marine kerogen and coals principally composed of either lacustrine freshwater algal (kerogen type I) or of freshwater or brackish higher land plant material (kerogen types II and III) (Sladen, 1997; Todd et al., 1997). According to Todd et al. (1997) roughly equal oil equivalent volumes of the two main petroleum types occur, although the lacustrine algal-rich mudstones are responsible for a much greater proportion of oil than the paralic deposits, primarily with kerogen type III, and the coals.

The carbonaceous lacustrine mudstones and lake-related facies were deposited in long-lived lakes with a stratified

water column in grabens and halfgrabens formed by crustal extension or extensional strike-slip movements, and are prominent in syn-rift successions of the numerous Cenozoic basins of the region. The key controlling factors for development of such lacustrine successions appear to be: (1) subsidence outpacing the sedimentation rate; (2) a hot and humid subtropical to tropical climate; and (3) a reduced input of siliciclastics due to a hinterland geology dominated by carbonate rocks and/or a drainage pattern away from the lake basins due to rift-shoulder uplift (Sladen, 1997).

The Palaeogene lacustrine mudstones characterised by kerogen type I are the dominant source rock in a number of prospective basins along the northern and western margin of the East Vietnam Sea (South China Sea). These include the Beibu Wan and Pearl River Mouth basins on the Chinese shelf (e.g. Wang and Sun, 1994; Zhu et al., 1999), and the Cuu Long Basin, located on the Vietnamese shelf off the Mekong River delta (Fig. 1), where geochemical data suggest a brackish lacustrine source rock (Todd et al., 1997). Biomarker data from oil samples from the Nam Con Son Basin farther to the southeast show a striking similarity to Lower Miocene coaly mudstones, suggesting

* Corresponding author.

E-mail address: hip@geus.dk (H.I. Petersen).

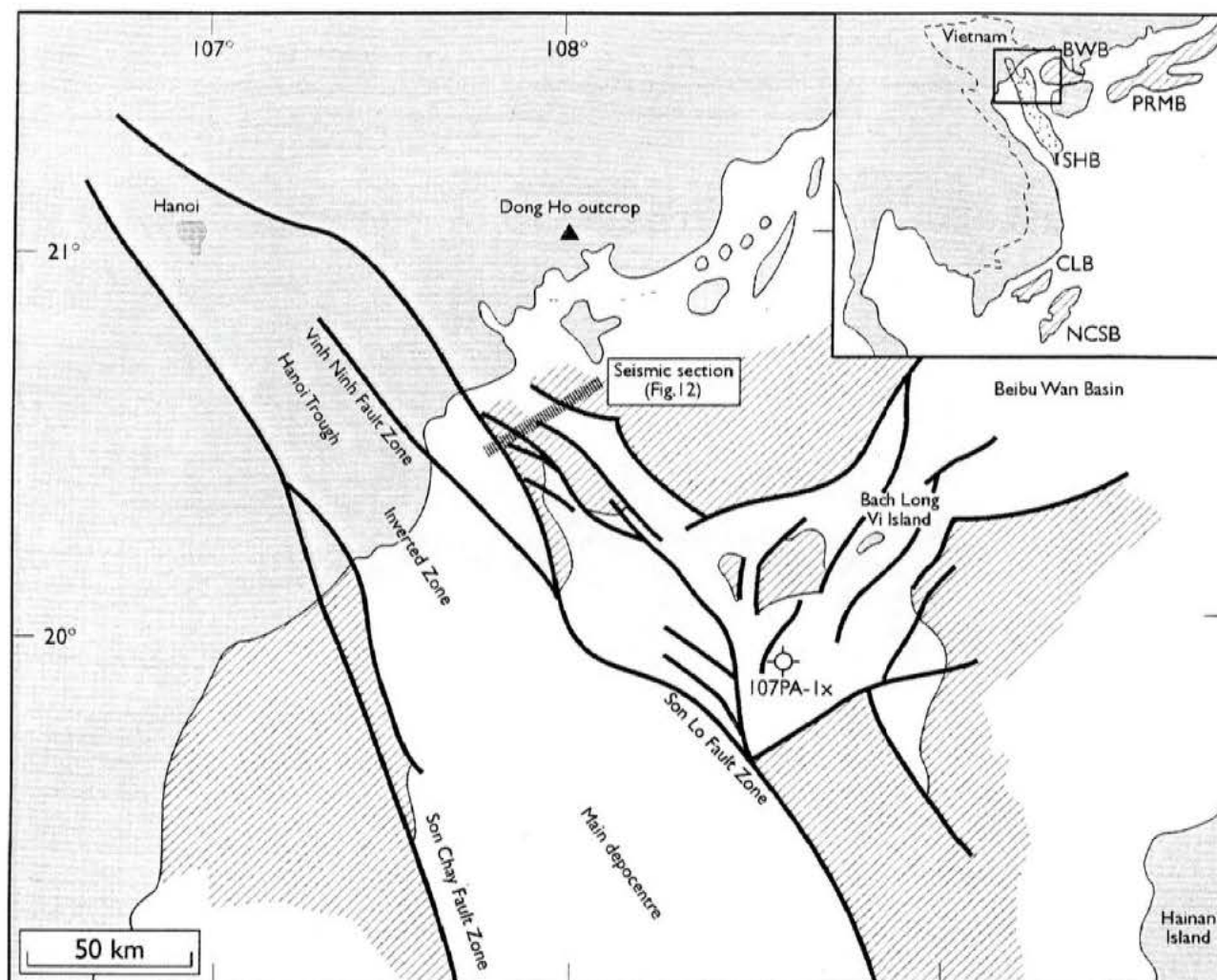


Fig. 1. Location map of the study area with the Dong Ho outcrop (isolated outlier), well 107 PA-1x, the seismic section shown in Fig. 12, and the structural outline of the northern part of the Song Hong Basin. Location of Cenozoic basins along the northern and western margin of the East Vietnam Sea mentioned in the text is also shown. BWB: Beibu Wan Basin; CLB: Cuu Long Basin; NCSB: Nam Con Son Basin; PRMB: Pearl River Mouth Basin; SHB: Song Hong Basin. Hatched areas: Post-rift sediments resting directly on pre-Cenozoic basement in the offshore area.

paralic carbonaceous mudstones and coastal plain coals as the main source rocks (Todd et al., 1997). However, the presence of an additional source rock facies, including lacustrine sediments deposited either in floodplain lakes or in earlier Palaeogene halfgrabens, has been suggested by Matthews et al. (1997).

In contrast to the above mentioned basins, the greater Song Hong (also called Bac Bo, Yinggehai or Red River) Basin is generally regarded to be mostly gas-prone as kerogen type III is the dominating organic matter in the thick Cenozoic basin-fill succession (Hao Fang et al., 1995, 1998; Ha, 1998; Chen Honghan et al., 1998; Nielsen et al., 1999). However, this basin, which extends from the Song Hong delta southeast into the Gulf of Tonking (Fig. 1), is in an early stage of exploration with only few wells drilled offshore. Several of the wells drilled onshore in the Hanoi Trough (Fig. 1), the onshore part of the greater Song Hong Basin, have encountered hydrocarbons. Geochemical

analyses and maturity modelling indicate that the hydrocarbons may have been generated from two possible source rocks in the Hanoi Trough area, namely Oligocene lacustrine sediments and Miocene coal seams (Nielsen et al., 1999). A number of undrilled Palaeogene halfgrabens has been mapped in the northeastern offshore part of the greater Song Hong Basin (Rangin et al., 1995; Andersen et al., 1998), where parts of the syn-rift deposits show seismic facies patterns that often are interpreted as lacustrine mudstones. A possible analogue to these potential source rocks crops out at Dong Ho, northern Vietnam (Fig. 1), where immature Oligocene carbonaceous mudstones and coals are exposed. The composition and petroleum generative potential of these sediments may thus provide valuable information on source rock quality and variability of deeply buried Palaeogene successions offshore.

The aim of this paper is to provide such information through (1) analysis of composition, depositional environment and

Stratigraphic column
Dong Ho outcrop, Quang Ninh Province, northern Vietnam



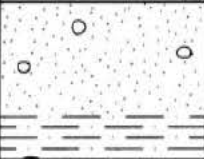



Age	Formation	Lithology	Thickness (m)	Remarks
Quaternary			5	Gravel and sands
Oligocene	Dong Ho		70	Claystones
			25	Sandstones with siltstones in lower part
			15	Carbonaceous mudstones with scattered coal beds (up to 5–15 cm). Subordinate siltstones. Upper part sampled.
			8	Conglomerates and sandstones
Triassic	Hon Gai			Sandstone, siltstone with coal beds

Fig. 2. Simplified stratigraphic column of the Oligocene outcrop at Dong Ho (after Thanh, 1997).

source potential of outcrop samples, (2) step-wise artificial maturation (hydrous pyrolysis) of selected samples, (3) determination of gas-to-oil ratios (GOR) of artificially matured samples, and (4) discussion of implications for petroleum exploration in the neighbouring offshore areas in the Gulf of Tonking.

2. The Dong Ho outcrop

The Dong Ho outcrop, located some 20 km northwest of the coastal city of Hon Gai and 3 km west of the village Hoanh Bo (approximately N21°05', E106°57') in the Ha Long Bay region (Fig. 1), consists of grey to black and dark brown faintly laminated to structureless organic-rich mudstones interbedded with thin muddy sandstones most likely deposited in a low energy, long-lasting lake site (Traynor and Sladen, 1997). Bedding planes often show scattered coal fragments. Coal seams up to 15 cm thick occur interbedded with the carbonaceous mudstones. The economic potential of the mudstones as an oil-shale deposit was studied during the late 1950s when a number of wells and pits were made. The deposits are part of a more than 100 m thick succession of sediments (assigned an Oligocene

age by Traynor and Sladen (1997)) dominated by sandstones and mudstones occurring as an outlier resting unconformably on the Triassic bedrock of sandstones and siltstones with anthracite beds belonging to the Hon Gai Formation (Fig. 2).

3. Methods

Five samples representing the lithological variability at the outcrop have been analysed in detail. They were sampled along the bank of a stream over a stratigraphic interval of a few metres within the upper part of the 15 m thick succession of mainly carbonaceous mudstones (Fig. 2). Samples Dong Ho 1 (DH 1), Dong Ho 2 (DH 2), and Dong Ho 6 (DH 6) are dark grey mudstones, the former slightly silty with plant fragments on bedding planes. Sample Dong Ho 3 (DH 3) and Dong Ho 4 (DH 4) are black structureless coals. Neither macroscopically nor microscopically the samples showed evidence of weathering or oxidation.

Particulate pellets suitable for optical analyses were prepared. Huminite reflectance measurements (random, oil immersion) were carried out on eu-ulminite using the Leica

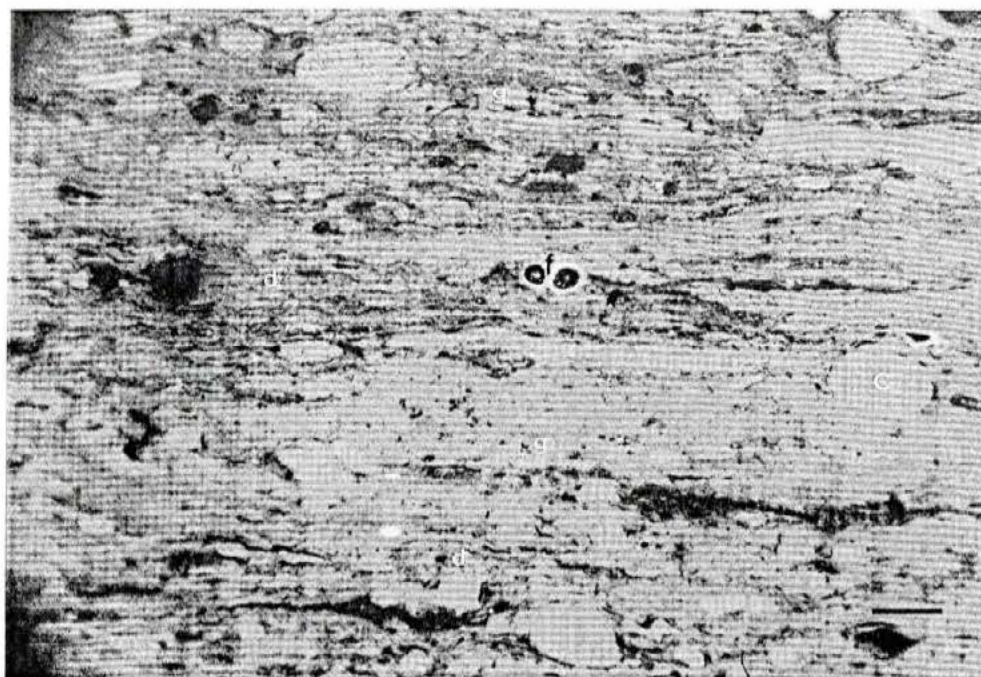


Fig. 3. Typical complex mixture of densinite (d), corpohuminite (c), and gelinite (g) in the humic coals. A funginite (f) with two chambers is observed. (DH 3, reflected white light, oil immersion, scale bar $\sim 30 \mu\text{m}$).

MPVGEOR software and a Leitz MPV-SP system. The samples were petrographically analysed in reflected white light and fluorescence-inducing blue light in oil immersion using a Zeiss incident light microscope. A total of 500 particles (macerals, minerals) were counted in each sample, and the brown coal classification was used. The petrographic analysis procedures and the brown coal maceral identification follow the standards outlined in ICCP (1971, 1975) and Taylor et al. (1998).

A LECO IR-212 induction furnace was used for total organic carbon (TOC) determination, and Rock-Eval pyrolysis, including determination of the activation energy distributions (E_a) and pre-exponential factors (A) (Optkin software), was carried out using Vinci Rock-Eval 5 equipment on non-extracted and extracted samples. The E_a -distributions are related to the chemical composition (bonding energies) of the organic matter, and the E_a -distributions are used to compare the petroleum generation characteristics of the samples.

Asphaltene-free solvent extracts were separated into saturated, aromatic and heteroatomic compounds by medium performance liquid chromatography (MPLC). Saturate fractions were analysed on a Hewlett Packard 5890 gas chromatograph (GC) fitted with a 25 m HP-1 WCOT column and FID, and by coupled gas chromatography/mass spectrometry (GC/MS) using a Hewlett Packard 5890 series II gas chromatograph equipped with a 25 m HP-5 WCOT column and coupled to a Hewlett Packard 5971A quadrupole mass spectrometer.

Temperature programmed pyrolysis-gas chromatography (Py-GC) was carried out on extracted samples using a

custom-made stainless steel pyrolysis unit coupled to a Hewlett Packard 5890A gas chromatograph, equipped with a 50 m Chrompack CP-Sil-8CB WCOT column and FID, using direct on-column injection. 1 m of pre-column, used for cold trapping of pyrolysis products in liquid nitrogen prior to chromatography, joined the pyrolysis unit and the column. Determination of the proportion of gas-range and oil-range components was done by splitting the integrated chromatogram into a C_{1-5} (gas) and C_{6+} (oil) fraction, and an estimate of the fractions of TOC of gas-prone, oil-prone and chemically inert carbon was computed by combining Rock-Eval and Py-GC data (Pepper and Corvi, 1995).

Stainless steel HPLC columns were used for hydrous pyrolysis. The columns were filled with 0.7–1.0 g of ground sample mixed with water and thoroughly stirred to remove any air. The sealed columns were heated for 72 h at 240, 270, 300 and 330°C. The hydrous-pyrolysed samples were afterward subjected to TOC determination, Rock-Eval pyrolysis and extraction followed by GC analysis of the saturate fractions. The E_a distributions of the samples pyrolysed at 330°C/72 h were likewise determined.

4. Results

4.1. Organic petrography of outcrop samples

The DH 3 and DH 4 coal samples contain high proportions of loosely compacted huminite, which is composed of a complex mixture of a variety of huminite macerals (Fig. 3;

Table 1
Petrographic compositions and huminite reflectance values of the outcrop samples

Maceral type	Dong Ho 1 (vol%)	Dong Ho 2 (vol%)	Dong Ho 3 (vol%)	Dong Ho 4 (vol%)	Dong Ho 6 (vol%)
Textinite	0.0	0.0	0.6	0.4	0.0
Textoulminite	0.0	0.0	1.8	4.4	0.0
Eu-ulminite	0.2	0.0	7.6	8.4	0.2
Attrinite	2.8	8.6 ^a	0.4	0.6	9.6
Densinite	1.2	1.0	54.6	56.4	1.0
Porigelinite	0.0	0.0	2.6	2.6	0.0
Corpohuminit	0.0	0.0	5.0	3.4	0.0
Gelinite	0.0	0.0	14.0	9.2	0.6
Sporinite	2.4	2.8	1.4	2.0	4.0
Cutinite	0.8	0.0	2.4	2.6	3.8
Resinite	0.0	0.0	0.2	0.0	0.0
Alginite	1.4	3.0	0.0	0.0	9.0
Liptodetrinite	8.0	8.2	6.6	7.6	27.0
Amorphous O.M. ^b	82.0	51.0	0.0	0.0	40.0
Fusinite	0.0	0.2	0.0	0.0	0.0
Semifusinite	0.0	0.0	0.0	0.0	0.0
Funginite	0.0	0.0	0.6	0.0	0.0
Inertodetrinite	0.0	4.4 ^a	0.0	0.8	0.0
Macrinite	0.0	0.0	0.0	0.0	0.0
Pyrite	1.2	2.2	0.4	0.0	2.2
Other minerals	0.0	18.6	1.8	1.6	2.6
HUMINITE	4.2	9.6	86.6	85.4	11.4
LIPTINITE	12.6	14.0	10.6	12.2	43.8
INERTINITE	0.0	4.6	0.6	0.8	0.0
MINERALS	83.2	71.8	2.2	1.6	44.8
%R ₀	—	—	0.41	0.37	—

^a Attrinite and inertodetrinite are extremely fine-grained and are thus very difficult to distinguish from each other.

^b Amorphous O.M., fluorescing amorphous organic matter; probably intimately associated with mineral matter.

Table 1). In both samples the primary huminite maceral is densinite followed by gelinite and eu-ulminite. The liptinite maceral group amounts to 10.6–12.2 vol% and is mainly composed of liptodetrinite (Table 1). The inertinite content is negligible and the mineral matter content very low. Small amounts of pyrite were recorded in DH 3. Huminite reflectance measurements on the coal samples yielded mean random reflectances of 0.41%R_r and 0.37%R_r, which correspond to the sub-bituminous C coal rank or thermal immaturity.

The remaining three samples are dominated by mineral matter, which to a large extent is intimately associated with yellowish-orange fluorescing amorphous organic matter (AOM) (Table 1). In sample DH 6 in particular the mineral matter is intimately mixed with small pieces of degraded liptinite (Fig. 4A,B). Angular quartz (?) particles constitute a part of the mineral matter in DH 1, and cutinite and sporinite are commonly seen bending around these particles due to compression (Fig. 4C). Pyrite, commonly as framboidal forms, is present in all three samples. The non-amorphous organic matter in the samples is primarily composed of liptinite (Table 1). The majority is liptodetrinite followed by a high proportion of strongly yellow fluorescing alginite with typical *Botryococcus*-morphology (Fig. 4A,B), which may reach a size up to approximately 95 µm. Sporinite, which in DH 6 often is identified as colpate pollen, and cutinite are also present (Fig. 4A,C; Table 1). Huminite is

a subordinate component in the three mudstones, while inertinite is absent in DH 1 and DH 6.

4.2. Organic geochemistry of outcrop samples

The TOC content varies from 6.48 wt% in the mudstones to 66.91 wt% in the coals (Table 2). *T*_{max} values range from 414 to 427°C. The thermally extracted and generated hydrocarbons, S₁ and S₂, range from 1.52 to 4.61 mg HC/g rock and 37.96–146.04 mg HC/g rock respectively, and the Hydrogen Index (HI) varies from 200 to 690 (Table 2).

The coal samples (DH 3, DH 4) have *E*_a-distributions centred around 58 and 62 kcal/mole (Fig. 5). The *E*_a-distributions are slightly asymmetric due to a 'tail' of high activation energies reaching up to 80 kcal/mole in DH 4. Samples DH 1 and DH 6 yield 'left-skewed' *E*_a-distributions with prominent peaks at 58 and 62 kcal/mole, respectively (Fig. 5).

The samples yield an extract amount between 37 and 88 mg soluble organic matter (SOM)/g OC, and the deasphalted solvent extracts are mainly composed of heteroatomic compounds (Table 3).

The gas chromatograms show that the saturate fractions of the DH 3 and DH 4 coals are characterised by an abundance of long-chain *n*-alkanes which maximise in the C_{25–31} range, moderate proportions of "Unresolved Complex Mixture" (UCM) with prominent asymmetric, heavy-end skewed terpane "humps", high proportions of C_{15–20} acyclic

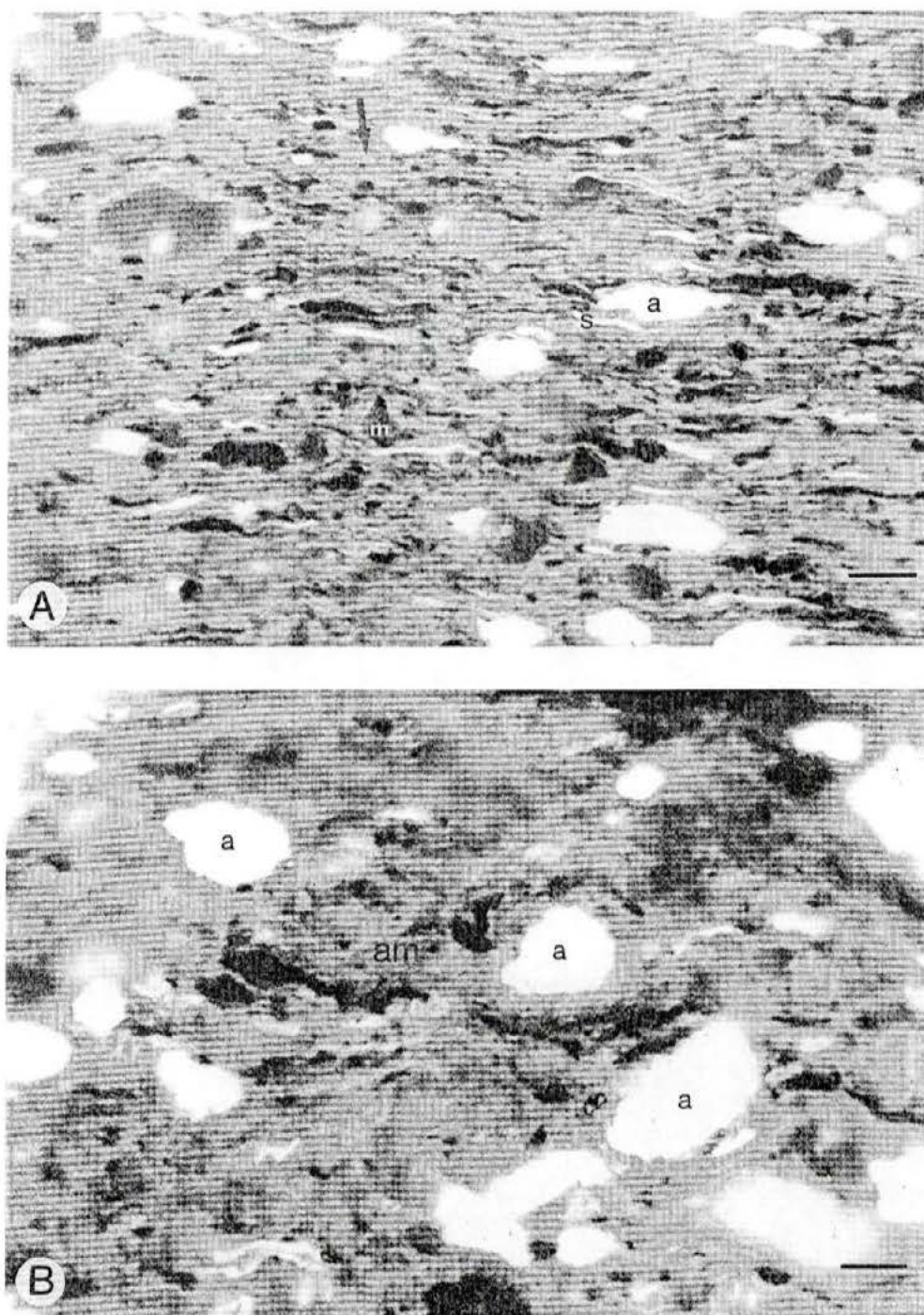


Fig. 4. (A) Intimately associated liptodetrinite (arrows), sporinite (s), alginite (a), and minerals (m) in a groundmass of fluorescing amorphous organic matter; (B) Alginite (a) with a morphology similar to the extant *Botryococcus* genus in a matrix of fluorescing amorphous organic matter (am) and mineral matter; (C) Cutinite (c) in a groundmass of fluorescing amorphous organic matter and mineral matter. Note cutinite 'bending' around angular quartz(?) grain. (A, B: DH 6; C: DH 1; reflected blue light, oil immersion, scale bar $\sim 30 \mu\text{m}$).

isoprenoids, and a tendency to a bimodal distribution (Fig. 6). There is a predominance of odd-carbon numbered *n*-alkanes with CPI_{22-32} (Carbon Preference Index; Bray and Evans, 1961; Cooper and Bray, 1963) values between 2.47 and 2.74 (Table 4). The pristane/phytane (Pr/Ph) ratio ranges from 3.10 to 3.27 (Table 4). Although the DH 1 sample shows characteristics very similar to the two coal

samples, differences are observed. The initial Pr/Ph is somewhat lower (2.83; Table 4) and the UCM envelope is slightly less prominent and more symmetric. The characteristics of the saturate fraction of the DH 6 sample also differ only slightly from those of the DH 1, DH 3 and DH 4 samples. However, the initial Pr/Ph ratio is rather low (2.41; Table 4), and UCM is largely absent.

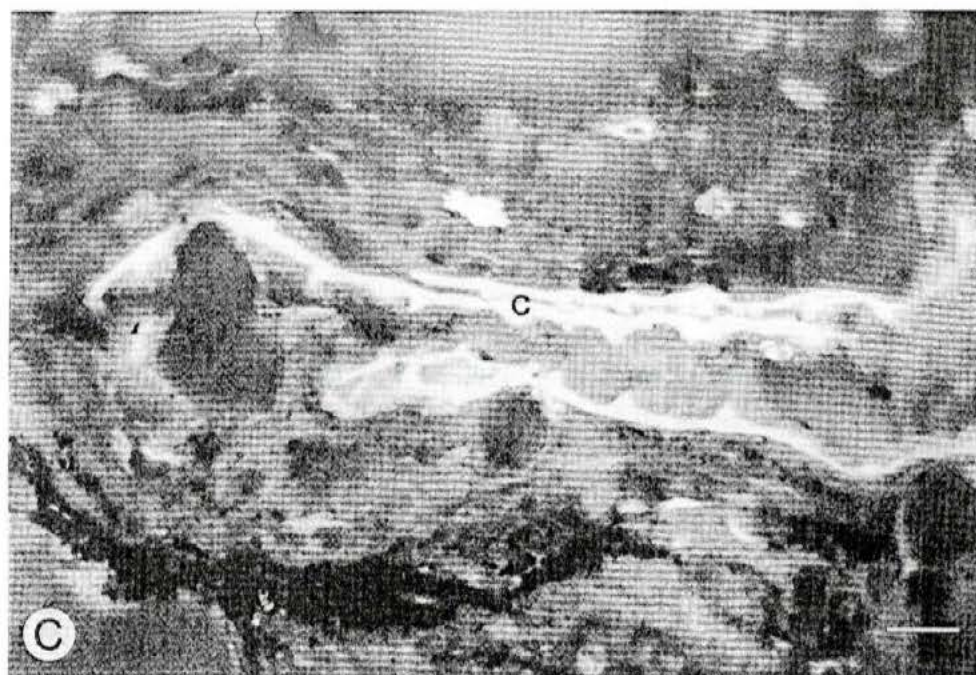


Fig. 4. (continued)

The m/z 191 mass fragmentograms are characterised by high proportions of oleanenes and abundance of $\beta\beta$ -hopanes, $\beta\alpha$ -hopanes (moretanenes) and hopanes (Petersen et al., 1998a), although the DH 6 sample contains much lower proportions of oleanene compared to the other samples. The $C_{31}\alpha\beta$ 22S/(22S + 22R) ratio is very low for the samples (0.02–0.03) (Table 4). Steranes are only present in negligible amounts and cannot be used to determine the relative proportions of steranes C_{27-29} .

4.3. Hydrous pyrolysis

The coal samples (DH 3, DH 4) more or less follow the kerogen type III maturation path on the HI versus T_{\max} diagram (Fig. 7). After hydrous pyrolysis of DH 3 and DH 4 at 330°C/72 h, T_{\max} has increased from initial 414°C to 452–453°C whereas HI has decreased from initial 200 to 138 (DH 3) and 242 to 144 (DH 4). Extracted samples have slightly higher T_{\max} temperatures and much lower HI values. For both samples, S_1 yields increase significantly during artificial maturation (Tables 2 and 5). S_2 shows a maximum at approximately 151–157 mg HC/g rock between 270 and

300°C/72 h before it decreases to values below the initial S_2 yields (Tables 2 and 5).

The carbonaceous mudstone samples (DH 1, DH 6) follow the maturation path of kerogen type II on the HI versus T_{\max} diagram (Fig. 7). The T_{\max} of DH 1 increases from initial 427 to 433°C after hydrous pyrolysis at 330°C/72 h whereas HI decreases from initial 586 to 344 (Fig. 7). Pyrolysed and extracted samples have much lower HI values and generally higher T_{\max} values than the non-extracted counterparts. During hydrous pyrolysis S_1 yields show a 7-fold increase, whereas S_2 yields are approximately halved (Tables 2 and 5).

The untreated DH 6 sample has a T_{\max} of 423°C, which increases to 436°C at a temperature of 330°C/72 h, and during artificial maturation the HI decreases from initial 690 to 390. Extracted samples have in general slightly higher T_{\max} values and much lower HI values than the non-extracted counterparts. However, HI from the extracted samples shows an increase for pyrolysis temperatures 240°C/72 h and 270°C/72 h compared to the untreated, extracted sample (Fig. 7). S_1 yields increase significantly, whereas S_2 yields are more than halved (Tables 2 and 5).

Table 2
Screening data and HI of outcrop samples

Sample	TOC (wt%)	T_{\max} (°C)	S_1 (mg HC/g rock)	S_2 (mg HC/g rock)	HI
Dong Ho 1	6.48	427	1.89	37.96	586
Dong Ho 2	14.90	427	1.52	70.32	472
Dong Ho 3	66.91	414	4.07	134.14	200
Dong Ho 4	60.35	414	3.95	146.04	242
Dong Ho 6	16.89	423	4.61	116.62	690

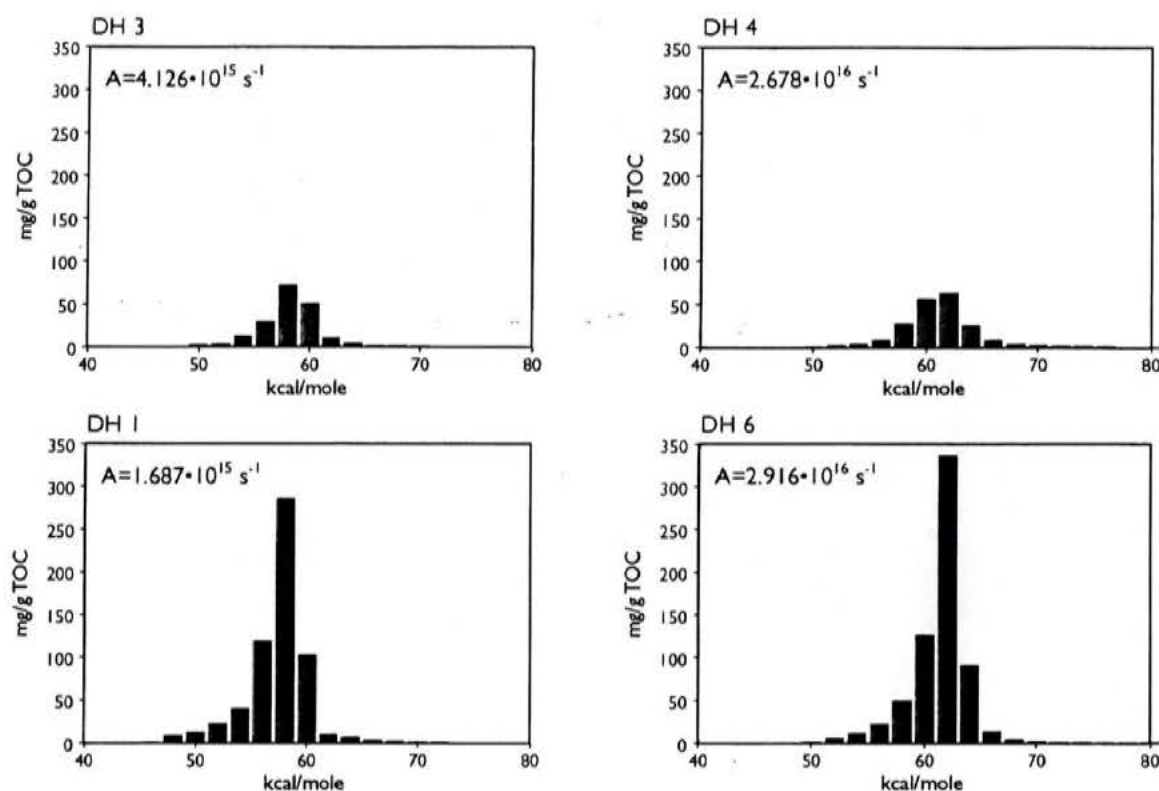


Fig. 5. Activation energy (E_a) distributions and pre-exponential factors (A) of the DH 3, DH 4, DH 1, and DH 6 samples. The broad E_a -distributions of DH 3 and DH 4 are typical for humic coals and kerogen type III. Although the E_a -distributions of DH 1 and DH 6 have a 'front' of low activation energies, the dominance of kerogen type I and II in the samples is reflected by the characteristic narrow span of dominant activation energies and a prominent principal E_a -value.

The E_a -distributions of samples DH 3 and DH 4 hydrous-pyrolysed at 330°C/72 h have E_a -peaks at 64 kcal/mole and high proportions of E_a -values above 64–66 kcal/mole (Fig. 8). Both E_a -distributions still have a 'front' of activation energies lower than the peak activation energy. The 'front' is however not present in the E_a -distributions of the extracted, pyrolysed samples (330°C/72 h) (Fig. 8).

The E_a -distribution of the hydrous-pyrolysed (330°C/72 h) DH 1 sample has more or less similar shape as the initial sample, but the E_a -peak position has moved to 60 kcal/mole and the magnitude of the E_a has decreased significantly (Fig. 8). The E_a -distribution of the hydrous-pyrolysed DH 6 is characterised by a significant decrease of E_a -values larger than 58 kcal/mole and an increase of the proportion of lower E_a -values, particularly manifested by the principal activation energy of 58 kcal/mole. After extraction of the hydrous-

pyrolysed DH 1 and DH 6 samples the majority of the low E_a -values disappear, and the resulting E_a -distributions are very narrow and practically restricted to the range 56–60 kcal/mole (Fig. 8).

The gas chromatograms of the saturated extract fractions of the DH 3 and DH 4 coals show very similar initial characteristics and development when subjected to hydrous pyrolysis (Fig. 6). With increasing hydrous pyrolysis temperature the initial bimodal shapes of the overall n -alkane distributions are gradually transformed into broad, heavy-end skewed unimodal distributions, which retain notable odd-number predominance in the nC_{22+} range. Acyclic isoprenoids are gradually masked by increasing proportions of lower carbon number range n -alkanes, Pr/Ph ratios pass through maxima of 8.07 and 6.97, and subsequently decrease to values of 5.25 and 5.29 after hydrous

Table 3
Solvent extract yields and extract compositions of outcrop samples

Sample	Extract yield (mg SOM/g OC)	Asphaltenes (%)	Saturates (%)	Aromatics (%)	Polars (%)
DH 1	88	36.6	16.4	6.7	76.9
DH 2	37	36.2	16.1	7.8	76.1
DH 3	57	55.8	4.0	6.5	89.4
DH 4	68	47.6	3.9	7.4	88.7
DH 6	84	36.7	2.9	13.2	83.9

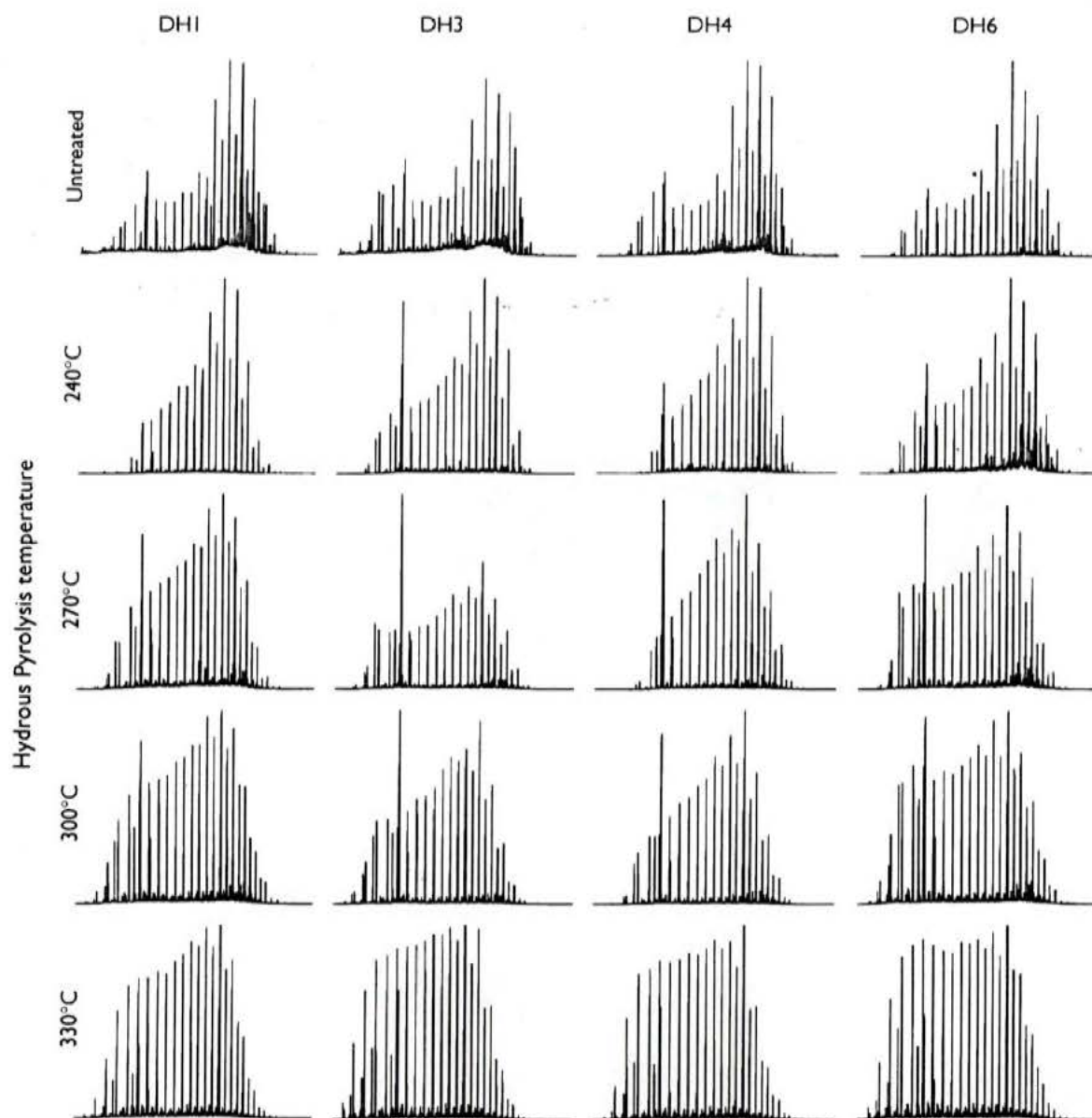


Fig. 6. Gas chromatograms of untreated and hydrous-pyrolysed samples. The chromatograms of the DH 3 and DH 4 coals are with increasing temperature gradually transformed into broad, heavy-end skewed unimodal distributions with an odd-over-even predominance in the C_{22+} range. The chromatograms of the DH 1 and DH 6 mudstones retain a slight bimodality.

pyrolysis at 330°C/72 h. Furthermore, the prominent UCM envelopes disappear.

The gas chromatograms of the DH 1 and DH 6 mudstones differ only slightly from the DH 3 and DH 4 coals (Fig. 6).

Table 4
Pr/Ph ratios, CPI values and C_{31} homohopane epimerization ratios of outcrop samples

Sample	Pr/Ph	CPI	$C_{31}\alpha\beta$ 227S/(22S + 22R)
Dong Ho 1	2.83	2.57	0.02
Dong Ho 2	2.84	2.87	0.02
Dong Ho 3	3.27	2.47	0.02
Dong Ho 4	3.10	2.74	0.03
Dong Ho 6	2.41	3.57	0.02

With increasing temperature of hydrous pyrolysis, the n -alkane distribution of DH 1 retains a slight bimodality, and the Pr/Ph ratio shows but a very slight increase to 2.94 through a maximum of 3.42. With increasing hydrous pyrolysis temperature, the Pr/Ph ratio of DH 6 increases to 3.07 through a maximum of 3.69, and the bimodality of the n -alkane distribution is enhanced. After hydrous pyrolysis at 330°C/72 h, the distribution is nearly symmetrical, centred at nC_{20} .

During hydrous pyrolysis a significant decrease in the amount of heteroatomic compounds in the maltene fractions from the samples is associated with a significant increase in the proportion of hydrocarbons (Fig. 9). The solvent extract yields of the DH 3 and DH 4 coal samples are doubled from

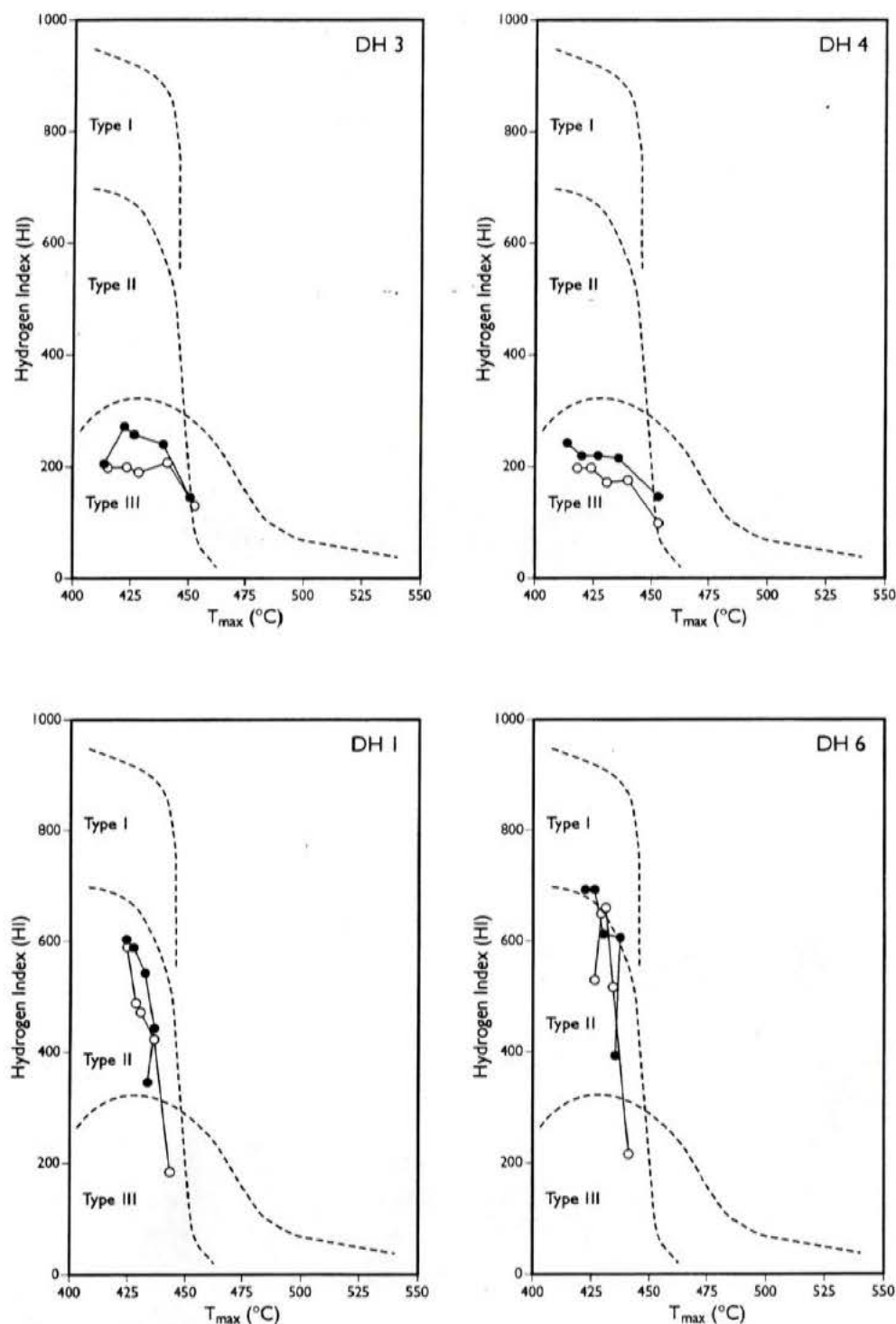


Fig. 7. HI vs T_{max} diagrams showing the evolution of the samples during artificial maturation (hydrous pyrolysis). The DH 3 and DH 4 coals follow the path of kerogen type III, whereas DH 1 and DH 6 mudstones containing kerogen types IIA and IIA/I, respectively, follow the path of kerogen type II. DH 1 and DH 6 represent very good source rocks that generate petroleum over a comparatively narrow temperature interval, which is in agreement with the narrow span of dominant activation energies and a prominent principal E_a -value. Dots: untreated samples; circles: solvent extracted samples.

the initial samples to the samples subjected to hydrous pyrolysis at $330^\circ\text{C}/72$ h (Tables 3 and 5). In contrast, the solvent extract yields from the DH 1 and DH 6 mudstone samples show a 8- to 10-fold increase after hydrous pyrolysis at $330^\circ\text{C}/72$ h (Tables 3 and 5).

4.4. Py-GC of outcrop and hydrous-pyrolysed samples

The DH 3 and DH 4 coals show a high degree of similarity. Pyrograms of solvent-extracted outcrop samples show that in the low molecular weight range (i.e. $<nC_{15}$)

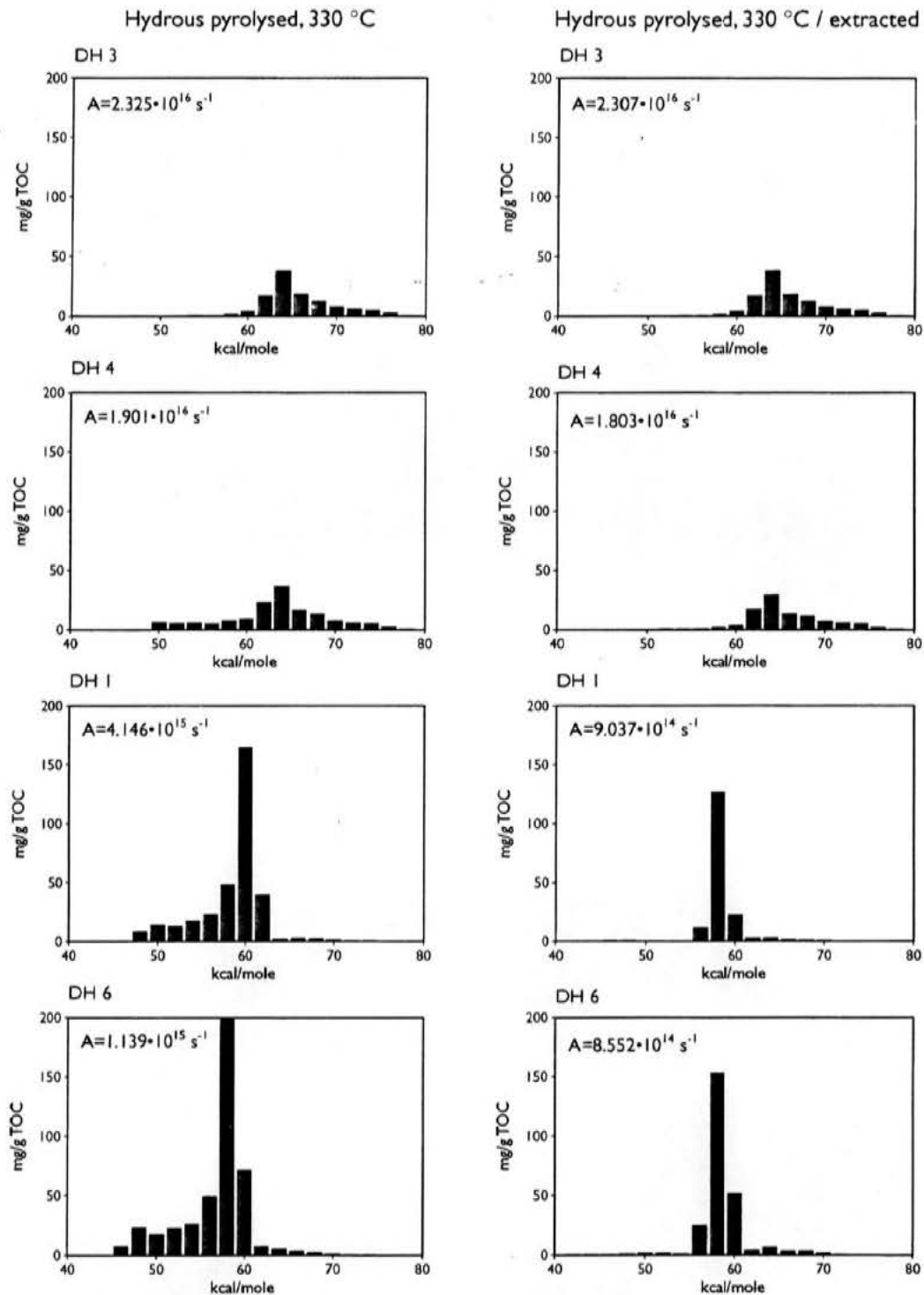


Fig. 8. The E_a -peak of the E_a -distributions of the hydrous-pyrolysed (330°C/72 h) DH 3 and DH 4 coals has, compared to the raw samples, moved to a higher value, and the distributions show a high proportion of activation energies above 64–66 kcal/mole. The low activation energies in the distribution of DH 4 is related to solvent extractable organic matter. Compared to the untreated samples, the hydrous-pyrolysed (330°C/72 h) DH 1 mudstone shows a significant decrease in the magnitude of the E_a -peak and a shift to 60 kcal/mole, and the DH 6 mudstone a significant decrease of activation energies above 58 kcal/mole and an increase of lower activation energies. The major part of the low activation energies are related to solvent extractable organic matter, and the solvent extracted samples have narrow E_a -distributions.

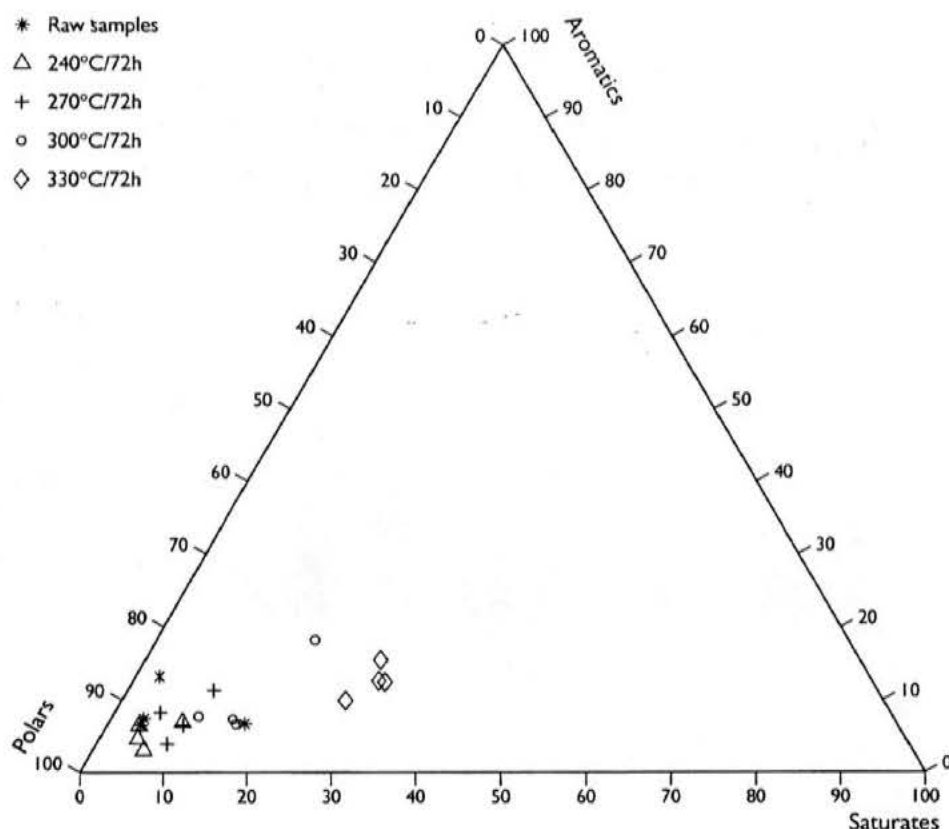


Fig. 9. Compositional evolution of the solvent extractable maltene fractions of the DH 1, DH 3, DH 4, and DH 6 samples during artificial maturation (hydrous pyrolysis). There is a clear tendency towards an increase of saturates in the extracts with increasing maturation.

pyrolysates are dominated by aromatic and phenolic compounds in various states of alkylation. In the nC_{10-15} range, an abundance of unknowns, which are tentatively identified as cresols, xylenols, and alkylated naphthalenes, are present together with naphthalene. The proportion of the total pyrolysate eluting in the nC_{15+} range is comparatively high, and dominated by alkane/alkene doublets extending to

a carbon number of at least 35. The n -alkanes show a slight odd-number predominance in the nC_{23-29} range. Little change is observed in compound distribution during artificial maturation by hydrous pyrolysis, although the proportions of unknowns (probably mainly heteroatomic compounds) decrease, as does the maximum observed alkane/alkene chain length. Such changes are most

Table 5

TOC contents, S_1 and S_2 yields, and solvent extract yields at the four hydrous pyrolysis temperatures

Sample	Temperature (°C)	TOC (wt%)	S_1 (mg HC/g rock)	S_2 (mg HC/g rock)	Extract yield (mg SOM/g OC)
Dong Ho 1	240	5.30	1.96	31.86	232
	270	6.24	3.17	33.64	248
	300	5.97	4.95	26.36	424
	330	5.20	13.22	17.92	690
Dong Ho 3	240	54.52	10.64	144.86	79
	270	62.38	16.76	157.50	85
	300	60.29	35.86	140.86	122
	330	74.62	51.14	103.22	103
Dong Ho 4	240	62.57	7.24	136.12	65
	270	68.54	13.00	150.28	71
	300	70.59	25.04	151.44	78
	330	65.38	52.33	94.06	132
Dong Ho 6	240	16.41	5.94	113.36	146
	270	16.47	10.00	100.38	212
	300	15.53	15.00	93.84	381
	330	13.19	31.08	51.40	808

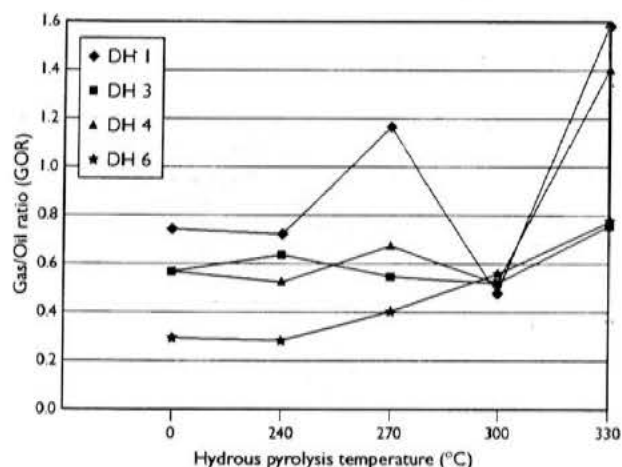


Fig. 10. Evolution of the GOR of the DH 1, DH 3, DH 4, and DH 6 with increasing maturity (hydrous pyrolysis). In general, the GOR are below 0.75 indicating a primary oil-generating capability of the samples, which is particularly evident for DH 6. At a pyrolysis-temperature of 330°C/72 h, the DH 1 and DH 4 samples have GOR of 1.57 and 1.40, respectively, which indicate a primary gas-generative potential at this maturity.

pronounced in the DH 4 sample. GOR (i.e. nC_{1-5}/nC_{6+} , total pyrolysate measured on blank-subtracted pyrograms) remain largely constant close to 0.6 until a hydrous pyrolysis temperature of 330°C/72 h, where an increase is observed (Fig. 10). "Generation diagrams" created by combining Py-GC and Rock-Eval data (method modified from Pepper and Corvi, 1995) show that only 16–17% of the organic carbon takes part in the formation of petroleum, and that both gas and oil-like products are generated over a wide range of thermal maturities (Fig. 11).

A detailed scrutiny of the pyrolysate composition of the untreated DH 1 mudstone shows a compound distribution largely indistinguishable from that yielded by the DH 4 coal as described above. Likewise, the evolution in pyrolysate composition during artificial maturation parallels that observed for the DH 4 coal, although DH 1 differs significantly with respect to generation characteristics. 40–50% of the organic carbon in the DH 1 mudstone participates in petroleum generation during maturation up to 300°C/72 h (Fig. 11). Despite this very high proportion of reactive constituents, the GOR is rather high (Fig. 10).

The DH 6 mudstone differs significantly from the samples described above. The pyrolysate is entirely dominated by *n*-alkane/alkene doublets which extend up to a chain length of at least 35 carbon atoms. Aromatic and phenolic compounds as well as functionalised unknowns appear of very subordinate importance. In general, the pyrogram is very similar to published pyrograms obtained from analysis of the Green River shale, torbanite, and other highly oil-prone, alginite-rich shales (e.g. Larter, 1985; Horsfield, 1989). The GOR yielded by the original sample is low, 0.3, and the initial proportion of generative organic carbon upon maturation is high, 45% (Figs. 10 and 11). Hydrous pyrolysis induces notable changes in pyrolysate composition, including an

overall reduction in the proportion of higher molecular weight pyrolysate components and in maximum *n*-alkyl chain length observed. After hydrous pyrolysis at 270°C/72 h, the potential for liquid petroleum generation decreases significantly and after hydrous pyrolysis at 330°C/72 h the generative potential is largely exhausted; only traces of *n*-alkyl components with chain lengths exceeding 12 are observed, and the principal recognisable components in the nC_{6+} fraction are benzene, *n*-heptane and toluene.

5. Discussion

5.1. Depositional environment

Samples DH 3 and DH 4 are humic coals with a TOC content of 66.91 and 60.35 wt% respectively, and with a petrographic composition consisting of about 98 vol% organic matter (Tables 1 and 2). The high proportion of huminite indicates that the coal originates from accumulation of large amounts of lignin- and cellulose-rich tissues from higher land plants. Pr/Ph ratios above 3, odd-over-even *n*-alkane predominance ($CPI_{22-32} = 2.47-2.74$), and an abundance of long-chain odd-numbered *n*-alkanes conform with this interpretation (Table 4). Significant proportions of oleanenes, which only occur in Late Cretaceous or younger rocks, are thought to be derived from angiosperms (e.g. Waples and Machihara, 1991; Peters and Moldowan, 1993), whereas the abundance of hopanes may indicate direct bacterial contribution to the biomass. Very low proportions of inertinite and abundant humified organic matter suggest continuously waterlogged mires with restricted oxygen availability and a low frequency of wild-fires. The absence or negligible content of pyrite points to a fresh water precursor mire (e.g. Casagrande, 1987).

Samples DH 1, DH 2, and DH 6 represent carbonaceous mudstones deposited in a more open environment. The mudstones have TOC contents from 6.48 to 16.89 wt%, and the petrographic analyses give a mineral matter content between 44.8 and 83.2 vol%. The organic matter is terrestrial and is mainly composed of detrital liptinite, sporinite, cutinite, alginite having a morphology very similar to the extant *Botryococcus* genus, and liptinitic AOM intimately associated with the mineral matrix (Fig. 4, Table 1). CPI_{22-32} values showing odd-over-even *n*-alkane predominance, abundance of odd-numbered long-chain *n*-alkanes and the presence of oleanenes support a strong terrestrial influence on the depositional environment. High proportions of fluorescing AOM, combined with low amounts of inertinite, and mineral matter mainly within the fine-grained size range, imply a low-energy, oxygen-deficient depositional environment, which favoured preservation of the organic matter. The presence of *Botryococcus*-like alginite (Fig. 4A,B) conforms with a mainly fresh water lake. However, the pyrite content, in particular the framboidal forms, may be related to activity of sulphur-metabolising bacteria during

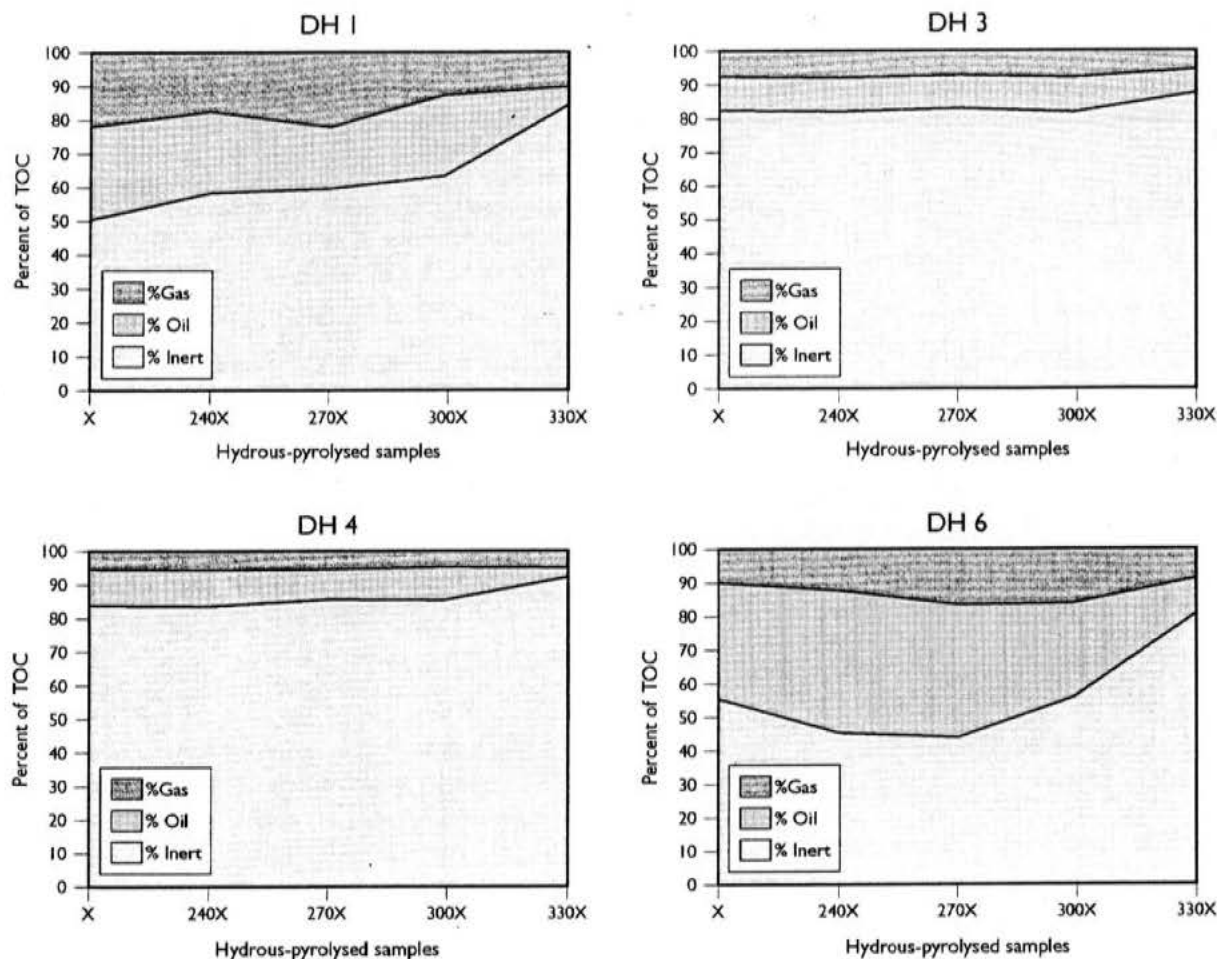


Fig. 11. The proportion of oil-prone, gas-prone, and inert carbon in the samples during artificial maturation (hydrous pyrolysis). A constant of 16–17% of the organic carbon in the DH 3 and DH 4 coals contributes to petroleum formation during maturation up to a pyrolysis-temperature of 300°C/72 h. The proportion of generative organic carbon in the DH 1 and DH 6 mudstones is much higher (initial samples 50 and 45%, respectively), and the majority of the generated petroleum will be liquid. In terms of hydrous pyrolysis conditions, the major part of the potential in DH 6 is realised over the interval 270°C/72 h to 330°C/72 h. X: extracted untreated sample; 240X: hydrous-pyrolysed at 240°C/72 h, extracted; 270X: hydrous-pyrolysed at 270°C/72 h, extracted; 300X: hydrous-pyrolysed at 300°C/72 h, extracted; 330X: hydrous-pyrolysed at 330°C/72 h, extracted.

saline water introduction (Cohen et al., 1984; Brown and Cohen, 1995), which implies proximity to the sea during deposition of the lacustrine carbonaceous mudstones.

Based on the limited number of samples available, the overall depositional environments of the Dong Ho sediments are freshwater peat-forming mires changing to oxygen-deficient principal freshwater lakes, which on occasion possibly were subject to marine influence. This interpretation conforms with the low-energy long-lived lake site depositional setting suggested by Traynor and Sladen (1997).

5.2. Thermal maturity of outcrop samples

The complex mixture of a variety of rather uncompact brown coal macerals in the humic coal samples (DH 3 and DH 4), and the yellowish fluorescence colour of the liptinite macerals in all five samples indicate a low thermal maturity of the organic matter. This is in agreement with T_{\max} values

of 414°C and huminite reflectance values of 0.37–0.41% R_o for the humic coals. The remaining three carbonaceous mudstone samples yield T_{\max} values between 423 and 427°C. However, these higher values may be caused by adsorption of the pyrolysate (S_2) onto the mineral matrix (Peters, 1986). Immaturity of the samples is further stressed by the presence of hopanes and $\beta\beta$ -hopanes in the solvent extracts, and by the very low C_{31} -homohopane epimerisation ratios of 0.02–0.03. The outcrop samples are thus thermally immature with respect to petroleum generation.

5.3. Source rock characteristics

The DH 3 and DH 4 coals correspond to kerogen type III, and the organic matter in the DH 1 and DH 2 mudstones can be classified as kerogen type IIA and that of DH 6 as kerogen type IIA/I according to the kerogen classification system of Mukhopadhyay et al. (1985).

The HI values of the humic coals and carbonaceous

mudstones span from 200 to 690 indicating a good to an excellent petroleum potential (Table 2). The principal controlling components on the HI of humic coals are the macerals collotelinite (derived from eu-ulminite in low rank coals), collodetrinite (derived from attrinite + densinite), liptodetrinite, the liptinite maceral group and the microlitho-type vitrite as shown in a study of 27 humic coal samples (including DH 3) of varying petrographic composition, rank, age and origin (Petersen and Rosenberg, 2000). The considerably higher HI values of the carbonaceous mudstones are related to the abundance of the highly hydrogen-rich constituents of the liptinite maceral group, including alginite (kerogen type I) and the mixture of detrital liptinite and fluorescing AOM in the mineral matrix.

The E_a -distributions of the initial samples conform well with published distributions of E_a of kerogen types II and III (Fig. 5) (e.g. Tissot et al., 1987; Ungerer and Pelet, 1987; Petersen and Rosenberg, 1998, 2000; Schenk and Horsfield, 1998; Boreham et al., 1999). The broad E_a -distributions of the DH 3 and DH 4 coals are related to the heterogeneous composition of coal and the aromatic nature of huminite/vitrinite, which is thermally robust (Tegelaar and Noble, 1994; Pepper and Corvi, 1995; Boreham et al., 1999). The DH 1 and DH 6 mudstones, containing kerogen types IIA and IIA/I respectively, would be expected to have more narrow E_a -distributions than the humic coals due to more uniform chemical bonds of the organic matter in kerogen I and II (Tissot et al., 1987). Thus, the 'front' of activation energies down to 48–50 kcal/mole reflect a complex petrographic composition with organic entities (possibly in the AOM) with low activation energies.

5.4. Petroleum generation characteristics (artificial maturation)

As expected from their petrography the DH 3 and DH 4 coals follow the maturation path for kerogen type III and the DH 1 and DH 6 mudstones the maturation path for kerogen type II during hydrous pyrolysis (Fig. 7). Comparison of the extracted and non-extracted samples in Fig. 7 shows that the generated bitumen influences both T_{max} and HI values. The trapped high molecular weight bitumen is comparatively labile compared to the kerogen and will thus result in lower T_{max} values and higher HI values. The low HI value of the original DH 3 coal compared to the sample hydrous-pyrolysed at 240°C/72 h may be related to suppression of the original HI by initial release of abundant oxygen groups (e.g. carboxyl and hydroxyl groups) from the coal matrix (Boudou et al., 1994) (Fig. 7).

After hydrous pyrolysis at 330°C/72 h the DH 3 and DH 4 coals yield T_{max} values just above 450°C, which according to Hunt (1996, cf. his fig. 10-38) corresponds to a vitrinite reflectance of approximately 1.1% R_o . Other T_{max} versus % R_o correlations suggest a slightly lower reflectance of about 1.0% R_o (Teichmüller and Durand, 1983; Veld et al., 1993). The DH 1 and DH 6 mudstones hydrous-pyrolysed at

330°C/72 h yield only T_{max} temperatures from 433 to 436°C. A narrow activation energy distribution, as in kerogen type I, typically results in a lack of change in T_{max} and a considerable petroleum formation during thermal maturation (Tissot et al., 1987). The lower T_{max} values obtained from the DH 1 and DH 6 mudstones hydrous-pyrolysed at 330°C/72 h may thus be related to their large principal E_a -values.

After hydrous pyrolysis at 330°C/72 h the humic coal samples still have broad E_a -distributions, and this does not change significantly for DH 3 after extraction (Fig. 8). In contrast, comparison of the non-extracted and extracted DH 4 coal reveals that extractable organic matter with activation energies between approximately 50 and 60 kcal/mole was formed during pyrolysis. The shift towards a higher principal E_a -value after artificial maturation is caused by depletion of lower activation energies; this is also well known from naturally matured coal series up to a vitrinite reflectance of 1.70% R_o (Schenk and Horsfield, 1998; Petersen and Rosenberg, 2000). During artificial maturation the majority of the organic carbon in the DH 3 and DH 4 coals remains inert with respect to petroleum generation as only about 16–17% of the organic carbon participates in petroleum formation (Fig. 11). However, the major part of the generated petroleum will be liquid as shown by the GOR (Fig. 10), and following Isaksen et al. (1998) the ability to generate C_{15+} n-alkanes (as shown by the Py-GC traces) indicate a potential for generation and expulsion of crude oil. The significant increase in the GOR at 330°C/72 h for DH 4 indicates that a primary gas generative potential has remained at this maturity (Fig. 10). Thus, despite a maturity corresponding to the late oil window for the hydrous-pyrolysed (330°C/72 h) DH 3 and DH 4 coals the HI values of 138 and 144 and the E_a -distributions show, that the humic coals have retained a petroleum generative potential at this maturity level. However, as shown by Schenk and Horsfield (1998) artificial maturation of coal may not be able to reproduce the structural changes of the coal matrix occurring during natural maturation. During natural maturation of coal, structural reorganisation of the organic matter by solid state aromatisation and condensation creates new petroleum potential, which is retained up to higher maturity levels (Schenk and Horsfield, 1998; Boreham et al., 1999). This conforms with Py-GC data obtained from naturally matured Middle Jurassic coals from the Danish North Sea that, despite a vitrinite reflectance of 1.3% R_o , are able to generate liquid petroleum upon further maturation (Petersen et al., 1998b).

Schenk and Horsfield (1998) showed that the critical solid state aromatisations first start in marine Toarcian shales (kerogen type II) when petroleum generation has come to an end, which, in contrast to coal, makes artificial experiments on kerogen type II more reliable with regard to replication of natural maturation. The E_a -distributions of the two hydrous-pyrolysed mudstones containing kerogen type IIA and IIA/I are at a first glance relatively broad. However, the very narrow E_a -distribution of the extracted

samples indicate that a large part of the E_a -values are related to solvent-extractable bitumen in the samples (Fig. 8). In contrast to the non-extracted samples the extracted ones show a typical kerogen type II distribution of E_a . The principal E_a -value has only shifted from 58 kcal/mole for the initial DH 1 sample to 60 kcal/mole for the hydrous-pyrolysed (330°C/72 h) counterpart, whereas the extracted hydrous-pyrolysed DH 6 shows a shift to a lower principal E_a -value compared to the initial sample. A possible explanation could be the small change in T_{\max} during artificial maturation due to extensive generation of bitumen (petroleum), related to the large principal E_a -values. In DH 1 about 45% of the organic carbon participates in petroleum formation during artificial maturation and the majority of the petroleum will be liquid (Figs. 10 and 11). The highly generative organic matter and the high proportion of mineral matrix can be expected to facilitate the expulsion of higher molecular weight petroleum products generated during thermal maturation. The significant increase of the GOR after hydrous pyrolysis at 330°C/72 h indicates that the potential for liquid petroleum is exhausted. The DH 6 mudstone represents an excellent, highly oil-prone source rock, capable of generating and expelling large quantities of crude waxy oil, as well as gas (Figs. 10 and 11). Hydrous pyrolysis data show that the main portion of the source potential is realised rather early during thermal maturation over a comparatively narrow maturity interval (Fig. 11), which conforms with the E_a -distribution of DH 6. Thus, in terms of hydrous pyrolysis conditions, the major part of the potential is realised over the interval 270°C/72 h to 330°C/72 h.

Lewan (1994) performed hydrous pyrolysis experiments on kerogen type II and showed that up to a hydrous pyrolysis temperature of about 330°C/72 h the kerogen decomposes to mainly high molecular weight bitumen, that forms a continuous network within the rock. Higher temperature (hydrous pyrolysis temperatures >330°C) results in decomposition of the bitumen to oil. According to these results the hydrous-pyrolysed mudstones of this study have reached the stage of maximum bitumen formation and only the beginning of oil expulsion due to partial decomposition of the bitumen. This fits well with a comparison of the E_a -distributions of the non-extracted and extracted DH 1 and DH 6 samples (Fig. 8), showing that a major part of the E_a -values can be related to trapped bitumen in the rocks.

As shown by the HI values of 344 and 390 and the E_a -distributions the mudstones still have a significant petroleum generative potential after hydrous pyrolysis. However, the conspicuous decrease in HI values from the initial to the hydrous-pyrolysed samples suggests that the kerogen of DH 1 and DH 6 is relatively more exhausted with respect to petroleum formation than the humic coals (DH 3 and DH 4).

Extract compositions change towards higher proportions of saturates with increasing hydrous pyrolysis temperature (Fig. 9). This maturation effect on the generated petroleum product, the ability of the samples to form C_{15+} n -alkanes,

and the selective expulsion of preferential long chain aliphatic compounds from humic coals in particular (due to the higher degree of adsorption of aromatic and heteroatomic compounds onto the coal matrix; Isaksen et al., 1998) would result in the formation of a waxy paraffinic crude oil.

5.5. Summary of source rock and generation characteristics

The petrography and organic geochemistry of the Dong Ho samples show that the outcrop contains two types of source rocks: humic coals/kerogen type III and kerogen types IIA and IIA/I. This is further stressed by the E_a -distributions. The implications of the E_a -distributions are that the two source rock types will have different generation characteristics. The HI values, extract yields, GOR and E_a -distributions of the DH 1 and DH 6 mudstones indicate that these samples will generate large quantities of crude oil (particularly DH 6) at a comparatively restricted temperature range (depth interval). In contrast the HI values, extract yields, GOR and E_a -distributions of the DH 3 and DH 4 coals indicate that they will generate crude oil, although minor quantities, over a wider temperature range (depth interval), and they will probably continue to generate after the mudstones have been completely depleted in petroleum potential. This is supported by the work of Tissot et al. (1987) who showed a progressive and slower transformation ratio of kerogen type III and coals of the Mahakam Delta compared to kerogen types I and II, where the transformation to hydrocarbons is completed over a shorter temperature/depth interval.

5.6. Extension of Palaeogene terrestrial source rocks into the offshore parts of the Song Hong Basin

The Song Hong Basin belongs to a left-lateral transtensional system developed along the Red River Fault Zone. It is a deep NW–SE elongated basin with the offshore part stretching for more than 500 km covering the entire Gulf of Tonking and the northern part of the central Vietnamese shelf. The depth to the base of the Cenozoic fill in the central depocentre may exceed 14 km (Hao Fang et al., 1995).

The basin development in the northern part of the Gulf of Tonking can be separated into a number of specific tectonic phases separated by basin-wide unconformities as described by Rangin et al. (1995) and Nielsen et al. (1999) among others. Palaeogene extension led to formation of widespread grabens and halfgrabens followed by a Late Oligocene to Early Miocene post-rift subsidence phase. During the Middle-Late Miocene the tectonic regime changed, and basement inversion took place leading to formation of conspicuous compression structures over the former depocentres between the major basin bounding faults: the Son Chay Fault Zone to the southwest and the Vinh Ninh and Son Lo Fault Zones to the northeast (Fig. 1). Basin inversion culminated in the Late Miocene with the formation of a significant unconformity that deeply truncates the inversion structures. Renewed basin subsidence is witnessed by a

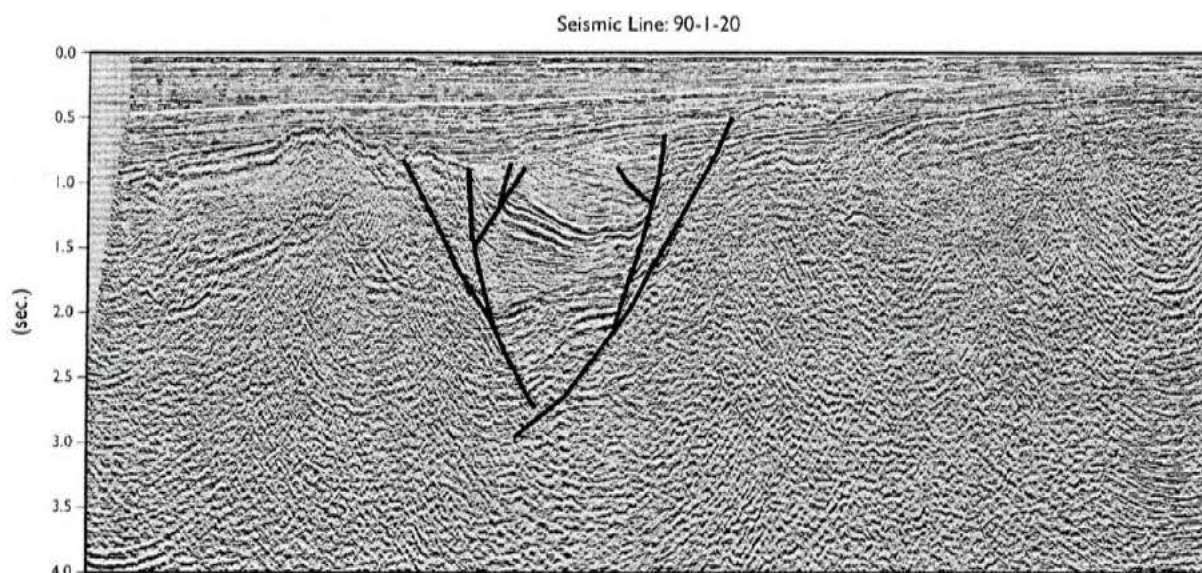


Fig. 12. SW–NE oriented seismic section (90-1-020) crossing the narrow Palaeogene Kiem An graben structure. For location, see Fig. 1. Note the interval of continuous, high amplitude reflections between 1.1–1.5 s in the syn-rift prism, possibly representing Lower Oligocene shales deposited in a lacustrine environment (after Andersen et al., 1998).

southward thickening, mostly undisturbed cover of uppermost Miocene to Pliocene and Quaternary sediments.

A number of NW–SE trending narrow Palaeogene grabens and halfgrabens has been mapped north-east of the Son Lo Fault Zone in the northernmost part of the Gulf of Tonking (Fig. 1). To the east this dominant trend is replaced by NE–SW trending structures connecting with the trend of the Palaeogene grabens in the Chinese Beibu Wan Basin. The syn-rift deposits may occasionally exceed a thickness of 5 km. The syn-rift prisms have only been partly penetrated in one well, 107 PA-1x (Fig. 1). Here massive conglomerates and sandstones are overlain by alternating sandstones, siltstones and mudstones deposited in a mixed alluvial-fluvial and lacustrine environment. The age of these syn-rift sediments have been dated as Eocene–Oligocene by the operator (Total Vietnam, 1991). The TOC content is low, mostly below 0.5 wt%, except for a few scattered high values caused by the occasional presence of thin coals. However, the seismic reflection pattern in the syn-rift succession at the well location differs considerably from the seismically correlating interval characterised by continuous, high amplitude reflections between 1.1–1.5 s in the Palaeogene graben structure displayed in Fig. 12 (for location of the seismic section, see Fig. 1). These reflections may originate from lacustrine shaly units embedded in an otherwise coarse-clastic dominated syn-rift succession by analogy to other Southeast Asian Cenozoic basins, e.g. the Pearl River Mouth Basin and the Gulf of Thailand (Leo, 1997). This shale-prone seismic facies is widespread in the NW–SE oriented grabens.

Successions of organic-rich lacustrine shales with minor coals similar to those exposed at Dong Ho may therefore be preserved in the Palaeogene syn-rift prisms in the offshore

halfgrabens. Although no direct ties can be made from the offshore Palaeogene successions to the isolated Dong Ho outcrop onshore, the postulated offshore extension of rich Palaeogene source rock intervals is further substantiated by similar high values of TOC, HI and S_2 yields obtained from Oligocene mudstones and silty mudstones recently sampled from the seabed and at outcrops on Bach Long Vi Island (Tri, 1997), located on a NE–SW trending inversion ridge (Fig. 1). Maturity modelling suggests that large parts of the undrilled, shale-prone Palaeogene interval characterised by continuous, high amplitude reflectors presently are in the oil and condensate window (Andersen et al., 1998; Nielsen et al., 1999). Therefore, an offshore Palaeogene source kitchen possibly exists in the syn-rift prisms in the northern part of the Gulf of Tonking northeast of the Song Lo Fault Zone.

6. Conclusions

1. The Oligocene deposits cropping out at Dong Ho, northern Vietnam, contain two source rocks: (a) carbonaceous mudstones, and (b) humic coals. The mudstones were deposited in low-energy, oxygen-deficient freshwater lakes, which on occasion were subjected to marine influence. The organic matter of the mudstones is primarily allochthonous. The humic coals represent in situ peat formation in wet, freshwater mires with a restricted oxygen availability and a low frequency of wildfires.
2. The carbonaceous mudstones have TOC contents from 6.48 to 16.89 wt%, and contain kerogen types IIA and IIA/I. The organic matter is terrestrial and is mainly composed of detrital liptinite, sporinite, cutinite, alginite with *Botryococcus*-morphology, and fluorescing AOM.

The mudstones yield Pr/Ph ratios slightly below 3, and show an odd-over-even *n*-alkane predominance and abundance of odd-numbered long-chain *n*-alkanes. The coals are dominated by huminite (kerogen type III) derived from woody tissues from higher land plants, which conforms with organic geochemical data (Pr/Ph ratios above 3, $CPI_{22-32} = 2.47-2.74$, abundance of long-chain odd-numbered *n*-alkanes). Significant proportions of oleanenes are thought to be derived from angiosperms.

3. The outcrop sediments are, with respect to petroleum formation, thermally immature. Huminite reflectances range between $0.37\%R_0$ and $0.41\%R_0$, C_{31} -homohopane epimerisation ratios are very low (0.02–0.03), and the solvent extracts contain the thermal unstable hopenes and $\beta\beta$ -hopanes.
4. The immature carbonaceous mudstones and coals have HI values from 472 to 690 and from 200 to 242, respectively. The E_a -distributions of the mudstones are characterised by a pronounced principal E_a , whereas the coals have broad E_a -distributions.
5. During artificial maturation the carbonaceous mudstones follow the path for kerogen type II and the coals the path for kerogen type III on the T_{max} versus HI diagram. The pronounced principal E_a -values of the carbonaceous mudstones result in a small change in T_{max} and considerable petroleum formation during maturation. The artificially matured mudstones have broad E_a -distributions, but narrow E_a -distributions of extracted samples show that a large part of the E_a -values are related to generated solvent-extractable organic matter. Maturation of the coals results in a shift towards a higher principal E_a -value, however, the E_a -distributions remain broad.
6. During artificial maturation about 16–17% of the organic carbon in the coals participated in petroleum formation. GOR in general between 0.50 and 0.75 show that the major part of the generated petroleum was liquid. In the DH 1 mudstone (kerogen type IIA) about 45% of the organic carbon participated in petroleum formation, which primarily was liquid. Up to about 55% of the organic carbon in the DH 6 (kerogen type IIA/I) participated in petroleum formation, and an initial GOR of 0.30 indicates significant generation of liquid petroleum. The main portion of the source potential is realised over a comparatively narrow maturity interval corresponding to a restricted temperature range or depth interval. The high generative capability of the carbonaceous mudstones is further stressed by a considerable increase in extract yields (up to nearly 10-times increase).
7. After hydrous pyrolysis at $330^\circ\text{C}/72\text{ h}$ the coals and the carbonaceous mudstones still have retained a significant petroleum generative potential, although the kerogen of the mudstones is relatively more exhausted with respect to petroleum formation than the coals.
8. The excellent generative capability of the two terrestrial source rock types at Dong Ho is very encouraging for

exploration of the Cenozoic Song Hong Basin where the plays rely on sourcing from rift-lake successions. The variable organic composition of the source rocks results in different generation characteristics, such as timing of petroleum generation, amount and composition of generated petroleum, which should be considered when the exploration potential of the basin is evaluated.

Acknowledgements

The results presented herein were obtained from a recently completed study on basin analysis and modelling of the Cenozoic Song Hong Basin. The project was jointly carried out by the Geological Survey of Denmark and Greenland (GEUS) and Vietnam Petroleum Institute (VPI), a subsidiary of the national state-owned oil company PetroVietnam. The Danish contribution has been funded through grants from the Danish Energy Research Programme (grants no. 1313/97-0034 and 1313/98-0022) and the Danish International Development Assistance (DANIDA). M. Gibling (Dalhousie University, Halifax, Canada) and F.G. Christiansen (GEUS) are thanked for their valuable comments on the paper. The paper is published with the permission of the Geological Survey of Denmark and Greenland.

References

- Andersen, C., Tiem, P.V., Mathiesen, A., Nielsen, L.H., 1998. Some new thermal maturity modelling results using Yüklér 1D software and seismic facies mapping in the northern part of the Song Hong Basin. In: Toan, T.N. (Ed.), Conference on Vietnam Petroleum Institute, 20 years development and prospects. Hanoi, May 1998, pp. 273–284.
- Boreham, C.J., Horsfield, B., Schenk, H.J., 1999. Predicting the quantities of oil and gas generated from Australian Permian coals, Bowen Basin using pyrolytic methods. *Marine and Petroleum Geology* 16, 165–188.
- Boudou, J.P., Espitalié, J., Bimer, J., Salbut, P.D., 1994. Oxygen groups and oil suppression during coal pyrolysis. *Energy and Fuels* 8, 972–977.
- Bray, E.E., Evans, E.D., 1961. Distribution of *n*-paraffins as a clue to recognition of source beds. *Geochimica et Cosmochimica Acta* 22, 2–15.
- Brown, K.E., Cohen, A.D., 1995. Stratigraphic and micropetrographic occurrences of pyrite in sediments at the confluence of carbonate and peat-forming depositional systems, southern Florida. *Organic Geochemistry* 22, 105–126.
- Casagrande, D.J., 1987. Sulphur in peat and coal. In: Scott, A.C. (Ed.), *Coal and coal-bearing strata: recent advances*. Geological Society London Special Publication 32, pp. 87–105.
- Chen Honghan, Li Sitian, Sun Yongchuan, Zhang Qiming, 1998. Two petroleum systems charge the YA13-1 gas field in Yinggehai and Qiongdongnan Basins, South China Sea. *American Association of Petroleum Geologists Bulletin* 82, 757–772.
- Cohen, A.D., Spackman, W., Dolsen, P., 1984. Occurrence and distribution of sulfur in peat-forming environments of southern Florida. *International Journal of Coal Geology* 4, 73–96.
- Cooper, J.E., Bray, E.E., 1963. A postulated role of fatty acids in petroleum formation. *Geochimica et Cosmochimica Acta* 27, 1113–1127.
- Ha, N.B., 1998. Studying source rocks in the Song Hong sedimentary Basin. In: Toan, T.N. (Ed.), *Conference on Vietnam Petroleum*

- Institute, 20 years development and prospects. Hanoi, May 1998, pp. 186–204.
- Hao Fang, Sun Yongchuan, Li Sitian, Zhang Qiming, 1995. Overpressure retardation of organic-matter maturation and petroleum generation: a case study from the Yinggehai and Qiongdongnan Basins, South China Sea. *American Association of Petroleum Geologists Bulletin* 79, 551–562.
- Hao Fang, Li Sitian, Sun Yongchuan, Zhang Qiming, 1998. Geology, compositional heterogeneities, and geochemical origin of the Yacheng gas field, Qiongdongnan Basin, South China Sea. *American Association of Petroleum Geologists Bulletin* 82, 1372–1384.
- Horsfield, B., 1989. Practical criteria for classifying kerogens: some observations from pyrolysis-gas chromatography. *Geochimica et Cosmochimica Acta* 53, 891–901.
- Hunt, J.M., 1996. *Petroleum geochemistry and geology*. Freeman, New York, p. 743.
- ICCP., 1971. Supplement to the 2nd edition of the International Handbook of Coal Petrography. Centre National de la Recherche Scientifique, Paris.
- ICCP., 1975. Supplement to the 2nd edition of the International Handbook of Coal Petrography. Centre National de la Recherche Scientifique, Paris.
- Isaksen, G.H., Curry, D.J., Yeakel, J.D., Jenssen, A.I., 1998. Controls on the oil and gas potential of humic coals. *Organic Geochemistry* 29, 23–44.
- Larter, S.R., 1985. Integrated kerogen typing in the recognition and quantitative assessment of petroleum source rocks. In: Thomas, B.M. (Ed.), *Petroleum geochemistry in exploration of the Norwegian shelf*. Graham & Trotman, London, pp. 269–286, for the Norwegian Petroleum Society.
- Lee, G.H., Watkins, J.S., 1998. Seismic sequence stratigraphy and hydrocarbon potential of the Phu Khanh Basin, offshore central Vietnam, South China Sea. *American Association of Petroleum Geologists Bulletin* 82, 1711–1735.
- Leo, C.T.A.M., 1997. Exploration in the Gulf of Thailand in deltaic reservoirs, related to the Bongkot Field. In: Fraser, A.J., Matthews, S.J., Murphy, R.W. (Eds.), *Petroleum geology of Southeast Asia*, Geological Society London Special Publication 126, pp. 77–87.
- Lewan, M.D., 1994. Assessing natural oil expulsion from source rocks by laboratory pyrolysis. In: Magoon, L.B., Dow, W.G. (Eds.), *The petroleum system — from source to trap*. American Association of Petroleum Geologists Memoir 60, pp. 201–210.
- Matthews, S.J., Fraser, A.J., Lowe, S.P., Todd, S.P., Peel, F.J., 1997. Structure, stratigraphy and petroleum geology of the SE Nam Con Son Basin, offshore Vietnam. In: Fraser, A.J., Matthews, S.J., Murphy, R.W. (Eds.), *Petroleum geology of Southeast Asia*, Geological Society London Special Publication 126, pp. 89–106.
- Mukhopadhyay, P.K., Hagemann, H.W., Gormly, J.R., 1985. Characterization of kerogens as seen under the aspect of maturation and hydrocarbon generation. *Erdöl und Kohle-Erdgas-Petrochemie vereinigt mit Brennstoff-Chemie* 38, 7–18.
- Nielsen, L.H., Mathiesen, A., Bidstrup, T., Vejrbæk, O.V., Dien, P.T., Tiem, P.V., 1999. Modelling of hydrocarbon generation in the Cenozoic Song Hong Basin, Vietnam: a highly prospective basin. *Journal of Asian Earth Sciences* 17, 269–294.
- Noble, R.A., Wu, C.H., Atkinson, C.D., 1991. Petroleum generation and migration from Talang Akar coals and shales off-shore NW Java, Indonesia. *Organic Geochemistry* 17, 363–374.
- Pepper, A.S., Corvi, P.J., 1995. Simple kinetic models of petroleum formation. Part 1: oil and gas generation from kerogen. *Marine and Petroleum Geology* 12, 291–319.
- Peters, K.E., 1986. Guidelines for evaluating petroleum source rock using programmed pyrolysis. *American Association of Petroleum Geologists Bulletin* 70, 318–329.
- Peters, K.E., Moldovan, J.M., 1993. *The biomarker guide — interpreting molecular fossils in petroleum and ancient sediments*. Prentice Hall, New Jersey, p. 363.
- Petersen, H.I., Rosenberg, P., 1998. Reflectance retardation (suppression) and source rock properties related to hydrogen-enriched vitrinite in Middle Jurassic coals, Danish North Sea. *Journal of Petroleum Geology* 21, 247–263.
- Petersen, H.I., Rosenberg, P., 2000. The relationship between the composition and rank of humic coals and their activation energy distributions for the generation of bulk petroleum. *Petroleum Geoscience* 6, 137–149.
- Petersen, H.I., Bojesen-Koefted, J.A., Nielsen, L.H., Nytoft, H.P., 1998a. Organic petrography and geochemistry of three samples from Dong Ho, Vietnam. EFP-project: Description of the petroleum system(s) of the Song Hong Basin, Vietnam. Danmarks og Grønlands Geologiske Undersøgelse Rapport 1998/49, 38 pp.
- Petersen, H.I., Andsbjerg, J., Bojesen-Koefted, J.A., Nytoft, H.P., Rosenberg, P., 1998b. Petroleum potential and depositional environments of Middle Jurassic coals and non-marine deposits, Danish Central Graben, with special reference to the Søgne Basin. *Geology of Denmark Survey Bulletin* 36, 78 pp.
- Rangin, C., Klein, M., Roques, D., Le Pichon, X., Truong, L.V., 1995. The Red River fault system in the Tongking Gulf, Vietnam. *Tectonophysics* 243, 209–222.
- Ratanasthien, B., Kandharosa, W., Chompusri, S., Chartprasert, S., 1999. Liptinite in coal and oil source rocks in northern Thailand. *Journal of Asian Earth Sciences* 17, 301–306.
- Schenk, H.J., Horsfield, B., 1998. Using natural maturation series to evaluate the utility of parallel reaction kinetics models: an investigation of Toarcian shales and Carboniferous coals, Germany. *Organic Geochemistry* 29, 137–154.
- Sladen, C., 1997. Exploring the lake basins of east and southeast Asia. In: Fraser, A.J., Matthews, S.J., Murphy, R.W. (Eds.), *Petroleum Geology of Southeast Asia*. Geological Society London, Special Publication 126, pp. 49–76.
- Taylor, G.H., Teichmüller, M., Davis, A., Diessel, C.F.K., Littke, R., Robert, P., 1998. *Organic petrology*. Gebrüder Borntraeger, Berlin, p. 704.
- Tegelaar, E.W., Noble, R.A., 1994. Kinetics of hydrocarbon generation as a function of the molecular structure of kerogen as revealed by pyrolysis-gas chromatography. *Organic Geochemistry* 22, 543–574.
- Teichmüller, M., Durand, B., 1983. Fluorescence microscopical rank studies on liptinites and vitrinites in peat and coals, and comparisons with results of the Rock-Eval pyrolysis. *International Journal of Coal Geology* 2, 197–230.
- Thanh, L., 1997. Dong Ho oil-shale outcrop. Unpublished internal report, Vietnam Petroleum Institute.
- Tissot, B.P., Pelet, R., Ungerer, P.H., 1987. Thermal history of sedimentary basins, maturation indices, and kinetics of oil and gas generation. *American Association of Petroleum Geologists Bulletin* 71, 1445–1466.
- Todd, S.P., Dunn, M.E., Barwise, A.J.G., 1997. Characterizing petroleum charge systems in the Tertiary of SE Asia. In: Fraser, A.J., Matthews, S.J., Murphy, R.W. (Eds.), *Petroleum Geology of Southeast Asia*, Geological Society London Special Publication 126, pp. 25–47.
- Total Vietnam, 1991. Final report, Well 107-PA-1x.
- Traynor, J.J., Sladen, C., 1997. Seepage in Vietnam — onshore and offshore examples. *Marine and Petroleum Geology* 14, 345–362.
- Tri, T.V., 1997. Geology of Bach Long Vi Island. *Geological Bulletin* 132 (in Vietnamese).
- Ungerer, P., Pelet, R., 1987. Extrapolation of the kinetics of oil and gas formation from laboratory experiments to sedimentary basins. *Nature* 327, 52–54.
- Veld, H., Fermont, W.J.J., Jegers, L.F., 1993. Organic petrological characterization of Westphalian coals from The Netherlands: correlation between T_{max} , vitrinite reflectance and hydrogen index. *Organic Geochemistry* 20, 659–675.
- Wan Hasiah, A., 1999. Oil-generating potential of Tertiary coals and other organic-rich sediments of the Nyalau Formation, onshore Sarawak. *Journal of Asian Earth Sciences* 17, 255–267.
- Wang, C., Sun, Y., 1994. Development of Paleogene depressions and deposition of lacustrine source rocks in the Pearl River Mouth Basin.

- northern margin of the South China Sea. *American Association of Petroleum Geologists Bulletin* 78, 1711–1728.
- Waples, D.W., Machihara, T., 1991. Biomarkers for geologists — a practical guide to the application of steranes and triterpanes in petroleum geology. *American Association of Petroleum Geologists Methods in Exploration Series* 9, 91 pp.
- Williams, H.H., Fowler, M., Eubank, R.T., 1995. Characteristics of selected Palaeogene and Cretaceous lacustrine source basins of Southeast Asia. In: Lambiase, J.J. (Ed.), *Hydrocarbon habitat in rift basins*, Geological Society London, Special Publication 80, pp. 241–282.
- Zhu, W., Li, M., Wu, P., 1999. Petroleum systems of the Zhu III Subbasin, Pearl River Mouth Basin, South China Sea. *American Association of Petroleum Geologists Bulletin* 83, 990–1003.

17 α ,21 α (H)-hopanes: natural and synthetic

Hans Peter Nytoft* and Jørgen A. Bojesen-Koefoed

Geological Survey of Denmark and Greenland, Thoravej 8, DK 2400 Copenhagen NV, Denmark

* Corresponding author. Tel.: + 45-38-142458; fax: + 45-38-142050.

E-mail adress: hpn@geus.dk (H.P. Nytoft).

Abstract

17 α ,21 α (H)-hopanes are found in low concentrations in sediments and oils, but C₃₀ 17 α ,21 α (H)-hopane is the only member of the series which can be detected in the *m/z* 191 mass chromatogram. The ratio of C₃₀ 17 α ,21 α (H)-hopane to C₃₀ 17 α ,21 β (H)-hopane is typically 0.02 - 0.04 in crude oils and mature sediments. Ratios up to 0.10 have been found in immature sediments with 22*S*/(22*S* + 22*R*) ratios of C₃₁-C₃₅ hopanes around 0.4. Compounds coeluting with 17 α ,21 α (H)-hopane are usually absent in samples of early oil window rank or higher maturity. 17 α ,21 α (H)-hopane and 17 α ,21 β (H)-hopane have almost identical mass spectra and response factors in the *m/z* 191 mass chromatogram. These features make 17 α ,21 α (H)-hopane an ideal internal standard for the quantification of hopanes in oils and sediments. 17 α ,21 α (H)-hopane can be obtained in high yield by hydrogenation of synthetic hopa-15,17(21)-diene.

Keywords: biomarkers; hopanes; 17 α ,21 α (H)-hopanes; hydrogenation; hop-17(21)-enes; hopa-15,17(21)-dienes; GC-MS analysis; internal standards.

1. Introduction

Textbooks on biomarkers (e.g. Philp, 1985; Waples and Machihara, 1991; Peters and Moldowan, 1993) state that hopanes exist as three series: the 17 β ,21 β (H)-hopanes ($\beta\beta$), the 17 α ,21 β (H)-hopanes ($\alpha\beta$) and the 17 β ,21 α (H)-hopanes ($\beta\alpha$) or moretanes (**1-3**; see Appendix for structures).

Hopanoids produced by living organisms are principally of the $\beta\beta$ -configuration. With increasing maturity the thermodynamically less stable $\beta\beta$ -hopanes are lost or converted to $\alpha\beta$ -hopanes and $\beta\alpha$ -hopanes. The former predominate in mature sediments. However, the possibility exists, that hopanes can have the $\alpha\alpha$ -configuration (4), but such hopanes have been largely ignored in the geochemical literature. Molecular mechanics calculations have shown that $\alpha\alpha$ -hopanes should be less stable than $\alpha\beta$ -hopanes and $\beta\alpha$ -hopanes but more stable than $\beta\beta$ -hopanes (Kolaczowska et al., 1990; van Duin et al., 1997). They have been considered as hypothetical intermediates in the interconversion of hopane isomers via free radicals (Seifert and Moldowan, 1980). Synthesis of the C_{29} - and C_{30} $\alpha\alpha$ -hopanes has been described (Corbett and Heng, 1971; Bauer et al., 1983) but there is to our knowledge no record of $\alpha\alpha$ -hopanes in sediments and crude oils. Peters and Moldowan (1993) state "Hopanes of the $\alpha\alpha$ series are not natural products and it is unlikely that they occur above trace levels in petroleum".

The main objective of this study was to examine if $\alpha\alpha$ -hopanes could be detected in oils and source rocks, and in order to do that we needed mass spectra and retention times of the complete series of $\alpha\alpha$ -hopanes. The first step was then to find a simple way to prepare these, and after having succeeded in doing so, the next step was to prove that $\alpha\alpha$ -hopanes occur in geological samples. It was expected that most of the $\alpha\alpha$ -hopanes would be obscured by other hopanes, and because the mass spectra of $\alpha\alpha$ -hopanes lacked features that could help identify them, it seemed futile just to analyse ordinary samples using GC-MS. Instead we used HPLC-fractions of triterpane concentrates which were available from previous studies. Knowing the approximate retention times of synthetic $\alpha\alpha$ -hopanes and other hopanes on various HPLC-columns it was possible to pick the relevant fractions and use GC-MS to identify the $\alpha\alpha$ -hopanes unambiguously by comparison with mass spectra of synthetic standards. Finally with the synthetic $\alpha\alpha$ -hopanes in hand it appeared that especially the C_{30} $\alpha\alpha$ -hopane was useful as internal standard for quantification of hopanes in sediments and oils.

The present paper describes the synthesis of $\alpha\alpha$ -hopanes and the occurrence of such compounds in oil and sediment samples, as well as the use of C_{30} $\alpha\alpha$ -hopane as internal standard for biomarker quantification.

2. Experimental

2.1. Samples

Triterpane concentrates were prepared from four crude oils. The concentrate was then subjected to preparative reverse phase HPLC-separation followed by GC-MS analysis in scan mode of most fractions. Two of the oils were from West Greenland (The Marraat oil and the Eqaalik oil). These oils have been described previously (Christiansen et al., 1996; Bojesen-Koefoed et al., 1999; Nytoft et al., 2000). The others were a North Sea oil (Mona-1 well) and a lacustrine oil from Vietnam. The saturate fraction from an immature shale extract (Vietnam) was HPLC-separated without prior concentration of triterpanes.

Samples analysed using GC-MS in SIM-mode were mainly crude oils and source rock extracts from the North Sea, including extracts of 15 coal samples which have been described recently (Petersen et al., 2000). Two carbonate sourced oils from Iran and Kuwait (exact location unknown) were obtained from a Danish refinery.

2.2. Extraction and separation

Sediments were extracted with a dichloromethane/methanol mixture (93:7 v/v) using a Soxtec system. The Marraat oil had been obtained by extraction of cores with toluene. The asphaltenes were removed from oils and extracts by precipitation in *n*-pentane, and the maltenes were fractionated by MPLC (Radke et al., 1980). When internal standard was used, synthetic $\alpha\alpha$ -hopane (0.01 or 0.02 mg in 1 ml isooctane) was added to the oil sample (35-160 mg). Most of the isooctane was then removed by evaporation before precipitation of asphaltenes.

2.3. Preparation of triterpane concentrates and HPLC-separation

The deasphalted fraction (15 g) from a crude oil (Mona-1 well, Danish North Sea) was separated in 100 mg portions using MPLC. During separation two saturate fractions were collected. The first half of the saturate peak contained mainly *n*-alkanes, whereas triterpanes were concentrated in the second half which was collected separately. The second half (sat. 2) was separated again giving two new saturate fractions (sat. 21 and 22). The latter was separated similarly two more times giving a

fraction (sat. 2222) almost free of *n*-alkanes and highly enriched in triterpanes. Since the oil had to be MPLC-separated anyhow to get the saturate fraction, the extra separations of the progressively smaller triterpane concentrate only increased the workload slightly. However, concentrates obtained this way are more enriched in triterpanes with a short or no side-chain than in compounds with a relatively long side chain such as tricyclics, steranes and hopanes with more than 30 carbon atoms. This method should therefore not be used as an alternative to treatment by urea adduction or molecular sieves for routine biomarker analyses.

The sat. 2222 fraction (0.4 g) was separated (40-50 mg at a time) using a Hyperprep ODS, 8 μ m, 10 x 250 mm column in an overloaded mode giving low molecular weight cyclic and branched compounds (206 mg), steranes and C₂₇-C₃₂ hopanes (127 mg) and finally hopanes > C₃₂ (32.5 mg). The mobile phase was acetone/acetonitrile 70:30 v/v at 3 ml/min. The middle fraction was separated into several smaller fractions using similar conditions but injecting only 10-20 mg at a time. Some of these fractions containing compounds of interest were rechromatographed on smaller columns having a different selectivity. A Vydac 201 TP, 5 μ m, 4.6 x 250 mm column was used with acetone/acetonitrile 80:20 v/v at 0.5 ml/min. Alternatively, a Hyperprep 300, 5 μ m, 4.6 x 250 mm column was used with acetone/acetonitrile 70:30 v/v at 0.5 ml/min. So far about 500 of the fractions have been analysed by GC-MS in scan mode giving clean mass spectra of even very minor compounds.

The Marraat oil and the Vietnamese oil were treated similarly, but only about 1.2 g of each was used. The Eqaalulik oil already had a very high content of hopanes and a two-stage MPLC-separation of only 100 mg oil was sufficient to obtain almost pure hopanes.

2.4. Gas chromatography (GC)

Gas chromatography was performed using a Hewlett-Packard 5890 instrument equipped with a splitless injector and an HP-1 capillary column (25 m x 0.20 mm i.d., film thickness 0.11 μ m). The temperature program was 5°C/min from 80 to 300°C, followed by 15 min at 300°C.

2.5. Gas chromatography-mass spectrometry (GC-MS)

Gas chromatography-mass spectrometry (GC-MS) was carried out on a Hewlett-Packard 5890 gas chromatograph connected to a HP5971 mass selective detector. The GC was fitted with a HP-5 capillary column (25 m x 0.20 mm i.d., film thickness 0.11 μm). The temperature program was 30°C/min from 70 to 100°C and 4°C/min from 100 to 300°C followed by 12 min at 300°C. A few of the samples were also analysed using a Zebron ZB-5 column (60 m x 0.25 mm i.d., film thickness 0.10 μm). The temperature program was 35°C/min from 50 to 150°C and 2°C/min from 150 to 320°C followed by 10 min at 320°C. The samples were dissolved in isooctane, and the concentration was usually 1 mg/100 μl . In case of HPLC-fractions containing few compounds, the concentration was only 0.1 mg/100 μl . Splitless injection was used. The MS was operated in electron impact (EI) mode with an electron energy of 70 eV. Analysis was done in the full data acquisition (SCAN) mode by scanning from 50 to 500 amu at 1.1 cycles/s and in the selected ion monitoring (SIM) or multiple ion detection mode with each of 20 ions being monitored for 30 ms dwell times.

2.6. Synthesis of hop-21(22)-ene and hop-22(29)-ene

22-hydroxyhopan-3-one (**5**) was isolated from dammar resin (Fluka) and converted to 22-hydroxyhopane (diplopterol) (**6**) by Wolff-Kishner reduction as described by Dunstan et al. (1957). Dehydration of 22-hydroxyhopane in phosphoroxchloride and pyridine (Dunstan et al., 1957) yielded a mixture of hop-22(29)-ene (**7**) and hop-21(22)-ene (**8**) in a 1:3 ratio. The hopenes were separated on a Vydac 201 TP, 5 μm , 250 x 4.6 mm column using acetone/acetonitrile 90:10 vol/vol at 0.6 ml/min. Traces of hop-17(21)-ene (**9b**) eluted first ($k' = 1.0$) followed by hop-21(22)-ene ($k' = 1.8$) and hop-22(29)-ene ($k' = 2.1$).

Hop-22(29)-ene was also prepared from the fern *Athyrium filix-femina*. Ferns leaves were collected oktober - november near Copenhagen. Dry leaves (1 kg) were chopped and extracted with hexane (3 x 4 l). A colourless fraction (300 mg) containing mainly *n*-alkanes and triterpenes was obtained by repeated chromatography on silica gel columns using hexane as eluent. This fraction was subjected to MPLC-separation, which gave (in order of elution) *n*-alkanes, fern-9(11)-ene (**10b**), hop-22(29)-ene and a C₃₀ tetracyclic diene. The crude hop-22(29)-ene was separated from traces of other triterpenes using reverse phase HPLC. 17 mg pure hop-22(29)-ene was obtained after recrystallisation from acetone.

2.7. Synthesis of C_{30} hop-17(21)-ene

Hop-17(21)-ene was made by combined dehydration and isomerization of crude 22-hydroxyhopane from the Wolff-Kishner reduction of 22-hydroxyhopan-3-one in a mixture of 0.1 N perchloric acid in acetic acid and ethylacetate (4:1). After 1h at 50°C, the mixture was cooled, neutralized with aqueous sodium hydroxide and extracted with hexane. The hexane solution was filtered through a short silica gel column. Evaporation of the hexane gave about 6 g 85-90 % pure hop-17(21)-ene/kg dammar resin. Pure hop-17(21)-ene was prepared by recrystallisation from acetone. Alternatively, hop-17(21)-ene was prepared by acid catalyzed isomerization of a mixture of hop-22(29)-ene and hop-21(22)-ene.

2.8. Synthesis of C_{29} and C_{31} - C_{35} hop-17(21)-enes

A mixture of hop-22(29)-ene and hop-21(22)-ene was oxidized using the method of Carlsen et al. (1981). A 200 ml flask was charged with hopene mixture (400 mg), carbon tetrachloride (16 ml), acetonitrile (16 ml) and water (24 ml). To the biphasic solution sodium metaperiodate (3.5 g) and ruthenium trichloride hydrate (40 mg) was added, and the entire mixture was stirred vigorously for 3 h at room temperature. The reaction mixture was diluted with water and extracted with pentane. The crude product was chromatographed on a silica gel column (50 ml). Elution with hexane 100 ml gave unreacted hopenes (68 mg). Diethylether/hexane 25:75 vol/vol (200 ml) eluted a mixture (194 mg) of 22,29,30-trinorhopan-21-ones (**11**), 30-norhopan-22-ones (**12**) and some minor compounds. Some of the ketone mixture was treated with excess ethyl magnesium bromide in diethylether. After 30 minutes dilute sulphuric acid was added to pH 2 and the mixture was extracted with diethyl ether. The crude product (a complex mixture of hopenes and hopanols) was dissolved in 0.1 N perchloric acid in acetic acid, and kept at 25°C for one hour. Neutralization with aqueous sodium hydrogen carbonate and extraction with *n*-pentane afforded a mixture consisting mainly of 30-norhop-17(21)-ene (**9a**) and homohop-17(21)-enes (**9c**). 30-norhop-17(21)-ene and 22*R*-homohop-17(21)-ene were prepared pure (>99.5 %) using reverse phase HPLC.

C_{31} and C_{32} hop-17(21)-enes (**9c-d**) and a mixture of C_{31} - C_{35} hop-17(21)-enes (**9c-g**) (41-46 % 22*S*, 54-59 % 22*R*) were prepared by oxidation of pure hop-22(29)-ene (prepared from ferns) to 30-

norhopan-22-ones followed by reaction with ethyl-, *n*-propyl- or a mixture of C₂-C₆ *n*-alkyl magnesium bromides.

2.9. Synthesis of hopa-15,17(21)-diene

Hop-17(21)-ene (200 mg) was dissolved in chloroform or methylene chloride (50 ml) and *m*-chloroperoxybenzoic acid (120 mg) was added. The solution was stirred for 1 h at room temperature, washed with 2N NaOH (2 x 20 ml) and finally with deionized water 3 x 20 ml. Evaporation of the solvent gave 17(21)-epoxyhopanes (**13b**) consisting of a major compound (90%) and a minor, later eluting isomer (10%). Both had identical mass spectra (as shown by Tritz et al., 1999). The epoxyhopane mixture was dissolved in hot ethanol (200 ml). Aqueous 37 % HCl (20 ml) was added, and the solution was refluxed for 2h. The solution was cooled, diluted with water and extracted with *n*-pentane. The crude product was purified on a silica gel column (20 ml). Elution with *n*-pentane (100 ml) gave hopa-15,17(21)-diene (**14b**) in 50-70 % yield. Impurities (< 10 %) were mainly unstable isomeric dienes (Morelli and Marsili 1970) which rapidly isomerized to the more stable hopa-15,17(21)-diene during the subsequent hydrogenation in acid solution. Mass spectrum of hopa-15,17(21)-diene (Nytoft et al., 1999): $m/z = 408$ (M^+ , 4%); 393 ($M^+ - CH_3$, 54 %); 187 (ring C cleavage, 100%); no other ions above 12%.

2.10. Hydrogenation of hopa-15,17(21)-diene

Hopa-15,17(21)-diene (30 mg) in ethyl acetate (3 ml) was added slowly (four hours) to 0.1 N perchloric acid in glacial acetic acid (5 ml) containing PtO₂ (200 mg). Hydrogen (2 l/h) was supplied using pieces of capillary GC-column (internal diameter 0.5 mm) and ordinary balloons as hydrogen reservoirs. Magnetic stirring was used. After addition of all the hopa-15,17(21)-diene, the hydrogenation was continued for 2 hours. The solution was pipetted from the catalyst which could be used again. Neutralization in aqueous sodium hydrogen carbonate and extraction with *n*-pentane afforded a hopane mixture containing 45-65 % $\alpha\alpha$ -hopane.

2.11. Purification of $\alpha\alpha$ -hopanes

C₂₉ hopanes (**1a-4a**) from hydrogenation of 30-norhop-17(21)-ene described in 3.1 were separated using reverse phase HPLC on a Vydac 201 TP 5 μ m, 250 x 4,6 mm column and acetone/acetonitrile 80:20 vol/vol at 0.5 ml/min. $\alpha\beta$: $k' = 2.5$ (Fig. 1), $\alpha\alpha$: $k' = 5.0$ (Fig. 1), $\beta\alpha$: $k' = 6.2$, $\beta\beta$: $k' = 10.6$. The C₃₀ hopanes from hydrogenation of hopa-15,17(21)-diene were purified on a short column containing silica by elution with *n*-pentane and then separated using reverse phase HPLC on two different columns. First a Hyperprep ODS, 8 μ m, 250 x 10 mm column was used with acetone at 2 ml/min, which separated $\alpha\beta$ -hopane ($k' = 1.83$) from $\alpha\alpha$ -hopane ($k' = 2.05$). The maximum amount that could be separated without overloading the column was about 3 mg. A second separation (0.3 mg/separation) on a Vydac 201 TP, 5 μ m, 250 x 4,6 mm column using acetone/acetonitrile 90:10 vol/vol at 0.6 ml/min separated the $\alpha\alpha$ -hopane ($k' = 1.56$)(Fig. 2) from the minor impurities: $\alpha\beta$ -hopane ($k' = 1.25$)(Fig. 2), 17 α (H)-diahopane ($k' = 1.45$) and $\beta\alpha$ -hopane ($k' = 1.49$). 34.0 mg $\alpha\alpha$ -hopane was obtained > 99.8 % pure. Mixtures of higher carbon number hopanes were not separated.

3. Results and discussion

3.1. Synthesis of $\alpha\alpha$ -hopanes

Corbett and Heng (1971) synthesized $\alpha\alpha$ -hopane and Bauer et al. (1983) prepared $\alpha\alpha$ -30-norhopane. Both syntheses used 22,29,30-trinorhopan-21-one obtained by degradation of 22-hydroxyhopan-3-one or 7 β -acetoxy-22-hydroxyhopane (**15**) as the starting substance. A series of reactions then added a side chain again with the desired stereochemistry at C17 and C21. These syntheses, although elegant, seemed too elaborate for the mere "production" of hopanes and a simpler procedure was sought. Since mass spectral data of all four C₂₉ hopanes and their relative GC-retention times were available (Bauer et al., 1983) it was easy to check if hydrogenation of 30-norhop-17(21)-ene gave $\alpha\alpha$ -30-norhopane in sufficient yield and if the other $\alpha\alpha$ -hopanes could be prepared similarly.

30-norhop-17(21)-ene was hydrogenated (PtO₂, 0.1 N perchloric acid in glacial acetic acid). GC-MS analysis (full scan) of the products showed three major peaks. The first eluting compound (53.6 %) was $\alpha\beta$ -30-norhopane. The next peak (38.9 %) had the same retention time as $\beta\alpha$ -30-norhopane in geological samples but with a *m/z* 177/191 ratio of only 0.38, which showed that it was mainly $\alpha\alpha$ -30-norhopane with only a small amount of coeluting $\beta\alpha$ -30-norhopane. The last peak (3.4 %)

was $\beta\beta$ -30-norhopane. Various C_{27} and C_{28} compounds accounted for the remaining 4.1 %. Hydrogenation using platinum (10 %) on charcoal in isooctane gave the same three peaks (76.5 %, 20.7 % and 2.8 %) and no lower carbon number byproducts. The middle peak had a m/z 177/191 ratio of 0.41, which indicated a higher content of $\beta\alpha$ -30-norhopane than in the previous experiment. HPLC was used to separate the four C_{29} hopanes. The m/z 177/191 ratios of the purified hopanes were $\alpha\alpha$: 0.33, $\alpha\beta$: 0.36, $\beta\alpha$: 1.17 and $\beta\beta$: 2.05. The values reported by Bauer et al. (1983) were 0.36, 0.42, 1.23 and 1.98 respectively.

It is known that the product stereochemistry can be influenced by the specific catalyst used for hydrogenation, the quantity of catalyst, the hydrogen pressure and the reaction medium (Augustine, 1972 and refs. therein). Palladium generally gives more of the thermodynamically stable product than other catalysts. Summons and Jahnke (1992) thus obtained in excess of 95% of $\alpha\beta$ -hopane by hydrogenation of hop-17(21)-ene in glacial acetic acid containing perchloric acid. The minor product was $\beta\alpha$ -hopane. Hydrogenation of hop-17(21)-ene in acidic solution with PtO_2 as catalyst is also known to preferentially yield $\alpha\beta$ -hopane (>55%) followed by $\beta\alpha$ -hopane (<40%) and $\beta\beta$ -hopane (6%). (Tsuda et al., 1967). $\alpha\alpha$ -hopane was apparently not detected in any of these experiments. We have hydrogenated hop-17(21)-ene in 0.1 N perchloric acid in acetic acid using PtO_2 as catalyst at atmospheric pressure, and similar to the hydrogenation of 30-norhop-17(21)-ene, four hopanes were obtained. When a large amount of catalyst (10 mg/0.1 mg hopene) was used, $\alpha\beta$ -hopane was the main product (70-75 %) followed by $\alpha\alpha$ -hopane (20-25 %) and only 2-3 % hopanes with the $\beta\alpha$ - and $\beta\beta$ stereochemistry. Attempts to scale up the hydrogenation (100 mg hopene) using relatively less catalyst (100 mg) led to a decreasing yield of $\alpha\alpha$ -hopane (5-10 %) and an increase in the yield of $\beta\alpha$ -hopane. Since pure $\alpha\alpha$ -hopane was the desired product and $\beta\alpha$ -hopane was the most difficult to remove using HPLC, we soon abandoned hop-17(21)-ene as a source and turned our attention towards hoba-15,17(21)-diene which was synthesized from hop-17(21)-ene (Berti et al., 1966; Morelli and Marsili, 1970).

Hydrogenation of hoba-15,17(21)-diene (PtO_2 , hexane) gave a mixture of (in order of elution) hop-17(21)-ene (**9b**), a hop-15-ene (**16**) and hop-16-enes (**17**) in a 3:1:6 ratio with traces of $\alpha\alpha$ - and $\alpha\beta$ -hopane. Complete hydrogenation was only possible in acidic solvents and the hopenes could be detected in the same ratio immediately after the hydrogenation was started. The hop-16-enes (two closely eluting peaks in a 100:1 ratio) had mass spectra almost identical to that reported by Shiojima and Ageta (1990) for hop-16-ene isolated from a fern. However, unlike the natural product the

major, early eluting synthetic hop-16-ene probably has the $21\alpha(\text{H})$ -stereochemistry. It was isolated pure using HPLC, and when hydrogenated (PtO_2 , 0.1 N perchloric acid in acetic acid) it yielded in excess of 60 % $\alpha\alpha$ -hopane. Hydrogenation of hoba-15,17(21)-diene (PtO_2 , 0.1 N perchloric acid in acetic acid) gave $\alpha\alpha$ -hopane (45-65 %), $\alpha\beta$ -hopane (30-45 %), $\beta\alpha$ -hopane (1-2 %), $\beta\beta$ -hopane (1-2 %) and $17\alpha(\text{H})$ -15 α -methyl-27-norhopane (**18**) (2-4 %). The latter compound which is better known as “ $17\alpha(\text{H})$ -diahopane” was formed because the hoba-15,17(21)-diene can (irreversibly) isomerize to a complex mixture of rearranged hopadienes. Most of these are then easily hydrogenated to a “diahop-13-ene” (**19**) (based on NMR) which in turn is slowly hydrogenated to $17\alpha(\text{H})$ -diahopane in almost quantitative yield. Acid treatment (6-12h) before the actual hydrogenation increased the content of diahopane to 20-40 %. We believe that most diahopanes in oils and mature sediments are formed this way from hoba-15,17(21)-dienes which are abundant in immature sediments (Nytoft et al., 1999) although alternative routes from hop-17(21)-enes have been found. Details will be reported elsewhere.

C_{31} , C_{32} and a mixture of C_{31} - C_{35} hop-17(21)-enes were hydrogenated (PtO_2 , 0.1 N perchloric acid in acetic acid) which yielded a distribution of isomers similar to that described for the C_{30} compounds, which also meant that the yield of $\alpha\alpha$ -hopanes did not exceed 25 %. The mixture of C_{31} - C_{35} hopanes is shown in Fig. 3. Retention times of $\beta\alpha$ -hopanes and $\beta\beta$ -hopanes which are not immediately apparent in the chromatogram are shown with arrows below the baseline.

3.2. Mass spectra of $\alpha\alpha$ -hopanes

The mass spectra of $\alpha\alpha$ -30-norhopane and $\alpha\beta$ -30-norhopane have been published previously (Philp, 1985; Peters and Moldowan, 1993). These spectra are largely identical to ours (Fig. 1), but the spectra in Peters and Moldowan (1993) have a different m/z 398/383 ratio, which could be due to different experimental conditions. The mass spectra of $\alpha\alpha$ -30-norhopane and $\alpha\beta$ -30-norhopane are at a first glance identical (Fig. 1). However, the more subtle details can be used to distinguish their mass spectra. The m/z 178/177 and 179/177 ratios are identical for $\alpha\alpha$ -30-norhopane but different for $\alpha\beta$ -30-norhopane. The same differences related to fragments from the ring D/E part of the molecule can also be seen in the mass spectra of the C_{31} - C_{35} hopanes. In the C_{30} hopanes these differences are masked by the presence of the m/z 191 fragment from the ring A/B part of the molecule (Fig. 2). These small mass spectral differences of the various C_{29} - C_{31} hopane isomers are

shown in Table 1. As pointed out by Bauer et al. (1983), the C₂₉ αα hopane has a slightly lower *m/z* 148+R/191 ratio than the C₂₉ αβ hopane. This difference is even more pronounced for the C₃₁-C₃₅ hopanes, e.g. *m/z* 205/191 = 0.3 for C₃₁ αβ and 0.2 for C₃₁ αα.

3.3. αα-hopanes in oils and sediments

αβ-hopane is the dominant C₃₀ hopane in all non biodegraded oils and mature extracts followed by the later eluting βα-hopane (moretane) and the moretane/hopane ratio is usually less than 0.15 (Seifert and Moldowan, 1980). The *m/z* 191 mass chromatogram of a typical North Sea crude oil (Fig. 4) shows both compounds as well as three minor peaks eluting between. 2α(CH₃),αβ-hopane (**20b**) can be seen on the trailing edge of the αβ-hopane. In oils from carbonate source rocks (Fig. 7) a C₃₀ 30-norhopane (**21c**) can also be found at this position (Subroto et al., 1991; Moldowan et al., 1992). The peak eluting almost half-way between αβ-hopane and βα-hopane has been tentatively assigned as the C₃₀ member of the 18α-neohopane series ("30Ts")(**22b**) based on relative retention time (Michaelsen and McKirdy, 1995) and statistical covariance with C₂₉ 18α-neohopane (Farrimond and Telnæs, 1996). Neohop-13(18)-ene (**23b**), which is the most likely precursor, has the same retention time, but is only found in immature samples. An unidentified C₂₉ compound often coelutes with 30Ts. This compound could be a C₂₉ fernane (Paull et al., 1998). However, the mass spectrum of the coeluting C₂₉ compound prepared almost pure from a crude oil (Mona-1 well, Danish North Sea) suggests another structure: *m/z* = 398 (M⁺, 11%); 383 (7%); no *m/z* 369; 245 (2%); 217 (2%); 205 (4%); 204 (4%); 191 (100%); 177 (62%).

A small peak can be seen between 30Ts and βα-hopane (Fig. 4) and this peak has been found in every oil or mature source rock that we have analysed (several hundred samples from all over the world) and it can be seen in most published *m/z* 191 mass chromatograms. The peak area is typically 2-4 % of the area of the αβ-hopane. This compound is probably the same as the unknown compound eluting immediately after 30Ts which was observed by Farrimond and Telnæs (1996), who also performed principal component analysis on a hopane data set (21 hopanes, 36 samples). It was found (Fig. 7 in Farrimond and Telnæs (1996)) that the unknown compound plotted between the C₃₀ hopane and C₃₀ moretane and away from three series of rearranged hopanes suggesting a relationship with the regular hopanes.

A very high content of hopanes has been found in the Eqaalulik oil from West Greenland (Bojesen-Koefoed et al., 1999; Nytoft et al., 2000). From this oil a fraction enriched in the unknown compound was obtained using MPLC and reverse phase HPLC. The compound coeluted with synthetic $\alpha\alpha$ -hopane, and had an identical mass spectrum (Fig. 2). A triterpane concentrate from the Marraat oil, West Greenland, (Christiansen et al., 1996) had previously been separated using two columns of different selectivities (First Hyperprep ODS and then Vydac 201 TP) and several hundred fractions were collected. 262 of these fractions had been analysed by GC-MS in scan mode with the purpose of identifying various terrigenous triterpanes, including lupane (Nytoft et al., 1997). In three consecutive fractions from the Hyperprep ODS column $\beta\alpha$ -30-norhopane was identified. The $\beta\alpha$ -30-norhopane peak in the last of these fractions had a m/z 177/191 ratio of only 0.9 versus 1.17 in pure $\beta\alpha$ -30-norhopane indicating coeluting $\alpha\alpha$ -30-norhopane. This was confirmed by a second separation of this fraction on the Vydac 201 TP column which yielded a compound with a GC retention time and mass spectrum identical to that of synthetic $\alpha\alpha$ -30-norhopane (Fig. 1). C_{30} $\alpha\alpha$ -hopane was found in the Marraat oil as well, and C_{32} $\alpha\alpha$ -hopanes were tentatively identified, whereas the C_{31} $\alpha\alpha$ -hopanes could not be identified with certainty. $\alpha\alpha$ -30-norhopane and $\alpha\alpha$ -hopane were identified similarly in a mature crude oil from the North Sea (Mona-1 well). C_{29} , C_{30} and C_{31} 22*R* $\alpha\alpha$ -hopane were identified in HPLC-fractions from an immature Oligocene shale and a lacustrine crude oil from Vietnam and C_{32} 22*R* $\alpha\alpha$ -hopane was also found in the oil. None of these samples were originally selected with the purpose of detecting $\alpha\alpha$ -hopanes, and $\alpha\alpha$ -hopanes can probably be found in most other oils and sediments using a combination of HPLC and GC/MS.

Because the mass spectra of $\alpha\alpha$ -hopanes do not show any characteristic fragments except m/z 191 and a small ring D + E fragment, which are also produced by most other hopanes, their identification in normal samples using GC-MS in SIM-mode is difficult, and even GC-MS-MS will not make a great difference. Only C_{30} $\alpha\alpha$ -hopane can be identified with certainty in the m/z 191 mass chromatogram (Figs. 4,5 and 7). In immature samples it coelutes with the $\beta\beta$ -30-norhopane, but at higher thermal maturity when the normal C_{31} - C_{35} $\alpha\beta$ -hopanes are close to equilibrium at C_{22} and $\beta\beta$ -hopanes have disappeared, coeluting compounds are almost absent (Fig. 5).

Several compounds either coelute with $\alpha\alpha$ -30-norhopane or immediately before or after (Fig. 4) making quantification impossible in most cases. Using synthetic compounds it was found that $\alpha\alpha$ -30-norhopane (m/z 177/191: 0.33) and $\beta\alpha$ -30-norhopane (m/z 177/191: 1.17) coelute. In analyses of

numerous oils and rock extracts Bauer et al. (1983) found m/z 177/191 ratios above 1 for the peak corresponding to C_{29} $\beta\alpha + \alpha\alpha$, which showed that C_{29} $\alpha\alpha$ was at most, a minor constituent of that peak. In many North Sea oils and source rock extracts the m/z 177/191 ratios for this peak can be well below 1. However, these samples often contain a complete series of 28-norhopanes (Nytoft et al., 2000) and $\beta\alpha$ -28-norhopane (**24b**), which also has a low m/z 177/191 ratio, coelutes with $\beta\alpha$ -30-norhopane. The " $\beta\alpha$ -30-norhopane" peak in Fig. 4 is actually about half $\beta\alpha$ -28-norhopane. The minor $\alpha\beta$ -28-norhopane (**25b**) elutes just before the " $\beta\alpha$ -30-norhopane" peak (Fig. 4) and should not be confused with another compound eluting slightly earlier, which has been tentatively identified as the C_{29} member of a series of 21-methyl-28-norhopanes (**26a**)(GEUS, work in progress). All members of this series have an extremely large m/z 369 fragment (~90 % of m/z 191). C_{29} 21-methyl-28-norhopane coelutes with two unidentified C_{30} compounds and can only be accurately quantified using the m/z 369 ion chromatogram. The first of the C_{30} compounds can be resolved from C_{29} 21-methyl-28-norhopane on a 60 m ZB-5 column (Fig. 4). A third C_{30} compound partly coelutes with $17\alpha(H)$ -diahopane (Fig. 4). A compound with an identical mass spectrum has been reported previously (Fig. 4b in Fowler et al., 1988) and it is probably the C_{30} member of a series of C-ring enlarged (involving the 27-Me) hopanes identified by Trendel et al. (1993) in a biodegraded petroleum. This series seems small and insignificant but may coelute with some of the $\alpha\alpha$ -hopanes. Using a 60m ZB-5 column the first eluting C_{31} member of the series (prominent ions at m/z 273, 245, 191 and 123) elutes on the trailing edge of $\alpha\alpha$ -hopane (Fig. 4). On a 25m HP-5 column it coelutes with $\beta\alpha$ -hopane. Another series of C-ring enlarged hopanes (involving the 26-Me) has been identified by Trendel et al. (1993). These $C(14a)$ -Homo-26-nor- 17α -hopanes are more abundant than the former series, but only the C_{30} compound (**27b**), which elutes slightly earlier than $\alpha\beta$ -30-norhopane (Fig. 4), can be routinely detected in the m/z 191 ion chromatogram. Mass spectra of the other members of the series do not show a significant m/z 191 fragment and they are more easily detected using their molecular ion in combination with m/z 369 and m/z 259. In extracts of Middle Jurassic coals from the North Sea and oils generated from these coals (Petersen et al., 2000) an unidentified C_{29} compound elutes on the trailing edge of the " $\beta\alpha$ -30-norhopane" peak, and in samples containing abundant diahopanes and neohopanes this later eluting peak can be almost as high as the " $\beta\alpha$ -30-norhopane" peak. In the North Sea crude oil (Fig. 4) it is almost absent.

28-Norhopanes are particularly abundant in the late Jurassic Hot Shales but are usually low in concentration elsewhere. 28-Norhopanes are found at 8500-8550 feet in the Bo-1 well, Danish

North Sea (Nytoft et al., 2000) but they are almost absent a few hundred feet below. m/z 191 mass chromatograms of extracts of the samples at 8700-8890 feet show a high content of C_{30} $\alpha\alpha$ -hopane ($\alpha\alpha/\alpha\beta$: 0.08-0.10) and a $\beta\alpha/\alpha\beta$ ratio that is only slightly higher. Close inspection of the $\beta\alpha$ -30-norhopane peak from the 8890' sample, which was analysed on both a 25 m HP-5 column and a 60 m ZB-5 column (Fig. 5) revealed a m/z 177/191 ratio of only 0.63. Since 28-norhopanes and other interfering compounds were largely absent, this could only be ascribed to an even higher amount of coeluting $\alpha\alpha$ -30-norhopane.

The ratio between 17 α (H)-diahopane and $\beta\alpha$ -30-norhopane "hopane X/(hopane X + normoretane)" has been used as a maturity parameter, especially for North Sea samples (Cornford et al., 1986; Karlsen et al., 1995; Ahsan et al., 1998; Bhullar et al., 1998). However, because of the various coeluting compounds, $\beta\alpha$ -30-norhopane should in our opinion not be used for anything, unless it is clear what is actually being measured.

C_{31} - C_{35} 22S $\alpha\alpha$ -hopanes and 22S $\beta\alpha$ -hopanes with the same carbon number coelute (Fig. 3) and low concentrations of the former will be impossible to detect in routine analyses. Furthermore, C_{31} - C_{33} 22R $\alpha\alpha$ -hopanes (**4c-e**) coelute with the isomeric C_{31} - C_{33} 22S $\alpha\beta$ -28-norhopanes (**25d-f**) (Compare Fig. 3 with Fig. 1 in Nytoft et al. 2000) making detection difficult in North Sea samples. C_{31} 22R $\alpha\alpha$ -hopane is clearly visible in the Bo-1 sample without 28-norhopanes (Fig. 5), but in most other cases the C_{31} 22R $\alpha\alpha$ -hopane peak (pure or not) is always very minor compared to that of the two coeluting C_{31} $\beta\alpha$ -hopanes. This indicates that C_{31} and higher carbon number $\alpha\alpha$ -hopanes occur in relatively lower concentrations than the C_{29} - C_{30} -members of the series. The aforementioned analytical difficulties have so far precluded any measurements of 22S/(22S+22R) ratios of the $\alpha\alpha$ -hopanes.

Fig. 6 shows the relative content of $\alpha\alpha$ -hopane and $\beta\alpha$ -hopane ($\alpha\alpha + \alpha\beta + \beta\alpha = 100$ %) versus C_{29} sterane 20S/(20S+20R) in 112 samples from the North Sea. The concentration of $\alpha\alpha$ -hopane is relatively high in immature samples but decreases to 2-4 % before the start of the oil window and remains almost constant. The increased scattering at high maturities is probably caused by a more noisy baseline making measurements more unreliable. The concentration of $\beta\alpha$ -hopane is always higher but much more variable. Samples with a high concentration of $\beta\alpha$ -hopane are usually from non-marine source rocks with a poor potential for oil generation. They also have increased proportions of Tm and $\alpha\beta$ -30-norhopane, a low content of neohopanes and a rapid decrease in abundance with increasing carbon number of extended hopanes. Samples from Greenland and other

parts of the world (not shown) seem to follow the pattern in Fig. 6, although the few crude oils from carbonate source rocks that we have analysed, show a lower than average content of $\alpha\alpha$ -hopane and especially $\beta\alpha$ -hopane. Such an oil (Iran, exact location unknown) is shown in Fig. 7.

3.4. C_{30} $\alpha\alpha$ -hopane as internal standard

Quantitative determination of biomarkers has always been a challenge, and biomarker analyses are often only presented as ratios of individual compounds within a compound class e.g. saturated steranes or hopanes. For quantitative work the best results are obtained using an internal standard. This has been described previously (Dahl et al., 1985; Requejo, 1992 and refs. therein). Various deuterated and non-deuterated steranes are commercially available for use as internal standards for quantification of steranes. Because suitable triterpane standards are not readily available, the same sterane standards are often used for quantification of triterpanes as well. This is far from ideal since they have different fragmentation patterns, which means that the m/z 191 response of hopanes and other triterpanes must be compared with e.g. m/z 221 of a deuterated sterane.

The natural content of $\alpha\alpha$ -hopane in early oil window rank and more mature samples is low and fairly constant ($\alpha\alpha/\alpha\beta$: 0.02-0.04) and coeluting compounds are usually absent. Furthermore, $\alpha\alpha$ -hopane has a fragmentation pattern very similar to that of $\alpha\beta$ -hopane and the other major hopanes. Mixtures of the three C_{30} hopanes found in mature samples ($\alpha\alpha$, $\alpha\beta$ and $\beta\alpha$) were analysed using GC-FID and GC-MS. Assuming identical response factors in GC-FID it was found that $\alpha\alpha$ -hopane yielded the lowest m/z 191 response per unit amount of compound. GC-MS response factors (peak areas, m/z 191) were: $\alpha\alpha = 1.0$, $\alpha\beta = 1.1$ and $\beta\alpha = 1.6$. A slightly biodegraded, early mature North Sea crude oil very similar to the one shown in Fig. 4 was analysed 6 times using $\alpha\alpha$ -hopane as internal standard. The standard was added to the whole (untopped) oil prior to precipitation of asphaltenes. Compensating for a natural m/z 191 $\alpha\alpha/\alpha\beta$ ratio of 0.04, the content of $\alpha\beta$ -hopane was measured to be 420 $\mu\text{g/g}$ oil with a standard deviation of 1.1 %.

4. Conclusions

$\alpha\alpha$ -hopanes have been considered absent in oils and source rocks because of their low stability compared to the $\alpha\beta$ - and $\beta\alpha$ isomers. They are nevertheless found in samples of all maturities,

although in low concentrations. Their presence in all hopane-containing samples probably means that they are produced by the same mechanisms as the $\alpha\beta$ and $\beta\alpha$ hopanes (mainly release from kerogen). $\alpha\alpha$ -hopane is the only member of the series that can be routinely measured in the m/z 191 mass chromatogram, whereas the others are masked by various coeluting compounds. The C_{30} $\alpha\alpha/\alpha\beta$ ratio is low and relatively constant (0.02-0.04) which means that synthetic $\alpha\alpha$ -hopane is an ideal internal standard for quantification of other hopanes. Hydrogenation of hop-17(21)-ene gives mainly $\alpha\beta$ -hopane, whereas $\alpha\alpha$ -hopane can be prepared in high yield by hydrogenation of hopa-15,17(21)-diene.

Acknowledgements

Samples from Vietnam were supplied by Petrovietnam and Vietnam Petroleum Institute. Hop-17(21)-ene and hopa-15,17(21)-diene were prepared by Toni Kennet Corleoné Jørgensen, Kate Lund, Steen Wendel Sørensen and Jens Valdemar Thomsen. Extraction of source rocks and MPLC-separation was done by Ditte Kiel-Dühring, Una Høegh-Guldberg, Ayoe Slot Hansen, Suzanne Wulff-Harslund and Simon Kopalski. Funding was provided by the Danish Energy Research Programme (EFP-98), grant 1313/98-0022. We thank A. Bishop, M. Moldowan and B.J. Keely for their constructive reviews.

References

Ahsan, S.A., Karlsen, D.A., Mitchell, A.W., Rothwell, N., 1998. Inter and intrafield hydrocarbon compositional variations in the Ula and the Gyda fields (Central Graben-North Sea)-implication for understanding the controls on hydrocarbon distribution within and between these fields. *Organic Geochemistry* 29, 429-448.

Augustine, R.L., 1972. Steroid hydrogenation. In: Fried, J., Edwards, J.A (Eds.), *Organic reactions in steroid chemistry*, Volume I, pp 111-144. Van Nostrand Reinhold Company.

- Bauer, P.E., Dunlap, N.K., Arseniyadis, S., Watt, D.S., Seifert, W.K., Moldowan, J.M., 1983. Synthesis of biological markers in fossil fuels. 1. 17α and 17β isomers of 30-norhopane and 30-normoretane. *The Journal of Organic Chemistry* 48, 4493-4497.
- Berti, G., Bottari, F., Marsili, A., Morelli, I., 1966. A triterpenoid epoxide from polypodium vulgare. *Tetrahedron Letters* 979-982.
- Bhullar, A.G., Karlsen, D.A., Holm, K., Backer-Owe, K., Le Tran, K., 1998. Petroleum geochemistry of the Frøy field and Rind discovery, Norwegian Continental Shelf. Implications for reservoir characterization, compartmentalization and basin scale hydrocarbon migration patterns in the region. *Organic Geochemistry* 29, 735-768.
- Bojesen-Koefoed, J.A., Christiansen, F.G., Nytoft, H.P., Pedersen, A.K., 1999. Oil seepage onshore West Greenland: evidence of multiple source rocks and oil mixing. In: Fleet, A.S., Boldy, S. (Eds.), *Petroleum Geology of NW-Europe: Proceedings of the 5th Conference*, Geological Society of London, London.
- Carlsen, P.H.J., Katsuki, T., Martin, V.S., Sharpless, K.B., 1981. A greatly improved procedure for ruthenium tetroxide catalyzed oxidations of organic compounds. *The Journal of Organic Chemistry* 46, 3936-3938.
- Christiansen, F.G., Bojesen-Koefoed, J.A., Dam, G., Nytoft, H.P., Larsen, L.M., Pedersen, A.K., Pulvertaft, T.C.R., 1996. The Marraat oil discovery on Nuussuaq, West Greenland: evidence for a latest Cretaceous - earliest Tertiary oil prone source rock in the Labrador Sea - Melville Bay region. *Bulletin of Canadian Petroleum Geology*. 44, 39-54.
- Corbett, R.E., Heng, C.K., 1971. Lichens and Fungi. Part IX. $17\alpha H$ -Hopane and $17\alpha H$ -Moretane and their Derivatives. *Journal of the Chemical Society. Section C: Organic Chemistry*, 1885-1888.

Cornford, C., Needham, C.E.J., De Walque, L., 1986. Geochemical habitat of North Sea oils. In: Spencer, A.M. et al. (Eds.), *Habitat of Hydrocarbons on the Norwegian Continental Shelf*. Norwegian Petroleum Society, 39-54.

Dahl, B., Speers, G.C., Steen, A., Telnæs, N., Johansen, J.E., 1985. Quantification of steranes and triterpanes by gas chromatographic-mass spectrometric analysis. In: Thomas, B.M. et al. (Eds.), *Petroleum Geochemistry in Exploration of the Norwegian Shelf*. Norwegian Petroleum Society, Graham & Trotman, London, 303-307.

Dunstan, W.J., Fazakerley, H., Halsall, T.G., Jones, E.R.H., 1957. The chemistry of the triterpenes and related compounds. Part XXXII. The chemistry of hydroxyhopanone. *Croatica Chemica Acta* 29, 173-182.

Farrimond, P., Telnæs, N., 1996. Three series of rearranged hopanes in Toarcian sediments (northern Italy). *Organic Geochemistry* 25, 165-177.

Fowler, M.G., Snowdon, L.R., Brooks, P.W., Hamilton, T.S., 1988. Biomarker characterisation and hydrous pyrolysis of bitumens from Tertiary volcanics, Queen Charlotte Islands, British Columbia, Canada. *Organic Geochemistry* 13, 715-725.

Karlsen, D.A., Nyland, B., Flood, B., Ohm, S.E., Brekke, T., Olsen, S., Backer-Owe, K., 1995. Petroleum geochemistry of the Haltenbanken, Norwegian continental shelf. In: Cubitt, J.M., England, W.A. (Eds.), *The Geochemistry of Reservoirs*. Geological Society London Special Publication, No. 86, pp. 203-256.

Kolaczowska, E., Slougui, N.-E., Watt, D.S., Maruca, R.E., Moldowan, J.M., 1990. Thermodynamic stability of various alkylated, dealkylated, and rearranged 17 α - and 17 β -hopane isomers using molecular mechanics calculations. *Organic Geochemistry* 16, 1033-1038.

Michaelsen, B.H., McKirdy, D.M., 1995. A C₃₀ 18 α -neohopane and its application to basin analysis. In: Grimalt, J.O., Dorronsoro, C. (Eds.), *Selected papers from the 17th International*

Meeting on Organic Geochemistry Donastia-San Sebastián, The Basque Country. Spain. 4th-8th September 1995, A.I.G.O.A. Donastia-San Sebastián, pp. 542-544.

Moldowan, J.M., Lee, C.Y., Sundararaman, P., Salvatori, T., Alajbeg, A., Gjukic, B., Demaison, G. J., Slougui, N.-E., Watt, D.S., 1992. Source correlation and maturity assessment of select oils and rocks from the Central Adriatic Basin (Italy and Yugoslavia). In: Moldowan, J. M., Albrecht, P., Philp, R.P. (Eds.), *Biological Markers in Sediments and Petroleum*. Prentice Hall. Englewood Cliffs, NJ., pp. 370-401.

Morelli, I., Marsili, A., 1970. The Dehydration of Some Triterpenoid Epoxides with Pyridinium Chloride. A Method for the Conversion of Tetrasubstituted Triterpenoid Olefins into Unrearranged Dienes. *The Journal of Organic Chemistry* 35, 567-570.

Nytoft, H.P., Bojesen-Koefoed, J.A., Christiansen, F.G., Fowler, M.G., 1997. HPLC-separation of coeluting lupane and oleanane - confirmation of the presence of lupane in oils derived from terrigenous source rocks of Cretaceous-Tertiary age. In: *Abstracts Part I from the 18th International Meeting on Organic Geochemistry, Maastricht, The Netherlands. 22-26 September 1997*, Forschungszentrum Jülich, pp. 313-314.

Nytoft, H.P., Thomsen, J.V., Jørgensen, T.K.C., Bojesen-Koefoed, J.A., Petersen, H.I., 1999. Hopa-15,17(21)-dienes in sediments: Precursors of diahopanes?. 19th International Meeting on Organic Geochemistry 6-10 September 1999 Istanbul - Turkey, *Abstracts Part I*, 13-14.

Nytoft, H.P., Bojesen-Koefoed, J.A., Christiansen, F.G., 2000. C₂₆ and C₂₈-C₃₄ 28-norhopanes in sediments and petroleum. *Organic Geochemistry* 31, 25-39.

Paull, R., Michaelsen, B.H., McKirdy, D.M., 1998. Fernenes and other triterpenoid hydrocarbons in *Dicroidum*-bearing Triassic mudstones and coals from South Australia. *Organic Geochemistry* 29, 1331-1343.

Peters, K.E., Moldowan, J.M., 1993. *The Biomarker Guide. Interpreting Molecular Fossils in Petroleum and Ancient Sediments*. Prentice-Hall, Englewood Cliffs, NJ.

Petersen, H.I., Andsbjerg, J., Bojesen-Koefoed J.A., Nytoft, H.P., 2000. Coal-generated oil: source rock evaluation and petroleum geochemistry of the Lulita Oilfield, Danish North Sea. *Journal of Petroleum Geology*, 23, 55-90.

Philp, R.P., 1985. *Fossil Fuel Biomarkers - Applications and Spectra. Methods in Geochemistry and Geophysics*, 23. Elsevier, 294 p.

Radke, M., Willsch, H., Welte, D.H., 1980. Preparative hydrocarbon group determination by automated Medium Pressure Liquid Chromatography. *Analytical Chemistry* 52, 406-411.

Requejo, A.G., 1992. Quantitative Analysis of Triterpane and Sterane Biomarkers: Methodology and Applications in Molecular Maturity Studies. In: Moldowan, J.M., Albrecht, P., Philp, R.P. (Eds.), *Biological Markers in Sediments and Petroleum*, Prentice Hall. Englewood Cliffs, NJ., pp. 222-240.

Seifert, W.K., Moldowan, J.M., 1980. The effect of thermal stress on source-rock quality as measured by hopane stereochemistry. *Physics and Chemistry of the Earth*. 12, Pergamon Press, Oxford, 229-237.

Shiojima, K., Ageta, H., 1990. Fern constituents: Two new triterpenoid hydrocarbons, hop-16-ene and isohop-22(29)-ene, isolated from *Davallia mariesii*. *Chemical and Pharmaceutical Bulletin* 38, 347-349.

Subroto, E.A., Alexander, R., Kagi, R.I., 1991. 30-Norhopanes: their occurrence in sediments and crude oils. *Chemical Geology* 93, 179-192.

Summons, R.E., Jahnke, L.L., 1992. Hopenes and hopanes methylated in ring-A: correlation of the hopanoids from extant methylotrophic bacteria with their fossil analogues. In: Moldowan, J.M.,

Albrecht, P., Philp, R.P. (Eds.), *Biological Markers in Sediments and Petroleum*. Prentice Hall. Englewood Cliffs, NJ., pp. 182-200.

Trendel, J-M., Graff, R., Wehrung, P., Albrecht, P., Dessort, D., Connan, J., 1993. *C*(14a)-Homo-26-nor-17 α -hopanes, a novel and unexpected series of molecular fossils in biodegraded petroleum. *Journal of the Chemical Society, Chemical Communications* 5, 461-463.

Tritz, J.-P., Herrmann, D., Bissere, P., Connan, J., Rohmer, M., 1999. Abiotic and biological hopanoid transformation: towards the formation of molecular fossils of the hopane series. *Organic Geochemistry* 30, 499-514.

Tsuda, Y., Isobe, K., Fukushima, S., Ageta, H., Iwata, K., 1967. Final clarification of saturated hydrocarbons derived from hydroxyhopanone, diploptene, zeorin and dustanin. *Tetrahedron Letters*. 23-28.

van Duin, A.C.T., Sinninghe Damsté, J.S., Koopmans, M.P., van de Graaf, B., de Leeuw, J.W., 1997. A kinetic calculation method of homohopanoid maturation: Applications in the reconstruction of burial histories of sedimentary basins. *Geochimica et Cosmochimica Acta* 61, 2409-2429.

Waples, D.W., Machihara, T., 1991. Biomarkers for Geologists. American Association of Petroleum Geologists. AAPG Methods in Exploration Series, No. 9, 91 p.

Figure captions

Fig. 1. Mass spectra of C_{29} hopanes: (A) $\alpha\alpha$ -30-norhopane, synthetic; (B) $\alpha\beta$ -30-norhopane, synthetic. Insets show details of the spectra. Part of the spectrum of $\alpha\alpha$ -30-norhopane from the Marraat oil, West Greenland is shown for comparison. m/z 178 and 179 have the same size in $\alpha\alpha$ -30-norhopane but are different in $\alpha\beta$ -30-norhopane.

Fig. 2. Mass spectra of C_{30} hopanes: (A) $\alpha\alpha$ -hopane, synthetic; (B) $\alpha\alpha$ -hopane, Eqalulik oil, West Greenland; (C) $\alpha\beta$ -hopane, synthetic.

Fig. 3. TIC (full scan) of C₃₁-C₃₅ hopanes produced by hydrogenation of synthetic C₃₁-C₃₅ hop-17(21)-enes. $\alpha\beta$ -hopanes are the major compounds (70-75 %) followed by $\alpha\alpha$ -hopanes (20-25 %). Retention times of the minor $\beta\alpha$ - and $\beta\beta$ -hopanes are shown with arrows below the baseline. A 25m HP-5 column was used.

Fig. 4. *M/z* 191 mass chromatograms of a crude oil from the M-2 well, Danish North Sea. Top: no internal standard; Bottom: 0.02 mg $\alpha\alpha$ -hopane / 72.4 mg oil. The main chromatograms were obtained using a 25m HP-5 column. Insets show details of the chromatograms on both sides of C₃₀ $\alpha\beta$ -hopane. Parts of chromatograms obtained on a 60m ZB-5 column are shown for comparison. On the 60m ZB-5 column two minor C₃₁ compounds coelute with $\alpha\alpha$ -hopane. Their retention times are indicated by small black peaks below the chromatograms.

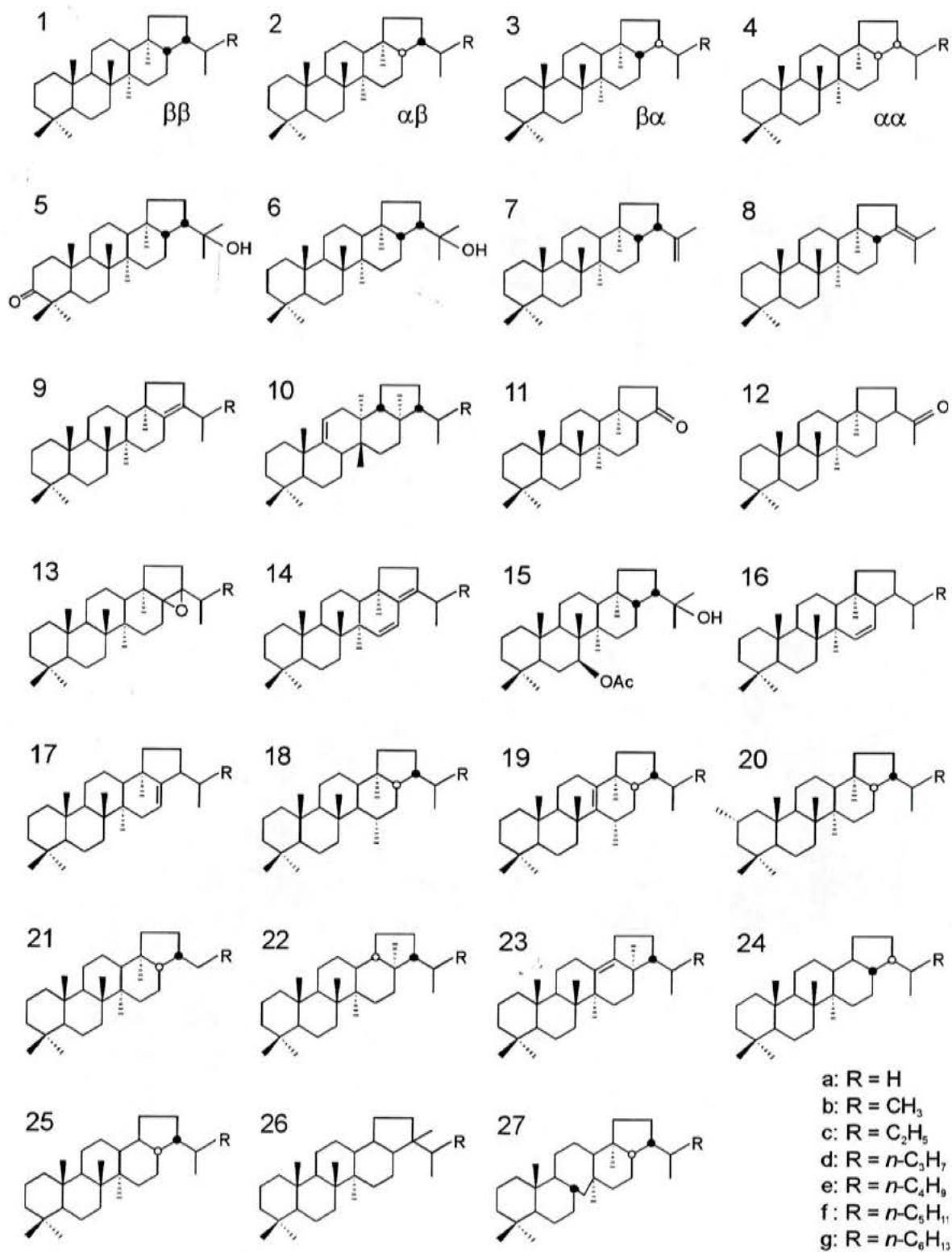
Fig. 5. *M/z* 191, 177 and 205 mass chromatograms (60m ZB-5 column) of an immature shale extract (Bo-1 well 8890', Danish North Sea). The *m/z* 191 mass chromatogram (top) shows almost equal amounts of C₃₀ $\beta\alpha$ -hopane and $\alpha\alpha$ -hopane. A *m/z* 177/191 ratio of only 0.63 in the " $\beta\alpha$ -30-norhopane" peak versus 1.17 of pure $\beta\alpha$ -30-norhopane indicates that it actually contains more coeluting $\alpha\alpha$ -30-norhopane.

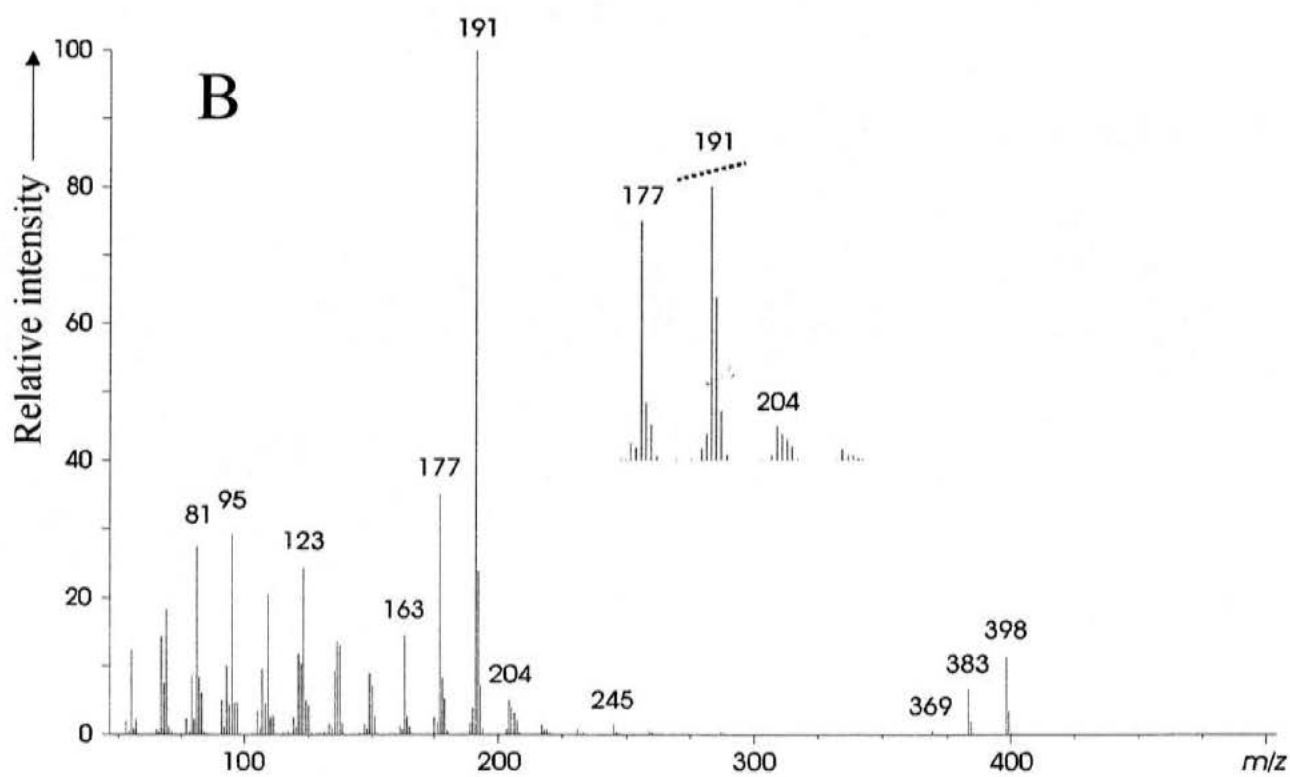
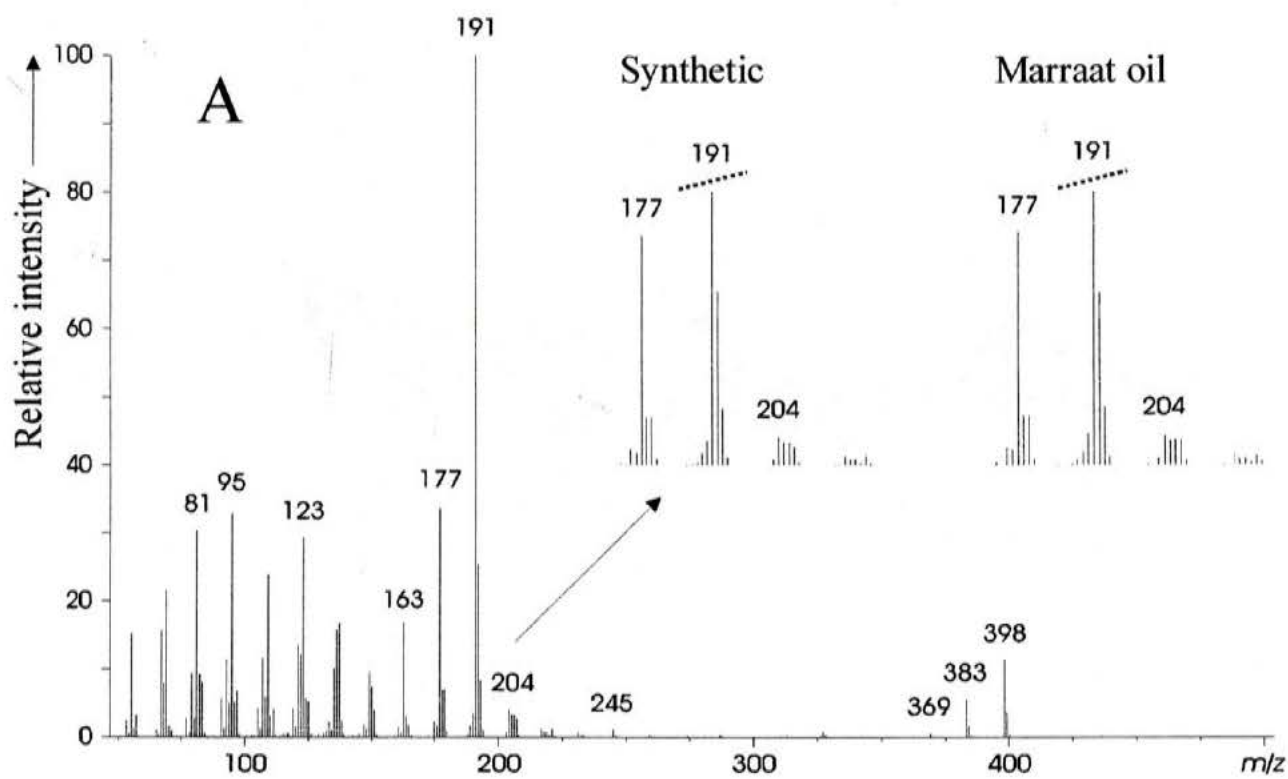
Fig. 6. Distribution of C₃₀ hopanes versus C₂₉ sterane 20*S* / (20*S* + 20*R*) in 9 crude oils and 103 source rock extracts from the Danish North Sea measured from *m/z* 191 and *m/z* 217 peak heights. The relative content of $\alpha\alpha$ -hopane in mature samples is relatively constant independent of source type, whereas the content of $\beta\alpha$ -hopane is more variable.

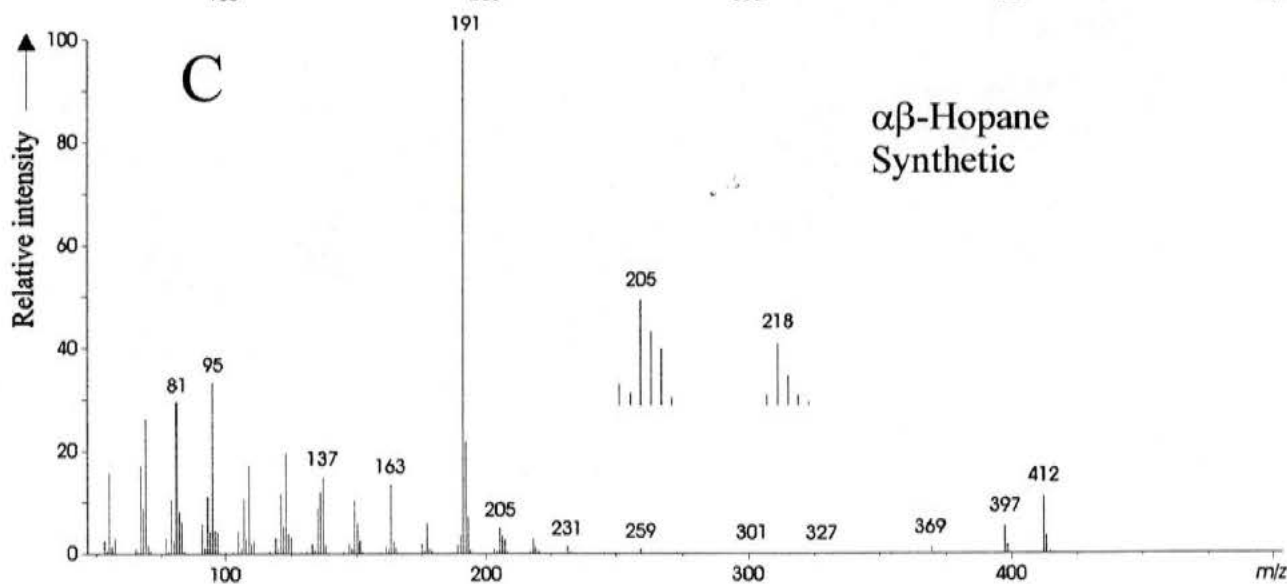
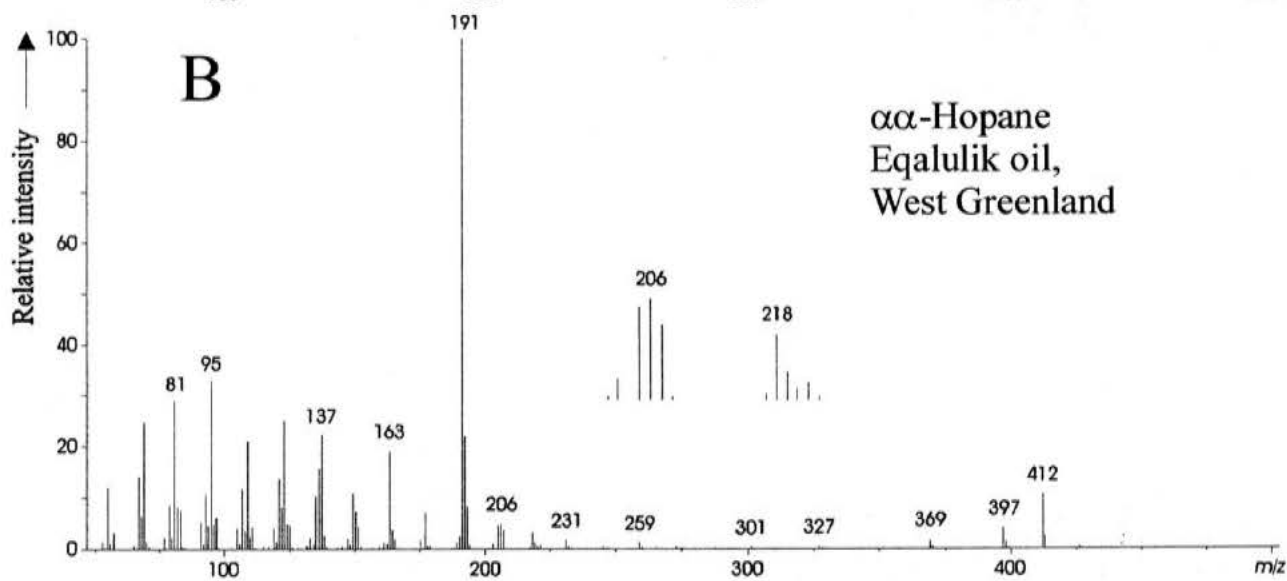
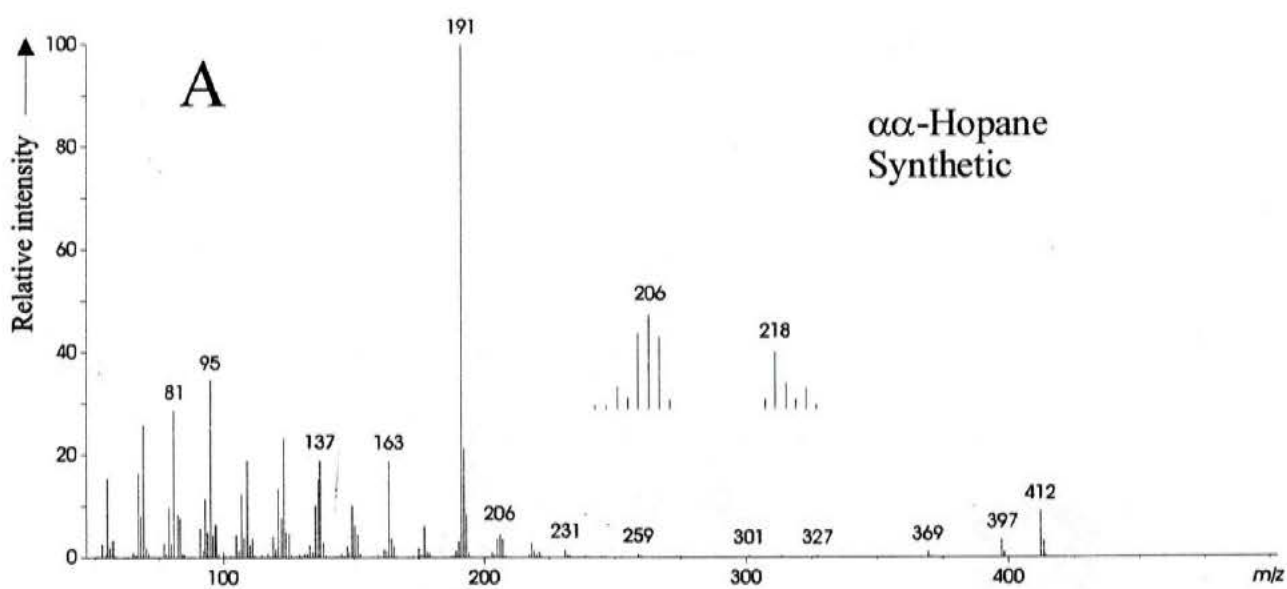
Fig. 7. *M/z* 191 mass chromatograms of a carbonate sourced crude oil from Iran (exact location unknown).

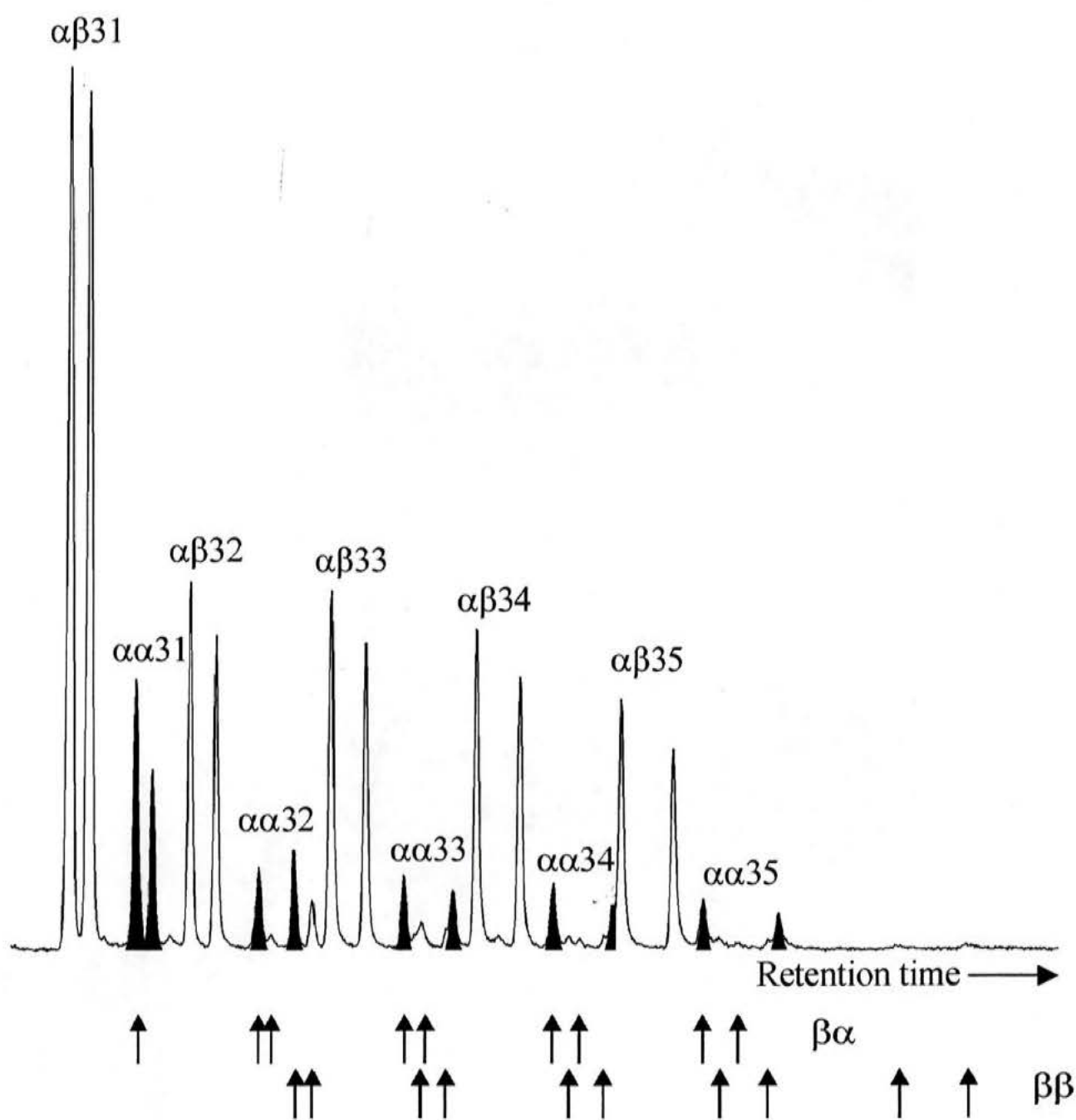
Table 1. Details from the mass spectra of C₂₉-C₃₁ hopanes. *: 148 + R + 1 / 148 + R, **: 148 + R + 2 / 148 + R, e.g. 178/177 and 179/177 for C₂₉ hopanes.

Appendix



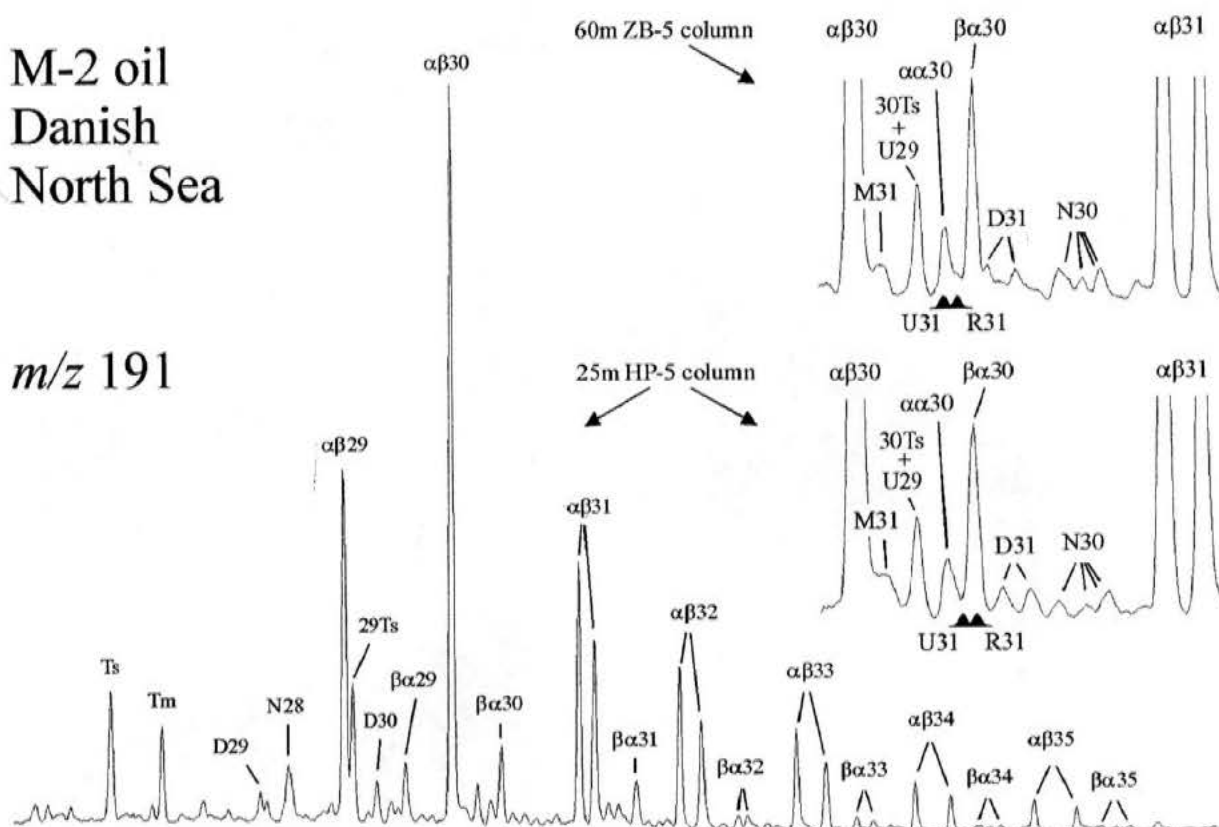




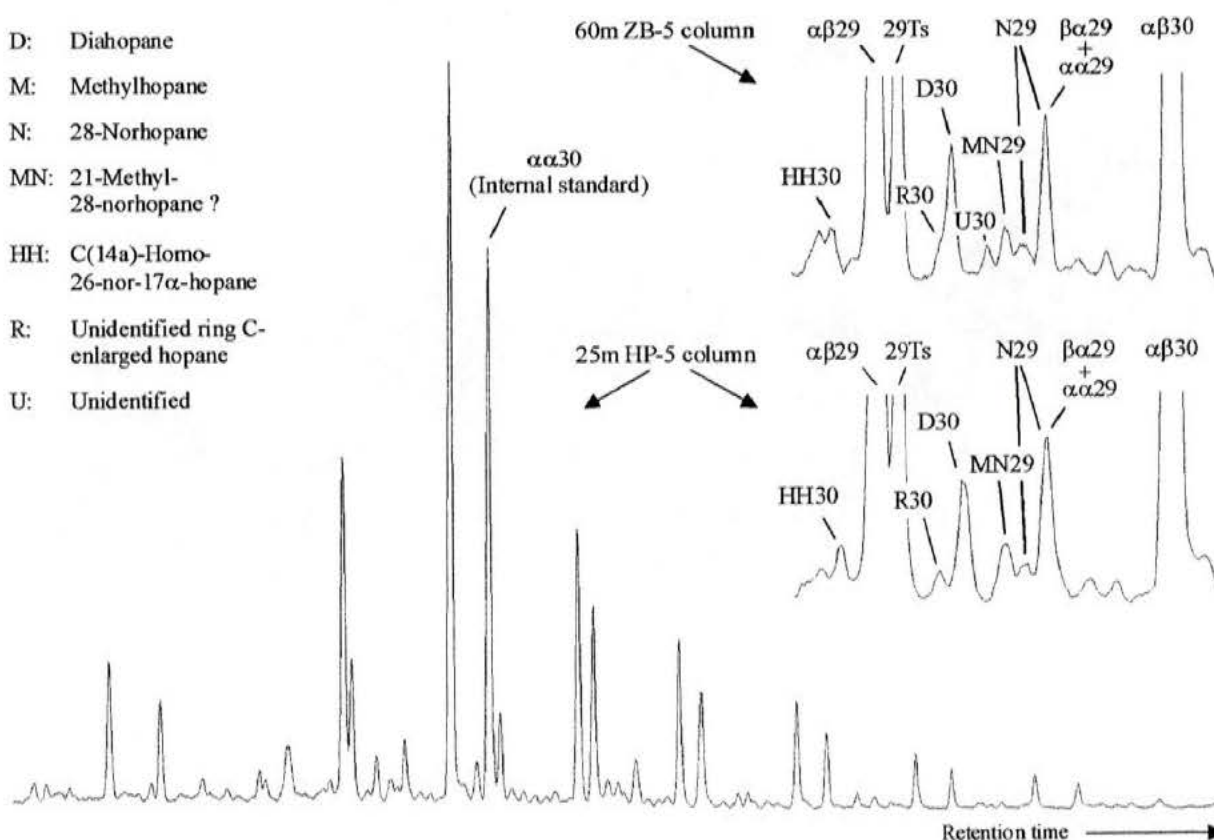


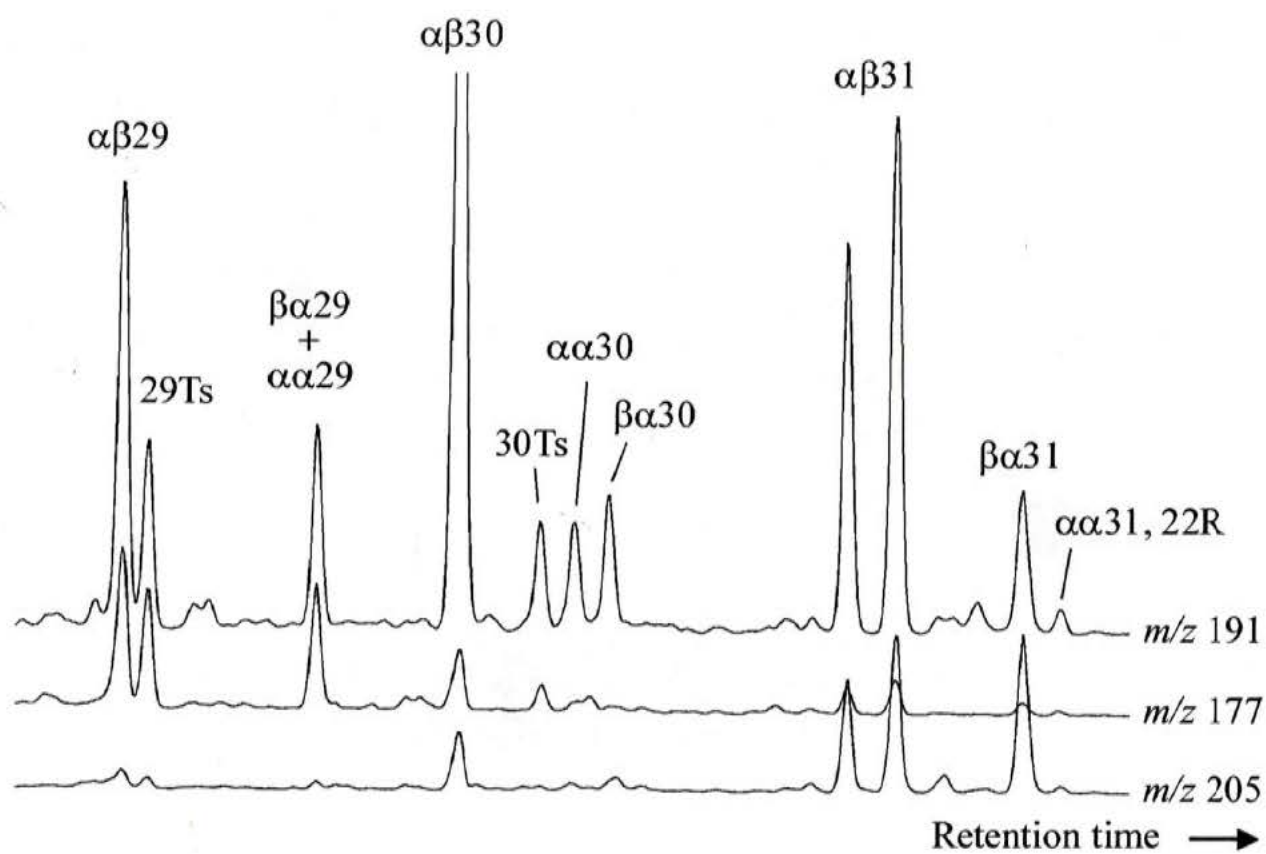
M-2 oil
Danish
North Sea

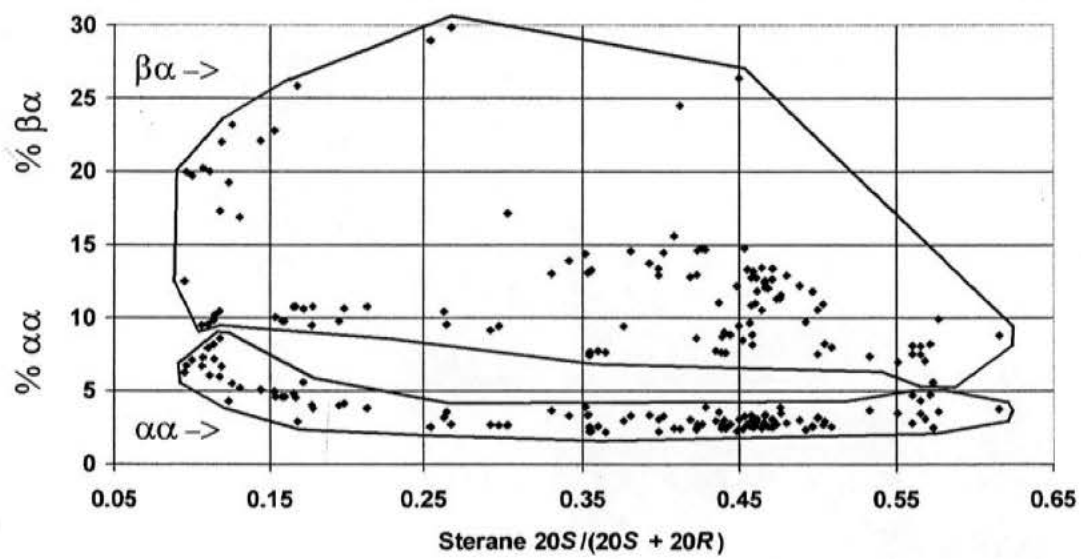
m/z 191

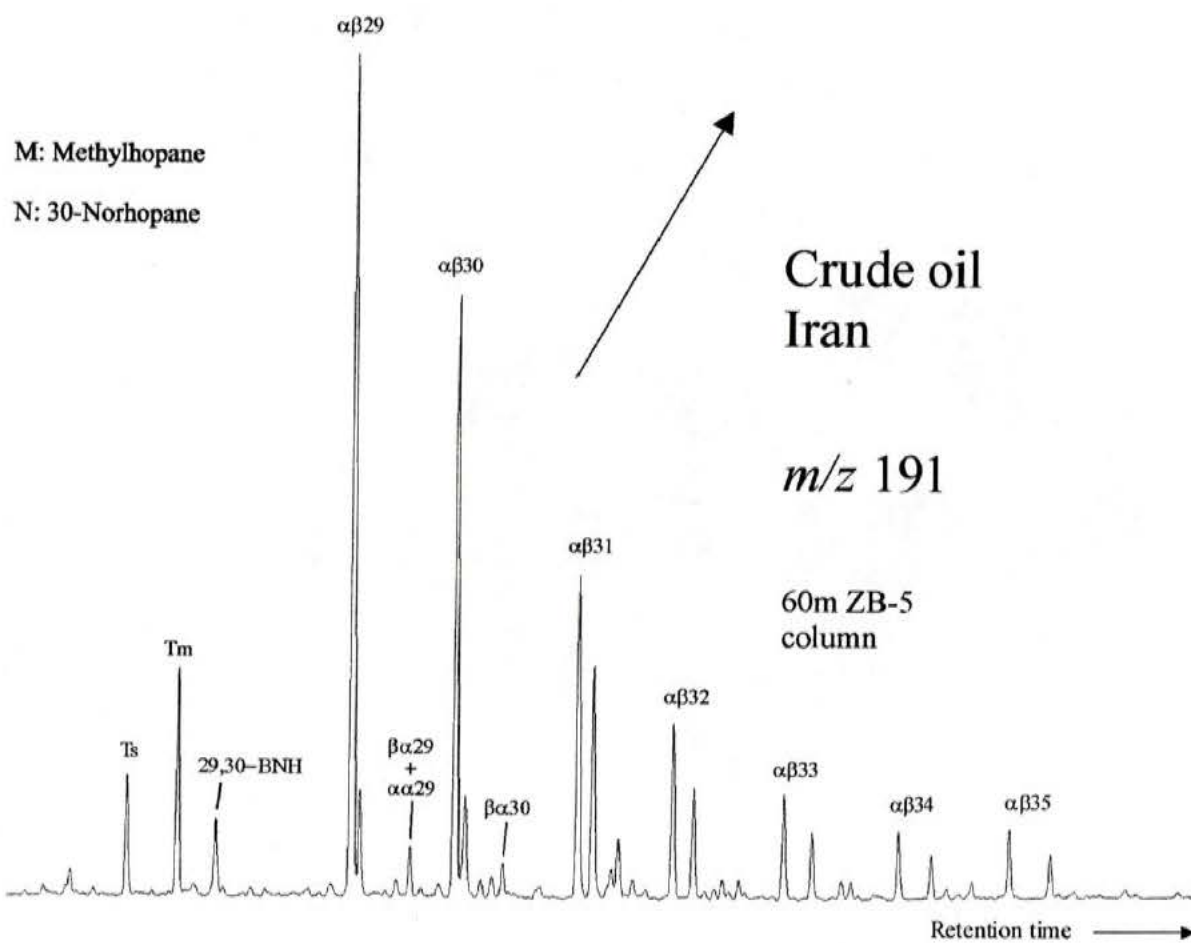
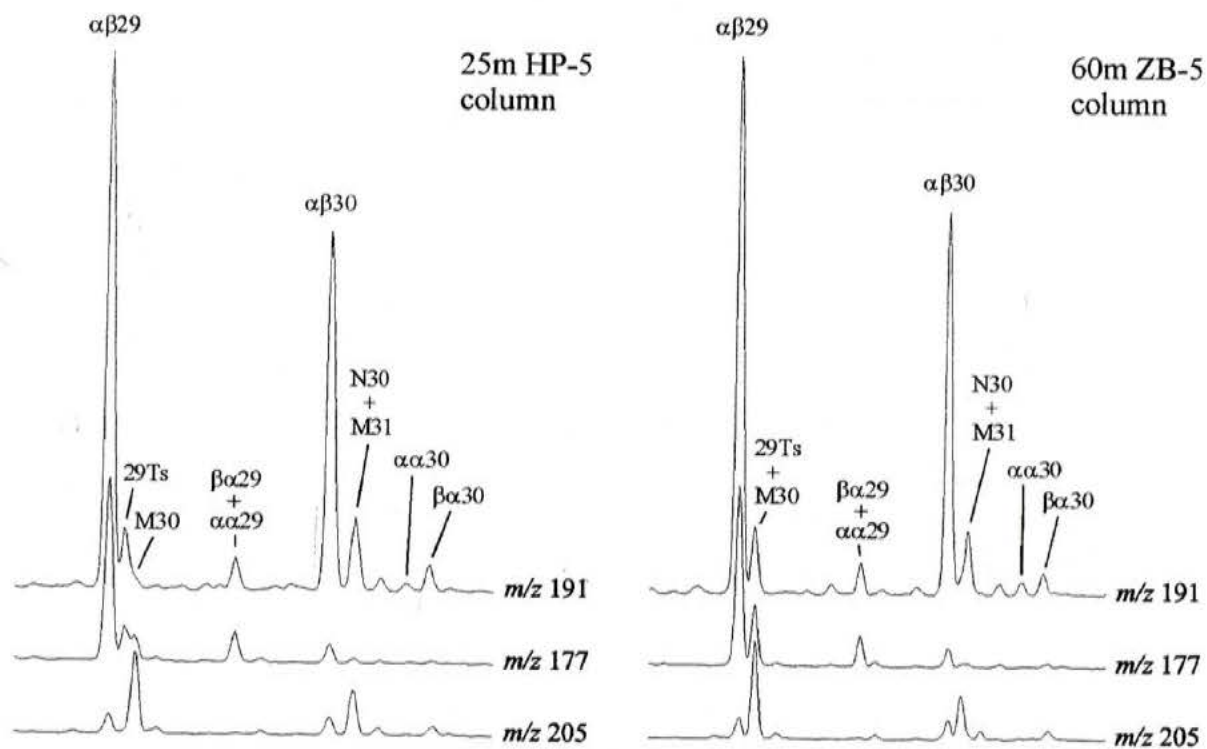


- D: Diahopane
M: Methylhopane
N: 28-Norhopane
MN: 21-Methyl-28-norhopane ?
HH: C(14a)-Homo-26-nor-17α-hopane
R: Unidentified ring C-enlarged hopane
U: Unidentified









	$\alpha\alpha$		$\alpha\beta$		$\beta\alpha$		$\beta\beta$	
	*	**	*	**	*	**	*	**
C_{29}	22	22	24	15	19	4	16	3
C_{30}	22	9	22	7	20	5	18	3
$C_{31}, 22S$	30	30	28	16	20	4	n.a.	n.a.
$C_{31}, 22R$	30	29	30	17	20	4	n.a.	n.a.

**Drowning of a nearshore peat-forming environment, Atane Formation
(Cretaceous) at Asuk, West Greenland: sedimentology, organic
petrography and geochemistry.**

Jørgen A. Bojesen-Koefoed^{1*}, Gregers Dam¹, Birgitte F. Hjortkjær¹, H. Peter
Nytoft¹, Gunver K. Pedersen² and Henrik I. Petersen¹

¹ Geological Survey of Denmark and Greenland (GEUS), 8 Thoravej, DK-2400
Copenhagen NV

² Geological Institute, University of Copenhagen, 10 Øster Voldgade , DK-1350
Copenhagen K

* Corresponding author. E-mail JBK@GEUS.DK

Abstract

The Cretaceous Atane Formation, Nuussuaq Basin, West Greenland is dominated by non-marine sandstones, shales, coals, and delta-front deposits. Marine incursions are frequent, however, and near Asuk, Qeqertarsuaq, a coal seam is encased in shallow marine deposits. Notable changes in both petrography and geochemistry occur through the seam. At the base and top of the seam, the proportions of inertinite and liptinite increase at the expense of the huminite maceral group, and within all maceral groups, proportions of detrital macerals increase. Geochemical changes include systematic variations in TOC, TS, n-alkane, acyclic isoprenoid, and di- and triterpenoid biomarker distributions. The variations reflect the changes in depositional environment going from shallow marine conditions, through fresh/brackish water mire on a coastal plain back to shallow marine conditions following gradual inundation of the peat-forming mire by marine waters.

Keywords: Coal, sedimentology, organic petrography, organic geochemistry, diterpanes, triterpanes, sea-level

Introduction

Peat deposition is governed by a complex interplay between organic matter accumulation and destruction, which in turn are dependent on a number of factors that in coastal areas include changes in relative sealevel. Hence, peat accumulation over prolonged periods of time will only occur under near steady state conditions, when autochthonous organic matter accumulation is balanced by a steady rise in the water-table, which in paralic settings is closely linked to relative sealevel. Stable relative sealevel will lead to cessation of peat accumulation, whereas falling relative sealevel will result in erosion and destruction of peat already accumulated. Conversely, if the rise in relative sealevel exceeds the accumulation rate of organic matter, peat formation will cease due to drowning, and the peat already deposited may be eroded and/or covered by minerogenic sediments (e.g. Banerjee et al., 1996; Petersen et al., 1998). For a comprehensive account of peat deposition and coal formation, the reader is referred to Taylor et al. (1998) and Diessel (1992).

A coal-bearing succession of the Atane Formation (Albian–Campanian) is exposed in a coastal cliff near Asuk (Fig. 1) on the north coast of Qeqertarsuaq (Disko), central West Greenland. The sediments record the drowning of a peat-forming depositional environment by a rising relative sealevel. The present paper documents the systematic changes in sediment character, organic petrography and organic geochemistry, that result from the process of drowning.

Geological setting

The Nuussuaq Basin is of Mesozoic–Tertiary age and contains at least 5 kilometres of Mesozoic sediments. The sediments were deposited in a rift basin dominated by N–S trending faults, and sediment thicknesses decrease towards the east.

The eastern portion of the basin may be part of a Late Cretaceous thermal subsidence basin (Chalmers et al., 1999). The deposits of the Atane Formation are exposed in coastal cliffs and ravines, especially in eastern Qeqertarsuaq (Disko) and southern Nuussuaq (Fig. 1).

The Atane Formation comprises non-marine to shallow marine sediments interpreted as having been deposited in a series of deltaic environments. Fluvial and distributary channel sandstones are interbedded with thin flood plain deposits in eastern Disko (Koppelhus and Pedersen, 1993). Relatively thick successions of non-marine shales interbedded with coal seams are exposed in NE Disko and SE Nuussuaq. The coals were mined at Qullissat until 1972, but except for a few reports (Sheckar et al., 1980; Schiener, 1976), The coals themselves have attracted little scientific interests. In central Nuussuaq, the Atane Formation is dominated by wave-rippled heterolithic delta-front deposits locally with abundant trace fossils and occasional marine fossils (Olsen and Pedersen, 1991; Pedersen and Pulvertaft, 1992). Palaeocurrents indicate overall sediment transport towards the west and northwest. Contemporaneous fully marine sediments (the "Itilli succession") are known from westernmost Nuussuaq and Svartenhuk (Dam and S nderholm,

1994), but the position of the palaeocoastline at any given period during deposition is difficult to determine. The Atane Formation is characterized by a cyclic depositional pattern, reflecting repeated phases of delta progradation, interrupted by periods of marine transgression. Hence, deposits showing marine influence are present at number of locations, including the coastal outcrops at Asuk.

The Atane Formation is poorly dated due to the scarcity of marine invertebrates, and the inherent difficulties attached to dating of non-marine sediments. Reconnaissance palynological studies demonstrate the dominance of terrestrial spores and pollen, many of which are long-ranging species. The available biostratigraphic data indicate ages in the range Albian to early Campanian (Olsen and Pedersen, 1991; Pedersen and Pulvertaft, 1992; Koppelhus and Pedersen, 1993; Nøhr-Hansen, 1996; Lanstorp, 1998; Dam et al., in press). This fits tolerably well with the (rather scanty) geochemical evidence (see below and Bojesen-Koefoed et al., 1999), which suggests a pre-Santonian age. The sedimentary succession youngs towards the northwest, i.e., the oldest deposits are found in the southeastern part of the basin.

Samples and methods

The coal seam exposed at Asuk has a total thickness of up to 15 centimetres, and may be followed for a few tens of metres along the coast. Sampling datum (0 cm) was picked at the base of the seam, i.e. at the marked change in colour

and lithology observed between the brownish rooted sandstone beneath the seam (the "seatearth") and the dark-brown to black organic-rich deposits of the seam itself (Table 1). The full thickness of the seam was sampled, and subdivided into subsamples, each of which integrates a specific interval above the datum (Table 1).

Samples were analysed for total organic carbon (TOC) using a LECO IR 212 carbon analyser and for total sulphur (TS) analyses using a LECO CS 200 carbon/sulphur analyser. Rock-Eval screening pyrolysis was carried out using a Rock-Eval 5 apparatus, following the procedures outlined by Espitalié et al. (1985). Sample splits were prepared for maceral analyses, and point counting (500 points per sample) was carried out on polished grains mounted in epoxy resin, using a Zeiss Photomicroscope III, oil immersion and incident white and fluorescence inducing blue light. Analytical procedures and maceral identification followed the standards outlined by ICCP (1971, 1975) and Taylor et al. (1998). Palynological preparation was carried out following modified standard palynological processing procedures (Poulsen et al., 1990; Desezar and Poulsen, 1994). The fraction greater than 10µm was prepared as scatter mounts in glycerine jelly and studied under a Leitz Diaplan microscope.

Solvent extraction was carried out by means of a Soxtech™ instrument, using dichloromethane/methanol (93+7 vol/vol) as solvent. Asphaltenes were precipitated by n-pentane, and maltene fractions were separated into saturated, aromatic and heteroatomic fractions by liquid chromatography, using a Waters HPLC instrument and a method modified from Radke et al. (1980). Saturated extract fractions were analysed by gas

chromatography (Hewlett-Packard 5890 Ser. II GC, 25 m HP-1 WCOT column, FID) and by coupled Gas Chromatography-Mass Spectrometry (Hewlett-Packard 5890 GC interfaced to a Hewlett-Packard 5871 quadropole mass selective detector, 25m HP-5 WCOT column) using selected ion monitoring.

Sedimentology

The exposure west of Asuk is a coastal cliff, approximately 10 metres high (Figs. 2, 3, 4). It consists of sand-streaked mudstones, heterolithic sandstones, sandstones and a thin coal seam, arranged in four coarsening-upward cycles (of which two are incomplete), each up to 1.6 m thick and a 4-6 metres thick fluvial sandstone unit. Four facies associations have been recognised: delta front, channel, transgressive sand sheet, and coastal plain. The former three associations, together with a delta plain association, are characteristic of the Atane Formation throughout the region. The coastal plain association discussed herein corresponds to a paralic development of the delta plain association. For details of the characteristics of the various facies associations and their interpretation, the reader is referred to Pedersen and Pulvertaft (1992) and Olsen (1993).

The delta front deposits comprise a continuous spectrum of facies ranging from sand-streaked mudstone and heterolithic sandstone to well-sorted sandstone. The sandstone streaks are usually less than 1 cm thick, have sharp bases and are normally graded. The heterolithic part of the succession is

characterised by wavy and lenticular beds with continuous and discontinuous mudstone drapes. The heterolithic beds are succeeded by sharply based sandstones (Figs 2, 4). Symmetrical ripple form-sets and structures typical of wave generation are common together with parallel-laminated, hummocky and swaley cross-stratification. Comminuted plant debris is present on bedding planes. Reworked calcareous concretions are present at the base of one sandstone bed. The degree of bioturbation is variable, but occasionally, bioturbation obscures the primary structures completely. Recognisable trace fossils include abundant *Ophiomorpha nodosa* and common *Thalassionides* sp. and *Taenidium serpentinum*. All internal structures of the delta front association show features diagnostic of wave and storm action. The general upwards increase in sand content and change in wave-generated structures reflect shallowing-upward tendency and an increase in wave energy (cf. Pedersen and Pulvertaft, 1992; Olsen, 1993). The sharp-based sandstones may suggest that progradation of the delta front took place during forced regressions (cf. Posamentier et al., 1992).

The channel deposits comprise a number of medium- to coarse-grained, cross-stratified sandstone beds with a total thickness of 4–6 metres. The sandstones is sharply-based and divided into two parts. The lowermost part show cross-lamination and mud drapes at the base and at the top, and a single low-angle cross-bedded set (Fig. 4). The upper part is sharply based and trough and planar cross-bedded. At the base, planar lamination and wave ripple cross-lamination is observed. The sets are up to 35 cm thick. The uppermost cross-sets show mudstone drapes on foresets and foreset dip

directions in succeeding beds are reversed. The fluvial sandstone is very similar to those reported from other sections of the Atane Formation (Pedersen and Pulvertaft, 1992; Olsen, 1993). According to Pedersen and Pulvertaft (1992) and Olsen (1993), the fluvial sandstones were deposited in straight to slightly sinuous distributary channels. The lower part is tentatively assigned to lateral accretion (point bar) cross-bedding. The presence of drapes along foresets and reverse foreset dip-directions are suggestive of tidal activity within the channel.

The channel sandstone is topped by a 30 cm thick sharply based medium-grained sandstone (Fig. 4). The sedimentary structures are nearly completely obliterated by rooting and the depositional environment cannot be determined with confidence, but based on the occurrence of *Ophiomorpha nodosa* burrows and other data, which are discussed in the following, the sandstone is believed to represent a transgressive sand sheet.

The coastal plain facies association corresponds to a paralic development of the "delta plain swamp and shallow lake association" of Pedersen and Pulvertaft (1992). The coastal plain facies association is represented by carbonaceous shale and coal. Root structures and the coal seam represents autochthonous and parautochthonous plant remains, formed and deposited in low-lying areas and mires on a low relief delta- or coastal plain during the initial base-level rise, when dammed groundwater in front of the rising sea created conditions favourable for peat accumulation. The sandy fills indicate that the plants had hollow roots characteristic of aquatic plants. Similar plant fossils have been observed in the Hettangian–Sinemurian of

Jameson Land, East Greenland and Bornholm, Denmark (Dam and Surlyk, 1993, 1998; Surlyk et al., 1995). Previously, root structures and coal seams in the Atane Formation have been assigned to delta plain deposits (Pedersen and Pulvertaft, 1992; Olsen, 1993). However, the presence of a transgressive sandstone below the coal seam and the organic geochemistry indicating a marine influence on the depositional environment suggests that it is more likely that the coals at Asuk were deposited in a coastal plain environment.

Based on sedimentological evidence, the development of the sedimentary succession observed at Asuk may be summarised as follows: Delta front deposits are succeeded by coarser sediments of a system of prograding fluvial channels. Mud drapes indicate tidal, i.e. marine influence, and the channel deposits are in turn covered by a marine transgressive sand sheet with scattered *Ophiomorpha nodosa* burrows. The top of the transgressive sand sheet marks a coinciding sequence boundary and flooding surface, where a fall in baselevel results in a seawards shift of facies, indicated by the overlying coals, which in turn mark the base of a transgressive systems tract, i.e. the onset of renewed base level rise (cf. Petersen et al., 1998) The rooted top of the transgressive sand sheet forms the seatearth of the overlying coal seam, which formed from peat deposited in low lying mires on a coastal plain. Peat deposition is initiated by incipient baselevel rise, which eventually leads to submersion of the mires, reestablishment of shallow marine conditions, and subsequent deposition of several coarsening-upwards deltafront packages.

Petrography

Detailed petrographic analyses were carried out on the the samples 440117 – 440121; analysis of sample 440122 was considered meaningless due to low TOC. The development of the peatforming mire is recorded by a dramatic increase in huminite group macerals until a maximum is reached in the central part of the seam, after which point a notable decrease follows towards the top of the seam (Fig. 5, Table 2). The inertinite and liptinite groups as well as pyrite show the opposite development, passing through minima in the central part of the seam. The changes in total inertinite are mainly caused by variations in inertodetrinite. In general, detailed maceral analyses show notable increases in the proportions of detrital macerals (attrinite, densinite, liptodetrinite and inertodetrinite) at the expense of 'structured' macerals near the base and the top of the seam (Table 2). Furthermore, the proportion of dark-coloured, low-reflecting euulminite particles ('ulminite A') increases towards the top of the seam. Huminite reflectance (R_o) was determined on three samples, yielding values close to 0.55% or 0.48%, depending on the type of ulminite selected (Table 3).

The changes in petrographic composition record the gradual shift in depositional conditions, and agree with the evolution observed in other marine-roofed coal-seams such as the Carboniferous Katharina-seam in Germany (e.g. Diessel, 1992). After the initial base-level rise and the establishment of a coastal mire, increases in huminite are expected as the floral system develops from herb-dominated to a more woody character.

However, as the transgression continues, the watertable rise in the mire outpaces peat accumulation, and higher pH- and Eh-levels in the waters restrict the humification process, render humic gels unstable, and alter the mechanisms of organic matter degradation. A combination of physical and chemical processes such as winnowing due to transport of organic matter, and changes in the mode of organic matter decomposition and deterioration in preservation potential due to changes in Eh and overall water chemistry, result in increasing proportions of detrital macerals, principally belonging to the refractory inertinite and liptinite groups. Rising pH-levels enhance bacterial activity, and increased availability of sulphate results in the formation of pyrite through bacterial sulphate reduction. Increased bacterial activity may also lead to the formation of low-reflecting, occasionally perhydrous, huminite ('ulminite A'), which shows increased abundance in the uppermost coal sample (440121), see also Petersen and Rosenberg (1998). However, the presence of low-reflecting ulminite-A may also be related to the original plant tissue type (Ting, 1977; Sykes et al., 1994). Differences of up to 0.24 % R_o between two types of ulminite in the same sample have been recorded in lignites (Sykes et al., 1994), but generally, high-reflecting huminite-B is used for determination of huminite reflectance (R_o). In the present case, the values obtained (approximately 0.55 %) are considerably higher than should be expected from geochemical parameters. If low-reflecting huminite-A is used instead, values of approximately 0.48 % R_o are obtained, but assessed from geochemical rank/maturity parameters, the 'true' R_o value of the Asuk samples is likely to be slightly above 0.40 %. It is conceivable that the variation in reflectance between

different types of ulminite is related to the precursor flora, and not just to the tissue type. The problem is presently unresolved, but the discrepancy observed emphasizes the need for caution when using huminite reflectance for rank/maturity assessment in low rank samples.

Palynology

Palynological analysis of the samples from Asuk shows that all samples are totally dominated by brown to dark/brown and black wood. Particles of amorphous organic matter (AOM) are present in all samples. In the lowermost and uppermost samples (440117 and 440122), the colour of the AOM is greyish to yellowish, whereas the central samples show darker colours. The proportion of palynomorphs is very low, but the preservation is in general good. With the exception of uppermost sample, the palynoflora consists of spores and coniferous pollen of no stratigraphic importance. However, the uppermost sample (440122) is dominated by coniferous pollen such as *Rugubivesciculites rugosus* Pierce 1961 and includes stratigraphically important spore species such as *Lycopodiacidites canaculiatus* Singh 1971 and *Triporoletes radiatus* (Dettman) Playford 1971. A few well-preserved specimens of the dinoflagellate cyst *Nyktericysta davisii* Bint 1986 are also present in sample 440122.

Unfortunately, palynological analyses were not able to demonstrate changes in vegetation during the evolution of the peat-forming mire. However, the few data obtained agree with petrographic and sedimentological

observations. In the lowermost and uppermost samples (440117 and 440122), the colour of the AOM is greyish to yellowish indicating a marine depositional environment (see Tyson, 1995). In the other samples the AOM seems to originate from degradation of ligneous particles. The lower and upper samples of the coal seam, (samples 440119 and 440121) show evidence of transportation of the organic particles. The presence of palynomorphs such as *Rugubivesciculites rugosus* Pierce 1961, *Lycopodiacidites canaculatus* Singh 1971 and *Triporoletes radiatus* (Dettman) Playford 1971 as well as the dinoflagellate cyst *Nyktericysta davisii* Bint 1986 indicate a late Albian to Cenomanian age of the sediment (Bint, 1986; Burden and Langille, 1991; Lanstorp, 1998). The presence of *Nyktericysta davisii* indicates a brackish-water depositional environment (Bint, 1986).

Rock-Eval/TOC/TS

Except for TOC and "Sulphur Index" ("SI": $TS \cdot 100 / TOC$), little variation in the various organic geochemical screening parameters is present (Table 3). The TOC shows a rapid rise from 8.5 % in the carbonaceous mudstone at the base of the seam to 69.2 % in the centre, followed by an equally rapid decrease to 3.6 % in the sandy shale overlying the coal (Fig. 5). The trend in SI is roughly opposite that of the TOC, but the sulphur content is generally not very high. The hydrogen index (HI) shows a slight initial increase followed by a steady decrease.

The trend in TOC records the establishment of a mire due to rise in water level, which in turn results in increased preservation of organic matter and to peat formation, until accumulation of authochthonous organic matter gradually ceases as the mire drowns, and marine waters eventually inundate the area. The trend in SI reflects the presence of sulphide minerals, principally pyrite, and of organically bound sulphur. Sequestering of sulphur is principally achieved through reduction of sulphate ions, which abound in marine water. Sulphate reduction is microbially mediated, and the relatively low proportions of sulphur observed (<1%) may have resulted from poor substrate quality, i.e. the humic organic matter could not sustain a dense population of sulphate-reducing microbes, thus limiting sequestering of sulphate. The change in Hydrogen Index is interpreted along the same lines: although the rising water level led to increasing proportions of both high-hydrogen liptinite, and low-hydrogen inertinite, the latter shows a relatively larger increase, leading to slightly decreasing values of HI, although the organic matter type remains largely the same.

Biological marker analyses

Gas chromatograms of the saturated extract fractions show overall similarity, but also slight systematic changes through the succession (Fig. 6). The samples 440117– 440121 show heavy-end skewed n-alkane distributions with strong odd-number predominance in the nC_{21-35} range and a pronounced

'biomarker hump' in the nC_{25-31} range; in some samples the 22R-homohopane, eluting fractionally earlier than nC_{32} , constitutes a prominent peak in the chromatogram. Samples 440117 and 440118 show enhancement of nC_{19} . Mass spectrometry data show this feature to be caused partly by coelution with the tricyclic diterpane 19-norisopimarane, although some enhancement of nC_{19} actually seems to be present. Sample 440119 shows enhancement of nC_{20} , in addition to enhancement of nC_{19} . This is caused by coelution of the tetracyclic diterpane phyllocladane with nC_{20} . Samples 440120 and 440121 show pronounced enhancement at nC_{20} and rather slight enhancement at nC_{19} . Coeluting isopimerane and phyllocladane contribute to the nC_{19} and nC_{20} peaks. Sample 440122, collected above the coal seam, shows a slightly bimodal n-alkane distribution with a prominent heavy-end apex centred at nC_{29} , and a minor apex centred at nC_{17} . Again, isopimerane and phyllocladane contribute to the nC_{19} and nC_{20} peaks. All samples show abundant acyclic isoprenoids, in particular pristane, and high pristane/phytane ratios. From base to top through the coal seam pristane/phytane ratios vary from 4.4 at the base (sample 440117) to 6.9 in the centre of the coal (440119) to 2.6 in the sandy shale overlying the coal (sample 440122). The concentration of C_{15-20} acyclic isoprenoids relative to C_{15-20} n-alkanes shows the opposite trend: an initial decrease from 1.2 at the base (sample 440117) to 0.8 in the centre (sample 440120) succeeded by an increase to 1.4 in the shale above the coal (sample 440122). Phyllocladane/eicosane ratios based on peak areas of these compounds in scaled m/z 71 (n-alkanes) and m/z 123 (diterpanes) ion fragmentograms show systematic evolution through the succession, comprising

an initial rise from 0.22 (sample 440117) to 4.07 in the centre of the seam (sample 440120) followed by a decrease to 0.72 (sample 440122) in the shale overlying the coal (Figs. 6 and 7). Conversely, little change is observed in isopimerane/nonadecane ratios (Fig. 6).

Hopane-family biological marker distributions are strongly influenced by the low level of thermal maturity, and show a prominence of 13(18)-neohopenes, $\beta\beta$ -hopanes, moretanes and 22R isomers of extended moieties, whereas $\alpha\beta$ -hopanes and 22S-isomers of extended hopanes are sparse (Fig. 7, Table 4). However, notable changes in relative distributions of these various compounds are observed through the succession (Fig. 7). The basal sample (440117) shows a hopanoid distribution comprising appreciable proportions of 28,30-bisnorhopane, 13(18)-neohopenes, $\beta\beta$ -hopanes, moretanes and 22R isomers of both homohopane and bishomohopane. Upwards through the succession 28,30-bisnorhopane disappears abruptly and the relative abundance of 22R-homohopane increases steadily until this compound, in the centre of the seam (sample 440119), becomes dominant, and more or less masks the presence of other hopanoids. Further upwards the evolution is reversed, and the uppermost sample (440122) shows very similar characteristics to those of the basal sample (440117), including an abundance of 28,30-bisnorhopane, although the proportion of 22R-homohopane is higher. Due to very high hopanoid to steroid ratios, interference from abundant hopenes render the sterane marker signal (m/z 217 and 218) useless. Hence sterane data are not available.

Data on n-alkanes, linear isoprenoids, and di- and triterpane biological markers agree with the evidence from sedimentology, petrography and Rock-Eval pyrolysis. Heavy-end skewed, high CPI n-alkane distributions are characteristic of terrigenous organic matter, but the bimodal distribution observed in the uppermost sample (440122) testifies to the marine influence by indicating a mixed organic matter source. High pristane/phytane ratios are also commonly observed in coals and terrigenous kerogen, but the variation through the succession, comprising an initial rise followed by a notable decrease, demonstrates the effects of marine waters at the base and top of the seam. This also goes for the trend in the ratio of C₁₅₋₂₀ acyclic isoprenoids to C₁₅₋₂₀ n-alkanes, where marine deposits generally show higher proportions of isoprenoids. Enhancement of n-alkanes in the nC₁₅₋₂₃ range is observed in a number of microalgae and bacteria (e.g. Clark and Bluhmer, 1967; Han and Calvin, 1969; Gelpi, 1970; Youngblood et al., 1971; Tissot and Welte, 1984), but isolated enhancement of nC₁₉ is somewhat enigmatic, and no explanation can be readily offered. The 440117 and 440122 samples, which were collected at the base of and above the coal seam respectively, contain appreciable proportions of 28,30-bisnorhopane, which is generally held to be a marine marker (Nytoft et al., in press; Moldowan et al., 1984), although it has also been observed in coals (N. Telnæs, oral communication 1999; GEUS unpublished data). The base of the seam shows marine influence on the biomarker distribution, which is otherwise a product of the "settlement-flora" of the incipient mire. Floral changes during the evolution of the mire and decreasing clay content are recorded by the biomarker distributions trend

through the seam, until a reversal takes place in the centre of the seam, from which level marine influence gradually resumes. Floral changes are probably the main cause for changes in diterpane distribution, whereas the variation in the relative proportions of $\alpha\beta$, $\beta\beta$, and $\beta\alpha$ -hopanes, diahopane and hopenes were probably mainly caused by variations in the availability of clay, the catalytic effect of which is important for molecular rearrangement (e.g. Nytoft et al., 1999). Very high proportions of homohopane is often observed in coaly sediments, which are generally depleted in the higher hopane homologues compared to marine sediments. The biological marker distribution yielded by the 440122 sample, collected above the seam, represents the combined signal of autochthonous marine organic matter and reworked material from the underlying peat.

Phyllocladane and isopimarane are known as a conifer markers (Philp, 1994; Blunt et al., 1988; Noble et al., 1986), although the latter compound is also found in angiosperms (Stefanova et al., 1995; Peters and Moldowan, 1993). Biological markers of indisputable angiosperm origin such as members of the oleanane, lupane or taraxastane families have neither been observed in the Asuk samples nor in other samples of the Atane Formation (GEUS, unpublished data). In central West Greenland, such biological markers are commonly present in sediments younger than the Santonian, as well as in oils presumably derived from them (Bojesen-Koefoed et al., 1999). The absence of angiosperm markers in samples of the Atane Formation may suggest an age older than the Santonian, at least for the samples analysed to date.

Discussion and conclusion

Even though the number of samples analysed from the Asuk outcrop is indeed limited, the data clearly and consistently demonstrate the nature of the changes in organic petrography and geochemistry, that would be expected to follow from the evolution in sedimentary conditions during the "life-time" of a coastal mire in the vicinity of a large fluvial system. Large fluvial/deltaic depositional systems are highly dynamic, and shifting of channels, abandonment, reactivation or formation of new delta-lobes have profound effects on depositional subenvironments in various parts of the entire system. This also includes coastal areas, which develop in response to the general evolution of the delta system (e.g. Tibert and Gibling, 1999). Emergence and submersion of low-lying coastal plains, often protected behind beach ridges are essential parts of this development. Occasional emergence and inundation of coastal plain areas in nearshore parts of the greater depositional system are thus not necessarily dependant on the regional relative sea-level, but are more likely to be governed by local phenomena. Although the drowning of the peat-forming mire at Asuk cannot be held to indicate a general transgression, the information gathered from the study of the outcrop is of general nature, since the effects of marine inundation are the same, irrespective of the cause. Hence, the present study has shown that a combination of sedimentological, petrographical, palynological, and organic geochemical data allow the tracing of the

establishment, evolution and eventual disruption of a nearshore peatforming environment. The data presented here consistently demonstrate the changes in the sedimentary environment going from a shallow marine, sand-dominated delta front environment through the formation of a peat-forming mire on a costal plain to the re-establishment of shallow marine conditions after the cessation of peat deposition due to inundation resulting from rising relative sea-level.

Acknowledgments

This paper is published with the permission of the Geological Survey of Denmark and Greenland (GEUS). Jon R. Ineson improved the english language of the text and provided valuable comments and suggestions. Stefan Sølberg and Jacob Lautrup prepared the figures. Samples were collected during a field campaign partly sponsored by the Bureau of Mineral Resources under the Greenland local government. Laboratory analyses were partly sponsored by the Danish Energy Research Programme, grant EFP-9813/13-0022. Mobilisation of field camps took place by m/s "Maja S." of Godhavn (Qeqertarsuaq), and the skipper Finn Steffens and his crew Peter Brandt and Peter Broberg are thanked for good seamanship, help, and pleasant company.

References

- Banerjee, I., Kalkreuth, W. and Davies, E. H., 1996. Coal seam splits and transgressive–regressive coal couplets: A key to stratigraphy of high-frequency sequences. *Geology* 24, 1001-1004
- Bint, A.N., 1986. Fossil Ceratiaceae: a restudy and new taxa from the mid-Cretaceous of the Western Interior, U.S.A. *Palynology*, 10, p. 135-180.
- Blunt, J. W, Czochanska, Z., Sheppard, C. M., Weston R. J. and Woolhouse, A. D., 1988. Isolation and structural characterisation of isopimarane in some New Zealand seep oils. *Organic Geochemistry* 12, 479-486
- Bojesen-Koefoed, J. A., Christiansen, F. G., Nytoft, H. P. and Petersen, A. K., 1999. Oil seepage onshore West Greenland: evidence of multiple source rocks and oil mixing. In Fleet, A.S. and Boldy, S. A. R. (eds): *Petroleum Geology of Northwest Europe: Proceedings of the 5th Conference*. Geological Society, London, 305-314
- Burden, E.T. and Langille, A.B., 1991. Palynology of Cretaceous and Tertiary strata, northeast Baffin Island, Northwest Territories, Canada: Implications for the history of the rifting in Baffin Bay. *Palynology* 15, 91-114.

Chalmers, J. A. Pulvertaft, T. C. R., Marcussen, C. and Pedersen, A. K. 1999, New insight into the structure of the Nuussuaq Basin, central West Greenland. *Marine and Petroleum Geology* 16, 197-224

Clark, R. C. and Blumer, M., 1967. Distribution of n-paraffins in marine organisms and sediment. *Limnology and Oceanography* 12, 79-87

Dam, G., Nøhr-Hansen, H., Pedersen, G. K. and Sønderholm, M., in press. Sedimentary and structural evidence of a new early Campanian rift phase the Nuussuaq Basin, West Greenland. *Cretaceous Research*.

Dam, G. and Surlyk, F., 1998. Stratigraphy of the Neill Klint Group; a Lower – lower Middle Jurassic tidal embayment succession, Jameson Land, East Greenland. *Geology of Greenland Survey Bulletin* 175, 80pp

Dam, G. and Surlyk, F., 1993. Cyclic sedimentation in a large wave and storm-dominated anoxic lake; Kap Stewart Formation (Rhaetian-Sinemurian), Jameson Land East Greenland. In: H. W. Posamentier, C. P. Summerhayes, B. U. Haq & G. P. Allen (eds), *Sequence stratigraphy and facies associations*. International Association of Sedimentologists Special Publications 18, 419-448

Dam, G. and Sønderholm, M., 1994. Lowstand slope channels of the Itilli succession (Maastrichtian–Lower Paleocene), Nuussuaq, West Greenland. *Sedimentary Geology* 94, 49-71

Desezar, Y. and Poulsen, N. E., 1994. On palynological preparation technique. American Association of Stratigraphic Palynologist, Newsletter. 27, 12-13.

Diessel, C. F. K., 1992. Coal-bearing depositional systems. Springer Verlag, Berlin, 721pp.

Espitalié, J., Deroo, G. and Marquis, F., 1985. La pyrolyse Rock-Eval et ses applications. Revue de l'Institut Français du Pétrole 40, 563-579

Gelpi, E., Schneider, H., Mann, J. and Oró, J., 1970. Hydrocarbons of geochemical significance in microscopic algae. Phytochemistry 9, 603-612

Han, J., and Calvin. M., 1969. Hydrocarbon distribution in algae and bacteria, and microbiological activity in sediments. Proceedings of the National Academy of Science 64, 436-443

ICCP, 1971. Supplement to the 2nd edition of the International Handbook of Coal Petrography. Centre National de la Recherche Scientifique, Paris

ICCP, 1975. Supplement to the 2nd edition of the International Handbook of Coal Petrography. Centre National de la Recherche Scientifique, Paris

Koppelhus, E. B. & Pedersen, G.K., 1993. A palynological and sedimentological study of Cretaceous floodplain deposits of the Atane Formation at Skansen and Igdlunguaq, Disko, West Greenland. *Cretaceous Research* 14, 707-734.

Lanstorpe, J., 1998. En palynologisk undersøgelse af Atane Formationen fra det sydøstlige Nuussuaq, Vestgrønland (in Danish). M.Sc. thesis, University of Aarhus, 135pp.

Moldowan, J. M., Seifert, W. K., Arnold, E. and Clardy, J., 1984. Structure proof and significance of stereoisomeric 28,30-bisnorhopanes in petroleum and petroleum source rocks. *Geochimica et Cosmochimica Acta* 48, 1651-1661

Noble, R. A., Alexander R., Kagi, R. I. and Knox, J., 1986. Identification of some diterpenoid hydrocarbons in petroleum. *Organic Geochemistry* 10, 825-829

Nytoft, H. P., Bojesen-Koefoed, J. A. and Christiansen, F. G., in press. C₂₆ and C₂₈₋₃₄ 28-norhopanes in sediment and petroleum. *Organic Geochemistry*

Nytoft, H. P., Thomsen, J. V., Jørgensen, T. K. C., Bojesen-Koefoed, J. A., and Petersen, H. I., 1999. Hopa-15,17(21)-dienes in sediments: Precursors of diahopanes?. 19th International Meeting on Organic Geochemistry, Istanbul, September 1999, Abstracts 13-14

Nøhr-Hansen, H., 1996. Upper Cretaceous dinoflagellate cyst stratigraphy, onshore West Greenland. Grønlands Geologiske Undersøgelse, Bulletin 170, 104 p.

Olsen, T., 1993. Large fluvial systems: The Atane Formation, a fluvio-deltaic example from the Upper Cretaceous of central West Greenland. In: Fielding, C. R. (ed.) Current research in fluvial sedimentology, Sedimentary Geology 85, 457-473

Olsen, T. and Pedersen, G. K., 1991. The occurrence of marine fossils in the Upper Cretaceous deltaic sediments at Pautût, central West Greenland. Bulletin of the Geological Society of Denmark 39, 111-122

Paull, R., Michaelsen, B. H. and McKirdy, D. M., 1998. Fernenes and other triterpenoid hydrocarbons in *Dicroidium*-bearing Triassic mudstones and coals from South Australia. Organic Geochemistry 29, 1331-1343

Pedersen, G. K. and Pulvertaft, T. C. R., 1992. The nonmarine Cretaceous of the West Greenland Basin, onshore West Greenland. Cretaceous Research 13, 263-272

Peters, K. E. and Moldowan J. M., 1993. The biomarker guide. Prentice Hall Englewood Cliffs, New Jersey, 363pp.

Petersen, H. I., Bojesen-Koefoed, J. A. , Nytoft, H. P., Surlyk, F, Therkelsen, J and Vosgerau, H., 1998. Relative sea-level changes recorded by paralic liptinite-rich coal facies cycles, Middle Jurassic Muslingebjerg Formation, Hochstetter Forland, Northeast Greenland. *International Journal of Coal Geology* 36, 1-30

Petersen, H. I. and Rosenberg, P., 1998. Reflectance retardation (suppression) and source rock properties related to hydrogen-enriched vitrinite in Middle Jurassic coals, Danish North Sea. *Journal of Petroleum Geology* 20, 247-263

Philp, R. P., 1994. Geochemical characteristics of oils derived predominantly from terrigenous source materials. In: Scott, A. C. and Fleet, A. J. (eds.) *Coal and coal-bearing strata as oil-prone source rocks?* Geological Society Special Publication 77, 71-91

Posamentier, H. W., Allen, G. P. & James, D. P., 1992. Forced regressions in a sequence stratigraphic framework: concepts, examples, and exploration significance. *Bulletin of the American Association of Petroleum Geologists* 76, 1687-1709

Poulsen, N. E., Gudmundsson, L., Hansen, J. M. and Husfeldt, Y., 1990. Palynological preparation techniques, a new maceration tank method and other modifications. Geological Survey of Denmark, Series C 10, 24 pp.

Radke, M., Willsch, H. and Welte, D. H., 1980. Preparative hydrocarbon group type determination by automated medium pressure liquid chromatography.

Analytical Chemistry 52, 406-411

Schiener, E. J., 1976. Coal geology. In: Escher, A. and Watt, W. S. (eds.)

Geology of Greenland, Geological Survey of Greenland, Copenhagen, 504-516

Shekhar, S. C, Frandsen, N. and Thomsen, E., 1982. Coal on Nûgssuaq, West Greenland. Geological Survey of Denmark

Stefanova, M., Magnier, C. and Velinova, D., 1995. Biomarker assemblage of some Miocene-aged Bulgarian lignitic lithotypes. Organic Geochemistry 23, 1067-1084

Surlyk, F., Arndorff, L., Hamann, N.-E., Hamberg, L., Johannesen, P. N., Koppelhus, E. B., Nielsen, L. H., Noe-Nygaard, N., Pedersen, G. K. and Petersen, H. I., 1995. High-resolution sequence stratigraphy of a Hettangian–Sinemurian paralic succession, Bornholm, Denmark. Sedimentology 42, 323-354

Sykes, R., Fowler, M. G., and Pratt, K. C., 1994. A plant tissue origin for ulminites A and B in Saskatchewan lignites and implications for R_o. Energy & Fuels 8, 1402-1416

Taylor, G. H., Teichmüller, M., Davis, A., Diessel, C. F. K., Littke, R., and Robert, P., 1998. Organic Petrology. Gebrüder Borntraeger, Berlin-Stuttgart, 704pp.

Tibert, N. E. and Gibling, M. R., 1999. Peat accumulation on a drowned coastal braidplain: the Mullins Coal (Upper Carboniferous), Sydney Basin, Nova Scotia. *Sedimentary Geology* 128, 23-38

Ting, F. T. C., 1977. Microscopical investigation of the transformation (diagenesis) from peat to lignite. *Journal of Microscopy* 109, 75-83

Tissot B. P. and Welte, D. H., 1984. Petroleum formation and occurrence. Springer Verlag, Berlin, 699pp

Tyson, R.V., 1995. Sedimentary Organic Matter. Chapman and Hall, London. 615 pp.

Youngblood, W. W., Blumerd, M., Guillard, R. L. and Fiore, F., 1971. Saturated and unsaturated hydrocarbons in marine benthic algae. *Marine Biology* 8, 190-201

Figure Captions

Fig. 1.

Generalised geological map of central West Greenland showing location map of the study area (large black dot) west of Asuk on the north coast of Qeqertarssuaq. Note that Qeqertarssuaq is the Inuit name for the island formerly known as "Disko" as well as for the town formerly known as "Godhavn" situated on the southern tip of the island.

Fig. 2.

Photo showing the outcrop at the coastal cliffs near Asuk, Qeqertarssuaq. Person for scale. The coal seam is arrowed.

Fig 3.

Photo showing coal seam at Asuk. Hammer for scale, handle points to the contact between the coal seam and the underlying rooted transgressive sand sheet.

Fig. 4

Sedimentary log of the measured section at Asuk, Qeqertarssuaq

Fig. 5

Overall petrographic composition in terms of huminite, inettinite, liptinite, pyrite and 'other minerals', in volume-percent from point counting (400 or 500 points

per sample). TOC in weight-percent. Sampling datum = 0 cm is picked at the contact between rooted sandstone and carbonaceous mudstone.

Fig. 6

Gas chromatograms, saturated extract fractions. Key: pr = pristane; filled triangle: nonadecane (nC_{19}) coeluting with 19-norisopimarane; filled circle = eicosane (nC_{20}) coeluting with phyllocladane; 25 = pentaicosane (nC_{25}), 35 = pentatriacontane (nC_{35}); PR/PH = pristane/phytane ratio; I/NA = C_{15-20} acyclic isprenoids/ C_{15-20} n-alkane ratio; CPI = Carbon Preference Index; NIP/ nC_{19} = 19-norisopimarane/n-nonadecane ratio, based on integrated peak areas in ion fragmentograms m/z 123 and m/z 71; PHYL/ nC_{20} = phyllocladane/n-eicosane ratio, based on integrated peak areas in ion fragmentograms m/z 123 and m/z 71. Note prominence of 22R-homohopane, eluting fractionally earlier than nC_{32} in samples 440119 – 440121. See text for discussion

Fig. 7

Ion fragmentograms m/z 191 (triterpanes and m/z 123 (diterpanes) samples 440117, 440119 and 440122. Compound identifications are shown in Table 4.

Table Captions

Table 1.

Sample identification

Table 2. Detailed petrographic compositions based on point counting (500 points per sample, except for sample 440117: 400 points). Numbers in percent

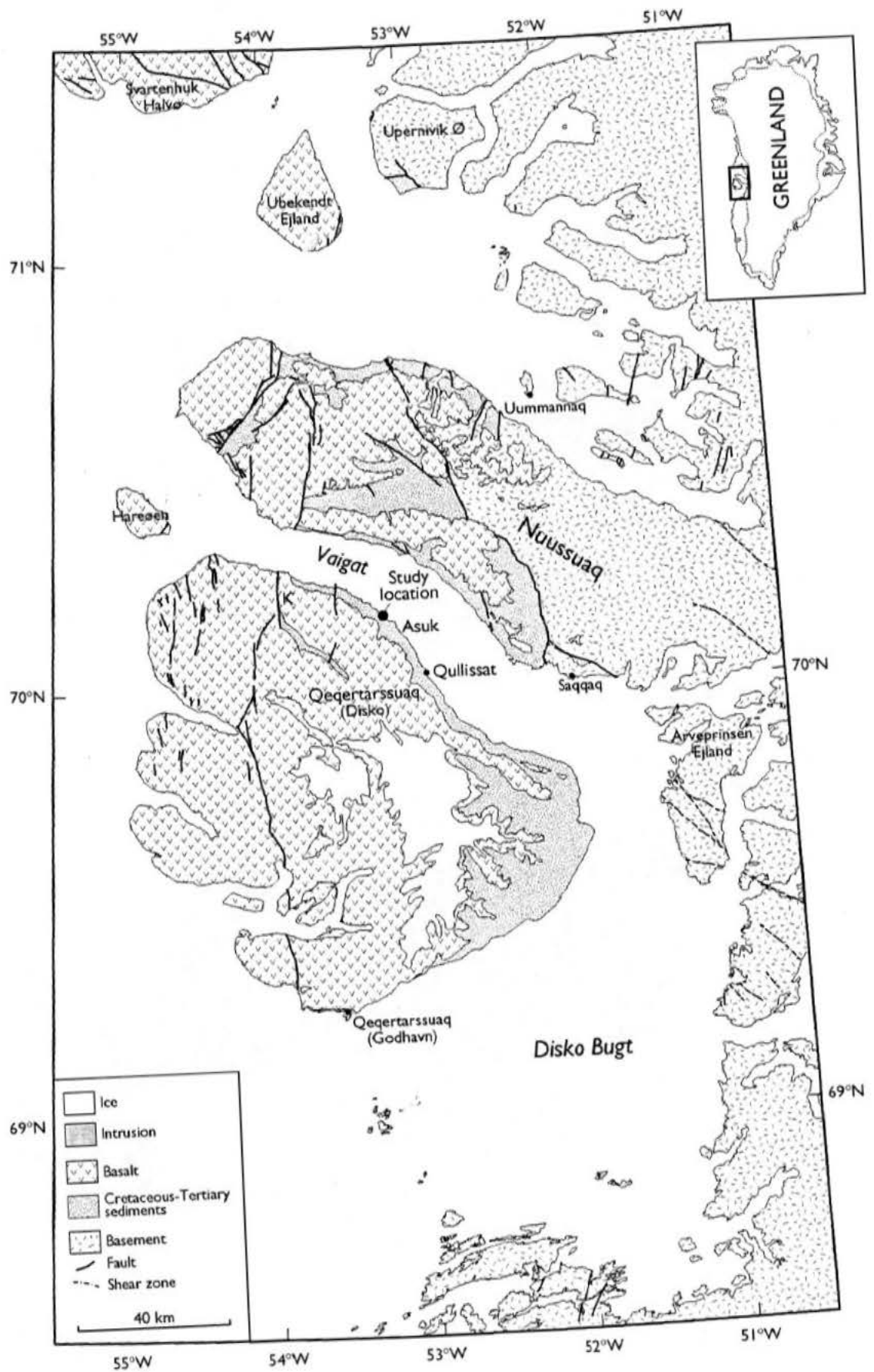
Table 3.

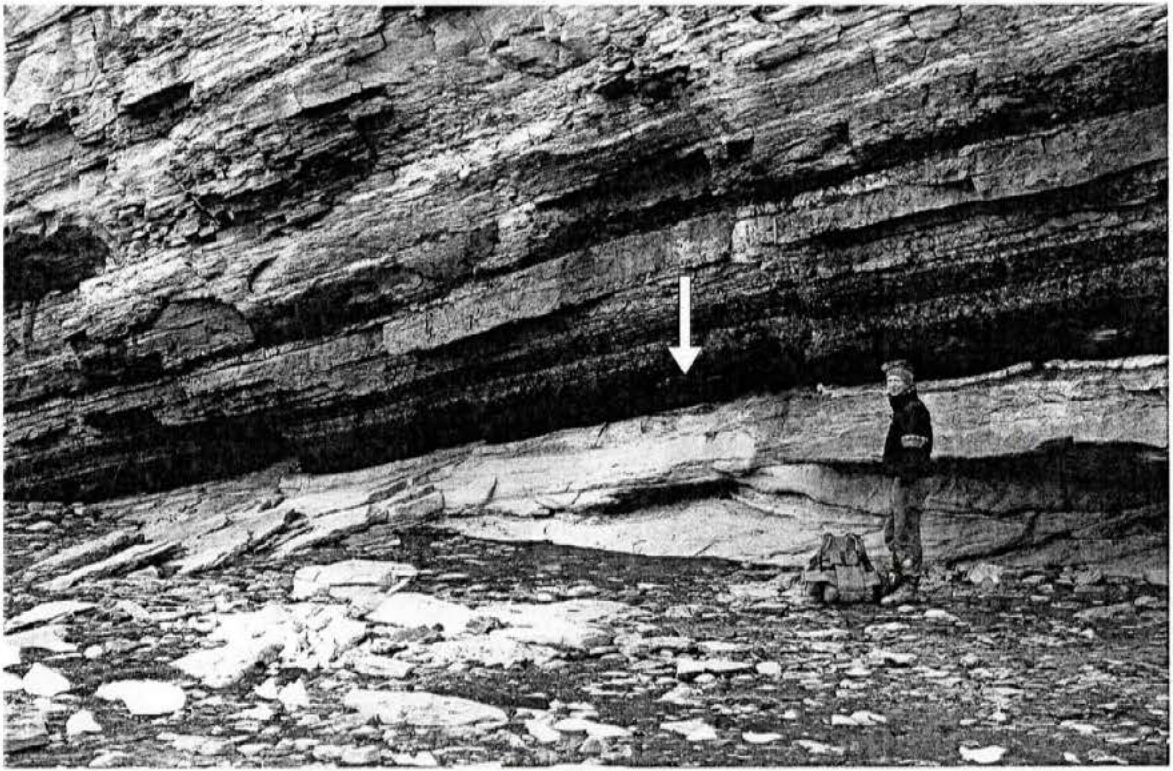
Rock-Eval/TOC/TS and R_o data. TOC and TS in weight-%. S1, S2, in mg HC/g rock, $SI = 100 \cdot TS/TOC$, $HI = 100 \cdot S2/TOC$, $SI = 100 \cdot TS/TOC$, R_o in %. Please note that two values of R_o are cited, measured on ulminite B and ulminite B (R_o ulminite-B / R_o ulminite-A), respectively, see text for discussion.

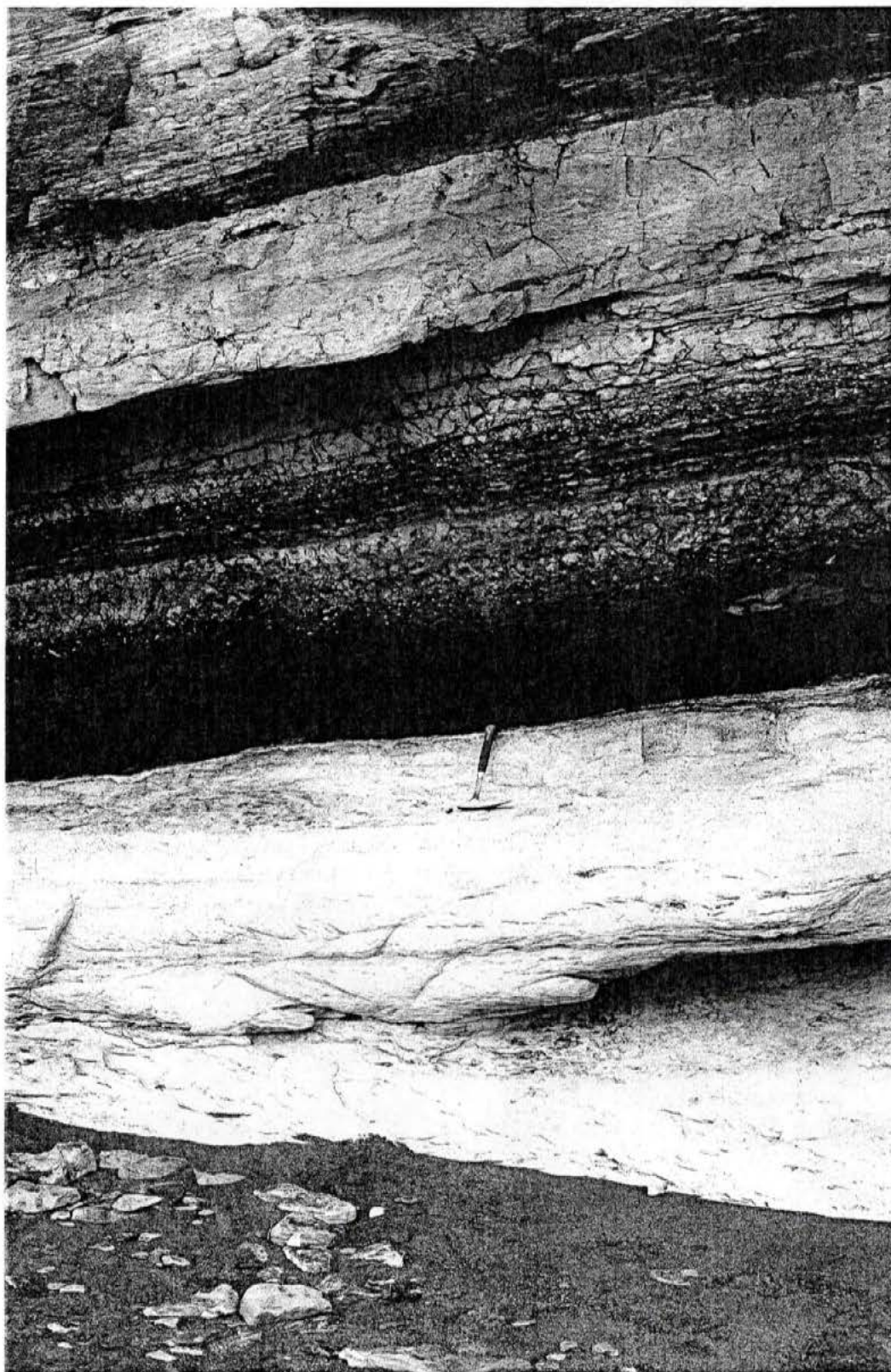
Table 4.

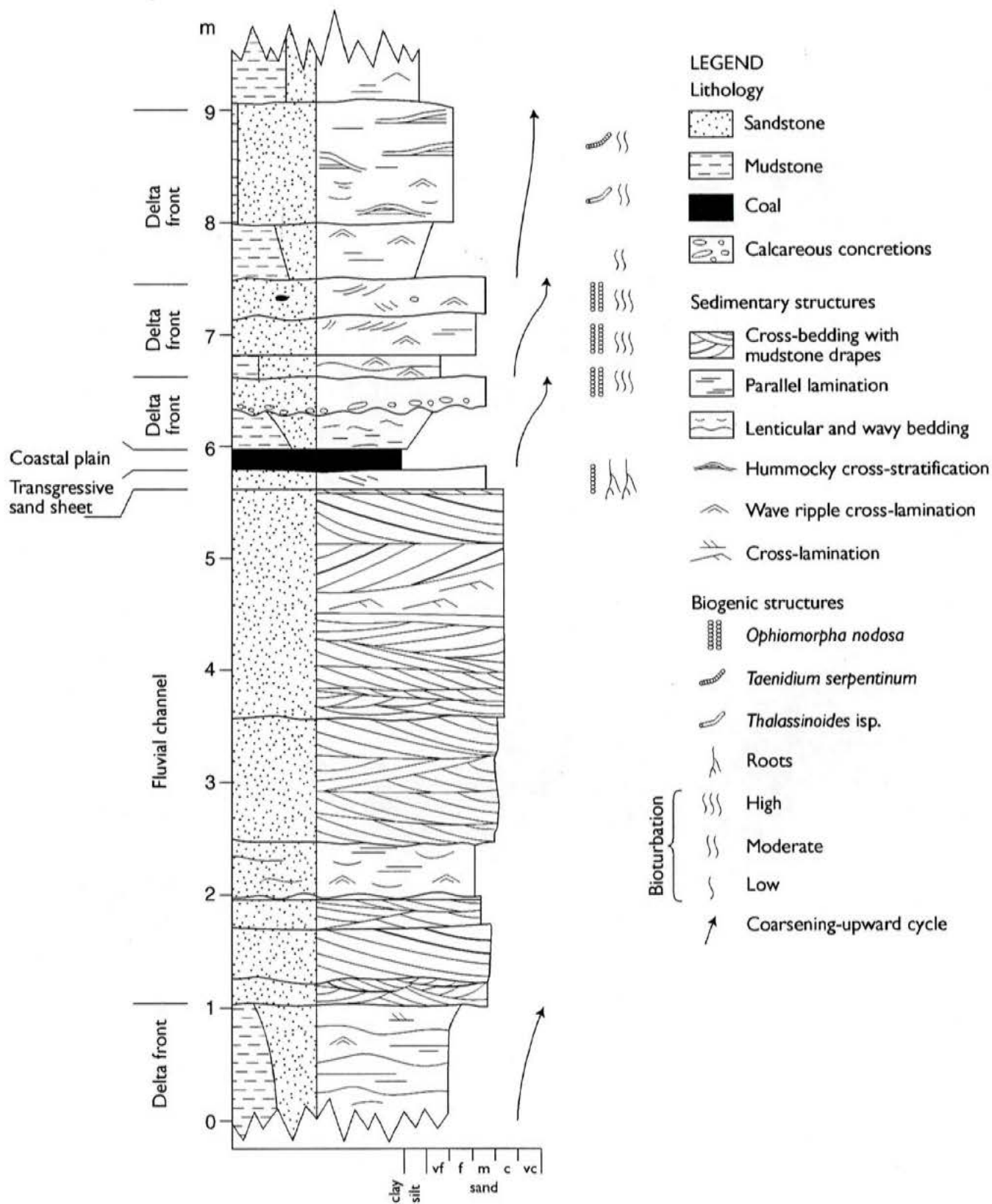
Compound identification for Fig. 7. Diterpanes m/z 123, triterpanes m/z 191.

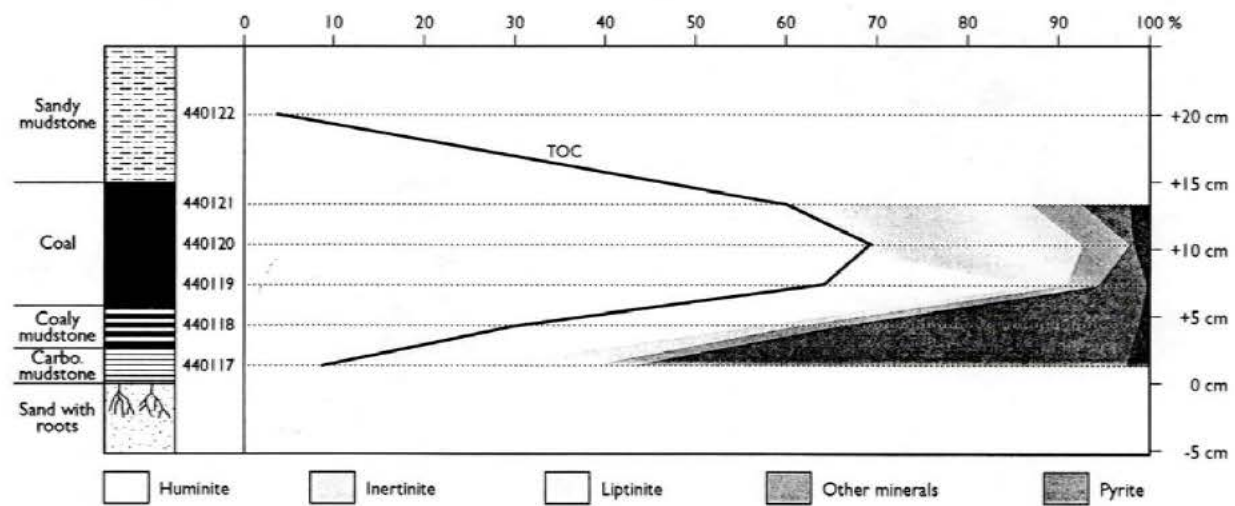
Unknown C_{29} triterpane coeluting with neohop-13(18)-ene may be identical to the C_{29} fernane tentatively identified by Paull et al. (1998)

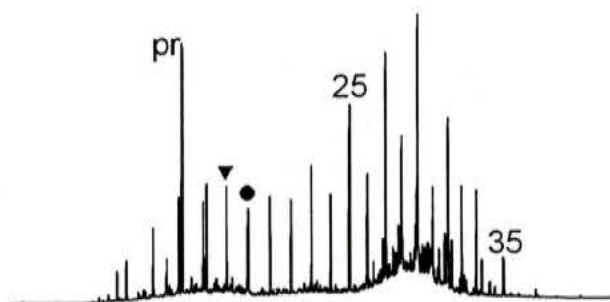












440122

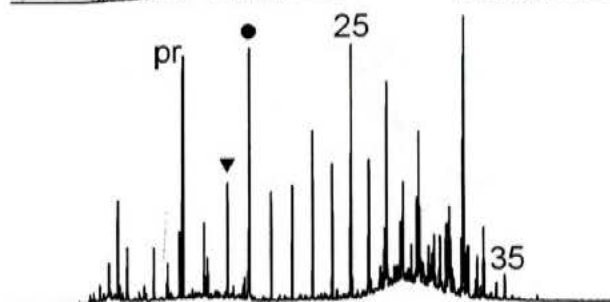
PR/PH = 2.59

I/NA = 1.38

CPI = 1.64

NIP/nC₁₉ = 0.04

PHYC/nC₂₀ = 0.72



440121

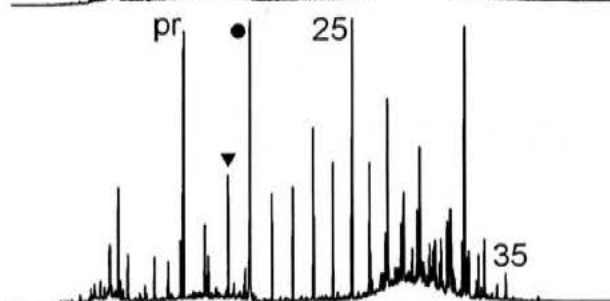
PR/PH = 6.59

I/NA = 0.81

CPI = 2.24

NIP/nC₁₉ = 0.04

PHYC/nC₂₀ = 2.88



440120

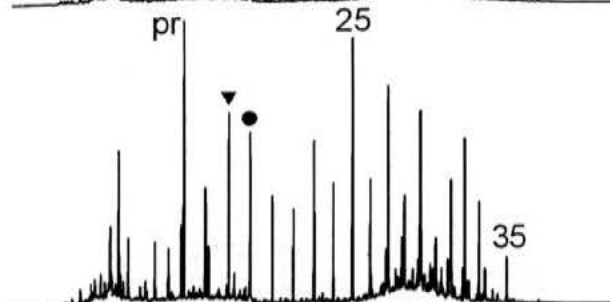
PR/PH = 6.38

I/NA = 0.76

CPI = 2.29

NIP/nC₁₉ = 0.04

PHYC/nC₂₀ = 4.07



440119

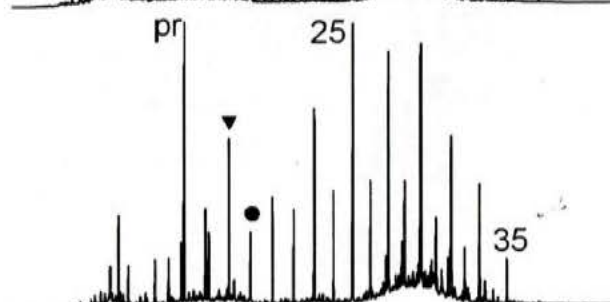
PR/PH = 6.87

I/NA = 1.05

CPI = 2.54

NIP/nC₁₉ = 0.04

PHYC/nC₂₀ = 1.53



440118

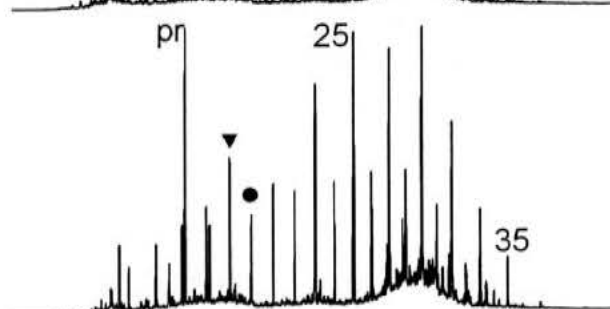
PR/PH = 5.32

I/NA = 1.29

CPI = 2.80

NIP/nC₁₉ = 0.05

PHYC/nC₂₀ = 0.37



440117

PR/PH = 4.35

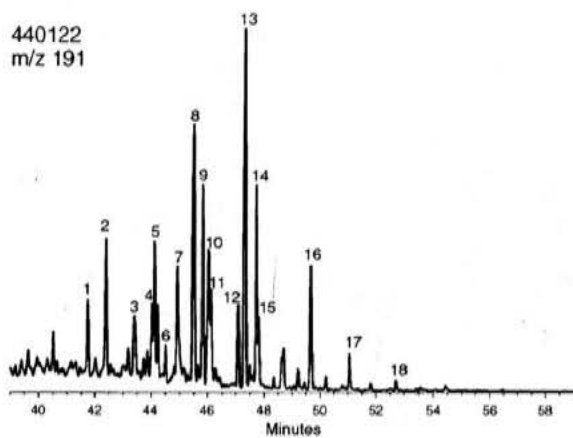
I/NA = 1.17

CPI = 3.97

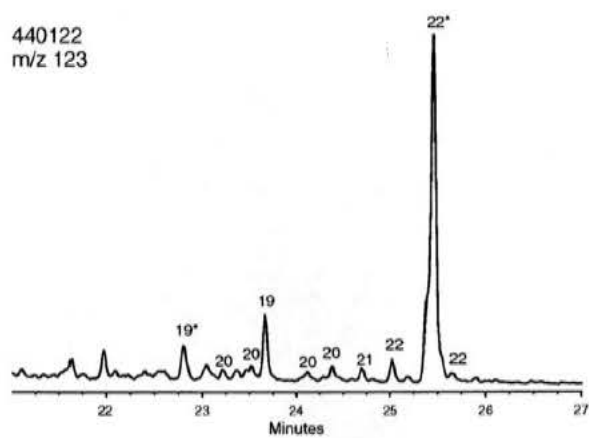
NIP/nC₁₉ = 0.06

PHYC/nC₂₀ = 0.22

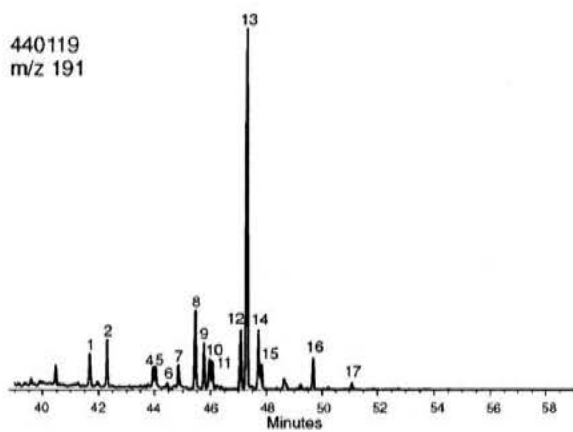
440122
m/z 191



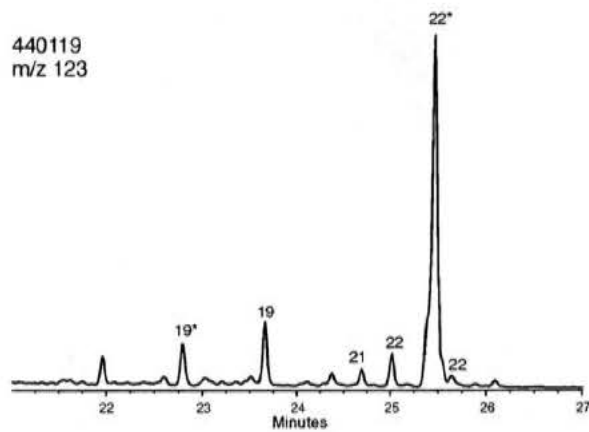
440122
m/z 123



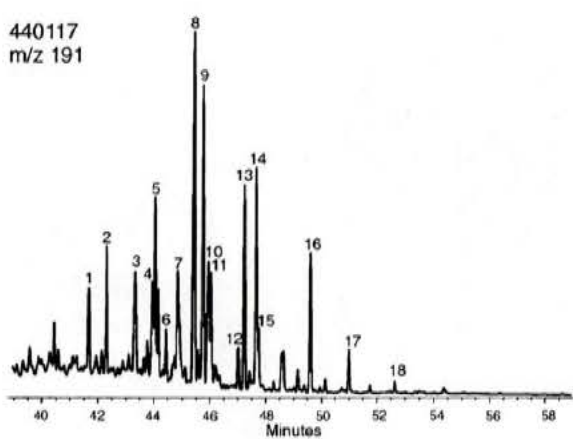
440119
m/z 191



440119
m/z 123



440117
m/z 191



440117
m/z 123

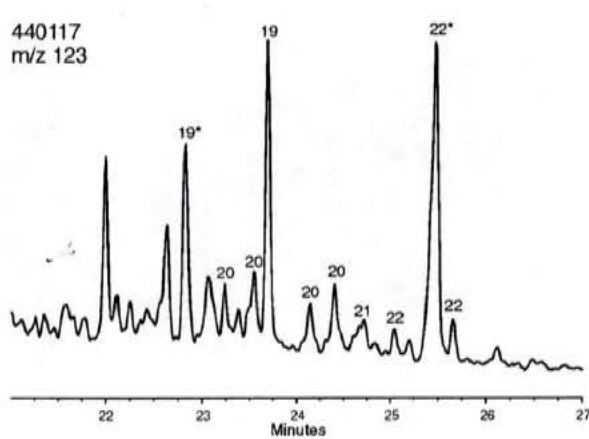


Table 1

Sample Number	Sample interval relative to datum (centimetres)	Lithology	Lithology interval relative to datum (centimetres)
no samples		Sandstone, brownish, chaotic, with abundant <i>Ophiomorpha nodosa</i> burrows	above c. 50 cm
440122	15-25	Sandy mudstone, brownish, upwards grading into burrowed sandstone	15-50
440121	12-15	Coal, bright, black	
440120	9-12	Coal, bright, black	
440119	6-9	Coal, bright, black	
440118	3-6	Coaly mudstone, black	
440117	0-3	Carbonaceous mudstone, brownish black, earthy	
no samples		Sandstone, faintly laminated. Upper c. 30 cm cm with abundant roots, up to 15 cm in length and up to c 0.3 cm in thickness	below datum

Table 2

Sample Number	Textinite	Textoulminite	Euulminite	Attrinite	Densinite	Porigelinite	Corpohuminite	Gelinite	Sporinite	Cutinite	Liptodetrinite	Resinite	Suberinite	Fusinite	Semifusinite	Inertodetrinite	Macrinite	Pyrite	Other minerals	Total
440121	0	0.6	9.8	0.8	28.6	0	0.2	1.6	1.8	0.6	3.2	0	0	5.2	3.8	32.4	4.0	2.2	5.2	100
440120	0	0.2	20.4	0	39.4	0.2	0.4	3.2	1	0.6	3.4	0	0	4.8	2.4	19.2	2.6	1.8	0.4	100
440119	0	2.4	48.4	0.4	22.0	0.8	3.0	10.2	0.2	2.4	0.6	0.2	0	0.2	0	3.2	0.4	0.2	5.4	100
440118	0.2	1.4	18.2	12.8	15.4	0	3.2	6.2	0.4	2.2	1.6	0.2	0	0	0	4.4	0	1.2	32.6	100
440117	0.75	0	6.25	9.25	8.0	0	0.5	1.75	2.75	1.25	1.25	0	0	0.5	0	10.0	1.5	2.5	54.75	100

Table 3

Sample Number	Sample interval relative to datum (centimetres)	TOC	TS	Tmax	S1	S2	HI	SI	R _o
440122	15-25	3.61	0.08	430	0.04	3.18	88	2.22	
440121	12-15	59.91	0.96	426	0.55	65.78	110	1.60	0.55/0.48
440120	9-12	69.18	0.81	425	1.13	86.20	125	1.17	
440119	6-9	64.18	0.69	427	0.40	80.68	126	1.07	0.55/0.48
440118	3-6	30.00	0.27	429	0.26	42.14	140	0.90	0.57/0.48
440117	0-3	8.52	0.12	434	0.05	8.38	98	1.41	

Table 4

Label	Compound
1	17 α (H)-trisnorhopane (Tm)
2	17 β (H)-trisnorhopane
3	28,30-bisnorhopane
4	30-norneohop-13(18)-ene
5	17 α (H),21 β (H)-30-norhopane
6	diahopane
7	17 β (H)21 α (H)-30-norhopane (normoretane)
8	17 α (H),21 β (H)-hopane
9	Neohop-13(18)-ene + unknown C29 triterpane ^a
10	17 β (H)21 β (H)-30-norhopane
11	17 β (H)21 α (H)-hopane (moretane)
12	17 α (H),21 β (H)-22S-homohopane
13	17 α (H),21 β (H)-22R-homohopane
14	17 β (H)21 β (H)-hopane
15	17 β (H)21 α (H)-homohopane (homomoretane)
16	17 β (H)21 β (H)-homohopane
17	17 β (H)21 β (H)-bishomohopane
18	17 β (H)21 β (H)-trishomohopane
19	isomers of norpimarane, 19* coelutes with nC ₁₉
20	isomers of norabietane
21	pimarane
22	isomers of phyllocladane, 21* coelutes with nC ₂₀

^a : See Paull et al. (1998)

Source Rock Evaluation of Middle Jurassic Coals, North-East Greenland, by Artificial Maturation: Aspects of Petroleum Generation from Coal

Henrik I. Petersen^{1,*}, Jørgen A. Bojesen-Koefoed and Hans P. Nytoft¹

¹Geological Survey of Denmark and Greenland, Thoravej 8, DK-2400 Copenhagen NV, Denmark

*corresponding author: Tel: +45 38142345; e-mail: hip@geus.dk

ACKNOWLEDGEMENTS

This study received financial support from the Danish Energy Research Programme (EFP-98), grant no. 1313/98-0022. T. C. R. Pulvertaft (GEUS) improved the English, and J. Halskov (GEUS) prepared the figures. This paper is published with the permission of the Geological Survey of Denmark and Greenland (GEUS).

ABSTRACT

Paralic liptinite-enriched coals and carbonaceous mudstones in North-East Greenland constitute potential highly oil-prone source rocks, whereas the humic coals may be marginal source rocks. The liptinite-rich coals are dominated by resinite or fluorescing amorphous organic matter and alginite, resulting in HI values generally above 300 and reaching up to 728. During artificial maturation up to 330°C/72h the coals follow the maturation paths of kerogen types I and II on a HI versus T_{\max} diagram, and calculations show that upon passage through the oil window roughly 85% of their generation potential will be realised. Activation energy (E_a) distributions with prominent principal E_a -values centred around 60–62 kcal/mole strongly influence the generation characteristics from 300°C/72h to 330°C/72h artificial maturation; important changes include: marked loss of liptinite fluorescence and increase in resinite reflectance; small change in T_{\max} ; significant decrease in HI; pronounced increase in extract yields; increased generation of saturates; generation of labile bitumen with low E_a -values. These observations indicate significant bitumen/petroleum formation from the coals

during a relatively narrow temperature range, which together with the petrographic composition may facilitate expulsion of a waxy crude oil. The coals demonstrate that under certain depositional conditions highly prolific coal source rocks can form with the capacity not only to generate but also to expel liquid petroleum.

INTRODUCTION

In the North Sea and the North Atlantic region the principal oil-generating source rock is generally accepted to be marine Upper Jurassic shales, i.e. Kimmeridge Clay Formation and equivalents. However, alternative, terrestrial-dominated source rocks are present in the region. These have been highlighted by evidence for contribution from the Middle Jurassic algal-rich Brora coals to the Beatrice oil field in the Inner Moray Firth area offshore Scotland (Peters et al., 1989), from Middle Jurassic lacustrine facies to the "Foinaven Complex" oils in the West of Shetlands area (Scotchman et al., 1998), and from the documented Middle Jurassic coal-generated petroleum in the Harald and Lulita fields in the Danish North Sea (Petersen et al., 1996, 1998a, 2000). In addition, the capability of coal-bearing and lacustrine strata to generate liquid petroleum is increasingly acknowledged worldwide due to discoveries, in particular in Asia and Australia, of hydrocarbon accumulations with typical terrestrial organic geochemical signatures.

East to North-East Greenland is an excellent area in which to study onshore source rocks which may have mature offshore equivalents in the North Atlantic region, and, in view of the above, the Middle Jurassic coal outcrops in North-East Greenland are of interest. Middle Jurassic coals are known from Kuhn Ø, Hochstetter Forland and Germania Land, and to the north, in Hertugen of Orleans Land, erratic coal blocks occur (Figure 1). The depositional environment and petrographic composition of the coals from Hochstetter Forland and Payer Dal on Kuhn Ø have attracted attention due to their unusual resinite-rich composition (Bojesen-Koefoed et al., 1996; Petersen et al., 1998b; Petersen and Vosgerau, 1999). These studies also indicated that mature equivalents of the coals could constitute prolific local source rocks with a significant potential to generate liquid petroleum.

This study aims to contribute to the recognition of alternative non-marine source rocks in the North Atlantic region by describing the petroleum generative potential of the coals from

Hochstetter Forland and Kuhn Ø, including hitherto unreported data from coals from a succession at Bastian Dal, Kuhn Ø, by (1) providing organic geochemical data of all samples, and (2) carrying out artificial maturation (hydrous pyrolysis) and activation energy distribution determinations of four selected samples. This has provided not only important information on the generation potential and characteristics of possible mature equivalents of the coals, but also adds to the understanding of the petroleum generative aspects of coal in general.

THE MIDDLE JURASSIC COALS ON HOCHSTETTER FORLAND AND KUHN Ø

The Middle Jurassic coal-bearing strata of Hochstetter Forland and Kuhn Ø belong to the Middle Jurassic Muslingebjerg Formation (Alsgaard et al., in press; Surlyk et al., in press). The coal-bearing succession of Hochstetter Forland is exposed in an isolated NW–SW oriented fault-block at the south-west coast of the peninsula (Figure 1). On Kuhn Ø approximately 40–50 km south of Hochstetter Forland the coals are exposed in Payer Dal and Bastian Dal (Figure 1). Despite complications caused by significant liptinite-induced suppression of huminite reflectance values, non-suppressed samples from both Kuhn Ø and Hochstetter Forland yield random huminite reflectance values of 0.49–0.53 %R_o (Petersen and Vosgerau, 1999), which conventionally imply thermal immaturity with respect to petroleum generation.

Kulhus, Hochstetter Forland

The coal-bearing Muslingebjerg Formation is exposed in the coastal cliff near Kulhus (Figure 1), and due to faulting the succession is repeated along the coast. The formation, which is estimated to be about 20 m thick at Kulhus, contains four coal seams (Figure 2). At present only seams 2, 3, and 4 are exposed and are 3.45 m, 1.15 m and 3.0 m thick respectively; a comprehensive description of the petrographic composition of these coal seams is given in Petersen et al. (1998b). Seam 1 (Joswa seam cf. H. Frebold) was recognised by Frebold (1932) but has not been exposed for many years and is therefore not included in the present study.

The coal-bearing Muslingebjerg Formation succession was deposited at the head of an embayment in the Jurassic Wollaston Forland rift basin of North-East Greenland during an overall Middle–Late Jurassic transgression which progressed from south to north (Surlyk, 1978, 1990; Surlyk and Clemmensen, 1983). The succession consists of a coastal plain facies association and a shoreface facies association with the coal seams belonging to the former facies association (Figure 2) (Clemmensen and Surlyk, 1976; Petersen et al., 1998b). The Muslingebjerg Formation succession is overlain by a tidal facies association. Accumulation of the precursor peats occurred in low-lying coastal mires and was governed by base-level rise linked to relative sea-level rise. The peat formation marks the onset of base-level rise, and in a sequence stratigraphic framework each coal seam represents the lower part of the transgressive systems tract (Petersen et al., 1998b). The coal seams contain organic facies (dulling-upward) cycles, and in general an organic facies cycle starts with bright or banded coal and ends with dull coal or carbonaceous mudstone. The dull coals are characterised by enrichment in liptinite, commonly resinite, which is a result of winnowing of huminitic components and concentration of liptinite during flooding. The carbonaceous mudstones may contain alginite and pyrite and may have high diasterane C_{27}/C_{29} ratios which suggest marine influence during drowning. Thus, the liptinite-enriched organic facies cycles record repeated outpacing of peat accumulation by watertable rises or inundations (Petersen et al., 1998b). In terms of sequence stratigraphy the coal facies cycles probably represent parasequences separated by lacustrine or marine-influenced flooding surfaces. These depositional conditions have resulted in a complex petrographic composition of the coals spanning from bright and banded coals with huminite contents >60 vol.% (mineral matter free, m.m.f.) to dull coals characterised by ca. 25–50 vol.% (m.m.f.) liptinite of which the majority is resinite (Petersen et al., 1998b) (Figure 3a).

Payer Dal and Bastian Dal, Kuhn Ø

The coal-bearing strata of the Muslingebjerg Formation in Bastian Dal and Payer Dal (Figure 1) on Kuhn Ø are less wellknown than the succession at Kulhus, Hochstetter Forland, since the coals on Kuhn Ø have only recently been sampled, and the coal-bearing outcrop in Bastian Dal was only discovered during fieldwork in 1994. The Bastian Dal outcrop contains

three coal seams, approximately 1.0–1.5 m thick, partially interbedded with fluvial deposits (Alsgaard et al., in press). In Payer Dal locally up to about 0.15 m thick coal overlies thin fluvial deposits or weathered crystalline basement. The coal samples from Payer Dal are highly enriched in liptinite (ca. 50–85 vol.%, m.m.f.), in particular resinite (ca. 30–70 vol.%, m.m.f.), and are petrographically comparable to the dull coal facies of the coals at Kulhus, Hochstetter Forland (Petersen and Vosgerau, 1999) (Figure 3b). The coals outcropping in Bastian Dal have only recently been sampled and analysed. These coals differ significantly from those from Payer Dal by containing generally less than 10 vol.% (m.m.f.) liptinite of which the major part is liptodetrinite (Figure 3b). Three samples contain considerably more liptinite, and again it is resinite which is dominant. Generally the coals contain >60 vol.% (m.m.f.) huminite and a large proportion of inertinite (up to 55 vol.%, m.m.f.) (Figure 3b).

ANALYTICAL METHODS

Total organic carbon (TOC) determination of a total of 132 samples was carried out on a Leco IR-212 or Leco CS-200 induction furnace. In addition the total sulphur (TS) content of the samples from Bastian Dal was determined using a Leco CS-200 induction furnace. Rock-Eval II or Rock-Eval 5 equipment was used for Rock-Eval pyrolysis of the samples.

The Rock-Eval 5 instrument was also used for determination of activation energy distributions (E_a) and pre-exponential factors (A) (Optkin software) of four selected samples. These four samples were subjected to hydrous pyrolysis in stainless steel HPLC columns filled with 0.7–1.0 g of ground sample mixed with water and thoroughly stirred to remove any air. The sealed columns were heated for 72 hrs at 240°C, 270°C, 300°C and 330°C. The hydrous-pyrolysed samples were subjected to TOC determination, Rock-Eval pyrolysis (including determination of E_a), solvent extraction followed by gas chromatography (GC) analysis of the saturate fractions, microscopic examination, and reflectance measurements on resinite and vitrinite.

Solvent extraction and separation of asphaltene-free extracts into saturated, aromatic and heteroatomic compounds was carried out by medium performance liquid chromatography (MPLC). GC analysis of the saturate fractions was performed on a Hewlett Packard 5890 gas chromatograph fitted with a 25 m HP-1 WCOT column and FID. The microscopic

examination of polished blocks was carried out in reflected white and blue light using a Zeiss incident light microscope, whereas the reflectance measurements were carried out using a Leitz MPV-SP system.

RESULTS

Rock-Eval screening of outcrop samples

The Hydrogen Index (HI) of samples from Kulhus, Hochstetter Forland, show a wide range of values from 87 to 728 (Figure 4a). However, the majority of the HI values are greater than 300 and a significant population can be defined within HI values of 260 and 480 (Figure 4a). The thermally extracted and generated hydrocarbons, S_1 and S_2 , range from 0.14 to 12.90 mg HC/g rock and 6.25 to 402.41 mg HC/g rock, respectively. However, about 68% of the samples yield S_2 amounts above 200 mg HC/ g rock.

The four resinite-rich coal samples from Payer Dal, Kuhn Ø, yield likewise high HI values, from 354 to 454 (Figure 4b). The S_1 and S_2 yields range from 6.25 to 10.97 mg HC/g rock and 224.68 to 286.62 mg HC/g rock, respectively. This contrasts with the HI values obtained from the coals from Bastian Dal, which only in a single case exceed 300. The major part of the HI values are within the range of 30 to 240 (Figure 4b). S_1 and S_2 yields are likewise lower: 18 to 3.98 mg HC/g rock and 3.22 to 211.38 mg HC/g rock, respectively. About 60% of the S_2 values are below 80 mg HC/g rock.

Hydrous pyrolysis (artificial maturation)

Four samples were selected for artificial maturation experiments, 071 and 144 from Kulhus, Hochstetter Forland, and C-8 and C-20 from Payer Dal, Kuhn Ø. The samples represent different facies of the coal seams. All samples are nearly free of inertinite and contain only limited amounts of huminite (Table 1). Samples 071 and 144 are rich in mineral matter, and 071 particularly in intimately associated fluorescing detrital liptinite and amorphous organic matter and mineral matter (Table 1). The TOC values are correspondingly low. Sample 071 has a relatively low content of well-defined liptinite macerals and in particular resinite,

whereas sample 144 contains much more well-defined liptinite, including significant proportions of both resinite and alginite. The two raw samples have HI values above 600. Samples C-8 and C-20 are extraordinarily liptinite-rich and mineral-poor, and accordingly have higher TOC values (Table 1). The liptinite is dominated by very high proportions of resinite. The HI values for these two raw samples are above 400.

Rock-Eval screening

Sample 071 follows the kerogen type II maturation path on the HI versus T_{\max} diagram (Figure 5a). After hydrous pyrolysis at 330°C/72h T_{\max} has increased from initial 427°C to 443°C and HI has decreased from initial 621 to 223. Extracted samples have in general higher T_{\max} values and much lower HI values (Figure 5a). During artificial maturation S_1 yields increase from initial 2.89 mg HC/g rock to 51.63 mg HC/g rock at 330°C/72h, whereas S_2 yields decrease from initial 182.01 mg HC/g rock to 59.80 mg HC/g rock at 330°C/72h (Table 2). S_2 values for extracted samples are significantly lower than the non-extracted counterparts (Table 2).

Sample 144 follows the maturation path of kerogen type I on the HI versus T_{\max} diagram (Figure 5b). The T_{\max} value increases from initial 426°C to 441°C after hydrous pyrolysis at 330°C/72h, but the change in T_{\max} of the samples hydrous-pyrolysed at 300°C/72h and 330°C/72h is insignificant. The HI decreases from initial 626 to 397 during hydrous pyrolysis. The samples hydrous-pyrolysed at 240°C/72h, 270°C/72h and 300°C/72h show higher HI values after extraction than the non-extracted counterparts, whereas the extracted sample hydrous-pyrolysed at 330°C/72h has a higher T_{\max} value and a significantly lower HI value (Figure 5b). There is an approximately 10-fold increase in the S_1 yield to 43.46 mg HC/g rock after hydrous pyrolysis at 330°C/72h and an associated decrease in S_2 yield from initial 143.33 mg HC/g rock to 62.54 mg HC/g rock (Table 2). Solvent-extracted samples yield lower S_2 values (Table 2).

Samples C-8 and C-20 follow a maturation path somewhere between kerogen types I and II (Figures 5c, d). Both samples (non-extracted) show a considerable increase in the HI values from the raw samples to the samples hydrous-pyrolysed at 270°C/72h, followed by a decrease.

During artificial maturation T_{\max} for sample C-8 increases from initial 428°C to 445°C after hydrous pyrolysis at 330°C/72h, whereas the HI actually shows a small increase from initial 402 to 427 at 330°C/72h. However, the extracted samples yield higher T_{\max} values and, in particular the sample hydrous-pyrolysed at 330°C/72h, significantly lower HI values (Figure 5c). S_1 shows an approximately 10-fold increase to 106.05 mg HC/g rock at a hydrous pyrolysis temperature of 330°C/72h, whereas S_2 increases to a maximum of 332.02 mg HC/g rock at 270°C/72h before it decreases to 270.38 mg HC/g rock (Table 2). S_2 values of extracted samples are initially higher than the non-extracted counterparts, but at the highest hydrous pyrolysis temperatures they are considerably lower (Table 2).

Sample C-20 shows an increase in T_{\max} from initial 421°C to 441°C after hydrous pyrolysis at 330°C/72h, but the change in T_{\max} between the two last hydrous pyrolysis steps is small (Figure 5d). The HI shows a significant initial increase from 454 of the raw sample to 632 after hydrous pyrolysis at 270°C/72h, followed by a decrease which is particularly pronounced for the last hydrous pyrolysis step (Figure 5d). Solvent extracted samples display lower HI values and similar or higher T_{\max} values. The S_1 yield shows a steady increase during artificial maturation to 134.36 mg HC/g rock at 330°C/72h, whereas S_2 increases to a maximum of 355.92 mg HC/g rock at 240°C/72h before it decreases to 241.72 mg HC/g rock (Table 2).

Petrographic changes

Qualitative microscopic examination of the hydrous-pyrolysed samples revealed a significant change with regard to fluorescence intensity of the organic matter with increasing temperature. From the outcrop samples to a hydrous pyrolysis temperature of 270°C/72h the change in fluorescence intensity is small. However, at 300°C/72h the fluorescence intensity of alginite, amorphous groundmass and resinite decreases markedly, and at 330°C/72h fluorescence is only just visible. In sample 144 the very dark, fluorescing amorphous groundmass in the outcrop sample has become grey at 330°C/72h, and fluorescing 'bubbles' together with exsudatinite/bitumen are observed in fractures. Resinite has become greyish and appears similar to vitrinite (Figure 6). Reflectance measurements on resinite in sample C-20 show a significant increase from an mean random reflectance of 0.06 % R_{resinite} for the outcrop sample to 0.21 % R_{resinite} after hydrous pyrolysis at 300°C/72h and to 0.59 % R_{resinite} after

hydrous pyrolysis at 330°C/72h (Figure 7). Reflectance measurements on two presumed vitrinite particles in the sample hydrous-pyrolysed at 330°C/72h both yield mean values of 1.11 %R_{vitrinite} (Figure 7).

Extract yields and composition

The yields of solvent extractable organic matter increase with increasing hydrous pyrolysis temperature, with a significant increase observed around 300°C/72h (Figure 8). Maltene fractions show a clear change in the relative distribution of aromatics, saturates, and NSO-compounds with increasing hydrous pyrolysis temperature, comprising an increase in the proportion of hydrocarbons, in particular of saturates, at the expense of heteroatomic moieties (Figure 9).

Gas chromatograms of the saturate fractions from the samples subjected to hydrous pyrolysis at 330°C/72h are shown in Figure 10. Samples 071 and 144 show very similar characteristics, comprising broad, slightly light-end skewed normal alkane distributions, with *n*-alkanes decreasing in abundance with increasing carbon number along a distinctly convex-up trend (Figure 10). The *n*-alkanes extend to at least *n*C₃₇. A slight odd-number predominance is observed in the *n*C₂₂₊ range, and minor enhancement of *n*C₁₅, *n*C₁₇, and perhaps *n*C₁₉ can be detected. Normal alkanes constitute the dominant component class, whereas acyclic isoprenoids, sesqui- and diterpanes and alkylcyclohexanes are scarce. “Unresolved Complex Mixture” (UCM) is negligible. The pristane/phytane (pr/ph) ratios are moderate, 2–4.

Samples C-8 and C-20 are characterised by rather irregular *n*-alkane distributions, which may be light-end skewed (C-20) or more or less bimodal (C-8) (Figure 10). Both samples show enhancement of *n*C₁₅, *n*C₁₇ and *n*C₁₉, whereas odd-number predominance in the *n*C₂₂₊ range only prevails in sample C-8. The proportions of acyclic isoprenoids relative to normal alkanes are moderate, although sample C-8 shows very high concentration of pristane, and consequently a very high pr/ph ratio (Figure 10). Sample C-8 shows the presence of moderate proportions of alkylcyclohexanes and methyl-alkylcyclohexanes (see also Bojesen-Koefoed et al., 1996), whereas these components are less prominent in sample C-20. In addition, in the *n*C_{18–20} range, a number of unknown peaks are present, which are tentatively assigned to

various tri- and tetracyclic diterpanes of the pimarane and phyllocladane series. These components are particularly prominent in sample C-8. The UCM is low for both samples.

Although notable differences exist between the compositions of hydrous pyrolysates of the four samples, they share a number of features, including the prominence of waxy *n*-alkanes (nC_{22+}), moderate to high pr/ph ratios, slight enhancement of nC_{15} , nC_{17} , and perhaps nC_{19} , and overall low to moderate proportions of acyclic isoprenoids, except perhaps for pristane.

Activation energy distributions

The activation energy (E_a) distributions of the raw samples are centred around prominent principal E_a -values of 60 kcal/mole (samples 144 and C-8) and 62 kcal/mole (samples 071 and C-20) (Figure 11). The E_a -distributions are broad, extending from 40 kcal/mole to 80 kcal/mole, but with the primary activation energies ranging from 50 kcal/mole to approximately 72 kcal/mole. The pre-exponential factors (A) range from $A = 5.855 \cdot 10^{15} \text{ s}^{-1}$ to $A = 3.249 \cdot 10^{16} \text{ s}^{-1}$ (Figure 11).

After hydrous pyrolysis the samples hydrous-pyrolysed at 300°C/72h have broad E_a -distributions with an apron of low activation energies between 44 kcal/mole and 50 kcal/mole (Figure 12). The principal E_a -values and the A factors have decreased. However, solvent extraction of the hydrous-pyrolysed samples result in a near total elimination of the low activation energies and (except for sample C-20) an increase in the principal E_a -value (Figure 12). At the highest hydrous pyrolysis temperature (330°C/72h) the solvent extracted samples have principal E_a -values of 60 kcal/mole and 62 kcal/mole, but the magnitude of the principal E_a -values has diminished significantly (Figure 12). In addition, the samples have a pronounced tail of activation energies above 66 kcal/mole.

DISCUSSION

Source rock potential

The coals from Kulhus, Hochstetter Forland, and Payer Dal, Kuhn Ø, are enriched in hydrogen-rich components, which have a profound influence on the HI values. At Kulhus frequent flooding of the precursor peats caused by relative sea-level-linked base-level rises in

the paralic depositional setting resulted in the formation of the unique coal source rocks (Petersen et al., 1998b). The concentration of hydrogen-rich components towards the top of the organic facies cycles is associated with an increase in HI, and a correlation exists between the coal facies type and the HI values (Petersen et al., 1998b). The highest HI values are derived from the resinite-rich dull coals (up to HI = 673) and carbonaceous mudstones (up to 728), which also have the highest average HI values of 464 and 459, respectively. The more huminite-rich bright and banded coals yield HI values up 541 and average values of 364 and 375; respectively. Altogether, a majority of HI values above 300 and values reaching up to 728 for the coals and carbonaceous mudstones from Kulhus indicate a very good to excellent potential for petroleum generation (Figure 4a). Combined with a cumulative coal seam thickness of minimum 7.6 m at Kulhus this suggests that, if thermally mature, the coals could constitute a very attractive, local source rock. This also applies to the samples from Payer Dal about 40–50 km south of Kulhus (Figures 1, 4b), although the total potential is restricted by a seam thickness of only 0.15 m. The formation of this prolific coal source rock is not understood at present. However, marine influence on coastal mires is known to enhance the source rock potential of the resulting coals, as for example demonstrated for the coals at Kulhus. Another example is the Middle Jurassic coals of the Bryne Formation in the Danish part of the North Sea, where a landward–seaward transect relative to the palaeoshoreline of the coal seams reveals that the low-lying, coastal reaches of the seams provide the best source rock (Petersen et al., 1996, 1998a, 2000).

In general the high HI values of the Kulhus and Payer Dal coals are related to the high content of liptinite macerals and in particular resinite, which corresponds to kerogen type II (Figures 3a, b). Two examples of such very resinite-rich coals (“dull coal facies”) are samples C-8 and C-20 (Table 1), both of which have been subjected to hydrous pyrolysis. In some cases very high HI values can be attributed to the presence of alginite and intimately associated fluorescing detrital liptinite and amorphous organic matter and mineral matter. Alginite with a morphology similar to the extant freshwater/brackish alga *Botryococcus* occurs in carbonaceous mudstones at the top of the coal facies cycles in the coals of Kulhus (Petersen et al., 1998b). This alginite corresponds to kerogen type I which has an excellent generative potential. The hydrous-pyrolysed sample 144 is an example of such a carbonaceous mudstone with alginite. The fluorescing amorphous organic matter may in part be derived

from degraded algal material, as recognisable alginite with *Botryococcus* morphology has been observed together with the amorphous organic material. Sample 071, used for hydrous pyrolysis, is an example of a coal with a high content of amorphous organic matter.

The coals from Bastian Dal, Kuhn Ø, have considerably lower HI, S₁ and S₂ values as could be expected from their significantly lower content of hydrogen-rich constituents (Figure 3b). Despite this the Bastian Dal coals cannot be disregarded as a source for petroleum although they may only represent a marginal source rock type. The petroleum potential of immature coals rich in humic organic matter (huminite) may be underestimated due to suppression of the HI by initial release of abundant oxygen groups from the coal matrix (Boudou et al., 1994). Middle Jurassic coals from the Søgne Basin, Danish North Sea, are vitrinite- and inertinite-rich and liptinite-poor (generally <5 vol.%), which conventionally would classify them as poor source rocks. Nevertheless, these coals are the source for the petroleum accumulations in the Harald and Lulita fields (e.g. Petersen et al., 1996, 1998a, 2000). A multivariate statistical evaluation of the correlation between the generative potential of these coals and their petrography, and another similar study based on 27 humic coals of varying composition, rank, age and origin (Petersen and Rosenberg, 2000) indicate that the maceral collotelinite is very important for the petroleum potential. Collotelinite is the hard coal equivalent to eu-ulminite in brown coals, and it is thus notable that the Bastian Dal coals can contain considerable proportions of this maceral (up to 56 vol.%). In addition, total sulphur (TS) data show that the TS content of the coals is rather high, ranging from 0.32 wt.% to 7.92 wt.% and averaging 2.60 wt.%, whereas the pyrite content varies between nil and only 0.6 vol.%, averaging 0.2 vol.%. This could suggest that much of the sulphur is organically bound, which may result in more thermally labile (lower activation energies) organic matter due to weak C-S bonds (e.g. Tissot et al., 1987; Tegelaar and Noble, 1994; Pepper and Corvi, 1995).

Baskin (1997) has devised a method for estimating the degree of organic matter (kerogen) conversion based on H/C ratios. It is assumed that wt.% carbon loss of kerogen during hydrocarbon formation can be calculated by assuming a continuous depletion of hydrogen and carbon in proportions equivalent to those found in typical hydrocarbon products. Thus during liquid hydrocarbon generation this proportion is equivalent to typical oils, in which the H/C ratio is about 1.85. During a full maturation process, i.e. at the end of dry-gas generation

(approximately 3.5% R_o), kerogen type I loses 80–85% of its organic carbon, kerogen type II 45–60% of its organic carbon and kerogen type III 10–20% of its organic carbon. Based on these considerations Baskin (1997) constructed curves illustrating wt.% carbon loss against the H/C ratio for typical kerogen types (figure 5 in Baskin, 1997). The H/C ratio of the initial immature kerogen is thus essential as the amount of conversion is approximated by dividing the actual carbon loss by the maximum carbon loss at full maturity. The H/C of a coal or kerogen can be estimated from the distribution of the maceral groups and a Van Krevelen diagram. An attempt has been made to give a rough estimate of the amount of hydrocarbons that would be generated from samples C-20 and 144 if they passed through the oil window (for convenience defined between 0.5% R_o and 1.3% R_o), using the method described above. The non-suppressed huminite reflectance of the coals is about 0.50% R_o (Petersen and Vosgerau, 1999). Thus, from Table 1 the maceral distribution of sample C-20 gives an estimated H/C ratio of 1.20 (Figure 13a). Assuming the fluorescing amorphous organic matter corresponds mainly to kerogen type I, a similar calculation for sample 144 gives an estimated H/C ratio of 1.17 (Figure 13b). Both these H/C ratios correspond to a kerogen type II. Maturation of the samples until the end of the oil window results in H/C ratios of approximately 0.85 for C-20 and 0.80 for sample 144 (Figure 13). According to the carbon loss curves of Baskin (1997) both samples would roughly have realised 85% of their generative potential at the end of the oil window, indicating that these coals to a large extent are highly oil-prone.

Generation characteristics

The loss of fluorescence observed during artificial maturation is well known from liptinite macerals naturally matured in nature (e.g. Taylor et al., 1998). Contemporaneous with the loss of fluorescence a 10-fold increase in the mean reflectance of resinite is seen from the outcrop sample (C-20) to the highest hydrous pyrolysis temperature (Figure 7). The difference in fluorescence intensity between the outcrop samples and the samples subjected to hydrous pyrolysis at 270°C/72h is minimal, whereas loss of fluorescence is observed at 300°C/72h. At 300°C/72h the mean resinite reflectance has increased to 0.21 % R_{resinite} (Figure 7), which approximately corresponds to a vitrinite reflectance of 0.75 % $R_{\text{vitrinite}}$ (Bustin et al., 1985). This

coincides with a significant increase in extract yields and a considerable drop in the HI (see below). This situation may represent an analogy to the so-called 'second coalification jump' of sporinite (0.8–1.0 % $R_{\text{vitrinite}}$), where maximum petroleum generation occurs from this maceral (Teichmüller, 1989), and to hydrocarbon generation and entrapment at the bituminisation coalification stage of Levine (1993). The mean reflectance of 0.59 % R_{resinite} at 330°C/72h corresponds to a vitrinite reflectance of approximately 1.1 % $R_{\text{vitrinite}}$ (Bustin et al., 1985), which is consistent with the measured vitrinite reflectance values of 1.11 % $R_{\text{vitrinite}}$. The reflectance values thus suggest that, in terms of thermal maturity after hydrous pyrolysis at 330°C/72h, the coals are well within the oil window. This is also consistent with the very weak to absent liptinite fluorescence at this pyrolysis temperature. The samples subjected to hydrous pyrolysis at 330°C/72h yield T_{max} values between 441°C and 445°C which corresponds to a vitrinite reflectance of approximately 0.85% R_o . This is in conflict with the observed loss of liptinite fluorescence and the measured reflectance value of vitrinite at the highest hydrous pyrolysis temperature. However, for samples 144 and C-20 the change in T_{max} between the last two hydrous pyrolysis steps is insignificant, and for sample 071 the change in T_{max} is small, which may be linked to the E_a -distributions of these samples. A narrow E_a -distribution typically results in a minor change of T_{max} during maturation (Tissot et al., 1987). The samples have relatively broad E_a -distributions which reflect the heterogeneous composition of the organic matter shown by the samples petrography (Table 1); in addition Tegelaar and Noble (1994) have shown that gymnosperm-derived diterpenoid resinite has broad E_a -distributions. However, despite the relatively broad E_a -distributions, prominent principal E_a -values, which is related to the dominance of specific kerogen type I and II entities in the samples, may be responsible for the very small observed change in T_{max} .

The increase in HI of samples C-8 and C-20 during hydrous pyrolysis may be caused by the suppression of the initial HI by release of abundant oxygen groups, which makes determination of HI of immature coals uncertain (Figures 5c, d). Loss of oxygen-bearing compounds would also result in an increase in S_2 yields due to a relative enrichment of hydrogen-rich constituents (Levine, 1993). A significant drop in the HI value is observed from 300°C/72h to 330°C/72h in samples 071, 144 and C-20, whereas C-8 shows a significant drop from 270°C/72h to 300°C/72h. This is consistent with the small changes in T_{max} already discussed, which together with the significant increase in extract yields (Figure 8) indicate

extensive petroleum (bitumen) generation. It also agrees with the maximum exsudatinitite formation from resinite between 280°C/72h and 290°C/72h hydrous pyrolysis temperatures demonstrated in a lignite from the Far East (Teerman and Hwang, 1991).

A comparison of the non-extracted and extracted hydrous-pyrolysed samples on the HI versus T_{\max} diagrams shows that generated bitumen influences the T_{\max} and HI values, in particular by increasing the HI values (Figures 5a–d). The E_a distributions of non-extracted and extracted samples subjected to hydrous pyrolysis at 300°C/72h clearly show that generated comparatively labile bitumen with activation energies between 44 kcal/mole and 50 kcal/mole has been trapped in the coals (Figure 12). Removal of the labile bitumen by solvent extraction results in a shift towards a higher principal E_a -value and pre-exponential factor. This is particularly evident in the samples subjected to hydrous pyrolysis at 330°C/72h, where a considerable petroleum/bitumen generation has occurred. The shift in the principal E_a -value is caused by depletion in kerogen components of lower activation energies during maturation, an evolution wellknown from naturally matured coal series up to a vitrinite reflectance of 1.70% R_o (Schenk and Horsfield, 1998; Petersen and Rosenberg, 2000).

Expulsion considerations

The unusual composition of the coals from Kulhus and Payer Dal is favourable for petroleum expulsion. The observations on bitumen generation are consistent with the work of Lewan (1994), who carried out hydrous pyrolysis of kerogen type II and demonstrated that up to 330°C/72h mainly high molecular weight bitumen is generated. The considerable bitumen formation will saturate the coal matrix and create a continuous network (Lewan, 1994), which may facilitate expulsion. Horsfield et al. (1988), for example, considered the saturating effect of in particular resinite to be essential for petroleum expulsion from the Talang Akar coals in the Adjuna Basin of north-west Java. Several studies have shown that the bitumen/petroleum generation from resinite starts at low maturities (approximately between 0.40% $R_{\text{vitrinite}}$ and 0.60% $R_{\text{vitrinite}}$) (Snowdon and Powell, 1982; Shanmugam, 1985; Khorasani, 1987), and this is supported by artificial maturation of resin/resinite and of ‘Cyrilla facies’ peat containing resin globes from the Okefenokee Swamp of Georgia (Stout, 1995; Cohen and Bailey, 1997). This suggests that saturation of the resinite-rich coals may be accomplished relatively rapidly,

leading to an early incipient expulsion of petroleum. Furthermore, Bojesen-Koefoed et al. (1996) state that up to 50% of some of the resinite-rich coals from Kulhus is converted to petroleum, which will significantly change the micropore system of the coals and limit the adsorptive capacity.

Lewan (1994) showed that not until above a hydrous pyrolysis temperature of 330°C/72h does *primary* oil generation start by partial decomposition of bitumen. Similarly Teerman and Hwang (1991) showed that *maximum* oil-pyrolysate generation and expulsion from a resinite-rich Far East lignite occurs at or above a hydrous pyrolysis temperature of 360°C/72h, which is 70–90°C above maximum bitumen formation. These indications of a late, considerable hydrocarbon formation may be supported by the composition of the solvent extracts from the samples subjected to hydrous pyrolysis which show a significant increase in saturates from a temperature of 300°C/72h to 330°C/72h (Figure 9). Likewise, Killips et al. (1998) noted that expulsion of paraffinic oil from vitrinite-rich coals occurs up to a vitrinite reflectance of approximately 1.1% $R_{\text{vitrinite}}$. The late primary petroleum formation and expulsion from the coals contrasts to some extent with the concept of Levine (1993), according to whom coals enter the debituminisation stage of coalification at the thermal maturity attained after hydrous pyrolysis at 330°C/72h (about 1.11% $R_{\text{vitrinite}}$). Levine (1993) assumed that most generated petroleum is trapped in the coal and first released as light hydrocarbons (gas) due to cracking during the stage of debituminisation. However, this generalisation seems to be too simplistic for coal source rocks, and could result in potential petroleum-producing areas being overlooked.

It is notable that the saturate-to-aromatic ratio decreases with increasing resinite content (Figure 9); the aromatic compounds are derived from resinite and may for example be alkyl naphthalenes and tricyclic diterpanes such as retene (e.g. Teerman and Hwang, 1991; Bojesen-Koefoed et al., 1996). However, despite the pronounced generation of aromatic compounds, Bojesen-Koefoed et al. (1996) showed by pyrolysis-gas chromatography that the coals from Kulhus are able to generate *n*-alkanes ranging up nC_{32} or more. According to Isaksen et al. (1998) long-chain *n*-alkanes are preferentially expelled from the coal matrix when excess of *n*-alkanes disturbs the equilibrium conditions of the generated petroleum constituents in the coal. In fact Teerman and Hwang (1991) showed that about 50% of the oil-pyrolysate derived from a liptinite-rich Far East lignite originated from the resinite.

Despite the differences in hydrous pyrolysate compositions of the four samples demonstrated herein, petroleum generated and expelled from coals and carbonaceous mudstones similar to those found at Payer Dal and Kulhus will share a number of characteristics. Whereas the composition of 'early oils', arising from early petroleum generation from resinite (e.g. Snowdon and Powell, 1982; Khorasani, 1987; Stout, 1995; Cohen and Bailey, 1997), can be expected to be strongly influenced by the high proportion of resinite in the coals, the effects of generation and expulsion combine at higher levels of maturity to produce mature oils of more uniform composition. Masking of the initial 'naphthenic' character of early resinite-generated oils by later generated *n*-alkanes, combined with preferential expulsion of such components (Isaksen et al., 1998), will result in petroleum compositions characterised by high HC/non-HC ratios, moderate to high saturate-to-aromatic ratios, high contents of waxy *n*-alkanes, high pr/ph ratios, and presence of a number of resinite related tri- and tetracyclic diterpanes (pimaranes, abietanes, phyllocladanes) and their aromatic counterparts (e.g. retene, methyl-phenanthrene), and perhaps also notable proportions of alkylcyclohexanes and methyl-alkylcyclohexanes (see also Bojesen-Koefoed et al., 1996 and references therein).

The petrographically more 'normal' humic coals of Bastian Dal will generally constitute a source rock end-member, and their ability to generate and expel petroleum is more speculative. However, approximately time-equivalent and petrographically similar coals from the Danish North Sea, which conventionally would be regarded as gas-prone coals at best, are the source for the gas/condensate and high-wax crude oil accumulations of the Harald and Lulita fields (Petersen and Rosenberg, 1998; Petersen et al., 1996, 1998a, 2000). These studies indicate that it is important to consider coal as a heterogeneous rock where a combination of the coal composition, the detailed chemistry of the vitrinite, a uniform distribution of source potential (HI), and the seam thickness may determine the generation characteristics and expulsion efficiency. All these parameters are related to the depositional conditions under which the precursor peats accumulated.

CONCLUSIONS

The majority of the HI values from the coals from Kulhus, Hochstetter Forland, and Payer Dal, Kuhn Ø, are greater than 300 and may reach 728, and S₂ yields are generally above 200 mg HC/g rock. These values indicate a high petroleum generative potential. The more conventional humic coals from Bastian Dal, Kuhn Ø, have in general HI values less than 240 and S₂ yields below 80 mg HC/g rock. During hydrous pyrolysis samples rich in resinite or fluorescing A.O.M. and alginite follow the maturation path of kerogen type II or I on the HI versus T_{max} diagram. After hydrous pyrolysis at 300°C/72h a reflectance of 0.21%R_{resinite} suggests that in terms of thermal maturity the samples are within the oil window (approximately 0.75%R_{vitrinite}), whereas reflectances of 0.59%R_{resinite} and 1.11%R_{vitrinite} after hydrous pyrolysis at 330°C/72h suggest the late oil window in terms of thermal maturity.

The outcrop samples have relatively broad activation energy distributions, but, importantly, they have prominent principal E_a-values centred around 60 kcal/mole and 62 kcal/mole. This seems to have a profound influence on the generation characteristics of the samples during artificial maturation above 270°C/72h, i.e. from 300°C/72h to 330°C/72h. The following important changes are observed:

- (1) a marked loss of fluorescence of the liptinite macerals and a significant increase in the reflectance of resinite and A.O.M.;
- (2) an insignificant or small change in T_{max}, rendering this parameter unsuitable for determining the thermal maturity in this case;
- (3) following an initial increase in HI, the HI exhibits a considerable decrease;
- (4) a very pronounced increase in extract yields;
- (5) a significant increase in the amount of saturates in the extracts, and an increase in the aromatic-to-saturate ratio with resinite content;
- (6) generation of labile solvent extractable bitumen which increases the HI values and produces an 'apron' of activation energies between 44 kcal/mole and 50 kcal/mole on the E_a-distributions. Extracted samples show the expected increase towards higher activation energies after artificial maturation.

These results indicate that significant bitumen/petroleum formation from the coals could take place during a relatively narrow temperature range (i.e. burial depth interval). A large

bitumen/petroleum generation is also suggested by a theoretical calculation of the chemical changes occurring in a resinite-rich coal and an A.O.M.- and alginite-rich carbonaceous mudstone during maturation. The calculations show that the coal and the mudstone would realise roughly 85% of their generative potential by passing through the oil window. The large quantities of generation-products over a restricted temperature range facilitate saturation of the coals to the expulsion threshold. The expelled crude oils will be characterised by high HC/non-HC ratios, moderate to high saturate-to-aromatic ratios, high contents of waxy *n*-alkanes, high pr/ph ratios and the presence of a number of resinite-related tri- and tetracyclic diterpanes and their aromatic counterparts.

Thus, if thermally mature the liptinite-rich coals and associated carbonaceous mudstones from Kulhus and Payer Dal may act as highly oil-prone, local source rocks offshore North-East Greenland. The cumulative coal seam thickness of minimum 7.6 m at Kulhus makes the coals from Hochstetter Forland the most attractive source rock. The humic coals from Bastian Dal, Kuhn Ø, may potentially constitute an additional but marginal source rock. The results also emphasise that depositional conditions similar to those during which the precursor peats of the coals from Kulhus, Hochstetter Forland, and Payer Dal, Kuhn Ø, accumulated are favourable for the formation of highly prolific coal source rocks with the capacity to not only generate but also expel liquid petroleum.

REFERENCES CITED

- Alsgaard, P. C., V. L. Felt, H. Vosgerau, and F. Surlyk, in press, The Jurassic of Kuhn Ø, North-East Greenland, *in* F. Surlyk and J. Ineson, eds., The Jurassic of Denmark and Greenland: Geology of Denmark Survey Bulletin.
- Baskin, D. K., 1997, Atomic H/C ratio of kerogen as an estimate of thermal maturity and organic matter conversion: AAPG Bulletin, v. 81, p. 1437–1450.
- Bojesen-Koefoed, J. A., F. G. Christiansen, H. I. Petersen, S. Piasecki, L. Stemmerik, and H. P. Nytoft, 1996, Resinite-rich coals of northeast Greenland – a hitherto unrecognized, highly oil-prone Jurassic source rock: Bulletin of Canadian Petroleum Geology, v. 44, p. 458–473.
- Boudou, J. P., J. Espitalié, J. Bimer, P. D. Salbut, 1994, Oxygen groups and oil suppression during coal pyrolysis: Energy and Fuels, v. 8, p. 972–977.
- Bustin, R. M., A. R. Cameron, D. A. Grieve, and W. D. Kalkreuth, 1985, Coal petrology - its principles, methods, and applications: Geological Association of Canada, Short Course Notes, v. 3, 230 p.
- Clemmensen, L. B. and F. Surlyk, 1976, Upper Jurassic coal-bearing shoreline deposits, Hochstetter Forland, East Greenland: Sedimentary Geology, v. 15, p. 193–211.
- Cohen, A. D. and A. M. Bailey, 1997, Petrographic changes induced by artificial coalification of peat: comparison of two planar facies (Rhizophora and Cladium) from the Everglades-mangrove complex of Florida and a domed facies (Cyrilla) from the Okefenokee Swamp of Georgia: International Journal of Coal Geology, v. 34, p. 163–194.
- Frebold, H., 1932, Geologie der Jurakohlen des Nördlichen Ostgrönland: Meddelelser fra Grønland, v. 84, 65 p.
- Horsfield, B., K. L. Yordy, and J. C. Crelling, 1988, Determining the petroleum-generating potential of coal using organic geochemistry and organic petrology: Organic Geochemistry, v. 13, p. 121–129.
- Isaksen, G. H., D. J. Curry, J. D. Yeakel, and A. I. Jenssen, 1998, Controls on the oil and gas potential of humic coals. Organic Geochemistry, v. 29, p. 23–44.

- Khorasani, G. K., 1987, Oil-prone coals of the Walloon Coal Measures (Jurassic), Surat Basin, Australia, *in* A. C. Scott, ed., Coal and coal-bearing strata: recent advances: Geological Society London Special Publication, v. 32, p. 303–310.
- Killops, S. D., R. H. Funnell, R. P. Suggate, R. Sykes, K. E. Peters, C. Walters, A. D. Woolhouse, R. J. Weston and J.-P. Boudou, 1998, Predicting generation and expulsion of paraffinic oil from vitrinite-rich coals: *Organic Geochemistry*, v. 29, p. 1–21.
- Levine, J. R., 1993, Coalification: the evolution of coal as source rock and reservoir rock for oil and gas, *in* B. E. Law and D. D. Rice, eds., *Hydrocarbons from coal: AAPG Studies in Geology*, v. 38, p. 39–77.
- Lewan, M. D., 1994, Assessing natural oil expulsion from source rocks by laboratory pyrolysis, *in* L. B. Magoon and W. G. Dow, eds., *The petroleum system – from source to trap: AAPG Memoir*, v. 60, p. 201–210.
- Pepper, A. S. and P. J. Corvi, 1995, Simple kinetic models of petroleum formation. Part I: oil and gas generation from kerogen: *Marine and Petroleum Geology*, v. 12, p. 291–319.
- Peters, K. E., J. M. Moldowan, A. R. Driscoll, and G. J. Demaison, 1989, Origin of Beatrice oil by co-sourcing from Devonian and Middle Jurassic source rocks, Inner Moray Firth, United Kingdom: *AAPG Bulletin*, v. 73, p. 454–471.
- Petersen, H. I. and P. Rosenberg, 1998, Reflectance retardation (suppression) and source rock properties related to hydrogen-enriched vitrinite in Middle Jurassic coals, Danish North Sea: *Journal of Petroleum Geology*, v. 21, p. 247–263.
- Petersen, H. I. and P. Rosenberg, 2000, The relationship between the composition and rank of humic coals and their activation energy distributions for the generation of bulk petroleum: *Petroleum Geoscience*.
- Petersen, H. I. and H. Vosgerau, 1999, Composition and organic maturity of Middle Jurassic coals, North-East Greenland: evidence for liptinite-induced suppression of huminite reflectance: *International Journal of Coal Geology*, v. 41, p. 257–274.
- Petersen, H. I., J. Andsbjerg, and J. A. Bojesen-Koefoed, 2000, Source rock evaluation and palaeoenvironment of oil-generating Middle Jurassic coals, Lulita Field, Danish North Sea: *Journal of Petroleum Geology*.

- Petersen, H. I., P. Rosenberg, and J. Andsbjerg, 1996, Organic geochemistry in relation to the depositional environments of Middle Jurassic coal seams, Danish Central Graben, and implications for hydrocarbon generative potential: AAPG Bulletin, v. 80, p. 47–62.
- Petersen, H. I., J. Andsbjerg, J. A. Bojesen-Koefoed, H. P. Nytoft, and P. Rosenberg, 1998a, Petroleum potential and depositional environments of Jurassic coals and non-marine deposits, Danish Central Graben, with special reference to the Søgne Basin: Geology of Denmark Survey Bulletin, v. 36, 78 p.
- Petersen, H. I., J. A. Bojesen-Koefoed, H. P. Nytoft, F. Surlyk, J. Therkelsen, and H. Vosgerau, 1998b, Relative sea-level changes recorded by paralic liptinite-enriched coal facies cycles, Middle Jurassic Muslingebjerg Formation, Hochstetter Forland, Northeast Greenland: International Journal of Coal Geology, v. 36, p. 1–30.
- Schenk, H. J. and B. Horsfield, 1998, Using natural maturation series to evaluate the utility of parallel reaction kinetics models: an investigation of Toarcian shales and Carboniferous coals, Germany: Organic Geochemistry, v. 29, p. 137–154.
- Scotchman, I. C., C. E. Griffith, A. J. Holmes, and D. M. Jones, 1998, The Jurassic petroleum system north and west of Britain: a geochemical oil-source correlation study: Organic Geochemistry, v. 29, p. 671–700.
- Shanmugam, G., 1985, Significance of coniferous rain forests and related organic matter in generating commercial quantities of oil, Gippsland Basin, Australia: AAPG Bulletin, v. 69, 1241–1254.
- Snowdon, L. R. and T. G. Powell, 1982, Immature oil and condensate – modification of hydrocarbon generation model for terrestrial organic matter: AAPG Bulletin, v. 66, p. 775–788.
- Stout, S. A., 1995, Resin-derived hydrocarbons in fresh and fossil dammar resins and Miocene rocks and oils in the Mahakam Delta, Indonesia, *in* K. B. Anderson and J. C. Crelling, eds., Amber, resinite, and fossil resins: ACS Symposium Series, v. 617, p. 43–75.
- Surlyk, F., 1978, Jurassic basin evolution of East Greenland: Nature, v. 274, p. 130–133.
- Surlyk, F., 1990, Timing, style and sedimentary evolution of Late Palaeozoic–Mesozoic

- extensional basins of East Greenland, *in* R. P. F. Hardman and J. Brooks, eds., Tectonic events responsible for Britain's oil and gas reserves: Geological Society London Special Publication, v. 55, p. 107–125.
- Surlyk, F. and L. B. Clemmensen, 1983, Rift propagation and eustasy as controlling factors during Jurassic inshore and shelf sedimentation in northern East Greenland: *Sedimentary Geology*, v. 34, p. 119–143.
- Surlyk, F., G. Dam, M. Engkilde, C. F. Hansen, M. Larsen, N. Noe-Nygaard, S. Piasecki, J. Therkelsen, and H. Vosgerau, *in press*, Jurassic stratigraphy of East Greenland, *in* F. Surlyk and J. Ineson, eds., *The Jurassic of Denmark and Greenland: Geology of Denmark Survey Bulletin*.
- Taylor, G. H., M. Teichmüller, A. Davis, C. F. K. Diessel, R. Littke, R., and P. Robert, 1998, *Organic petrology*: Gebrüder Borntraeger, Berlin, Stuttgart, 704 p.
- Teerman, S. C. and R. J. Hwang, 1991, Evaluation of the liquid hydrocarbon potential of coal by artificial maturation techniques: *Organic Geochemistry*, v. 17, p. 749–764.
- Tegelaar, E. W. and R. A. Noble, 1994, Kinetics of hydrocarbon generation as a function of the molecular structure of kerogen as revealed by pyrolysis-gas chromatography: *Organic Geochemistry*, v. 22, p. 543–574.
- Teichmüller, M., 1989, The genesis of coal from the viewpoint of coal petrology: *International Journal of Coal Geology*, v. 12, p. 1–87.
- Tissot, B. P., R. Pelet, and PH. Ungerer, 1987, Thermal history of sedimentary basins, maturation indices, and kinetics of oil and gas generation: *AAPG Bulletin*, v. 71, p. 1445–1466.

Figure captions

Figure 1. Map of North-East Greenland showing the position of the Middle Jurassic coal outcrops at the Kulhus locality on Hochstetter Forland and in Bastian Dal and Payer Dal on Kuhn Ø.

Figure 2. Sedimentological log of the coal-bearing Muslingebjerg Formation at Kulhus, Hochstetter Forland, showing the paralic nature of the succession. 'Shoreface facies association': 1a, transgressive lag; 1b, runnels or rip channels; 1c, uppermost shoreface or foreshore. 'Coastal plain facies association': 2a and 2b, lakes or lagoons; 2c, washover or crevasse splays. 'Tidal facies association': 3a, tidal channel lag; 3b, tidal channel. TRS: tidal ravinement surface; WRS: wave ravinement surface. (After Petersen et al., 1998b).

Figure 3. The maceral group composition on a mineral matter free (m.m.f.) basis of the coals from (A) the Kulhus outcrop (76 samples), Hochstetter Forland, and (B) the outcrops in Bastian Dal (14 samples) and Payer Dal (4 samples), Kuhn Ø. Note the high liptinite content of the Payer Dal and the majority of the Kulhus samples.

Figure 4. HI versus T_{\max} plots of the coal samples from (A) the Kulhus outcrop (86 samples), and (B) the outcrops in Bastian Dal (42 samples) and Payer Dal (4 samples), Kuhn Ø. The samples from Payer Dal and majority of the samples from Kulhus have HI values above 300. In contrast only one sample from Bastian Dal exceeds a HI of 300.

Figure 5. HI versus T_{\max} plots of the samples subjected to hydrous pyrolysis showing the evolution of HI and T_{\max} with increasing artificial maturation temperature (240°C/72h, 270°C/72h, 300°C/72h and 330°C/72h) of (A) sample 071 from Kulhus, (B) sample 144 from Kulhus, (C) sample C-8 from Payer Dal, and (D) sample C-20 from Payer Dal. Note the significant decrease in HI from 300°C/72h to 330°C/72h and the associated insignificant change in T_{\max} for samples 071, 144 and C-20.

Figure 6. Resinite (R) particle after hydrous pyrolysis at 330°C/72h. Fluorescence has more or less disappeared and the mean random reflectance has increased to 0.59% R_{resinite} . The associated reflectance of vitrinite is 1.11% $R_{\text{vitrinite}}$. Photomicrograph taken in reflected white light and oil immersion; scale bar $\approx 30 \mu\text{m}$).

Figure 7. Increase in mean random reflectance of resinite with increasing hydrous pyrolysis temperature.

Figure 8. Increase in extract yields during artificial maturation. A significant increase is observed above 270°C/72h.

Figure 9. Evolution in extract composition during artificial maturation. A significant increase in the content of saturates is observed from 300°C/72h to 330°C/72h. However, it is evident that the aromatic-to-saturate ratio increases with increasing resinite content.

Figure 10. Gas chromatograms (saturate fraction) of the four samples subjected to hydrous pyrolysis at 330°C/72h. Characteristic features include a high proportion of waxy *n*-alkanes ($n\text{C}_{22+}$), moderate to high pr/ph ratios, slight enhancement of $n\text{C}_{15}$, $n\text{C}_{17}$ and perhaps $n\text{C}_{19}$, and overall low to moderate proportions of acyclic isoprenoids. Numbers refer to carbon number; pr: pristane; ph: phytane; dots: alkylcyclohexanes; triangles: methylalkylcyclohexanes.

Figure 11. Activation energy distributions of outcrop samples showing prominent principal E_a -values centred around 60 kcal/mole and 62 kcal/mole.

Figure 12. Activation energy distributions of artificially matured samples. Comparison of the non-extracted and extracted samples 071 and 144 (300°C/72h) reveals the generation of solvent extractable organic matter (bitumen/petroleum) with low E_a -values (44–50 kcal/mole). Samples hydrous-pyrolysed at 330°C/72h show the expected shift towards higher principal E_a -values and reduced magnitudes of the activation energies.

Figure 13. Estimation of H/C ratios of the coals on the basis of petrographic composition using the method by Baskin (1997). The maturity of the coals corresponds to a reflectance of $0.50\%R_{\text{vitrinite}}$ (Petersen and Vosgerau, 1999). (A) estimated H/C ratio of sample C-20 is 1.20, and (B) estimated H/C ratio of sample 144 is 1.17. Solid triangles show the approximately evolution of the samples as they pass through the oil window (from about $0.50\text{--}1.3\%R_{\text{vitrinite}}$) at which time samples C-20 and 144 will have H/C ratios of roughly 0.85 and 0.80 respectively.

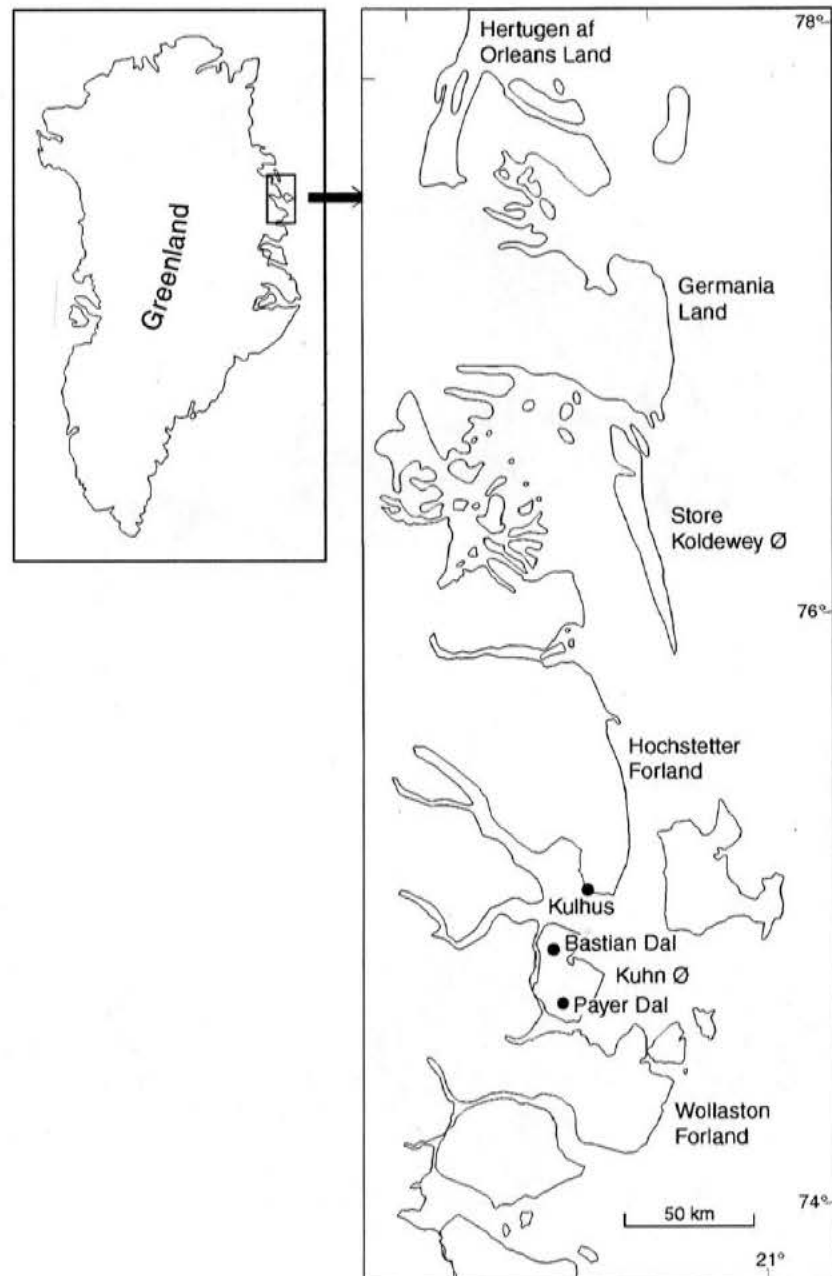


Fig 1

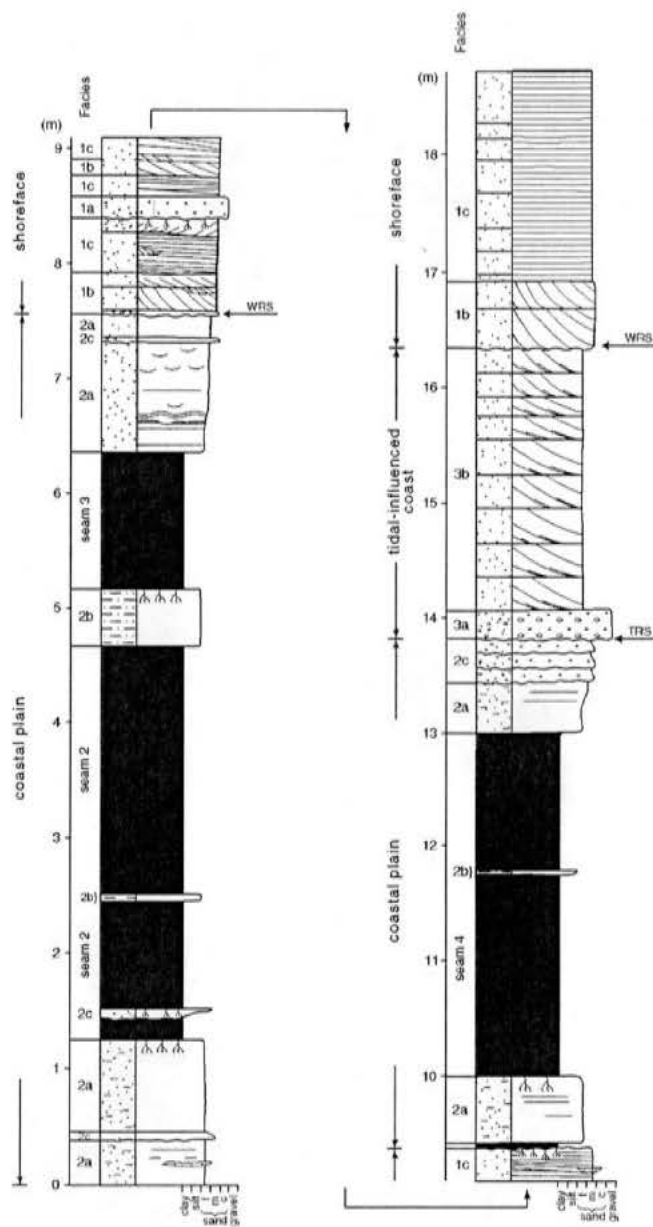
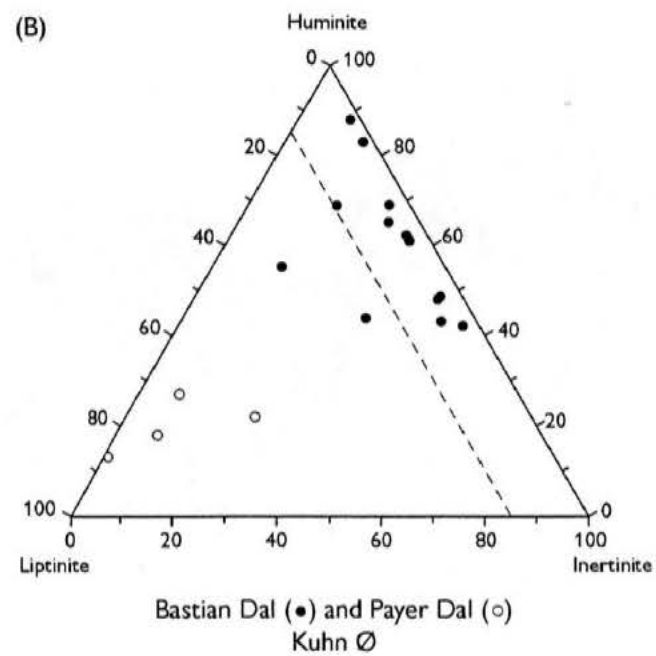
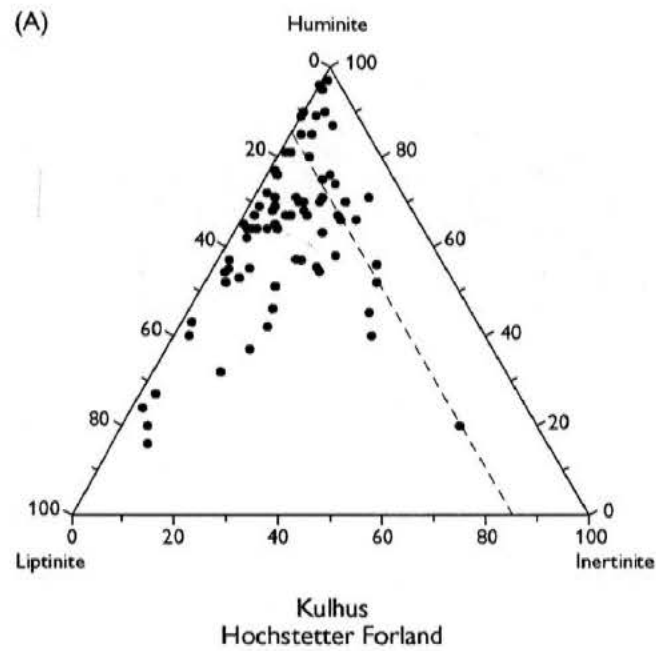
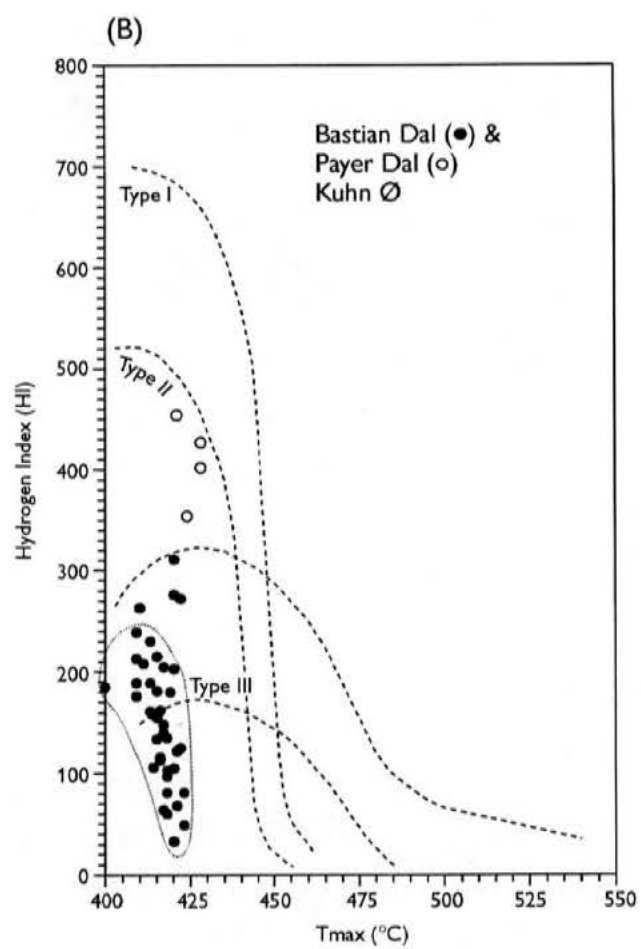
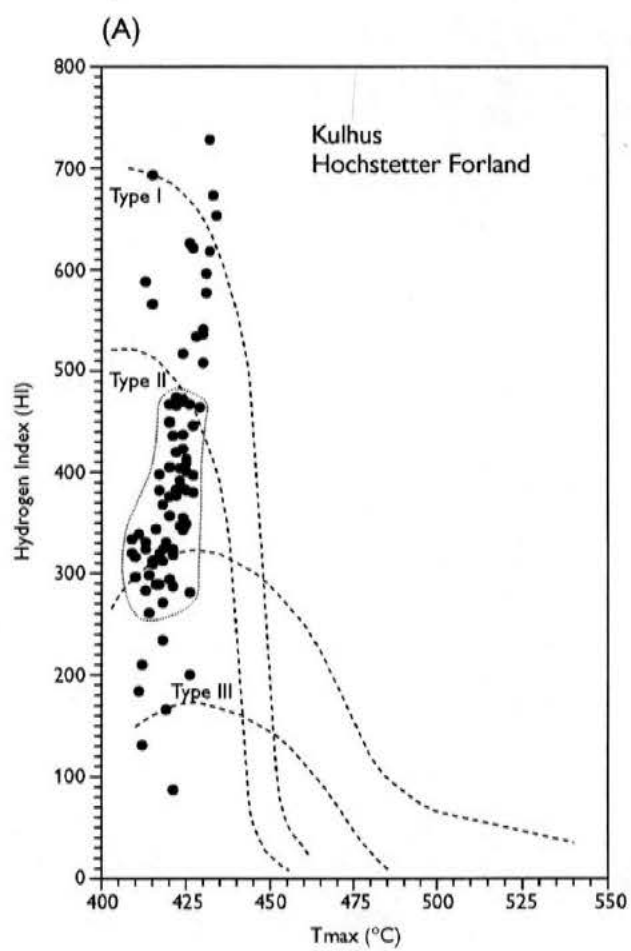


Fig. 2





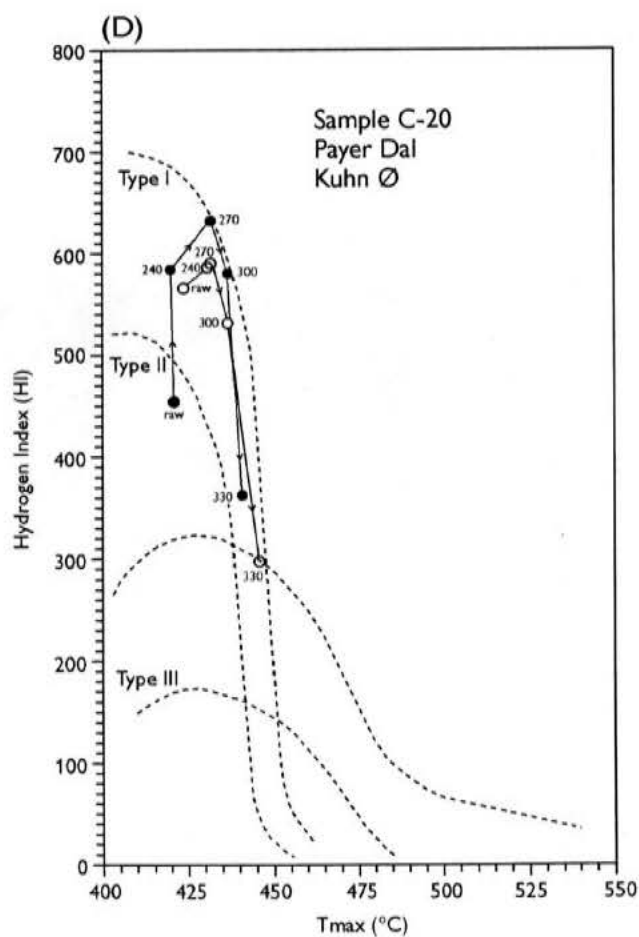
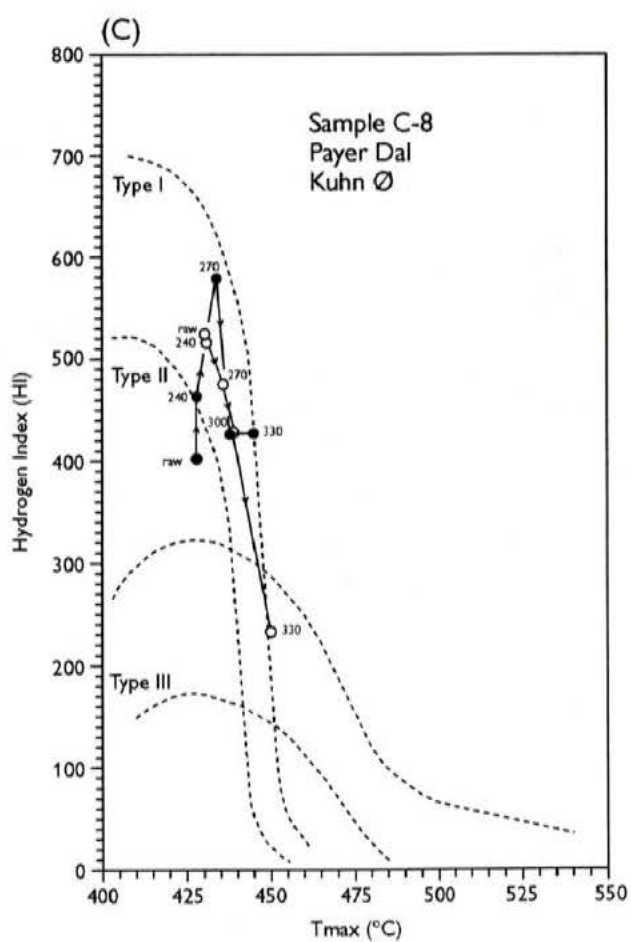
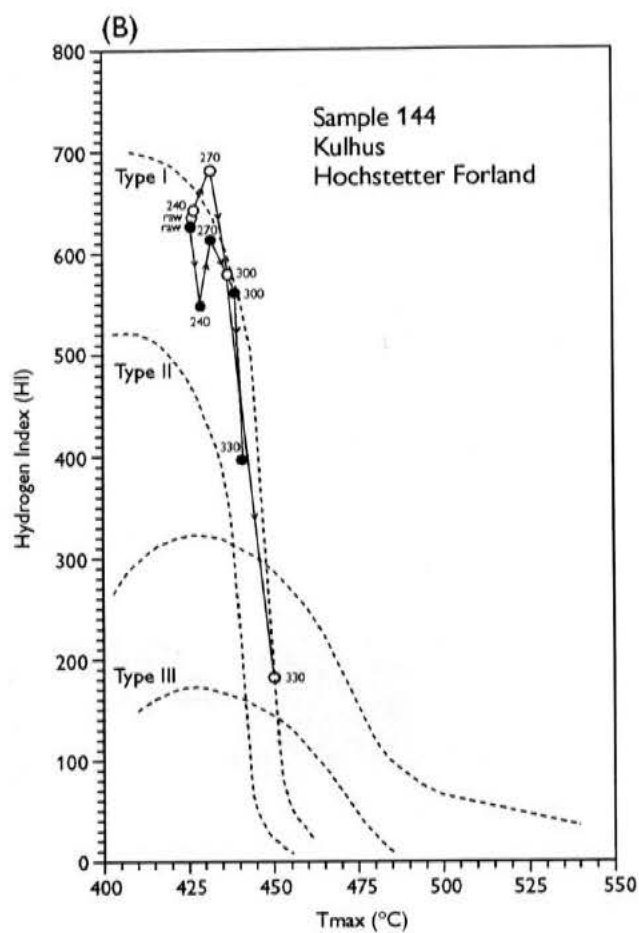
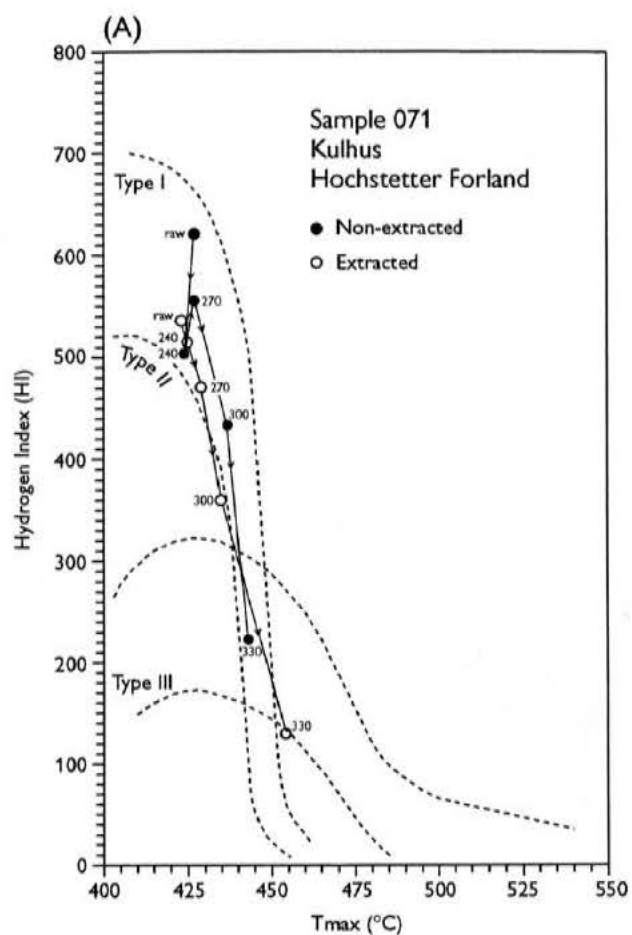


Fig 5

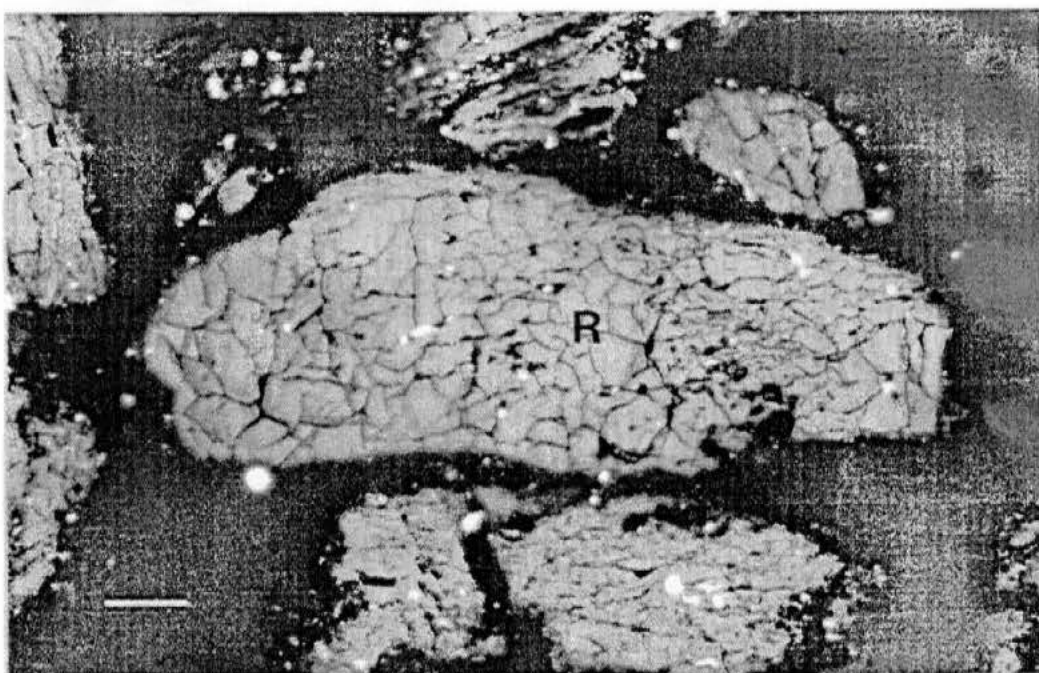
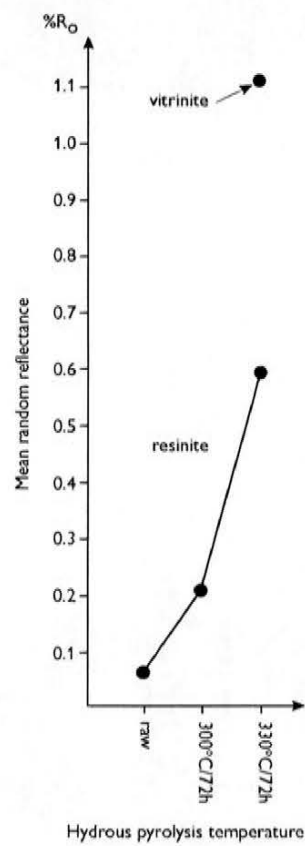
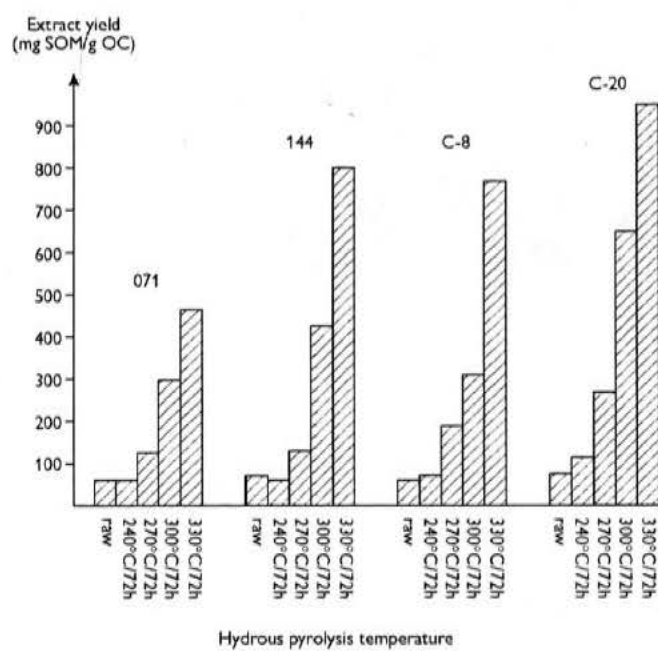
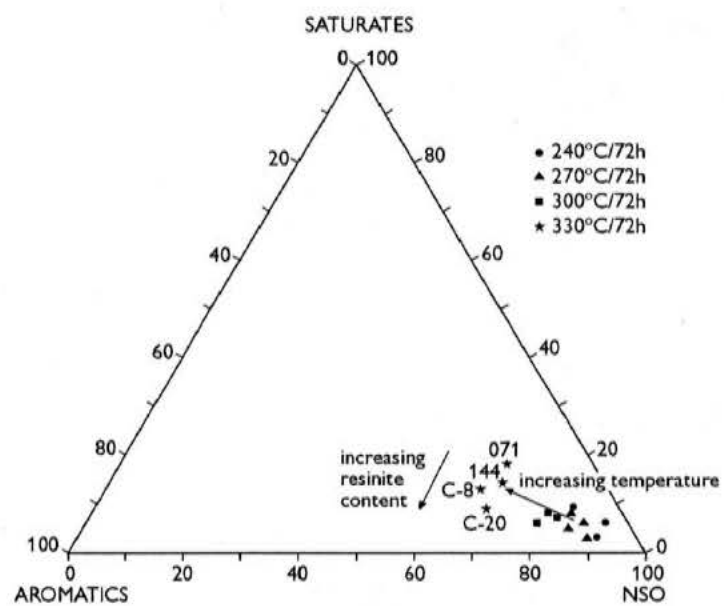
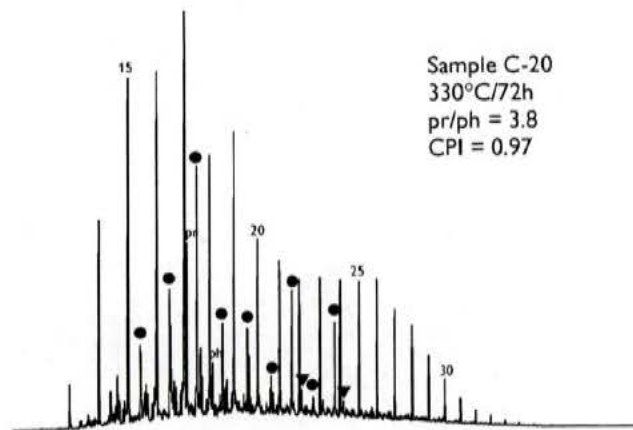
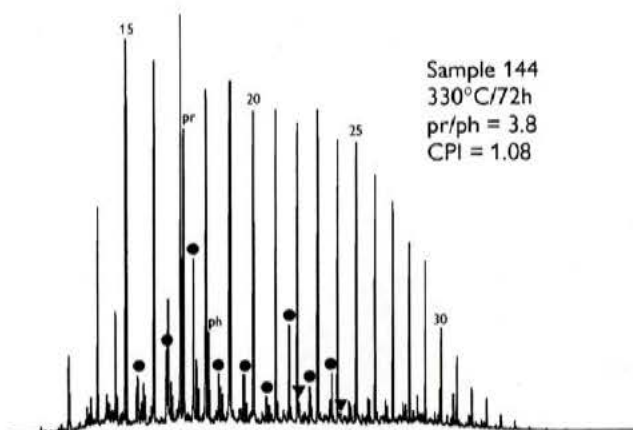
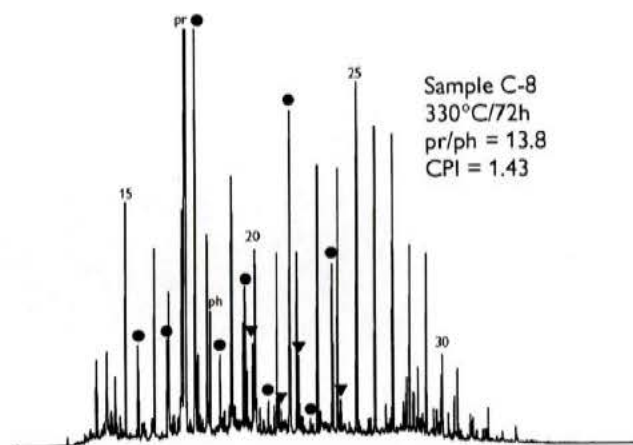
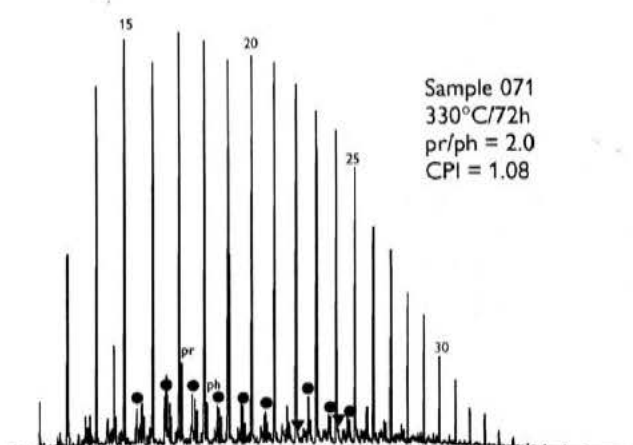


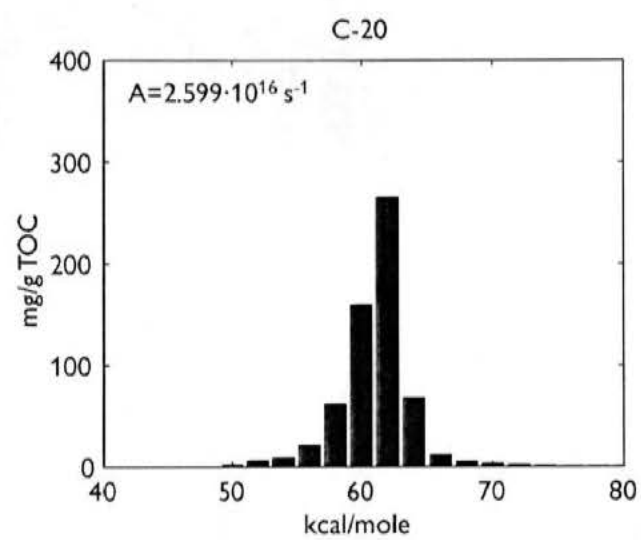
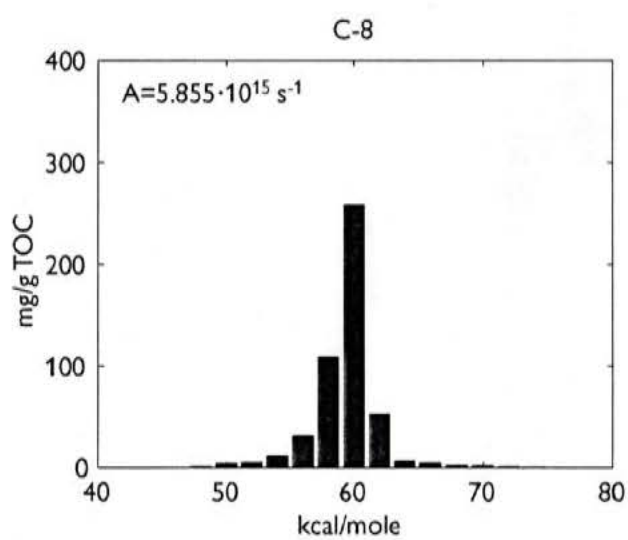
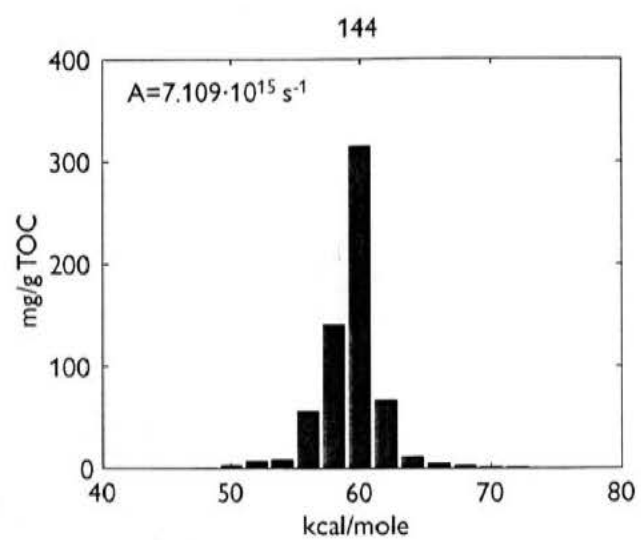
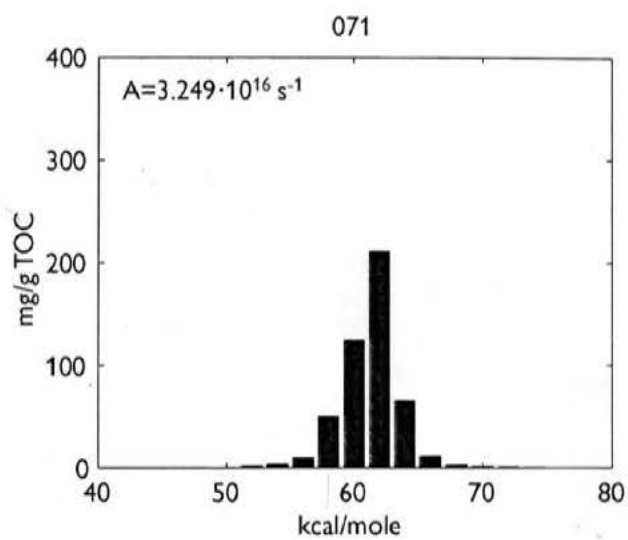
Fig. 6

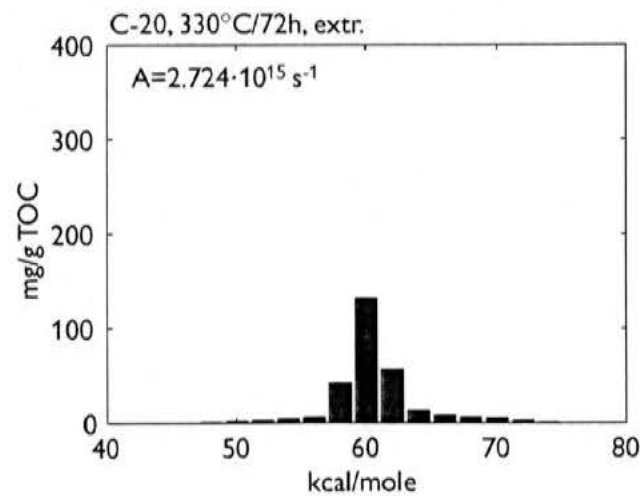
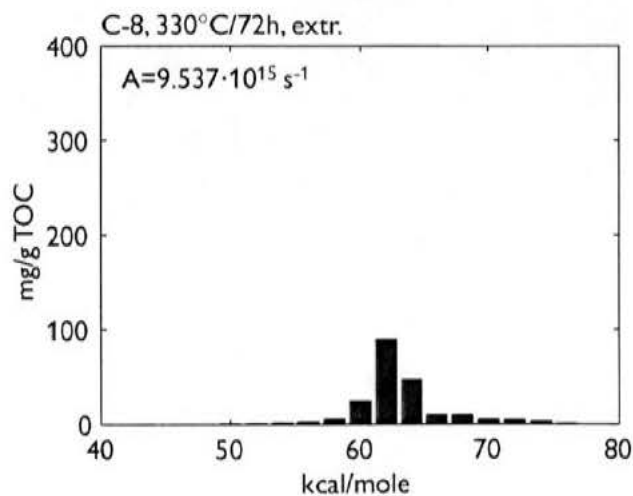
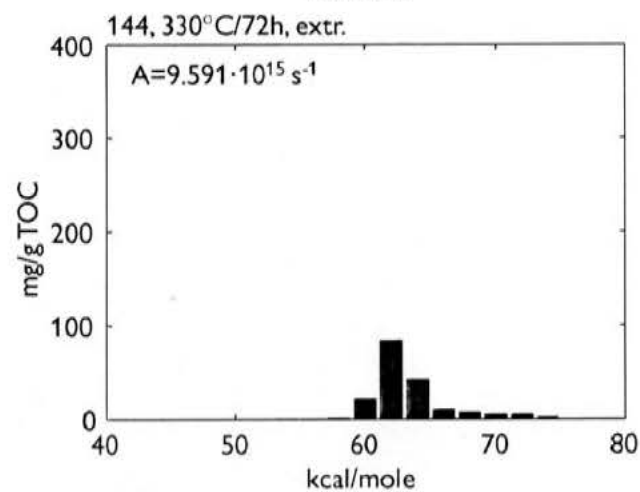
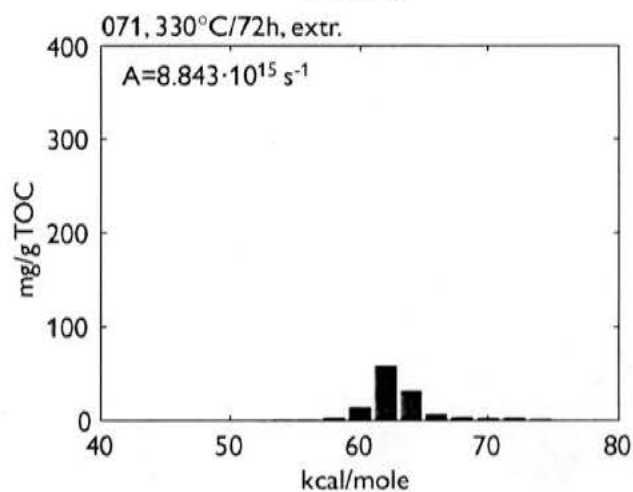
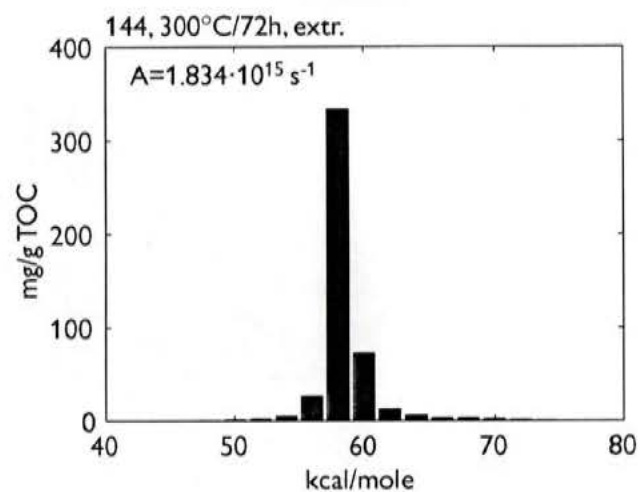
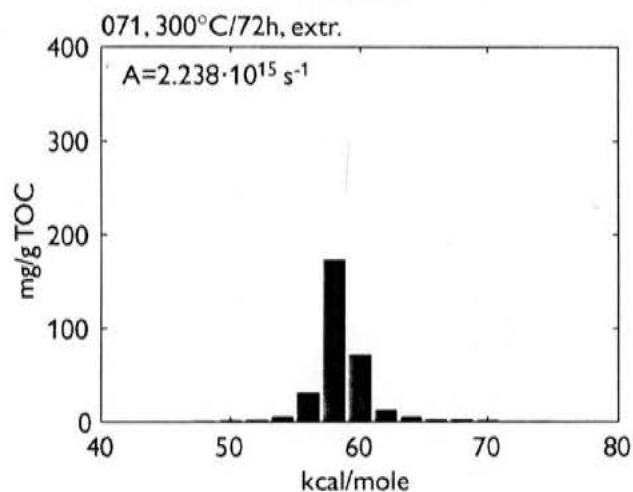
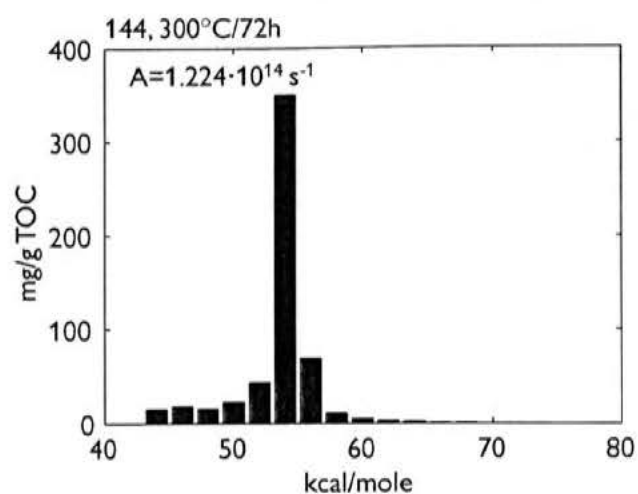
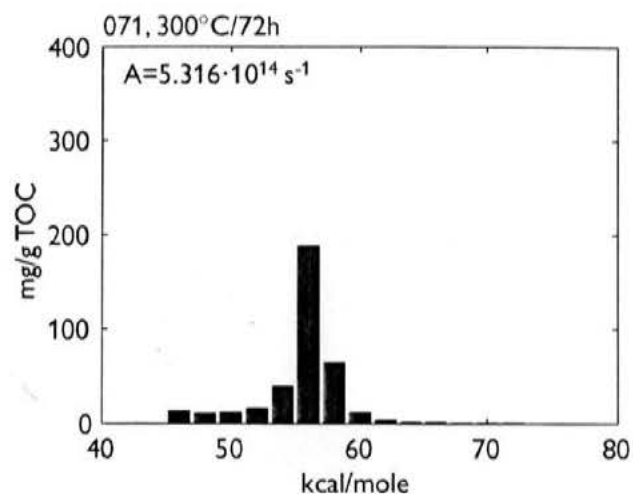












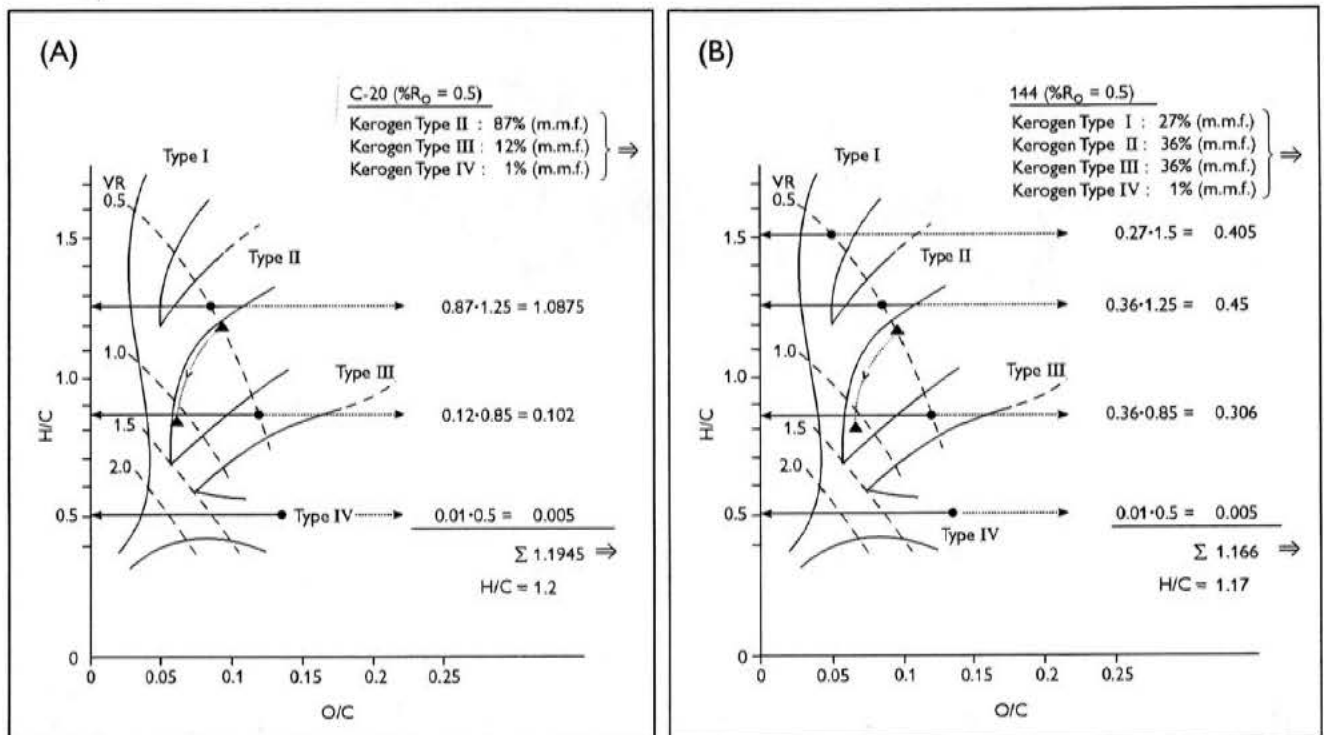


Table 1. Composition of samples subjected to hydrous pyrolysis

Composition	071	144	C-8	C-20
Huminite (vol.%)	20	26	18	12
Liptinite (vol.%)	15	31	74	85
resinite (vol.%)	3	11	54	69
alginate (vol.%)	0	5	0	0
Inertinite (vol.%)	1	1	8	1
Fluore. A.O.M. (vol.%)*	37	15	0	0
Pyrite (vol.%)	11	4	0	0
Other minerals (vol.%)	16	23	0	2
TOC (wt.%)	29.32	22.91	71.36	58.54
S ₁ (mg HC/g rock)	2.89	4.28	10.97	10.84
S ₂ (mg HC/g rock)	182.01	143.33	286.62	265.56
Hydrogen Index	621	626	402	454

*Matrix of minerals and fluorescing amorphous organic matter

Table 2. Evolution of S_1 and S_2 with increasing hydrous pyrolysis temperature

Sample		071	144	C-8	C-20
Raw	S_1 , non-extr. ^a	2.89	4.28	10.97	10.84
	S_1 , extr. ^b	0.78	0.98	3.04	3.16
	S_2 , non-extr.	182.01	143.33	286.62	265.56
	S_2 , extr.	144.20	123.32	347.22	326.02
240°C/72h	S_1 , non-extr.	3.93	4.11	14.21	21.06
	S_1 , extr.	0.52	0.37	0.82	1.23
	S_2 , non-extr.	168.48	161.76	297.36	355.92
	S_2 , extr.	159.20	146.78	318.64	341.84
270°C/72h	S_1 , non-extr.	9.31	8.92	33.20	37.85
	S_1 , extr.	0.50	0.28	1.04	0.89
	S_2 , non-extr.	159.14	144.70	332.02	351.42
	S_2 , extr.	145.08	150.96	312.08	334.14
300°C/72h	S_1 , non-extr.	27.38	22.59	69.05	63.89
	S_1 , extr.	0.37	0.39	0.81	2.01
	S_2 , non-extr.	131.02	125.86	321.50	332.64
	S_2 , extr.	97.00	110.18	282.20	295.04
330°C/72h	S_1 , non-extr.	51.63	43.46	106.05	134.36
	S_1 , extr.	0.39	0.29	0.85	1.06
	S_2 , non-extr.	59.80	62.54	270.38	241.72
	S_2 , extr.	23.02	22.46	143.04	116.98

^anon-extr.: non-extracted

^bextr.: solvent extracted

Cretaceous source rocks in the Arctic: hydrous pyrolysis of black shales from Ellesmere Island, Northwest Territories, Canada – implications for exploration on- and offshore West Greenland and in the Melville Bay region.

Jørgen A. Bojesen-Koefoed¹, Flemming G. Christiansen¹, L. Koldo Núñez-Betulu², H. Peter Nytoft¹ and Henrik I. Petersen¹

¹ Geological Survey of Denmark and Greenland (GEUS), 8 Thoravej, DK-2400 Copenhagen NV, Denmark

² Department of Stratigraphy and Paleontology, Faculty of Sciences, University of the Basque Country, P. O. Box 644, 48080 Bilbao, The Basque Country, Spain

Acknowledgments

This study received financial support from the Danish Energy Research Programme (EFP-98), grant 1313/98-0022. Laboratory assistance by Ditte Kiel-Dühring and Lisbeth Løvig Nielsen is gratefully acknowledged. Jens Bisgaard built the pyrolysis unit used for Pyrolysis-GC. Jette Halskov

prepared the map shown in Figure 1. T. C. R. Pulvertaft improved the English language of the text. This paper was published with the permission of the Geological Survey of Denmark and Greenland (GEUS).

Abstract

Organic-rich mudstones occur in the Hassel Formation (Albian) and the basal 'Bituminous Member' of the Kanguk Formation (Cenomanian–Maastrichtian) in Ellesmere Island, Northwest Territories, Canada. From a database comprising approximately 600 Rock-Eval/TOC analyses from these units, two thermally immature samples ($\% R_o = 0.45$ and 0.32 , $T_{max} = 419^\circ\text{C}$ and 411°C) were selected for detailed study by organic petrography, hydrous pyrolysis, pyrolysis-GC, pseudo-activation energy distribution, and distribution of biological markers. Both units comprise excellent petroleum source rocks. The Hassel Formation contains predominantly terristrial type III kerogen, whereas the Bituminous Member contains predominantly marine type II kerogen. Although the initial petroleum generation potential of the two samples is very similar, the samples vary with respect to their generation characteristics, as well as with respect to the composition of petroleum products formed upon maturation. The type II kerogen sample will generate gas and low wax oil

over a relatively narrow maturity interval and exclusively gas at higher maturities. Conversely, The type III kerogen sample will generate both gas and waxy oil over a somewhat broader maturity interval. The results reported are important for future petroleum exploration in the Melville Bay area, as well as in areas on- and offshore central West Greenland.

Introduction

Enrichment in organic matter is observed in several intervals within Aptian–Coniacian marine sections in many sedimentary basins around the world, and this observation has given rise to the concept of “Cretaceous Oceanic Anoxic Events” (Schlanger and Jenkyns, 1976; Arthur et al., 1987; Hallam, 1987; Schlanger et al., 1987). Furthermore, in many parts of the world these mid-Cretaceous organic-rich sediments constitute prolific source rocks for oil, and they are held to be the source of 29% of the world’s original petroleum reserves (Ulmishek and Klemme, 1990; Klemme and Ulmishek, 1991).

In present-day lower latitude regions, these organic-rich sediments often consist of limestones or marlstones (e.g. Kuhnt and Wiedmann, 1995), whereas in higher latitude and polar regions, decreasing proportions of carbonate result in the organic-rich sediments being developed as typical

black shales. Since the relative positions of relevant land masses have not changed more than 10–15° in a north–south direction since the Albian (e.g. Rowley and Lottes, 1988), this variation in sediment type is related to the palaeolatitudes of the sediments in question.

Data on the source rock potential of Cretaceous sediments in arctic and North Atlantic regions are sparse, although such information would be very influential in the assessment of the prospectivity of these regions. This is not least the case on- and offshore central West Greenland, where recent discoveries of oil seeps in the Cretaceous–Palaeogene Nuussuaq Basin (Figure 1) have revived interest in petroleum exploration in this region (Christiansen et al., 1996, 1998; Bojesen-Koefoed et al., in press). Furthermore, interpretation of seismic data from the Melville Bay region (Figure 1) has revealed the presence of thick sedimentary successions of likely Cretaceous age and large potential trap structures (Whittaker et al., 1997), leaving the occurrence of high quality source rocks as the main remaining risk factor in this region.

An opportunity to study potential source rocks of Cretaceous age in an arctic region is provided by outcrops in the eastern part of the Sverdrup Basin on Ellesmere Island, Northwest Territories, Canada. Here both the uppermost Cenomanian–Turonian 'Bituminous Member' (informal unit) at the base of the Kanguk Formation and the upper part of the underlying Upper Albian Hassel Formation (Figure 2) consist of papery, black, marine

shales with intervals highly enriched in organic matter (Núñez-Betulu, 1993, 1994). The present paper reports some results of organic geochemical and petrographic analysis and of artificial maturation experiments using hydrous pyrolysis carried out on samples from the Hassel Formation and the 'Bituminous Member' of the Kanguk Formation.

Geological Setting

The Sverdrup Basin, extending over most of the Canadian Arctic, contains a very thick sedimentary succession comprising deposits of Carboniferous to Tertiary age (Embry, 1991) (Figure 1). Both the extent and shape of the basin have varied through time due to tectonic movements and sea-level fluctuations. Sedimentation in the Sverdrup Basin was brought to an end by the Eurekan Orogeny, which probably terminated in the earliest Oligocene (Okulitch and Trettin, 1991; Ricketts, 1994). The Eurekan Orogeny resulted from the opening of the Baffin Bay, which involved a pivotal rotation and northerly movement of the Greenland craton away from North America and to its subsequent collision with northeastern Ellesmere Island (Embry, 1991, De Paor et al., 1989). The Hassel and Kanguk formations crop out over most of the Sverdrup Basin, but the present study only considers samples from the easternmost part of this

vast area (Figure 1). Over most of the Sverdrup Basin, the Kanguk Formation rests unconformably on the Hassel Formation, although in some areas it rests unconformably on older strata. Thus, the Hassel and Kanguk formations are separated by a notable hiatus, which is probably of tectonic origin (Embry, 1991). A simple stratigraphic column of the succession on Ellesmere Island is shown in Figure 2.

Over the greater part of the Sverdrup basin, the Late Albian Hassel Formation consists predominantly of interbedded fine- to coarse-grained sandstone, siltstone, shale and minor coal of delta-plain origin (Embry 1991). However, on Axel Heiberg Island and on Ellesmere Island the Hassel Formation consists of sandstone-dominated coarsening-upwards cycles of marine shelf origin, overlain by a thick (90 m) marine shale-siltstone succession.

The Kanguk Formation was deposited over a period extending from the latest Cenomanian to the earliest Maastrichtian (Embry, 1991; Núñez-Betulu, 1994). The lower portion of the formation consists predominantly of papery bituminous shales, which represent starved offshore shelf deposits. The shales become gradually lighter and siltier upwards through the formation, and the uppermost part consists of prodelta deposits (Embry, 1991). In marginal settings, glauconitic sandstones are present. Informally, the Kanguk Formation has been divided into three members, viz. the Bituminous Member, the Mount Bridgman

Member, and the Remus Creek Member (Núñez-Betulu, 1994). Due to deformation of the basin during the Eureka Orogeny, the position of the palaeocoastline is not known, but since shoreline and near-shore facies are present in the easternmost outcrops of the Kanguk Formation, relative proximity to the palaeocoastline is inferred for the study area (Núñez-Betulu, 1994).

Samples and methods

Núñez-Betulu (1993) lists results of Rock-Eval pyrolysis of several hundred samples of the Kanguk and Hassel formations on Ellesmere Island. Based on these data, one sample from the Fosheim Anticline section, representing the Hassel Formation, and one sample from the Bay Fiord section, representing the Bituminous Member of the Kanguk Formation, were selected for hydrous pyrolysis. Samples were selected to meet the following criteria: the samples should be rich in organic matter and of low thermal maturity. A flow-chart of the organic geochemical analyses performed is shown in Figure 3.

Vitrinite reflectance (R_o) was measured on polished blocks of both samples prior to hydrous pyrolysis, as well as on the suite of pyrolyzed samples of the Hassel Formation. The petrography of the two selected

samples was determined by standard point-counting of polished blocks using both white light and fluorescence-inducing blue light. Maceral identification and sample preparation follow the standards outlined by Stach, et al., (1982). During analysis of the Bituminous Member sample, the informal term "organo-mineral matrix" was used to describe intimately associated organic and mineral matter.

For hydrous pyrolysis, stainless steel HPLC-columns were used as reactors. In several stages the columns were filled with 0.7-1.0 grams of finely ground rock, mixed with water and thoroughly stirred to remove any bubbles of air present. Sealed columns were heated for 72h at seven different temperatures in the range from 220 °C to 330 °C. All samples were run in duplicate.

Rock-Eval pyrolysis (incl. TOC) was carried out in accordance with the guidelines published by Espitalié et al., (1985), using cycle 1.

Determination of pseudo-activation energy distributions was carried out using a Rock-Eval 5 instrument and the "Optkin" software package.

Solvent extraction was carried out by means of a "Soxtec" apparatus, using dichloromethane/methanol (93 + 7 vol./vol.) as solvent.

Asphaltenes were precipitated using n-pentane. MPLC fractionation of the maltene fractions was carried out using a procedure modified from Radke et al., (1980a).

Gas-chromatography was carried out using a Hewlett-Packard 5890 gas-chromatograph, fitted with a 25m HP1 WCOT column and FID.

Biomarker analyses were performed using a Hewlett-Packard 5890 Ser. II gas-chromatograph furnished with a 25m HP5 WCOT column, coupled to a Hewlett-Packard 5971A Quadropole Mass Selective Detector.

Pyrolysis-gas chromatography was done by means of a custom made pyrolysis system (25 °C/minute from 300°C to 550°C, N_{2(liq.)} cold trap, on-column injection), coupled to a Hewlett-Packard 5890 gas chromatograph fitted with a 50m Chrompack CP-Sil-8CB WCOT column and FID. Gas-Oil Ratios (GOR) of pyrolysis products were estimated from integration areas of products in the C₁₋₅ fraction ("gas") and the C₆₊ fraction ("oil") in blank-subtracted pyrograms.

Results and discussion

According to the data of Núñez-Betulu (1993, 1994) the sediments of both the Hassel and the Kanguk formations are generally immature with respect to petroleum generation, but Rock-Eval screening data show the presence of highly prolific source rock intervals within the succesions, although the amount of data from the Hassel Formation is limited (Figure 4).

Initial sample compositions

Petrographic analyses show that the composition of the organic matter in the samples is significantly different (Table 1). The Hassel Formation sample is dominated by huminite and inertinite, which together account for 82% of the organic matter. Liptinite accounts for 11% of the organic matter, with liptodetrinite as the dominant constituent. Thus, the organic matter in the Hassel Formation sample is dominated by terrigenous higher land plant debris. On the basis of this observation combined with the Rock-Eval pyrolysis data, the Hassel Formation kerogen can be described as type III, or perhaps as an intermediate kerogen type II/III. In contrast, the Bituminous Member sample contains mainly liptinite, which constitute 63% of the organic matter, with liptodetrinite as the dominant constituent. Huminite and inertinite account for 13%, and a significant proportion of 'amorphous' organo-mineral matrix is present (24%). Hence, although some terrigenous higher land plant debris is present, a predominantly marine algal/bacterial origin of the organic matter is assumed, and the Bituminous Member kerogen is tentatively classified as type II.

Organic richness and pyrolysis yield show very wide variation in both units. Table 2 shows Rock-Eval/TOC screening data on untreated samples as well as on samples subjected to hydrous pyrolysis. The samples selected for hydrous pyrolysis were 1) a sample collected from the Hassel

Formation at the Fosheim Anticline section, 6 metres below the unconformity at the base of the Kanguk Formation, and showing the following characteristics: TOC: 17.83%, T_{\max} : 419°C, S1: 1.95 mg/g, S2: 59.46 mg/g, Hydrogen Index: 333, and 2) a sample collected from the Bituminous Member at the Bay Fiord section, 12 metres above the base of the Kanguk Formation, which showed the following characteristics: TOC: 9.61%, T_{\max} : 411°C, S1: 1.31 mg/g, S2: 34.36 mg/g, Hydrogen Index: 358. The somewhat tentative kerogen type classification provided by the petrographic analyses and Rock-Eval pyrolysis data, is supported by pyrolysis-GC studies. Pyrolysis-gas chromatograms of the two samples show marked differences (Figure 5). The Hassel Formation sample shows high proportions of unresolved components in the higher carbon number range, and abundant long chain normal alkane/alkene doublets (at least up to C_{34}), which do not seem to decrease in abundance with increasing carbon number in a systematic manner. The Bituminous Member sample shows fair proportions of long chain normal alkane/alkene doublets, the abundance of which decreases with increasing carbon number (at least up to C_{32}) along a more or less linear trend. Aromatic and phenolic moieties are not very prominent, but a number of unknowns are tentatively identified as alkylated thiophenes. Compared to the Hassel Formation sample, aromatic and phenolic moieties are less abundant, and a number of

unknowns present in the C_{15-20} carbon number range, tentatively identified as sesqui- and diterpenoid compounds, are not prominent.

The differences between the samples are further substantiated by analyses of solvent extracts of the samples (Tables 3, 4 and 5). The Hassel Formation sample displays a heavy-end skewed, high CPI normal alkane distribution with abundant sesqui- and diterpanes, high pristane/phytane ratio, absence of tricyclic triterpanes, and a pronounced predominance of C_{29} regular steranes. In contrast, the Bituminous Member sample shows a light-end skewed, low CPI normal alkane distribution, few sesqui- and diterpanes, low pristane/phytane ratio, significant proportions of tricyclic triterpanes, and a clear predominance of C_{27} regular steranes. Both samples contain abundant 28,30-bisnorhopane; the triterpanes of the Bituminous Member sample are dominated by this compound, which is even discernable in the gas chromatogram and also in the m/z 217 ion fragmentogram where it elutes between the C_{29} $\alpha\alpha\alpha$ -20S and $\alpha\beta\beta$ -20R regular steranes. This phenomenon is particularly evident in the Hassel Formation sample which has a high hopane/sterane ratio.

Both the Hassel Formation and the Bituminous Member samples are thermally immature, but represent excellent potential petroleum source rocks. Immaturity is further indicated by low huminite reflectance values $R_o = 0.45\%$ and $R_o = 0.32\%$, respectively, and hopane and sterane epimerization ratios far below equilibrium values (Tables 4 and 5).

Evolution of kerogen characteristics during hydrous pyrolysis

From the foregoing it is evident that all the data acquired during this study consistently show notable differences in kerogen and solvent extract composition between the two samples. In the following, it will be demonstrated that although most characteristics of the samples change dramatically during hydrous pyrolysis, differences between the samples remain clear, both with respect to kerogen composition and the composition of petroleum products generated during hydrous pyrolysis. Furthermore, differences in generation characteristics are noted.

Upon hydrous pyrolysis-induced artificial maturation, the Hassel Formation sample, which is dominated by terrigenous kerogen (Table 1), will roughly follow the type III evolution path in the T_{\max} vs. Hydrogen Index diagram (Figure 6). The initial Hydrogen Index of 333 mg/g OC (extracted sample 297 mg/g OC) decreases to 206 mg/g OC (extracted sample 155 mg/g OC) concurrently with an increase in T_{\max} from 419°C (extracted sample 417°C) to 449°C (extracted sample 452°C) (Table 2). Notable generation potential remains after hydrous pyrolysis at 330°C/72h, as shown by the Hydrogen Index and S2 parameters (206 mg/g OC and 40.23 mg/g, respectively).

Upon hydrous pyrolysis at increasing temperatures, the characteristics of the Bituminous Member sample, which is assumed to be dominated by marine kerogen (Table 1), closely follows the type II evolution path in the T_{\max} vs. Hydrogen Index diagram (Figure 6). The initial Hydrogen Index of 358 mg/g OC (extracted sample 352 mg/g OC) decreases to 106 mg/g OC (extracted sample 80 mg/g OC) concurrently with an increase in T_{\max} from 411°C (extracted sample 409°C) to 442°C (extracted sample 452°C) (Table 2). Hydrous pyrolysis at 250°C/72h apparently results in a slight increase in generation potential (S2 and Hydrogen Index) relative to the untreated sample. A similar observation was made by Bojesen-Koefoed et al. (1995), and may probably be explained by release of abundant heteroatomic compounds from very immature kerogen during the initial phases of thermal maturation (e.g. Tissot and Welte, 1984), leading to relative increases in hydrogen content. After hydrous pyrolysis at 330°C/72h, the generation potential is close to being exhausted, as shown by Hydrogen Index: 106 mg/g OC (extracted sample: 80 mg/g OC), and S2: 9.69 mg/g (extracted sample: 5.55 mg/g).

For both samples, pyrolysis-gas chromatography data show gradual compositional changes with increasing temperature of hydrous pyrolysis, including decreasing proportions of high carbon number range components, particularly n-alkanes/alkenes, and increasing proportions gas- and gasoline range components and increasing proportions of aromatic/phenolic moieties

(Figure 5). After hydrous pyrolysis at 330°C/72h, oil-range compounds are very sparse in pyrograms of the Bituminous Member sample, whereas in the Hassel Formation sample, notable proportions of oil range compounds persist (Figure 5). In both the Bituminous Member sample and the Hassel Formation sample, GOR's estimated from pyrolysis-gas chromatography data increase with hydrous pyrolysis temperature from 0.4 to 1.8, and from 0.3 to 0.6, respectively.

By combining Rock-Eval/TOC and pyrolysis-gas chromatography data, the fractions of 'inert', 'oil-prone' and 'gas-prone carbon in the kerogen can be calculated (Pepper and Corvi, 1995). If this calculation is carried out for each sample at the various hydrous pyrolysis temperatures used, generation diagrams can be constructed (Figure 7). The results indicate that for both samples, approximately 30% of the original TOC will participate in the generation of petroleum products, and that the proportions of oil relative to gas are very similar for the two samples, irrespective of the prominent differences in kerogen composition observed. However, notable differences in generation characteristics are observed. Generation of petroleum products from the Bituminous Member sample takes place over a comparatively narrow maturity range, and after hydrous pyrolysis at 330°C/72h the potential for oil generation is largely exhausted while a minor potential for gas generation remains. In contrast, the Hassel Formation sample will generate both oil and gas over a rather wide range

of thermal maturities, and even after hydrous pyrolysis at 330°C/72h when the sample shows $\%R_o = 1.34$, corresponding to the base of the oil window by normal standards, a considerable potential for generation of both oil and gas remains. These results are in perfect agreement with published observations concerning petroleum generation from marine ('type II'), and terrigenous ('type III') kerogen (see e.g. Bordenave et al., 1993).

Pseudo-activation energy distributions further support these results. Prior to hydrous pyrolysis, the Bituminous Member sample displays a pseudo-activation energy distribution that indicates that the main part of the generation potential is realized over a comparatively narrow E_a -range. Only a very minor proportion of the total generation potential is realized in the higher E_a range (Figure 8). This distribution is very similar to published E_a distributions for type II kerogen (e.g. Tissot et al., 1987; Huc, 1990). On the other hand, the Hassel Formation sample displays a pseudo-activation energy distribution very similar to published E_a -distributions of 'type III' kerogen (e.g. Tissot et al., 1987; Huc, 1990), with higher proportions of the total generation potential in both the low E_a - and high E_a -ranges. For both samples, however, the distribution maximum is at a slightly higher E_a than observed in the data of Tissot et al. (1987) and Huc (1990). During hydrous pyrolysis at increasing temperatures, generation potential in the lower E_a -ranges is progressively eliminated, but even after hydrous

pyrolysis at 330°C/72h the differences in E_a -distributions between the two samples are retained (Figure 9).

In general, the composition of solvent extractable organic matter present in samples subjected to hydrous pyrolysis corresponds well to the nature of the kerogen in the two samples. Both samples show increasing extract yields with increasing temperature of hydrous pyrolysis. This is particularly true for the Bituminous Member sample, which shows very high extract yields (Table 3). The solvent extract compositions change, leading to higher proportions of hydrocarbons, but the main portion of the extracts remains in the asphaltene and NSO fractions, even after hydrous pyrolysis at 330°C/72h. Figure 9 shows the gradual evolution in composition of the saturate extract fractions during hydrous pyrolysis, as revealed by the gas chromatograms. Chromatograms of saturated extract fractions of untreated samples and of hydrous pyrolysates obtained after 330°C/72h are shown at a larger scale in Figure 5, together with m/z 191 and m/z 217 ion fragmentograms and pyrolysis-GC traces. Initial biomarker and saturate fraction characteristics of the two samples were described previously. During hydrous pyrolysis, a number of features of the two samples converge, but overall sample characteristics remain clearly different. CPI gradually approaches unity in both samples, but even after hydrous pyrolysis at 330°C/72h, the Hassel Formation sample retains CPI clearly greater than 1. The n-alkanes distributions grow increasingly light-end

skewed for both samples. The Bituminous Member sample shows the 'concave-up' decreasing trend in n-alkane abundance with increasing carbon number which is typical of many marine oils, whereas the Hassel Formation sample shows higher abundance of long-chain n-alkanes, leading to a more or less linear or slightly 'convex-up' decreasing trend in n-alkane abundance with increasing carbon number. Such distributions are common in terrigenous oils. Pristane/phytane ratios change markedly during hydrous pyrolysis. In the Hassel Formation sample, a notable decrease is observed, whereas in the Bituminous Member sample a less dramatic, but still significant increase is noted. Changes in pristane/phytane ratios with maturity are well known (e.g. Radke et al., 1980b, and references therein), and have been attributed to variable rates of formation of pristane and phytane from the parent kerogen. However, the dissimilarity of the changes observed in the two samples may suggest that in the present case, coelution of unknown components and/or catalytic effects of different mineral components may also influence the pristane/phytane ratio.

Thermal maturity indicators

In the present context, 'thermal maturity indicators' include the parameters T_{max} , % R_o , and homohopane and sterane epimerization ratios. Due to the

very small particle size and low concentration of huminite/vitrinite in the Bituminous Member, %R_o was not measured on the subsamples from this unit that were subjected to hydrous pyrolysis.

The Hassel Formation sample contains abundant vitrinite, and %R_o increases regularly with increasing hydrous pyrolysis temperature (Figure 10). The untreated sample yields an initial %R_o of 0.45, whereas after hydrous pyrolysis at 330°C/72h, a value of 1.34 is obtained. A parallel change is noted in T_{max}, which increases from 417°C to 452°C. Little difference in data from raw and extracted samples is noted, showing that suppression of T_{max} is not occurring (Snowdon, 1995). Furthermore, the correlation of %R_o and T_{max} agrees with published data on type III kerogen (Espitalié, 1986; Espitalié and Joubert, 1987).

The Bituminous Member sample also shows a regular increase in T_{max} with increasing hydrous pyrolysis temperature (Figure 10). However, although the trend in evolution of T_{max} with increasing temperature of hydrous pyrolysis is similar for both samples, values yielded by the Bituminous Member sample are somewhat lower than the values obtained from the Hassel Formation sample. At hydrous pyrolysis temperatures greater than approximately 285°C, notable suppression of T_{max} is evident from the ever more pronounced difference in T_{max} values yielded by untreated and solvent extracted samples, respectively, corresponding to

increasing bitumen-saturation with increasing level of thermal maturity (Snowdon, 1995).

Homohopane and bishomohopane 22S/(22S + 22R) epimerization ratios increase with hydrous pyrolysis temperature, and for both samples thermodynamic equilibrium distribution is attained after hydrous pyrolysis at 330°C/72h (Table 4). No significant differences between the two samples are noted. Conversely, significant differences are evident in the C₂₉ regular sterane 20S/(20S + 20R) epimerization ratio (Figure 11, Table 5). The Bituminous Member sample shows a steady increase in sterane epimerization ratio with increasing temperature of hydrous pyrolysis, until a near-equilibrium distribution is attained after hydrous pyrolysis at 330°C/72h. Conversely, the Hassel Formation sample shows considerable retardation in evolution of the C₂₉ regular sterane 20S/(20S + 20R) epimerization ratio. A marked decrease in sterane epimerization ratio is noted after hydrous pyrolysis at 220°C/72h. This is most likely due to coelution of some unknown labile compound present in the untreated sample, but no data are available to support this hypothesis. With higher temperatures of hydrous pyrolysis, the C₂₉ regular sterane 20S/(20S + 20R) epimerization ratio increases steadily, but after hydrous pyrolysis at 330°C/72h, the ratio is still far from thermodynamic equilibrium (Figure 12, Table 5). Similar differences between samples containing marine (type II) and terrigenous (type III) kerogen have been observed previously, and have

been attributed to variable catalytic effects of different mineral matrices (Strachan et al., 1989). Furthermore, kinetic calculations indicate that these differences are also dependent on heating rate. Allegedly, at low heating rates, the sterane epimerization will proceed faster in rocks containing type III kerogen than in rocks containing type II kerogen, whereas at high heating rates the opposite is true (Strachan et al., 1989). Hence, hydrous pyrolysis is indeed expected to produce the very marked differences observed. However, studies of absolute biomarker concentrations in coals and vitrinite concentrates of various ranks indicate that the sterane epimerization ratio is not merely a conversion of one isomer to its more stable counterpart in response to the prevailing thermodynamic regime (Dzou et al., 1995), and the observations of Strachan et al. (1989) certainly do not provide a fully satisfactory explanation. However, the observations of Strachan et al. (1989) and Dzou et al. (1995) as well as the data reported here call for caution when using sterane epimerization ratios as thermal maturity indicators in sedimentary successions containing rocks with varying kerogen types.

Conclusions

Excellent potential petroleum source rocks are present in both the Albian and Cenomanian–Turonian successions on Ellesmere Island, Northwest Territories, Canada. Although both successions were deposited in marine environments, the Albian Hassel Formation contains predominantly terrigenous type III kerogen, whereas the Cenomanian–Turonian Bituminous Member (informal) of the Kanguk Formation contains predominantly marine type II kerogen.

Simulated thermal maturation by means of hydrous pyrolysis shows that upon maturation, both the generation characteristics and the products formed are widely different for the two samples. The Hassel Formation source rocks will generate both gas and wax-rich oil over a wide range of thermal maturities, whereas the Bituminous Member source rocks will generate both gas and low-wax oil over a somewhat narrower maturity range, and only gas at higher levels of maturity.

After hydrous pyrolysis at 330°C/72h, the type II kerogen sample shows considerable suppression of T_{max} due to bitumen impregnation, whereas the type III kerogen sample shows notable retardation in C_{29} regular sterane 20S/(20S + 20R) epimerization, calling for caution in the assessment of the level of thermal maturity in successions containing varying kerogen types.

The results draw attention to the importance of generation of liquid petroleum from terrigenous kerogen, which according to long held notions has been regarded as gas-prone only. Furthermore, the presence of highly

oil-prone source rocks in the Cretaceous succession on Ellesmere Island is very encouraging for ongoing petroleum exploration on- and offshore central West Greenland, and for possible future exploration in the Melville Bay and Baffin Bay. Moreover, the results reported herein may be important for exploration in deep-water basins in North Atlantic areas where the Mesozoic succession is imperfectly known.

References

- Arthur M. A., S. O. Schlanger, and H. C. Jenkyns, 1987. The Cenomanian – Turonian Oceanic Anoxic Event II. Palaeoceanographic controls on organic matter production and Preservation. In: Brooks, J. and Fleet, A. J. (eds): Marine Petroleum Source Rocks. Geological Society Special Publication No. 26, p. 401-420
- Bojesen-Koefoed, J. A., H. P. Nytoft and M. A. Dejkam, 1995. Hydrous pyrolysis of Upper Farsund Formation (Volgian–Ryazanian) "hot shales" from the southern Central Trough, German North Sea Sector. In: Grimalt, J. O. and Dorronsoro, C. (eds.) Organic Geochemistry: developments and applications to energy, climate, environment and human history - Selected papers from the 17th International Meeting on Organic Geochemistry 4-8th September 1995, Donastia - San Sebastian, p. 530-531
- Bojesen-Koefoed, J. A., F. G. Christiansen, H. P. Nytoft and A. K. Pedersen, in press. Oil seepage onshore West Greenland: evidence of multiple source rocks and oil mixing. In: A. S. Fleet and S. Boldy (eds): Petroleum Geology of NW-Europe, proceedings of the 5th Conference, Geological Society of London

Bordenave, M. L., J. Espitalié, P. Leplat, J. L. Oudin and M.

Vandenbroucke, 1993. Screening techniques for source rock evaluation. In: M. L. Bordenave (ed.), Applied petroleum geochemistry, Editions Technip, Paris, p. 219-278

Christiansen, F. G., J. Bojesen-Koefoed, G. Dam, H. P. Nytoft, L. M.

Larsen, A. K. Pedersen and T. C. R. Pulvertaft, 1996a: The Marraat oil discovery on Nuussuaq, West Greenland: evidence for a latest Cretaceous–earliest Tertiary oil prone source rock in the Labrador Sea–Melville Bay region. Bulletin of Canadian Petroleum Geology v. 44, p. 39-54.

Christiansen, F. G., A. Boesen, J. A. Bojesen-Koefoed, F. Dalhoff, G. Dam, P. S. Neuhoff, A. K. Pedersen, G. K. Pedersen, L. S. Stannius, and K. Zinck-Jørgensen, 1998. Petroleum geological activities onshore West Greenland in 1997. Geology of Greenland Survey Bulletin v. 180, p. 10-17

- De Paor, D. G., D. C. Bradley, G. Eisenstadt and S. M. Phillips, 1989. The Arctic Eureka Orogen: A most unusual fold-and-thrust belt. Geological Society of America Bulletin v. 101, p. 952-967
- Dzou, L. I. P., R. A. Noble and J. T. Senftle, 1995. Maturation effects on absolute biomarker concentration in a suite of coals and associated vitrinite concentrates. Organic Geochemistry v. 23, p. 681-697
- Embry, A. F. 1991. Mesozoic History of the Arctic Islands. In: H. P. Trettin (ed.), Geology of the Inuitian Orogen and Arctic Platform of Canada and Greenland. Geological Survey of Canada, Geology of Canada v. 3, chp. 14, p. 369-432 (Also: Geological Society of America. The Geology of North America, vol. E)
- Espitalié, J. 1986. Use of Tmax as a maturation index for different types of organic matter. Comparison with vitrinite reflectance. In: J. Burrus (ed.) Thermal modelling in sedimentary basins. Editions Technip, Paris, p. 475-496.
- Espitalié J., G. Deroo and F. Marquis, 1985. La pyrolyse Rock-Eval et ses applications. Première partie. Revue de l'institut Français du Pétrole v. 40, p. 563-579

- Espitalié, J. and L. Joubert ,1987. Use of Tmax as a maturation index in petroleum exploration. In: Kumar-Ruby, K., P. Dwivedi, V. Bannerjee and V. Gupta (eds): Petroleum geochemistry and exploration in the Afro-Asian region. Balkema, Rotterdam, p. 67-73
- Hallam, A. 1987. Mesozoic marine organic-rich shales. In: J. Brooks. and A. J. Fleet (eds): Marine Petroleum Source Rocks, Geological Society Special Publication No. 26, p. 251-261
- Huc, A. Y. 1990. Understanding organic facies: A key to improved quantitative petroleum evaluation of sedimentary basins. In: A. Y. Huc (ed.): Deposition of organic facies. AAPG Studies in geology v. 30, p. 1-11
- Klemme, H. D. and G. F. Ulmishek, 1991. Effective petroleum source rocks of the world: Stratigraphic distribution and controlling factors. AAPG Bulletin v. 75, p. 1809-1851
- Kuhnt, W. and J. Wiedmann, 1995. Cenomanian–Turonian source rocks: paleobiogeographic and paleoenvironmental aspects. In: A. Y. Huc

(ed.): Paleogeography, paleoclimate and source rocks, AAPG Studies in geology v. 40, p. 213-231

Núñez-Betulu, L. K., 1993. Rock-Eval/TOC pyrolysis data from the Kanguk Formation (Upper Cretaceous), Axel Heiberg and Ellesmere Islands, Canadian Arctic. Geological Survey of Canada Open File v. 2727, 30pp.

Núñez-Betulu, L. K., 1994. Sequence stratigraphy of a coastal to offshore transition, Upper Cretaceous Kanguk Formation: a palynological, sedimentological and Rock-Eval characterization of a depositional sequence, northeastern Sverdrup Basin, Canadian Arctic. Ph.D Dissertation, University of Calgary, 569pp.

Pepper, A. S. and P. J. Corvi, 1995. Simple kinetic models of petroleum formation. Part 1: oil and gas generation from kerogen. Marine and Petroleum geology v. 12, P. 291-319

Okulitch, A. V. and H. P. Trettin, 1991. Late Cretaceous - Early Tertiary deformation, Arctic Islands. In: H. P. Trettin (ed.), Geology of the Inuitian Orogen and Arctic Platform of Canada and Greenland. Geological Survey of Canada, Geology of Canada v. 3, chp. 17, p.

469-489 (Also: Geological Society of America. The Geology of North America, vol. E)

Radke M., H. Willsch and D. H. Welte, 1980a. Preparative hydrocarbon group determination by automated Medium Pressure Liquid Chromatography, *Analytical Chemistry* v. 52, p. 406-411

Radke, M., R. G. Schaefer, D. Leythaeuser and M. Teichmüller 1980b. Composition of soluble organic matter in coals: relation to rank and liptinite fluorescence, *Geochimica et Cosmochimica Acta* v. 44, p. 1787-1800

Ricketts, B. D. 1994. Basin analysis, Eureka Sound Group, Axel Heiberg and Ellesmere Islands, Canadian arctic archipelago. Geological Survey of Canada Memoir 439, 119 pp.

Rowley, D. B. and A. L. Lottes, 1988. Plate-kinematic reconstructions of the North Atlantic and Arctic: Late Jurassic to Present, *Tectonophysics* v. 155, p. 73-120

Schlanger, S. O. and H. C. Jenkyns, 1976. Cretaceous anoxic events: causes and consequences. *Geologie en Mijnbouw* v. 55, p. 179-184

Schlanger, S. O., M. A. Arthur, H. C. Jenkyns and P. A. Scholle, 1987.

The Cenomanian–Turonian Oceanic Anoxic Event I. Stratigraphy and distribution of organic carbon-rich beds and the marine $\delta^{13}\text{C}$ excursion.

In: J. Brooks and A. J. Fleet (eds): Marine Petroleum Source Rocks, Geological Society Special Publication No. 26, p. 251-261

Snowdon, L. R. 1995. Rock-Eval T_{max} suppression: documentation and amelioration. AAPG Bulletin v. 79, p. 1337-1348

Stach, E., M.-Th. Mackowsky, M. Teichmüller, G. H. Taylor, D. Chandra and R. Teichmüller, 1982. Stach's textbook of coal petrology. Gebrüder Borntraeger, Berlin, 535 pp.

Strachan, M. G., R. Alexander, W. van Bronswijk and R. Kagi, 1989.

Source and heating rate effects upon maturity parameters based on ratios of 24-ethylcholestane diastereomers, Journal of geochemical exploration v. 31, p. 285-294

Tissot, B. P., R. Pelet and Ph. Ungerer, 1987. Thermal history of sedimentary basins, maturation indices, and kinetics of oil and gas generation. AAPG Bulletin v. 71, p. 1445-1466

Tissot, B. P. and D. H. Welte, 1984. Petroleum formation and occurrence.

2nd edition, Springer, Berlin, 699 pp.

Ulmishek G. F. and H. D. Klemme, 1990. Depositional Controls,

Distribution, and Effectiveness of World's Petroleum Source Rocks.

United States Geological Survey Bulletin 1931, 59pp. + enclosures.

Whittaker, R. C., N. E. Hamann and T. C. R. Pulvertaft, 1997. A new

frontier province offshore Northwest Greenland: structure, basin

development, and petroleum potential of the Melville Bay area. AAPG

Bulletin v. 81, p. 978-998

Figure captions:

Figure 1. Map of western Greenland and northeastern Canada.

Approximate outline of the Sverdrup Basin is indicated by stippled line.

Sampling locations on Ellesmere Island are indicated by filled circles

Figure 2. Simple stratigraphic chart showing the Ellesmere Island

succession. In other areas the Kanguk Formation may rest unconformably

on strata older than the Hassel Formation. E.S. Gp. = Eureka Sound Group

Modified from Núñez-Betulu (1994).

Figure 3. Flow chart showing analytical programme.

Figure 4. Crossplots of T_{max} vs. Hydrogen Index and TOC vs. S2 for

samples of the Bituminous Member of the Kanguk Formation (upper part)

and the Hassel Formation (lower part). Data compiled from Núñez-Betulu

(1993). Samples selected for hydrous pyrolysis experiments are indicated by arrows.

Figure 5. Gas chromatograms, ion fragmentograms m/z 191 and m/z 217,

and pyrolysis gas chromatograms for the Bituminous Member and Hassel

Formation samples. Upper part: untreated samples. Lower part: after

hydrous pyrolysis at 330°C/72h. Key: (GC data): 25: nC_{25} , H28: 28,30-bisnorhopane; (m/z 191): Tm: 17 α (H)-trisnorhopane, 17 β TNH: 17 β (H)-trisnorhopane, H28: 28,30-bisnorhopane, H29: 30-norhopane, M29: 30-normoretane, H30: hopane, M30: moretane, H31: homohopane (22S and 22R epimers indicated), H33: trishomohopane (22S and 22R epimers indicated); (m/z 217): H28: 28,30-bisnorhopane, S29: ethylcholestane (5 α (H)14 α (H)17 α (H)20S, 5 α (H)14 β (H)17 β (H)20R, 5 α (H)14 β (H)17 β (H)20S and 5 α (H)14 α (H)17 α (H)20R epimers indicated); (Pyrolysis-GC): T: Toluene, X: M + P-xylene, 10: nC_{10} alkene/alkane doublet.

Figure 6. T_{max} versus hydrogen Index diagrams for samples subjected to hydrous pyrolysis. Left: Hassel Formation sample. With increasing thermal maturity induced by hydrous pyrolysis, the kerogen composition changes roughly following the type III evolution path. Note that significant generation potential remains after hydrous pyrolysis at 330°C/72h (Hydrogen Index 206 mg/g OC, extracted sample 155 mg/g OC). Right: Bituminous Member sample. With increasing thermal maturity induced by hydrous pyrolysis, the kerogen composition changes along the type II evolution path. Note that after hydrous pyrolysis at 330°C/72h, the generation potential is largely exhausted (Hydrogen Index: 106 mg/g OC, extracted sample 80 mg/g OC). Also note initial increase in Hydrogen

Index, probably due to release of high proportions of heteroatomic gaseous compounds (H_2O , CO , CO_2 etc.) during early stages of thermal maturation.

Figure 7. "Generation diagrams" constructed by combining Rock-Eval/TOC and GOR data from pyrolysis gas chromatography following the procedures of Pepper and Corvi (1995). Note differences in generation characteristics: after hydrous pyrolysis at 330°C/72H, the capacity for generation of liquid petroleum is largely exhausted in the marine type II kerogen Bituminous Member sample, whereas in the terrigenous type III kerogen Hassel Formation sample, potential for generation of both liquid and gaseous petroleum products persists.

Figure 8. Pseudo-activation energy distributions for untreated samples and for samples after hydrous pyrolysis at 330°C/72H. Note slightly higher total potential and narrower distribution of the marine type II kerogen Bituminous Member sample, as compared to the terrigenous type III kerogen Hassel Formation sample. After hydrous pyrolysis at 330°C/72H, notably higher generation potential remains in the terrigenous type III kerogen Hassel Formation sample compared to the marine type II kerogen Bituminous Member sample.

Figure 9. Gas chromatograms showing changes in saturate fraction compositions with increasing temperature of hydrous pyrolysis for the marine type II kerogen Bituminous Member sample and the terrigenous type III kerogen Hassel Formation sample.

Figure 10. Evolution in T_{max} and vitrinite reflectance (Hassel Formation sample only) with increasing temperature of hydrous pyrolysis.

Fig 11. Evolution in regular sterane 20S/(20S + 20R) epimerization ratio with increasing temperature of hydrous pyrolysis.

Tables:

Table 1. Organic matter composition in samples from the Hassel Formation and the Bituminous Member, mineral free basis. The distribution is based on point-counting (500 points).

Table 2. Rock-Eval screening data, untreated samples and samples subjected to hydrous pyrolysis and solvent extraction.

Table 3. Extraction and gas chromatography data, untreated samples and samples subjected to hydrous pyrolysis. Extract yield in mg/g TOC. Asphaltenes in wt-% of total extract. Saturates, aromatics and NSO's in wt-% of maltene fraction. Isopren/n-alkane = sum of C_{15-20} acyclic isoprenoids/sum of C_{15-20} n-alkanes.

Table 4. Triterpane biomarker ratios, untreated samples and samples subjected to hydrous pyrolysis. T_{23} : C23 tricyclic triterpane; Ts: 18 α (H)-trisnorhopane; Tm: 17 α (H)-trisnorhopane; 17 β : 17 β (H)-trisnorhopane; H_{28} : 28,30-bisnorhopane H_{29} : 30-norhopane H_{30} : hopane; H_{31} : homohopane (22S and 22R epimers); H_{32} : bishomohopane (22S and 22R epimers); M_{30} : moretane

Table 5. Sterane biomarker ratios, untreated samples and samples subjected to hydrous pyrolysis. S_{29} (S/S + R): ethylcholestane $\alpha\alpha\alpha 20S / (\alpha\alpha\alpha 20S + \alpha\alpha\alpha 20R)$; S_{29} ($\beta\beta / \beta\beta + \alpha\alpha$): ethylcholestane $\alpha\beta\beta / (\alpha\beta\beta + \alpha\alpha\alpha)$; S_{27}/S_{29} : cholestane/ethylcholestane, calculated as $C_{27}\alpha\alpha\alpha 20R / C_{29}\alpha\alpha\alpha 20R$.

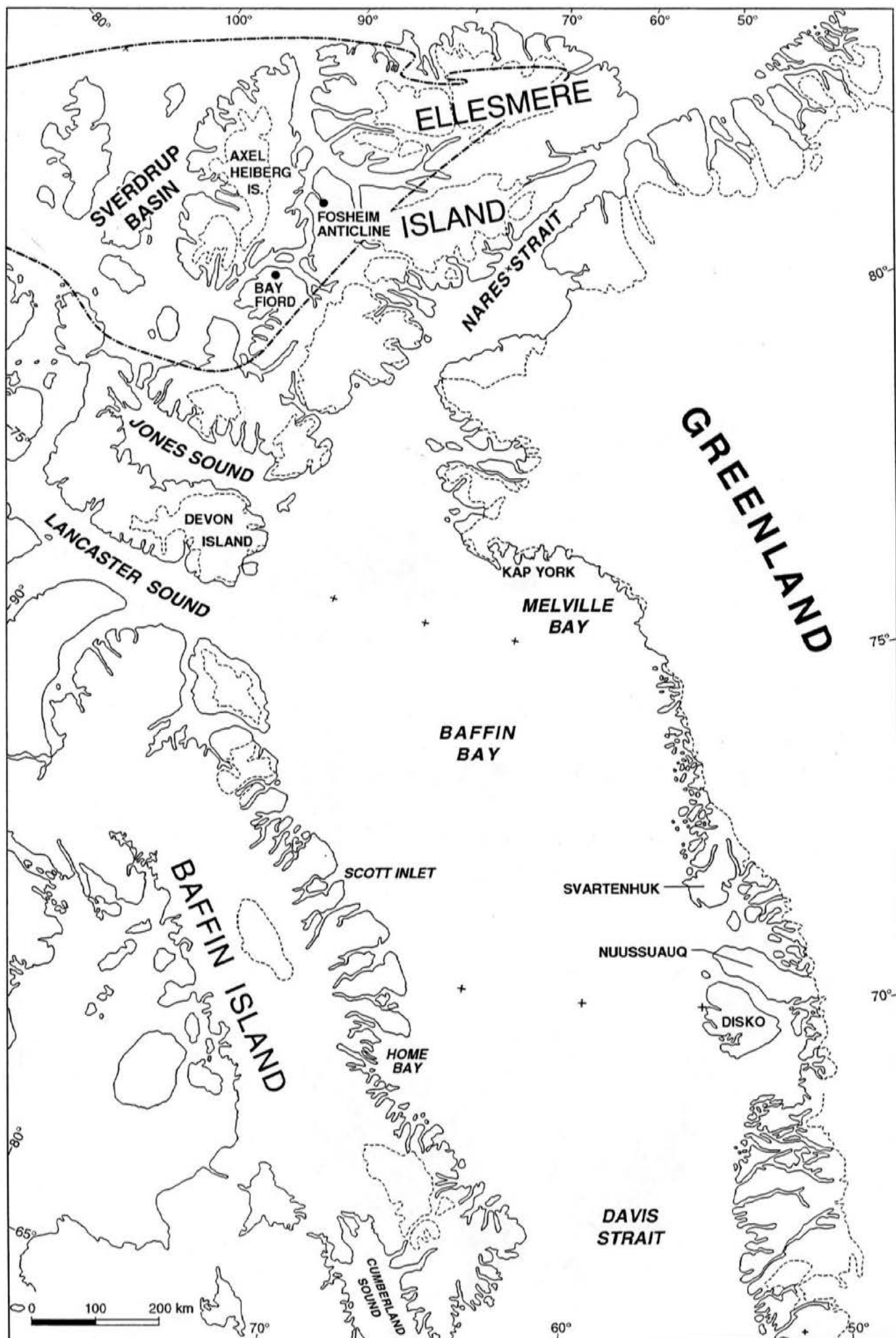


Fig. 1

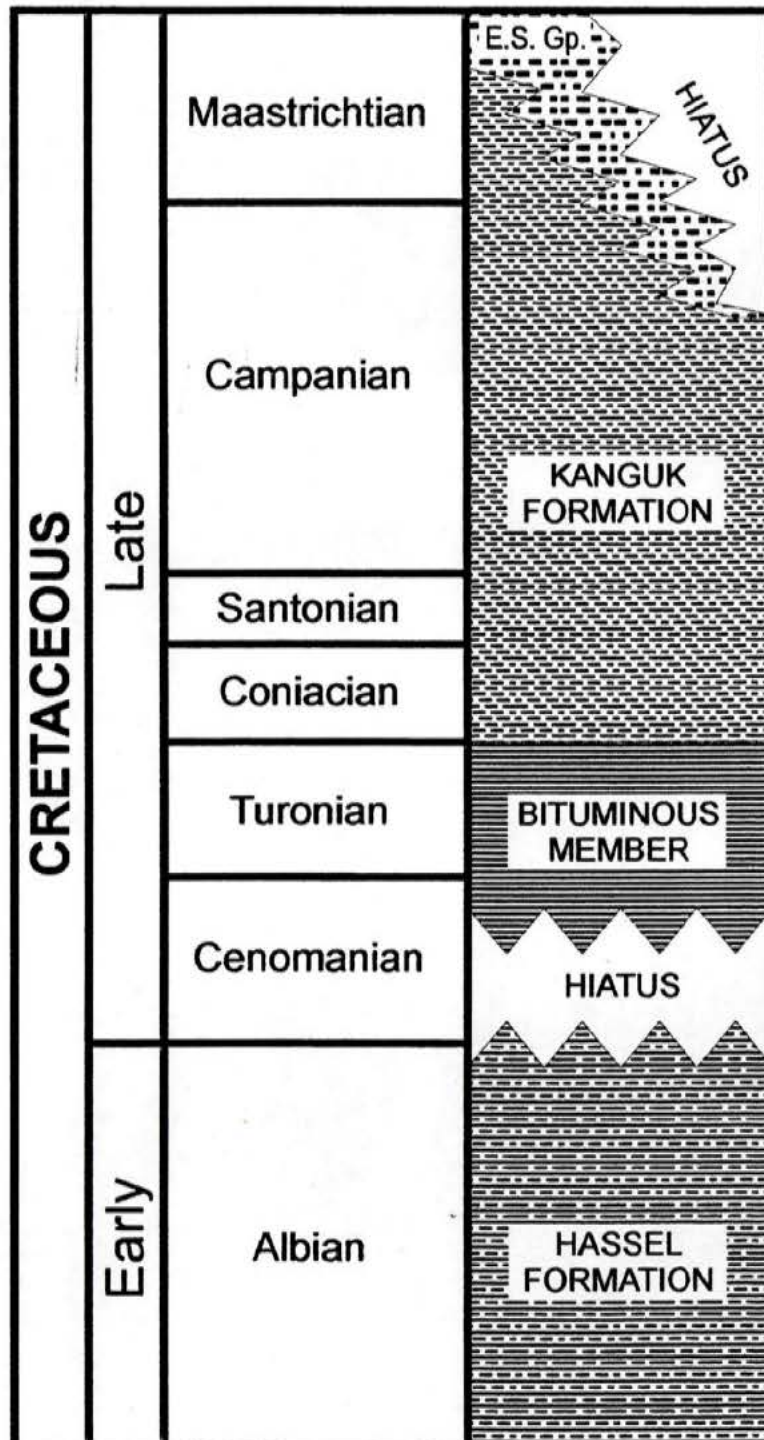


Fig. 2.

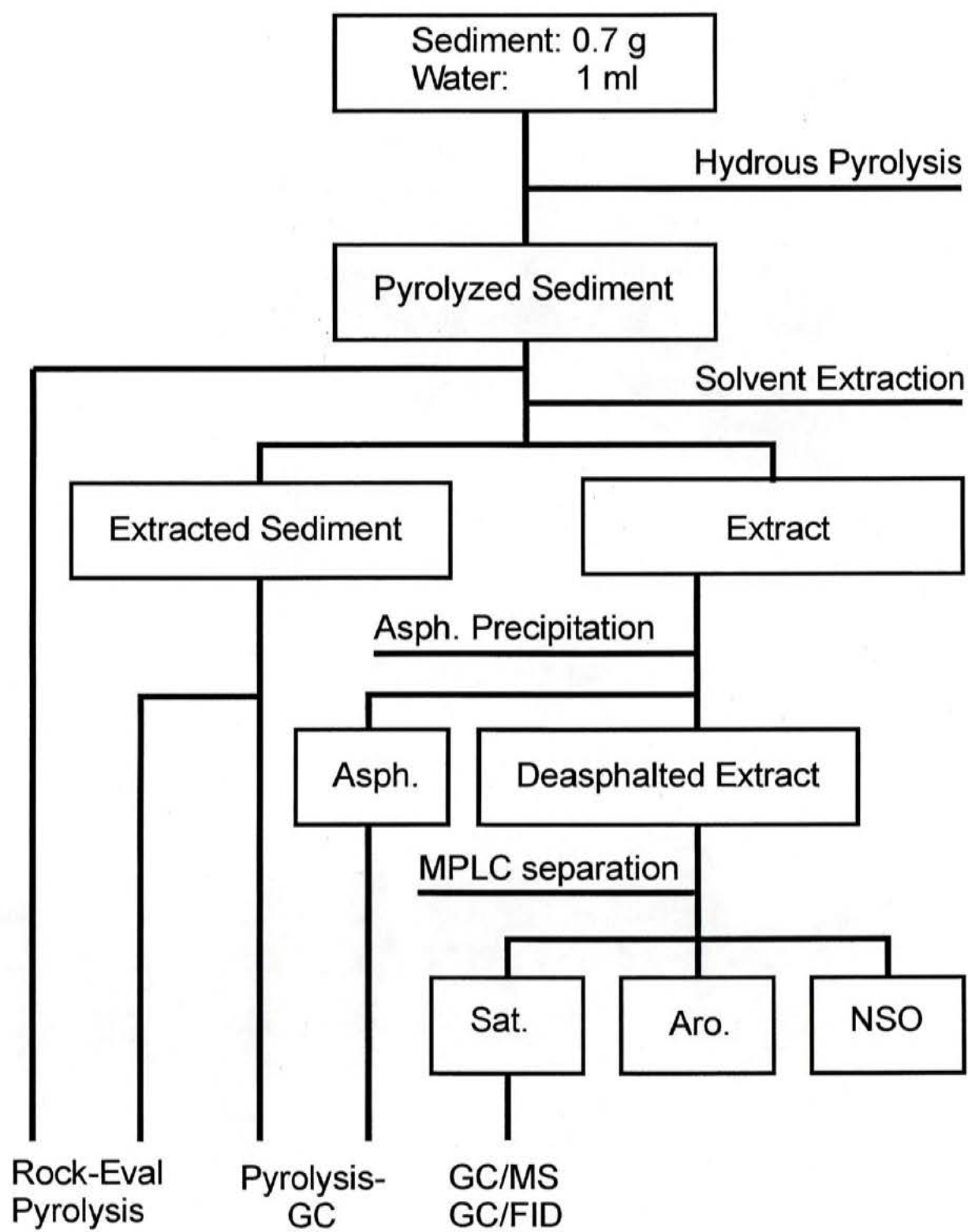
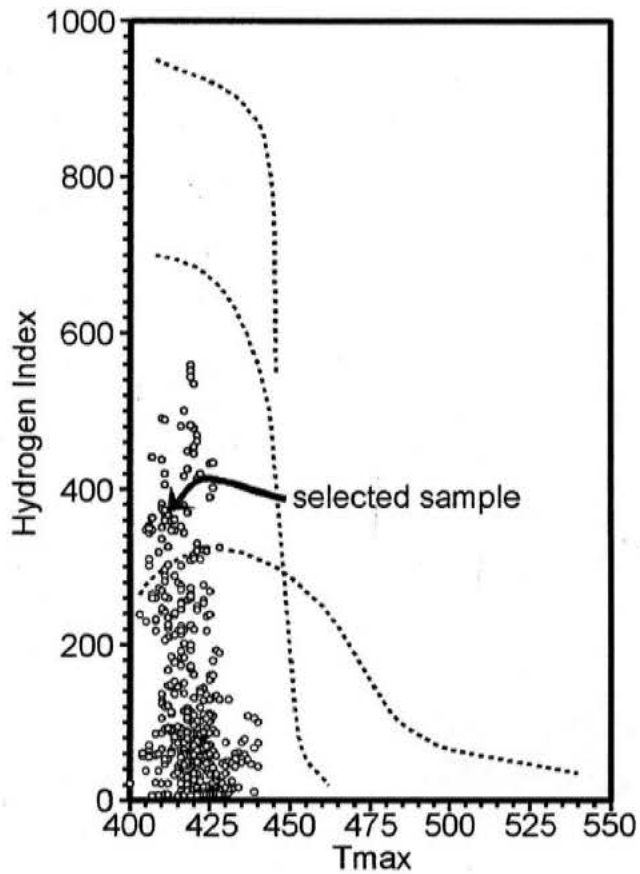
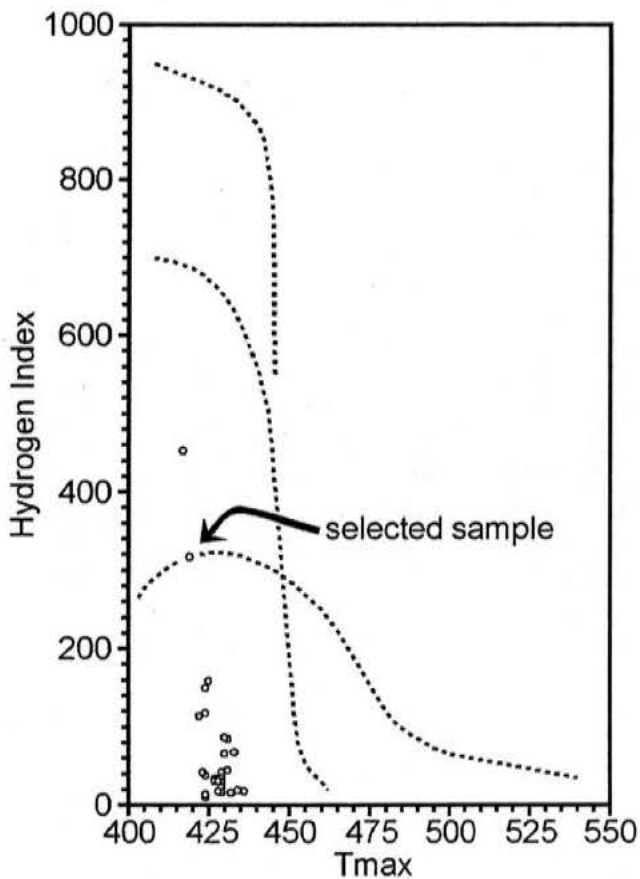
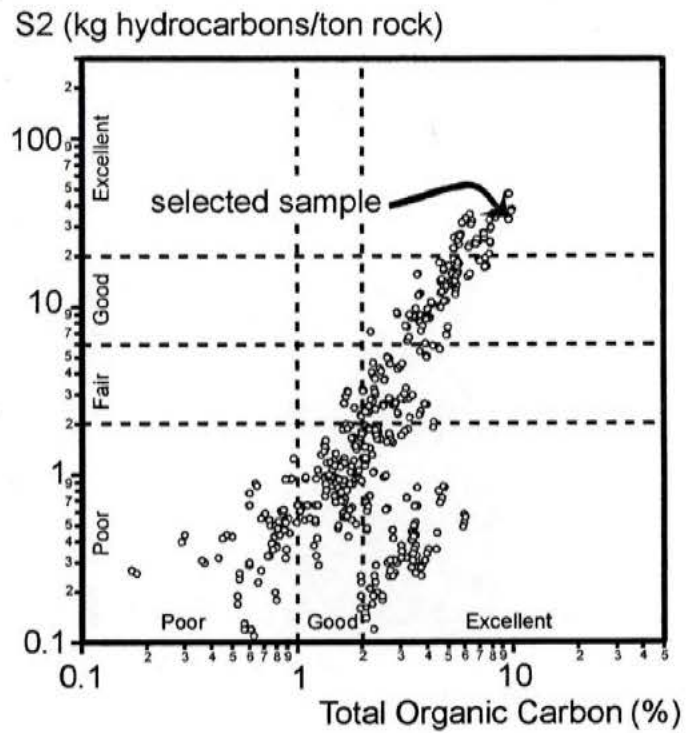


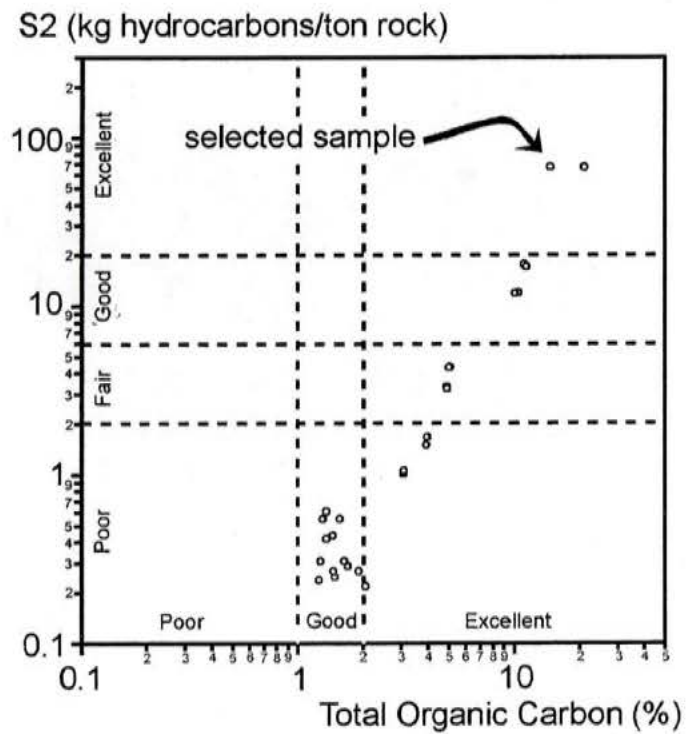
Fig. 3



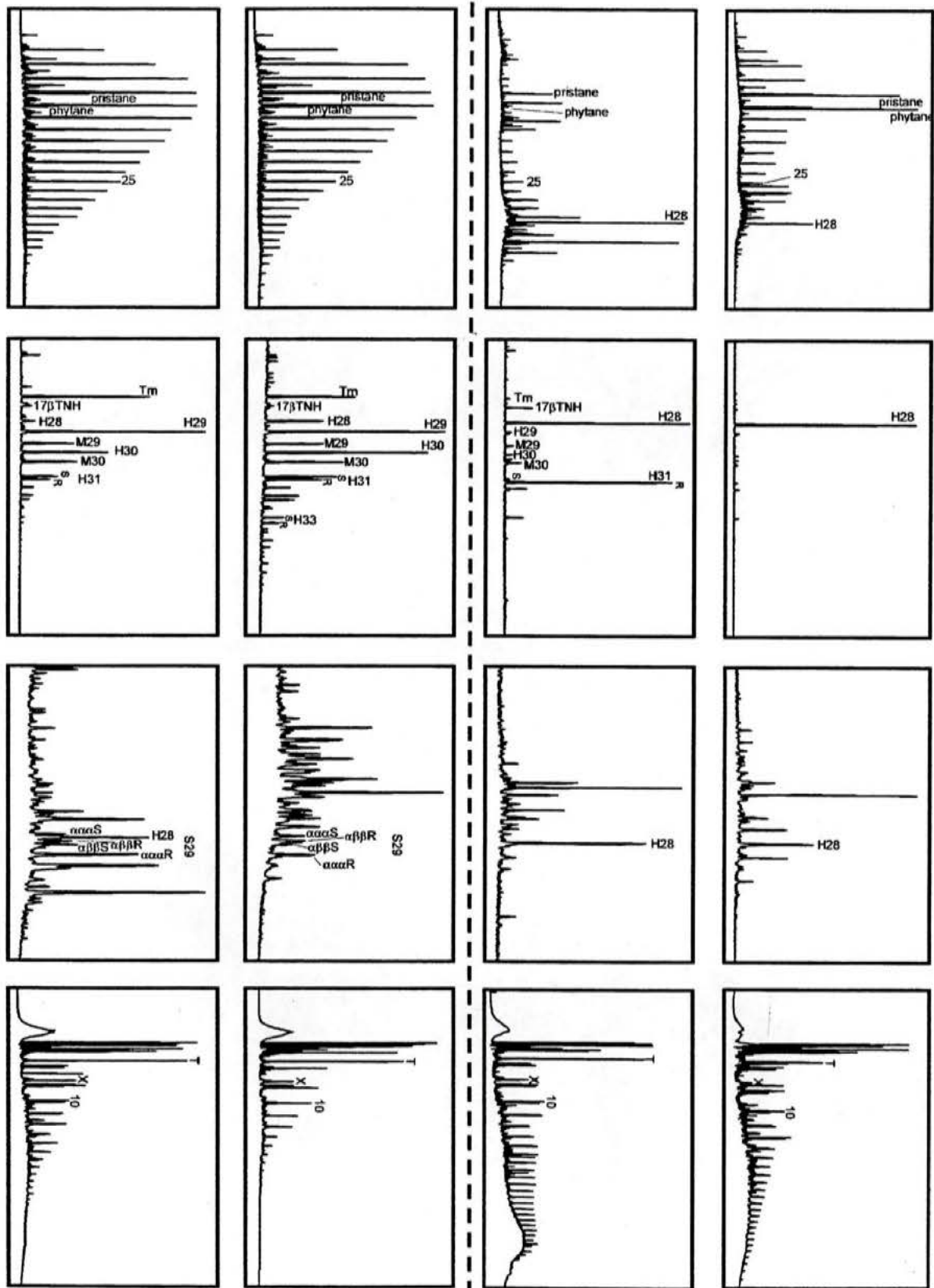
Kunguk Fm., Bituminous Mb.



Hassel Fm.



Fr. 5



Gas chromatograms

Triterpanes, m/z 191

Steranes, m/z 217

Pyrolysis-gas chromatograms

Hassel Fm.

Bituminous Mb.

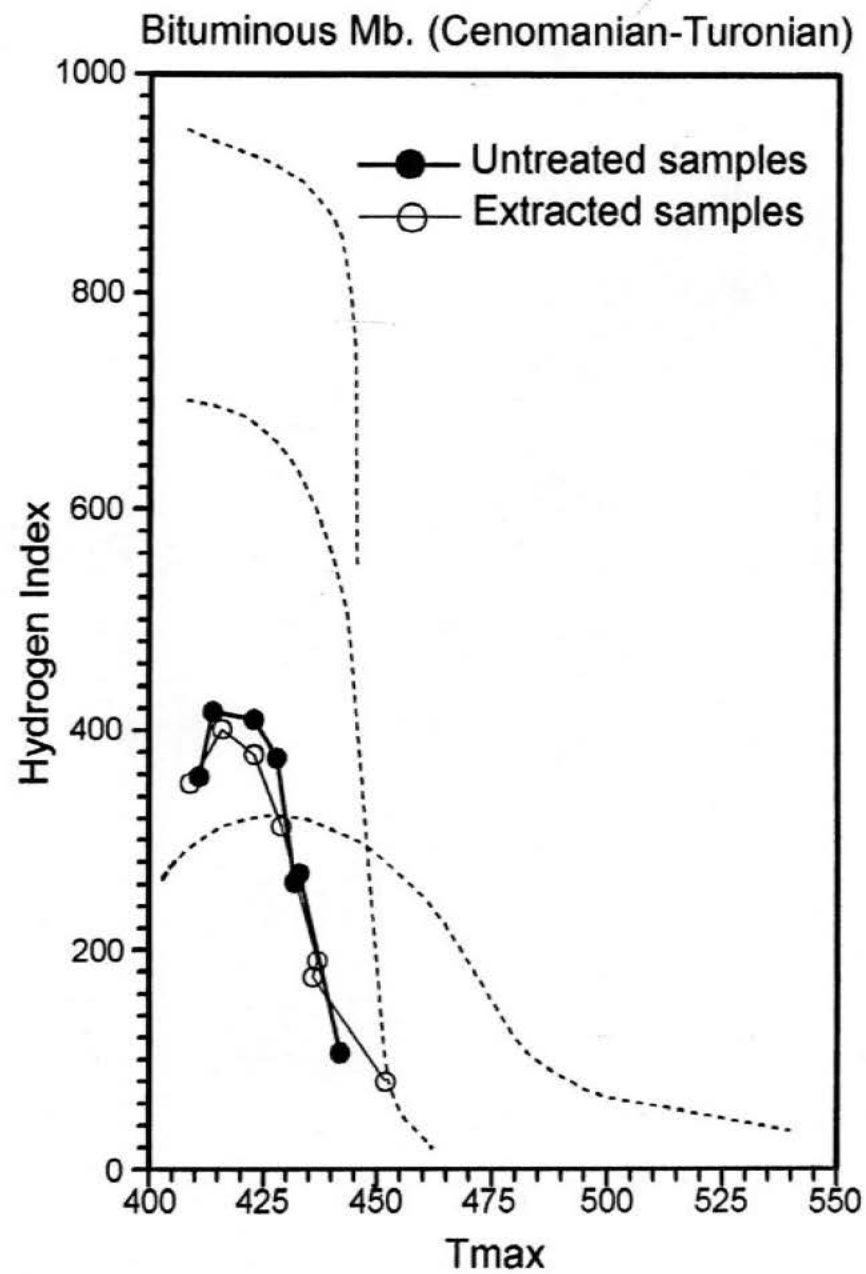
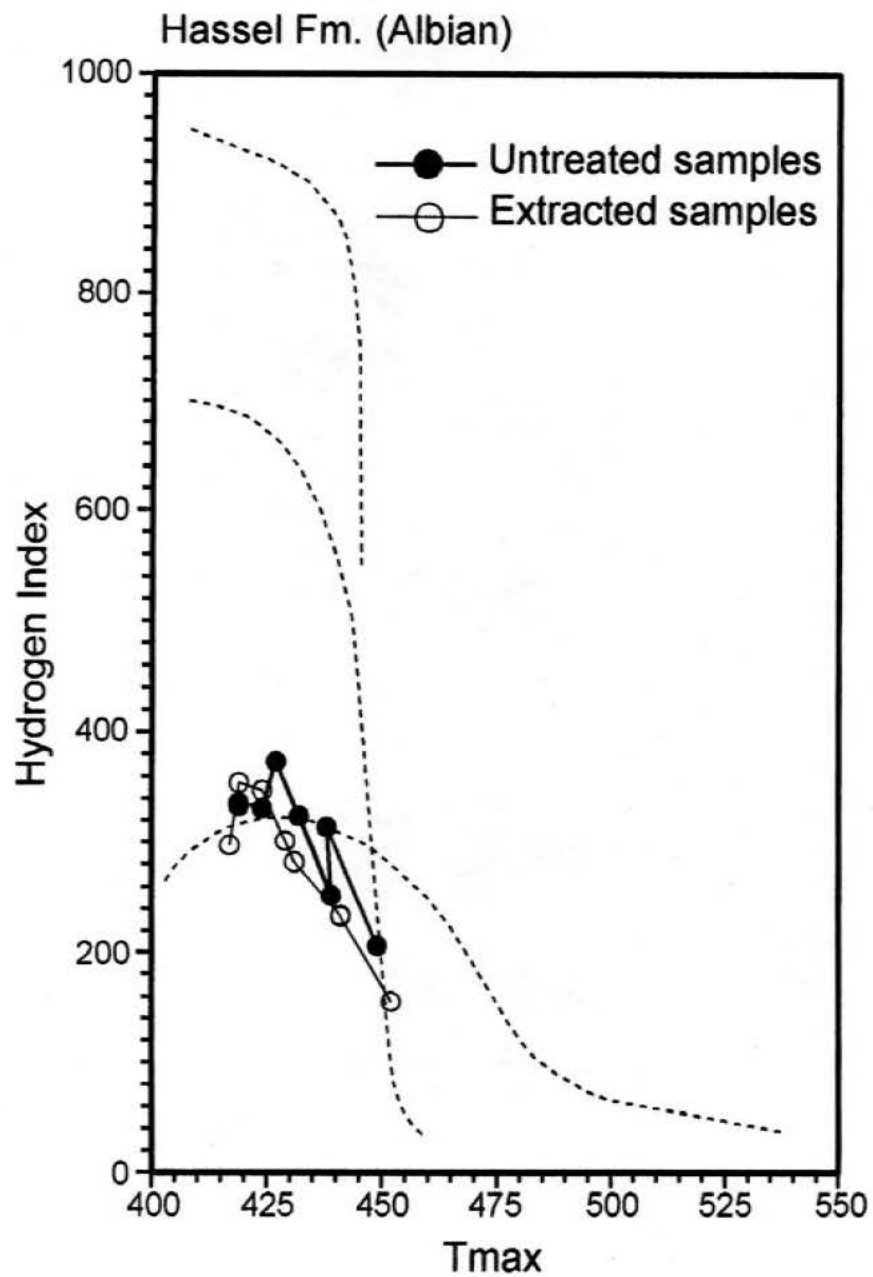
Hassel Fm.

Bituminous Mb.

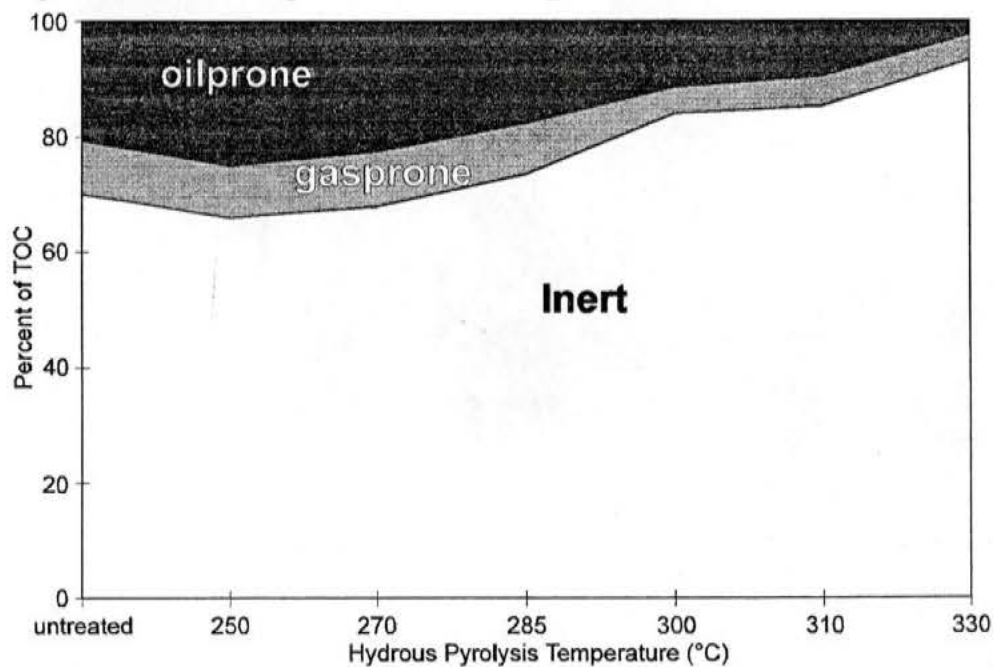
Hydrous pyrolysis
at 330°C/72h

Untreated sample

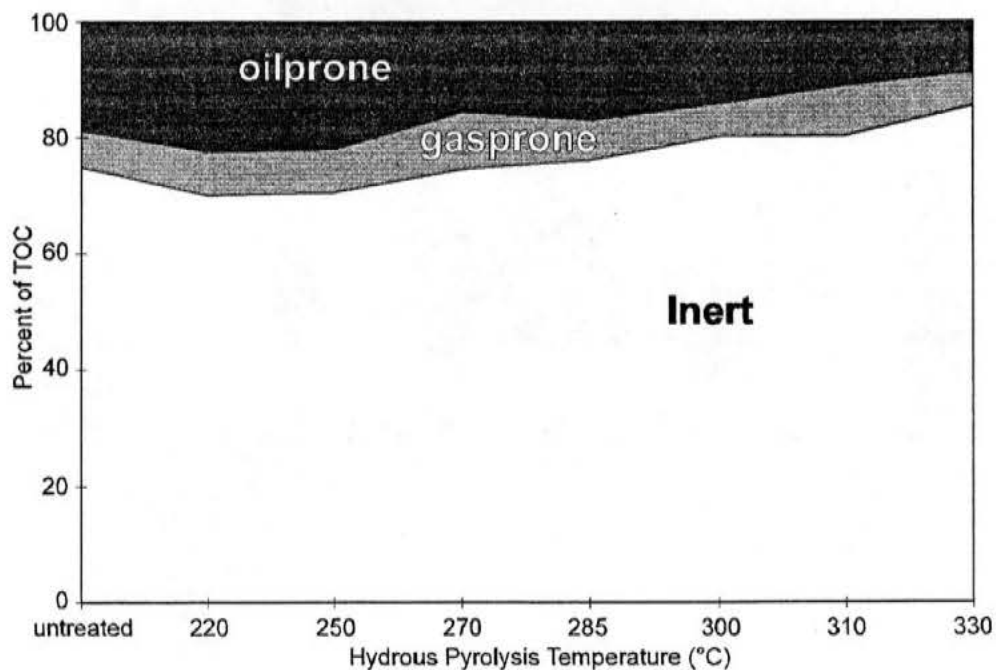
Fig. 6.



Kanguk Fm., Bituminous Mb. (Cenomanian - Turonian),
predominantly marine kerogen:



Hassel Formation (Albian),
predominantly terrigenous kerogen:



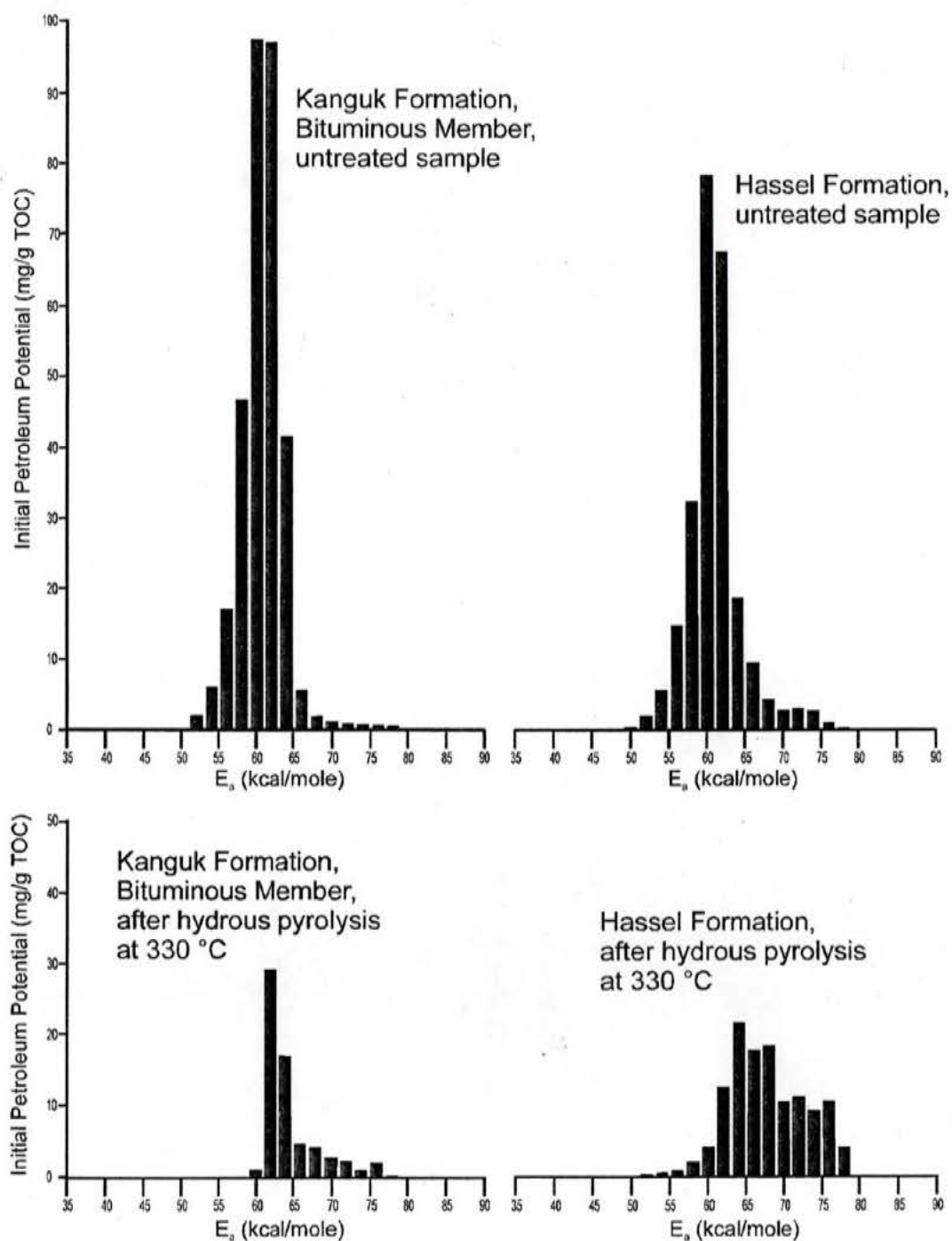
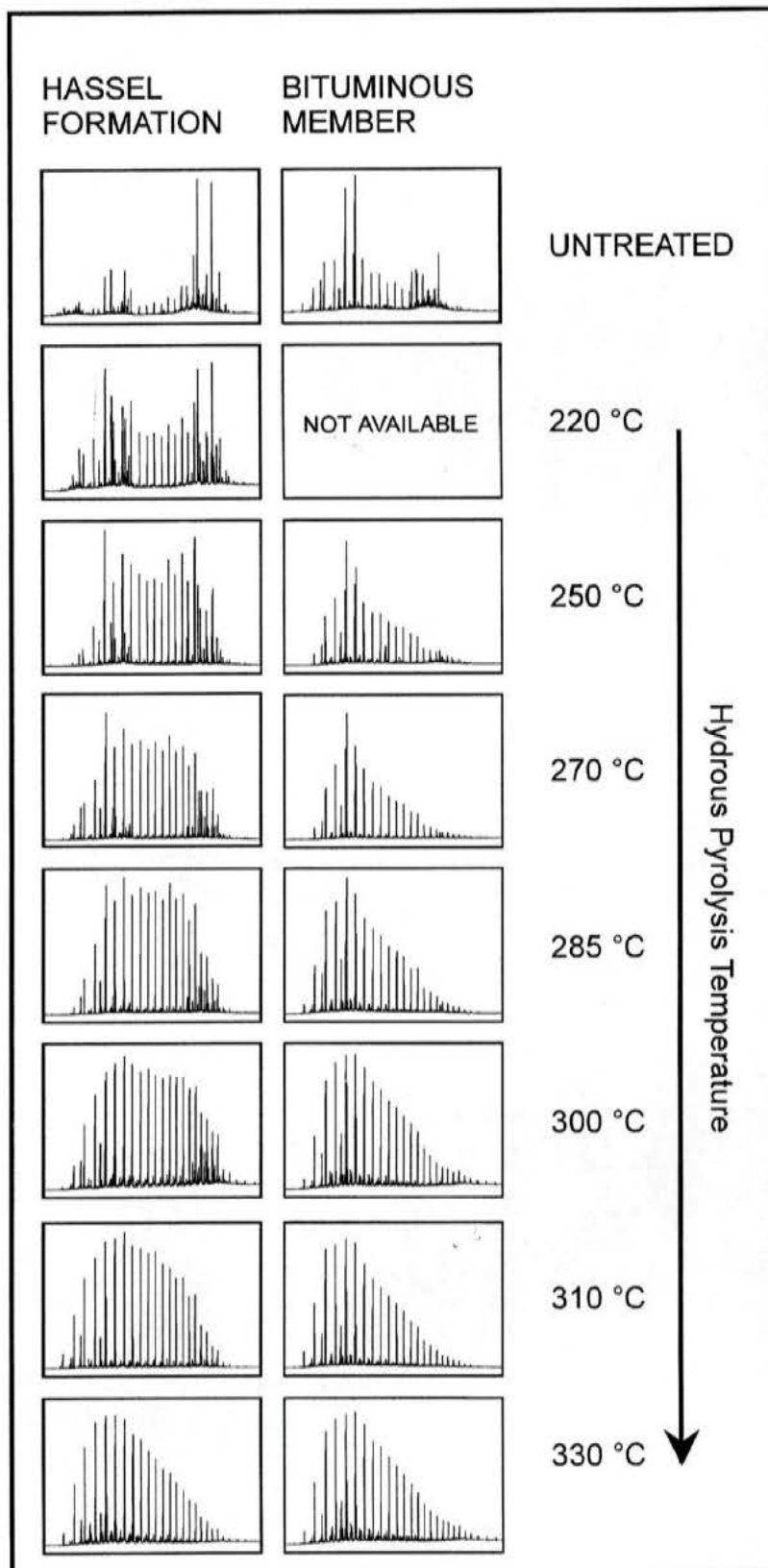


Fig. 8



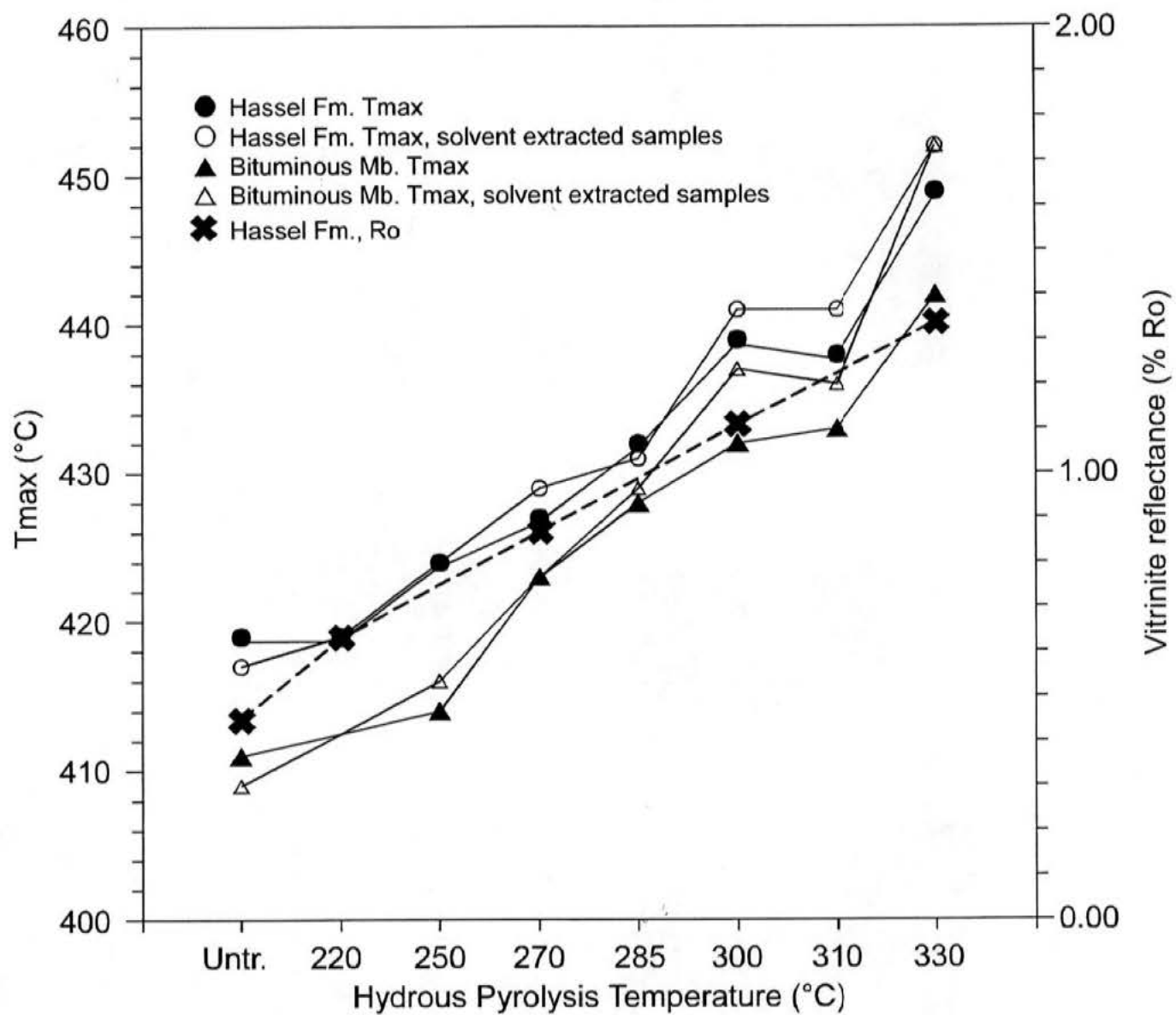


Fig. 10

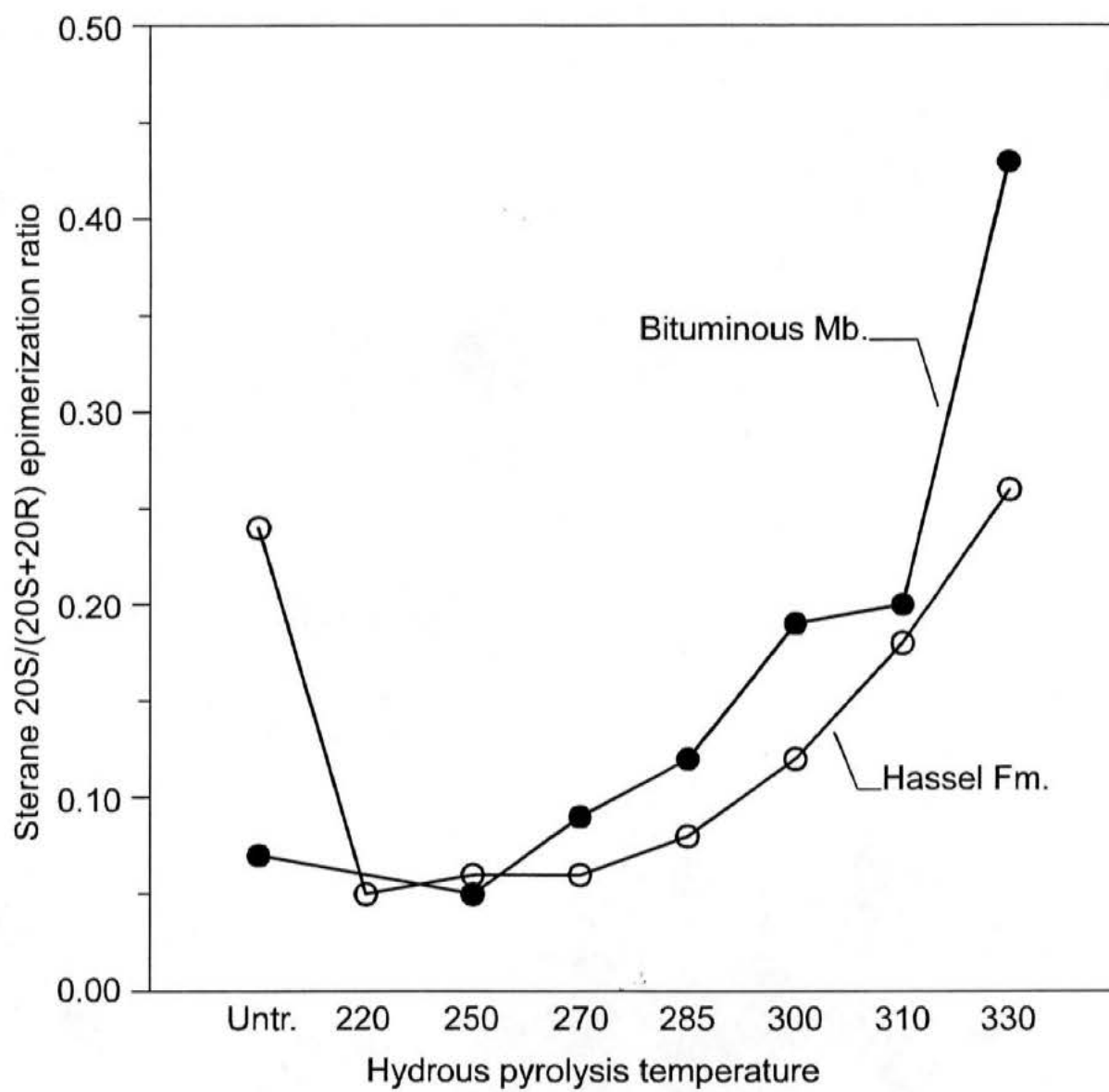


Fig. 11

	Hassel Formation		Bituminous Member	
	(% vol. mineral-free)		(% vol. mineral-free)	
Huminite	31		8	
Inertinite	51		5	
Sporinite	2	Total	5	Total
Cutinite	1	liptinite:	5	liptinite:
Liptodetrinite	8	11	53	63*
Organo-mineral matrix	7		24	

* Probably minimum due to presence of very fine-grained dispersed liptinite. Alginite has been observed.

Table 1.

SAMPLE	TOC	Tmax	S1	S2	PI	HI
Hassel Fm., Untreated	17,83	419	1,95	59,46	0,03	333
Hassel Fm., 220°C/72h	19,80	419	1,93	66,53	0,03	336
Hassel Fm., 250°C/72h	20,43	424	3,22	67,55	0,05	331
Hassel Fm., 270°C/72h	17,91	427	3,75	66,83	0,05	373
Hassel Fm., 285°C/72h	19,98	432	5,07	64,76	0,07	324
Hassel Fm., 300°C/72h	20,60	439	8,99	51,96	0,15	252
Hassel Fm., 310°C/72h	16,48	438	7,29	51,80	0,12	314
Hassel Fm., 330°C/72h	19,49	449	17,44	40,23	0,30	206
Hassel Fm. Untreated, Extracted	17,63	417	1,38	52,29	0,03	297
Hassel Fm., 220°C/72h, Extracted	17,13	419	0,96	60,56	0,02	354
Hassel Fm., 250°C/72h, Extracted	16,94	424	1,13	58,86	0,02	347
Hassel Fm., 270°C/72h, Extracted	19,64	429	1,12	59,10	0,02	301
Hassel Fm., 285°C/72h, Extracted	20,15	431	1,17	56,86	0,02	282
Hassel Fm., 300°C/72h, Extracted	18,50	441	1,13	43,33	0,03	234
Hassel Fm., 310°C/72h, Extracted	17,84	441	0,94	41,49	0,02	233
Hassel Fm., 330°C/72h, Extracted	17,40	452	1,13	26,91	0,04	155
Bituminous Mb., Untreated	9,61	411	1,31	34,36	0,04	358
Bituminous Mb., 250°C/72h	10,46	414	1,12	43,60	0,03	417
Bituminous Mb., 270°C/72h	10,32	423	1,96	42,32	0,04	410
Bituminous Mb., 285°C/72h	10,07	428	2,91	37,73	0,07	375
Bituminous Mb., 300°C/72h	9,44	432	3,13	24,69	0,11	262
Bituminous Mb., 310°C/72h	9,46	433	3,94	25,58	0,13	270
Bituminous Mb., 330°C/72h	9,13	442	4,36	9,69	0,31	106
Bituminous Mb., Untreated, Extracted	9,98	409	0,81	35,16	0,02	352
Bituminous Mb., 250°C/72h, Extracted	9,66	416	0,19	38,73	0,00	401
Bituminous Mb., 270°C/72h, Extracted	9,05	423	0,12	34,17	0,00	378
Bituminous Mb., 285°C/72h, Extracted	8,55	429	0,12	26,74	0,00	313
Bituminous Mb., 300°C/72h, Extracted	8,23	437	0,11	15,64	0,01	190
Bituminous Mb., 310°C/72h, Extracted	7,86	436	0,12	13,72	0,01	175
Bituminous Mb., 330°C/72h, Extracted	6,96	452	0,07	5,55	0,01	80

Table 2.

SAMPLE	Extract	Asph.	Sat.	Aro.	NSO	pristane	isopren	Sum nC ₁₅₋₂₂	CPI
	Yield	(%)	(%)	(%)	(%)	phytane	n-alkane	Sum nC ₂₃₋₃₀	
Hassel Fm., Untreated	107	40	9	7	84	6,08	1,15	n.a.	n.a.
Hassel Fm., 220°C/72h	48	33	n.a.	n.a.	n.a.	5,71	0,69	n.a.	1,26
Hassel Fm., 250°C/72h	n.a.	19	11	6	83	4,14	0,58	0,75	1,39
Hassel Fm., 270°C/72h	79	38	5	5	90	5,78	0,57	0,88	1,29
Hassel Fm., 285°C/72h	69	33	n.a.	n.a.	n.a.	5,31	0,46	0,84	1,28
Hassel Fm., 300°C/72h	93	36	11	11	78	5,37	0,33	1,02	1,20
Hassel Fm., 310°C/72h	96	41	n.a.	n.a.	n.a.	4,67	0,23	1,39	1,17
Hassel Fm., 330°C/72h	136	35	13	14	73	2,70	0,11	2,62	1,10
Bituminous Mb., Untreated	64	51	4	9	87	0,83	1,53	2,07	0,66
Bituminous Mb., 250°C/72h	92	30	3	6	91	1,27	0,88	2,58	0,99
Bituminous Mb., 270°C/72h	132	38	n.a.	n.a.	n.a.	1,70	0,74	3,30	0,94
Bituminous Mb., 285°C/72h	202	41	4	13	83	1,93	0,58	3,17	0,91
Bituminous Mb., 300°C/72h	225	46	8	10	82	1,78	0,34	3,11	1,00
Bituminous Mb., 310°C/72h	250	45	8	12	80	1,95	0,33	3,38	0,97
Bituminous Mb., 330°C/72h	332	51	14	16	70	1,81	0,22	3,08	1,04

Table 3

SAMPLE	T ₂₃ /H ₃₀	Ts/Ts+Tm	Tm/Tm+17β	H ₂₈ /H ₂₉	H ₂₉ /H ₃₀	M ₃₀ /H ₃₀	H ₃₁ (S/S+R)	H ₃₂ (S/S+R)
Hassel Fm., Untreated	0,00	0,00	0,20	7,41	0,89	0,58	0,06	0,00
Hassel Fm., 220°C/72h	0,00	0,00	0,23	8,94	0,74	0,65	0,06	0,00
Hassel Fm., 250°C/72h	0,00	0,00	0,31	4,90	0,97	0,84	0,08	0,13
Hassel Fm., 270°C/72h	0,00	0,00	0,52	1,91	1,35	1,00	0,16	0,06
Hassel Fm., 285°C/72h	0,00	0,00	0,68	0,96	1,81	1,08	0,29	0,16
Hassel Fm., 300°C/72h	0,00	0,01	0,79	0,36	1,63	0,88	0,45	0,38
Hassel Fm., 310°C/72h	0,00	0,01	0,92	0,19	2,14	1,03	0,50	0,52
Hassel Fm., 330°C/72h	0,06	0,08	0,92	0,08	2,13	0,65	0,56	0,59
Bituminous Mb., Untreated	0,17	0,00	0,40	12,60	1,67	0,83	0,09	n.a.
Bituminous Mb., 250°C/72h	0,10	0,00	0,56	13,13	1,15	0,60	0,14	n.a.
Bituminous Mb., 270°C/72h	0,11	0,00	0,59	6,29	1,37	0,63	0,16	0,14
Bituminous Mb., 285°C/72h	0,13	0,00	0,78	2,56	1,31	0,67	0,20	0,19
Bituminous Mb., 300°C/72h	0,34	0,10	0,82	0,98	1,36	0,62	0,34	0,33
Bituminous Mb., 310°C/72h	0,18	0,08	0,88	1,14	1,06	0,53	0,37	0,35
Bituminous Mb., 330°C/72h	0,47	0,10	0,90	0,34	1,10	0,50	0,55	0,53

Table 4.

SAMPLE	S ₂₉ (S/S+R)	S ₂₉ ($\beta\beta/\beta\beta+\alpha\alpha$)	S ₂₇ /S ₂₉
Hassel Fm., Untreated	0,24	n.a	0,39
Hassel Fm., 220°C/72h	0,05	n.a	0,26
Hassel Fm., 250°C/72h	0,06	n.a	0,07
Hassel Fm., 270°C/72h	0,06	n.a	0,04
Hassel Fm., 285°C/72h	0,08	0,22	0,06
Hassel Fm., 300°C/72h	0,12	0,15	0,05
Hassel Fm., 310°C/72h	0,18	0,20	0,06
Hassel Fm., 330°C/72h	0,26	0,39	0,19
Bituminous Mb., Untreated	0,07	n.a.	3,10
Bituminous Mb., 250°C/72h	0,05	0,33	3,78
Bituminous Mb., 270°C/72h	0,09	0,30	3,68
Bituminous Mb., 285°C/72h	0,12	0,26	3,28
Bituminous Mb., 300°C/72h	0,19	0,27	3,44
Bituminous Mb., 310°C/72h	0,20	0,29	3,10
Bituminous Mb., 330°C/72h	0,43	0,41	3,35

Table 5.